The Visual Pigments of Deep-Sea Crustaceans

Jeremy Kent

A thesis submitted to the University of Bristol in accordance with the requirements of the degree of Doctor of Philosophy in the Faculty of Science.

School of Biological Sciences
University of Bristol

June 1997

ABSTRACT

The deep-sea presents a unique visual environment. Due to spectral filtering by overlying water, the downwelling light is reduced to homochromatic blue light. At greater depths and at night, downwelling sunlight is insignificant and the visual environment is limited to bioluminescent emissions. The suggestion that deep-sea animals have their retinal spectral sensitivities matched to the light available at depth, the Sensitivity Hypothesis, has largely been investigated using species of deep-sea fishes. To test the hypothesis further it has now been applied to another taxon which inhabits the same environment. This thesis is presented as a comparative study of the visual pigments of deep-sea crustaceans, concentrating on the caridean and penaeidean decapods.

During RRS Challenger cruise 122 (September to October 1995) and a cruise on the RV New Horizon (May 1996) a total of thirty six species of deep-sea crustaceans were collected. Specimens included twenty nine species of decapods, six mysids and a single amphipod. On board ship, specimens were sorted under dim red illumination, the eyes removed and preserved by rapid freezing. Following the cruises, at the University of Bristol, frozen eyes were sectioned on a cryostat and the spectral absorbances of the rhabdomeric visual pigments were measured using a purpose-modified microspectrophotometer. Computer spread-sheet based analysis methods were written to fully characterise the visual pigments present.

Most deep-sea crustaceans investigated have a single visual pigment with a wavelength of peak absorbance (λ_{max}) between 482 and 509 nm, on average *ca.* 10 nm longer than those of the deep-sea fishes. Thus, on first investigation, deep-sea crustacean visual pigments are not matched to the spectrum of downwelling sunlight available in the deep-sea, nor the wavelength of maximum bioluminescent emissions. No correlation is apparent with depth and the total range of pigments is limited. However, simple modelling describing the viewing of bioluminescence suggests that, due to the asymmetries of both visual pigment and bioluminescent spectra, these pigments are, in fact, spectrally located to maximise photon capture. This model also reveals a correlation between rhabdom length and rhodopsin pigment which may explain differences in visual pigment complement between species.

In contrast to the majority of species, four Oplophorid species also have a second, short wavelength sensitive visual pigment (λ_{max} *ca.* 414 nm), conferring broader spectral sensitivity and the potential for hue discrimination. The demonstration of such a pigment in a bathypelagic, non-vertically migrating species which lacks photophores questions the use of such a pigment in mediating daily migrations and conspecific recognition. However, its presence still indicates its possible advantage in increasing perception to, and distinguishing between, different sources of bioluminescence.

Dedicated to my friends

ACKNOWLEDGEMENTS

I thank my advisor, Julian Partridge, for his help and encouragement during my time as both an undergraduate and postgraduate here at Bristol. My Ph.D. would not have been possible without him. To my second advisor, Peter Herring, I express my gratitude and respect.

While not reflected in this thesis, over a year of this project was concerned with the setting up of equipment. As such, the research I subsequently achieved would not have occurred without the help of numerous technicians. Above all, Linda Teagle gave me the continued help, support and encouragement I needed.

My fellow 'vision scientists' have proved a welcoming group and I especially thank Tom Cronin and Justin Marshall for showing me many of the experimental procedures used in this study. Other scientists I thank include Peter Shelton, Magnus Johnson, Pat Hargreaves, Ron Douglas and family, and Jim Childress for allowing a 'Brit' on his cruise. This work would not have been possible without the captains and the crew of RRS Discovery, RRS Challenger and RV New Horizon and I thank everyone who has made these trips such a rewarding yet friendly experience. The MBA, Plymouth and the Sea-Life Centres at Weston-super-Mare and Weymouth are acknowledged for supplying me with specimens during the beginning of this study.

Over the past few years it is my friends who have kept me going. I am fortunate in having many close friends and in particular I thank Tamsin Knight, Clare Gilmore, Neil Ranson and Sally Magher, members of the diving club too numerous to mention, the 98 Dove Street 'lads' Simon Williams and Paul Fisher, and my colleagues in this department, including Andy Hope, Paula Wood, Nathan Hart, Sarah Hunt, Rohan Powell, Jamie Stevens, Abi Gannicott, Gail Lambourne and especially Jeanne Pimenta.

Financial support for this project was provided by the Natural Environment Research Council.

AUTHOR'S DECLARATION

The work described in this thesis is my own, unless otherwise stated, and has not previously been submitted for consideration for a higher degree at this or any other university.

The views expressed in this dissertation are my own and not those of the University.

Jeremy Kent

June 1997

TABLE OF CONTENTS

TITLE i

ABSTRACT ii
ACKNOWLEDGEMENTS iv
AUTHOR'S DECLARATION v
TABLE OF CONTENTS vi
LIST OF FIGURES ix
LIST OF TABLES xii
ABBREVIATIONS AND SYMBOLS xiv

CHAPTER ONE - VISUAL PIGMENTS AND SPECTRAL SENSITIVITIES OF THE CRUSTACEA 1

1.1 INTRODUCTION 2

1.2 VISUAL PIGMENTS 4

1.3 TECHNIQUES USED TO MEASURE VISUAL PIGMENTS 8

1.4 THE ECOLOGY OF VISUAL PIGMENTS 21

1.4.1 The aquatic photic environment 21
1.4.2 Previous crustacean visual pigment studies 24
1.4.3 The mantis shrimps 27
1.4.4 The crabs and lobsters 31
1.4.5 *Ligia*, an exception to the two visual pigment 'rule' 35
1.4.6 Adaptations to freshwater 36
1.4.7 Ontogenetic changes 38
1.4.8 Deep-sea shrimps 39
1.4.9 Conclusions and speculations on polarization sensitivity 47

1.5 THIS STUDY 50

CHAPTER TWO - MATERIALS AND METHODS 51

2.1 SPECIMEN COLLECTION AND PREPARATION 52

2.1.1 Animal collection 52
2.1.2 Animal maintenance 53
2.1.3 Tissue preservation 53
2.1.4 Tissue preparation for microspectrophotometry 54
2.1.5 Cryosection thickness 55

2.2 MICROSPECTROPHOTOMETRY 56

2.2.1 The microspectrophotometer 56
2.2.2 Microspectrophotometer illumination spectra 59
2.2.3 Protocol for microspectrophotometry 65
2.2.4 Difference spectra 66

2.3 DATA ANALYSIS 67

2.3.1 Data selection 67
2.3.2 Estimating the rhodopsin and metarhodopsin absorbances 69

CHAPTER THREE - RESULTS 70

3.1 PRELIMINARY STUDY: *HOMARUS* AND *NEPHROPS* 71

3.2 DEEP-SEA SHRIMPS 83

3.2.1 General observations 84
3.2.2 *Parapasiphaea sulcatifrons* 86

CHAPTER FOUR - MICROSPECTROPHOTOMETRIC MEASUREMENT AND ANALYSIS OF VISUAL PIGMENT DATA 192

4.1 MICROSPECTROPHOTOMETRIC DATA 193
4.1.1 Absorbance precision 193
4.1.1.1 Extrinsic noise 194
4.1.1.2 Intrinsic, signal-induced noise 196
4.1.1.3 Intrinsic versus extrinsic noise 196
4.1.1.4 In-scan photoconversion and photobleaching 197
4.1.1.5 Estimation of absorbance precision 199
4.1.2 Absorbance accuracy 200
4.1.3 Other sources of distortions 202
4.1.4 Wavelength precision and accuracy 203
4.2 DATA ANALYSIS OF VISUAL PIGMENT ABSORBANCE SPECTRA 205
4.2.1 Computer based analysis software 207
4.2.2 Data normalisation 208
4.2.2.1 Finding a maximum 208
4.2.2.2 Finding a minimum 209
4.2.3 Bandwidth 212
4.2.4 Finding the λ_{max} 213
4.2.4.1 Using a rhodopsin template 213
4.2.4.2 Template longwave tails 216
4.2.4.3 Shortwave visual pigments 219
4.2.4.4 Shifting β-band 222
4.2.4.5 Generating rhodopsin templates 228
4.2.4.6 The 'correct' rhodopsin template 231
4.2.5 Estimation of signal to noise ratios 233
4.2.5.1 The variability of the data 233
4.2.5.2 The noise of the data 234
4.2.5.3 Signal to noise ratios 237
4.2.6 The running average 238
4.2.6.1 Modelling the effect of the running average 238
4.2.6.2 Optimising the running average 242
4.2.6.3 Running average optimisation and microspectrophotometric data 246
4.2.7 Averaging microspectrophotometric data 248
4.2.7.1 Average files 248
4.2.7.2 A note on pseudoreplication 250
4.2.7.3 File averages 251
4.2.7.4 The 'average' λ_{max} value 253
4.2.7.5 The 'average' extinction ratio 256
4.2.7.6 Average files versus file averages 256
4.3 CHARACTERISING THE RHODOPSIN AND METARHODOPSIN 257
4.3.1 Analysing visual pigment mixtures with template fitting programs 257
4.3.2 Estimating the metarhodopsin 259
4.3.2.1 Calculation of the metarhodopsin 261
4.3.2.2 Metarhodopsin estimates calculated in this study 264
4.3.3 Estimating the rhodopsin 266
4.3.3.1 Metarhodopsin fluorescence 270
4.3.3.2 Characterising the visual pigments of the R8 cells 273
4.3.3.3 'Anchoring' the metarhodopsin 277
4.3.3.4 Photoconversion difference spectra 278
4.3.3.5 Rhodopsin estimates calculated in this study 281
4.3.4 Summary 284

CHAPTER FIVE - THE VISUAL PIGMENTS OF DEEP-SEA CRUSTACEANS **286**

5.1 PRELIMINARY STUDY: *HOMARUS* AND *NEPHROPS* 287

5.2 THE SPECTRAL SENSITIVITIES OF DEEP-SEA CRUSTACEANS 290

5.2.1 Previous studies 290
5.2.2 Deep-sea fishes 296
5.2.3 Taxonomic and depth comparisons 297
5.2.4 Spectral sensitivities versus visual pigment absorptions 300
5.2.5 *Gnathophausia* visual pigments 302
5.2.6 The effect of metarhodopsin on spectral sensitivity 303
5.2.7 Metarhodopsin spectral location 309
5.2.8 Specific absorbances 312
5.2.9 Metarhodopsin to rhodopsin extinction ratios 316
5.2.10 Consequences of the presence of metarhodopsin 317
5.2.11 Metarhodopsin levels *in vivo* 320
5.2.12 Near-UV pigments 323
5.2.13 Other pigments within the compound eye 326

5.3 THE SENSITIVITY HYPOTHESIS 328

5.3.1 Photon capture 329
5.3.2 Modelling photon capture 331
5.3.3 Perception of point sources 340
5.3.4 Signal to noise optimisation 343
5.3.5 Modelling conclusions 345

5.4 SUMMARY 348

REFERENCES **350**

APPENDIX I - PHOTOGRAPHS OF SELECTED DECAPODS **373**

APPENDIX II - ABSTRACTS OF CONFERENCE POSTERS **379**

LIST OF FIGURES

Figure 1.1 Normalised photon flux at various depths in Jerlov type IB ocean water. 23
Figure 1.2 A–C. Image formation in crustacean compound eyes. 25
Figure 2.1 Diagrammatic view of the microspectrophotometer. 57
Figure 2.2 A–C. Microspectrophotometer light fluxes, calculated as they occur at the specimen plane. 61
Figure 2.3 Light flux of the red-filtered head-torch. 64
Figure 3.1 A–E. Results from the main rhabdoms of *Homarus gammarus*. 79
Figure 3.2 A–E. Results from the main rhabdoms of *Nephrops norvegicus*. 81
Figure 3.3 A–E. Results from the main rhabdoms of *Bentheogennema intermedia*. 110
Figure 3.4 A–E. Results from the main rhabdoms of *Bentheogennema pasithea*.. 112
Figure 3.5 A–E. Results from the main rhabdoms of *Gennadas sp.* 114
Figure 3.6 A–E. Results from the main rhabdoms of *Gennadas valens*. 116
Figure 3.7 A–E. Results from the main rhabdoms of *Petalidium suspirosum*. 118
Figure 3.8 A–E. Results from the main rhabdoms of *Plesiopenaeus armatus*. 120
Figure 3.9 A–E. Results from the main rhabdoms of *Sergestes curvatus*. 122
Figure 3.10 A–E. Results from the main rhabdoms of *Sergestes similis*. 124
Figure 3.11 A–E. Results from the main rhabdoms of *Sergia maximus*. 126
Figure 3.12 A–E. Results from the main rhabdoms of *Sergia phorcus*. 128
Figure 3.13 A–E. Results from the main rhabdoms of *Sergia robustus*. 130
Figure 3.14 A–E. Results from the main rhabdoms of *Sergia splendens*. 132
Figure 3.15 A–E. Results from the main rhabdoms of *Acanthephyra curtirostris*. 134
Figure 3.16 A–E. Results from the main rhabdoms of *Acanthephyra microphthalma*. 136
Figure 3.17 A–E. Results from the main rhabdoms of *Acanthephyra purpurea*. 138
Figure 3.18 A–E. Results from the main rhabdoms of *Acanthephyra stylorostratis*. 140
Figure 3.19 A–E. Results from the main rhabdoms of *Hymenodora frontalis*. 142
Figure 3.20 A–E. Results from the main rhabdoms of *Hymenodora glacialis*. 144
Figure 3.21 A–E. Results from the main rhabdoms of *Meningodora miccyla*. 146
Figure 3.22 A–E. Results from the main rhabdoms of *Meningodora vesca*. 148
Figure 3.23 A–E. Results from the main rhabdoms of *Oplophorus spinosus*. 150
Figure 3.24 A–D. Results from the rhabdomeres of the 8th retinular cells of *Oplophorus spinosus*. 152
Figure 3.25 A–E. Results from the main rhabdoms of *Systellaspis braueri*. 154
Figure 3.26 A–D. Results from the rhabdomeres of the 8th retinular cells of *Systellaspis braueri*.. 156
Figure 3.27 A–E. Results from the main rhabdoms of *Systellaspis cristata*.. 158
Figure 3.28 A–D. Results from the rhabdomeres of the 8th retinular cells of *Systellaspis cristata*. 160
Figure 3.29 A–E. Results from the main rhabdoms of *Systellaspis debilis*. 162
Figure 3.30 A–D. Results from the rhabdomeres of the 8th retinular cells of *Systellaspis debilis*. 164
Figure 3.31 A–E. Results from the main rhabdoms of *Stylopandalus richardii*. 166

Figure 3.32 A–E. Results from the main rhabdoms of *Plesionika maritus*. 168
Figure 3.33 A–E. Results from the main rhabdoms of *Parapasiphaea sulcatifrons* (Atlantic-caught)..... 170
Figure 3.34 A–E. Results from the main rhabdoms of *Parapasiphaea sulcatifrons* (Pacific-caught). 172
Figure 3.35 A–E. Results from the main rhabdoms of *Pasiphaea chacei*..... 174
Figure 3.36 A–E. Results from the main rhabdoms of *Pasiphaea emarginata*..... 176
Figure 3.37 A–E. Results from the main rhabdoms of *Chalaraspidium alata*..... 178
Figure 3.38 A–E. Results from the main rhabdoms of *Eucopia australis*..... 180
Figure 3.39 A–E. Results from the main rhabdoms of *Eucopia sculpticauda*..... 182
Figure 3.40 A–E. Results from the main rhabdoms of *Gnathophausia gigas*..... 184
Figure 3.41 A–E. Results from the main rhabdoms of *Gnathophausia gracilis*. 186
Figure 3.42 A–E. Results from the main rhabdoms of *Gnathophausia ingens*..... 188
Figure 3.43 A–E. Results from the main rhabdoms of *Cyphocaris richardi*..... 190
Figure 4.1 Signal to noise ratio versus signal of the microspectrophotometer used in this study. 198
Figure 4.2 Linearity of the microspectrophotometer used in this study. 201
Figure 4.3 The absorbance spectrum of a didymium filter..... 204
Figure 4.4 A, B. Examples of the rhodopsin visual pigment template given by Stavenga *et al.* (1993). 215
Figure 4.5 A, B. The rhodopsin template given by Stavenga *et al.* (1993) with and without an added longwave tail..... 218
Figure 4.6 The 'offset' needed to shift the λ_{max} of the α-band as predicted by the polynomial given by Partridge and DeGrip (1991) to the α-peak value needed to produce a rhodopsin template as given by Stavenga *et al.* (1993) with the same λ_{max} as that of the original data..... 221
Figure 4.7 A, B. A series of rhodopsin visual pigment spectra plotted at 25 nm λ_{max} intervals from 350 to 600 nm, generated using the equation given by Stavenga *et al.* (1993). 223
Figure 4.8 A, B. A series of rhodopsin visual pigment spectra plotted at 25 nm λ_{max} intervals from 350 to 600 nm, generated using the equation given by Stavenga *et al.* (1993) and expressed on a λ_{max}/λ abscissa. 224
Figure 4.9 The percentage of the absorbance due to the β-band at the λ_{max} of a series of rhodopsin template spectra. 226
Figure 4.10 The FWHM bandwidths of a series of rhodopsin template spectra.. 227
Figure 4.11 The shortwave shift of the template λ_{max} relative to the λ_{max} of the α-band for a series of rhodopsin template spectra. 229
Figure 4.12 A, B. How the noise of a microspectrophotometric scan is calculated. 235
Figure 4.13 A, B. The effect of an incorrect running average at the peak absorbance..... 240
Figure 4.14 A, B. The effect of varying the number of points in the running average on the maximum corrected absorbance and the mean λ_{max}. 241
Figure 4.15 A, B. The average effect of increasing noise on the estimates of the maximum corrected absorbance and the mean λ_{max}..... 245

Figure 4.16 The absorbance spectrum of a mixture of two visual pigments compared to a rhodopsin template spectrum with the same λ_{max} 258

Figure 4.17 A, B. The shortwave shift in λ_{max} and the increase in the extinction coefficient between mix_2 and the estimated metarhodopsin. 267

Figure 4.18 A, B. The similarity between photoconversion difference spectra when normalised 271

Figure 4.19 The change in λ_{max} and extinction coefficient of the rhodopsin estimate versus the F_R in mix_1. 279

Figure 4.20 The effect of the F_R in mix_1 on the template generated photoconversion difference spectra... 283

Figure 5.1 Histograms showing the distributions of the λ_{max} values of rhodopsin and metarhodopsin pigments recorded in the photoreceptors of deep-sea crustaceans by microspectrophotometry. 295

Figure 5.2 A, B. The change in rhabdomeric absorptance with increasing levels of metarhodopsin, modelled as overlying the remaining rhodopsin. 305

Figure 5.3 A, B. The change in rhabdomeric absorptance with increasing levels of metarhodopsin homogeneously mixed with the rhodopsin. 307

Figure 5.4 A plot of metarhodopsin λ_{max} versus rhodopsin λ_{max} values for visual pigments as measured by microspectrophotometry.. 311

Figure 5.5 A, B. A simple model to show the relative photon catch when observing a typical deep-sea fish bioluminescence emittance spectrum 333

Figure 5.6 The effect of varying the rhodopsin λ_{max} on the relative photon capture of a typical deep-sea fish bioluminescent emission, given two different photoreceptor lengths 336

Figure 5.7 A, B. The rhodopsin λ_{max} values of 14 species of deep-sea decapods plotted against rhabdomeric absorbance and rhabdom length 339

Figure 5.8 The normalised relative photon capture of 14 species of deep-sea decapods. 341

Figure 5.9 A, B. The normalised relative sensitivities and normalised signal to noise ratios of 14 species of deep-sea decapods. 344

Figure 6.1 *Bentheogennema intermedia* (Family Penaeidae). 374

Figure 6.2 *Gennadas valens* (Family Penaeidae). 374

Figure 6.3 *Sergestes curvatus* (Family Sergestidae). 375

Figure 6.4 *Sergia maximus* (Family Sergestidae). 375

Figure 6.5 *Acanthephyra purpurea* (Family Oplophoridae). 376

Figure 6.6 *Meningodora vesca* (Family Oplophoridae). 376

Figure 6.7 *Oplophorus spinosus* (Family Oplophoridae) 377

Figure 6.8 *Systellaspis debilis* (Family Oplophoridae). 377

Figure 6.9 *Stylopandalus richardii* (Family Pandalidae). 378

Figure 6.10 *Parapasiphaea sulcatifrons* (Family Pasiphaeidae). 378

LIST OF TABLES

Table 1.1 Spectral sensitivities measured in the subphylum Crustacea....9
Table 3.1 Species measured in preliminary study....72
Table 3.2 Preliminary study: scan information....72
Table 3.3 Preliminary study: analysis results for the mix_1 averaged data....73
Table 3.4 Preliminary study: analysis results for the mix_2 averaged data....73
Table 3.5 Preliminary study: specific absorbances and the extinction coefficient ratios of the averaged data....74
Table 3.6 Preliminary study: deviation and signal to noise ratios of the mix_1 and mix_2 averaged data and the number of points used in the running averages....74
Table 3.7 Preliminary study: calculation of the metarhodopsin estimate....75
Table 3.8 Preliminary study: calculation of the rhodopsin estimate....75
Table 3.9 Preliminary study: summary of averaged data and the rhodopsin and metarhodopsin estimates. 76
Table 3.10 List of deep-sea species studied, presented in taxonomic order, with the number of specimens sampled and the number of eye sections successfully scanned....87
Table 3.11 Deep-sea species: scan information....89
Table 3.12 Deep-sea species: results for the mix_1 difference spectra which were analysed and accepted for subsequent averaging....91
Table 3.13 Deep-sea species: results for the mix_2 difference spectra which were analysed and accepted for subsequent averaging....93
Table 3.14 Deep-sea species: analysis results for the mix_1 averaged data....95
Table 3.15 Deep-sea species: analysis results for the mix_2 averaged data....97
Table 3.16 Deep-sea species: specific absorbances and the extinction coefficient ratios of the averaged data....99
Table 3.17 Deep-sea species: deviation and signal to noise ratios of the mix_1 and mix_2 averaged data and the number of points used in the running averages....101
Table 3.18 Deep-sea species: calculation of the metarhodopsin estimate....103
Table 3.19 Deep-sea species: calculation of the rhodopsin estimate....105
Table 3.20 Deep-sea species: summary of averaged data and the rhodopsin and metarhodopsin estimates. 107
Table 4.1 The effect of varying the number of points in the running average on the longwave offset absorbance, with the longwave offset wavelength both fixed and allowed to shift....211
Table 4.2 Optimum number of points needed in the running average to smooth data with the signal to noise ratios indicated....244
Table 4.3 The effect of the absorbance template employed on the estimate of the metarhodopsin....260
Table 4.4 The effect of varying ϕ on the estimate of the metarhodopsin....265

Table 4.5 Estimation of the rhodopsin and metarhodopsin pigments present in the R8 cells of the deep-sea species studied. 275
Table 5.1 Spectral sensitivities of the deep-sea shrimps measured in this and previous studies. 292
Table 5.2 The rhodopsin λ_{max} values, specific absorbances, rhabdom lengths and calculated rhabdomeric absorbances of 14 species of deep-sea decapods. 337
Table 5.3 The eye parameters of 14 species of deep-sea decapods used to calculate relative sensitivities and relative signal to noise levels. 342

ABBREVIATIONS AND SYMBOLS

A	aperture diameter
$A_i(\lambda)$	absorptance of pigment *i*
$\alpha_i(\lambda)$	molecular absorbance of pigment *i*
$a(\lambda)$	absorbance of a mixture of rhodopsin and metarhodopsin, divided by pathlength and pigment concentration
B	behavioural study
BP	behavioural/phototaxis study
c	concentration
ca.	circa
CS	calculated sensitivity
D	optical density
d.f.	degrees of freedom
$E(\lambda)$	molar absorption coefficient
EON	extracellular/optic nerve electrophysiology
ERG	electroretinogram
EX	visual pigment extract
$\varepsilon(\lambda)$	spectral sensitivity
f	focal length
ϕ	quantum efficiency ratio of rhodopsin ⇔ metarhodopsin photoconversion
F_M	fraction of metarhodopsin in a visual pigment mixture
F_R	fraction of rhodopsin in a visual pigment mixture
FWHM	full width at half maximum
IC	intracellular electrophysiology
HT	high tension
I_{abs}	intensity of light absorbed by a substance
I_{inc}	intensity of light incident on a substance
I_{trans}	intensity of light transmitted by a substance
l	pathlength
λ	wavelength
λ_{max}	wavelength of maximum absorbance
$\lambda_{max,i}$	wavelength of maximum absorbance of the *i*-band
M	metarhodopsin
mix_1	initial mixture of rhodopsin and metarhodopsin pigments
mix_2	mixture of rhodopsin and metarhodopsin pigments present post red/blue light treatment
MSP	microspectrophotometer/microspectrophotometry
N	noise
n	number (of data points)
NA	numerical aperture
OP	optical physiology
PC	personal computer
R	rhodopsin
R1–7	retinular cells 1 to 7
R8	eighth retinular cell
RMS	root-mean squared
S	signal
S/N	signal to noise (ratio)
s.d.	standard deviation
S_{max}	wavelength of maximum spectral sensitivity
sr	steradian
T	transmittance
UV	ultraviolet
V/F	voltage to frequency converter

Chapter One

Visual Pigments and Spectral Sensitivities of the Crustacea

1.1 INTRODUCTION

In all aspects of their biology, crustaceans exhibit a remarkable degree of variation. The subphylum Crustacea includes a diverse range of forms which reflects the ecological demands of different lifestyles and habitats and extends to include a great variety of eye designs (Land, 1981a). As stated by Land (1984) in his review; "Although one usually thinks of the Crustacea as linked to the insects by the presence of an exoskeleton and compound eyes, there is actually a much greater diversity of eye types in the Crustacea than in the insects or any other invertebrate group".

Crustaceans are found in all reaches of the marine environment from the seashore to the deepest ocean, in freshwater habitats and on land. They may live in bright tropical sun, or in habitats such as caves and the deep ocean where daylight does not penetrate. The importance of the visual sense can thus vary from the complete absence of compound eyes in some deep-sea species (Van Dover, Szuts, Chamberlain and Cann, 1989) to the high levels of development in the stomatopods (mantis shrimps; see Cronin, Marshall and Land, 1994a). Many species are demonstrably highly visual with vision being central to their survival, feeding and courtship both as adults and planktonic larvae (for a review see Rebach and Dunham, 1983). Often a variety of tasks must be performed at different times of the day and the need for effective vision under these broad ranging conditions has produced several different eye design strategies (Land, 1984 and 1990).

As well as the huge range of light intensities (10^{13} photons cm^{-2} sr^{-1} nm^{-1} to less than 10 photons cm^{-2} sr^{-1} nm^{-1}) experienced by crustaceans in different habitats, the colour and polarization content of light also varies considerably. While this study concentrates on one aspect of crustacean vision, their spectral sensitivities, it must be noted that the perception of the polarization of light may be even more important to many crustacean species than that of colour (e.g. Waterman, 1981; Marshall, Land, King and Cronin, 1991a). Crustaceans experience light which varies in its chromatic content from the broad 'white' sunlight of the reef-top to the narrow, blue waveband of oceanic midwater, the green of coastal water and even the yellow and red which predominates in some freshwater environments (Lythgoe, 1972; Jerlov, 1976). In common with fish, their

vertebrate neighbours in these habitats, one might expect crustacean spectral sensitivities to be adapted to suit these different requirements. While this appears true to some extent, given their diversity of eye designs and based on present data, most crustaceans seem to be surprisingly conservative in their spectral sampling capabilities. Most crustaceans possess only a single or more frequently two photoreceptor types, which operate under a number of different conditions irrespective of habitat. In a comparison between species, these are restricted to relatively narrow spectral sensitivity ranges. Thus, most have a photoreceptor population maximally sensitive to blue–green light between 480 nm and 540 nm and in some species a secondary set of UV–blue sensitive photoreceptors, maximally sensitive near 400 nm (see Table 1.1).

Due to biological interest, availability, and experimental factors, most of the crustaceans examined to date fall into three large groups: the crabs, stomatopods and the deep-sea shrimps. Either in taxonomic or environmental terms this is not a broad cross section and care must be taken if generalising about the subphylum. The fish, with which the Crustacea are frequently compared, have received more attention and a number of ecological trends with regard to the tuning of their visual pigments are well documented (Lythgoe, 1966, 1972 and 1979; Dartnall, 1975; Partridge, 1990). At present it seems that fish, which occupy almost precisely the same habitats as the Crustacea, possess a greater diversity of photoreceptor types (between 1 and 5 per species) with broader ranging peak sensitivities (340 to 560 nm; see Bowmaker, 1990; Partridge, 1990). The apparently more basic plan adopted by most crustaceans may be due not to spectral limitations, but the apparatus needed for polarization vision as has been suggested for the insects (Wehner, 1983; Seliger, Lall and Biggley, 1994).

A few exceptions to this conservatism are known but by far the most spectacular are the stomatopods. These hoplocarid crustaceans appear in the fossil record and have been in their own limb of the evolutionary tree for 400 million years (Caldwell and Dingle, 1976). During this time they followed a very different visual strategy to other crustaceans. Species from 2 of the 5 existing superfamilies possess up to 16 different photoreceptor types in their eyes, each with its own spectral sensitivity, and sample light from 312 nm to over 700 nm (Marshall, 1988; Cronin and Marshall, 1989a, b; Cronin, Marshall and

Caldwell, 1994b; Marshall, Land, Oberwinkler, Jones, Horwood, and Cronin, 1994). Further, polarization vision has been shown (Marshall *et al.*, 1991a) giving stomatopods the most complicated retinal spectral and polarization analyser known in *any* animal (Cronin and Marshall, 1989a, b; Osorio and Vorobyev, 1997).

When attempting to draw broad conclusions about the visual ecology of such a taxon it is important not to overlook the individuality of animals. Many species live in microhabitats, which both in geographical and behavioural terms may not be obvious to us. Furthermore, the spectral sensitivity of photoreceptors is not just a function of environmental factors. For instance, most crustacean visual pigments have λ_{max} values below 512 nm and this may be due to a number of factors such as thermal instability of visual pigments (Barlow, 1988) or evolutionary inertia (see Goldsmith, 1991, for a discussion of this). Apparent phylogenetic restrictions to λ_{max} positions are known in crustaceans (Cronin, 1990) as they are in fish (Partridge, Shand, Archer, Lythgoe and Groningen-Luyben, 1989; Douglas and Partridge, 1997). Also, as noted by Dartnall and Lythgoe (1965), visual pigment sensitivity peaks from a variety of animals seem to be clustered around certain regularly spaced modal values which are probably set by the interactions between the molecular components of visual pigments (Nathans, Thomas and Hogness, 1986; see also Partridge *et al.*, 1989). As a result of all these factors, any interpretation of photoreceptor spectral sensitivity just in terms of ecological factors is fraught with complications.

1.2 VISUAL PIGMENTS

Information about the visual environment is transferred to the internal, physiological environment of an organism at the point where photons are absorbed by the visual pigments. All the information available to the animal is contained in the number of photons 'counted' by the photoreceptors, and no subsequent analysis can add information that is not originally harvested by the visual pigments. As a result, knowledge of the

absorbance[1] spectra of visual pigments is fundamental to many facets of the study of vision.

In nearly all invertebrates, including crustaceans, visual pigment molecules are situated on stacks of tube shaped membranes or microvilli. Microvilli constitute the photoreceptive portion (rhabdom) of the retinal (retinular) cells and are the direct equivalent of the plate-shaped visual pigment bearing membranes of outer segments in vertebrate rods and cones. All known vertebrate and invertebrate photoreceptors, both visual and extraretinal, depend on visual pigments which comprise a protein (opsin) and a derivative of vitamin A (the chromophore). The absorbance spectra of visual pigments are asymmetrically bell-shaped, rising to a peak absorbance at a wavelength known as the λ_{max}. The spectral position of the λ_{max} depends on both the amino acid sequence of the opsin (Nathans *et al.*, 1986) and the nature of the chromophore. The latter is based on one of four derivatives, but the initial results with extracts encouraged the assumption that only the 11-*cis* isomer of retinal, a derivative of vitamin A_1, would be found in crustaceans. Thus all crustacean visual pigments would be A_1 visual pigments, or 'rhodopsins' (Goldsmith, 1972). However, 3-dehydroretinal (a vitamin A_2 derivative) was then discovered in the eyes of freshwater crayfish (Suzuki, Makino-Tasaka and Eguchi, 1984). This chromophore produces A_2 visual pigments, or 'porphyropsins', with absorption spectra shifted to longer wavelengths relative to rhodopsins employing the same opsin (Bridges and Yoshikama, 1970; Partridge, 1990). This visual adaptation is also found in freshwater fish (Bowmaker, 1990; Partridge, 1990) and amphibia (Bridges, 1972) and extends the range of possible λ_{max} values and therefore the longwave spectral sensitivity limit of the Crustacea.

---

[1] The amount of light absorbed by a substance (I_{abs}) is given by the intensity of the light incident on the substance (I_{inc}) minus the intensity of light transmitted through it (I_{trans}). A graph plotting light absorbed against wavelength is called an *absorptance spectrum*. The shape of the absorptance spectrum depends upon the concentration of the absorbing material and upon the length of the path that the light travels through it. Alternatively absorption is defined by specifying the *optical density* of the material, its *absorbance*. Absorbance is a logarithmic measure of absorption, which means that absorbances are additive: doubling the pathlength doubles the absorbance but, when normalised, the shape of the absorbance spectrum remains unchanged. Absorbance is defined as $\log_{10}(I_{inc}/I_{trans})$, or $-\log_{10}(T)$ where T is the *transmittance* (i.e. $I_{trans} = 1 - I_{abs}$).

A distinctive characteristic of known invertebrate pigments is their formation of an intermediate, non-dissociated, thermally stable state (the 'metarhodopsin') upon conversion of the visually active form (the 'rhodopsin'). Once formed, the metarhodopsin can be 'photoconverted' back to rhodopsin on the absorption of photons (Stavenga and Schwemer, 1984). Thus, the visual pigment may be recycled many times; however, only the rhodopsin to metarhodopsin transition leads to visual excitation (see Cronin and Goldsmith, 1982a). Typically, the metarhodopsin has a greater peak absorption coefficient than the rhodopsin, and the two pigments have absorbance spectra of very similar shape, but with maximal absorption at different wavelengths (see Cronin, 1986a). The intermediate states in the rhodopsin to metarhodopsin and metarhodopsin to rhodopsin pathways are discussed by Cronin and Goldsmith (1982b) and Stavenga and Schwemer (1984).

Active photoreceptors will always contain some metarhodopsin and the presence of this stable intermediate has two consequences. The first is the impediment presented to the process of maintaining maximum sensitivity: invertebrates seem to lack enzymatic systems for directly regenerating rhodopsin from metarhodopsin (Cronin and Goldsmith, 1984; Schwemer, 1984). In order to restore the photopigment content of the photoreceptors to 100% rhodopsin, it appears that at least the arthropods, and probably molluscs as well, must regularly replace their photoreceptor membranes and thus insert newly synthesised rhodopsin (see Blest, 1980; Stowe, 1980a, 1981; Piekos and Waterman, 1983; Waterman and Piekos, 1983). Large changes in rhabdom volume associated with changing light intensity have been found in many species including a 10- to 20-fold night-time increase in the crab *Grapsus grapsus* (Nässel and Waterman, 1979) and a three- to four-fold increase in *Nephrops norvegicus* (Shelton, Gaten and Chapman, 1985). These membrane turnover events are commonly associated with the ambient light:dark cycle, with periods of rhabdom synthesis and degradation at dusk and dawn respectively, and could be tied to mechanisms for measuring photoperiod (Cronin, 1986a).

Secondly, the presence of metarhodopsin will alter the spectrum of the ambient light as it passes down the photoreceptor (Goldsmith, 1978a). Coloured photostable accessory

pigments are also found in and around the rhabdom which filter the spectrum of light reaching the photoreceptor (Goldsmith, 1978a; Marshall, Land, King and Cronin, 1991b). These may sharpen or even shift the photoreceptor's spectral sensitivity spectrum away from the absorption of the rhodopsin alone (Snyder, Menzel and Laughlin, 1973; Goldsmith, 1978a; Stowe, 1980b; Cronin and Marshall, 1989a). Indeed a heterogeneous distribution of screening pigments can provide the capacity for hue discrimination in a retina containing a single visual pigment (Leggett, 1979; Kong, Yau and Wasserman, 1980). In contrast, long photoreceptors, which are common in invertebrates and substantially increase sensitivity, will tend to result in broadened sensitivity functions (Snyder *et al.*, 1973).

Ultimately the spectral sensitivity of a crustacean photoreceptor is dependent on multiple factors: the visual pigment's λ_{max} and density, filtering by a variety of photostable pigments in series or lateral to the photoreceptor, self screening within each photoreceptor by rhodopsin and its photoproducts such as metarhodopsin, screening by the visual pigments of distally placed photoreceptors, the properties of reflecting pigments or tapeta, and the dimensions of the photoreceptor itself. It is worth emphasising that λ_{max} values of visual pigments alone, and the best-fit template spectra one often sees illustrating them, are not inclusive of such important factors. As a result, they may be a misleading representation of the real spectral sensitivity of the photoreceptor considered as a whole, especially when considering evolutionary optimisation or ecological tuning. For example, some peak sensitivity values of stomatopod photoreceptors are shifted over 100 nm to longer wavelengths from the visual pigment λ_{max} by spectral filtering (Cronin and Marshall, 1989a). Unfortunately visual pigment λ_{max} values are often the only information available and therefore must form the basis of any speculation. From here on the term λ_{max} is used for photoreceptor peak sensitivity based only on microspectrophotometric data and S_{max} is used for data from electrophysiological or behavioural studies, or sensitivity maxima calculated to include filtering.

1.3 TECHNIQUES USED TO MEASURE VISUAL PIGMENTS

To date, spectral sensitivity measurements have been obtained from over 240 different photoreceptors in at least 105 species of crustaceans. These are listed with the original authors in Table 1.1. Four principal methods have been used to gather these data: 1) electrophysiology, involving the measurement of the electrical responses of photoreceptors, either in the whole eye using the electroretinogram (ERG - e.g. Frank and Case, 1988a, b), extracellularly on the optic nerve (EON - e.g. Smith and Macagno, 1990), or intracellularly in single photoreceptor cells (IC - e.g. Martin and Mote, 1982); 2) behavioural measures, usually involving phototactic action spectra (B and BP - e.g. Hyatt, 1975; Stearns, 1975; Stearns and Forward, 1984; Frank and Widder, 1994a); and measurement of absorption spectra of visual pigments either 3) extracted in solution using a spectrophotometer (EX - e.g. Kampa, 1955; Goldsmith and Bruno, 1973; Denys, 1982; Denys and Brown, 1982); or 4) *in situ*, in isolated photoreceptor cells by microspectrophotometry (MSP - e.g. Cronin and Forward, 1988; Cronin and Marshall, 1989a).

All techniques have their own merits, however, behavioural measures are generally not very precise, making a comparison between behavioural and other methods problematic. It is also recognised that it is hard to isolate invertebrate visual pigments in detergent-solubilized extracts without including non-visual pigments which contaminate the results (see Bruno and Goldsmith, 1974, and Denys and Brown, 1982, for discussions of this). Hence, this method has largely been abandoned. A non-invasive physiological method examining retinal screening pigment movements in response to different wavelengths of light has also been used, but obviously can only be used with live specimens (OP - Cronin, 1989; Cronin and King, 1989). Similarly, electrophysiology data are dependent on the condition of the specimen. In this study the technique of microspectrophotometry was chosen to determine the absorbance spectra of deep-sea crustacean visual pigments. This allowed isolated eyes to be collected and preserved by freezing for subsequent measurement of the visual pigments *in situ* (i.e. in their photoreceptors) after the research cruises during which the specimens were collected. The machine used for measurement is detailed in Section 2.2.1 and the procedures of tissue preparation and measurement are

Table 1.1 Visual spectral sensitivities measured in the subphylum Crustacea.

Species	Method of study	λ_{max} of R or S_{max} (nm)	λ_{max} of M (where measured) (nm)	Author(s)
Subphylum Crustacea				
Class Branchiopoda				
Subclass Diplostraca				
Order Cladocera				
Daphnia magna	BP	405, 440, 570 & 690	-	Buchanan & Goldberg, 1981
	B	365-400, 440 & 527	-	Consi & Macagno, 1985
	EON	348, 434, 525 & 608	-	Smith & Macagno, 1990
Subclass Sarsostraca				
Order Anostraca				
Artemia salina	BP	430, 505 & 535	-	Aiken & Hailman, 1978
	ERG	410	-	Hertel, 1980
	BP	400 & 520	-	Bradley & Forward, 1984
Class Maxillopoda				
Subclass Copepoda				
Acartia tonsa	BP	450-520	-	Stearns & Forward, 1984
Mesocylcops edax	BP	480-580	-	Swift & Forward, 1983
Subclass Cirripedia				
Order Thoracica				
Suborder Balanomorpha				
Balanus amphitrite	MSP	532	492	Minke & Kirschfield, 1978
	ERG	532	492	Hillman, Dodge, Hochstein, Knight & Minke, 1973
	ERG	532	492	Minke, Hochstein & Hillman, 1973
Balanus balanoides (nauplius)	BP	510-530	-	Barnes & Klepal, 1972
Balanus eburneus	MSP	532	492	Minke & Kirschfield, 1978
	ERG	532	492	Hillman, Dodge, Hochstein, Knight & Minke, 1973
	ERG	532	492	Minke, Hochstein & Hillman, 1973

Table 1.1 (Continued).

Species	Method of study	λ_{max} of R or S_{max} (nm)	λ_{max} of M (where measured) (nm)	Author(s)
Balanus improvisus (larva)	BP	480	-	Lang, Forward & Miller, 1979
Class Malacostraca				
Subclass Eumalacostraca				
Superorder Hoplocarida				
Order Stomatopoda				
Superfamily Squilloidea				
Cloridopsis dubia	MSP	510	-	Cronin, Marshall & Caldwell, 1993
Squilla empusa	MSP	517	-	Cronin, Marshall & Caldwell, 1993
	OP	360 & 500	-	Cronin, 1989
	MSP	507	503	Cronin, 1985
Squilla mantis	IC	535-555	-	Schiff, 1963
Superfamily Gonodactyloidea				
Gonodactylus aloha	MSP	400 to 551 (11)	-	Cronin, Marshall & Caldwell, 1996b
Gonodactylus curacaoensis	MSP	400 to 520 (8)	-	Cronin, Marshall & Caldwell, 1996b
Gonodactylus oerstedii	CS	400 to 695 (11)	-	Cronin, Marshall, Caldwell & Shashar, 1994b
	MSP	325	460	Cronin, Marshall, Quinn, & King, 1994c
	IC	312 to 710	-	Marshall, Land, Oberwinkler, Jones, Horwood & Cronin, 1994
	OP	360 & 500	-	Cronin, 1989
	MSP	400 to 551 (11)	-	Cronin & Marshall, 1989b
Hemisquilla ensigera	MSP	414 to 535 (11)	-	Cronin, Marshall, Caldwell & Shashar, 1994b
	CS	440 to 625 (11)	-	Cronin, Marshall, Caldwell & Shashar, 1994b
	MSP	330	-	Cronin, Marshall, Quinn, & King, 1994c
Odontodactylus brevirostris	MSP	402 to 535 (11)	-	Cronin, Marshall, Caldwell & Shashar, 1994b
	CS	400 to 623 (11)	-	Cronin, Marshall, Caldwell & Shashar, 1994b
Odontodactylus havanensis	MSP	407 to 520 (8)	-	Cronin, Marshall & Caldwell, 1996b

Table 1.1 (Continued).

Species	Method of study	λ_{max} of *R* or S_{max} (nm)	λ_{max} of *M* (where measured) (nm)	Author(s)
Odontodactylus scyllarus	MSP	400 to 546 (11)	-	Cronin, Marshall & Caldwell, 1994d
	CS	425 to 655 (11)	-	Cronin, Marshall & Caldwell, 1994d
Pseudosquilla ciliata	CS	400 to 680 (11)	-	Cronin, Marshall, Caldwell & Shashar, 1994b
	MSP	400 to 539 (11)	-	Cronin & Marshall , 1989b
	OP	360 & 500	-	Cronin, 1989
Superfamily Lysiosquilloidea				
Coronis scolopendra	MSP	407 to 533 (11)	-	Cronin, Marshall, Caldwell & Shashar, 1994b
	CS	425 to 620 (11)	-	Cronin, Marshall, Caldwell & Shashar, 1994b
Lysiosquilla maculata	MSP	330	-	Cronin, Marshall, Quinn, & King, 1994c
Lysiosquilla sulcata	MSP	397 to 538 (11)	-	Cronin, Marshall, Caldwell & Shashar, 1994b
	CS	410 to 620 (11)	-	Cronin, Marshall, Caldwell & Shashar, 1994b
Superorder Eucarida				
Order Euphausiacea				
Euphausia pacifica	MSP	483	489	Widder, Hiller-Adams & Case, 1987
	ERG	460-515	-	Boden, Kampa & Abbott, 1961
	EX	462	-	Kampa, 1955
Euphausia superba	EX	462	-	Denys, 1982
	EX	485	493	Denys & Brown, 1982
Meganyctiphanes norvegica	MSP	488	495	Denys & Brown, 1982
	EX	462	-	Fisher, 1967
	B	*ca.* 480	-	Kay, 1965
	ERG	460-515, 490	-	Boden, Kampa & Abbott, 1961
	EX	460-465	-	Fisher & Goldie, 1959
Nematoscelis megalops	EX	465	-	Fisher & Goldie, 1961
Stylocheiron maximum	EX	470	-	Fisher & Goldie, 1961
Thysanoessa raschii	EX	460-465	-	Fisher & Goldie, 1961
Thysanopoda acutifrons	EX	480	-	Fisher & Goldie, 1961

Table 1.1 (Continued).

Species	Method of study	λ_{max} of *R* or S_{max} (nm)	λ_{max} of *M* (where measured) (nm)	Author(s)
Order Decapoda				
Suborder Dendrobranchiata				
Infraorder Penaeidea				
Penaeus duorarum	EX	516	475	Fernandez, 1965
Family Sergestidae				
Sergestes tenuiremis	MSP	495	487	Hiller-Adams, Widder & Case, 1988
Suborder Pleocyemata				
Infraorder Caridea				
Family Oplophoridae				
Acanthephyra curtirostris	ERG	510	-	Frank & Case, 1988a
	MSP	485	480	Hiller-Adams, Widder & Case, 1988
Acanthephyra smithi	ERG	510	-	Frank & Case, 1988a
	MSP	491	482	Hiller-Adams, Widder & Case, 1988
Janicella spinicauda	ERG	400 & 500	-	Frank & Case, 1988a
Notostomus elegans	ERG	490	-	Frank & Case, 1988a
Notostomus gibbosus	ERG	490	-	Frank & Case, 1988a
Oplophorus gracilirostris	ERG	400 & 500	-	Frank & Case, 1988a
Oplophorus spinosus	ERG	400 & 500	-	Frank & Case, 1988a
Systellaspis debilis	MSP	410 & 498	474 & 484	Cronin & Frank, 1996
	B	nr-UV & blue-green	-	Frank & Widder, 1994a
	ERG	400 & 500	-	Frank & Case, 1988a
	MSP	493	481	Hiller-Adams, Widder & Case, 1988
Family Palaemonidae				
Palaemonetes palludosus	EX	539	497	Fernandez, 1965
Palaemonetes pugio (larva)	BP	500 & 560-580	-	Douglass, 1986

Table 1.1 (Continued).

Species	Method of study	λ_{max} of R or S_{max} (nm)	λ_{max} of M (where measured) (nm)	Author(s)
Palaemonetes vulgaris	ERG	390 & 540	-	Wald & Seldin, 1968
Family Pandalidae				
Pandalus borealis (nauplius)	ERG	475-500	-	Eaton & Brown, 1970
Family Alvinocarididae				
Rimicaris exoculata	EX	500	-	van Dover, Szuts, Chamberlain & Cann, 1989
Infraorder Astacidea				
Astacus fluviatilis	MSP	530	500	Hamacher & Kohl, 1981
Astacus leptodactylus	MSP	530	-	Hamacher & Stieve, 1984
Cambarellus schufeldtii	MSP	526	-	Crandall & Cronin, in press
Cambarus ludovicianus	MSP	529	-	Crandall & Cronin, in press
Engaeus cunicularius	MSP	522	-	Crandall & Cronin, in press
Homarus americanus	MSP	515	-	Bruno, Barnes & Goldsmith, 1977
	EX	515	490	Wald & Hubbard, 1957
Nephrops norvegicus	MSP	498	484	Loew, 1976
Orconectes rusticus	MSP	535	510	Cronin & Goldsmith, 1982
	MSP	530	515	Goldsmith, 1978b
Procambarus clarkii	MSP	533 (A_1), 567 (A_2)	510 (A_1), 537 (A_2)	Zeiger & Goldsmith, 1989
	IC	440 & 530	-	Cummins & Goldsmith, 1981
	MSP	535	510	Cronin & Goldsmith, 1982
	MSP	525	515	Goldsmith, 1978b
Procambarus milleri	MSP	522	-	Crandall & Cronin, in press
Infraorder Palinura				
Panulirus argus	ERG	370 & 510	-	Cummins, Chen & Goldsmith, 1984
	EX	504	495	Fernandez, 1965

Table 1.1 (Continued).

Species	Method of study	λ_{max} of R or S_{max} (nm)	λ_{max} of M (where measured) (nm)	Author(s)
Infraorder Anomura				
Pleuroncodes planipes	EX	503	-	Fernandez, 1973
	IC	523	-	Fernandez, 1973
Superfamily Paguridea				
Family Diogenidae				
Clibanarius vittatus	MSP	510	481	Cronin & Forward, 1988
Dardanus fucosus	MSP	511	490	Cronin & Forward, 1988
Petrochirus diogenes	MSP	508	490	Cronin & Forward, 1988
Family Coenobitidae				
Coenobita clypeatus	MSP	508	495	Cronin & Forward, 1988
Coenobita rugosa	MSP	491	487	Cronin & Forward, 1988
Family Paguridae				
Pagurus annulipes	MSP	495	491	Cronin & Forward, 1988
Pagurus beringanus (larva)	BP	400, 480 & 580	-	Forward, 1987
Pagurus granosimanus (larva)	BP	400, 500 & 600-620	-	Forward, 1987
Pagurus longicarpus	MSP	515	490	Cronin & Forward, 1988
Pagurus pollicaris	MSP	515	491	Cronin & Forward, 1988
Infraorder Brachyura				
Pinnotheres ostreum (larva)	BP	360, 460-500	-	Forward & Cronin, 1979
Section Oxystomata				
Family Calappidae				
Calappa flammea	MSP	486	509	Cronin & Forward, 1988
Hepatus epheliticus	MSP	487	498	Cronin & Forward, 1988

Table 1.1 (Continued).

Species	Method of study	λ_{max} of R or S_{max} (nm)	λ_{max} of M (where measured) (nm)	Author(s)
Section Oxyrhyncha				
Family Majidae				
Libinia dubia	MSP	489	501	Cronin & Forward, 1988
Libinia emarginata	MSP	493	-	Hays & Goldsmith, 1969
	MSP	493	498	Briggs, 1961
Libinia sp.	MSP	493	-	Goldsmith & Bruno, 1973
Section Cancridea				
Cancer gracilis (larva)	BP	400 & 500	-	Forward, 1987
Cancer irroratus	MSP	496	489	Cronin & Forward, 1988
Section Brachyrhyncha				
Family Portunidae				
Arenaeus cribrarius	MSP	498	498	Cronin & Forward, 1988
Callinectes ornatus	MSP	501	498	Cronin & Forward, 1988
Callinectes sapidus	MSP	503	503	Cronin & Forward, 1988
	IC	440 & 508	-	Martin & Mote, 1982
	EX	477	-	Bruno & Goldsmith, 1974
	MSP	500	-	Bruno & Goldsmith, 1974
	IC	508	-	Scott & Mote, 1974
	MSP	500	-	Goldsmith & Bruno, 1973
Carcinus maenas	IC	440 & 508	-	Martin & Mote, 1982
	MSP	508	505	Bruno, Mote & Goldsmith, 1973
	MSP	504	-	Goldsmith & Bruno, 1973
	B	508	-	Horridge, 1967
Ovipales stephensoni	MSP	505	506	Cronin & Forward, 1988
Portunus spinimanus	MSP	483	-	Cronin & Forward, 1988
Scylla serrata	MSP	490	-	Leggett, 1979

Table 1.1 (Continued).

Species	Method of study	λ_{max} of R or S_{max} (nm)	λ_{max} of M (where measured) (nm)	Author(s)
Family Xanthidae				
Eurypanopeus depressus	MSP	490	502	Cronin & Forward, 1988
Lophopanopeus b. bellus (larva)	BP	400 & 500	-	Forward, 1987
Menippe mercenaria	MSP	494	497	Cronin & Forward, 1988
Panopeus herbstii (larva)	BP	460-500	-	Forward & Cronin, 1979
(adult)	MSP	493	494	Cronin & Forward, 1988
Panopeus obesus	MSP	493	495	Cronin & Forward, 1988
Pilumnus sayi	MSP	489	492	Cronin & Forward, 1988
Rhithropanopeus harrisii (larva)	BP	420 & 500	-	Forward & Cronin, 1979
(adult)	MSP	495	507	Cronin & Forward, 1988
Rhithropanopeus sp. (larva)	B	Colour vision	-	Via & Forward, 1975
	B	Colour vision	-	Forward & Costlow, 1974
Family Geryonidae				
Geryon quinquendens	MSP	473	473	Cronin & Forward, 1988
Family Grapsidae				
Hemigrapsus edwardsii	EX	513	495	Briggs, 1961
Hemigrapsus oregonensis (larva)	BP	420 & 500	-	Forward, 1987
Leptograpsus variegtus	IC	484	-	Stowe, 1980
	EX	513	495	Briggs, 1961
Sesarma cinereum (larva)	BP	360 & 500-520	-	Forward & Cronin, 1979
(adult)	MSP	492	505	Cronin & Forward, 1988
Sesarma reticulatum (larva)	BP	360 & 500	-	Forward & Cronin, 1979
(adult)	MSP	493	496	Cronin & Forward, 1988
	IC	508	-	Scott & Mote, 1974
Family Ocypodidae				
Uca minax (larva)	BP	420-540	-	Forward & Cronin, 1979

Table 1.1 (Continued).

Species	Method of study	λ_{max} of *R* or S_{max} (nm)	λ_{max} of *M* (where measured) (nm)	Author(s)
Uca pugilator (larva)	BP	420 & 460-500	-	Forward & Cronin, 1979
(adult)	IC	508	-	Scott & Mote, 1974
	EX	480	-	Purple & Goldsmith, unpublished [a]
Uca pugnax	B	Colour vision	-	Hyatt, 1975
	IC	508	-	Scott & Mote, 1974
	EX	480	-	Purple & Goldsmith, unpublished [a]
Family Gecarcinidae				
Gecarcinus lateralis	MSP	487	498	Cronin & Forward, 1988
	ERG	510	-	Lall & Cronin, 1987
Superorder Peracarida				
Order Mysida				
Gnathophausia ingens	ERG	*ca.* 510	-	Frank & Case, 1988b
Mysis relicta	ERG	*ca.* 550-570		Lindström & Nilsson, 1988
Order Isopoda				
Ligia exotica	ERG	330, 460 & 520	-	Hariyama, Tsukahara & Meyer-Rochow, 1993
Order Amphipoda				
Pontoporeia affinis	MSP	548	500	Donner, Langer, Lindström & Schlecht, 1994

[a] reported by Bruno and Goldsmith (1974).

Table 1.1 (Continued).

Abbreviations as follows: MSP - microspectrophotometry; EX - visual pigment extract; OP - optical physiology; ERG - electroretinogram; EON - extracellular/optic nerve; IC - intracellular electrophysiology; B - behavioural; BP - behavioural/phototaxis; CS - calculated sensitivity. Where microspectrophotometry and visual pigment extracts have been used λ_{max} values are quoted, the rest represent S_{max} values from a variety of methods. For the stomatopoda, where known, both λ_{max} and S_{max} values (calculated from the λ_{max} and intrarhabdomal filtering) are given. A dash separating two values indicates the range of maximum spectral sensitivity measured. Where two values are separated by 'to' this indicates the range over which a number of distinct spectral sensitivity classes were found, with their total number indicated in the parentheses.

described in Sections 2.1.3, 2.1.4 and 2.2.3.

As a direct consequence of the necessity to use light to measure visual pigments, which by their very nature are photolabile, measurement records often suffer from low signal to noise ratios (for a discussion regarding microspectrophotometric records see Section 4.1). To improve signal to noise ratios, many spectra from both the same and different photoreceptors, or areas of the retinal tissue, can be averaged together (see Section 4.2.7). However, to avoid the inclusion of 'distorted' measurements into averaged spectra, the raw data are often subjected to selection criteria (Hárosi, 1975; Levine and MacNichol, 1985; MacNichol, 1986; Partridge, 1986). These selection criteria often involve the use of template spectra to describe the idealised absorbance spectrum of visual pigments. The analysis methods used in this study are described and discussed in Section 4.3.

The first such template curve was the 'nomogram' of Dartnall (1953), an empirically derived function describing the absorbance spectra of retinal-based visual pigments with λ_{max} values between 470 and 530 nm (Greenberg, Honig and Ebrey, 1975; Ebrey and Honig, 1977; Dawis, 1981). Although derived from measurements of vertebrate visual pigments such templates are routinely employed for comparisons with invertebrate absorption data (e.g. Goldsmith, 1972; Cronin and Goldsmith, 1982a; Stavenga and Schwemer, 1984; Cronin, 1985; Cronin and Forward, 1988). This was convenient both because the λ_{max} of most invertebrate rhodopsins is near 500 nm and because no separate empirical spectrum for invertebrates seemed to be necessary. In 1985, Mansfield proposed an invariant form of the visual pigment absorption spectrum based on an abscissa transform of the reciprocal of the wavelength (frequency or wavenumber) divided by the frequency or wavenumber of the absorbance maximum of that spectrum. This invariant form was then shown to apply to a wide range of vertebrate visual pigments (MacNichol, 1986) and, later, to invertebrate (in particular, crustacean) visual pigments (Lipetz and Cronin, 1988).

The use of an invariant form offers a number of advantages over the original nomograms. First, unlike the various nomogram curves that each match the visual pigment spectra for only one peak wavelength (Ebrey and Honig, 1977), the invariant form may be applied to

all retinal-based visual pigments whose λ_{max} lies within the visible spectrum. (Originally, it was thought that invariant forms would apply to *all* visual pigments based on the same chromophore, however, UV sensitive pigments have proved to warrant their own template; see Palacios, Goldsmith and Bernard, 1996, and Section 4.2.4.3.) Of more fundamental significance is the theoretical basis for the shape of the invariant form. Thus, crustaceans appear to use identical mechanisms to those of vertebrates to tune the wavelength ranges of their visual pigments, and the linkages of their chromophores to the opsins appear to be the same in both groups. Moreover, the electronic transition of the 11-*cis* chromophore remains much the same whether the pigment is in the rhodopsin form or the metarhodopsin form. Thus, the environment of the chromophore is held remarkably constant as it undergoes various conformational alterations (Lipetz and Cronin, 1988).

Many templates have now been proposed, some constructed as the sum of mathematical formulae (Hárosi, 1976; Levine and MacNichol, 1985, Partridge and DeGrip, 1991; Stavenga, Smits and Hoenders, 1993), others based on transformed measurements of carefully measured visual pigment (e.g. Bowmaker, Loew and Liebman, 1975; Lamb, 1995), the majority of both being of invariant forms based on different abscissa transformations. Due to the findings of Lipetz and Cronin (1988), two 'vertebrate' rhodopsin visual pigment templates have been used throughout this study; a modified version of the template given by Stavenga *et al.* (1993) (see Palacios *et al.*, 1996, and Section 4.2.4.1), and, where the longwave tail region was of importance, that given by Lamb (1995) (see Section 4.2.4.2). Both templates are based on the absorbance spectrum of purified bovine rhodopsin presented by Partridge and DeGrip (1991). For the analysis of the near-UV pigments found in certain species from the Family Oplophoridae, another modified version of the template given by Stavenga *et al.* (1993) was used (see Palacios *et al.*, 1996, and Section 4.2.4.3).

1.4 THE ECOLOGY OF VISUAL PIGMENTS

Natural selection has modified visual systems for high performance in the tasks for which they are most required. In other words, visual systems are generally thought to be highly adaptive and subject to substantial selective pressure. This optimisation extends to the visual pigments, including the spectral location at which each absorbs light. Their maximum absorption may be matched to the wavelengths of light having greatest photon flux in the animal's environment, to provide the greatest possible sensitivity (the 'Sensitivity Hypothesis', reviewed by Lythgoe, 1972). Alternatively, the absorption maximum may be placed to optimise contrast between viewed objects and the background spacelight (the 'contrast hypothesis', reviewed by Lythgoe, 1979). The possession of multiple visual pigments, each having a different spectral sensitivity, can then further aid contrast enhancement against monochromatic backgrounds (Lythgoe, 1966, 1968), and eventually lead to the evolution of colour vision (McFarland and Munz, 1975a, b). Other evolutionary constraints may act as well; for example, animals using species-specific colours for intraspecific communication may have special visual pigments for that task (Levine, Lobel and MacNichol, 1980).

1.4.1 The aquatic photic environment

The passage of light through water is affected by both the scattering of light and by the spectral absorptions of: 1) water itself, 2) chlorophyll, and 3) the breakdown products of plants, known as Gelbstoff or 'dissolved organic matter'. The relative importance of these factors varies considerably in different waters, both fresh and marine, leading to a wide variation in light transmission and spectral irradiance[2] at different depths. In pure

[2] When a beam of light is shone through air or water, it is reduced in intensity partly by absorption and partly by being scattered into other directions by the molecules of the medium itself and larger particles in the light path. The intensity of a narrow beam of light including only light from the direction of the source is termed *radiance*. Radiance is defined as the radiant flux per unit solid angle per unit projected area of surface. The total light incident on a surface, including both scattered (diffuse) light and directional (image-forming) light is termed *irradiance*. Irradiance is defined as the radiant flux incident on an infinitesimal element of surface containing the area under consideration divided by the area of that element. Luminance

water the attenuation coefficient (which takes into account both absorption and scattering) is lowest in the blue region of the spectrum and maximum transmission occurs at wavelengths close to 460 nm, a property which is unaffected by dissolved salts (Morel, 1974). As a result, the open oceans and a few oligotrophic, freshwater lakes appear blue in colour (Tyler, 1959; Jerlov, 1968, 1976; Tyler and Smith, 1970). As the depth increases in such waters the daylight available for vision is reduced both in intensity and spectral bandwidth, tending to the blue region of the spectrum (see Figure 1.1). In coastal waters, where phytoplankton and run-off from the land increase the levels of chlorophylls, Gelbstoff and particulate matter, the water colour is changed to green or yellow as the maximum transmission is shifted to longer wavelengths. The levels of these factors vary dramatically within short periods and plankton blooms and variations in run-off cause unpredictable and extreme variations in spectral transmission and hence in the light available for vision.

Fishes have long been the focus of spectral sensitivity studies (see Partridge, 1990) as they are outstanding among vertebrates for the diversity of the visual environments in which they live. Between the darkness at depth and the full sunlight at the surface there is a continuous range of luminous environments that vary in both colour and intensity. Further, underwater light has highly modified angular distributions which, together with spectral distributions, vary not only with depth but also over the course of the day (McFarland, 1986). In such a natural laboratory one encounters a wide variety of visual systems. Though these environments are often equally, if not more, heavily populated by invertebrates, especially the crustaceans, the body of invertebrate research is more scarce (for reviews see Stavenga and Schwemer, 1984; Cronin, 1986a; Cronin and Forward, 1988). Previously, only the visual pigments of fishes have been studied in sufficient detail to address the issue of sensory optimisation. In general, deep-water species, or species most active at twilight or night, have visual pigments matched to the light available for maximum sensitivity (Lythgoe, 1972; Munz and McFarland, 1973; Hobson, McFarland and Chess, 1981; Crescitelli, McFall-Ngai and Horwitz, 1985). Shallow-

---

and illuminance are the psychometric equivalents of radiance and irradiance (i.e. integral to each of them is the spectral sensitivity of the human eye).

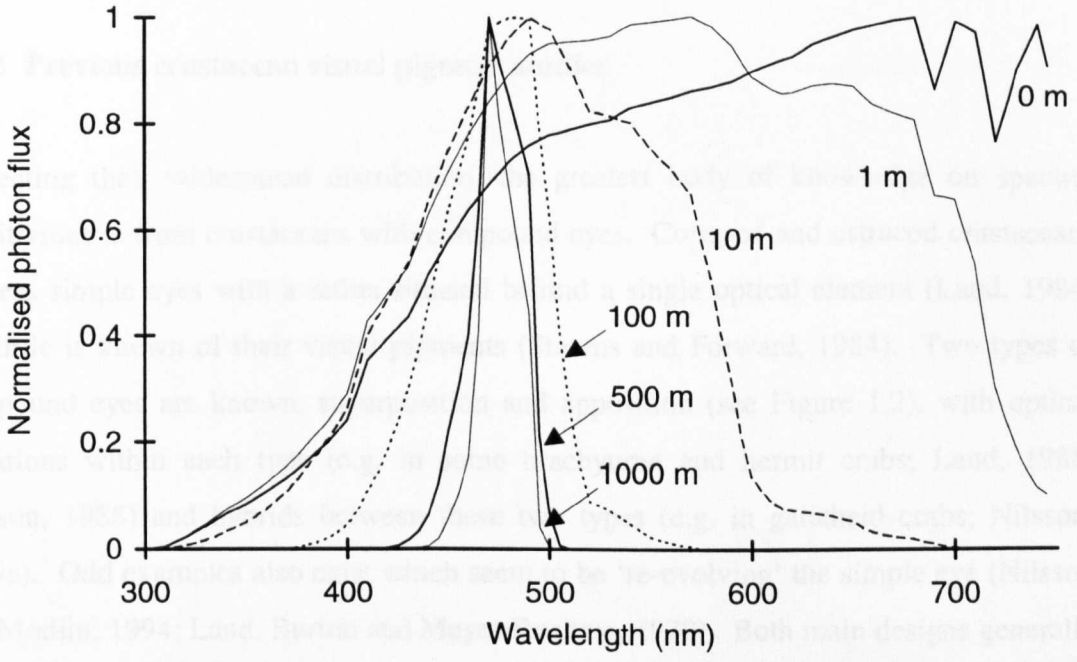

Figure 1.1 Normalised photon flux at various depths in Jerlov type IB ocean water. The spectrum at the surface (0 m) is taken from Moon (1940) and the rest calculated from spectral diffuse attenuation coefficients given by Jerlov (1976).

water, diurnal fishes often combine a matched scotopic (dim light[3]) visual system with an offset, contrast sensitive photopic (bright light[3]) system frequently capable of hue discrimination (McFarland and Munz, 1975b; Loew and Lythgoe, 1978; Levine *et al.*, 1980).

1.4.2 Previous crustacean visual pigment studies

Reflecting their widespread distribution, the greatest body of knowledge on spectral sensitivities is from crustaceans with compound eyes. Copepod and ostracod crustaceans possess simple eyes with a retina situated behind a single optical element (Land, 1984) but little is known of their visual pigments (Stearns and Forward, 1984). Two types of compound eyes are known, superposition and apposition (see Figure 1.2), with optical variations within each type (e.g. in some brachyuran and hermit crabs; Land, 1988; Nilsson, 1988) and hybrids between these two types (e.g. in galatheid crabs; Nilsson, 1989a). Odd examples also exist which seem to be 're-evolving' the simple eye (Nilsson and Modlin, 1994; Land, Burton and Meyer-Rochow, 1979). Both main designs generally consist of many hundred or thousand individual units or ommatidia and are well reviewed by Land (1980, 1981a, 1989a) and Nilsson (1989a, b, 1990a). The range of compound eye optical designs found in the Crustacea and their evolutionary adaptations are discussed by Land (1981b) and Cronin (1986b).

Largely due to their optical arrangement, superposition eyes are around 1000 times more sensitive than apposition eyes and are found in animals living in dim, scotopic conditions (Land, 1981a). The dioptric apparatus found in reflecting superposition eyes is

---

[3] The terms scotopic and photopic are normally used to describe vision in humans. Thus, scotopic vision is vision mediated primarily by rods, while photopic vision is due primarily to cones. The transition between the two is not an abrupt one and is known as mesopic vision. To apply these terms to other vertebrates the light levels at which the rods/cones are activated should be known. These terms lose distinction when applied to invertebrates which possess a completely different photoreceptor structure and mechanisms of dark-adaptation. However, they are still of use to differentiate between vision in dim light when visual systems are concerned primarily with sensitivity (i.e. scotopic vision) and vision in brighter conditions when other visual tasks such as resolution and hue determination may be achieved (i.e. photopic vision).

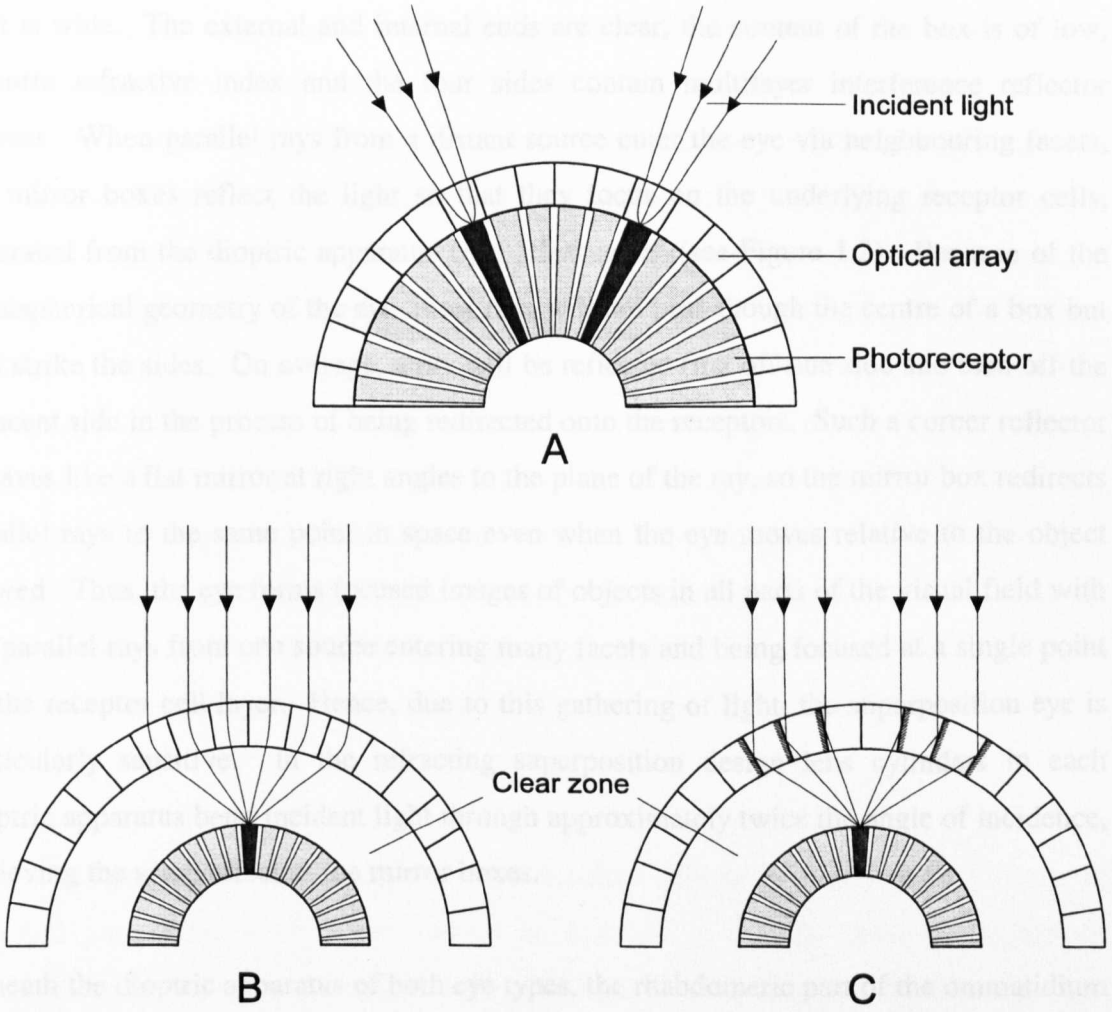

Figure 1.2 A–C. Image formation in crustacean compound eyes. (**A**) Apposition design. Individual ommatidia are optically isolated from each other by regions of pigment, and the aperture for each receptor is generally small. (**B**) Refracting superposition design. Lens cylinders in each dioptric apparatus bend incident light through twice the angle of incidence, and each receptor receives light over a wide aperture. (**C**) Reflecting superposition design. Instead of lens cylinders, each dioptric apparatus uses multilayer interference mirrors or total internal reflection to redirect light to the receptor layer. Otherwise, the design operates analogously to the refracting type (all after Land, 1981a).

particularly fascinating, using the 'corner reflector principle' (Vogt, 1975, 1977, 1980; Land, 1976, 1978). Behind each square corneal facet is a mirror box that is twice as long as it is wide. The external and internal ends are clear, the content of the box is of low, uniform refractive index and the four sides contain multilayer interference reflector mirrors. When parallel rays from a distant source enter the eye via neighbouring facets, the mirror boxes reflect the light so that they focus on the underlying receptor cells, separated from the dioptric apparatus by a 'clear zone' (see Figure 1.2). Because of the hemispherical geometry of the eye, most rays will not pass though the centre of a box but will strike the sides. On average, a ray will be reflected first off one side and then off the adjacent side in the process of being redirected onto the receptors. Such a corner reflector behaves like a flat mirror at right angles to the plane of the ray, so the mirror box redirects parallel rays to the same point in space even when the eye moves relative to the object viewed. Thus, the eye forms focused images of objects in all parts of the visual field with the parallel rays from one source entering many facets and being focused at a single point on the receptor cell layer. Hence, due to this gathering of light, the superposition eye is particularly sensitive. In the refracting superposition design lens cylinders in each dioptric apparatus bend incident light through approximately twice the angle of incidence, achieving the same effect as the mirror boxes.

Beneath the dioptric apparatus of both eye types, the rhabdomeric part of the ommatidium consists of 8 retinular cells in nearly all crustaceans (Eakin, 1972). In the Crustacea, seven of these (R1–7) generally fuse to form the bulk of the rhabdom, while the remaining cell (R8) is smaller and situated distally in the rhabdom making the whole photoreceptor a 2-tiered structure. It is the R1–7 cells that contain the blue–green sensitive visual pigments (λ_{max} between 480 and 540 nm) and the R8 cells the UV–violet sensitive visual pigments (λ_{max} near 400 nm). It is reasonable to assume this relationship holds for most crustaceans with two photoreceptor types. Interestingly, the axons projecting from the R8 cells terminate in a different optic neuropil (the medulla externa) to those of the R1–7 cells (which terminate in the lamina ganglionaris; Cummins and Goldsmith, 1981; Martin and Mote, 1982), potentially suggesting different functions for these two cell populations.

1.4.3 The mantis shrimps

By far the greatest body of work has been done on the stomatopod crustaceans (commonly named mantis shrimps) due to the unique design of their compound eyes (for an overview see Cronin *et al.*, 1994a). In terms of their spectral sampling abilities, the stomatopods are unsurpassed in the animal kingdom. From microspectrophotometry members of two of the existing five superfamilies (Manning and Camp, 1983) are known to possess at least 11 visual pigments (Cronin and Marshall, 1989a, b; Cronin *et al.*, 1994b). Recent electrophysiological data suggest there may be as many as 16 different S_{max} values (the wavelengths of maximal spectral sensitivity), one for each morphological type of photoreceptor cell in the retina (Marshall *et al.*, 1991a), each probably based on a different visual pigment (Marshall *et al.*, 1994). Photoreceptors can be divided into: colour receptors (12), polarization receptors (2) and those for spatial vision (2), although there may be some overlap in function. Colour and polarization receptors are found in the mid-band, a specialised zone of ommatidia that are obvious by external examination of the eye.

The mid-band in gonodactyloid and lysiosquilloid stomatopods contains 6 rows of enlarged ommatidia, 4 of which (rows 1 to 4, labelling dorsally downwards) contain rhabdoms adapted for colour vision, the remaining 2 (rows 5 and 6) containing structural adaptations which suggest they are sensitive to polarized light (Marshall, 1988; Cronin and Marshall, 1989a; Marshall *et al.*, 1991a). Colour vision has recently been confirmed behaviourally in the gonodactyloid mantis shrimp *Odontodactylus scyllarus* (Marshall, Jones and Cronin, 1996). The remainder of the eye, the 'periphery', contains photoreceptors much like those of other crustaceans with a short R8 cell distally placed over a longer R1–7 rhabdom tier, and is for spatial analysis of the world, possibly including monocular stereopsis (Exner, 1891; Marshall and Land, 1993).

The R1–7 cells of rows 1 to 4 are highly modified for their role in colour vision. Adaptations include tiering of photoreceptor segments (beneath the R8 cells into a 3 or 4 cell section made from the R1–7 cells), coloured intrarhabdomal filters in between tiers in rows 2 and 3, different visual pigments in each photoreceptor tier (demonstrated by

microspectrophotometry; Cronin and Marshall, 1989a; Cronin *et al.*, 1994b), and different screening pigments including, in some species, coloured lateral filters used in spectral tuning (Marshall *et al.*, 1991b; Cronin and Marshall, in press). The intrarhabdomal filters, a unique adaptation amongst the Crustacea, consist of densely coloured blocks of varying length (5–70 μm) made from vesicles containing carotenoid pigment (Marshall, 1988; Marshall *et al.*, 1991b; Cronin *et al.*, 1994b). They may be red, orange, yellow, blue or pink and are situated either between the R8 and the top tier of the R1–7 cells (distal filters) or between the two tiers formed by the R1–7 cells (proximal filters).

The tiering of photoreceptors and inclusion of coloured filters in rows 2 and 3 mean that as light passes down the rhabdom, through each photoreceptor tier or filter, its spectrum is modified. Specifically, each tier, whether colour filter or visual pigment, acts as a long-pass filter passing increasingly longer wavelengths to the tiers below. This results in the sensitivity of each retinal area beneath the first tier being very sharply tuned and shifted from the visual pigment λ_{max} to an S_{max} at longer wavelengths, in some cases displaced by over 100 nm (Cronin and Marshall, 1989a; Cronin *et al.*, 1994b). One can calculate the result of this filtering and show that the sensitivities of the photoreceptors in some species are spread to sample most of the visible spectrum.

R8 cells are present in all areas of the stomatopod eye and have also become modified for reception of polarized light in rows 5 and 6 (Marshall *et al.*, 1991a) and for colour vision in rows 1 to 4 (Marshall *et al.*, 1991b; Marshall *et al.*, 1996). At present the R8 photoreceptors of this system are not fully characterised but, as in other crustaceans, are sensitive to UV–violet wavelengths (Cronin, Marshall, Quinn and King, 1994c). However, in the stomatopods there may be as many as six different S_{max} values resulting from these cells and, from the partial classification of R8 cells in *Gonodactylus oerstedii* (Marshall *et al.*, 1994), it is known that these cells sample a range of light from 400 nm down to 312 nm. They are unusually long in mid-band rows 1 and 4 and will therefore act as UV–violet absorbing filters, resulting in more sharply tuned violet–blue R1–7 sensitivities beneath (Marshall *et al.*, 1991a, gives an example of this). In turn, this is thought to be important for spectral tuning of this system to the environmental light available to each species.

Eight spectral sensitivities, in R1–7 of rows 1 to 4, are only found in stomatopods living at, or relatively near to, the surface. Members of the superfamily Bathysquilloidea are deep water benthic animals (different species inhabiting depths from *ca.* 250 to 1000 m; Manning, 1969), possess no mid-band and in some cases reduced eyes (Manning, Schiff and Abbott, 1984). Nothing is known of their spectral sensitivities but they are likely to be tuned close to the wavelengths of downwelling light or bioluminescence, as in other deep-sea animals (see Section 1.4.8). Stomatopods from the superfamily Squilloidea dig burrows in muddy turbid areas and may be found at several hundred meters. In such a limited light environment a retina with the full spectral coverage of the gonodactyloids and lysiosquilloids would be functionless. As a result the squilloids have also 'lost' the six rowed mid-band presumed present in ancestral species. That this is a loss of the mid-band in this group seems likely as they do retain what appears to be a rudimentary 2 row mid-band, these ommatidia containing photoreceptors identical to those in the hemispheres (Cronin, Marshall and Caldwell, 1993). Squilloid rhabdoms have R8 cells which are uncharacterised due to their small size (Marshall *et al.*, 1991a) and R1–7 cells with λ_{max} values around 500 nm. Their long lengths give these photoreceptors high sensitivities from 400 to 600 nm, ideal for their murky habitat (Cronin *et al.*, 1993).

Four classes of adaptations are known in stomatopods living in dim light conditions. In all species the range of S_{max} values is reduced (compared with shallower living species) in order to match the long and short wavelength limits of the spectrum of available light. This is achieved by: 1) Changing filter colour, and thereby tuning its longwave pass, towards shorter wavelengths. 2) Using filters of similar spectral type in any one row. In a shallow water stomatopod, proximal filters pass longer wavelengths than the distal filters. Using filters of the same absorption, this shift is reduced and the sensitivity of the proximal photoreceptors kept to shorter wavelengths (Cronin, Marshall and Caldwell, 1994b, d). 3) 'Loss' of proximal filters to reduce the extent to which the sensitivities of the proximal tier is pushed to long wavelengths. 4) Reduction in the spectral spread of visual pigment λ_{max} positions at either end of the sensitivity range. As the final S_{max} of a photoreceptive tier is dependent on the λ_{max} of its visual pigment and, if it is a proximal tier, the visual pigment in the distal tier above it, this reduces the spread of sensitivities from either end of the spectrum. It is implemented particularly by the short wavelength

photoreceptors of row 1 and 4 to shift the short wavelength sensitivities in towards the centre of the spectrum, away from 400 nm.

The adaptations detailed above, coupled with the attenuation and irradiance spectra which have been measured in the environment of certain species at the actual depths and times of activity where the individuals were observed, suggest that the retinas of stomatopods are specialised to operate at similar levels of stimulation while maintaining the greatest possible potential for spectral coverage and discrimination (Cronin, Marshall, Caldwell and Shashar, 1994e). Finally, rows 5 and 6 of the mid-band (which in all species possess identical visual pigments) and the peripheral retina also exhibit R1–7 sensitivities correlated to environmental conditions. These photoreceptors are so long that their visual pigments absorb very efficiently between 400 nm and their long wavelength limb. It is the position of this long wavelength limb which shows environmental tuning.

Possible explanations for designing a colour vision system with multiple sharp tuned sensitivities, rather than three broad functions like our own, are often complex and fully presented in Cronin and Marshall (1989a), Marshall *et al.* (1991b), Marshall *et al.* (1996), Osorio and Vorobyev (1997) and Osorio, Marshall and Cronin (in press). In brief, colour, colour signalling and aggression plays an important part in the life of many stomatopods which inhabit tropical seas and reefs where their surroundings contain much colour detail. Individual species often have a distinguishing colour spot (the meral spot) which is displayed to con- and heterospecific rivals in competition for food, holes in the reef to live in, or during sexual encounters (Caldwell and Dingle, 1976). Mantis shrimps are so called because they have a raptorial limb similar to that of the preying mantis but capable of far greater force. It is used for prey capture or in battles with other stomatopods. A single blow could kill an opponent (Caldwell and Dingle, 1976) and their meral spot colour signals may be a way to communicate important information prior to any potential combat. Colour has therefore become an integral part of the lives of these animals.

Maintaining the effectiveness of their colour signals is therefore important to stomatopods. The perception of body colours will be greatly influenced both by environmental conditions and the efficacy of stomatopod vision. Maintaining colour

constancy with increasing depth or other light-limiting factors is hard. To our visual system red at the surface appears muddy green at 10 m, an example of colour constancy failure. It is due both to strong absorbance of red light by water and the relative insensitivity of the human visual system at this end of the spectrum. One way to better maintain colour constancy is to use sharply tuned sensitivities. These give higher colour contrast ratios, with some dependence on the colour being looked at. It may be the stomatopod's need to maintain colour constancy in order to interpret colour signals over a variety of ecological conditions that has driven the evolution of this unique visual system (Osorio and Vorobyev, 1997; Osorio *et al.*, in press).

1.4.4 The crabs and lobsters

The mantis shrimps aside, spectral sensitivity data from other species reveal that crustaceans as a group are restricted in their visual pigment and spectral sensitivity range. The spectral sensitivities of the crabs and lobsters have also been well studied (Cronin and Forward, 1988; Forward, Cronin and Douglass, 1988; Martin and Mote, 1982). Compared to deep-sea crustaceans, the majority of crabs dwell in shallower, more complex and diverse habitats and experience far more varied light regimes. It is therefore surprising to find that the λ_{max} values of crab visual pigments are as conservative as those of the deep-sea shrimps (see Section 1.4.8), the λ_{max} of their R1–7 cells of different species averaging around 494 nm and spreading no more than 20 nm either side of this. As mentioned before, it is possible that visual pigment λ_{max} values do not reflect the true sensitivity of the animal and filtering and/or screening by photostable pigments may shift spectral sensitivity and even mediate colour vision (Goldsmith, 1978a; Hyatt, 1975; Leggett, 1979; Kong *et al.*, 1980; Stowe, 1980b). These claims are, however, difficult to interpret and have yet to be confirmed. Colour vision in the fiddler crabs, for example, is a particularly attractive possibility as the males are well known for their claw waving display, often involving brightly coloured claws (Hyatt, 1975).

Two species of crab, *Callinectes sapidus* and *Carcinus maenas* (Martin and Mote, 1982), a crayfish, *Procambarus clarkii* (Cummins and Goldsmith, 1981) and one species of

caridean shrimp, *Palaemonetes vulgaris* (Wald and Seldin, 1968) have also been shown to possess a second sensitivity maximum in the short wavelength or ultraviolet region. The significance of this peak is still not clear; in some cases it may be used in hue discrimination (Hyatt, 1975), whilst in others it may offer contrast sensitivity or simply broaden spectral sensitivity. Indeed, there has been something of a paradox regarding the potential for colour vision in marine brachyuran crabs, various researchers claiming evidence of single (Bruno, Mote and Goldsmith, 1973; Scott and Mote, 1974) or multiple visual pigment systems (Horridge, 1967; Wald, 1968; Forward and Costlow, 1974; Hyatt, 1975; Via and Forward, 1975) using a variety of techniques. Thus, colour vision could result from this potential dichromacy but, again, this has never been examined thoroughly. R8 cells are often small and not easy to measure by microspectrophotometry so have frequently been overlooked in the past. Their existence in crabs may be the norm rather than the exception (Lall and Cronin, 1987).

Cronin and Forward (1988) investigated the visual pigments of 27 species of crabs from a variety of habitats by microspectrophotometry. In the second of this pair of papers (Forward, Cronin and Douglass, 1988), the authors describe the photic characteristics of the marine and estuarine environments of the species studied and discuss the evolutionary adaptations of the visual pigments of the crab species inhabiting them. Estuarine and algal, silt-laden coastal waters generally transmit proportionally more light at longer, 'green–yellow', wavelengths than oceanic water (Jerlov, 1976; Lythgoe, 1976) and the total light is likely to be reduced. This is also true in many freshwater habitats (Jerlov, 1976; Munz and McFarland, 1977; Loew and McFarland, 1990). However, the sort of adaptation to the freshwater or estuarine photic environments one finds in fish, where λ_{max} values are generally at longer wavelengths than ocean species, are disappointingly absent in crabs. The following λ_{max} ranges were found, arranged here according to Forward *et al.* (1988), by environment:

Semi-terrestrial	487 to 508 nm,
Estuarine	489 to 515 nm,
Coastal	483 to 515 nm,
Continental shelf	473 nm.

Only a single species, *Geryon quinquidens* a deep living continental shelf species, is well matched to the predominant wavelengths of light (at *ca.* 475 nm) in its habitat. It is notable that most species appear poorly adapted to the spectrum of light available at midday so, for this time of day, the Sensitivity Hypothesis is apparently not well founded in crabs. That is, the visual pigments of estuarine and coastal crabs are not tuned to absorb as many photons as possible at midday. No attempt was made by the authors to explain the discrepancy between the metarhodopsins of the Hermit crabs (Anomura, Paguridea) absorbing hypochromically to their rhodopsins (i.e. metarhodopsin λ_{max} values at shorter wavelengths than the rhodopsin λ_{max} values), in contrast to the bathochromatic location of the Brachyuran metarhodopsins (i.e. with metarhodopsin λ_{max} values at longer wavelengths than the rhodopsin λ_{max} values).

The remaining data on decapod spectral sensitivities have been collected by a number of authors using a variety of techniques (see Table 1.1). In general these agree well when comparing the same species as measured by different authors and/or techniques, species from within the same family and when compared to the species studied by microspectrophotometry by Cronin and Forward (1988). Most inconsistencies between *in vitro* and *in vivo* studies have been explained by the fact that chemical extraction procedures can alter the visual pigment causing artifactual shifts in apparent absorption maxima of as much as 20 nm (Bruno and Goldsmith, 1974; Denys and Brown, 1982), which is why its use has largely been superseded by microspectrophotometry. Further, as has already been pointed out for the mantis shrimps (Section 1.4.3), the presence of screening pigments can dramatically shift the S_{max} of a photoreceptor from the λ_{max} of its visual pigment explaining discrepancies between methods used to measure photoreceptor sensitivities (e.g. ERGs) and visual pigment absorbances (e.g. MSP). Thus, though it may be proposed that all non-deep-sea decapods studied to date are as poorly adapted for maximal photon capture as those measured by Cronin and Forward (1988), in many cases both their calculated spectral sensitivities and the necessary information concerning their visual environments is lacking.

Though the Sensitivity Hypothesis does not seem to be supported, neither is it obvious that crab photoreceptor sensitivities are deliberately offset to maximise contrast. This will

only work for bright objects viewed horizontally against relatively dark backgrounds (Lythgoe, 1972; McFarland and Munz, 1975a; Forward *et al.*, 1988). A crab on the sea-bed or seashore is faced with several different angles of view, from centimetres in front to the open space above, all containing different objects and backgrounds. A matched visual pigment will actually perform better for most visual tasks here (Forward *et al.*, 1988). Thus, this apparent ecological mismatch is still unexplained, though it is worth re-emphasising the importance of treating individual species as individuals and being cautious of generalisations.

Activity period and time of day have also been considered to explain the λ_{max} values recorded. During twilight, the underwater spectrum is narrowed and shifted towards the blue (Munz and McFarland, 1973). Thus, many crab species seem better adapted to this photic environment (see Lythgoe, 1972 and 1976; McFarland and Munz, 1975b for a discussion of this in fish) and this is particularly striking in the estuarine habitat. On land, the proportional reduction in yellow and orange light during twilight produces a bimodal spectrum which peaks in the blue and red (Munz and McFarland, 1973). Of the terrestrial crabs only one species, *Gecarcinus lateralis*, has been examined and was found to have visual pigment with a λ_{max} at 485 nm (Cronin and Forward, 1988). This is not a good match to the light available around sunset. However, as this land crab is active throughout the day (Lall and Cronin, 1987) its single visual pigment may represent a compromise between the light available by day and at sunrise/sunset. There is some evidence for a broader sensitivity in this species, possibly due to the presence of an R8 cell (Lall and Cronin, 1987). In all the habitats encountered, more light is available in the 425 to 525 nm range during the day, which encompasses the sensitivity maxima of crab photoreceptors, than at twilight. Therefore the light available at midday is probably not the main selective pressure regulating λ_{max} position. Also, in common with the deep-sea shrimps, many crabs have photoreceptors several hundred microns long (e.g. Stowe, 1980b; Arikawa, Kawamata, Suzuki and Eguchi, 1987) resulting in broad sensitivity functions. More probably, it is for vision at light-limited times that the photoreceptors of crabs, and indeed many other crustaceans, are optimised.

Crabs, lobsters and other crustaceans are often more active during dawn and dusk, and at night. In some species there is a substantial increase in rhabdom size (to boost sensitivity) which occurs every night (Arikawa *et al.*, 1987). Dawn and dusk in reef habitats have been shown to be critical periods with much activity and increased predation occurring (McFarland and Munz, 1975a) and this is likely to be the case elsewhere. Being able to see well at this time of the day may therefore be more important than at any other time. The spectral distribution of moonlight in clear tropical water is maximal at 570 nm (Munz and McFarland, 1973). No crustaceans yet examined are well matched to this, although the night active lobsters, *Homarus gammarus, H. americanus* and *Panulirus argus*, all have λ_{max} values greater than 500 nm (see Table 1.1). Perhaps during the darkest hours, other sense organs are more important.

Two patterns in crab λ_{max} values apparently not related to ecology are 'clustering' of maximal sensitivities around certain modal points and a loose phylogenetic trend. A plot of all crab photoreceptors examined reveals that their visual pigments tend to cluster near 490 and 510 nm. The diogenid (hermit) crabs generally fall in the latter group and brachyura the former, both groups including species from diverse habitats (Cronin, 1990). Some degree of phylogenetic constraint on λ_{max} values is also known in fish (Douglas and Partridge, 1997). Cluster points are noted at approximately 5 nm or 10 nm intervals in deep-sea fish, e.g. at 442, 452, 463, 470, 477, 483, 490, 501, 505, 511, 519, and 524 nm (Partridge *et al.*, 1989), and other vertebrates (e.g. Dartnall and Lythgoe, 1965). These imply a degree of molecular constraint on the position of λ_{max} values, probably relating to the opsin-chromophore interaction which sets visual pigment sensitivities (Bridges, 1964; Dartnall and Lythgoe, 1965; Partridge *et al.*, 1989).

1.4.5 *Ligia*, an exception to the two visual pigment 'rule'

Ligia exotica is a beach dwelling isopod active during the day and therefore exposed to a broad spectrum of light. Its ommatidia contain only 7 retinular cells but three distinct spectral sensitivities have been recorded by electroretinogram, with S_{max} values at 340, 460 and 520 nm (Hariyama, Tsukahara and Meyer-Rochow, 1993). It is not known how

these sensitivities integrate in the life of *Ligia* but the occurrence of a UV sensitive photoreceptor lends support to the likelihood that short wavelength receptors are common in the Crustacea (for a review of the distribution and function of UV sensitivity throughout the animal kingdom see Tovee, 1995). Chittka (1996) has recently suggested that the possession of three visual pigments such as this is the plesiomorphic condition for many crustaceans as well as the insects.

1.4.6 Adaptations to freshwater

A number of crustacean species live in freshwater and of these crayfish and cladoceran spectral sensitivities are known. Structurally crayfish eyes are much like the superposition eyes of related marine crustaceans. In all species investigated the rhabdoms include an R8 cell and in *Procambarus clarkii* it is known to be UV–violet sensitive with a λ_{max} at 440 nm (Cummins and Goldsmith, 1981). As with marine crustaceans, few suggestions exist as to the function of these cells. The light environment in freshwater is very variable but, in general, peak transmission is shifted to longer wavelengths, usually due to dissolved organic matter and chlorophyll in the water which absorb short wavelengths preferentially (see Lythgoe, 1966 and 1972). Many crayfish species are partially terrestrial and are often found in clear water, both being spectral environments where UV–violet is abundant and possibly maintaining the evolutionary pressure for their UV–violet sensitivity.

Conversely, the sensitivities of the R1–7 cells of crayfish are apparently adapted to the relatively long wavelengths which penetrate turbid freshwater and, as not all shortwave photons are absorbed by the water, the R8 cells may still function in such waters. Freshwater fish and amphibians use 3-dehydroretinal, the vitamin A_2 derived chromophore, to construct longwave sensitive visual pigments, the 'porphyropsins' (Bridges and Yoshikama, 1970). Intriguingly, this is also the mechanism used by the crayfish *P. clarkii* (and three other crayfish genera; Suzuki and Eguchi, 1987) to produce a visual pigment with λ_{max} at 562 nm (Suzuki *et al.*, 1984; Zeiger and Goldsmith, 1989).

How the pigment is distributed in retina is not known and it is not found in all crayfish. Nonetheless all λ_{max} values, whether A_1 or A_2 derived, are greater than 520 nm.

In common with fish such as the brown trout, *Salmo trutta* (Muntz and Mouat, 1984; Bowmaker, 1990), or the bullfrog (Reuter, White and Wald, 1971), there are seasonal variations in the amount of porphyropsin in the eyes of *P. clarkii*, more being present in winter months (Suzuki, Arikawa and Eguchi, 1985). This is perhaps an adaptation to increased water turbidity as a result of increased rainfall in winter. Unfortunately, little information exists on the habitats and habits of any crayfish and it is even unclear if spectral irradiance shifts to longer wavelengths in winter in their habitats.

The water flea, *Daphnia magna*, has only 22 ommatidia in its compound eye, each containing 8 rhabdomeres as found in other crustaceans. Since the work of von Frisch (von Frisch and Kupelwieser, 1913), followed by Smith and Baylor (1953) and Stearns (1975), a number of species of *Daphnia* have been known to respond in characteristic ways to different wavelengths of light. These 'colour dances' (Smith and Baylor, 1953) apparently enable avoidance of damaging short wavelengths and swarming in areas of food (phytoplankton) and may be more akin to the wavelength specific behaviours known for some insects (Menzel, 1981) than to colour vision *per se*. A recent electrophysiological investigation of *D. magna* has unearthed 4 spectrally distinct photoreceptors within one ommatidium (Schehr, 1984; Smith and Macagno, 1990), their S_{max} values at 348, 434, 525 and 608 nm. *Daphnia* live in the shallow depths of freshwater ponds where the spectral distribution of light may not be very different to air, but with the UV wavelengths decaying most rapidly with depth. Smith and Macagno (1990) in fact suggest that the UV photoreceptor in *Daphnia* may enable them to detect proximity to the surface or its direction to enable the body to be orientated with respect to it.

It is hard to believe *Daphnia* would need tetrachromatic vision although this has yet to be experimentally ruled out. A more parsimonius explanation of their spectral sampling diversity is that each photoreceptor type is 'hard wired' into a specific behaviour related to a narrow wavelength range. The early 'colour dance' observations (Smith and Baylor,

1953), which recorded stereotyped behaviours, such as clustering or sideways migration, in response to narrow bandwidth light stimuli, support this hypothesis. Wavelength specific behaviours, where a direct correlation exists between wavelengths of light encountered and individual photoreceptors, should provide a particularly clear-cut relationship between ecological influences and spectral sensitivities. Unfortunately the *Daphnia* visual micro-environmental and behavioural data needed are unknown.

1.4.7 Ontogenetic changes

A number of fish and amphibia undergo changes in spectral sensitivity during development or maturation (Bowmaker and Kunz, 1987), invariably associated with a change in habitat and often, although not always, the result of a migration from freshwater to seawater or from water to land (e.g. Wood, Partridge and DeGrip, 1992; Shand, 1993). Many crustaceans also undergo dramatic changes in lifestyle as their larvae leave the plankton to take up adult life on the sea-bed, in more defined niches in midwater, or on land. The visual demands of the adult are therefore likely to be very different. Descriptions of embryonic and larval eyes of crustaceans are limited (for a review see Gaten and Herring, 1995), but all larval decapods are thought to possess hexagonal facets and, therefore, are presumed to use apposition optics (Fincham, 1980). Those that use superposition optics as adults must undergo a major optical transformation during their development (Land, 1981b; Nilsson, 1983, 1989a; Fincham, 1984; Cronin, Marshall, Caldwell and Pales, 1995a). Thus after metamorphosis the gradual squaring of the eye facets, begun during the larval phase, is completed. This is an essential prerequisite for the functioning of the facultative superposition reflecting optics found in the long-bodied decapods (i.e. shrimps, prawns and lobsters) both coastal (Fincham, 1984; Douglass and Forward, 1989) and deep-sea (Gaten and Herring, 1995), and some Anomura. One might expect concomitant spectral sensitivity changes.

The behavioural sensitivity peaks found in a number of crustacean larvae all lie within the blue–green (Forward and Costlow, 1974; Forward and Cronin, 1979; Forward and Douglas, 1989). Anatomically, R8 cells are known in the larval eye of some stomatopods

(Cronin *et al.*, 1995a) and these are likely to be UV–violet sensitive although their spectral sensitivities are, as yet, unknown. In fact, the spectral sensitivities of the R1–7 cells of the larvae of just one crab, *Callinectes sapidus* (Cronin and Marshall, 1995), and one stomatopod, *Gonodactylus aloha* (Cronin *et al.*, 1995a), are known. Given the abundance and spectral coverage of adult visual pigments, one might expect to find stomatopod larval visual pigments occurring in one of the spectral classes of the adult. Surprisingly this is not so and suggests that the ecological tuning of larval spectral sensitivity is rather precise. Alternatively, as the adult eye is a radically new structure, replacing the larval eye completely on metamorphosis (Cronin *et al.*, 1995a), the differences in λ_{max} may be due to developmental constraints.

1.4.8 Deep-sea shrimps

Despite being some of the most inaccessible animals in the world, deep-sea fish have been a focus of attention for vision research for several decades (see Partridge, 1989; Partridge, Archer and Van Oostrum, 1992). More recently, deep-sea crustaceans have become the target of study, particularly the 'deep-sea shrimps' (e.g. Frank and Case, 1988a, b; Shelton, Gaten and Herring, 1992). These include the decapod sergestids (e.g. Hiller-Adams, Widder and Case, 1988), oplophorids (e.g. Cronin and Frank, 1996) and penaeids (e.g. Fernández, 1965), the mysid *Gnathophausia ingens* (Frank and Case, 1988b) and the euphausiids (Kampa, 1955 and 1965; Denys, 1982; Denys and Brown, 1982; Widder, Hiller-Adams and Case, 1987) (see Table 1.1). An excellent review of the photoecology of pelagic decapods is presented by Herring and Roe (1988).

The habitat of these deep-sea animals extends from a few hundred meters to benthic depths well below 1000 m (the average depth of the open ocean is *ca.* 4.5 km) and should be considered as several niches rather than a single one as it often is. Also, although the spectrum of downwelling light is relatively narrow compared to the broad spectrum experienced by day on land, it is a mistake to treat the mesopelagic depths (i.e. between *ca.* 300 and 1000 m) as 'monochromatic'. It has been regarded as such in the past, partly because it looks blue to us and partly because it has previously been quantified with

relatively insensitive instruments. Recently, Frank and Widder (1996) have demonstrated that sufficient UV wavelengths penetrate to allow shortwave-vision to several hundred meters. Downwelling irradiance is thus centred about the blue region of the spectrum but is not restricted to it, UV light being present at visually significant levels well into the depth ranges of many deep-sea shrimps. Further, different behaviours and modes of life exist within this habitat. Some mesopelagic decapods, such as *Systellaspis debilis* and *Oplophorus spinosus* for example, are part of the massive diurnal vertical migration undertaken by deep-sea shrimp, fish and other animals (Frank and Case, 1988a). Others such as *Notostomus gibbosus* and *Acanthephyra curtirostris* apparently stay at the same depth regardless of time of day (Frank and Widder, 1994b) or reside close to the bottom, e.g. *Plesiopenaeus armatus*. Compared to other crustaceans, however, the habitat of deep-sea shrimps is a relatively simple one, both in spectral and spatial terms.

As daylight penetrates into the sea it is absorbed and scattered, and its intensity diminishes rapidly with depth. Even in clear oceanic water the intensity, as measured by an upward facing irradiance meter, falls by approximately a tenth for about every 75 m increase in depth even for those wavelengths that penetrate best (Jerlov, 1976; Denton, 1990). Several adaptations including superposition optics, tapeta and enlarged eyes have evolved to catch as many incident photons as possible (Land, 1990; Shelton *et al.*, 1992; Gaten, Shelton and Herring, 1992). With such adaptations, and in the clearest tropical oceans, it is likely that some deep-sea animals can detect daylight down to about 1000 m (Denton, 1990). An alternative source of light below 1000 m, and also above this depth, is bioluminescence. Indeed, it is presumed that anything living below 1000 m will only see light produced by other animals and the fact that many highly visual animals exist below this depth demonstrates the importance of bioluminescence (Herring, 1977).

Along with optical adaptations (see Land, 1981a, b, and 1990) one might also expect the sensitivity of visual pigments to be tuned to the blue light which penetrates best in the ocean (Jerlov, 1976). Alternatively, their sensitivity may match bioluminescence which is also usually blue in order to match the downwelling light or to carry information over a long distance (Herring, 1977; Latz, Frank and Case, 1988). This is the Sensitivity Hypothesis first proposed separately by both Clarke (1936) and Bayliss, Lythgoe and

Tansley (1936) (see Lythgoe, 1972, and McFarland and Munz, 1975a, for a discussions of this). While true to an extent, in that the visual pigments of most deep-sea animals have λ_{max} values clustered between 450 nm and 500 nm, it is nevertheless an over-simplification.

Studies using microspectrophotometry have been able to characterise both the rhodopsin and metarhodopsin states of the visual pigments present. Four mesopelagic species, *Systellaspis debilis*, *Acanthephyra curtirostris*, *A. smithi* and *Sergestes tenuiremis*, were found to possess rhodopsins ranging from 485 to 495 nm λ_{max} and metarhodopsins from 480 to 487 nm λ_{max} (Hiller-Adams *et al.*, 1988). Due to the spectral location of the metarhodopsins, the authors concluded that the spectral characteristics of the rhodopsins and metarhodopsins permit high photosensitivity and facilitate photoregeneration in a nearly monochromatic environment. Further, photic regeneration of rhodopsins from the deep-sea environment was demonstrated, and data were obtained which are consistent with the occurrence of dark-regeneration (Hiller-Adams *et al.*, 1988).

Electroretinograms have also been used to determine the spectral sensitivities of dark-captured specimens of eight deep-sea shrimps from the decapod Family Oplophoridae (Frank and Case, 1988a). *Notostomus gibbosus* and *N. elegans* were maximally sensitive at 490 nm, and chromatic adaptation experiments indicated that a single visual pigment was present. Peak sensitivities of *Acanthephyra smithi* and *A. curtirostris* were at 510 nm, a longer wavelength than expected for such deep-sea dwellers and in contrast to the respective rhodopsin λ_{max} values of 491 nm and 485 nm recorded by Hiller-Adams *et al.* (1988) by microspectrophotometry. The latter highlights potential discrepancies between visual pigment λ_{max} and photoreceptor S_{max} values, though in the 'dark-adapted' superposition eyes of such deep-sea shrimps screening pigments are reduced and filtering and/or screening thought to be minimal (Gaten *et al.*, 1992). Electroretinography on the deep-sea mysid *Gnathophausia ingens* (Family Lophogastridae) found high sensitivity to orange light (S_{max} at *ca.* 510 nm), an unexpected result for a species whose adult members are never found above 400 m (Frank and Case, 1988b). Further, results of chromatic adaptation and silent substitution experiments were not compatible with either a one or

two pigment visual system, making this one of the more unusual visual pigment systems ever described.

Many deep-sea shrimps do not, as has often been assumed, inhabit Jerlov type I water, the clearest of the seawater types classified by Jerlov (1976). One has only to move to Jerlov type III water to find a minimum attenuation at 500 nm. Moreover, such a bulk classification of a water column takes no account of vertical heterogeneity or the seasonal variation in phytoplankton which will tend to push minimum attenuation to longer wavelengths. More importantly, even if not occupying different microhabitats deep-sea shrimp species will at least, in all likelihood, exhibit different 'micro-adaptations'. Considering species living in Jerlov I, others in Jerlov II or III, some tuned through evolution to search for bioluminescent sources emitting maximally at 450 nm and others that emit maximally at 500 nm, there is more than enough potential visual adaptation to account for the variation seen. One must know which visual stimuli are most relevant to the animal (i.e. which stimuli are associated with selective pressure) and very little detailed observation of this kind exists (Frank and Widder, 1994a, b; Land, Marshall and Diebel, 1995).

One argument put forward by Lythgoe (1972) and developed by McFarland and Munz (1975a, b) to explain the λ_{max} of some fish visual pigments is the 'offset' or contrast enhancing visual pigment. This hypothesis suggests that it is better to view a bright object against a dark background (as often occurs in surface waters) with a visual pigment whose λ_{max} is not matched to the background light. In the depths of the sea many animals are either very black, effectively black (by being red) or good reflectors of the ambient illumination by being silver (Denton, 1990). Thus they either appear dark against the brighter background of downwelling light or, if silver, match the background from nearly all angles. Under these conditions, a matched visual pigment is best (McFarland and Munz, 1975a) and applying the offset idea to deep-sea shrimp visual pigments is therefore hard.

Animals living in midwater, either deep or a few meters below the surface, do not experience even illumination, either in terms of the spectrum or intensity. In the

mesopelagic zone upwelling light is around 200 times dimmer than downwelling light (Denton, 1990; Land, 1990) and contains relatively more shortwave light due to particulate scatter being more effective at the shortwave end of the spectrum (Jerlov, 1976). Essentially the underwater world is divided into the narrow, bright window of downwelling light against which silhouettes might appear and a rapidly darkening violet–blue view beneath, punctuated by occasional bioluminescent flashes. Several mesopelagic animals including fish (Land, 1990), polychete worms (Wald and Rayport, 1977) and crustaceans, notably certain euphausiids (Land *et al.*, 1979) and hyperiid amphipods (Land, 1989b), have divided their eyes into upward and downward and looking regions. There are also adaptive optical trends with increasing depth (see Land *et al.*, 1979; Land 1989b), and one might predict different spectral sensitivities in the two eye regions. However, in the euphausiids at least (see Table 1.1; Denys and Brown, 1982; Boden, Kampa and Abott, 1961; Widder *et al.*, 1987), it appears that the λ_{max} of visual pigments in dorsal and ventral eye regions are the same. What may differ are screening pigments which potentially tune photoreceptor sensitivity. The hyperiid *Platyscelus ovoides* for instance has red pigment in its ventral eye and yellow pigment in its dorsal eye (Land *et al.*, 1995). Alternatively, if the task of the dorsal eye is to receive downwelling light and that of the ventral eye is to see bioluminescence, which itself is usually blue, the spectral requirements of the dorsal and ventral eye may well be the same.

An increasing number of crustaceans, including certain deep-sea shrimps, are being shown to possess more than one visual pigment (Cummins and Goldsmith, 1981; Martin and Mote, 1982; Frank and Case, 1988a; Frank and Widder, 1994a; Cronin and Frank 1996). Of the deep-sea shrimps, four photophore-bearing, vertically migrating species of the Family Oplophoridae, *Systellaspis debilis*, *Janicella spinicauda*, *Oplophorus spinosus* and *O. gracilirostris*, were measured using electroretinograms and found to have sensitivity maxima at 400 and 500 nm, chromatic adaptation experiments indicating the presence of two visual pigments (Frank and Case, 1988a). The behavioural responses exhibited by *S. debilis* specimens to changes in ambient light observed by Frank and Widder (1994a), led the authors to propose that this organism's migratory behaviour might be controlled by light.

Anatomical studies have shown the existence of both R8 and R1–7 photoreceptors in the eyes of certain members of the Family Oplophoridae (Gaten *et al.*, 1992). Recently, Cronin and Frank (1996) demonstrated by microspectrophotometry that those of *S. debilis* contain visual pigments maximally sensitive to 410 and 498 nm, respectively. Although it does not possess externally divided eyes, the relative lengths of the R8 and R1–7 receptors change within the eye such that in receptors looking upwards the R8 length to R1–7 length ratio is 0.15 whereas for downward looking receptors this ratio is 0.8. This is achieved by both a shortening of the R1–7 and elongation of the R8 in the ventral retina (Gaten *et al.*, 1992). Many deep-sea shrimp also possess a tapetum, a reflective layer proximal to the rhabdoms which increases sensitivity by reflecting light back through the photoreceptors. In the shallow living Oplophorid species, such as *S. debilis*, the tapetum is more extensive in the downward looking region which, together with the greater R8 to R1–7 length ratio also found, presumably increases sensitivity in the part of the eye viewing the darkest part of the visual field (Shelton *et al.*, 1992). A reduced or absent upward-pointing tapetum may also minimise upward eyeshine which is potentially visible to downward-looking predators (Shelton *et al.*, 1992). (This is supported by the counter intuitive observation that deeper living species, such as *Acanthephyra purpurea*, possess a reduced tapetum, and thus reduced sensitivity, despite the reduction in downwelling light. However, tapetal reflection of bioluminescent flashes will presumably be more visible in deeper waters becoming the most significant factor affecting its visibility to other organisms. The reduction of eyeshine is therefore thought to be adaptive, reducing visibility to predators (Shelton *et al.*, 1992).) The eye can therefore be viewed as a 'matched filter' to the distribution of light around the animal. Gaten *et al.* (1992) propose that the enlarged ventral R8 cells are spectrally adapted to the relatively more abundant UV–violet wavelengths in light scattered back from the depths.

Systellaspis debilis produces two spectrally differing bioluminescent emissions in the form of a defensive secretion and from ventral photophores for counter-illumination camouflage (Herring, 1977; Frank and Case, 1988a). Many of its cohabitants are also bioluminescent and it has been suggested that the UV–violet photoreceptors of *S. debilis* (and others, see Table 1.1) may aid in visualising this source of light or even distinguishing different bioluminescent sources which may be quite spectrally diverse

(Frank and Case, 1988a; Widder, Latz and Case, 1983; Latz *et al.*, 1988). This may be particularly useful in vertically migrating species with cuticular photophores, such as *S. debilis*, which undertake this journey in congener swarms (Gaten *et al.*, 1992). That is, being able to see the light produced by members of the same and different species may help swarms to remain together, an advantage in the expanse of the deep-sea.

Cronin, Kent, Frank, Widder, Partridge, Herring and Robinson (1996a) have calculated that the spectral sensitivities of the R8 and R1–7 photoreceptors of *S. debilis* are optimally placed for maximum contrast (i.e. the stimulation ratio of the R8 to R1–7 cells) when viewing bioluminescence. It is not clear at this stage if this putative task is also linked to the dorsal/ventral differences of the eye of *S. debilis*. It is known that the ventral eyes of hyperiid amphipods can be used for tracking blue bioluminescent-like sources (Land *et al.*, 1995), while the dorsal eyes are optically adapted for identifying small silhouettes against downwelling light (Land, 1989b). Further uses for dichromacy in the deep-sea are colour vision, for which no direct evidence exists, or more simply as a depth gauge. The ratio of UV–violet and blue–green light (i.e. those wavelengths to which the R8 and R1–7 cells are tuned) was thought to change with both depth and time of day and thus may have been used by vertical migrators (Frank and Case, 1988a). However, recent measurements of light in the deep-sea demonstrate that below the euphotic zone there is little change in spectral shape with time or depth (Frank and Widder, 1996) and this hypothesis has now been discarded. Nevertheless, there is clearly an advantage in possessing more than one visual pigment for some deep-sea fish as, out of the 183 species studied, 19 are multi-pigment species (Douglas and Partridge, 1997).

Rhabdom morphology also appears to be correlated with irradiance level, and therefore depth. Banded fusiform rhabdoms are commonly seen in the superposition eyes of decapods from shallower water, but were only found in the most dorsal regions of the Oplophorid species with the shallowest daytime ranges examined, *Oplophorus spinosus* and *S. debilis* (Gaten *et al.*, 1992). The fusiform shape helps to contain incident light within the target rhabdom, so limiting the spread of light within the rhabdom layer and maintaining resolution. In contrast, shrimps from deeper water, such as *S. cristata* and species of *Acanthephyra*, the ventral regions of *O. spinosus* and *S. debilis* eyes and the

refracting superposition eyes of the mesopelagic penaeid shrimp *Gennadas* (Meyer-Rochow and Walsh, 1977; Nilsson, 1990b) all possess stellate, interdigitating rhabdoms. With adjacent ommatidia so closely apposed there is little mechanism to limit the extent of light spread within the rhabdom layer and this is presumably an adaptation to increase the absolute sensitivity of the eye (Gaten *et al.*, 1992). Further, the accompanying loss of resolution may not be as great a problem for mesopelagic animals viewing small objects against a uniform background (Land, 1989b). Finally, the absence of alternating layers of orthogonally orientated microvilli is unusual in decapods and prohibits any sensitivity to polarized light (see Waterman, 1981 and Section 5.2.8).

Deep-sea shrimps also exhibit ontogenetic changes. In particular, Gaten and Herring (1995) propose that ontogenetic changes in eye morphology within the oplophorid shrimps can be correlated to their reproductive strategies. Any larval stages growing in the plankton would be best served by transparent apposition eyes. In this situation camouflage is maintained and the apposition ommatidia obtain enough light from all directions. As the growing juveniles move to deeper water, superposition optics are employed to improve the photon capture in the low-light mesopelagic zone. Apposition optics are retained in some species, however, for viewing the downwelling light. In contrast, species which complete much of their development within the egg, hatch with their eyes already developing superposition optics. They are thus well-adapted to life in the mesopelagic zone, avoiding the hazards that accompany a planktonic larval phase. No research has yet been done to investigate if there are parallel changes in the organisms' visual pigments.

Several benthic decapods (e.g. *Plesiopenaeus armatus*) have well developed eyes. However, *Rimicaris exoculata*, a deep-sea caridean shrimp which lives in large swarms around volcanic hydrothermal vents at depths in the ocean where no sunlight penetrates, has evolved a unique ocular morphology. The retinae of *R. exoculata* have migrated from the eye stalk and spread throughout the carapace (van Dover *et al.*, 1989). Reasons for this unusual structural reorganisation are not clear, although intriguingly it is paralleled in other crustaceans (Land, 1989c) and *Ipnops* a benthic deep-sea fish (Marshall, 1979). The function of the 'eye', however, may be to warn the shrimp as they cluster close to the

super heated plumes of water (350 °C) found at such sites. The visual pigment, whose λ_{max} is 500 nm, may be sensitive enough to see the black-body radiation produced by heat (Pelli and Chamberlain, 1989) and, although the eye is non-directional and lacks optical components, it may allow the detection of plumes, attracting the shrimps to feeding areas and deterring them from plunging into water hot enough to kill them (van Dover *et al.*, 1989; Land, 1989c). Very little bioluminescence is reported from the hydrothermal vents, lending support to this unusual claim.

1.4.9 Conclusions and speculations on polarization sensitivity

Influences determining crustacean spectral sensitivity fall into a variety of categories, none mutually exclusive. Thus, the final spectral position of a photoreceptor's visual pigment and, more importantly, its spectral sensitivity may be the result of a variety of factors. Ecological factors are integral to the Sensitivity and offset/contrast hypotheses. The first proposes that spectral sensitivity is matched to, and therefore dependent on, the spectral distribution of the light available taking into account behavioural factors such as the time of day that the organism is active and periods of significance, e.g. dawn and dusk. The latter is only applicable for viewing bright objects against darker backgrounds and so is probably limited to the lower half of the visual field in surface dwellers. Behaviourally significant tasks, specific events or tasks of importance, such as colour communication of aggressive intent, sexual display or bioluminescence, and depth determination are also potentially important in determining photoreceptor properties.

While phylogenetic trends in crustacean visual pigments are only notable in crabs this apparent exception may be due to the fact that in other cases there is insufficient data. Biochemical constraints may also influence spectral sensitivities: chromophore-opsin interaction may explain the observed clustering of λ_{max} values and opsin/porphyropsin exchange results in short and long wavelength families of visual pigments. Noise and thermodynamic considerations may set the longwave limit of visual pigment λ_{max} values, long wavelength S_{max} being achieved instead by filtering (e.g. in the stomatopods). Evolutionary inertia is sometimes used to explain visual pigment λ_{max} positions,

specifically the lack of red sensitivities (Goldsmith, 1991). In the light of new evidence, however, it seems that visual pigment evolution (Cronin, Marshall and Caldwell, 1996b) and eye evolution (Nilsson and Pelger, 1994) can occur rapidly. This implies that the spectral sensitivities observed today may well be optimal for the animal in question. The challenge in visual ecology is to determine which factor, or more likely which combination of factors, generates this solution.

In conclusion, decapod crustaceans usually possess two types of photoreceptors with different spectral sensitivities, one maximally sensitive around 500 nm (the blue–green sensitive R1–7 cells) and the other around 400 nm (the UV–violet sensitive R8 cells). Their small size and short wavelength sensitivity means R8 cells are often overlooked or hard to measure but, at least in the deep-sea crustaceans, may not always be present. The euphausiids and amphipods, despite often having divided eyes, probably possess only a single visual pigment (as do other crustaceans from the minor groups listed in Table 1.1). In contrast, the stomatopods, perhaps the mysids, *Daphnia* and *Ligia* all have more than two spectral sensitivities.

The combination of UV–violet and blue–green sensitivities in different photoreceptor populations is used by a surprisingly diverse assemblage of crustaceans in many different habitats. No such basic pattern exists in the fish whose number of visual pigments per species and spectral range exceeds the basic crustacean design. Coupled with the complexity of the stomatopod eyes, this questions the true constraints of crustacean phylogeny, biochemistry and unknown ecological factors, no matter how real these are. The answer may lie in polarization, rather than spectral, sensitivity. The microvillar design of crustaceans makes them inherently sensitive to the E-vector[4] of polarized light

[4] Light consists of electric and magnetic fields which oscillate perpendicular to the direction of travel. These transverse waves are in turn perpendicular to each other and have the same frequency and phase. The electric field (E) in a light wave affects a photographic plate and causes fluorescence, while the magnetic field, though present, plays no part in these effects of a light wave. On this account the *direction of light vibrations* is usually defined to be that of the electric vector (*E-vector*). The *plane of polarization* is then defined as the plane containing the light ray and the E-vector. The term *polarized light* refers to photons of electromagnetic radiation in the visible spectrum whose electric components all oscillate in a restricted plane, perpendicular to the direction of propagation.

(Waterman 1981). That they are concerned with maintaining this sensitivity is suggested by the regular array of orthogonal microvilli in R1–7 cells and occasional regular arrays in the R8 cells also (Eguchi and Waterman, 1973; Waterman, 1981; Krebs and Lietz, 1982; Marshall *et al.*, 1991a).

There is a significant amount of polarized light above and particularly below the water produced mainly by reflection and particle scattering (Ivanoff and Waterman, 1958). Functionally, its overall pattern in the sky is known to be used for navigation (Wehner, 1983) and it may enhance resolution in scattering media such as turbid waters (Lythgoe, 1976). Also, crustacean and other animal body patterns may selectively reflect polarized light making it a potential signal (Neville and Luke, 1971; Marshall *et al.*, 1991a; Cronin, Shashar and Wolff, 1995b; Shashar, Rutledge and Cronin, 1996). Behaviourally a number of crustaceans are known to respond to polarized light (e.g. Goddard and Forward, 1991) and, beneath the retina, signals from cells sensitive to orthogonal E-vectors appear separated until the first neural integration site, the lamina, where differential signals may then be integrated (Nässel, 1976; Glantz, 1996). In stomatopods, the advanced colour system seems to 'borrow' this plesiomorphic wiring system, possibly to achieve dichromatic opponency (Marshall *et al.*, 1991b; Marshall *et al.*, 1996). Further, stomatopods are also known to discriminate E-vectors (N.J. Marshall, unpublished observations).

The degree to which light is polarized in water is known to be wavelength dependent with a minimum at 450 to 500 nm (Ivanoff and Waterman, 1958). That is, the least attenuated light (in clear waters) shows the lowest polarization (Jerlov, 1976). Therefore, it may be that efficient perception of polarized light affects the spectral tuning of crustacean photoreceptors, their S_{max} values often lying on either side of this polarization minimum. Similar explanations have been suggested for the spectral positioning of insect photoreceptors known to be used for polarized light perception (Wehner, 1983; Seliger *et al.*, 1994). Given the apparent emphasis crustaceans place on this sensory modality, perhaps the perception of polarized light should be looked at more closely as a functional explanation of their spectral sensitivities.

1.5 THIS STUDY

Three principle objectives were identified during this study:

1) To test the Sensitivity Hypothesis by comparing the visual pigments of previously studied deep-sea fishes with those of deep-sea shrimps which inhabit the same environment.
2) To compare the visual pigments of deep-sea shrimps of different taxa.
3) To develop analysis procedures with which to determine the rhodopsin and metarhodopsin pigments present in a measured unknown mixture.

To achieve these aims, the visual pigments of 36 deep-sea shrimp species were examined by microspectrophotometry.

Chapter Two

Materials and Methods

2.1 SPECIMEN COLLECTION AND PREPARATION

2.1.1 Animal collection

Live specimens of the common lobster, *Homarus gammarus*, caught off of the south west coast, were obtained from a local fishmongers. Specimens of the Norway lobster, *Nephrops norvegicus*, were kindly donated by Dr. Peter Shelton, Leicester University. The latter had been caught at night in Scotland and maintained in the dark during all transits to stop permanent light damage to the eyes (see Loew, 1976; Shelton *et al.*, 1985). The investigation of specimens of these two species constituted the initial, preliminary study. Deep-sea crustaceans were collected during RRS Challenger cruise 122 (21st September to 20th October 1995, stationed off of Portugal and near Madeira) and during a cruise on the RV New Horizon (12th to 26th May 1996, off the coast of southern California). Exhaustive collections were made of all of the species of decapod crustaceans encountered during both cruises. In addition, specimens of six species of mysid and one species of amphipod were collected.

The majority of the specimens obtained while on RRS Challenger were mesopelagic and were collected in a light-tight closing cod-end (CCE) attached to a rectangular midwater trawl of 8 m^2 aperture (RMT 8; see Roe and Shale, 1979; Wild, Darlington and Herring, 1985). Two epibenthic species, *Acanthephyra microphthalma* and *Plesiopenaeus armatus*, were caught using a semi-balloon otter trawl (OTSB14; Merrett and Marshall, 1981). In total, eighteen species were obtained in sufficient numbers to allow full microspectrophotometric investigation in Bristol, namely: *Acanthephyra microphthalma*, *A. purpurea*, *A. stylorostratis*, *Bentheogennema intermedia*, *Gennadas valens*, *Gnathophausia gigas*, *Hymenodora glacialis*, *Meningodora miccyla*, *M. vesca*, *Oplophorus spinosus*, *Parapasiphaea sulcatifrons*, *Plesiopenaeus armatus*, *Sergestes curvatus*, *Sergia maximus*, *S. robustus*, *S. splendens*, *Stylopandalus richardii* and *Systellaspis debilis*. Meso- and bathypelagic species were collected while on RV New Horizon, all specimens being caught with an opening/closing 3.1 m Tucker Trawl, fitted with a thermally protected, light-tight collecting container (see Childress, Barnes, Quetin and Robison, 1977; Childress and Price, 1978). Specimens of nineteen different species

were obtained, namely: *Acanthephyra curtirostris*, *Bentheogennema pasithea*, *Chalaraspidium alata*, *Cyphocaris richardi*, *Eucopia australis*, *E. sculpticauda*, *Gennadas sp.*, *Gnathophausia gracilis*, *G. ingens*, *Hymenodora frontalis*, *Parapasiphaea sulcatifrons*, *Pasiphaea chacei*, *P. emarginata*, *Petalidium suspirosum*, *Plesionika maritus*, *Sergestes similis*, *Sergia phorcus*, *Systellaspis braueri* and *S. cristata*.

2.1.2 Animal maintenance

Specimens of *Homarus* and *Nephrops* were maintained in marine aquaria at the University of Bristol. In all cases animals were used within one week of collection, usually within two days. *Nephrops* were kept in a temperature controlled room (10 °C) and in absolute darkness to avoid light damage to the eyes. *Homarus* were maintained on a 12 h light:dark cycle at 12–13 °C. Due to their short maintenance time the specimens were not fed.

Deep-sea crustaceans could not be maintained on board the ships and tissue preparations were made immediately following retrieval of the net. The collecting containers used on both cruises were closed at depth and the contents subsequently examined and sorted under dim red light (see Section 2.2.2). Experimental animals were maintained in chilled seawater (*ca.* 5 °C) in light proof containers and all tissue preparations carried out within 4 h of capture (see Section 2.1.3 below). Preventing any exposure to surface light is essential when working with the visual systems of deep-sea species, which can be damaged by even low levels of light (Frank and Case, 1988a; see also Loew, 1976; Nilsson and Lindström, 1983; Shelton *et al.*, 1985).

2.1.3 Tissue preservation

Since deep-sea shrimps could not be maintained on board ship (and specimens were often dead when the net was retrieved) ocular tissue was preserved by rapid freezing. Microspectrophotometry of the tissue was then carried out up to three months later at the

University of Bristol. All preservation was carried out under dim red light (see Section 2.2.2) and involved the removal, orientation and mounting of each eye in a plastic well filled with cryomount (Tissue-Tek OCT Compound, Miles Inc., Elkhart, IN, USA) which was then rapidly frozen with fluorocarbon spray (Cryospray 22, Bright Instrument Co. Ltd., Cambridge, England, UK). The eyes were mounted with the lateral surface uppermost to allow longitudinal sections of rhabdoms to be obtained from all regions of the eye. The frozen blocks were individually sealed in plastic bags to avoid desiccation, placed in light-tight aluminium tubes, and maintained in the -70 °C freezers on board. The aluminium tubes were transported from the ships packed in dry-ice and stored at the University of Bristol in a -80 °C freezer.

The carapace lengths (from the back of the eye orbit to the posterior point of carapace, excluding expansions) and total lengths (from the tip of the rostrum to the tip of the telson) of all specimens collected were recorded. These data were not used in this study and are thus not presented. The eyeless bodies of certain specimens were stored in 10% formalin in seawater for subsequent identification. In addition, 'intact' examples of each species were preserved and retained for reference, particularly regarding the orientation of the eyes when attached to the body. Finally, macro-photographs were taken of some of the decapod specimens in an unfixed state and are presented in Appendix I.

2.1.4 Tissue preparation for microspectrophotometry

Specimens of *Homarus* and *Nephrops* were dark-adapted for 12 to 24 h prior to experimentation. In the dark, or under dim red illumination (see Section 2.2.2), the eyes were removed and the specimens killed by immersion in boiling water. To prepare a retinal sample from *Homarus*, the eyes were removed, slits cut in the corneal surface and each eye was left in artificial seawater with 2.5% glutaraldehyde for up to 1 h. This initial fixation allowed the eye to be bisected and the exposed tissue fixed for a further 2 to 3 h. Three distinct bands of tissue were then readily identified; a dark band representing the pigment surround the crystalline cones, the light clear zone, and a dark band representing the rhabdoms. The tissue was removed from the eye, teased apart with mounted needles

and the retinal tissue isolated and resuspended in artificial seawater. A drop of this suspension was placed on a 22 x 50 mm No. 1 coverslip and sealed using a ring of silicone grease and a second, 19 mm diameter No. 1 coverslip.

Initially, rhabdom cell suspensions were prepared from *Nephrops* specimens as described for *Homarus* but without the need for glutaraldehyde fixation. Later preparations, and those of the deep-sea shrimps, were made using a cryostat. Hence, eyes were removed and mounted in a well of Tissue-Tek and frozen with fluorocarbon spray. Frozen eyes were sectioned on a cryostat at a temperature of *ca.* -20 °C and a thickness of *ca.* 15 μm. Cut sections were transferred to a 22 x 50 mm No. 1 coverslip, mounted in artificial seawater and again sealed using a ring of silicone grease and a second, 19 mm diameter No. 1 coverslip. Sectioning proceeded from the region of the cornea opposite the eyestalk toward the centre of the eye. No axial scans of photoreceptors were taken, with most sections used representing longitudinal sections relative to the long axis of the rhabdoms, the actual angle depending on the depth of the section being examined.

2.1.5 Cryosection thickness

Knowing the thickness of the sections cut is necessary to calculate the specific absorbances of the visual pigments present (see Section 5.2.8). To do this the calibration of the focusing of a standard laboratory microscope was attempted. First both sides of a standard microscope slide were marked with a marker pen. Imaging both sides under the microscope (using a 10x eyepiece and a 100x objective) the number of units turned on the marked focusing knob was noted. This was repeated due to the subjective nature of determining when the markings were in focus and an average taken. The slide was then measured using a pair of electronic digital callipers and found to be 0.98 mm thick throughout. Dividing this distance by the number of units turned on the focusing knob it was calculated that each unit represents approximately 1.9 μm. Freshly cut sections from the cryostat were then placed under the microscope and the depth of focus between the top and the bottom of the section estimated. In practice this was difficult to judge and, again, averages were taken to take into account variations between sections and

judgement of focus. In the end it was estimated that the sections were of approximately 10 focusing units or less. This corresponds to a thickness of 19 μm or less.

It was therefore not possible to accurately determine the thickness of the sections cut on the cryostat but it was confirmed that they are approximately as indicated by the cryostat. Hence, for subsequent calculations the thickness of the sections was assumed to be that as set on the cryostat knife. It must also be noted that the sections 'collapse' to an unknown extent when thawing on the microscope slide. While this will inevitably reduce the thickness of the section, the original thickness of the frozen cut section should still be used when calculating the specific absorbances as this represents the distance over which the visual pigment present was originally distributed.

2.2 MICROSPECTROPHOTOMETRY

2.2.1 The microspectrophotometer

The microspectrophotometer used to measure the visual pigment absorption spectra in this study is a new single-beam, wavelength-scanning, computer-controlled instrument. It is similar in design to the one described in detail by Partridge (1986) but with significant improvements and additions for measuring invertebrate pigments. The machine is shown diagrammatically in Figure 2.1.

The microspectrophotometer's measuring beam consists of the light produced by a 100 W quartz-halogen bulb powered by a stabilised 12 V DC power supply (Oriel Corporation, USA). The filament of the bulb is focused onto the entrance slit (1 mm) of a Jobin Yvon H-1061 VIS grating monochromator (Instruments S.A. Ltd., Middlesex, UK), and the output (8 nm full width at half maximum, FWHM, bandwidth) focused onto an adjustable aperture. This consists of two sets of opposable slits which control the vertical and horizontal dimensions of the beam. The aperture housing also contains a calcite crystal which linearly polarizes the light passing through the aperture, a feature that enables the dichroic absorption properties of photoreceptor cells to be exploited. The measuring

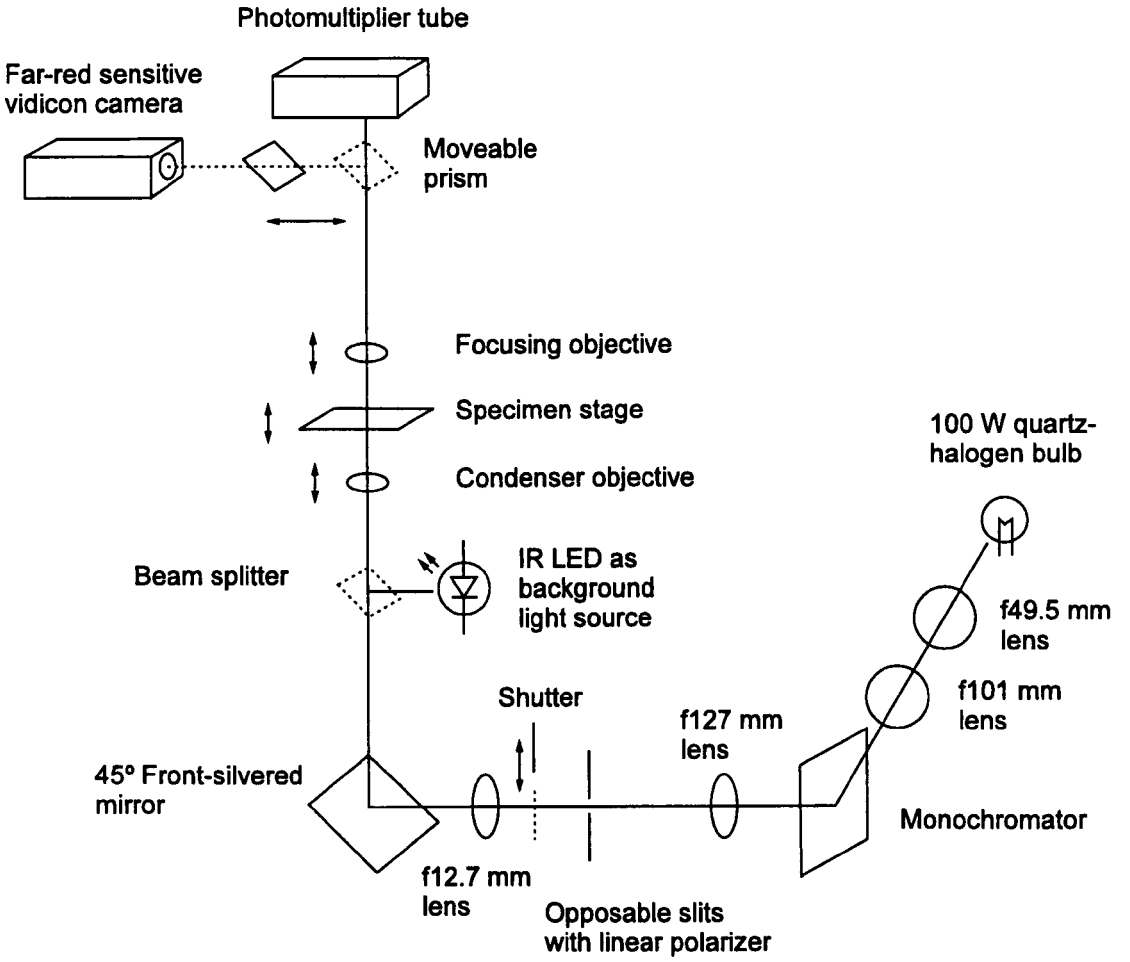

Figure 2.1 Diagrammatic view of the microspectrophotometer.

beam is focused, directed by a moveable front-silvered mirror and then demagnified into the plane of the specimen on a microscope stage by a Zeiss Ultrafluar 32x objective used as a condenser lens (numerical aperture, NA, 0.4). Above the stage, an Olympus 100x DApo 100UV objective (set to a NA of 1.3) focuses the beam emergent from the specimen towards the 'headstage'.

At the headstage the beam either falls directly onto a small area of the photocathode of a Hamamatsu R928 photomultiplier or, by use of a sliding prism, is directed towards a far-red sensitive vidicon camera (75 series miniature CCTV Camera 3; Insight Vision Systems Ltd., Malvern, UK). The latter is connected to a monochrome video monitor and allows viewing of the specimen without bleaching or photoconversion taking place. Background illumination is provided by an infra-red LED, the light from which is introduced to the light path by a beam-splitter positioned below the condenser lens. The passage of the measuring beam can be interrupted before reaching the specimen by an electric shutter controlled either manually or automatically via the computer. The modified microscope and headstage of the microspectrophotometer are housed within a light-tight box to keep stray light from bleaching the sample or reaching the photomultiplier. As a precaution, however, all light from the monitor, PC and electronics is red-filtered.

A substage condenser assembly, with a 100 W tungsten filament bulb, is situated beneath the movable front-silvered mirror allowing a direct optical path to the specimen stage. Together with a sliding filter tray and adjustable iris, this provides the saturating light needed to photoconvert or bleach samples using a greater intensity than that available from the monochromator. The spectra of the light used for photoconversion and photobleaching are presented in Section 2.2.2. Finally, a clear acetate overlay, calibrated by placing a graticule on the specimen stage of the microspectrophotometer, was produced to measure structures imaged on the video monitor.

To measure an absorption spectrum, the retinal section or individual photoreceptor cell is focused by moving the specimen stage up or down. The measuring beam, typically 3 x 5 μm, is then focused (at 730 nm) using the 'condenser' lens in an area adjacent to the

photoreceptor or outside of the eye section, the infra-red background illumination extinguished, and the light path directed to the photomultiplier. A 'baseline' scan is recorded as the computer-controlled stepper motor drives the monochromator from 730 to 350 nm and back again. Light hitting the photocathode induces a nanoamp (nA) current in the photomultiplier which is converted to a voltage in the headstage amplifier. This voltage is amplified and fed into an analogue multiplier together with the output from a digital to analogue converter, which receives a variable 'gain' signal from the PC, to give an approximately constant voltage at all wavelengths. This voltage is then amplified, inverted and low-pass filtered with a Butterworth 2-stage active filter, and fed to a voltage to frequency (V/F) converter. Decrease in light results in a linear increase in frequency output to a maximum of 2 MHz. After a short delay at each wavelength to allow the filtered signal to settle, the frequency output at each odd wavelength on the 'downward' long- to shortwave spectral pass (or each even wavelength on the 'upward' short- to longwave spectral pass) is integrated over *ca.* 10.8 ms using a CTM-05 counter/timer board (MetraByte Co., Taunton, MA, USA) in the PC. A single scan takes approximately 15 s and, like all other automated procedures, is controlled by a Microsoft QuickBASIC program. Having recorded a baseline scan the photoreceptor or retinal section is moved into the measuring beam and a 'sample' scan made in the same way. Baseline and sample data are recorded, along with summary file information, as a comma delimited text file for later analysis.

2.2.2 Microspectrophotometer illumination spectra

The spectra of the various light sources used in the microspectrophotometer were scanned using a Macam SR3010A spectroradiometer (Macam Photometrics Ltd., Livingston, Scotland, UK) with the irradiance sensor resting on a No. 1 coverslip placed on the microscope stage. Due to the relatively low photon fluxes, when measuring the light from the monochromator the neutral density filter (used to limited the photon flux of the measuring beam) was removed and the slits fully opened. Nevertheless, there was still insufficient light to measure the measuring beam at wavelengths below *ca.* 430 nm. The transmission of the neutral density filter (peak absorbance of 1.07) was measured using a

Shimadzu UV-2101PC scanning spectrophotometer (Shimadzu Scientific Instruments Inc., Columbia, MD, USA) and the actual light flux used during experimentation calculated by multiplying its spectral transmittance by the light fluxes measured. When measuring the illumination from the substage light source the photon flux was sufficient for direct measurement.

When the irradiance sensor is evenly illuminated the Macam SR3010A is calibrated to give readings in W m^{-2} nm^{-1} (i.e. the energy of the light at that wavelength which would fall on a square metre area if it was illuminated evenly at the same photon flux density as that sampled by the sensor). However, because neither the measuring beam nor the condenser illumination filled the irradiance sensor, measured values were multiplied by the ratio of the sensor area divided by the area illuminated. Specifically, the circular sensor has a diameter of 15.38 mm (a surface area of 185.78 mm^2) and, at the specimen plane, the measuring beam had dimensions of 16 by 16 µm (an area of 0.000256 mm^2), and the condenser illumination had a diameter of 0.4 mm (an area of 0.1257 mm^2). By converting all readings into quantal units, all the spectra measured from the microspectrophotometer are presented in photons m^{-2} s^{-1} (see Figure 2.2).

Figure 2.2A clearly shows the fall off of light available at short wavelengths, primarily due to the lack of shortwave photons produced by the quartz-halogen bulb which acts as the measuring beam's source. The *ca.* 8 nm FWHM bandwidth of the monochromator output is also apparent. In comparison, the maximum light fluxes per nanometer (in photons m^{-2} s^{-1}) produced by the substage condenser assembly are approximately two orders of magnitude above the maximum light fluxes per nanometer of the measuring beam (i.e. comparing Figure 2.2A and B). Hence, the light fluxes used to measure the visual pigments are of much lower intensity than those used to bleach or photoconvert the visual pigments, as expected to minimise in-scan photoconversion and/or in-scan photobleaching (see Section 4.1.1.4). The 'white' light produced by the unfiltered output of the monochromator set at its blaze angle was not used for visual pigment bleaching during this study but is included here for reference (Figure 2.2C).

The irradiance from the red-filtered head-torch used to illuminate the specimens during

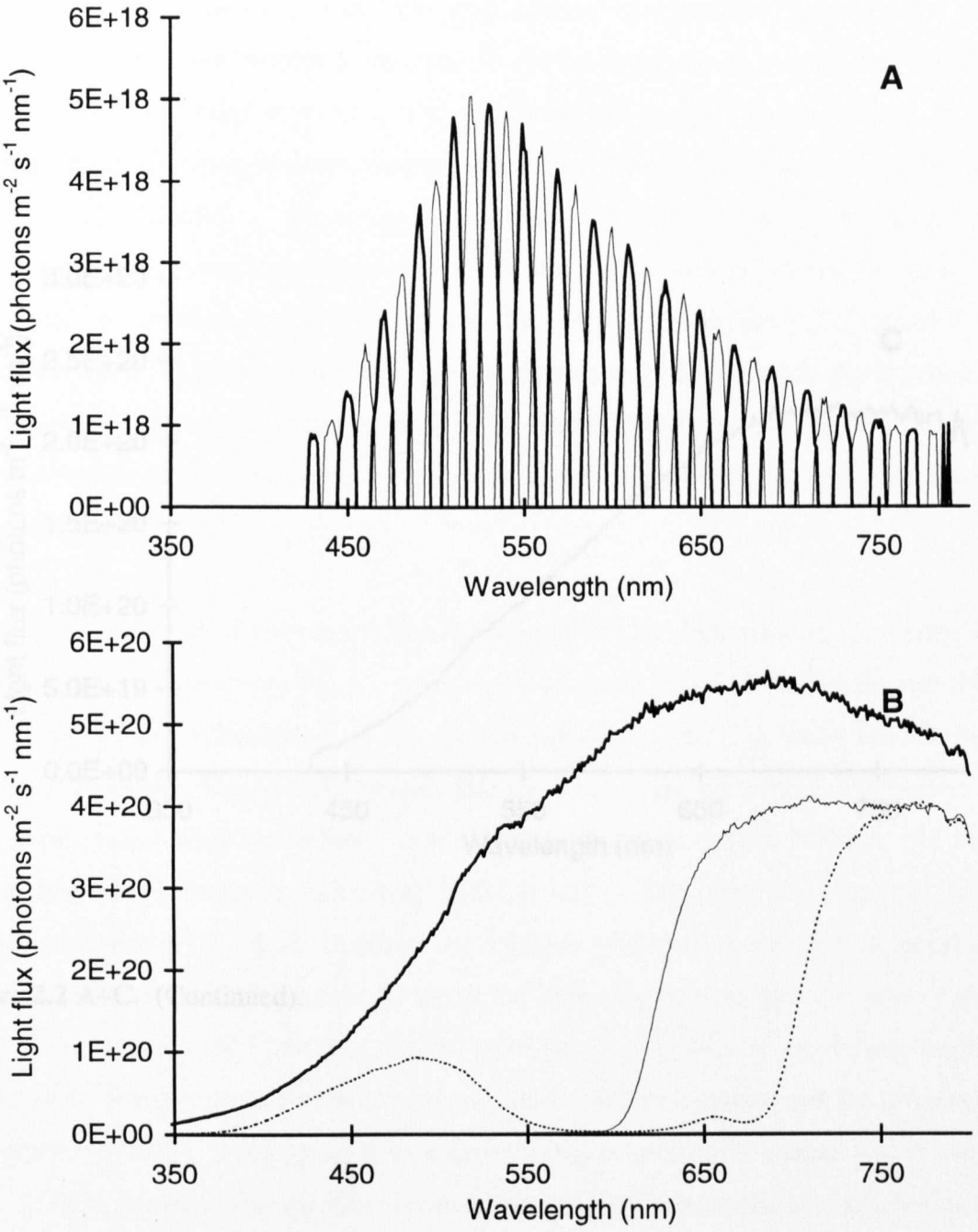

Figure 2.2 A–C. Microspectrophotometer light fluxes, calculated as they occur at the specimen plane. (**A**) The light flux of the measuring beam as used during scanning, recorded at 10 nm intervals (alternating bold and light traces). The *ca.* 8 nm bandwidth of the monochromator output is apparent. (**B**) Irradiances produced by the substage condenser source, unfiltered (bold trace), with the red filter (light trace) and with the blue filter (dotted trace). (**C**) The light flux of the monochromator when set at the grating's blaze angle, i.e. 'white' light output, with no neutral density filter in the light path.
Note, the apparent sudden falls of shortwave irradiance in (**A**) and (**C**) are due to the light fluxes dropping below the sensitivity threshold of the Macam SR3010A used to measure these spectra.

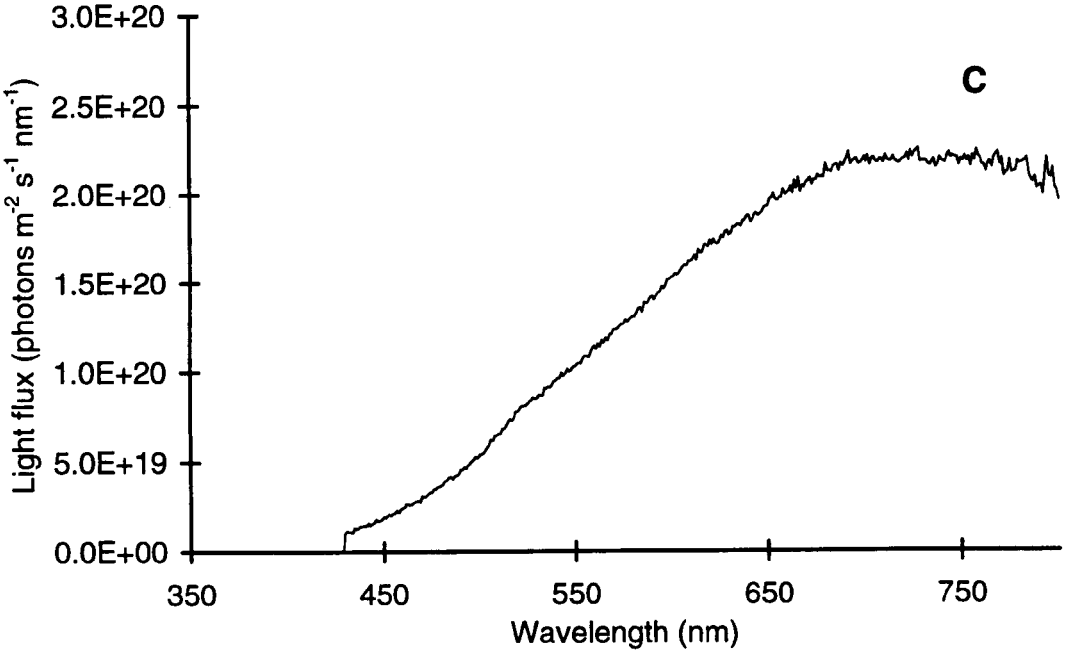

Figure 2.2 A–C. (Continued).

examination and selection, and the eyes during preparation, preservation and cryosectioning was also measured. Specifically, as the beam can be focused and the light source would have been at varying distances from the sample, the irradiance of the brightest part of the beam was measured at distances of 25 and 50 cm, with the beam both focused and diffused. These are presented in Figure 2.3. As with the microspectrophotometer light fluxes, the irradiance spectra are shown in units of photons m^{-2} s^{-1} measured at 1 nm intervals, though even with the light output fully diffused it is not of equal intensity over the area illuminated. However, as the specimens, and specifically their eyes, could all have been illuminated within the central, brightest region of the beam, this was the area measured and the equivalent light flux per square metre calculated from this.

A cursory comparison of the photon flux densities of the red light used to illuminate the samples during preparation etc. (i.e. using the head-torch; Figure 2.3) and the red light used to photoconvert the sample in the microspectrophotometer (i.e. using the substage condenser assembly; Figure 2.2B) reveals that the latter is approximately three orders of magnitude greater than the former. Indeed, integrating over 350 to 800 nm, the total quanta from the head-torch focused at 25 cm is over 3000 times less than that from substage condenser. Dartnall, Goodeve and Lythgoe (1936) have shown that, provided the absorbance of a visual pigment is low at the bleaching wavelength (not greater than *ca.* 0.1) the kinetics of bleaching can be represented very closely by an exponential relationship. For a given pigment its photosensitivity will be constant and the proportion of pigment remaining at any given time is then linearly related to the intensity of the light used. Hence, doubling the intensity, for example, halves the time taken to reach a given degree of bleaching with the amount of bleaching governed by the product of time and intensity, i.e. the total quanta received by the pigment (see also Knowles and Dartnall, 1977).

Though photoconversion between the rhodopsin and the metarhodopsin of invertebrate pigments involves the continuous conformational change of a population of molecules, it is still a light governed reaction and the time course to reach a photo-steady state also follows an exponential 'decay' or 'growth' (see Cronin and Goldsmith, 1981). Hence the

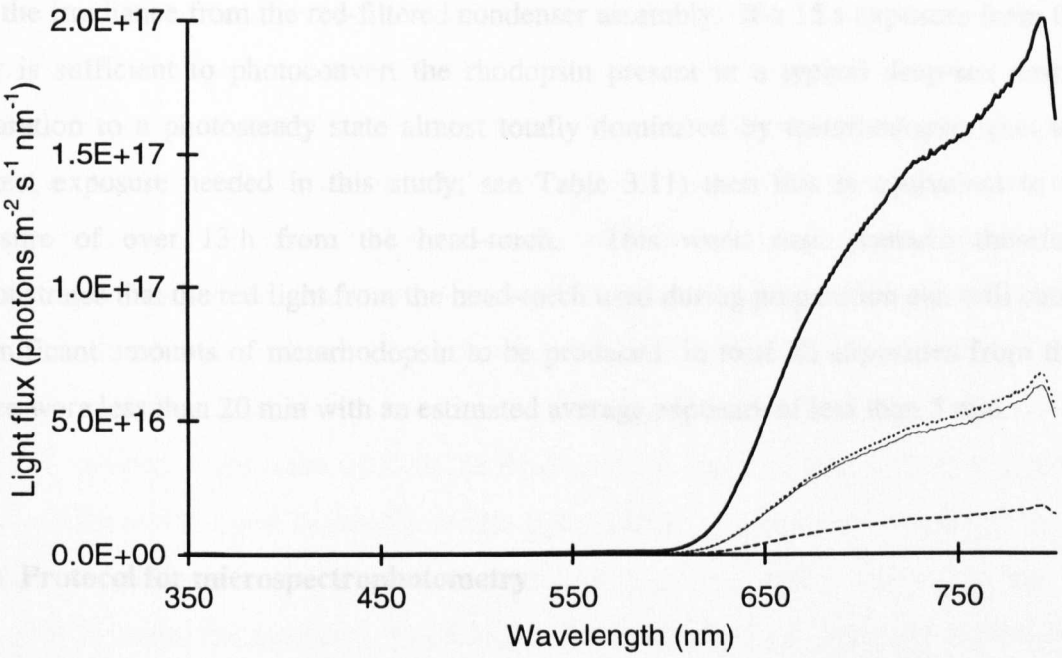

Figure 2.3 Light flux of the red-filtered head-torch. Irradiance spectra were measured at 25 cm with the beam both focused (bold trace) and diffused (light trace), and again at 50 cm with the beam both focused (dotted trace) and diffused (dashed trace).

same relationship as shown for photobleaching will apply for photoconversion. However, with photoconversion the proportions of the pigments present in the steady state mixture will depend on the spectrum of the light used, irrespective of intensity. Thus, assuming the shapes of the spectra are equal, the maximum irradiance from the red-filtered head-torch (i.e. focused at 25 cm) will take 3000 times longer to create a photosteady mixture than the irradiance from the red-filtered condenser assembly. If a 15 s exposure from the latter is sufficient to photoconvert the rhodopsin present in a typical deep-sea retinal preparation to a photosteady state almost totally dominated by metarhodopsin (i.e. the shortest exposure needed in this study; see Table 3.11) then this is equivalent to an exposure of over 13 h from the head-torch. This worst case scenario therefore demonstrates that the red light from the head-torch used during preparation etc. will cause insignificant amounts of metarhodopsin to be produced: in total all exposures from this source were less than 20 min with an estimated average exposure of less than 5 min.

2.2.3 Protocol for microspectrophotometry

Photoreceptor samples, either mounted cell suspensions or cryosections, were placed on the microscope stage of the microspectrophotometer and the measuring beam focused within the specimen plane. This was initially located outside of the photoreceptor cell and a 'background' scan taken. Specimens were then moved such that the beam was placed within a photoreceptor and the transmitted light was again measured. The ratio between these scans gave the transmission spectrum of the photoreceptor, from which the absorbance spectrum of any visual pigment present was calculated (see Partridge, 1986). The data were recorded on the microspectrophotometer's PC as comma delimited files of wavelength, baseline and sample, with 'file header' information noting experimental variables and comments.

These initial 'sample' scans were repeated to check their stability. If there was no difference in underlying signal between these scans (i.e. subtracting one scan from the other produced a flat spectrum with no wavelength dependent changes beyond the range of the noise), the photoreceptors were treated using a series of exposures to filtered light

from the substage condenser (each exposure of about 15 s duration) and scanned between each. This was continued until there was no difference in the recorded signal between successive scans, indicating that a photosteady state mixture of rhodopsin and metarhodopsin had been formed. Main rhabdoms were treated with red light and R8 rhabdomeres were exposed to blue light in order to maximise the fraction of metarhodopsin in the mixtures created. The photoreceptor samples were finally photobleached by exposure to unfiltered 'white' light from the substage condenser. Again this was done via successive exposures (each of about 10 min) until there was no further change in absorption. By continually scanning the sample at regular intervals any absorption changes due to other pigments or fluctuations in the microspectrophotometer (e.g. the light flux, or the specimen being moved between scans) could be observed and these scans rejected (see Section 2.3.1 below).

Note that this procedure relies on both the rhodopsin and metarhodopsin being thermally stable, yet bleaching when exposed to bright light. These properties are characteristic of crustacean visual pigments but many researchers have resorted to prior fixation in aldehydes to make the pigments unstable for the bleaching (see Hays and Goldsmith, 1969; Bruno, Barnes and Goldsmith, 1977, Goldsmith, 1978b; Cronin, 1985). During the bright light exposures from the substage condenser, the field diaphragm was closed down, producing a spot with a diameter of *ca.* 0.4 mm at the level of sample, to minimise local heating of the preparation. However, it is likely that the temperature of the preparation was still increased and some of the bleaching is due to this. Further, it is inevitable that some proportion of the visual pigment will be bleached by the red/blue light treatments (see Cronin, 1985). No attempt was made to correct for this as the level was estimated to be less than the inherent noise of the scans (see Section 4.1.1.4).

2.2.4 Difference spectra

Each section/photoreceptor scanned yielded approximately 8 to 10 data files (i.e. 2 'initial' scans, 3 to 4 'red/blue treatment' scans, and 3 or 4 successive 'white light' scans) with three pairs identical in all but noise. The absorption spectra (or 'difference spectra')

of the initial mix of rhodopsin and metarhodopsin present within the photoreceptor ('mix_1') were calculated as the difference between the two initial scans and the two final, post-bleach scans. The absorption spectra of the mixture of rhodopsin and metarhodopsin created by the red/blue light treatment ('mix_2') were then calculated as the difference between the final two red- or blue-treatment scans and the two final, post-bleach scans. Thus, using all possible combinations, each section/photoreceptor scanned yielded 8 difference spectra: four mix_1 and four mix_2 spectra.

For this calculation to be done 'on-line', new subroutines were added to the Microsoft QuickBasic programme controlling the microspectrophotometer. Though the values are calculated using pairs of absorption values at each wavelength, baseline and sample values are reconstructed and the difference spectra again recorded on the microspectrophotometer's PC as comma delimited files, with the 'file header' information noting experimental variables and the original files used to calculate it. Thus all of the files obtained, measured spectra and difference spectra, have a common format and both could be analysed by the analysis software described in Section 4.2.

2.3 DATA ANALYSIS

2.3.1 Data selection

For each type of photoreceptor, data were selected for inclusion into an average by analysing individual records and employing selection criteria. Analysis was automated using computer, spreadsheet based, software purposely written for this study and described, in brief, below. A full discussion of the analysis of visual pigment absorbance spectra obtained using microspectrophotometry is presented in Section 4.2.

The comma delimited microspectrophotometric data file is read into the Microsoft Excel 5.0c based analysis program and absorbance values calculated from the recorded baseline and sample frequencies. A 'box-car' running average is passed through the absorbance values and the peak value noted with its corresponding wavelength. Sample scans

recorded by the microspectrophotometer are frequently offset from the baseline scans due largely to the way in which the sample changes the focus of the measuring beam on the photocathode of the photomultiplier tube. Thus, it is often necessary to introduce an offset when normalising the absorbances. This is calculated at the longwave end of the spectrum where there is no absorbance due to the visual pigment. The maximum corrected absorbance is then calculated as the peak absorbance minus the longwave offset absorbance and the data are normalised to this range for subsequent calculations and display. The FWHM bandwidth is equal to the difference between the wavelengths corresponding to 50% maximum absorbance on the short- and longwave limbs of the data smoothed by the running average.

The polynomial given by Partridge and DeGrip (1991) is then used to fit the rhodopsin template spectrum given by Stavenga *et al.* (1993), with a shifting β-band (after Palacios *et al.*, 1996), to the data. Specifically, each point on the longwave limb between 80% and 20% of the normalised absorbance is used to estimate the λ_{max}. In effect, the template is moved mathematically to intersect each valid data point on the longwave limb (see Bowmaker *et al.*, 1975). The average of these estimations is then taken as the best estimate of the λ_{max} of the data. Only the longwave limb of a visual pigment absorbance spectrum is used to estimate the λ_{max} because this part of the spectrum is least affected by photoproduct build up, short wavelength light scattering and avoids the overlapping regions of the α- and β-bands which occurs at wavelengths shorter than *ca.* 430 nm.

Visual pigment absorbance spectra were accepted for inclusion in an average if: 1) the template spectrum fell within the peak noise of the data points between 80% and 20% of the maximum absorbance on the longwave limb, 2) the maximum was well defined and, 3) the absorbance spectra were flat for *ca.* 100 nm beyond the wavelength at which the longwave limb first falls to an absorbance of zero. Average mix_1 and mix_2 difference spectra were calculated using the selected individual difference spectra by taking the average absorbance value at each wavelength interval. These average spectra were then filed, re-analysed and used to estimate the absorbance spectra of the rhodopsin and metarhodopsin pigments present in the photoreceptor measured.

2.3.2 Estimating the rhodopsin and metarhodopsin absorbances

Various authors have detailed methods to estimate the λ_{max} of the metarhodopsin given the absorption spectra of the rhodopsin and of the rhodopsin and metarhodopsin mixture resulting from the post-red light treatment (e.g. Hochstein, Minke, Hillman and Knight, 1978; Cronin and Goldsmith, 1982a; Stavenga and Schwemer, 1984; Cronin and Forward, 1988). In brief, templates are fitted to the rhodopsin and mixture absorption spectra and the fraction of rhodopsin in the photosteady state mixture is estimated by comparing the total absorptions of the two templates in the region of the saturating, red light exposure. This fraction is then subtracted from the mixture and a new template fitted to this metarhodopsin estimate as before.

In this study, however, it was not possible to dark-adapt the deep-sea specimens and thus the mix_1 scans also potentially represent unknown mixtures of rhodopsin and metarhodopsin. Considerable effort was made to overcome this and is discussed in Section 4.3. In brief, for each photoreceptor type the above method was used to estimate the metarhodopsin absorbance spectrum by assuming mix_1 was 100% rhodopsin. This metarhodopsin estimate was then scaled and subtracted from the mix_1 averaged difference spectrum to produce a range of rhodopsin absorbance spectra given an assumed fraction of metarhodopsin in mix_1. This was repeated assuming different fractions of metarhodopsin in mix_1 and a series of rhodopsin estimates thus created. Photoconversion difference spectra (the absorbance of mix_2 minus mix_1, representing the change in absorbance between the two states) of these estimates and of the data were calculated and scaled appropriately, and the estimate curve which produced the least sum of squared differences with the data points was selected. Hence the estimates of the rhodopsin and metarhodopsin absorbance spectra were selected.

Chapter Three

Results

3.1 PRELIMINARY STUDY: *HOMARUS* AND *NEPHROPS*

The protocol and analysis outlined above (Sections 2.2 and 2.3) were successfully applied to specimens of the common lobster, *Homarus gammarus*, and the Norway lobster, *Nephrops norvegicus*. Specifically, data were obtained from *H. gammarus* rhabdom suspensions and from both rhabdom suspensions and cryosections of the eyes of *N. norvegicus*. For each species over 200 scans were made and over 100 difference spectra calculated. These represent recordings from over 30 R1–7 cells from at least four specimens of each species. However, mostly due to the fine-tuning of various aspects of the protocol during this time, but also due to the 'normal' rejection of those spectra which show excessive noise and/or variations from the accepted templates, only 8 difference spectra were selected and averaged for each pigment (i.e. the rhodopsin and metarhodopsin). Further, the initial results obtained for *N. norvegicus* using rhabdom suspensions were rejected in favour of the scans of the cryosections. None of the rejected scans indicated the presence of contrary or additional pigments. No attempt was made to identify or scan putative R8 cells.

The data obtained are listed in Tables 3.1 to 3.9 and the average spectra presented in Figures 3.1 and 3.2. Specifically, the numbers of sections/rhabdom suspensions successfully scanned and subsequently included for averaging are given together with the numbers of specimens from which they were obtained (Table 3.1). The average light treatments used to photoconvert and photobleach these samples is given (Table 3.2) and may be of use in the future modelling of photoreceptor sensitivities (see Section 5.3.5). The analysis of the mix_1 and mix_2 averaged data are presented (Tables 3.3 and 3.4) including the λ_{max} of the data (i.e. the running average λ_{max}), the λ_{max} of the best-fit template, the maximum corrected absorbance loss for the photobleach and the FWHM bandwidths of the averaged absorbance spectra. Specific absorbances were calculated for *N. norvegicus* (Table 3.5) but not for *H. gammarus* due to the unknown widths of the rhabdoms scanned. The extinction ratios of the mix_2 to mix_1 averaged files were calculated using those mix_1 and mix_2 scans recorded in the same photoreceptor (Table 3.5) and hence are not equal to the ratio of the mix_1 and mix_2 averaged files maximum corrected absorbances (i.e. the mix_1 and mix_2 average files include data where only one of

Table 3.1 Species measured in preliminary study.

Species	No. of specimens sampled	No. of sections accepted
Superorder Eucarida		
Order Decapoda		
Suborder Pleocyemata		
Infraorder Astacidea		
Homarus gammarus	2	8
Nephrops norvegicus	3	8

Table 3.2 Preliminary study: scan information.

Species	Average red light exposure (s) (± s.d., n)		Average final bleach exposure (mins.) (± s.d., n)	
Superorder Eucarida				
Order Decapoda				
Suborder Pleocyemata				
Infraorder Astacidea				
Homarus gammarus	20	(± 8.86, 8)	3.8	(± 1.82, 8)
Nephrops norvegicus	32.5	(± 14.14, 8)	2.38	(± 0.96, 8)

Table 3.3 Preliminary study: analysis results for the mix_1 averaged data.

Species	Running average λ_{max} (nm)	Best-fit template λ_{max} (nm) (± s.d., n)	Maximum corrected absorbance (± s.d., n)	FWHM bandwidth (nm)
Superorder Eucarida Order Decapoda Suborder Pleocyemata Infraorder Astacidea				
Homarus gammarus	529	522.4 (± 2.5, 37)	0.0624 (± 0.0030, 23)	92
Nephrops norvegicus	498	497.6 (± 0.9, 40)	0.0593 (± 0.0016, 17)	97

Table 3.4 Preliminary study: analysis results for the mix_2 averaged data.

Species	Running average λ_{max} (nm)	Best-fit template λ_{max} (nm) (± s.d., n)	Maximum corrected absorbance (± s.d., n)	FWHM bandwidth (nm)
Superorder Eucarida Order Decapoda Suborder Pleocyemata Infraorder Astacidea				
Homarus gammarus	485	481.8 (± 0.9, 38)	0.0538 (± 0.0012, 17)	100
Nephrops norvegicus	478	478.9 (± 0.8, 39)	0.0603 (± 0.0013, 17)	94

Table 3.5 Preliminary study: specific absorbances and the extinction coefficient ratios of the averaged data.

Species	Section thickness (μm)	Mix_1 specific absorbance (μm^{-1})	Mix_2 specific absorbance (μm^{-1})	Extinction ratio: $\varepsilon_{max\ mix_2} / \varepsilon_{max\ mix_1}$ (± s.d., n)
Superorder Eucarida Order Decapoda Suborder Pleocyemata Infraorder Astacidea				
Homarus gammarus	-	-	-	1.017 (± 0.081, 4)
Nephrops norvegicus	18.5	0.0033	0.0031	1.062 (± 0.332, 7)

Table 3.6 Preliminary study: deviation and signal to noise ratios of the mix_1 and mix_2 averaged data and the number of points used in the running averages.

Species	Mix_1 mean template deviation	Mix_1 S/N ratio	Mix_1 no. pts. in run. av.	Mix_2 mean template deviation	Mix_2 S/N ratio	Mix_2 no. pts. in run. av.	PC spectrum no. pts. in run. av.
Superorder Eucarida Order Decapoda Suborder Pleocyemata Infraorder Astacidea							
Homarus gammarus	0.0011	24.3 [a]	23	0.0016	53.9	17	17
Nephrops norvegicus	0.0033	61.4	17	0.0046	58.9	17	17

[a] The noise of the data was normally estimated between 80% shortwave normalised absorbance and the longwave offset (0.5% longwave normalised absorbance). However, where the data significantly deviated from the template the range was restricted to between 80% and 20% longwave normalised absorbance.

Table 3.7 Preliminary study: calculation of the metarhodopsin estimate.

Species	Mix_1 λ_{max} ($\equiv R$) (nm)	F_R in mix_2	Est. M λ_{max} (nm)	Extinction ratio: $\varepsilon_{max} M / \varepsilon_{max} mix_1$
Superorder Eucarida Order Decapoda Suborder Pleocyemata Infraorder Astacidea				
Homarus gammarus	522.4	0.011	481.5	1.020
Nephrops norvegicus	497.6	0.073	477.8	1.074

Table 3.8 Preliminary study: calculation of the rhodopsin estimate.

Species	F_R in mix_1	Est. R λ_{max} (nm)	Est. M λ_{max} (nm)	Extinction ratio: $\varepsilon_{max} M / \varepsilon_{max} R$
Superorder Eucarida Order Decapoda Suborder Pleocyemata Infraorder Astacidea				
Homarus gammarus	1.00	522.3	481.5	1.020
Nephrops norvegicus	0.95	498.7	477.8	1.070

Table 3.9 Preliminary study: summary of averaged data and the rhodopsin and metarhodopsin estimates.

Species	Mix_1 λ_{max} (nm)	Mix_2 λ_{max} (nm)	Extinction ratio: ε_{max} mix_2 / ε_{max} mix_1	Est. *R* λ_{max} (nm)	Est. *M* λ_{max} (nm)	Extinction ratio: ε_{max} *M* / ε_{max} *R*
Superorder Eucarida						
Order Decapoda						
Suborder Pleocyemata						
Infraorder Astacidea						
Homarus gammarus	522.4	481.8	1.017	522.3	481.5	1.020
Nephrops norvegicus	497.6	478.9	1.062	498.7	477.8	1.070

the visual pigment mixtures was selected for inclusion in an average). The signal to noise (S/N) ratios of the averaged files and the number of points used in the running averages used to smooth them are also given (Table 3.6).

The data concerning the estimation of the rhodopsin (*R*) and metarhodopsin (*M*) spectra are presented in Tables 3.7 and 3.8. The λ_{max} of the metarhodopsin estimate and its extinction ratio to mix_1 (assumed to be 100% rhodopsin in this analysis) are given, together with the rhodopsin λ_{max} value used and the calculated fraction of this pigment which would have been present in mix_2 (i.e. F_R in mix_2; Table 3.7). This metarhodopsin estimate was then used to estimate the rhodopsin pigment and the λ_{max} of the latter is given, together with the new metarhodopsin to rhodopsin extinction ratio and the estimated proportion of rhodopsin originally present in the mix_1 averaged file (i.e. F_R in mix_1; Table 3.8). Finally these data are summarised in Table 3.9 where the λ_{max} values of mix_1 and mix_2, and of the rhodopsin and metarhodopsin estimates are given, together with their respective extinction ratios.

The absorption spectra recorded from the main rhabdoms (retinular cells 1–7) of *H. gammarus* and *N. norvegicus* are presented in Figures 3.1 and 3.2 and displayed using the following charts: (A) Average absorbance spectra as measured by the microspectrophotometer; trace 1 (bold) showing the absorbance of the retina in its initial state, trace 2 (light) the absorbance following saturating red light irradiation, and trace 3 (dotted) the absorbance following photobleaching with bright white light. (B) Photoconversion difference spectrum derived from trace 2 minus trace 1 above (jagged trace), showing the change in absorbance induced by red light treatment of the photoreceptors in their initial state. The smooth trace is the photoconversion difference spectrum produced from the estimated rhodopsin and metarhodopsin templates. (C) Average difference spectra for the initial photoreceptor photobleaching derived from trace 1 minus trace 3 (i.e. mix_1; bold jagged trace), and following saturating red light irradiation derived from trace 2 minus trace 3 (i.e. mix_2; light jagged trace). Smooth solid traces are the best-fit template spectra to the data, the smooth dashed trace is the estimated metarhodopsin template, and the smooth dotted trace is the estimated rhodopsin template

(if different from mix_1). All spectra are normalised to the average absorbance loss for the initial state photobleach (mix_1).

Histograms are also presented to show the distribution of the average λ_{max} values of the templates which; (D) best-fit the mix_1 difference spectra calculated per section scanned, and (E) best-fit the mix_2 difference spectra per section scanned. For each species, the legend indicates the species name, the number of sections scanned from which data were subsequently selected for analysis, the total number of scans that constitute the difference spectra of mix_1 and mix_2, the λ_{max} values of the best-fit templates for mix_1 and mix_2, the λ_{max} values of the rhodopsin and metarhodopsin estimates, the estimated metarhodopsin to rhodopsin extinction ratio, and the average maximum corrected absorbance loss for the mix_1 photobleach. All template visual pigment absorbance spectra were generated using the equation given by Stavenga *et al.* (1993) for rhodopsin pigments, modified to incorporate a shifting β-band (after Palacios *et al.*, 1996).

[Note that all of the absorption spectra originally measured within this study represent data obtained at 1 nm intervals. Hence all spectra, both as measured and those calculated from these, should be presented as distinct data points. However, to improve the display data points have been joined with straight lines.]

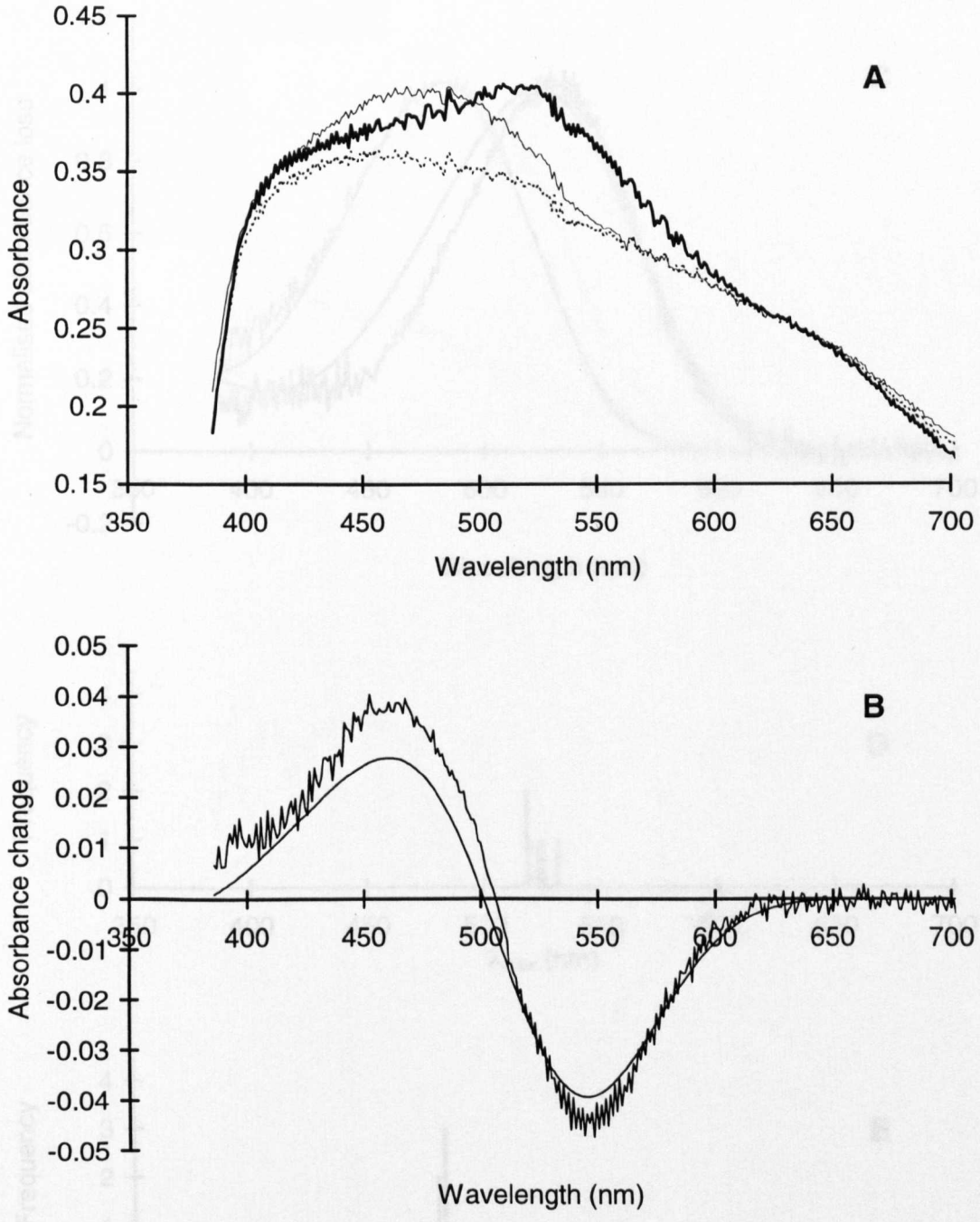

Figure 3.1 A–E. Results from the main rhabdoms (retinular cells 1–7) of *Homarus gammarus*. The absorbance spectra from eight sections were selected, with just one pair of mix_1 and mix_2 difference spectra calculated per section for inclusion in the file averages. The λ_{max} values of the best-fit templates for mix_1 and mix_2 are 522.4 and 481.8 nm, and the λ_{max} values of the *R* and *M* estimates are 522.3 and 481.5 nm with an estimated *M* to *R* extinction ratio of 1.020. The average maximum corrected absorbance loss for the mix_1 photobleach is 0.0624.

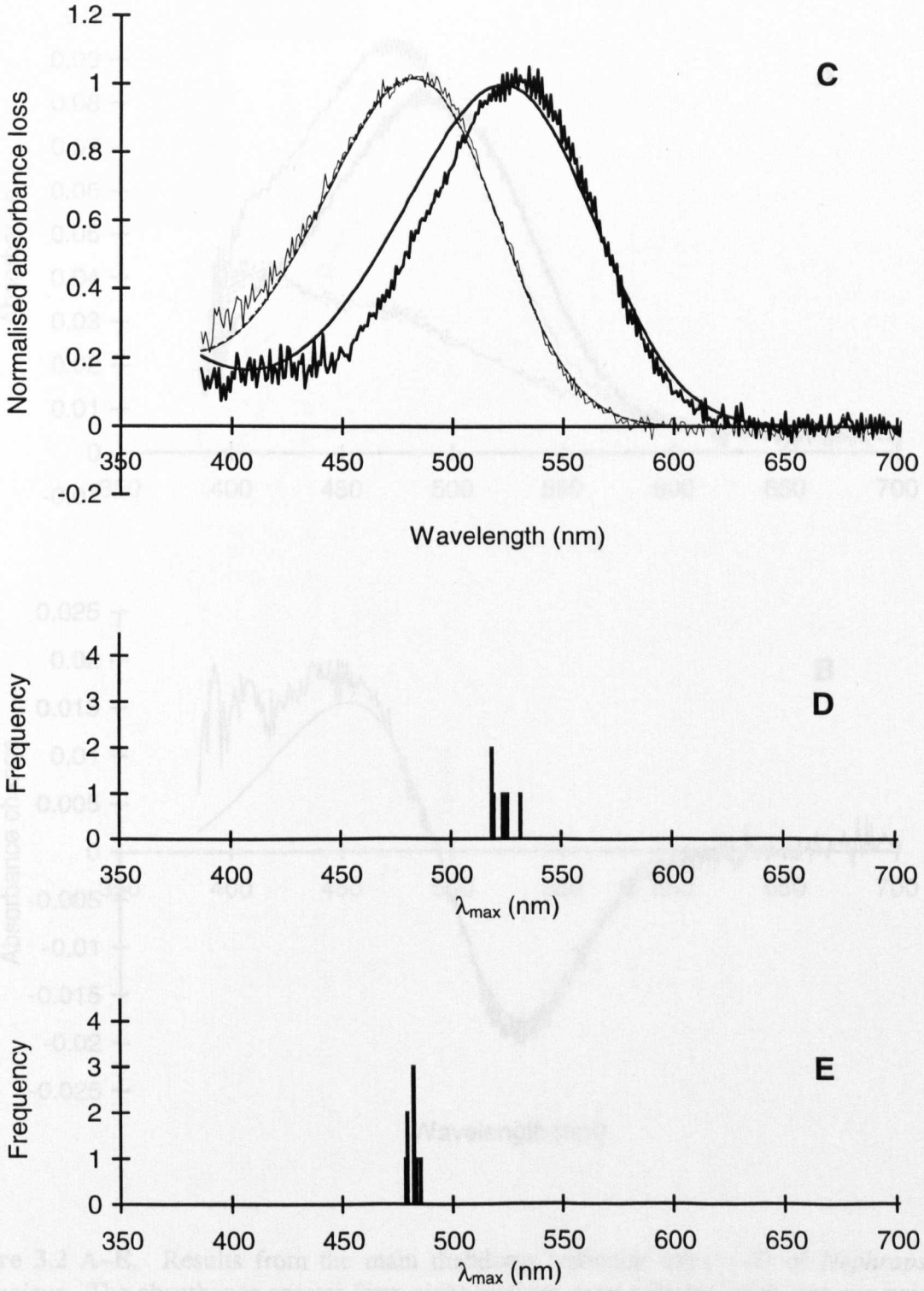

Figure 3.1 A–E. (Continued).

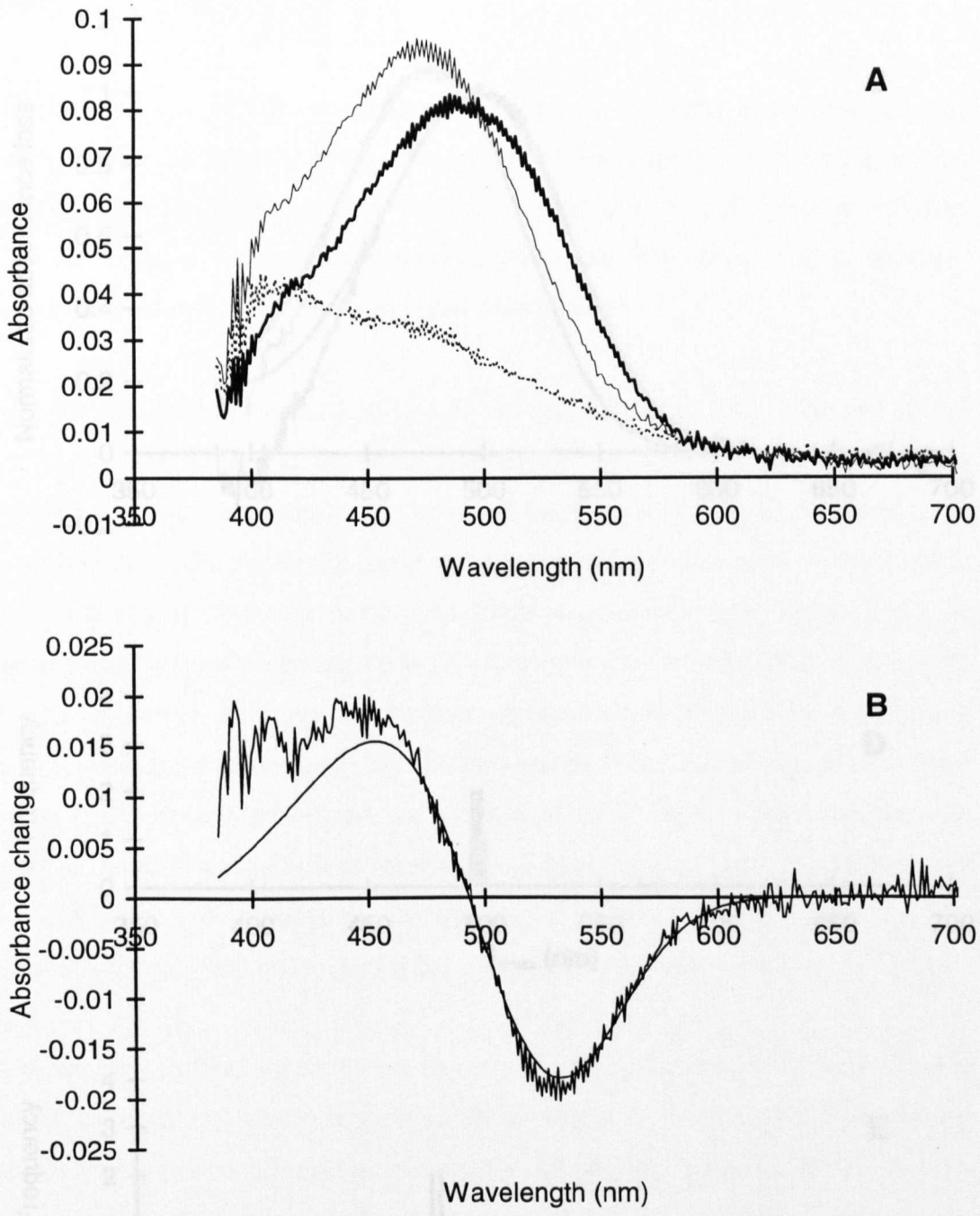

Figure 3.2 A–E. Results from the main rhabdoms (retinular cells 1–7) of *Nephrops norvegicus*. The absorbance spectra from eight sections were selected, with just one pair of mix_1 and mix_2 difference spectra calculated per section for inclusion in the file averages. The λ_{max} values of the best-fit templates for mix_1 and mix_2 are 497.6 and 478.9 nm, and the λ_{max} values of the *R* and *M* estimates are 498.7 and 477.8 nm with an estimated *M* to *R* extinction ratio of 1.070. The average maximum corrected absorbance loss for the mix_1 photobleach is 0.0593.

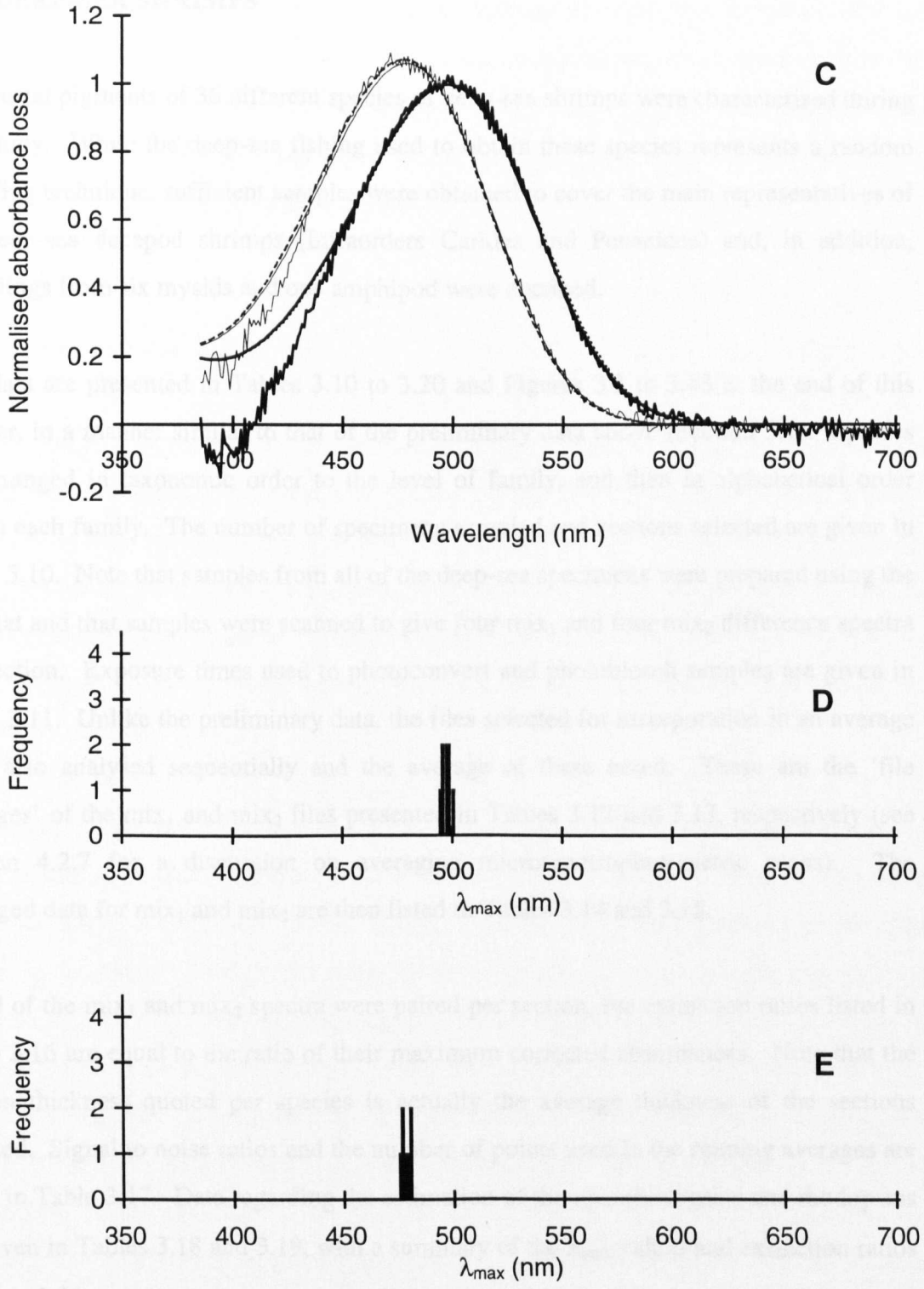

Figure 3.2 A–E. (Continued).

3.2 DEEP-SEA SHRIMPS

The visual pigments of 36 different species of deep-sea shrimps were characterised during this study. While the deep-sea fishing used to obtain these species represents a random sampling technique, sufficient samples were obtained to cover the main representatives of the deep-sea decapod shrimps (Infraorders Caridea and Penaeidea) and, in addition, recordings from six mysids and one amphipod were obtained.

The data are presented in Tables 3.10 to 3.20 and Figures 3.3 to 3.43 at the end of this chapter, in a manner similar to that of the preliminary data above (Section 3.1). Species are arranged in taxonomic order to the level of family, and then in alphabetical order within each family. The number of specimens sampled and sections selected are given in Table 3.10. Note that samples from all of the deep-sea specimens were prepared using the cryostat and that samples were scanned to give four mix_1 and four mix_2 difference spectra per section. Exposure times used to photoconvert and photobleach samples are given in Table 3.11. Unlike the preliminary data, the files selected for incorporation in an average were also analysed sequentially and the average of these noted. These are the 'file averages' of the mix_1 and mix_2 files presented in Tables 3.12 and 3.13, respectively (see Section 4.2.7 for a discussion on averaging microspectrophotometric scans). The averaged data for mix_1 and mix_2 are then listed in Tables 3.14 and 3.15.

As all of the mix_1 and mix_2 spectra were paired per section, the extinction ratios listed in Table 3.16 are equal to the ratio of their maximum corrected absorbances. Note that the section thickness quoted per species is actually the average thickness of the sections selected. Signal to noise ratios and the number of points used in the running averages are listed in Table 3.17. Data regarding the estimation of the metarhodopsins and rhodopsins are given in Tables 3.18 and 3.19, with a summary of the λ_{max} values and extinction ratios in Table 3.20.

The absorption spectra recorded from both the main rhabdoms (retinular cells 1–7) and from the eighth rhabdomeres (R8) of the deep-sea species are presented in Figures 3.3 to 3.43. For the R1–7 cells the charts used to display this data are identical to those in

the preliminary study and the key repeated on the page preceding these figures. For the R8 cells, mix_2 was not itself analysed and hence no histogram is presented to show the distribution of mix_2 λ_{max} values (see Section 4.3.3.2). The methods used to analyse the absorption spectra measured and estimate the rhodopsin and metarhodopsin present are detailed and discussed in Sections 4.2 and 4.3.

3.2.1 General observations

Every attempt was made to ensure that different photoreceptor classes were not missed during the investigation of a particular species. When found, the R8 cells were situated distal to the main rhabdoms (i.e. closer to the crystalline cones) and were noted to have a less granular appearance on the video monitor. Further, though the greatest absorptions were often measured towards the base of the main rhabdoms, scans were frequently initially taken from the distal end of the rhabdom to check for the presence of an unidentified R8 cell.

Depending on the depth and plane of the ocular sections, rhabdoms were often presented as longitudinal sections and the eye as a whole presented as bands of tissues radiating from the centre. In this way, dorsal, ventral, anterior and posterior regions of the eyes could be scanned. Though this was not investigated for every species, no regional differences were ever found. Using such longitudinal sections, care had to be taken not to section below the level of the basal membrane as the centre of compound eyes often contains substantial amounts of non-visual pigments. If this region was included in the section these non-visual pigments were often mobilised and slowly leached into the rest of the section. This then altered the absorbance of the section during its measurement, affecting the post-bleach scan and thus all of the difference spectra. Further these pigments may also bleach to an unknown extent during the white light exposures contributing to the apparent photobleach of the visual pigment present. All such 'contaminated' scans were rejected and not included in the average files. Consequently all sections, from all species, were initially checked on the video monitor for their structural integrity and scanning proceeded as quickly as possible.

Apparent differences between the eyes of these deep-sea species were often more the consequence of the initial state of the eye post-capture. This was reflected in the frequently marked difference between the quality of the results obtained from different specimens of the same species. Unfortunately, because all initial sorting and examination was done under dim red illumination with minimum exposure, it was not always possible to assess possible damage to the specimens' eyes at this time. It was possible to assess the eyes on initial sectioning and many were rejected before scanning was even attempted because of internal structural damage. However, investigation during this study has estimated that the intensity and spectrum of the red light used is such that it would take many hours to photoconvert a significant fraction of the rhodopsin initially present in the specimens (Section 2.2.2). Thus in future studies more time could be taken to assess the specimens selected, particularly using the eyeshine of superposition eyes as an indication of possible internal damage to the eye. No quantitative differences were found between specimens of the same species indicating the absence of visual pigment polymorphism within species.

Though morphological differences between the eyes of the species studied were not investigated they were often marked and affected the 'ease' of obtaining absorbance spectra. For example, *Plesiopenaeus armatus* possesses large reflecting superposition eyes (*ca.* 5 mm in diameter) which contained very little accessory screening pigment. Indeed, on the video monitor of the microspectrophotometer the rhabdom tissue was not distinguishable from the clear zone above it, and the measuring beam was simply located near to the basal membrane. Difference spectra for both mix_1 and mix_2 were undistorted and the averaged files have approximately average signal to noise ratios compared to the others obtained in this study (see Figure 3.8 and Table 3.17).

In contrast the eyes of *Hymenodora glacialis* are reduced with little, or no, optics. The rhabdoms are wider and shorter than those found in most deep-sea species (see Table 5.3) and appear to be optically separated with large deposits of screening pigment. All of the sections were disrupted and even if a rhabdom was found it was normally heavily covered with screening pigment. In the end only one photoreceptor was successfully scanned despite sectioning 4 eyes in total. With *P. armatus* the *best* 7 sections were selected for

averaging (i.e. those with the highest signal to noise ratios and the least deviations from the best-fit template). As a consequence the difference spectra presented for *H. glacialis* (Figure 3.20) have some of the lowest signal to noise ratios obtained in this study (Table 3.17). However, by averaging the four difference spectra obtained for each pigment mixture from that one section, the noise is still acceptable and the templates are clearly a good-fit, particularly about the peak and the longwave limb.

3.2.2 *Parapasiphaea sulcatifrons*

One species, *Parapasiphaea sulcatifrons*, was collected on both RRS Challenger Cruise 122 and RV New Horizon. Thus both Atlantic and Pacific specimens of the same species were sampled. Beyond specific identification no attempt was made to differentiate between members of the two populations and thus all recordings and analyses were separated. Intraspecific variation of visual pigments is known in the vertebrates (e.g. Archer, Endler, Lythgoe and Partridge, 1987; Archer, 1988), however, the tabulated data clearly indicates very similar λ_{max} values for both the mixtures scanned and the rhodopsin and metarhodopsin estimates (see Table 3.20). In contrast, slightly greater difference is seen in the extinction ratios but other, experimental factors may be responsible for this (see Section 5.2.9). No attempt was made to prove the similarity of these values statistically as the averaged data for each species population is effectively one independent data point (see Section 4.2.7.2). However, in the general discussion (Section 5.2) no distinction is made between the two populations.

Table 3.10 List of deep-sea species studied, presented in taxonomic order, with the number of specimens sampled and the number of eye sections successfully scanned.

Species	No. of specimens sampled	No. of sections accepted
Superorder Eucarida		
Order Decapoda		
Suborder Dendrobranchiata		
Family Penaeidae		
Bentheogennema intermedia	1	5
Bentheogennema pasithea	2	7
Gennadas sp.	1	3
Gennadas valens	3	7
Petalidium suspirosum	2	5
Plesiopenaeus armatus	2	7
Family Sergestidae		
Sergestes curvatus	2	8
Sergestes similis	1	5
Sergia maximus	1	5
Sergia phorcus	2	6
Sergia robustus	1	4
Sergia splendens	1	9
Suborder Pleocyemata		
Infraorder Caridea		
Family Oplophoridae		
Acanthephyra curtirostris	2	6
Acanthephyra microphthalma	1	4
Acanthephyra purpurea	2	6
Acanthephyra stylorostratis	1	4
Hymenodora frontalis	2	5
Hymenodora glacialis	1	1
Meningodora miccyla	1	6
Meningodora vesca	1	5
Oplophorus spinosus		
- R8	2	4
- Main rhabdom	1	6
Systellaspis braueri		
- R8	1	4
- Main rhabdom	2	4
Systellaspis cristata		
- R8	1	4
- Main rhabdom	2	5
Systellaspis debilis		
- R8	2	5
- Main rhabdom	3	6

Table 3.10 (Continued).

Species	No. of specimens sampled	No. of sections accepted
Family Pandalidae		
Stylopandalus richardii	1	5
Plesionika maritus	1	6
Family Pasiphaeidae		
Parapasiphaea sulcatifrons (Atl)	1	6
Parapasiphaea sulcatifrons (Pac)	2	3
Pasiphaea chacei	1	6
Pasiphaea emarginata	1	6
Superorder Percaridia Order Mysida		
Chalaraspidium alata	2	6
Eucopia australis	1	4
Eucopia sculpticauda	2	4
Gnathophausia gigas	1	5
Gnathophausia gracilis	2	6
Gnathophausia ingens	2	5
Order Amphipoda		
Cyphocaris richardi	2	3

Table 3.11 Deep-sea species: scan information.

Species	Average red light exposure (s) (± s.d., n)		Average final bleach exposure (mins.) (± s.d., n)	
Superorder Eucarida				
Order Decapoda				
Suborder Dendrobranchiata				
Family Penaeidae				
Bentheogennema intermedia	36	(± 13.42, 5)	26	(± 4.18, 5)
Bentheogennema pasithea	27.86	(± 10.35, 7)	35.71	(± 10.18, 7)
Gennadas sp.	15	-	28.33	(± 2.89, 3)
Gennadas valens	34.29	(± 16.69, 7)	17.86	(± 7.56, 7)
Petalidium suspirosum	18	(± 6.71, 5)	21	(± 2.24, 5)
Plesiopenaeus armatus	36.43	(± 8.02, 7)	27.86	(± 4.88, 7)
Family Sergestidae				
Sergestes curvatus	35.63	(± 7.76, 8)	28.13	(± 7.53, 8)
Sergestes similis	21	(± 8.22, 5)	29	(± 2.24, 5)
Sergia maximus	24	(± 13.42, 5)	27	(± 4.47, 5)
Sergia phorcus	20	(± 7.75, 6)	30	(± 5.48, 6)
Sergia robustus	37.5	(± 8.66, 4)	27.5	(± 2.89, 4)
Sergia splendens	30	(± 7.5, 9)	28.33	(± 6.61, 9)
Suborder Pleocyemata				
Infraorder Caridea				
Family Oplophoridae				
Acanthephyra curtirostris	32.5	(± 11.29, 6)	31.67	(± 5.16, 6)
Acanthephyra microphthalma	26.25	(± 22.5, 4)	20	(± 4.08, 4)
Acanthephyra purpurea	37.5	(± 8.22, 6)	22.5	(± 2.74, 6)
Acanthephyra stylorostratis	30	(± 12.25, 4)	38.75	(± 4.79, 4)
Hymenodora frontalis	27	(± 12.55, 5)	35	(± 11.18, 5)
Hymenodora glacialis	30	-	30	-
Meningodora miccyla	35	(± 7.75, 6)	25.83	(± 4.92, 6)
Meningodora vesca	45	(± 10.61, 5)	31	(± 8.22, 5)
Oplophorus spinosus				
- R8	10 [a]	(± 5.77, 4)	30	(± 4.08, 4)
- Main rhabdom	37.5	(± 8.22, 6)	25	(± 3.16, 6)
Systellaspis braueri				
- R8	15 [a]	-	50	(± 14.14, 4)
- Main rhabdom	30	(± 12.25, 4)	36.25	(± 4.79, 4)
Systellaspis cristata				
- R8	15 [a]	-	60	(± 7.07, 4)
- Main rhabdom	30	(± 10.61, 5)	25	(± 5, 5)
Systellaspis debilis				
- R8	6 [a]	(± 2.24, 5)	12.2	(± 6.46, 5)
- Main rhabdom	42.5	(± 11.29, 6)	25	(± 8.94, 6)

Table 3.11 (Continued).

Species	Average red light exposure (s) (± s.d., n)	Average final bleach exposure (mins.) (± s.d., n)
Family Pandalidae		
Stylopandalus richardii	35 (± 7.75, 5)	36.67 (± 6.06, 5)
Plesionika maritus	20 (± 7.75, 6)	40 (± 5.48, 6)
Family Pasiphaeidae		
Parapasiphaea sulcatifrons (Atl)	30 (± 9.49, 6)	24.17 (± 9.7, 6)
Parapasiphaea sulcatifrons (Pac)	20 (± 8.66, 3)	35 (± 13.23, 3)
Pasiphaea chacei	25 (± 12.25, 6)	33.33 (± 11.69, 6)
Pasiphaea emarginata	15 -	24.17 (± 3.76, 6)
Superorder Percaridia Order Mysida		
Chalaraspidium alata	25 (± 7.75, 6)	33.33 (± 4.08, 6)
Eucopia australis	15 -	23.75 (± 2.5, 4)
Eucopia sculpticauda	26.25 (± 7.5, 4)	75 (± 19.15, 4)
Gnathophausia gigas	21 (± 8.22, 5)	43 (± 8.37, 5)
Gnathophausia gracilis	22.5 (± 8.22, 6)	25.83 (± 6.65, 6)
Gnathophausia ingens	24 (± 13.42, 5)	33 (± 9.75, 5)
Order Amphipoda		
Cyphocaris richardi	35 (± 8.66, 3)	30 -

[a] Saturating blue light was used to create the R8 rhodopsin and metarhodopsin photosteady mixes (i.e. mix_2).

Table 3.12 Deep-sea species: results for the mix_1 difference spectra which were analysed and accepted for subsequent averaging.

Species	Number of individual spectra (n)	Mean running average λ_{max} (nm) (± s.d.)	Mean best-fit template λ_{max} (nm) (± s.d.)	Mean maximum corrected absorbance (± s.d.)
Superorder Eucarida				
Order Decapoda				
Suborder Dendrobranchiata				
Family Penaeidae				
Bentheogennema intermedia	18	488.1 (± 2.0)	492.3 (± 1.2)	0.0810 (± 0.0236)
Bentheogennema pasithea	28	498.3 (± 9.6)	500.2 (± 8.2)	0.0448 (± 0.0116)
Gennadas sp.	12	491.7 (± 7.8)	493.3 (± 3.9)	0.0632 (± 0.0120)
Gennadas valens	24	493.6 (± 4.5)	493.7 (± 2.4)	0.0744 (± 0.0250)
Petalidium suspirosum	20	498.6 (± 6.9)	500.3 (± 6.4)	0.0593 (± 0.0101)
Plesiopenaeus armatus	22	489.9 (± 3.9)	492.1 (± 3.1)	0.0570 (± 0.0161)
Family Sergestidae				
Sergestes curvatus	26	489.8 (± 2.7)	492.0 (± 2.0)	0.1177 (± 0.0272)
Sergestes similis	20	491.1 (± 3.5)	492.3 (± 1.5)	0.1032 (± 0.0315)
Sergia maximus	20	492.3 (± 2.8)	492.8 (± 1.9)	0.1024 (± 0.0110)
Sergia phorcus	24	494.7 (± 5.1)	494.8 (± 5.2)	0.0944 (± 0.0327)
Sergia robustus	16	493.6 (± 1.5)	493.8 (± 1.2)	0.1078 (± 0.0230)
Sergia splendens	36	492.6 (± 2.2)	493.8 (± 2.5)	0.1635 (± 0.0569)
Suborder Pleocyemata				
Infraorder Caridea				
Family Oplophoridae				
Acanthephyra curtirostris	24	482.9 (± 4.2)	484.2 (± 3.4)	0.1069 (± 0.0327)
Acanthephyra microphthalma	9	482.1 (± 2.3)	481.7 (± 1.6)	0.0572 (± 0.0102)
Acanthephyra purpurea	24	487.5 (± 2.5)	490.4 (± 1.1)	0.0749 (± 0.0177)
Acanthephyra stylorostratis	16	488.0 (± 2.8)	488.4 (± 3.0)	0.0879 (± 0.0133)
Hymenodora frontalis	20	491.4 (± 5.6)	494.3 (± 5.3)	0.0628 (± 0.0240)
Hymenodora glacialis	4	501.0 (± 4.7)	497.8 (± 1.2)	0.0323 (± 0.0040)
Meningodora miccyla	24	483.0 (± 4.1)	485.5 (± 1.3)	0.0737 (± 0.0200)
Meningodora vesca	18	486.8 (± 2.3)	486.8 (± 1.4)	0.1243 (± 0.0475)
Oplophorus spinosus				
- R8	16	411.9 (± 4.1)	- -	0.0270 (± 0.0235)
- Main rhabdom	24	492.0 (± 1.7)	492.1 (± 1.1)	0.1041 (± 0.0206)
Systellaspis braueri				
- R8	16	408.6 (± 5.4)	- -	0.0726 (± 0.0232)
- Main rhabdom	16	500.5 (± 6.5)	499.0 (± 3.1)	0.0661 (± 0.0246)
Systellaspis cristata				
- R8	16	413.4 (± 2.8)	- -	0.0996 (± 0.0353)
- Main rhabdom	20	496.9 (± 4.1)	496.1 (± 1.3)	0.0736 (± 0.0223)
Systellaspis debilis				
- R8	10	418.5 (± 1)	- -	0.0688 (± 0.0170)
- Main rhabdom	21	494.3 (± 3.6)	495.3 (± 1.3)	0.1286 (± 0.0504)

Table 3.12 (Continued).

Species	Number of individual spectra (n)	Mean running average λ_{max} (nm) (± s.d.)	Mean best-fit template λ_{max} (nm) (± s.d.)	Mean maximum corrected absorbance (± s.d.)
Family Pandalidae				
Stylopandalus richardii	20	490.2 (± 1.1)	491.3 (± 0.8)	0.1488 (± 0.0282)
Plesionika maritus	24	499.8 (± 4.5)	497.3 (± 3.2)	0.0425 (± 0.0141)
Family Pasiphaeidae				
Parapasiphaea sulcatifrons (Atl)	20	500.0 (± 5.8)	499.2 (± 3.4)	0.0676 (± 0.0360)
Parapasiphaea sulcatifrons (Pac)	12	500.4 (± 7.4)	502.2 (± 6.4)	0.0505 (± 0.0288)
Pasiphaea chacei	24	506.6 (± 10.4)	507.1 (± 6.6)	0.0331 (± 0.0224)
Pasiphaea emarginata	24	495.4 (± 3.9)	496.5 (± 3.4)	0.0589 (± 0.0049)
Superorder Percaridia Order Mysida				
Chalaraspidium alata	24	489.6 (± 2.8)	493.4 (± 2.4)	0.0776 (± 0.0227)
Eucopia australis	16	504.9 (± 3.9)	513.1 (± 3.4)	0.0951 (± 0.0069)
Eucopia sculpticauda	16	489.1 (± 3.2)	493.1 (± 0.7)	0.0859 (± 0.0323)
Gnathophausia gigas	20	489.5 (± 4.8)	491.5 (± 1.7)	0.0702 (± 0.0197)
Gnathophausia gracilis	24	489.9 (± 4.3)	494.1 (± 2.2)	0.0697 (± 0.0250)
Gnathophausia ingens	20	489.6 (± 3.9)	491.9 (± 3.2)	0.0811 (± 0.0072)
Order Amphipoda				
Cyphocaris richardi	12	485.8 (± 3.4)	481.9 (± 0.9)	0.1178 (± 0.0130)

Table 3.13 Deep-sea species: results for the mix_2 difference spectra which were analysed and accepted for subsequent averaging.

Species	Number of individual spectra (n)	Mean running average λ_{max} (nm) (± s.d.)	Mean best-fit template λ_{max} (nm) (± s.d.)	Mean maximum corrected absorbance (± s.d.)
Superorder Eucarida				
Order Decapoda				
Suborder Dendrobranchiata				
Family Penaeidae				
Bentheogennema intermedia	18	476.9 (± 2.0)	482.0 (± 1.6)	0.0996 (± 0.0375)
Bentheogennema pasithea	28	486.3 (± 6.2)	488.5 (± 7.1)	0.0610 (± 0.0130)
Gennadas sp.	12	475.4 (± 3.9)	479.7 (± 1.6)	0.0758 (± 0.0133)
Gennadas valens	24	476.8 (± 3.8)	478.9 (± 2.5)	0.0902 (± 0.0290)
Petalidium suspirosum	20	492.6 (± 3.1)	492.0 (± 2.8)	0.0779 (± 0.0155)
Plesiopenaeus armatus	22	483.0 (± 2.1)	482.4 (± 1.9)	0.0687 (± 0.0181)
Family Sergestidae				
Sergestes curvatus	26	485.9 (± 1.9)	485.5 (± 0.9)	0.1429 (± 0.0362)
Sergestes similis	20	486.7 (± 2.0)	485.8 (± 2.3)	0.1296 (± 0.0218)
Sergia maximus	20	484.6 (± 2.0)	484.1 (± 1.3)	0.1315 (± 0.0167)
Sergia phorcus	24	486.4 (± 3.7)	484.9 (± 4.6)	0.1083 (± 0.0405)
Sergia robustus	16	486.0 (± 1.5)	485.4 (± 0.6)	0.1368 (± 0.0401)
Sergia splendens	36	486.6 (± 1.5)	486.3 (± 2.1)	0.2046 (± 0.0608)
Suborder Pleocyemata				
Infraorder Caridea				
Family Oplophoridae				
Acanthephyra curtirostris	24	481.7 (± 3.1)	482.3 (± 2.8)	0.1350 (± 0.0361)
Acanthephyra microphthalma	9	479.9 (± 3.0)	481.1 (± 1.0)	0.0654 (± 0.0139)
Acanthephyra purpurea	24	482.3 (± 2.0)	482.9 (± 1.3)	0.1012 (± 0.0267)
Acanthephyra stylorostratis	16	485.3 (± 2.0)	485.9 (± 2.6)	0.1064 (± 0.0158)
Hymenodora frontalis	20	484.2 (± 2.6)	485.0 (± 1.3)	0.0775 (± 0.0273)
Hymenodora glacialis	4	484.0 (± 1.2)	484.0 (± 0.8)	0.0496 (± 0.0018)
Meningodora miccyla	24	482.3 (± 2.5)	482.5 (± 1.1)	0.0753 (± 0.0175)
Meningodora vesca	18	480.7 (± 2.5)	482.1 (± 0.8)	0.1576 (± 0.0554)
Oplophorus spinosus				
- R8	16	- -	- -	- -
- Main rhabdom	24	484.8 (± 1.2)	482.9 (± 0.7)	0.1333 (± 0.0283)
Systellaspis braueri				
- R8	16	- -	- -	- -
- Main rhabdom	16	488.3 (± 1.7)	487.6 (± 0.8)	0.0804 (± 0.0255)
Systellaspis cristata				
- R8	16	- -	- -	- -
- Main rhabdom	20	470.0 (± 3.0)	477.8 (± 2.9)	0.0858 (± 0.0298)
Systellaspis debilis				
- R8	10	- -	- -	- -
- Main rhabdom	21	483.6 (± 1.4)	484.0 (± 1.5)	0.1853 (± 0.0717)

Table 3.13 (Continued).

Species	Number of individual spectra (n)	Mean running average λ_{max} (nm) (± s.d.)	Mean best-fit template λ_{max} (nm) (± s.d.)	Mean maximum corrected absorbance (± s.d.)
Family Pandalidae				
Stylopandalus richardii	20	488.3 (± 1.1)	488.3 (± 0.4)	0.1787 (± 0.0232)
Plesionika maritus	24	491.3 (± 3.5)	490.4 (± 3.4)	0.0680 (± 0.0186)
Family Pasiphaeidae				
Parapasiphaea sulcatifrons (Atl)	20	483.8 (± 1.7)	483.7 (± 1.6)	0.0906 (± 0.0241)
Parapasiphaea sulcatifrons (Pac)	12	484.9 (± 2.8)	483.7 (± 4.0)	0.0676 (± 0.0332)
Pasiphaea chacei	24	486.8 (± 4.3)	487.6 (± 4.7)	0.0483 (± 0.0247)
Pasiphaea emarginata	24	484.9 (± 4.3)	486.0 (± 3.4)	0.0609 (± 0.0138)
Superorder Percaridia Order Mysida				
Chalaraspidium alata	24	490.0 (± 1.8)	489.8 (± 1.8)	0.1021 (± 0.0282)
Eucopia australis	16	490.7 (± 1.8)	494.3 (± 1.7)	0.1101 (± 0.0067)
Eucopia sculpticauda	16	487.4 (± 2.0)	490.2 (± 1.2)	0.1068 (± 0.0360)
Gnathophausia gigas	20	488.7 (± 3.9)	489.7 (± 1.8)	0.0831 (± 0.0207)
Gnathophausia gracilis	24	484.4 (± 2.4)	486.2 (± 2.6)	0.0828 (± 0.0284)
Gnathophausia ingens	20	489.2 (± 3.0)	490.0 (± 2.3)	0.0982 (± 0.0081)
Order Amphipoda				
Cyphocaris richardi	12	482.7 (± 1.8)	479.6 (± 0.6)	0.1328 (± 0.0133)

Table 3.14 Deep-sea species: analysis results for the mix_1 averaged data.

Species	Running average λ_{max} (nm)	Best-fit template λ_{max} (nm) (± s.d., n)	Maximum corrected absorbance (± s.d., n)	FWHM bandwidth (nm)
Superorder Eucarida				
Order Decapoda				
Suborder Dendrobranchiata				
Family Penaeidae				
Bentheogennema intermedia	487	492.2 (± 0.3, 38)	0.0806 (± 0.0009, 13)	104
Bentheogennema pasithea	494	499.2 (± 1.2, 43)	0.0437 (± 0.0009, 17)	101
Gennadas sp.	490	493.0 (± 0.9, 38)	0.0624 (± 0.0012, 17)	96
Gennadas valens	494	493.8 (± 0.7, 38)	0.0717 (± 0.0009, 15)	98
Petalidium suspirosum	499	498.6 (± 1.1, 44)	0.0579 (± 0.0009, 17)	96
Plesiopenaeus armatus	490	491.5 (± 0.6, 38)	0.0570 (± 0.0006, 15)	102
Family Sergestidae				
Sergestes curvatus	490	492.1 (± 0.3, 39)	0.1173 (± 0.0009, 15)	98
Sergestes similis	490	492.3 (± 0.5, 40)	0.1034 (± 0.0014, 15)	103
Sergia maximus	492	492.8 (± 0.5, 39)	0.1025 (± 0.0010, 15)	94
Sergia phorcus	494	493.6 (± 0.8, 38)	0.0939 (± 0.0010, 17)	94
Sergia robustus	494	493.9 (± 0.5, 38)	0.1083 (± 0.0008, 15)	98
Sergia splendens	492	494.2 (± 0.6, 38)	0.1587 (± 0.0010, 15)	99
Suborder Pleocyemata				
Infraorder Caridea				
Family Oplophoridae				
Acanthephyra curtirostris	484	484.8 (± 0.5, 39)	0.1067 (± 0.0010, 15)	100
Acanthephyra microphthalma	482	481.6 (± 0.5, 38)	0.0573 (± 0.0011, 17)	86
Acanthephyra purpurea	488	490.5 (± 0.5, 42)	0.0744 (± 0.0012, 15)	98
Acanthephyra stylorostratis	486	488.3 (± 0.8, 40)	0.0875 (± 0.0011, 15)	93
Hymenodora frontalis	491	493.1 (± 1.0, 43)	0.0622 (± 0.0011, 17)	101
Hymenodora glacialis	501	498.4 (± 1.6, 41)	0.0323 (± 0.0012, 23)	94
Meningodora miccyla	483	485.9 (± 0.5, 41)	0.0730 (± 0.0007, 15)	98
Meningodora vesca	487	487.2 (± 0.2, 40)	0.1237 (± 0.0009, 13)	99
Oplophorus spinosus				
- R8	413	413 -	0.0265 (± 0.0014, 21)	-
- Main rhabdom	491	492.0 (± 0.3, 39)	0.1043 (± 0.0007, 13)	97
Systellaspis braueri				
- R8	413	411 -	0.0720 (± 0.0022, 15)	-
- Main rhabdom	500	498.1 (± 1.1, 37)	0.0658 (± 0.0010, 17)	100
Systellaspis cristata				
- R8	414	414 -	0.1000 (± 0.0020, 13)	-
- Main rhabdom	496	496.4 (± 1.1, 38)	0.0737 (± 0.0009, 17)	97
Systellaspis debilis				
- R8	417	417 -	0.0694 (± 0.0013, 13)	-
- Main rhabdom	494	495.6 (± 0.5, 40)	0.1264 (± 0.0009, 15)	98

Table 3.14 (Continued).

Species	Running average λ_{max} (nm)	Best-fit template λ_{max} (nm) (± s.d., n)	Maximum corrected absorbance (± s.d., n)	FWHM bandwidth (nm)
Family Pandalidae				
Stylopandalus richardii	491	491.2 (± 0.5, 38)	0.1482 (± 0.0009, 13)	96
Plesionika maritus	498	497.1 (± 2.4, 37)	0.0417 (± 0.0012, 23)	94
Family Pasiphaeidae				
Parapasiphaea sulcatifrons (Atl)	498	499.6 (± 0.3, 41)	0.0660 (± 0.0005, 15)	100
Parapasiphaea sulcatifrons (Pac)	499	499.8 (± 0.8, 39)	0.0498 (± 0.0012, 17)	102
Pasiphaea chacei	505	507.5 (± 1.0, 43)	0.0325 (± 0.0010, 17)	109
Pasiphaea emarginata	494	495.8 (± 0.6, 41)	0.0583 (± 0.0008, 15)	99
Superorder Percaridia Order Mysida				
Chalaraspidium alata	489	493.4 (± 1.2, 41)	0.0774 (± 0.0013, 17)	101
Eucopia australis	506	513.0 (± 1.6, 47)	0.0950 (± 0.0009, 15)	116
Eucopia sculpticauda	491	493.0 (± 1.5, 42)	0.0858 (± 0.0015, 17)	105
Gnathophausia gigas	489	491.4 (± 1.0, 40)	0.0699 (± 0.0011, 17)	101
Gnathophausia gracilis	490	494.5 (± 0.8, 42)	0.0694 (± 0.0008, 15)	102
Gnathophausia ingens	491	491.7 (± 1.1, 39)	0.0810 (± 0.0010, 17)	101
Order Amphipoda				
Cyphocaris richardi	485	481.8 (± 1.2, 37)	0.1181 (± 0.0018, 17)	85

Table 3.15 Deep-sea species: analysis results for the mix_2 averaged data.

Species	Number of individual scans (n)	Mean running average λ_{max} (nm) (± s.d.)	Mean best-fit template λ_{max} (nm) (± s.d.)	Mean maximum corrected absorbance (± s.d.)
Superorder Eucarida				
Order Decapoda				
Suborder Dendrobranchiata				
Family Penaeidae				
Bentheogennema intermedia	18	476.9 (± 2.0)	482.0 (± 1.6)	0.0996 (± 0.0375)
Bentheogennema pasithea	28	486.3 (± 6.2)	488.5 (± 7.1)	0.0610 (± 0.0130)
Gennadas sp.	12	475.4 (± 3.9)	479.7 (± 1.6)	0.0758 (± 0.0133)
Gennadas valens	24	476.8 (± 3.8)	478.9 (± 2.5)	0.0902 (± 0.0290)
Petalidium suspirosum	20	492.6 (± 3.1)	492.0 (± 2.8)	0.0779 (± 0.0155)
Plesiopenaeus armatus	22	483.0 (± 2.1)	482.4 (± 1.9)	0.0687 (± 0.0181)
Family Sergestidae				
Sergestes curvatus	26	485.9 (± 1.9)	485.5 (± 0.9)	0.1429 (± 0.0362)
Sergestes similis	20	486.7 (± 2.0)	485.8 (± 2.3)	0.1296 (± 0.0218)
Sergia maximus	20	484.6 (± 2.0)	484.1 (± 1.3)	0.1315 (± 0.0167)
Sergia phorcus	24	486.4 (± 3.7)	484.9 (± 4.6)	0.1083 (± 0.0405)
Sergia robustus	16	486.0 (± 1.5)	485.4 (± 0.6)	0.1368 (± 0.0401)
Sergia splendens	36	486.6 (± 1.5)	486.3 (± 2.1)	0.2046 (± 0.0608)
Suborder Pleocyemata				
Infraorder Caridea				
Family Oplophoridae				
Acanthephyra curtirostris	24	481.7 (± 3.1)	482.3 (± 2.8)	0.1350 (± 0.0361)
Acanthephyra microphthalma	9	479.9 (± 3.0)	481.1 (± 1.0)	0.0654 (± 0.0139)
Acanthephyra purpurea	24	482.3 (± 2.0)	482.9 (± 1.3)	0.1012 (± 0.0267)
Acanthephyra stylorostratis	16	485.3 (± 2.0)	485.9 (± 2.6)	0.1064 (± 0.0158)
Hymenodora frontalis	20	484.2 (± 2.6)	485.0 (± 1.3)	0.0775 (± 0.0273)
Hymenodora glacialis	4	484.0 (± 1.2)	484.0 (± 0.8)	0.0496 (± 0.0018)
Meningodora miccyla	24	482.3 (± 2.5)	482.5 (± 1.1)	0.0753 (± 0.0175)
Meningodora vesca	18	480.7 (± 2.5)	482.1 (± 0.8)	0.1576 (± 0.0554)
Oplophorus spinosus				
- R8	16	- -	- -	- -
- Main rhabdom	24	484.8 (± 1.2)	482.9 (± 0.7)	0.1333 (± 0.0283)
Systellaspis braueri				
- R8	16	- -	- -	- -
- Main rhabdom	16	488.3 (± 1.7)	487.6 (± 0.8)	0.0804 (± 0.0255)
Systellaspis cristata				
- R8	16	- -	- -	- -
- Main rhabdom	20	470.0 (± 3.0)	477.8 (± 2.9)	0.0858 (± 0.0298)
Systellaspis debilis				
- R8	10	- -	- -	- -
- Main rhabdom	21	483.6 (± 1.4)	484.0 (± 1.5)	0.1853 (± 0.0717)

Table 3.15 (Continued).

Species	Number of individual scans (n)	Mean running average λ_{max} (nm) (± s.d.)	Mean best-fit template λ_{max} (nm) (± s.d.)	Mean maximum corrected absorbance (± s.d.)
Family Pandalidae				
Stylopandalus richardii	20	488.3 (± 1.1)	488.3 (± 0.4)	0.1787 (± 0.0232)
Plesionika maritus	24	491.3 (± 3.5)	490.4 (± 3.4)	0.0680 (± 0.0186)
Family Pasiphaeidae				
Parapasiphaea sulcatifrons (Atl)	20	483.8 (± 1.7)	483.7 (± 1.6)	0.0906 (± 0.0241)
Parapasiphaea sulcatifrons (Pac)	12	484.9 (± 2.8)	483.7 (± 4.0)	0.0676 (± 0.0332)
Pasiphaea chacei	24	486.8 (± 4.3)	487.6 (± 4.7)	0.0483 (± 0.0247)
Pasiphaea emarginata	24	484.9 (± 4.3)	486.0 (± 3.4)	0.0609 (± 0.0138)
Superorder Percaridia Order Mysida				
Chalaraspidium alata	24	490.0 (± 1.8)	489.8 (± 1.8)	0.1021 (± 0.0282)
Eucopia australis	16	490.7 (± 1.8)	494.3 (± 1.7)	0.1101 (± 0.0067)
Eucopia sculpticauda	16	487.4 (± 2.0)	490.2 (± 1.2)	0.1068 (± 0.0360)
Gnathophausia gigas	20	488.7 (± 3.9)	489.7 (± 1.8)	0.0831 (± 0.0207)
Gnathophausia gracilis	24	484.4 (± 2.4)	486.2 (± 2.6)	0.0828 (± 0.0284)
Gnathophausia ingens	20	489.2 (± 3.0)	490.0 (± 2.3)	0.0982 (± 0.0081)
Order Amphipoda				
Cyphocaris richardi	12	482.7 (± 1.8)	479.6 (± 0.6)	0.1328 (± 0.0133)

Table 3.16 Deep-sea species: specific absorbances and the extinction coefficient ratios of the averaged data.

Species	Section thickness (μm)	Mix_1 specific absorbance (μm^{-1})	Mix_2 specific absorbance (μm^{-1})	Extinction ratio: $\varepsilon_{max}\ mix_2 / \varepsilon_{max}\ mix_1$ (± s.d.)
Superorder Eucarida				
Order Decapoda				
Suborder Dendrobranchiata				
Family Penaeidae				
Bentheogennema intermedia	15	0.0054	0.0066	1.227 (± 0.033)
Bentheogennema pasithea	14	0.0031	0.0043	1.390 (± 0.048)
Gennadas sp.	14	0.0045	0.0054	1.220 (± 0.040)
Gennadas valens	15	0.0048	0.0058	1.216 (± 0.030)
Petalidium suspirosum	14	0.0041	0.0055	1.341 (± 0.046)
Plesiopenaeus armatus	16.36	0.0035	0.0042	1.214 (± 0.030)
Family Sergestidae				
Sergestes curvatus	15	0.0078	0.0094	1.207 (± 0.018)
Sergestes similis	14	0.0074	0.0092	1.242 (± 0.031)
Sergia maximus	15	0.0068	0.0088	1.284 (± 0.024)
Sergia phorcus	14	0.0067	0.0077	1.152 (± 0.028)
Sergia robustus	15	0.0072	0.0091	1.260 (± 0.022)
Sergia splendens	15	0.0106	0.0131	1.239 (± 0.014)
Suborder Pleocyemata				
Infraorder Caridea				
Family Oplophoridae				
Acanthephyra curtirostris	14	0.0076	0.0096	1.266 (± 0.022)
Acanthephyra microphthalma	15	0.0038	0.0044	1.141 (± 0.042)
Acanthephyra purpurea	15	0.0050	0.0067	1.358 (± 0.036)
Acanthephyra stylorostratis	14	0.0062	0.0076	1.216 (± 0.026)
Hymenodora frontalis	14	0.0044	0.0055	1.248 (± 0.034)
Hymenodora glacialis	15	0.0022	0.0033	1.527 (± 0.094)
Meningodora miccyla	15	0.0049	0.0050	1.022 (± 0.020)
Meningodora vesca	15	0.0082	0.0104	1.267 (± 0.020)
Oplophorus spinosus				
- R8	11	0.0024	-	- -
- Main rhabdom	15	0.0070	0.0089	1.282 (± 0.021)
Systellaspis braueri				
- R8	14	0.0036	-	- -
- Main rhabdom	12	0.0051	0.0062	1.222 (± 0.033)
Systellaspis cristata				
- R8	14	0.0071	-	- -
- Main rhabdom	12	0.0061	0.0071	1.164 (± 0.029)
Systellaspis debilis				
- R8	18	0.0039	-	- -
- Main rhabdom	16.47	0.0077	0.0109	1.424 (± 0.022)

Table 3.16 (Continued).

Species	Section thickness (μm)	Mix_1 specific absorbance (μm^{-1})	Mix_2 specific absorbance (μm^{-1})	Extinction ratio: $\varepsilon_{max}\ mix_2 / \varepsilon_{max}\ mix_1$ (± s.d.)
Family Pandalidae				
Stylopandalus richardii	15	0.0099	0.0119	1.207 (± 0.017)
Plesionika maritus	14	0.0030	0.0048	1.626 (± 0.080)
Family Pasiphaeidae				
Parapasiphaea sulcatifrons (Atl)	15	0.0044	0.0060	1.368 (± 0.019)
Parapasiphaea sulcatifrons (Pac)	14	0.0036	0.0048	1.351 (± 0.061)
Pasiphaea chacei	14	0.0023	0.0034	1.483 (± 0.066)
Pasiphaea emarginata	14	0.0042	0.0043	1.042 (± 0.037)
Superorder Percaridia Order Mysida				
Chalaraspidium alata	14	0.0055	0.0073	1.319 (± 0.038)
Eucopia australis	14	0.0068	0.0079	1.157 (± 0.025)
Eucopia sculpticauda	14	0.0061	0.0076	1.241 (± 0.040)
Gnathophausia gigas	14	0.0050	0.0059	1.185 (± 0.047)
Gnathophausia gracilis	14	0.0050	0.0059	1.194 (± 0.026)
Gnathophausia ingens	14	0.0058	0.0070	1.211 (± 0.029)
Order Amphipoda				
Cyphocaris richardi	14	0.0084	0.0095	1.129 (± 0.036)

Table 3.17 Deep-sea species: deviation and signal to noise ratios of the mix_1 and mix_2 averaged data and the number of points used in the running averages.

Species	Mix_1 mean template deviation	Mix_1 S/N ratio	Mix_1 no. pts. in run. av.	Mix_2 mean template deviation	Mix_2 S/N ratio	Mix_2 no. pts. in run. av.	PC spectrum no. pts. in run. av.
Superorder Eucarida							
Order Decapoda							
Suborder Dendrobranchiata							
Family Penaeidae							
Bentheogennema intermedia	-0.0039	147.0 [a]	13	-0.0001	85.9 [c]	15	17
Bentheogennema pasithea	0.0067	46.9	17	0.0049	61.2	17	19
Gennadas sp.	0.0018	65.5	17	0.0046	54.9	17	17
Gennadas valens	0.0006	83.8	15	0.0034	81.0	15	15
Petalidium suspirosum	0.0053	62.1	17	0.0008	99.6	15	17
Plesiopenaeus armatus	0.0021	83.2	15	-0.0024	85.0	15	19
Family Sergestidae							
Sergestes curvatus	0.0018	99.9	15	-0.0005	135.4	13	17
Sergestes similis	0.0012	94.5	15	-0.0019	95.7	15	17
Sergia maximus	-0.0019	95.3	15	-0.0007	127.4	13	15
Sergia phorcus	-0.0048	61.9	17	-0.0021	76.5 [a]	15	19
Sergia robustus	-0.0026	80.6	15	-0.0013	151.4	13	17
Sergia splendens	-0.0016	76.2	15	-0.0018	216.1	13	19
Suborder Pleocyemata							
Infraorder Caridea							
Family Oplophoridae							
Acanthephyra curtirostris	0.0015	98.8	15	0.0023	135.9	13	19
Acanthephyra microphthalma	-0.0021	**76.4**	**17**	0.0005	94.4	15	31
Acanthephyra purpurea	0.0037	85.5	15	0.0015	153.6	13	17
Acanthephyra stylorostratis	-0.0009	94.0	15	-0.0006	97.2	15	23
Hymenodora frontalis	0.0067	61.2	17	0.0032	79.3	15	19
Hymenodora glacialis	0.0026	36.1	23	0.0030	36.8	23	17
Meningodora miccyla	0.0041	88.0	15	-0.0008	148.7	13	19
Meningodora vesca	0.0012	137.4	13	0.0014	202.6	13	17
Oplophorus spinosus							
- R8	-	-	21	-	-	21	15
- Main rhabdom	0.0000	146.7	13	0.0021	131.4 [a]	13	15
Systellaspis braueri							
- R8	-	-	15	-	-	15	15
- Main rhabdom	0.0006	55.3	17	-0.0036	83.8	15	19
Systellaspis cristata							
- R8	-	-	13	-	-	13	11
- Main rhabdom	-0.0011	55.5	17	0.0006	49.9 [c]	17	17
Systellaspis debilis							
- R8	-	-	13	-	-	13	15
- Main rhabdom	0.0010	83.5	15	0.0009	146.8	13	13

Table 3.17 (Continued).

Species	Mix_1 mean template deviation	Mix_1 S/N ratio	Mix_1 no. pts. in run. av.	Mix_2 mean template deviation	Mix_2 S/N ratio	Mix_2 no. pts. in run. av.	PC spectrum no. pts. in run. av.
Family Pandalidae							
Stylopandalus richardii	0.0010	104.0	15	-0.0013	127.7	13	21
Plesionika maritus	0.0017	28.3	23	0.0036	60.8	17	21
Family Pasiphaeidae							
Parapasiphaea sulcatifrons (Atl)	0.0058	93.3	15	0.0013	135.9	13	13
Parapasiphaea sulcatifrons (Pac)	0.0030	48.9	17	0.0004	64.6	17	17
Pasiphaea chacei	0.0073	47.9	17	0.0088	42.8	17	15
Pasiphaea emarginata	0.0036	81.8	15	0.0035	**76.1**	**15**	19
Superorder Percaridia Order Mysida							
Chalaraspidium alata	-0.0011	62.6 [a]	17	0.0011	82.6	15	21
Eucopia australis	0.0026	82.4 [b]	15	-0.0024	62.5 [c]	17	15
Eucopia sculpticauda	0.0023	52.5 [a]	17	0.0060	61.1	17	25
Gnathophausia gigas	0.0022	55.4	17	0.0023	58.8	17	31
Gnathophausia gracilis	0.0013	83.7 [a]	15	0.0066	**74.1**	**15**	19
Gnathophausia ingens	0.0045	56.4	17	0.0033	82.5	15	27
Order Amphipoda							
Cyphocaris richardi	0.0063	48.7 [a]	17	0.0069	61.3 [a]	17	33

The noise of the data was normally estimated between 80% shortwave normalised absorbance and the longwave offset (0.5% longwave normalised absorbance). However, in cases where the data significantly deviated from the template the following, restricted ranges were used: [a] noise calculated between the running average λ_{max} and the offset end, [b] noise calculated between 550 nm and the offset end and, [c] noise calculated between 80% and 20% longwave normalised absorbance.

Bold text indicates those files which, when re-analysed using the indicated number of points in the running average, had a new S/N ratio which suggests a different number of points should be used. See text for more detail (Section 4.2.5).

Table 3.18 Deep-sea species: calculation of the metarhodopsin estimate.

Species	Mix$_1$ λ_{max} ($\equiv R$) (nm)	F_R in mix$_2$	Est. M λ_{max} (nm)	Extinction ratio: $\varepsilon_{max}\, M$ / ε_{max} mix$_1$
Superorder Eucarida				
Order Decapoda				
Suborder Dendrobranchiata				
Family Penaeidae				
Bentheogennema intermedia	492.2	0.191	480.5	1.288
Bentheogennema pasithea	499.2	0.193	486.3	1.492
Gennadas sp.	493.0	0.138	478.2	1.263
Gennadas valens	493.8	0.124	477.9	1.255
Petalidium suspirosum	498.6	0.282	489.9	1.481
Plesiopenaeus armatus	491.5	0.196	480.1	1.273
Family Sergestidae				
Sergestes curvatus	492.1	0.266	483.9	1.287
Sergestes similis	492.3	0.261	483.6	1.333
Sergia maximus	492.8	0.229	482.4	1.375
Sergia phorcus	493.6	0.186	482.2	1.193
Sergia robustus	493.9	0.229	483.7	1.344
Sergia splendens	494.2	0.243	484.8	1.322
Suborder Pleocyemata				
Infraorder Caridea				
Family Oplophoridae				
Acanthephyra curtirostris	484.8	0.428	481.6	1.466
Acanthephyra microphthalma	481.6	0.442	480.4	1.253
Acanthephyra purpurea	490.5	0.271	481.3	1.498
Acanthephyra stylorostratis	488.3	0.391	484.4	1.357
Hymenodora frontalis	493.1	0.227	482.9	1.327
Hymenodora glacialis	498.4	0.159	482.7	1.637
Meningodora miccyla	485.9	0.301	480.9	1.034
Meningodora vesca	487.2	0.329	480.8	1.402
Oplophorus spinosus				
- R8	-	-	-	-
- Main rhabdom	492.0	0.217	481.1	1.368
Systellaspis braueri				
- R8	-	-	-	-
- Main rhabdom	498.1	0.180	485.8	1.278
Systellaspis cristata				
- R8	-	-	-	-
- Main rhabdom	496.4	0.079	476.5	1.186
Systellaspis debilis				
- R8	-	-	-	-
- Main rhabdom	495.6	0.194	482.5	1.535

Table 3.18 (Continued).

Species	Mix$_1$ λ_{max} ($\equiv R$) (nm)	F_R in mix$_2$	Est. M λ_{max} (nm)	Extinction ratio: $\varepsilon_{max}\,M$ / ε_{max} mix$_1$
Family Pandalidae				
Stylopandalus richardii	491.2	0.374	486.8	1.333
Plesionika maritus	497.1	0.345	488.5	1.964
Family Pasiphaeidae				
Parapasiphaea sulcatifrons (Atl)	499.6	0.122	482.4	1.429
Parapasiphaea sulcatifrons (Pac)	499.8	0.132	483.5	1.413
Pasiphaea chacei	507.5	0.098	487.3	1.546
Pasiphaea emarginata	495.8	0.164	484.1	1.056
Superorder Percaridia Order Mysida				
Chalaraspidium alata	493.4	0.378	488.1	1.516
Eucopia australis	513.0	0.079	493.0	1.178
Eucopia sculpticauda	493.0	0.384	488.6	1.394
Gnathophausia gigas	491.4	0.417	488.7	1.318
Gnathophausia gracilis	494.5	0.225	484.7	1.257
Gnathophausia ingens	491.7	0.418	488.7	1.363
Order Amphipoda				
Cyphocaris richardi	481.8	0.381	478.6	1.210

Table 3.19 Deep-sea species: calculation of the rhodopsin estimate.

Species	F_R in mix$_1$	Est. R λ_{max} (nm)	Est. M λ_{max} (nm)	Extinction ratio: $\varepsilon_{max}\,M$ / $\varepsilon_{max}\,R$
Superorder Eucarida				
Order Decapoda				
Suborder Dendrobranchiata				
Family Penaeidae				
Bentheogennema intermedia	0.90	494.0	480.5	1.321
Bentheogennema pasithea	0.95	500.3	486.3	1.525
Gennadas sp.	0.90	495.3	478.2	1.286
Gennadas valens	0.95	494.9	477.9	1.264
Petalidium suspirosum	0.85	501.2	489.9	1.605
Plesiopenaeus armatus	0.90	493.2	480.1	1.304
Family Sergestidae				
Sergestes curvatus	0.95	492.6	483.9	1.305
Sergestes similis	0.85	494.6	483.6	1.406
Sergia maximus	0.90	494.5	482.4	1.426
Sergia phorcus	0.90	495.2	482.2	1.212
Sergia robustus	0.90	495.5	483.7	1.389
Sergia splendens	0.85	496.7	484.8	1.390
Suborder Pleocyemata				
Infraorder Caridea				
Family Oplophoridae				
Acanthephyra curtirostris	1.00	484.7	481.6	1.466
Acanthephyra microphthalma	1.00	481.5	480.4	1.253
Acanthephyra purpurea	0.90	492.2	481.3	1.577
Acanthephyra stylorostratis	0.95	488.5	484.4	1.382
Hymenodora frontalis	0.90	494.7	482.9	1.370
Hymenodora glacialis	0.95	499.9	482.7	1.681
Meningodora miccyla	1.00	485.8	480.9	1.034
Meningodora vesca	1.00	487.1	480.8	1.402
Oplophorus spinosus				
- R8	-	-	-	-
- Main rhabdom	0.90	493.8	481.1	1.416
Systellaspis braueri				
- R8	-	-	-	-
- Main rhabdom	0.90	500.0	485.8	1.308
Systellaspis cristata				
- R8	-	-	-	-
- Main rhabdom	0.95	497.7	476.5	1.187
Systellaspis debilis				
- R8	-	-	-	-
- Main rhabdom	0.95	496.7	482.5	1.572

Table 3.19 (Continued).

Species	F_R in mix$_1$	Est. R λ_{max} (nm)	Est. M λ_{max} (nm)	Extinction ratio: ε_{max} M / ε_{max} R
Family Pandalidae				
Stylopandalus richardii	1.00	491.1	486.8	1.333
Plesionika maritus	0.90	499.3	488.5	2.185
Family Pasiphaeidae				
Parapasiphaea sulcatifrons (Atl)	0.95	501.0	482.4	1.450
Parapasiphaea sulcatifrons (Pac)	0.95	501.1	483.5	1.435
Pasiphaea chacei	0.95	509.2	487.3	1.573
Pasiphaea emarginata	0.90	497.2	484.1	1.057
Superorder Percaridia Order Mysida				
Chalaraspidium alata	1.00	493.3	488.1	1.516
Eucopia australis	0.95	514.3	493.0	1.179
Eucopia sculpticauda	1.00	492.9	488.6	1.394
Gnathophausia gigas	1.00	491.3	488.7	1.318
Gnathophausia gracilis	0.85	496.9	484.7	1.305
Gnathophausia ingens	1.00	491.6	488.7	1.363
Order Amphipoda				
Cyphocaris richardi	1.00	481.7	478.6	1.210

Table 3.20 Deep-sea species: summary of averaged data and the rhodopsin and metarhodopsin estimates.

Species	Mix_1 λ_{max} (nm)	Mix_2 λ_{max} (nm)	Extinction ratio: ε_{max} mix_2 / ε_{max} mix_1	Est. *R* λ_{max} (nm)	Est. *M* λ_{max} (nm)	Extinction ratio: ε_{max} *M* / ε_{max} *R*
Superorder Eucarida						
Order Decapoda						
Suborder Dendrobranchiata						
Family Penaeidae						
Bentheogennema intermedia	492.2	482.1	1.227	494.0	480.5	1.321
Bentheogennema pasithea	499.2	487.9	1.390	500.3	486.3	1.525
Gennadas sp.	493.0	479.6	1.220	495.3	478.2	1.286
Gennadas valens	493.8	479.3	1.216	494.9	477.9	1.264
Petalidium suspirosum	498.6	491.6	1.341	501.2	489.9	1.605
Plesiopenaeus armatus	491.5	481.8	1.214	493.2	480.1	1.304
Family Sergestidae						
Sergestes curvatus	492.1	485.6	1.207	492.6	483.9	1.305
Sergestes similis	492.3	485.3	1.242	494.6	483.6	1.406
Sergia maximus	492.8	484.1	1.284	494.5	482.4	1.426
Sergia phorcus	493.6	483.9	1.152	495.2	482.2	1.212
Sergia robustus	493.9	485.4	1.260	495.5	483.7	1.389
Sergia splendens	494.2	486.5	1.239	496.7	484.8	1.390
Suborder Pleocyemata						
Infraorder Caridea						
Family Oplophoridae						
Acanthephyra curtirostris	484.8	482.7	1.266	484.7	481.6	1.466
Acanthephyra microphthalma	481.6	480.9	1.141	481.5	480.4	1.253
Acanthephyra purpurea	490.5	483.0	1.358	492.2	481.3	1.577
Acanthephyra stylorostratis	488.3	485.7	1.216	488.5	484.4	1.382
Hymenodora frontalis	493.1	484.6	1.248	494.7	482.9	1.370
Hymenodora glacialis	498.4	484.1	1.527	499.9	482.7	1.681
Meningodora miccyla	485.9	482.4	1.022	485.8	480.9	1.034
Meningodora vesca	487.2	482.4	1.267	487.1	480.8	1.402
Oplophorus spinosus						
- R8	413	-	-	413	*ca.* 475	*ca.* 1.45
- Main rhabdom	492.0	482.8	1.282	493.8	481.1	1.416
Systellaspis braueri						
- R8	411	-	-	411	*ca.* 475	*ca.* 1.45
- Main rhabdom	498.1	487.4	1.222	500.0	485.8	1.308
Systellaspis cristata						
- R8	414	-	-	414	*ca.* 475	*ca.* 1.45
- Main rhabdom	496.4	477.6	1.164	497.7	476.5	1.187
Systellaspis debilis						
- R8	417	-	-	417	*ca.* 475	*ca.* 1.45
- Main rhabdom	495.6	484.1	1.424	496.7	482.5	1.572

Table 3.20 (Continued).

Species	Mix_1 λ_{max} (nm)	Mix_2 λ_{max} (nm)	Extinction ratio: ε_{max} mix_2 / ε_{max} mix_1	Est. *R* λ_{max} (nm)	Est. *M* λ_{max} (nm)	Extinction ratio: ε_{max} *M* / ε_{max} *R*
Family Pandalidae						
Stylopandalus richardii	491.2	488.2	1.207	491.1	486.8	1.333
Plesionika maritus	497.1	490.2	1.626	499.3	488.5	2.185
Family Pasiphaeidae						
Parapasiphaea sulcatifrons (Atl)	499.6	483.7	1.368	501.0	482.4	1.450
Parapasiphaea sulcatifrons (Pac)	499.8	484.8	1.351	501.1	483.5	1.435
Pasiphaea chacei	507.5	488.4	1.483	509.2	487.3	1.573
Pasiphaea emarginata	495.8	485.8	1.042	497.2	484.1	1.057
Superorder Percaridia Order Mysida						
Chalaraspidium alata	493.4	489.6	1.319	493.3	488.1	1.516
Eucopia australis	513.0	494.1	1.157	514.3	493.0	1.179
Eucopia sculpticauda	493.0	490.0	1.241	492.9	488.6	1.394
Gnathophausia gigas	491.4	489.7	1.185	491.3	488.7	1.318
Gnathophausia gracilis	494.5	486.4	1.194	496.9	484.7	1.305
Gnathophausia ingens	491.7	489.8	1.211	491.6	488.7	1.363
Order Amphipoda						
Cyphocaris richardi	481.8	479.7	1.129	481.7	478.6	1.210

Figures 3.3 to 3.43: (**A**) Average absorbance spectra as measured by the microspectrophotometer; trace 1 (bold) showing the absorbance of the retina in its initial state, trace 2 (light) the absorbance following saturating red light irradiation, and trace 3 (dotted) the absorbance following photobleaching with bright white light. (**B**) Photoconversion difference spectrum derived from trace 2 minus trace 1 above (jagged trace), showing the change in absorbance induced by red light treatment of the photoreceptors in their initial state. The smooth trace is the photoconversion difference spectrum produced from the estimated rhodopsin and metarhodopsin templates. (**C**) Average difference spectra for the initial photoreceptor photobleaching derived from trace 1 minus trace 3 (i.e. mix_1; bold jagged trace), and following saturating red light irradiation derived from trace 2 minus trace 3 (i.e. mix_2; light jagged trace). Smooth solid traces are the best-fit template spectra to the data, the smooth dashed trace is the estimated metarhodopsin template, and the smooth dotted trace is the estimated rhodopsin template (if different from mix_1). All spectra are normalised to the average absorbance loss for the initial state photobleach (mix_1).

Histograms are presented to show the distribution of the average λ_{max} values of the templates which; (**D**) best-fit the mix_1 difference spectra per section scanned, and (**E**) best-fit the mix_2 difference spectra per section scanned. For each species, the legend indicates the species name, the number of sections scanned from which data were subsequently selected for analysis, the total number of scans that constitute the difference spectra of mix_1 and mix_2, the λ_{max} values of the best-fit templates for mix_1 and mix_2, the λ_{max} values of the rhodopsin and metarhodopsin estimates, the estimated metarhodopsin to rhodopsin extinction ratio, and the average maximum corrected absorbance loss for the mix_1 photobleach. All template visual pigment absorbance spectra were generated using the equation given by Stavenga *et al.* (1993) for rhodopsin pigments, modified to incorporate a shifting β-band (after Palacios *et al.*, 1996).

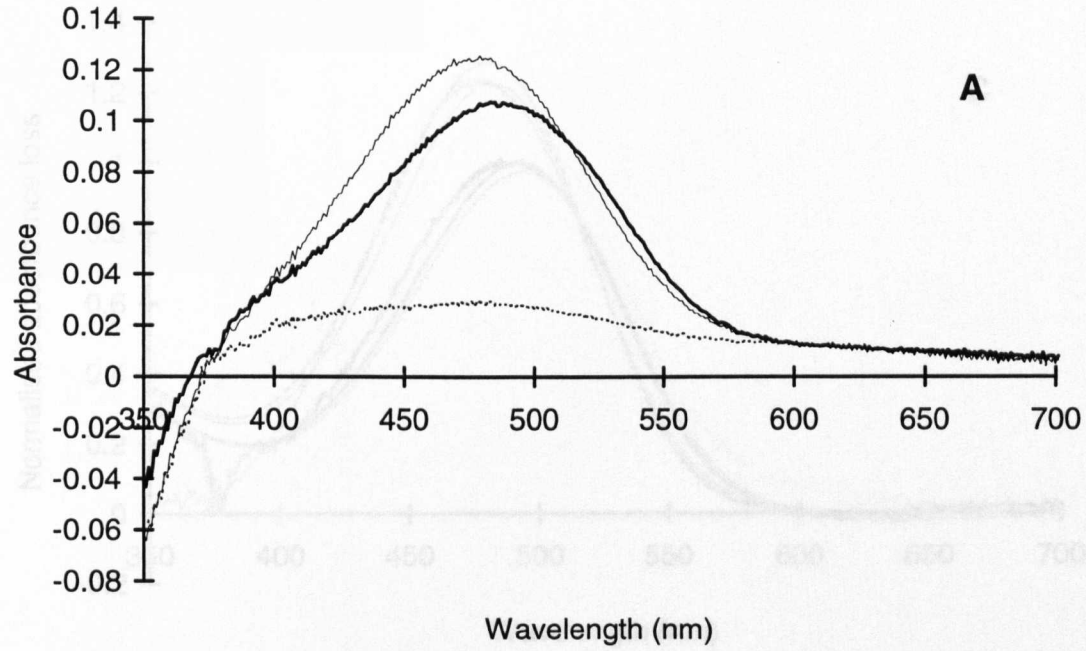

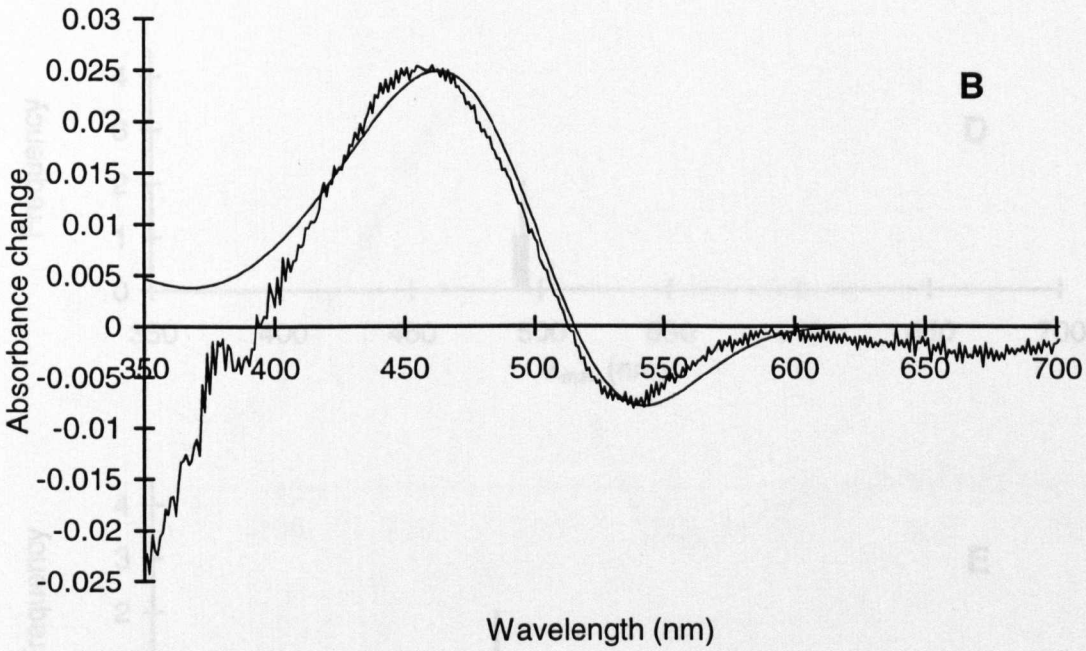

Figure 3.3 A–E. Results from the main rhabdoms (retinular cells 1–7) of *Bentheogennema intermedia*. The absorbance spectra from five sections were selected to give a total of 18 difference spectra which constitute the average files of mix_1 and mix_2. The λ_{max} values of the best-fit templates for mix_1 and mix_2 are 492.2 and 482.1 nm, and the λ_{max} values of the *R* and *M* estimates are 494.0 and 480.5 nm with an estimated *M* to *R* extinction ratio of 1.321. The average maximum corrected absorbance loss for the mix_1 photobleach is 0.0806.

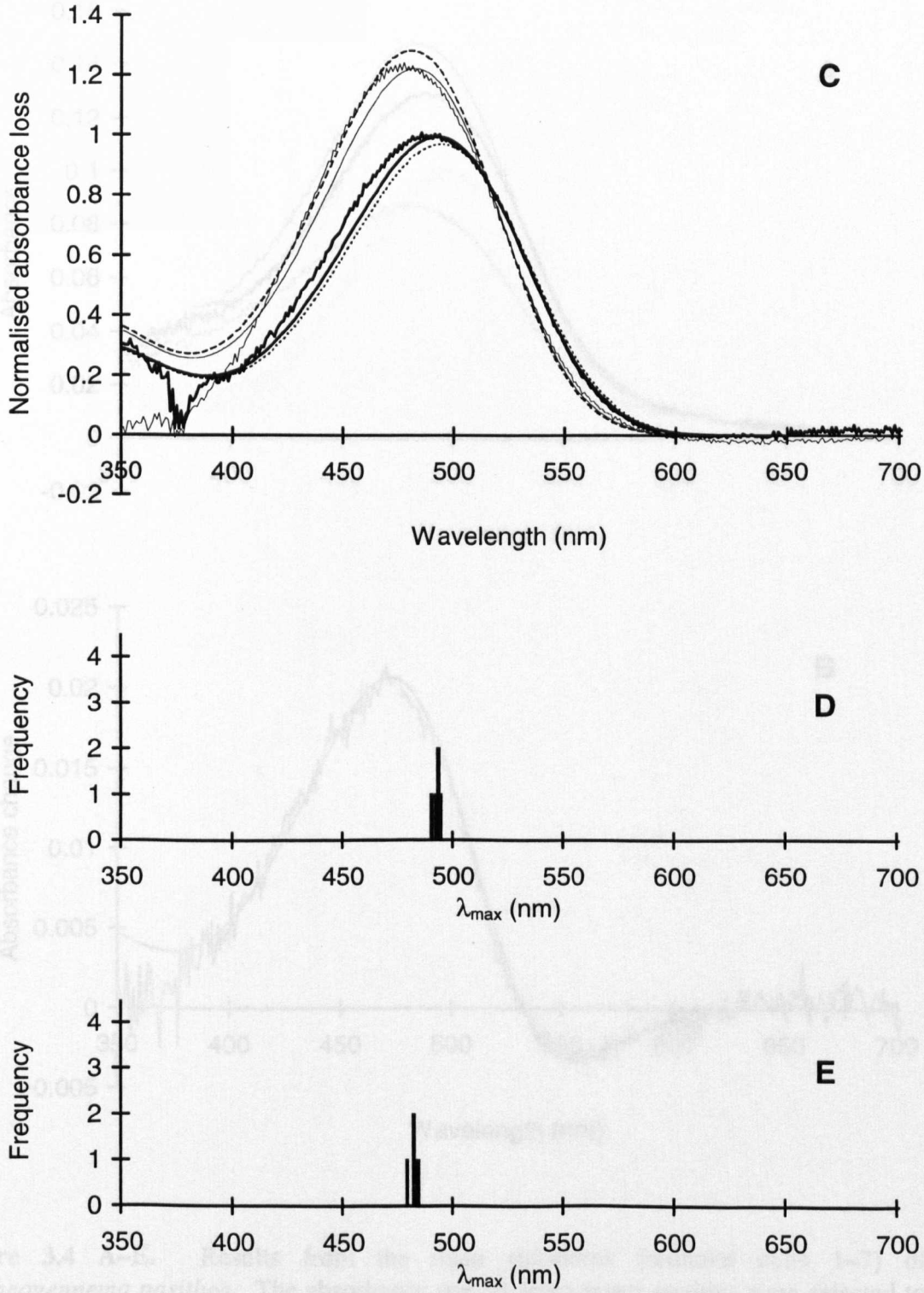

Figure 3.3 A–E. (Continued).

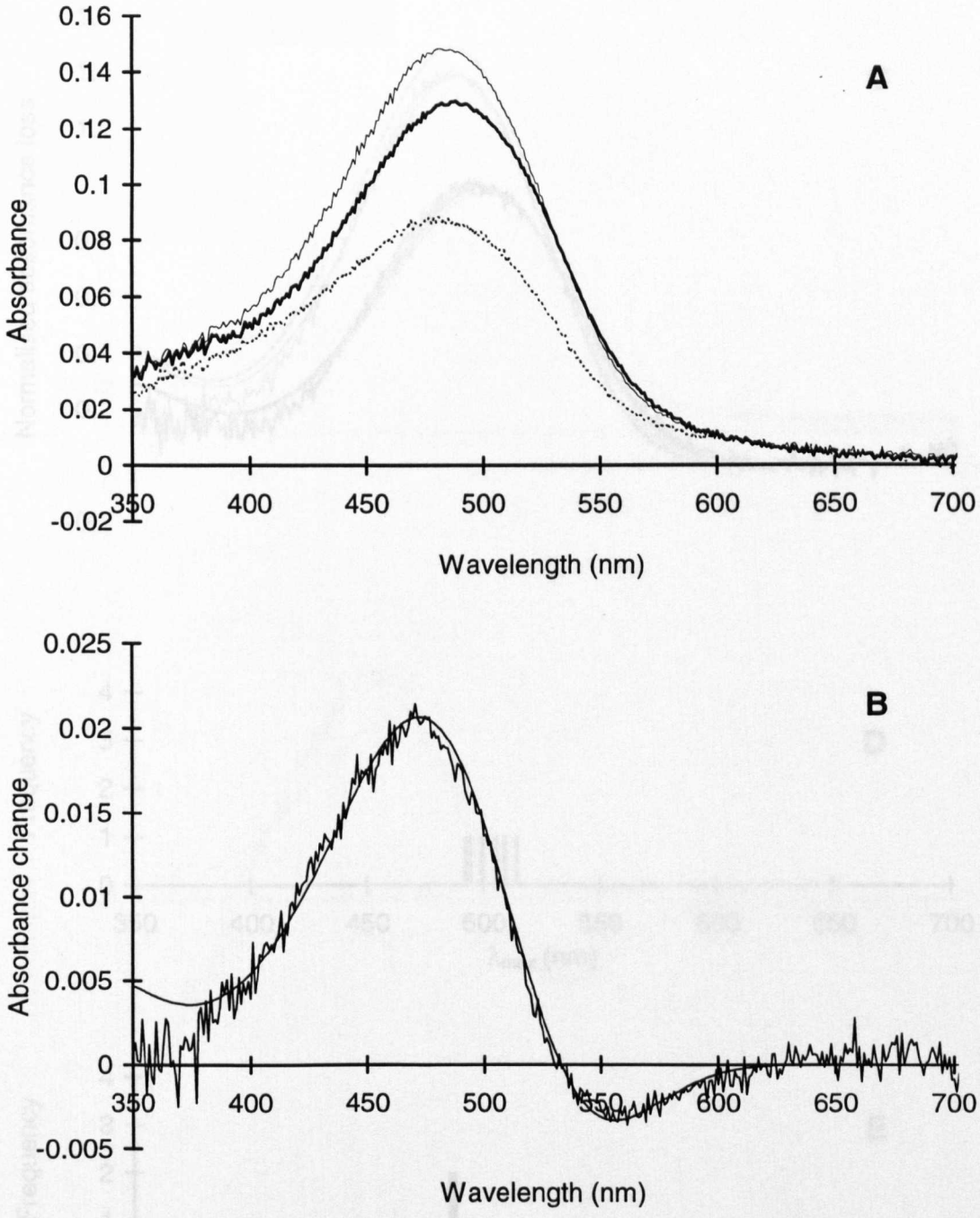

Figure 3.4 A–E. Results from the main rhabdoms (retinular cells 1–7) of *Bentheogennema pasithea*. The absorbance spectra from seven sections were selected to give a total of 28 difference spectra which constitute the average files of mix_1 and mix_2. The λ_{max} values of the best-fit templates for mix_1 and mix_2 are 499.2 and 487.9 nm, and the λ_{max} values of the *R* and *M* estimates are 500.3 and 486.3 nm with an estimated *M* to *R* extinction ratio of 1.525. The average maximum corrected absorbance loss for the mix_1 photobleach is 0.0437.

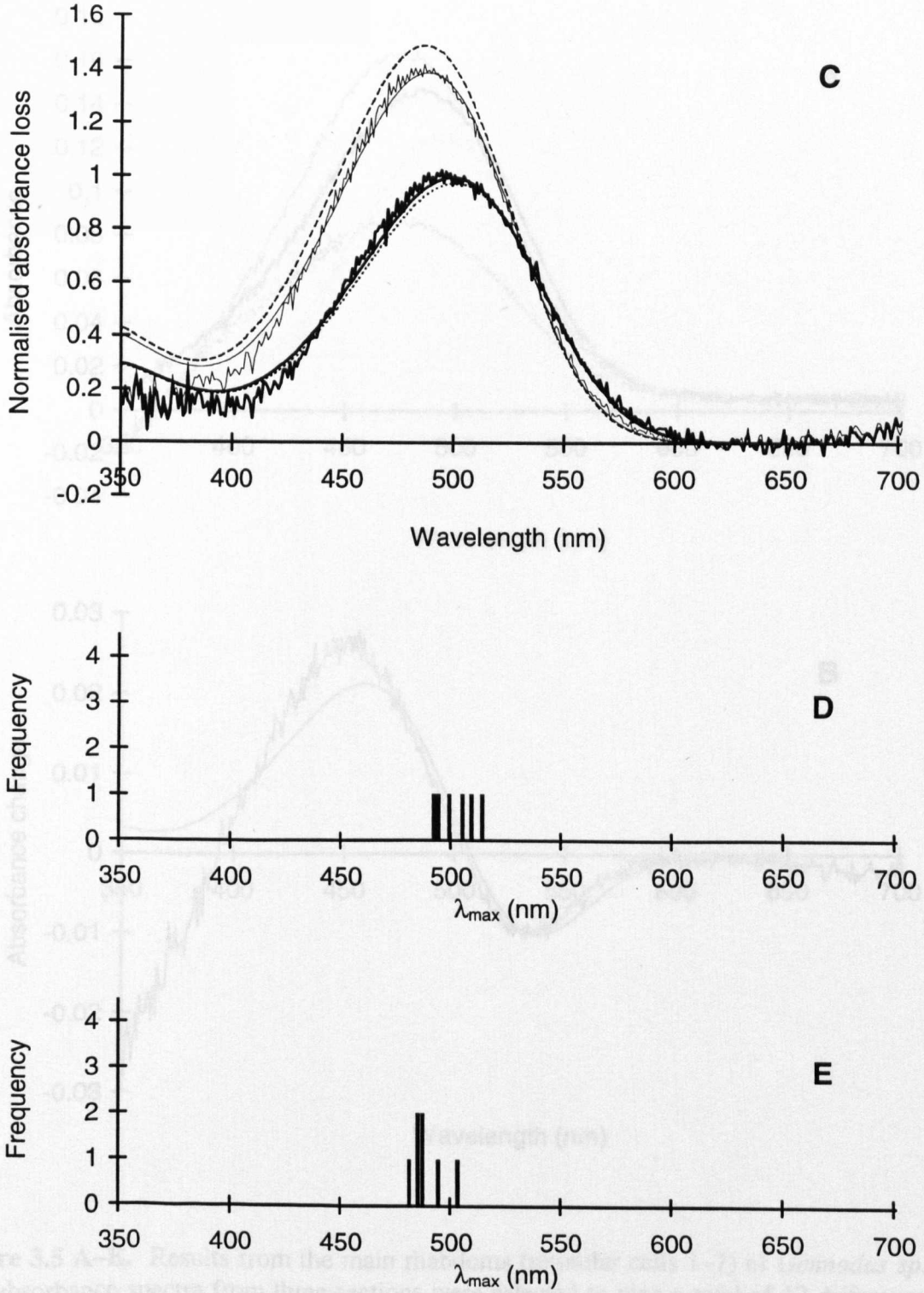

Figure 3.4 A–E. (Continued).

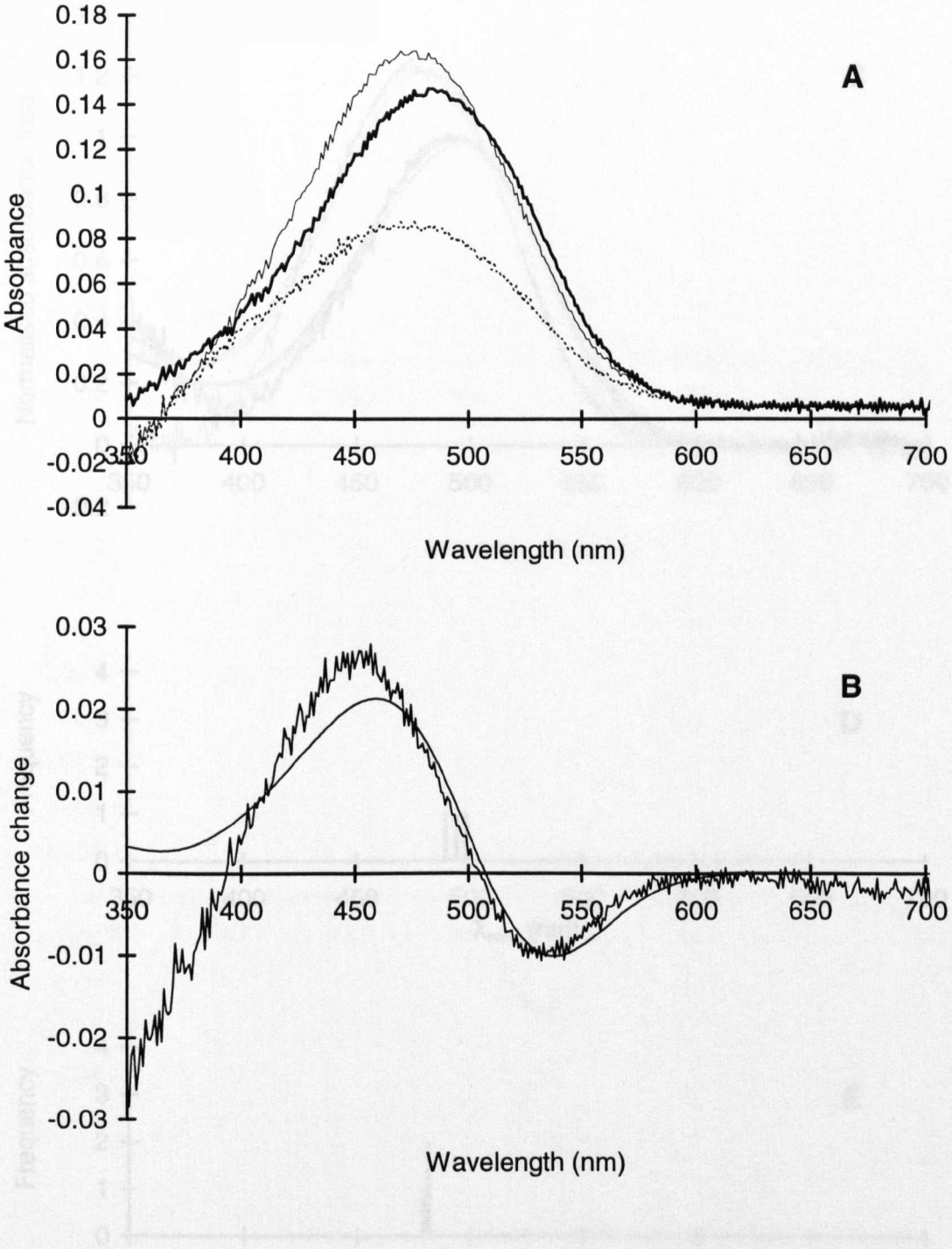

Figure 3.5 A–E. Results from the main rhabdoms (retinular cells 1–7) of *Gennadas sp.* The absorbance spectra from three sections were selected to give a total of 12 difference spectra which constitute the average files of mix_1 and mix_2. The λ_{max} values of the best-fit templates for mix_1 and mix_2 are 493.0 and 479.6 nm, and the λ_{max} values of the *R* and *M* estimates are 495.3 and 478.2 nm with an estimated *M* to *R* extinction ratio of 1.286. The average maximum corrected absorbance loss for the mix_1 photobleach is 0.0624.

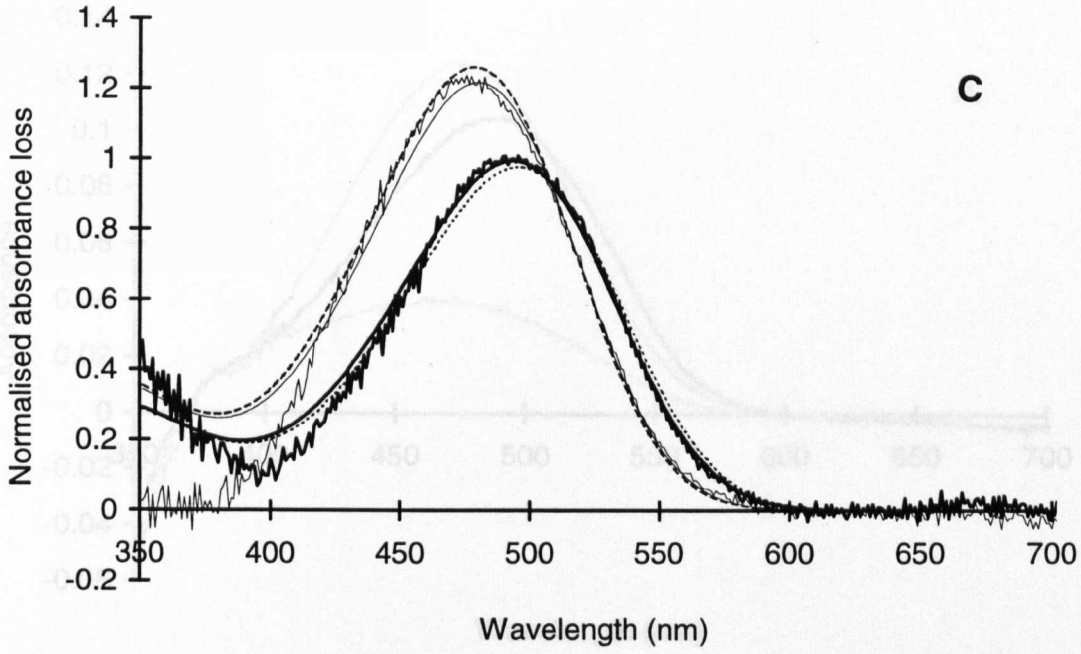

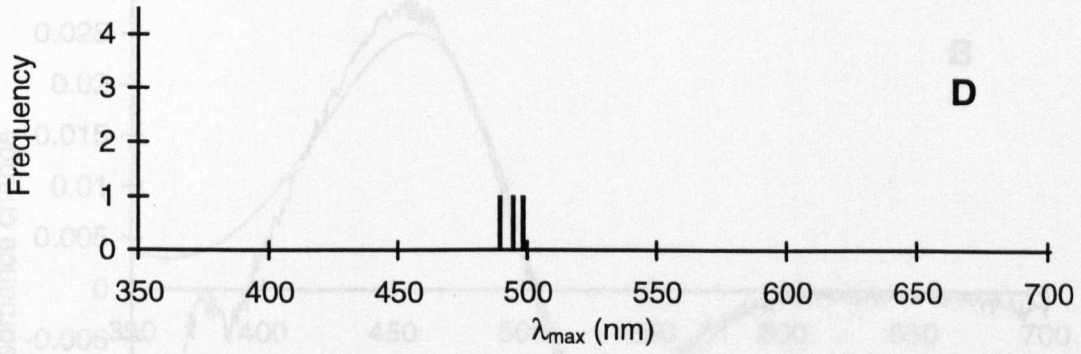

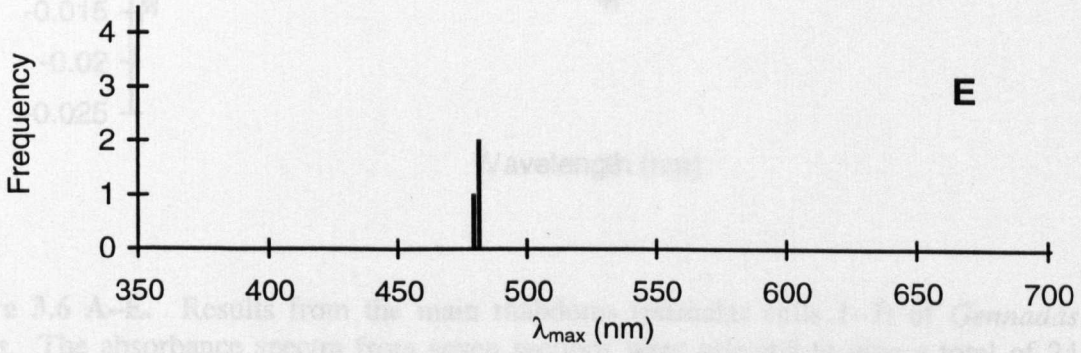

Figure 3.5 A–E. (Continued).

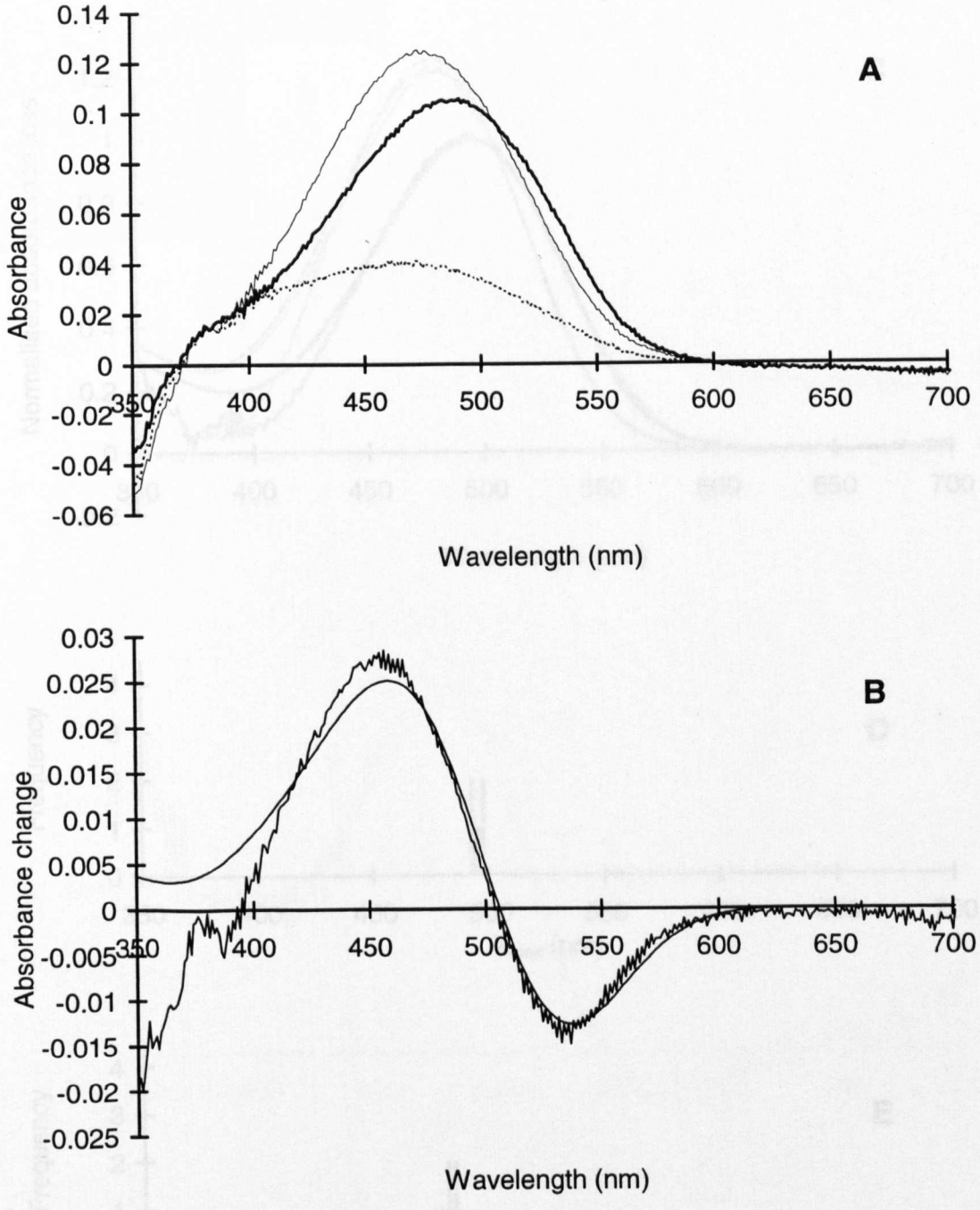

Figure 3.6 A–E. Results from the main rhabdoms (retinular cells 1–7) of *Gennadas valens*. The absorbance spectra from seven sections were selected to give a total of 24 difference spectra which constitute the average files of mix_1 and mix_2. The λ_{max} values of the best-fit templates for mix_1 and mix_2 are 493.8 and 479.3 nm, and the λ_{max} values of the *R* and *M* estimates are 494.9 and 477.9 nm with an estimated *M* to *R* extinction ratio of 1.264. The average maximum corrected absorbance loss for the mix_1 photobleach is 0.0717.

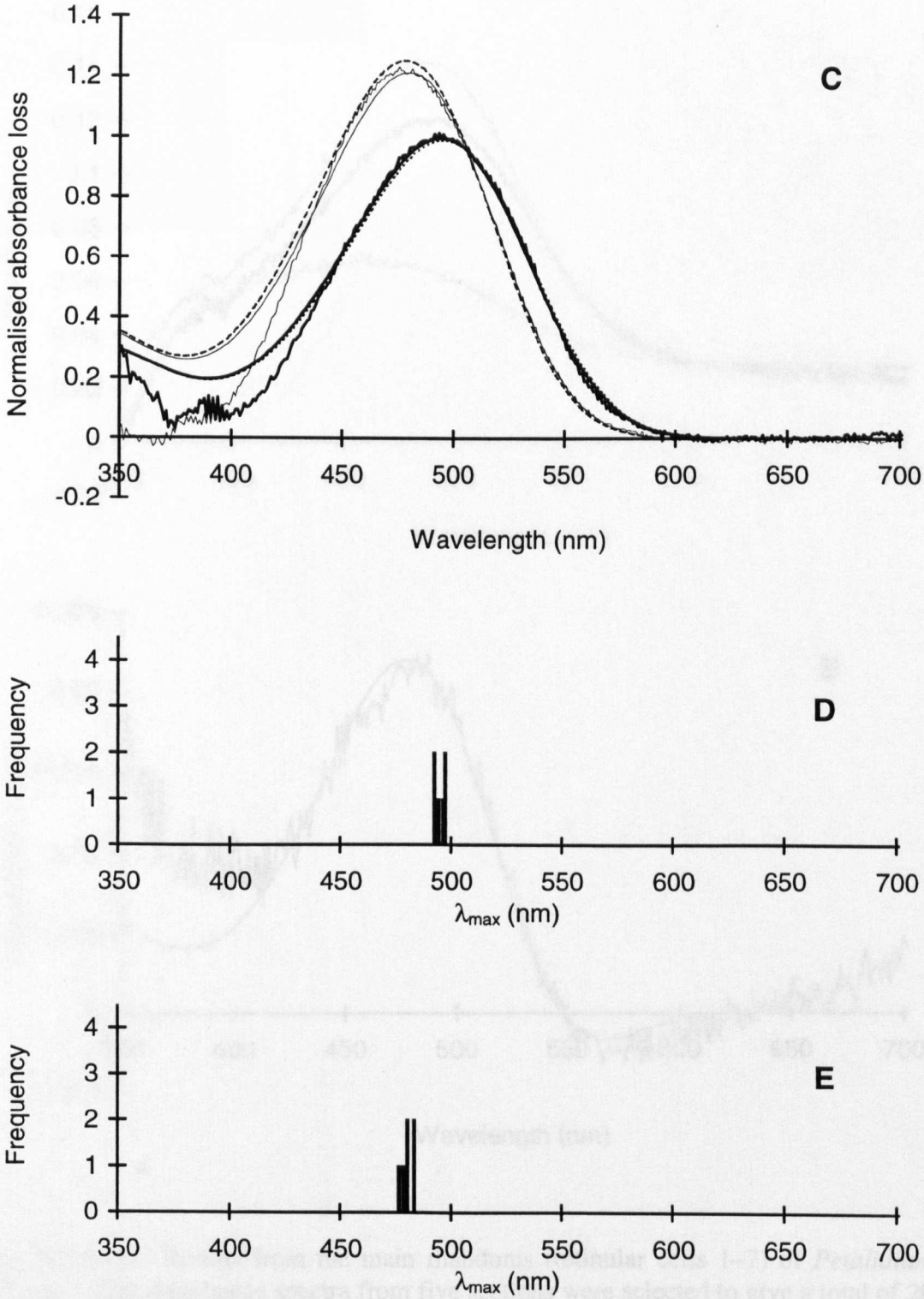

Figure 3.6 A–E. (Continued).

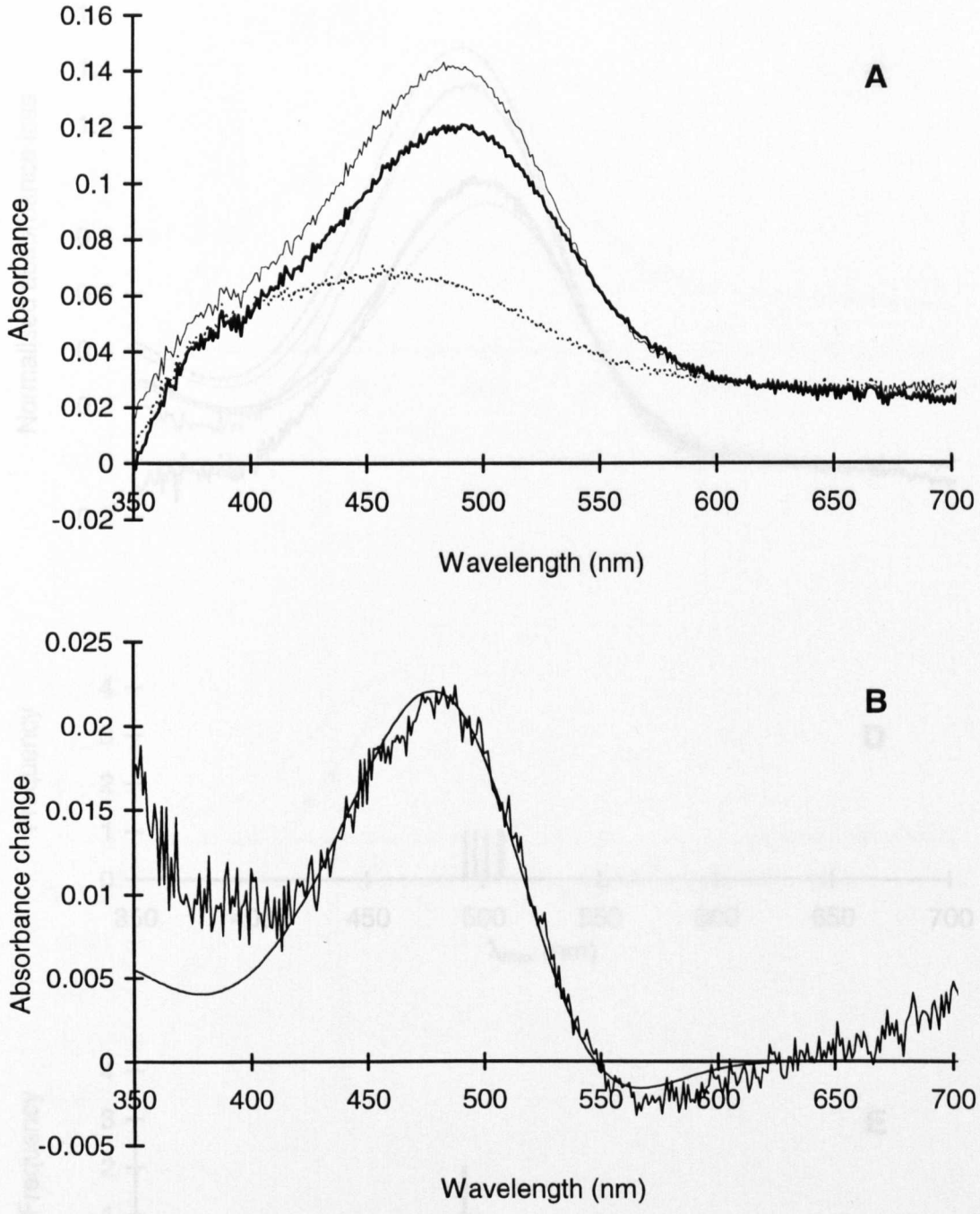

Figure 3.7 A–E. Results from the main rhabdoms (retinular cells 1–7) of *Petalidium suspirosum*. The absorbance spectra from five sections were selected to give a total of 20 difference spectra which constitute the average files of mix_1 and mix_2. The λ_{max} values of the best-fit templates for mix_1 and mix_2 are 498.6 and 491.6 nm, and the λ_{max} values of the *R* and *M* estimates are 501.2 and 489.9 nm with an estimated *M* to *R* extinction ratio of 1.605. The average maximum corrected absorbance loss for the mix_1 photobleach is 0.0579.

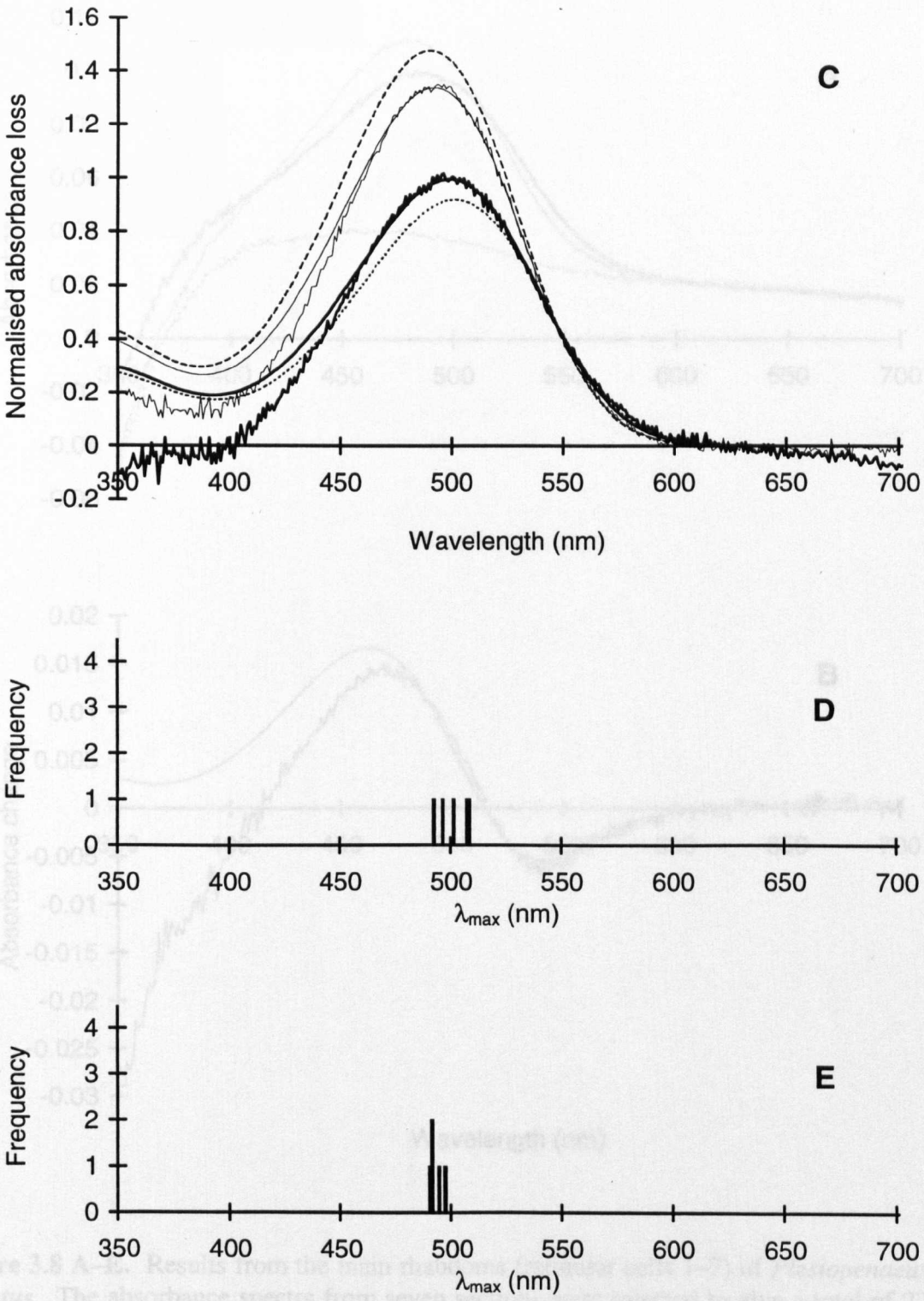

Figure 3.7 A–E. (Continued).

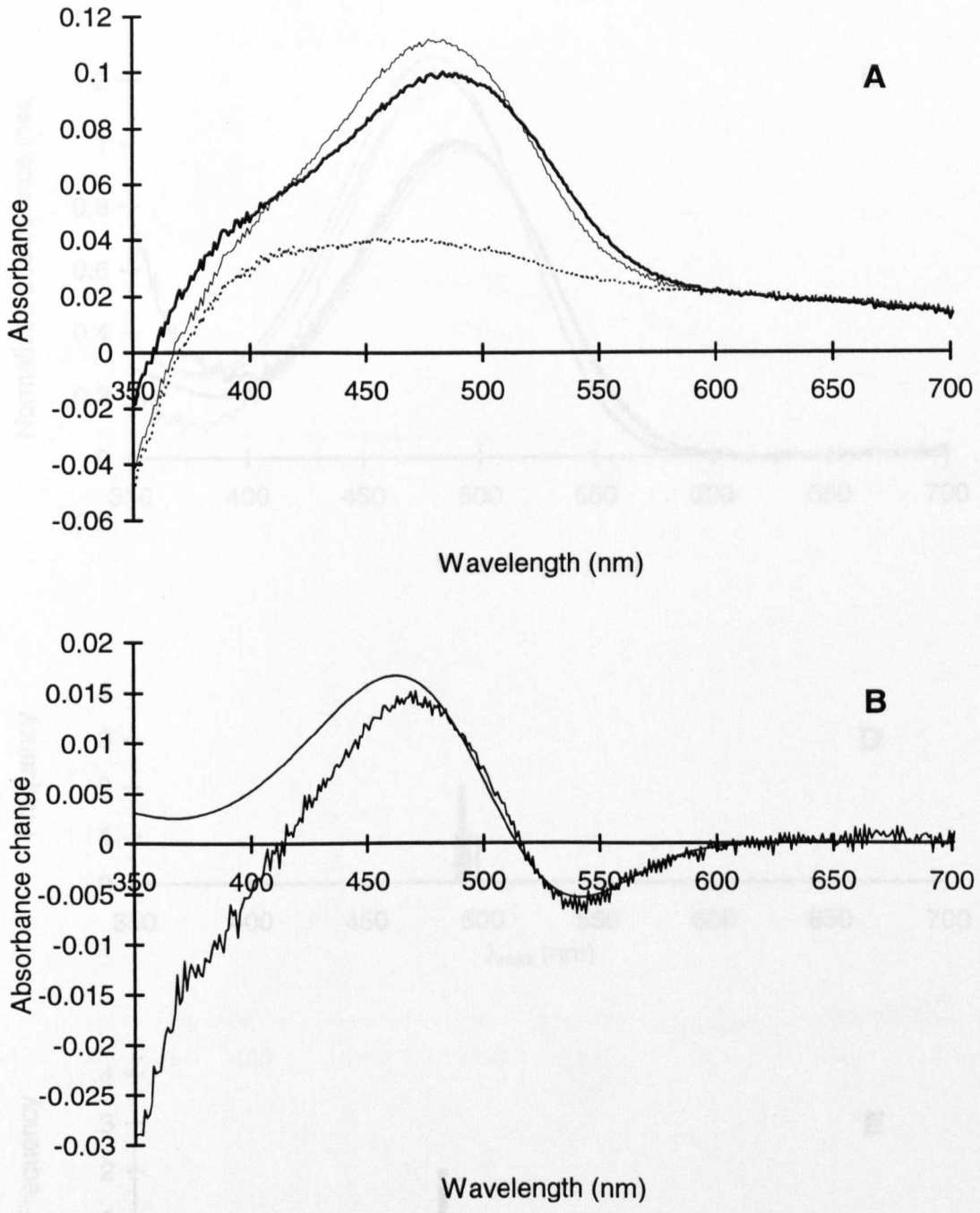

Figure 3.8 A–E. Results from the main rhabdoms (retinular cells 1–7) of *Plesiopenaeus armatus*. The absorbance spectra from seven sections were selected to give a total of 22 difference spectra which constitute the average files of mix_1 and mix_2. The λ_{max} values of the best-fit templates for mix_1 and mix_2 are 491.5 and 481.8 nm, and the λ_{max} values of the *R* and *M* estimates are 493.2 and 480.1 nm with an estimated *M* to *R* extinction ratio of 1.304. The average maximum corrected absorbance loss for the mix_1 photobleach is 0.0570.

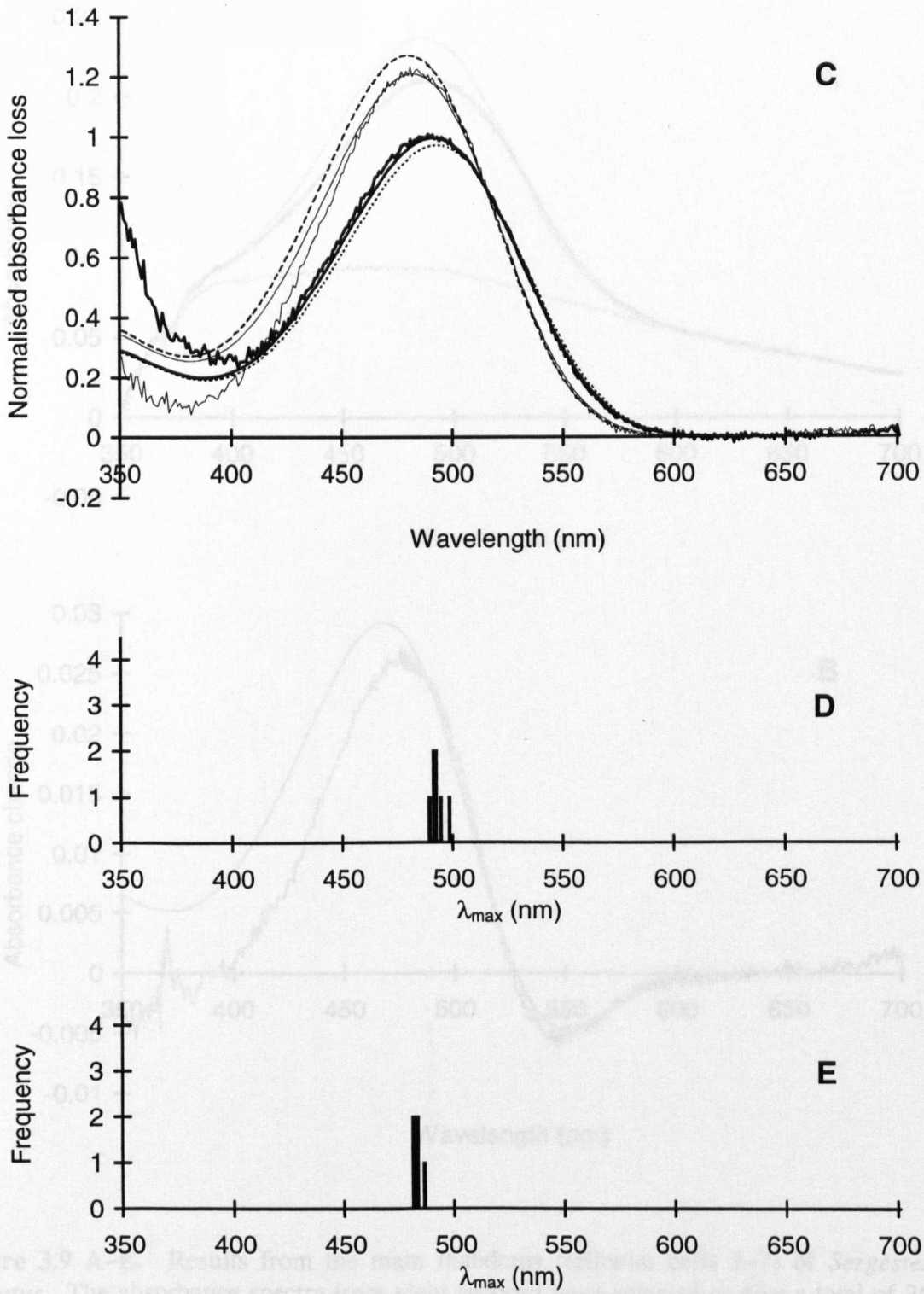

Figure 3.8 A–E. (Continued).

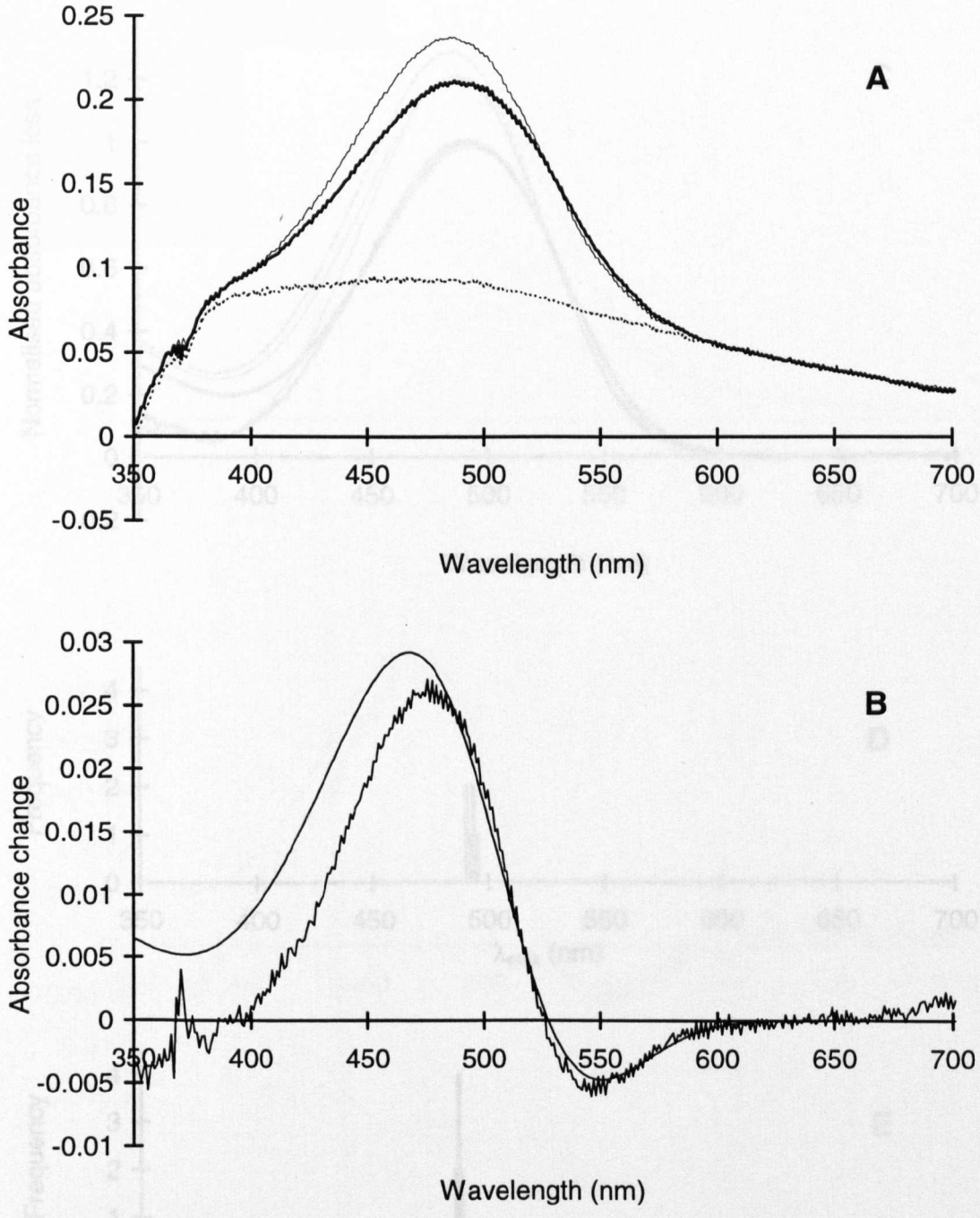

Figure 3.9 A–E. Results from the main rhabdoms (retinular cells 1–7) of *Sergestes curvatus*. The absorbance spectra from eight sections were selected to give a total of 26 difference spectra which constitute the average files of mix_1 and mix_2. The λ_{max} values of the best-fit templates for mix_1 and mix_2 are 492.1 and 485.6 nm, and the λ_{max} values of the *R* and *M* estimates are 492.6 and 483.9 nm with an estimated *M* to *R* extinction ratio of 1.305. The average maximum corrected absorbance loss for the mix_1 photobleach is 0.1173.

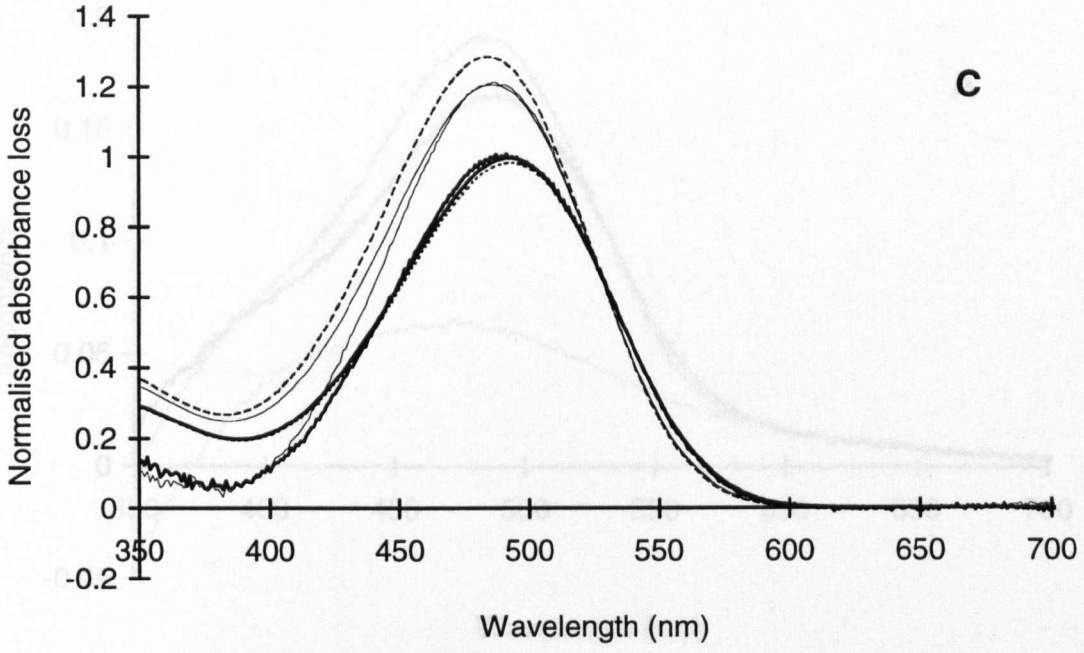

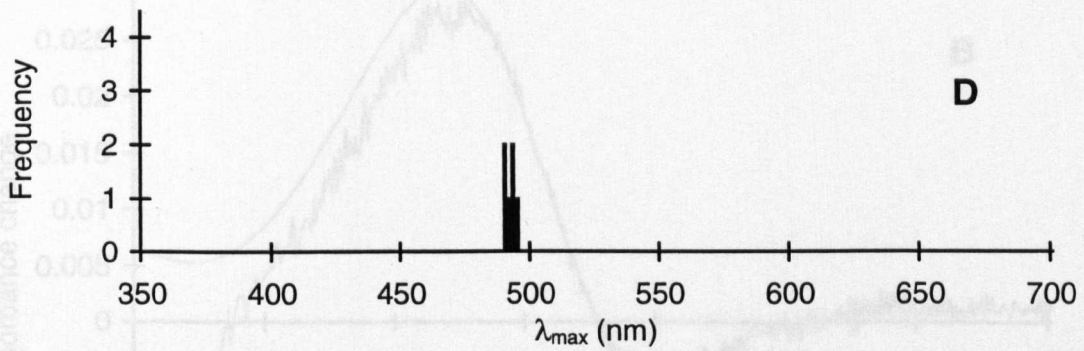

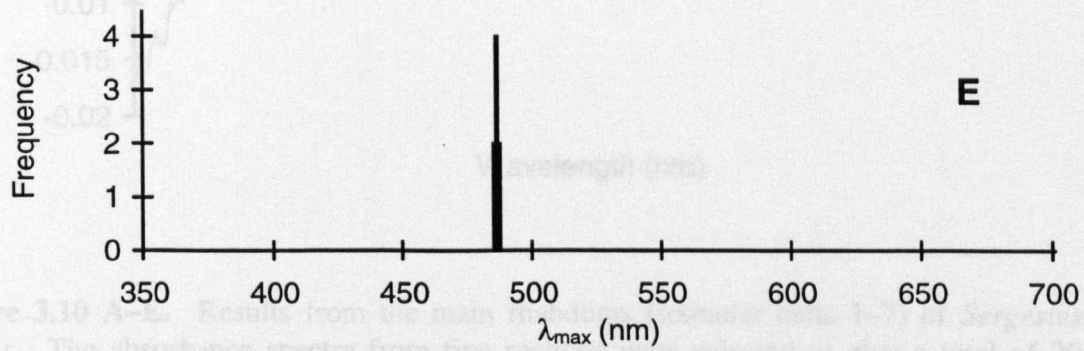

Figure 3.9 A–E. (Continued).

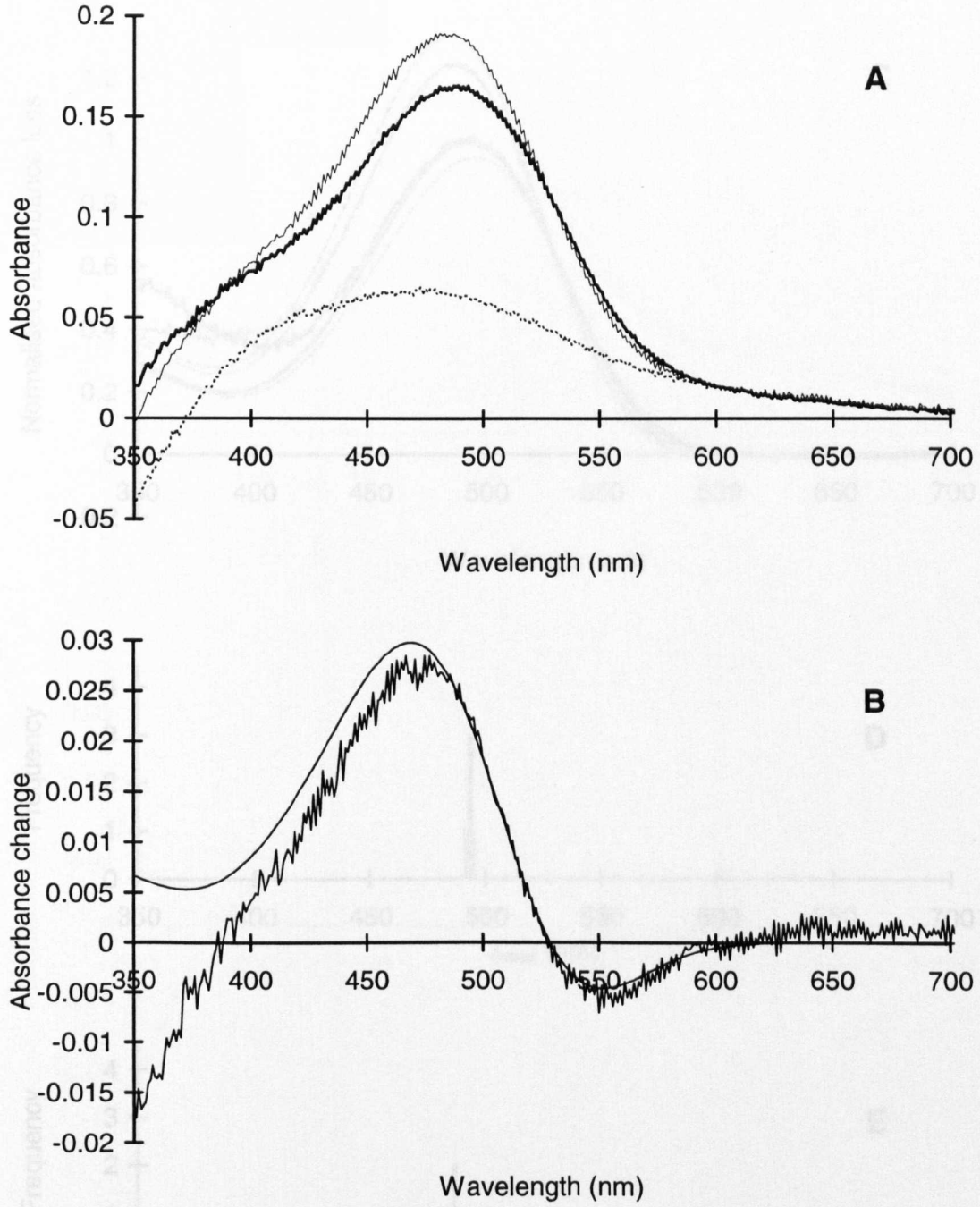

Figure 3.10 A–E. Results from the main rhabdoms (retinular cells 1–7) of *Sergestes similis*. The absorbance spectra from five sections were selected to give a total of 20 difference spectra which constitute the average files of mix_1 and mix_2. The λ_{max} values of the best-fit templates for mix_1 and mix_2 are 492.3 and 485.3 nm, and the λ_{max} values of the *R* and *M* estimates are 494.6 and 483.6 nm with an estimated *M* to *R* extinction ratio of 1.406. The average maximum corrected absorbance loss for the mix_1 photobleach is 0.1034.

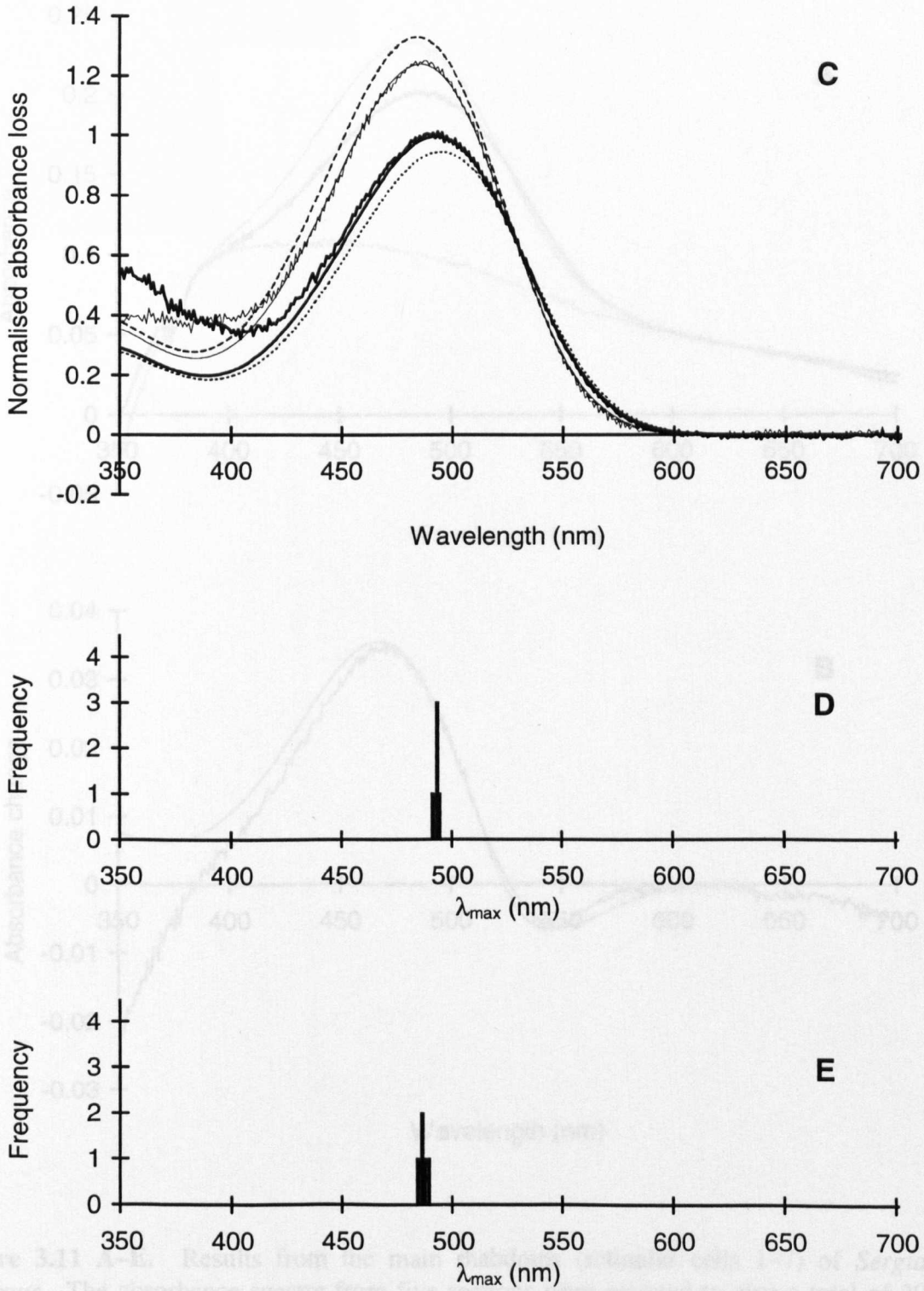

Figure 3.10 A–E. (Continued).

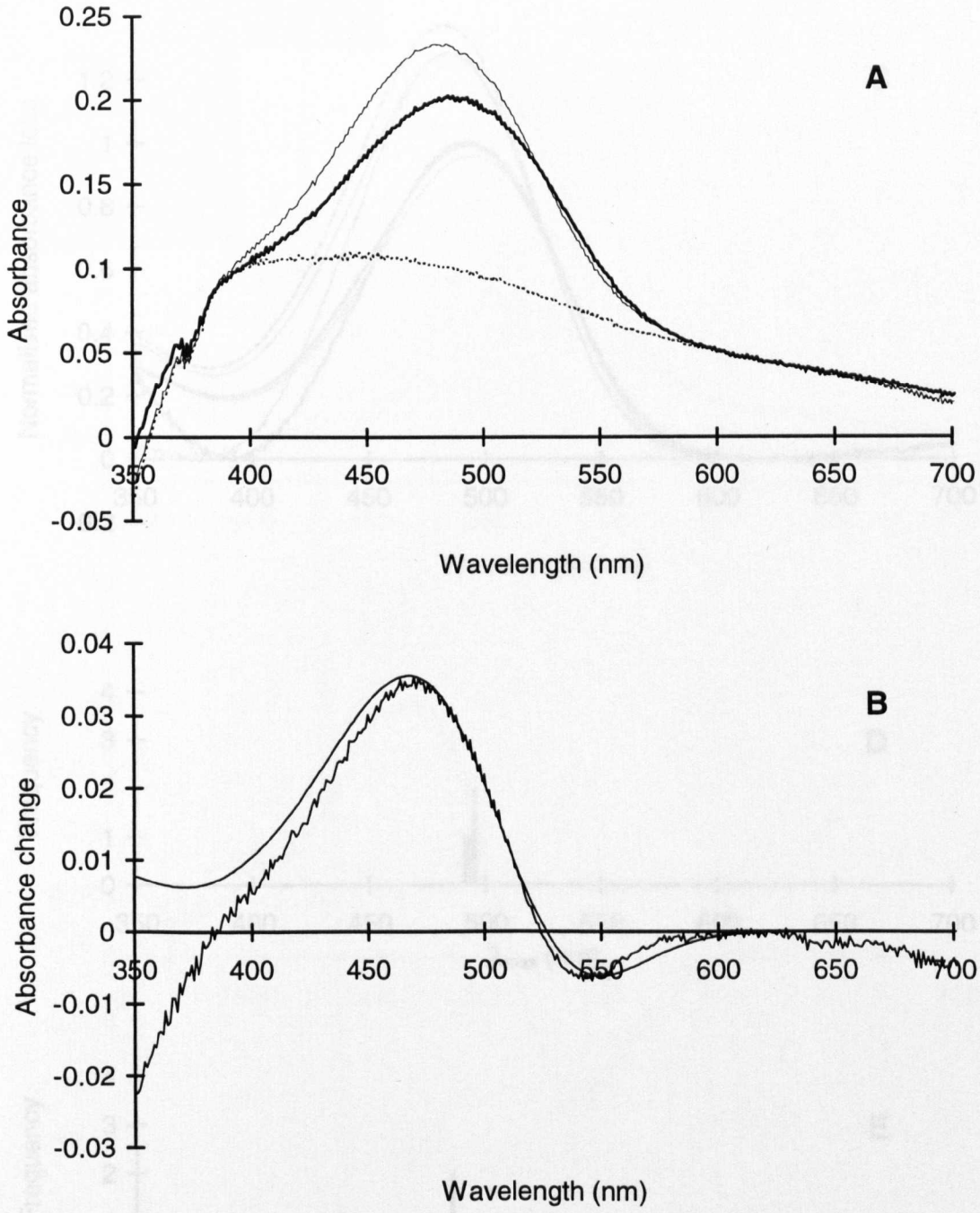

Figure 3.11 A–E. Results from the main rhabdoms (retinular cells 1–7) of *Sergia maximus*. The absorbance spectra from five sections were selected to give a total of 20 difference spectra which constitute the average files of mix_1 and mix_2. The λ_{max} values of the best-fit templates for mix_1 and mix_2 are 492.8 and 484.1 nm, and the λ_{max} values of the *R* and *M* estimates are 494.5 and 482.4 nm with an estimated *M* to *R* extinction ratio of 1.426. The average maximum corrected absorbance loss for the mix_1 photobleach is 0.1025.

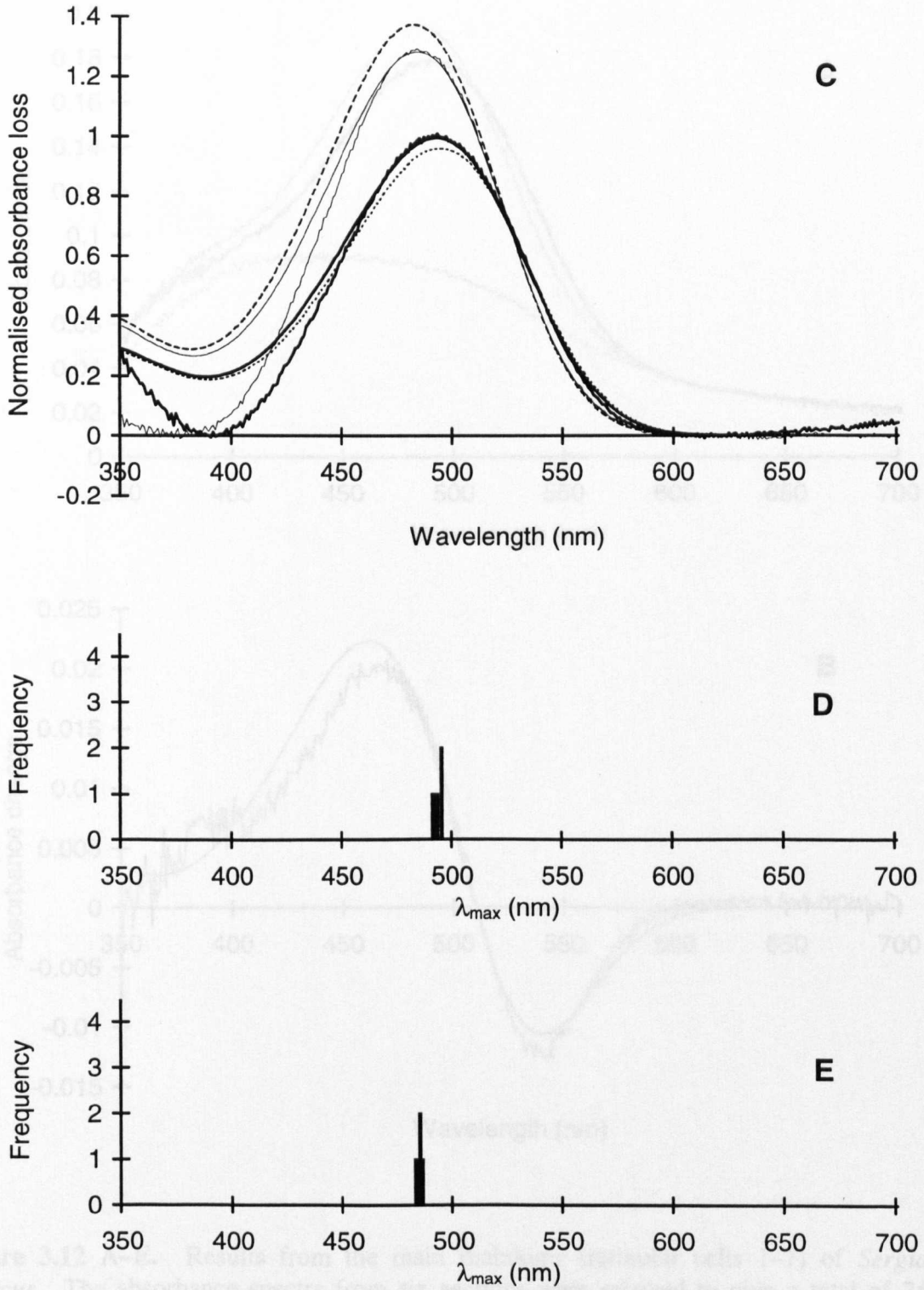

Figure 3.11 A–E. (Continued).

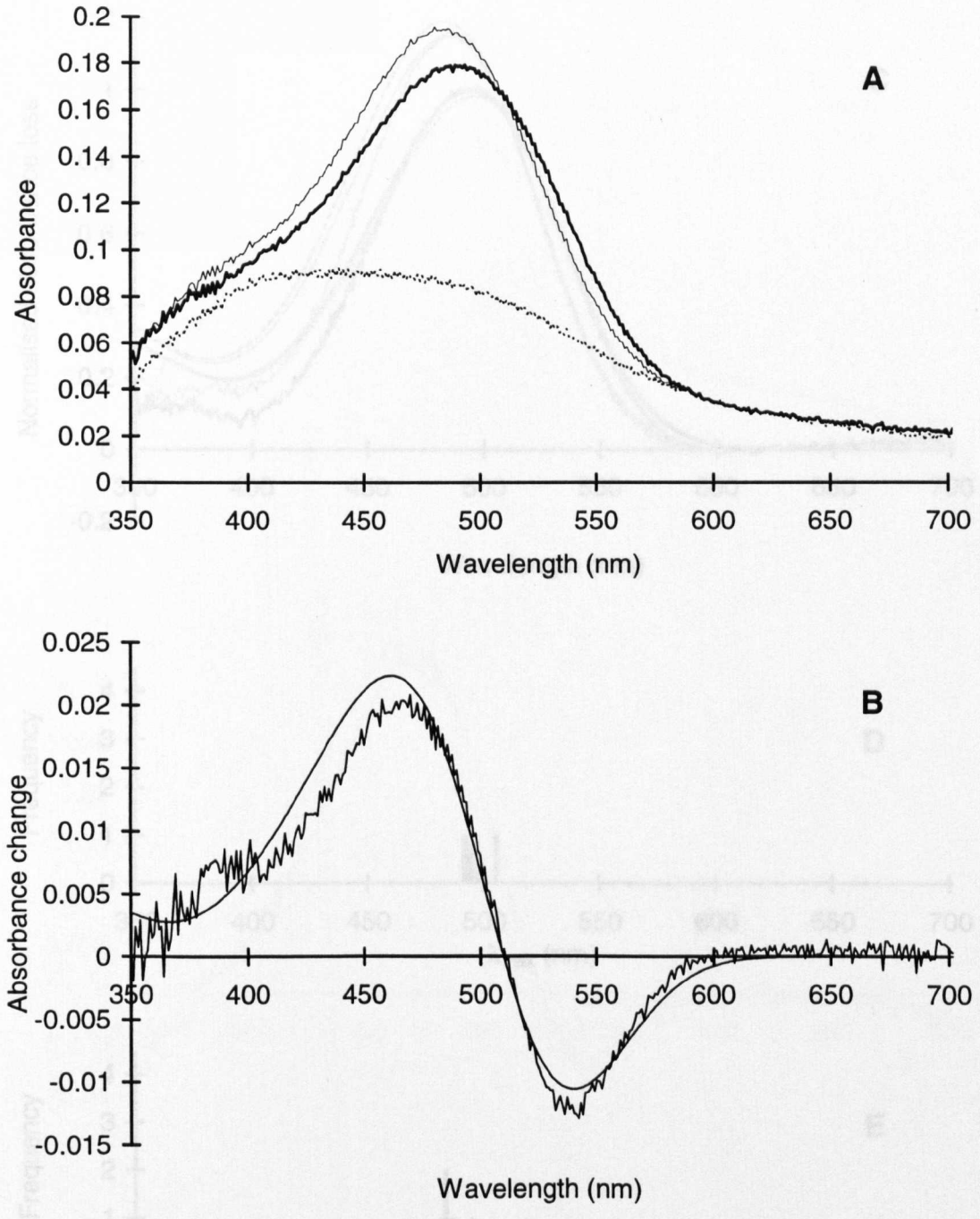

Figure 3.12 A–E. Results from the main rhabdoms (retinular cells 1–7) of *Sergia phorcus*. The absorbance spectra from six sections were selected to give a total of 24 difference spectra which constitute the average files of mix_1 and mix_2. The λ_{max} values of the best-fit templates for mix_1 and mix_2 are 493.6 and 483.9 nm, and the λ_{max} values of the *R* and *M* estimates are 495.2 and 482.2 nm with an estimated *M* to *R* extinction ratio of 1.212. The average maximum corrected absorbance loss for the mix_1 photobleach is 0.0939.

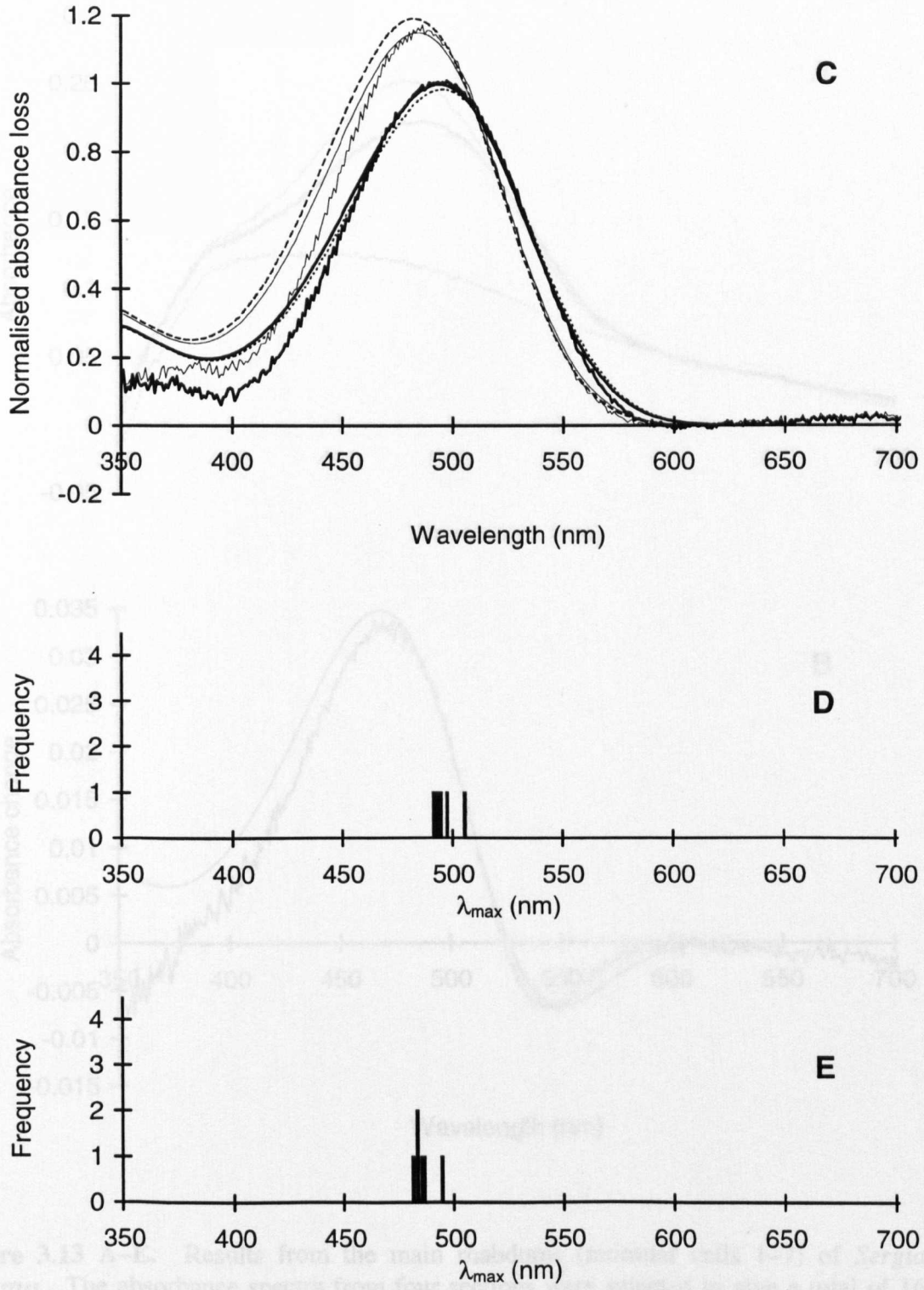

Figure 3.12 A–E. (Continued).

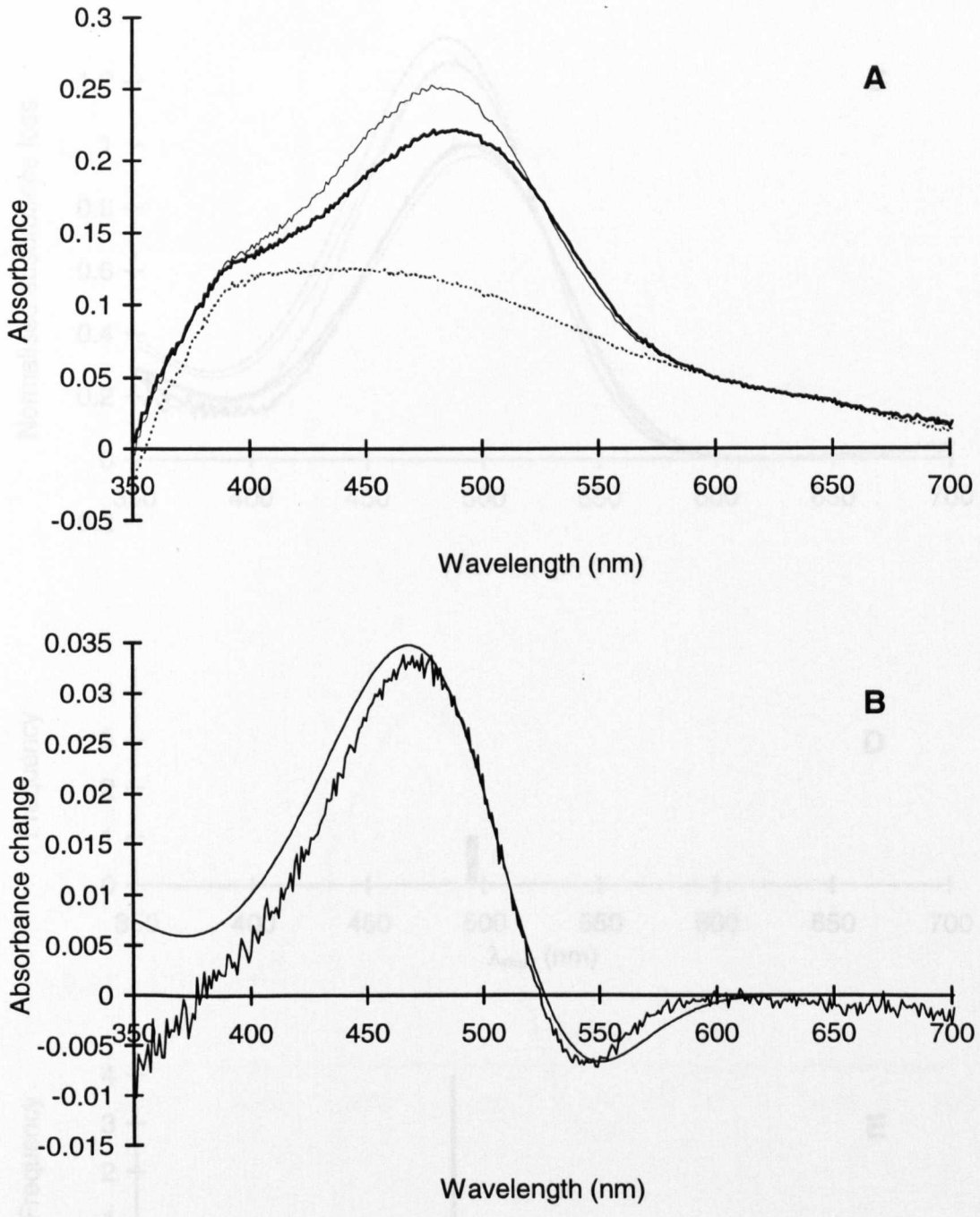

Figure 3.13 A–E. Results from the main rhabdoms (retinular cells 1–7) of *Sergia robustus*. The absorbance spectra from four sections were selected to give a total of 16 difference spectra which constitute the average files of mix_1 and mix_2. The λ_{max} values of the best-fit templates for mix_1 and mix_2 are 493.9 and 485.4 nm, and the λ_{max} values of the *R* and *M* estimates are 495.5 and 483.7 nm with an estimated *M* to *R* extinction ratio of 1.389. The average maximum corrected absorbance loss for the mix_1 photobleach is 0.1083.

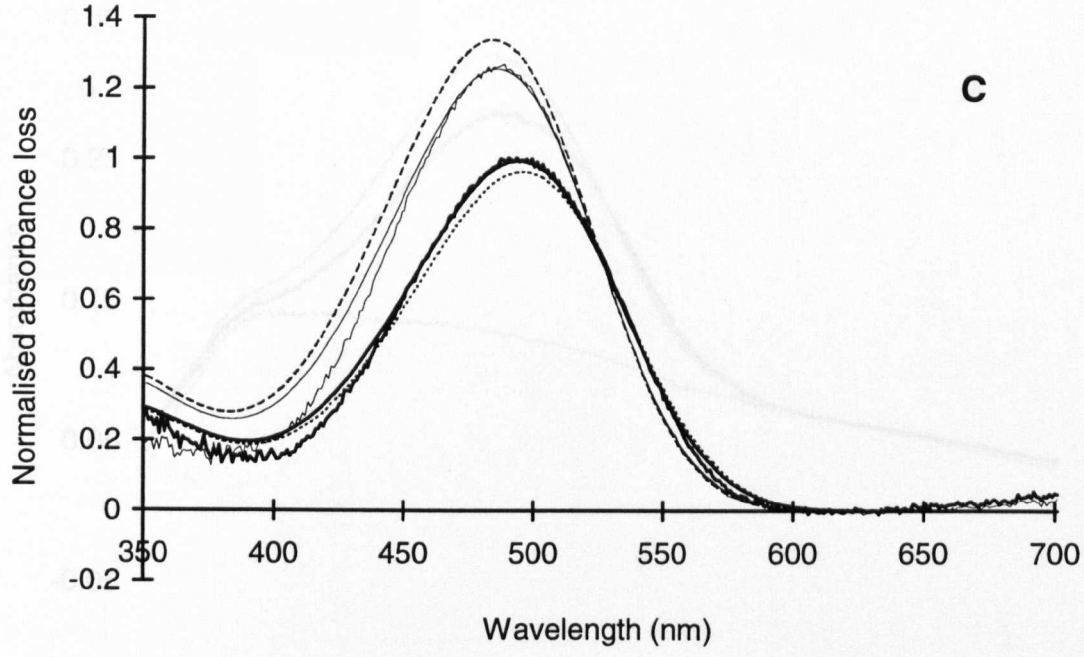

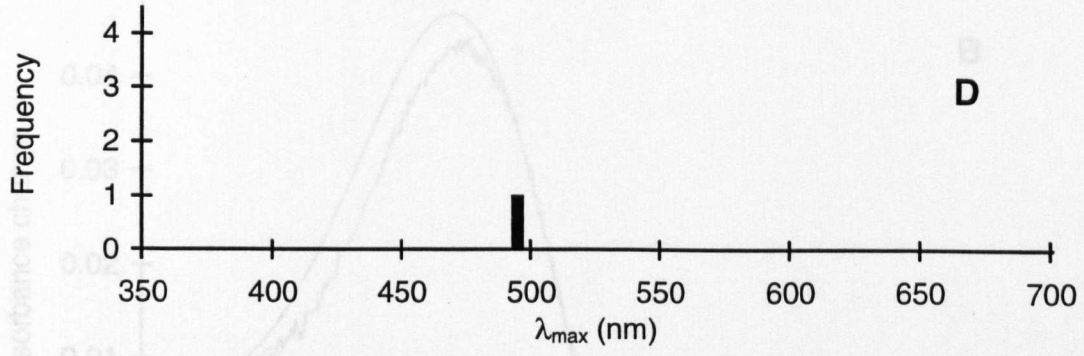

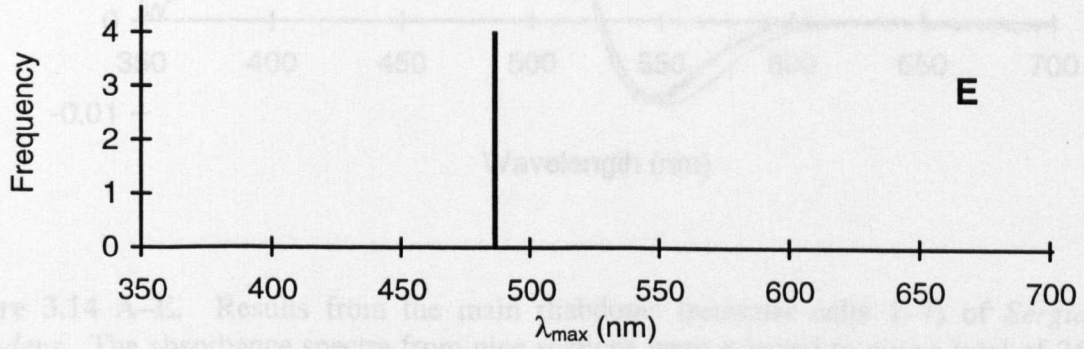

Figure 3.13 A–E. (Continued).

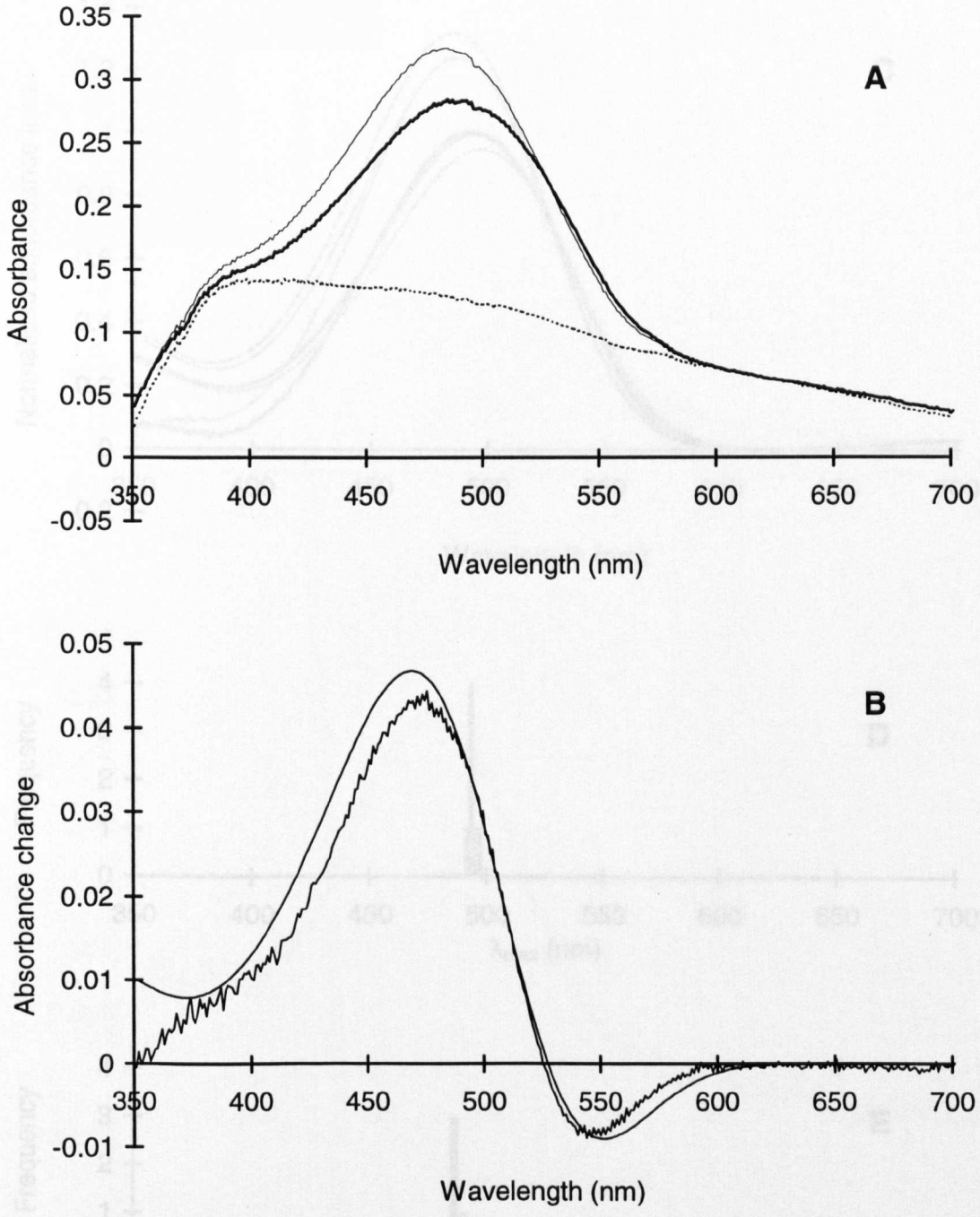

Figure 3.14 A–E. Results from the main rhabdoms (retinular cells 1–7) of *Sergia splendens*. The absorbance spectra from nine sections were selected to give a total of 36 difference spectra which constitute the average files of mix_1 and mix_2. The λ_{max} values of the best-fit templates for mix_1 and mix_2 are 494.2 and 486.5 nm, and the λ_{max} values of the *R* and *M* estimates are 496.7 and 484.8 nm with an estimated *M* to *R* extinction ratio of 1.390. The average maximum corrected absorbance loss for the mix_1 photobleach is 0.1587.

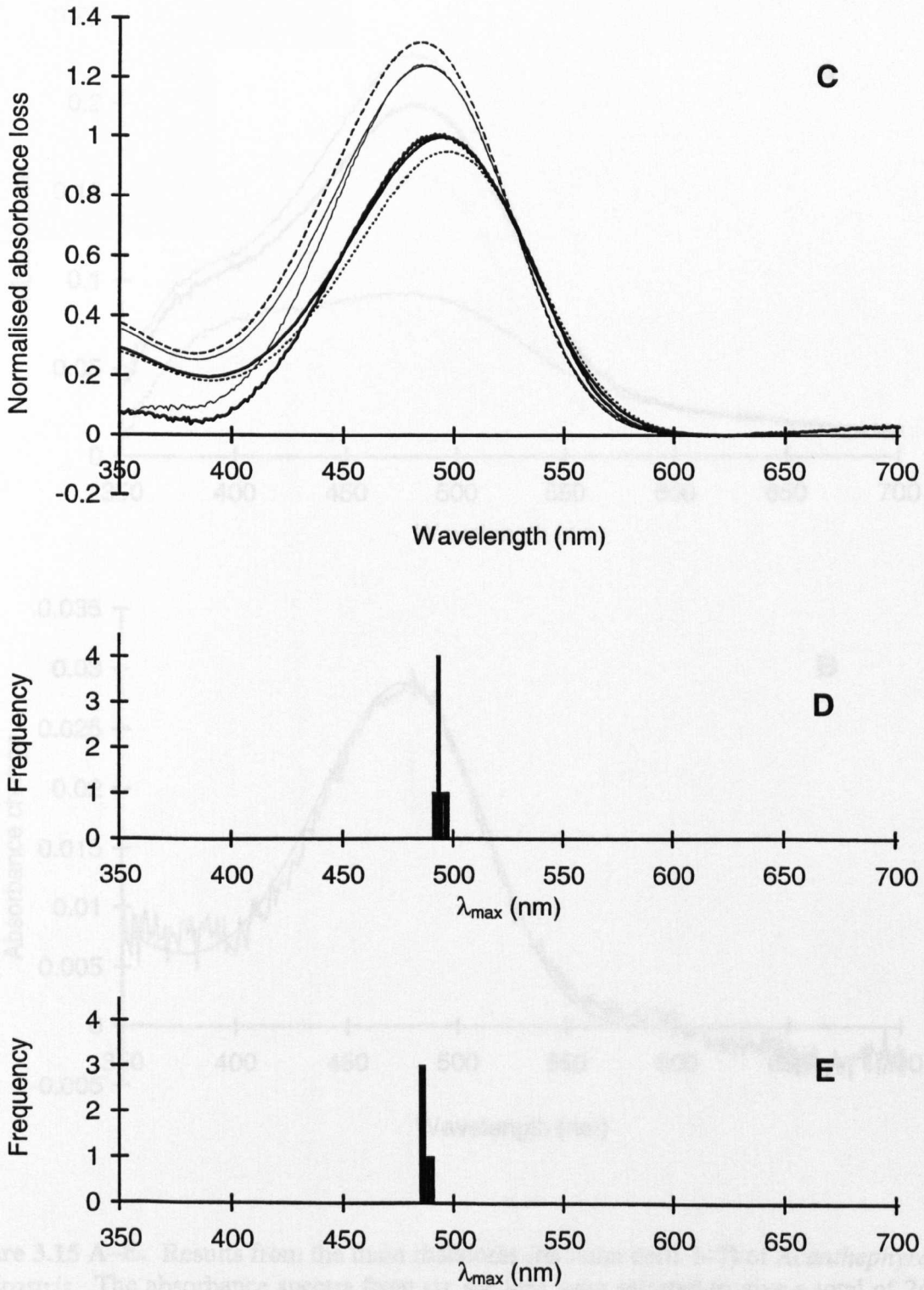

Figure 3.14 A–E. (Continued).

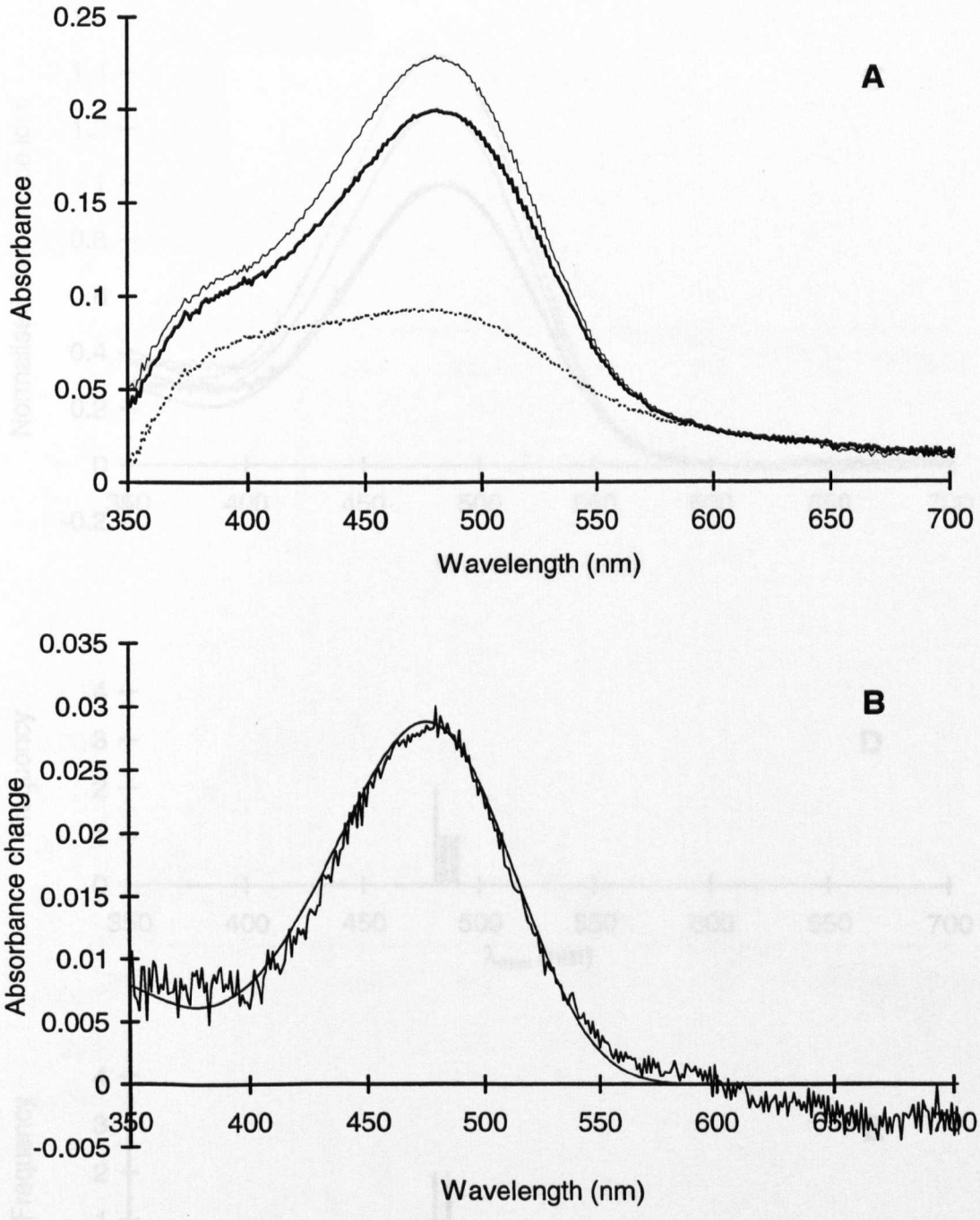

Figure 3.15 A–E. Results from the main rhabdoms (retinular cells 1–7) of *Acanthephyra curtirostris*. The absorbance spectra from six sections were selected to give a total of 24 difference spectra which constitute the average files of mix_1 and mix_2. The λ_{max} values of the best-fit templates for mix_1 and mix_2 are 484.8 and 482.7 nm, and the λ_{max} values of the *R* and *M* estimates are 484.7 and 481.6 nm with an estimated *M* to *R* extinction ratio of 1.466. The average maximum corrected absorbance loss for the mix_1 photobleach is 0.1067.

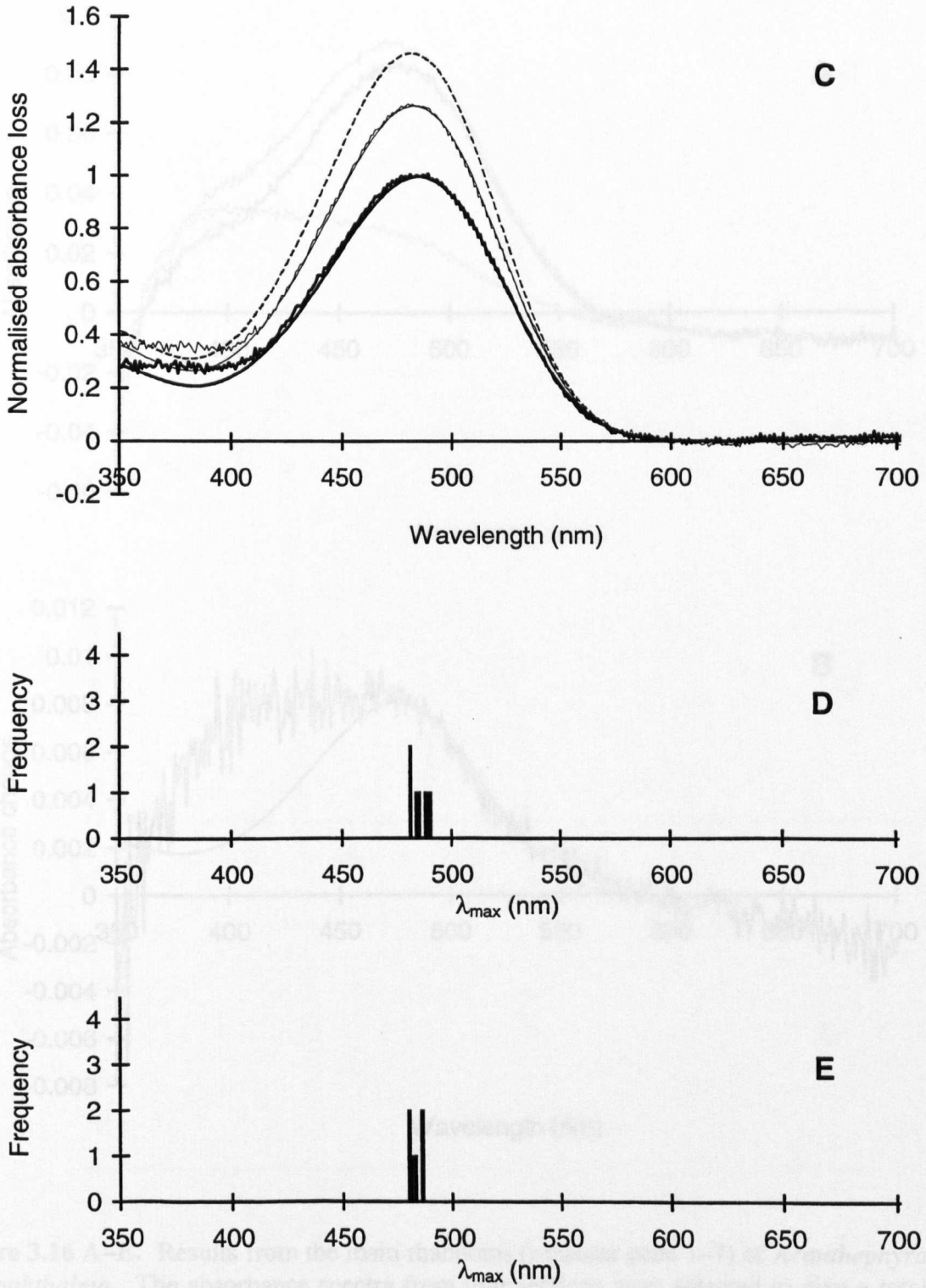

Figure 3.15 A–E. (Continued).

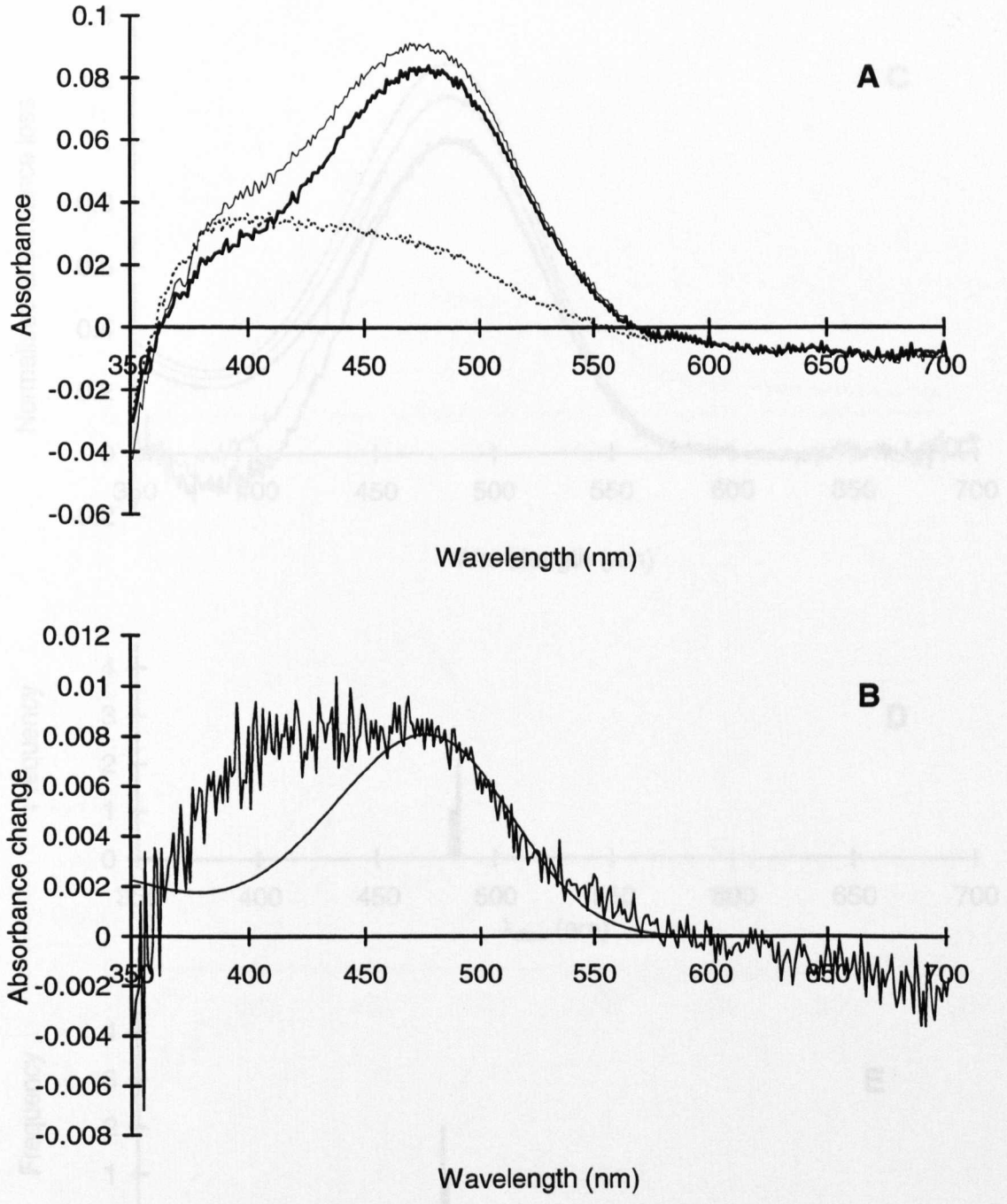

Figure 3.16 A–E. Results from the main rhabdoms (retinular cells 1–7) of *Acanthephyra microphthalma*. The absorbance spectra from four sections were selected to give a total of 9 difference spectra which constitute the average files of mix_1 and mix_2. The λ_{max} values of the best-fit templates for mix_1 and mix_2 are 481.6 and 480.9 nm, and the λ_{max} values of the *R* and *M* estimates are 481.5 and 480.4 nm with an estimated *M* to *R* extinction ratio of 1.253. The average maximum corrected absorbance loss for the mix_1 photobleach is 0.0573.

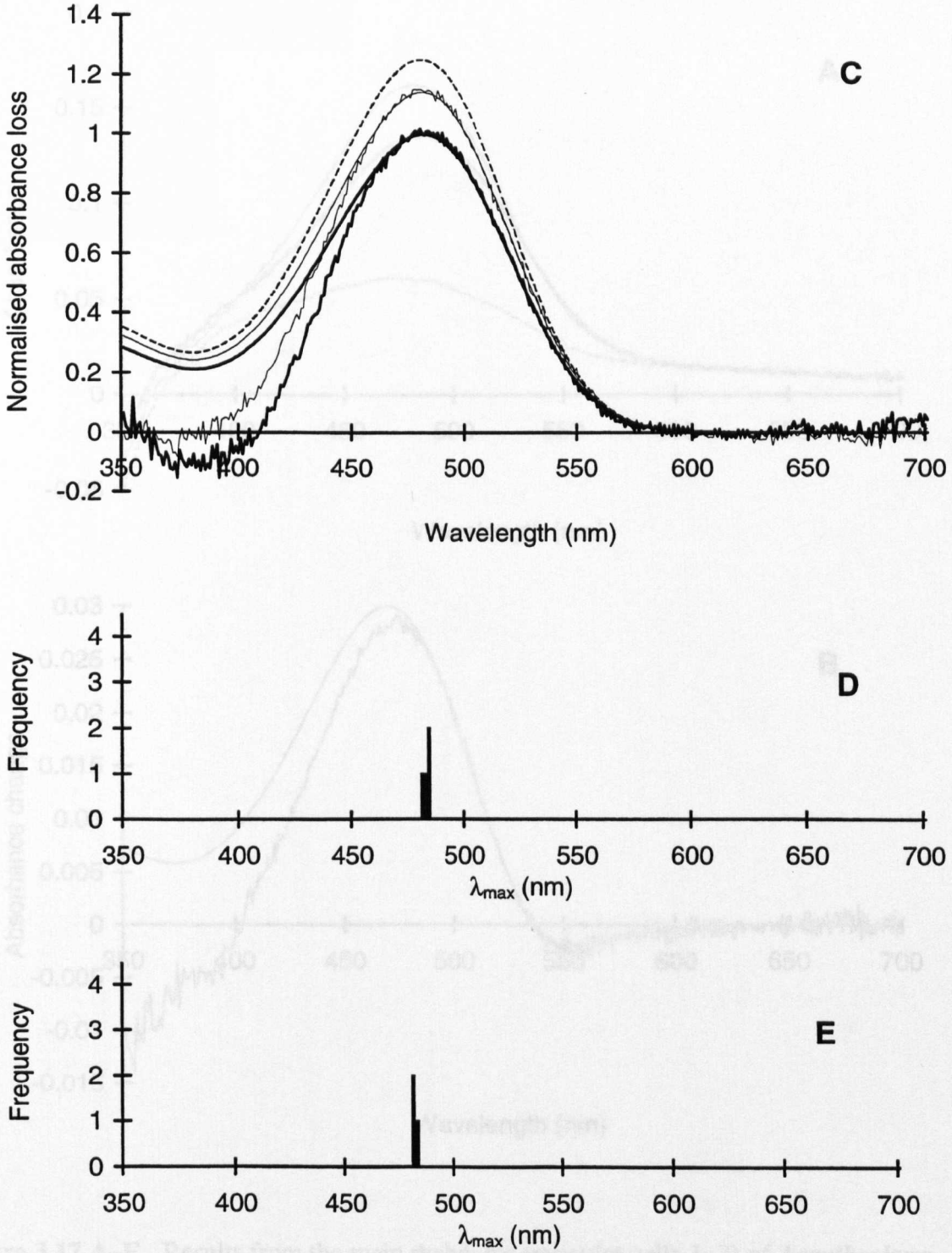

Figure 3.16 A–E. (Continued).

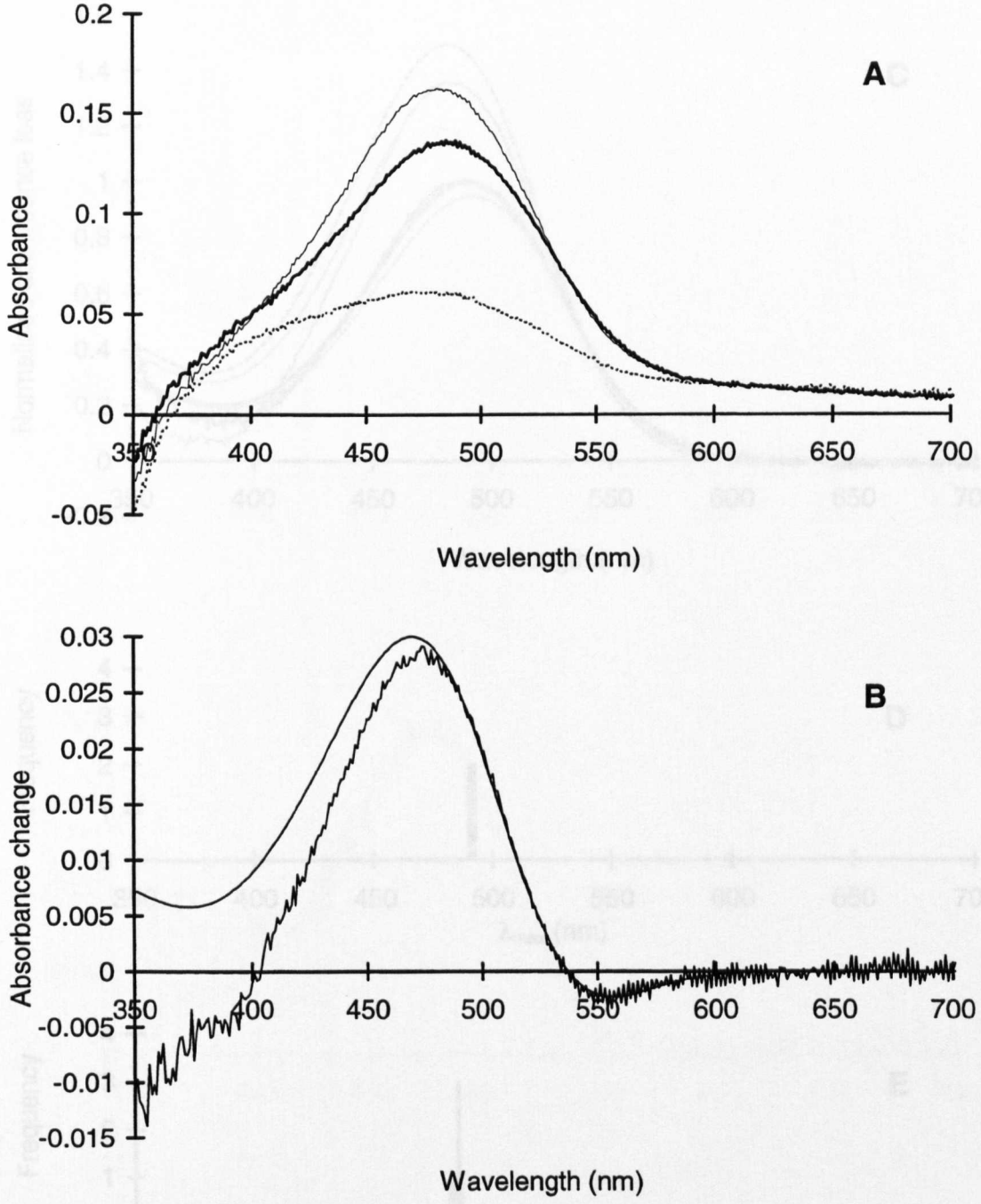

Figure 3.17 A–E. Results from the main rhabdoms (retinular cells 1–7) of *Acanthephyra purpurea*. The absorbance spectra from six sections were selected to give a total of 24 difference spectra which constitute the average files of mix_1 and mix_2. The λ_{max} values of the best-fit templates for mix_1 and mix_2 are 490.5 and 483.0 nm, and the λ_{max} values of the *R* and *M* estimates are 492.2 and 481.3 nm with an estimated *M* to *R* extinction ratio of 1.577. The average maximum corrected absorbance loss for the mix_1 photobleach is 0.0744.

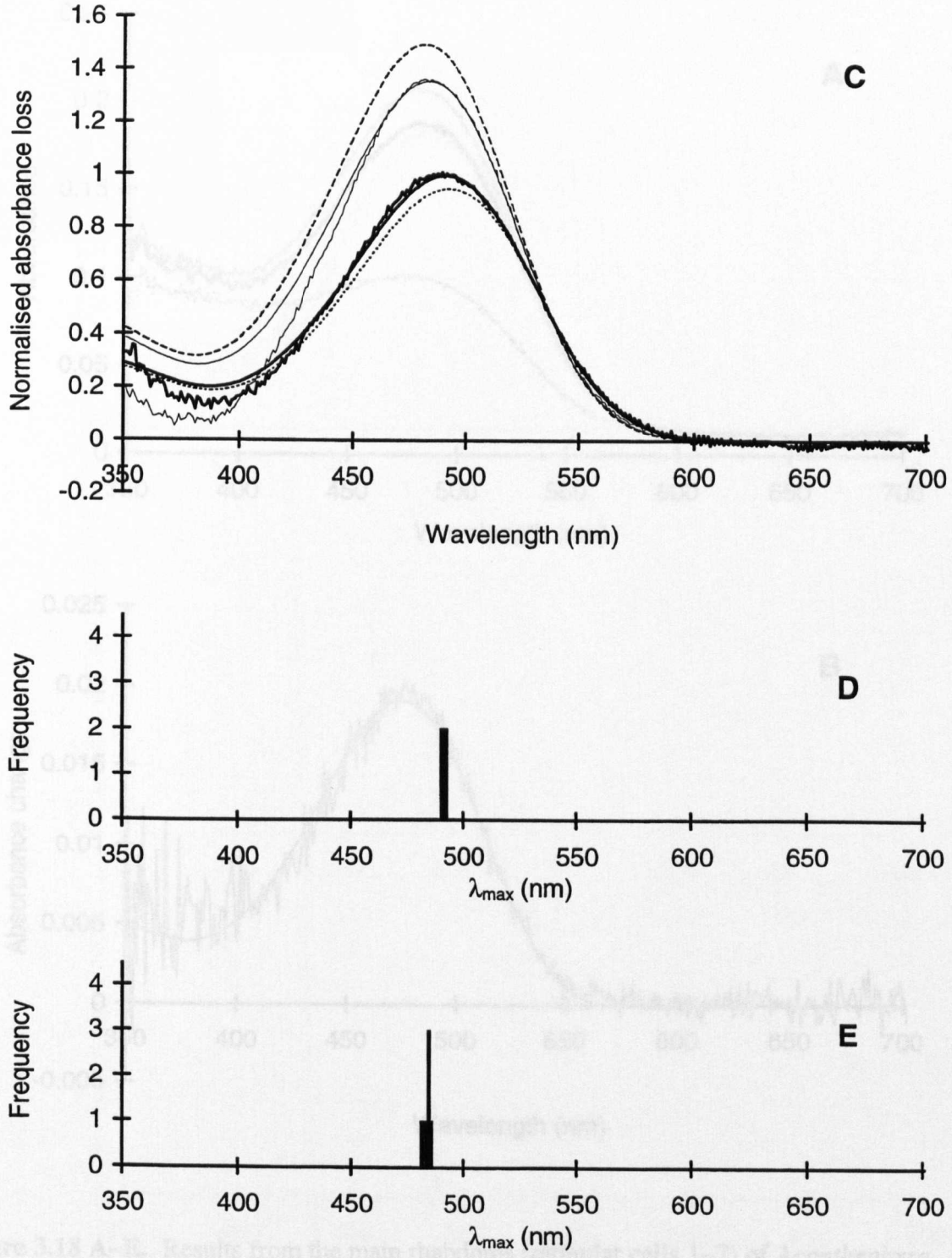

Figure 3.17 A–E. (Continued).

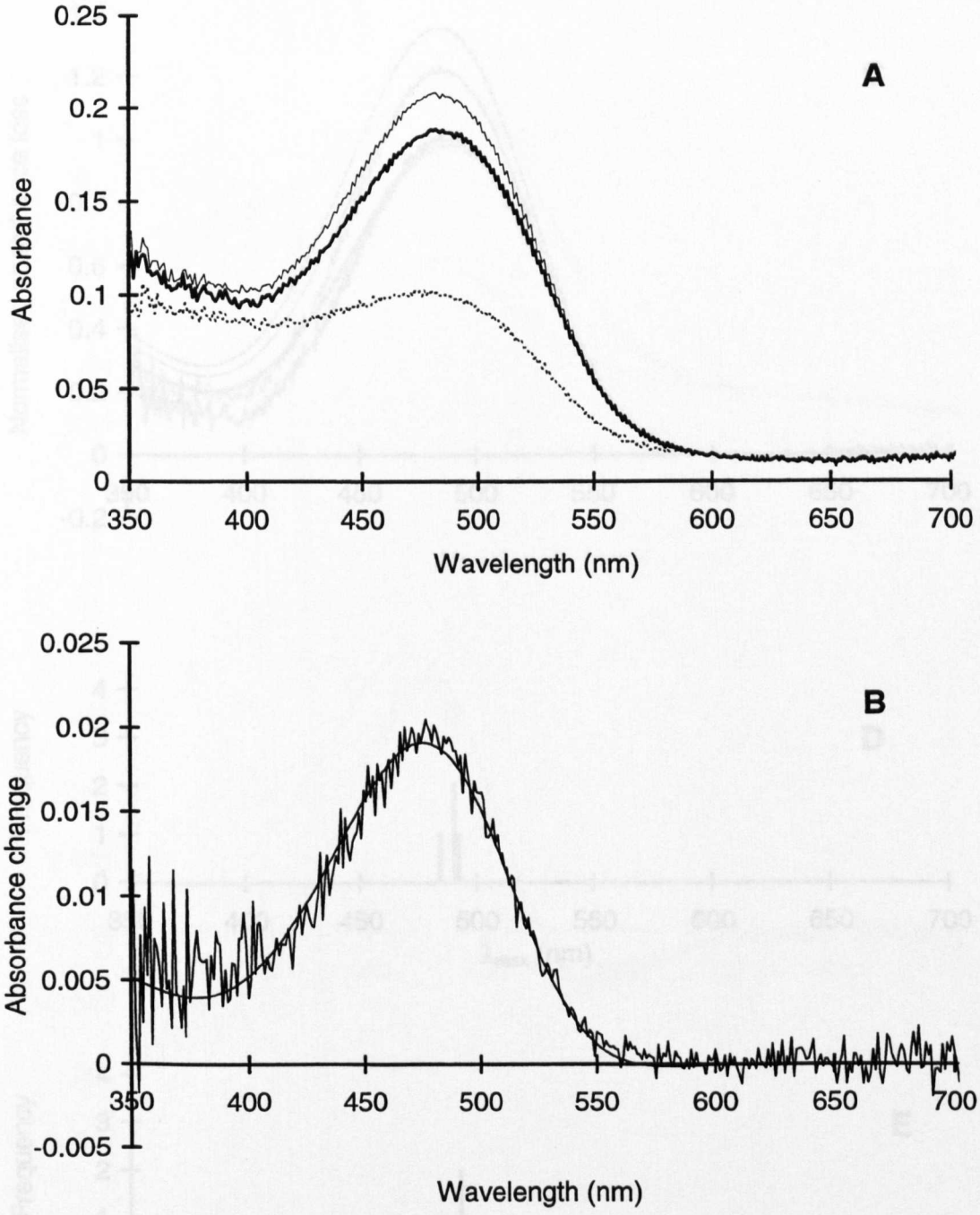

Figure 3.18 A–E. Results from the main rhabdoms (retinular cells 1–7) of *Acanthephyra stylorostratis*. The absorbance spectra from four sections were selected to give a total of 16 difference spectra which constitute the average files of mix_1 and mix_2. The λ_{max} values of the best-fit templates for mix_1 and mix_2 are 488.3 and 485.7 nm, and the λ_{max} values of the *R* and *M* estimates are 488.5 and 484.4 nm with an estimated *M* to *R* extinction ratio of 1.382. The average maximum corrected absorbance loss for the mix_1 photobleach is 0.0875.

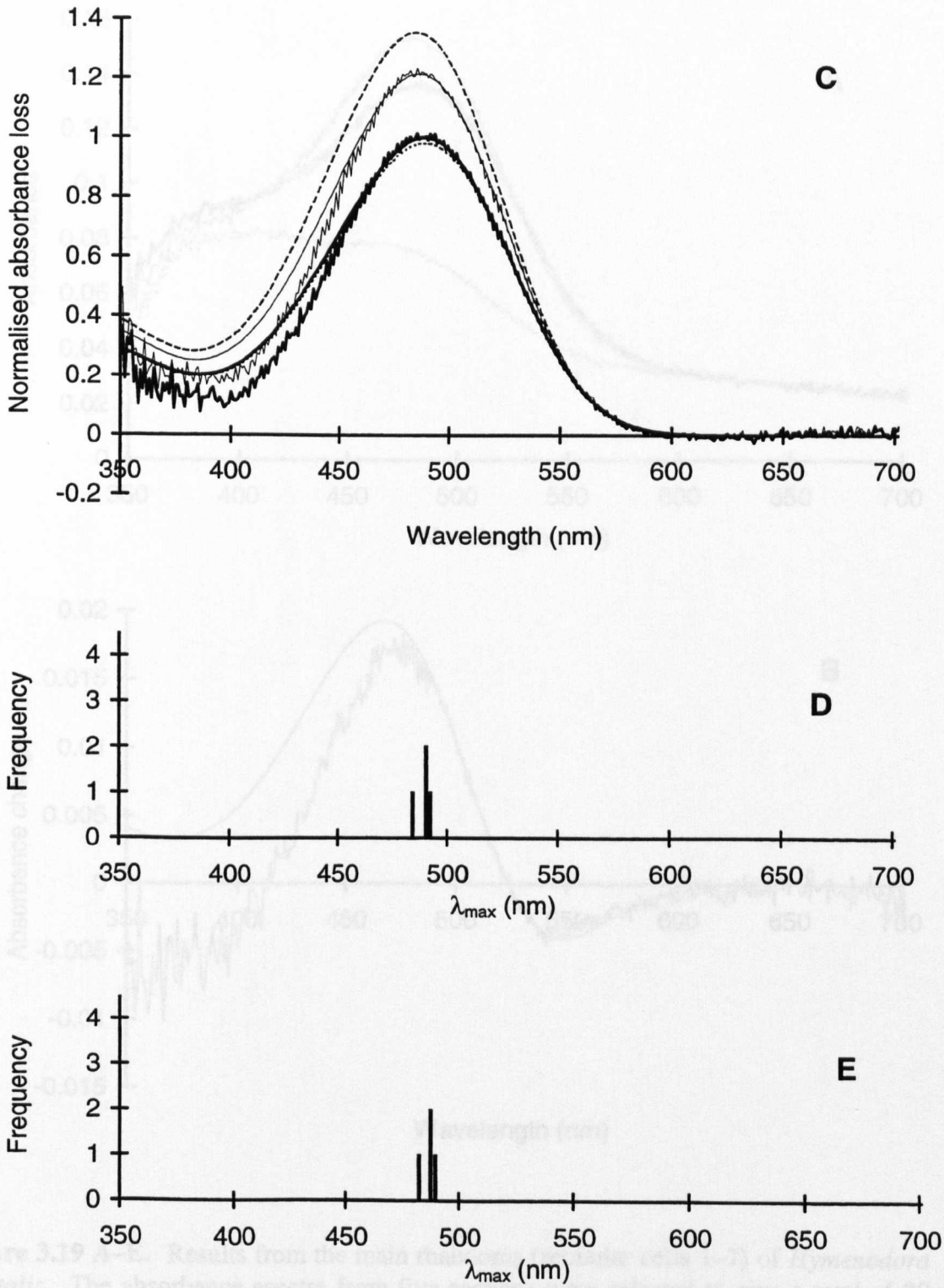

Figure 3.18 A–E. (Continued).

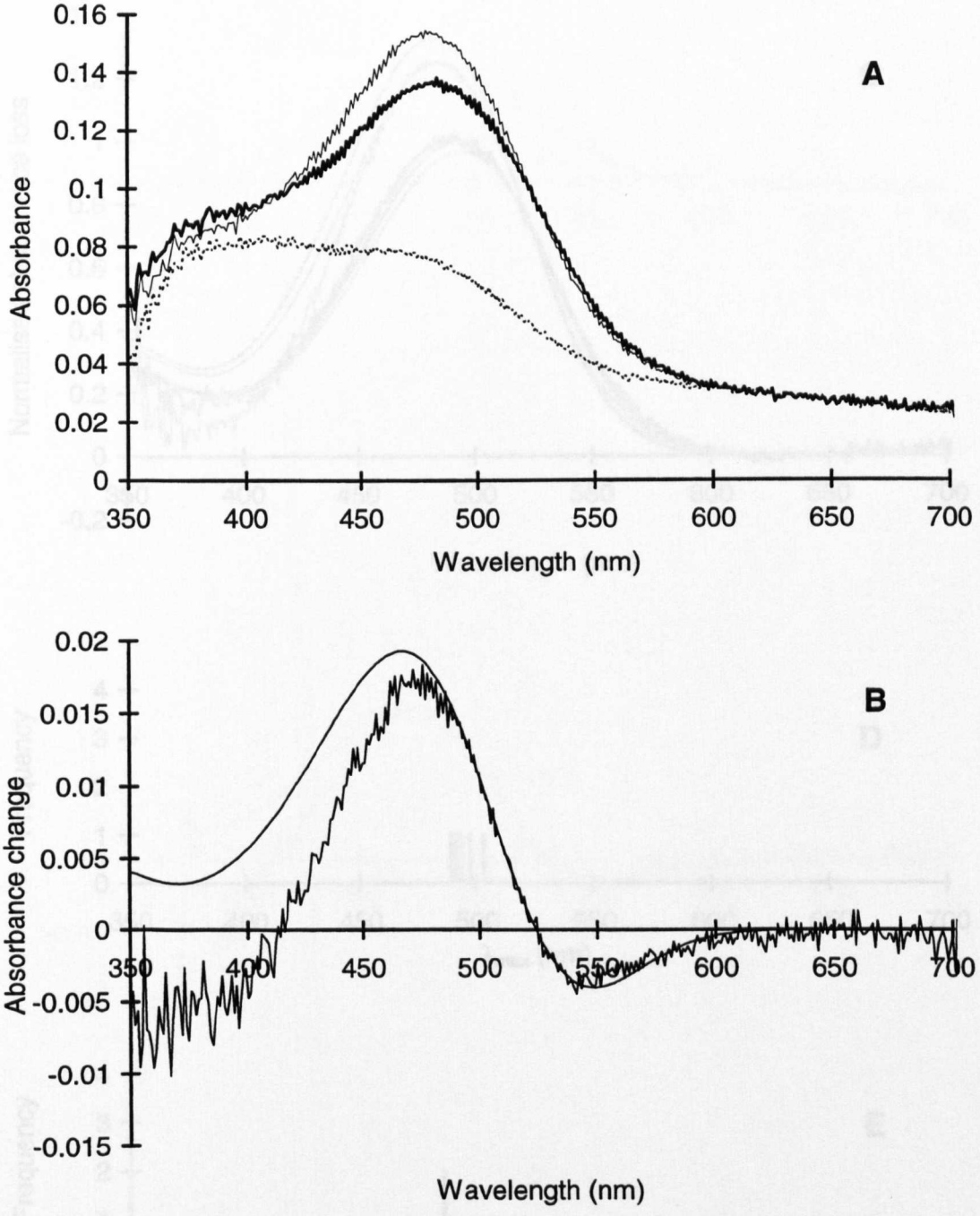

Figure 3.19 A–E. Results from the main rhabdoms (retinular cells 1–7) of *Hymenodora frontalis*. The absorbance spectra from five sections were selected to give a total of 20 difference spectra which constitute the average files of mix_1 and mix_2. The λ_{max} values of the best-fit templates for mix_1 and mix_2 are 493.1 and 484.6 nm, and the λ_{max} values of the *R* and *M* estimates are 494.7 and 482.9 nm with an estimated *M* to *R* extinction ratio of 1.370. The average maximum corrected absorbance loss for the mix_1 photobleach is 0.0622.

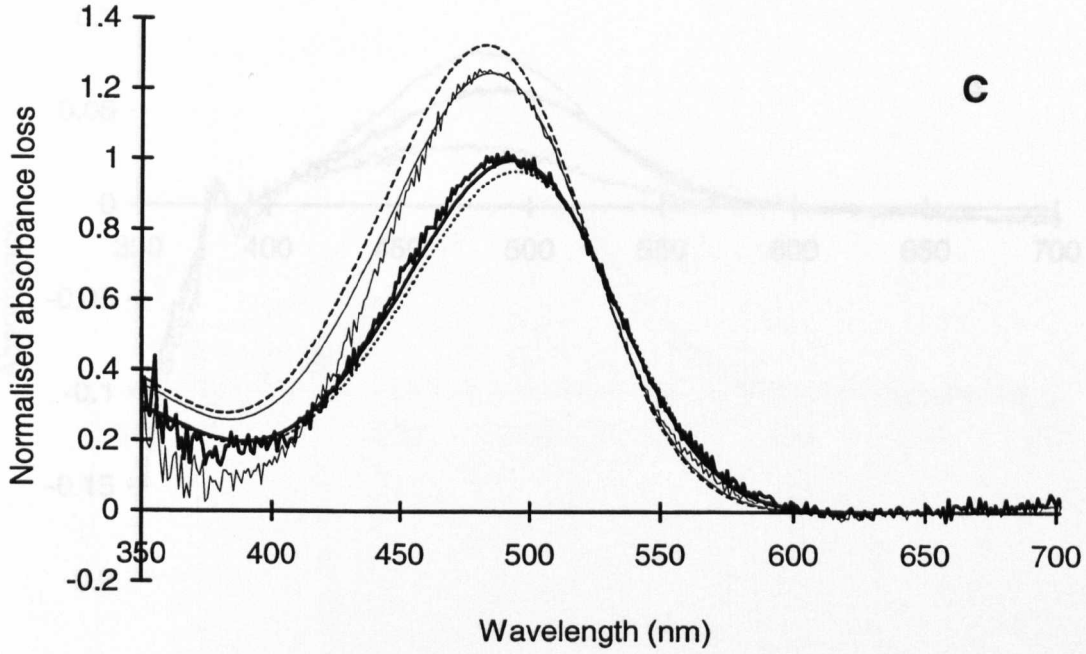

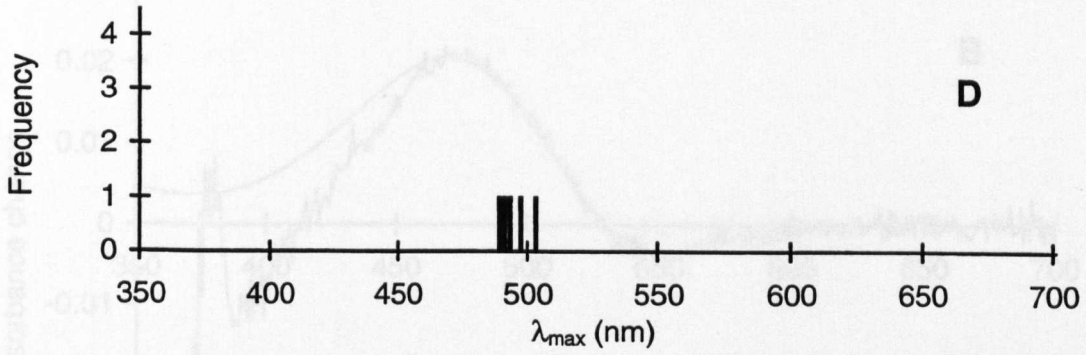

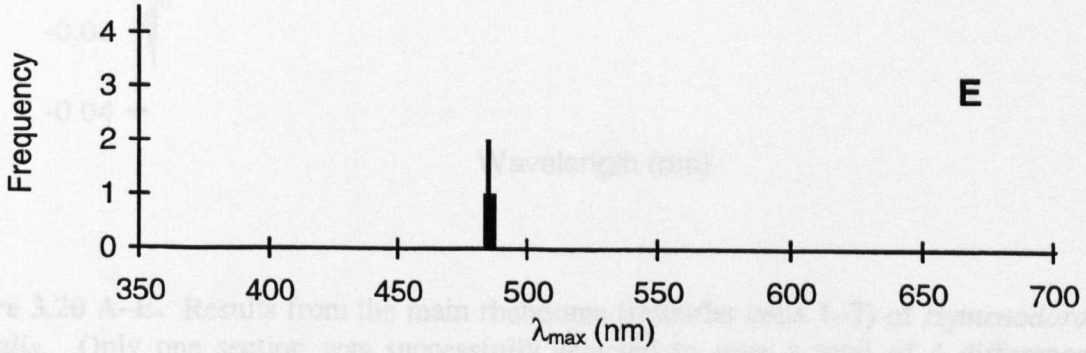

Figure 3.19 A–E. (Continued).

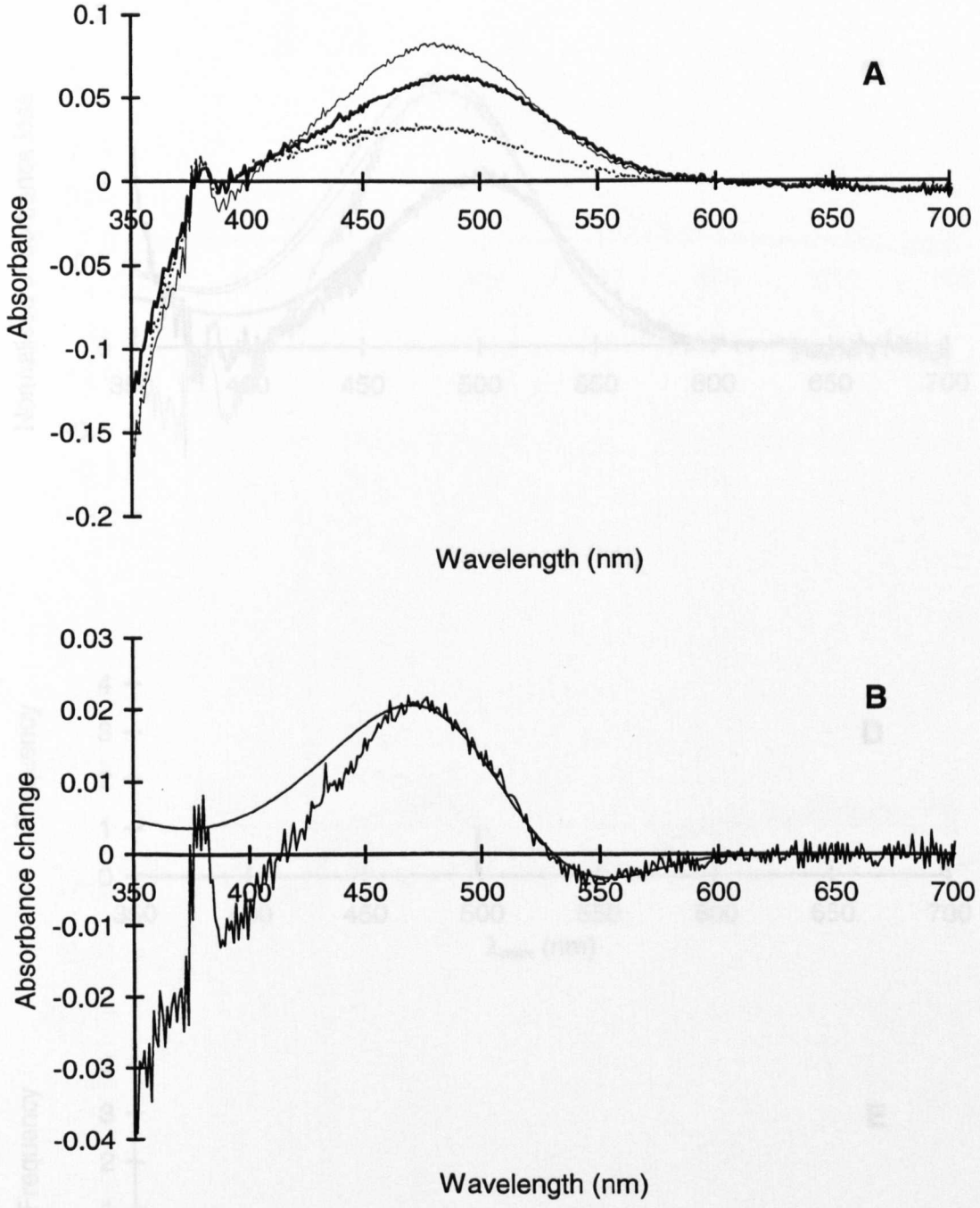

Figure 3.20 A–E. Results from the main rhabdoms (retinular cells 1–7) of *Hymenodora glacialis*. Only one section was successfully selected to give a total of 4 difference spectra which constitute the average files of mix_1 and mix_2. The λ_{max} values of the best-fit templates for mix_1 and mix_2 are 498.4 and 484.1 nm, and the λ_{max} values of the *R* and *M* estimates are 499.9 and 482.7 nm with an estimated *M* to *R* extinction ratio of 1.681. The average maximum corrected absorbance loss for the mix_1 photobleach is 0.0323.

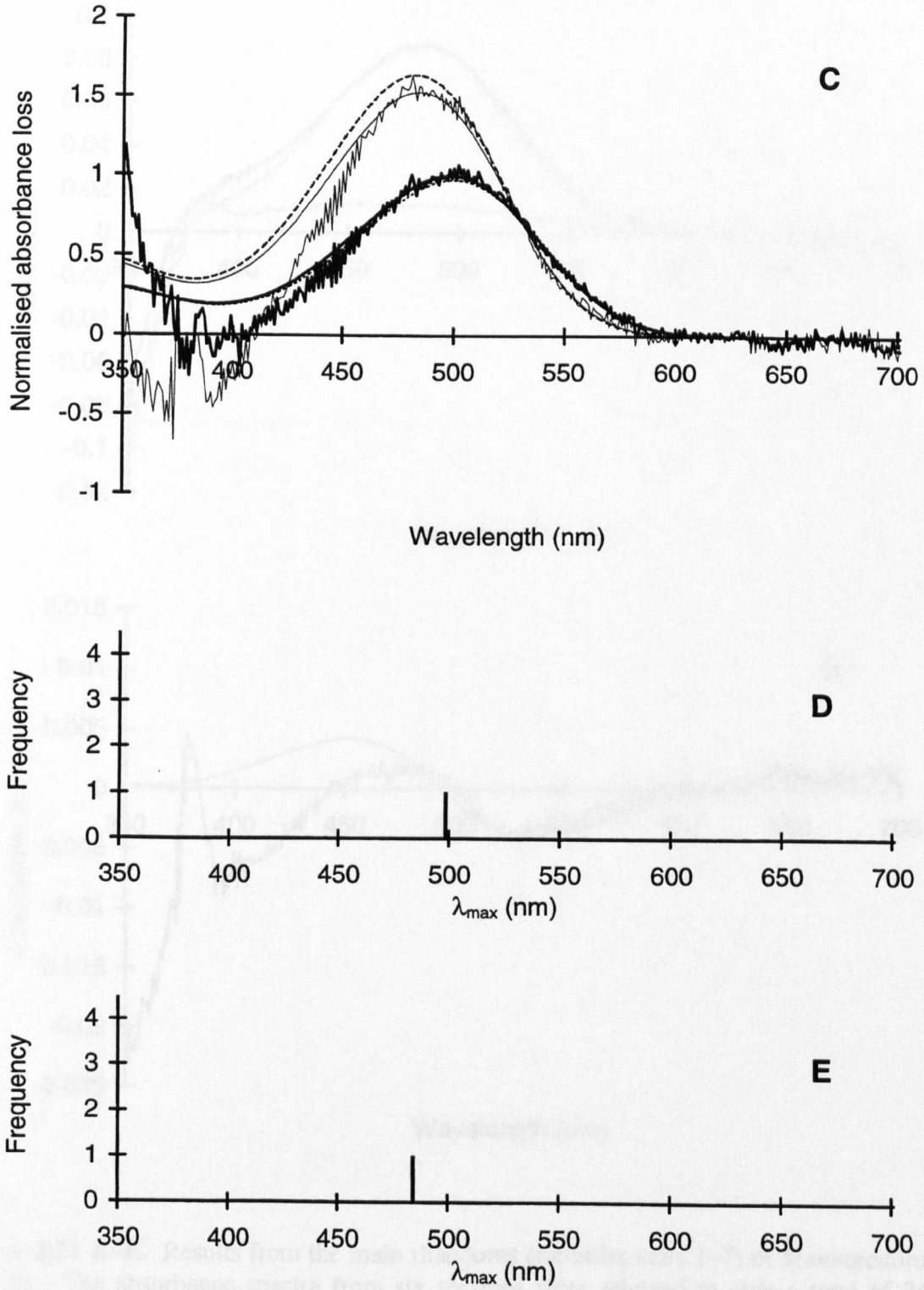

Figure 3.20 A–E. (Continued).

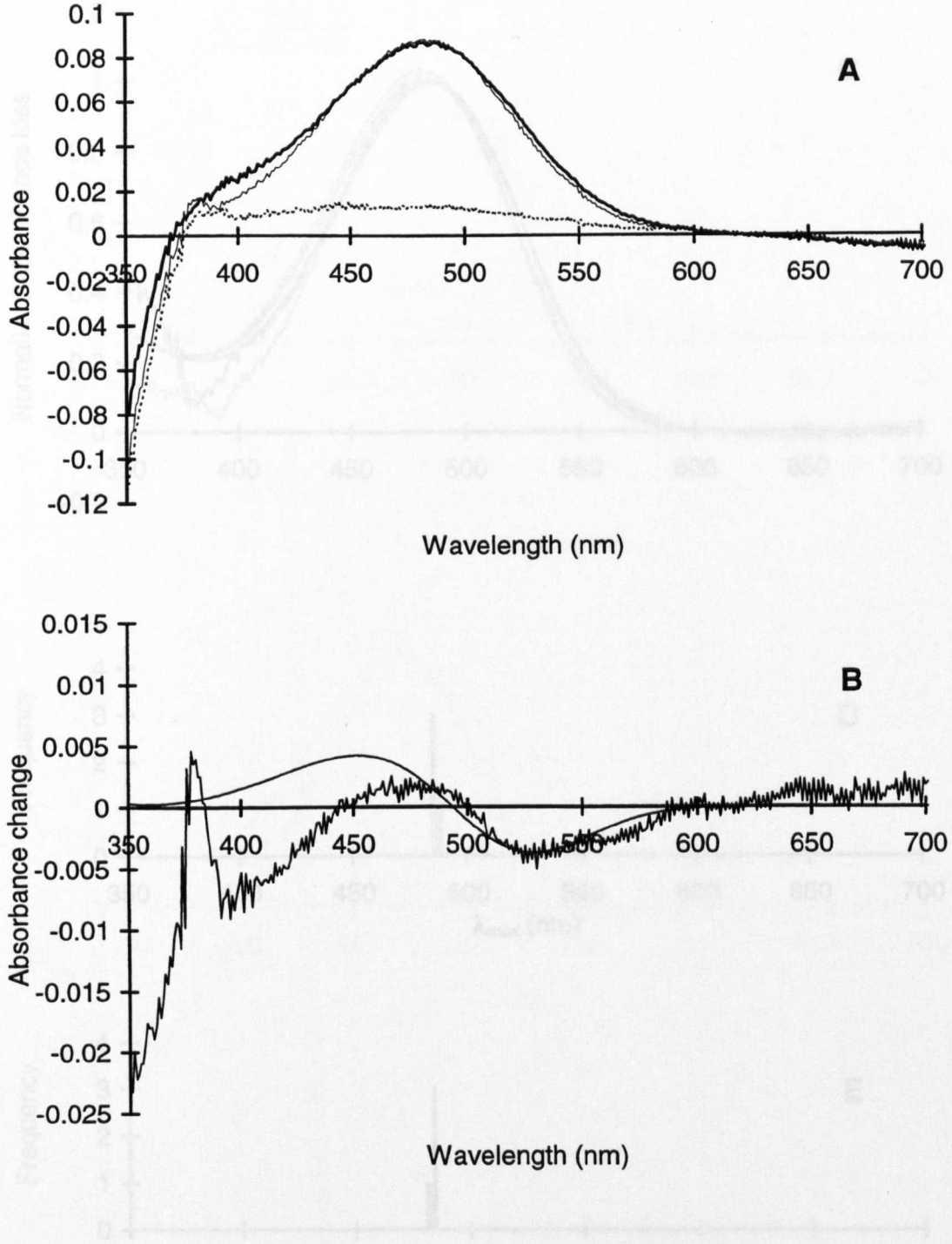

Figure 3.21 A–E. Results from the main rhabdoms (retinular cells 1–7) of *Meningodora miccyla*. The absorbance spectra from six sections were selected to give a total of 24 difference spectra which constitute the average files of mix_1 and mix_2. The λ_{max} values of the best-fit templates for mix_1 and mix_2 are 485.9 and 482.4 nm, and the λ_{max} values of the *R* and *M* estimates are 485.8 and 480.9 nm with an estimated *M* to *R* extinction ratio of 1.034. The average maximum corrected absorbance loss for the mix_1 photobleach is 0.0730.

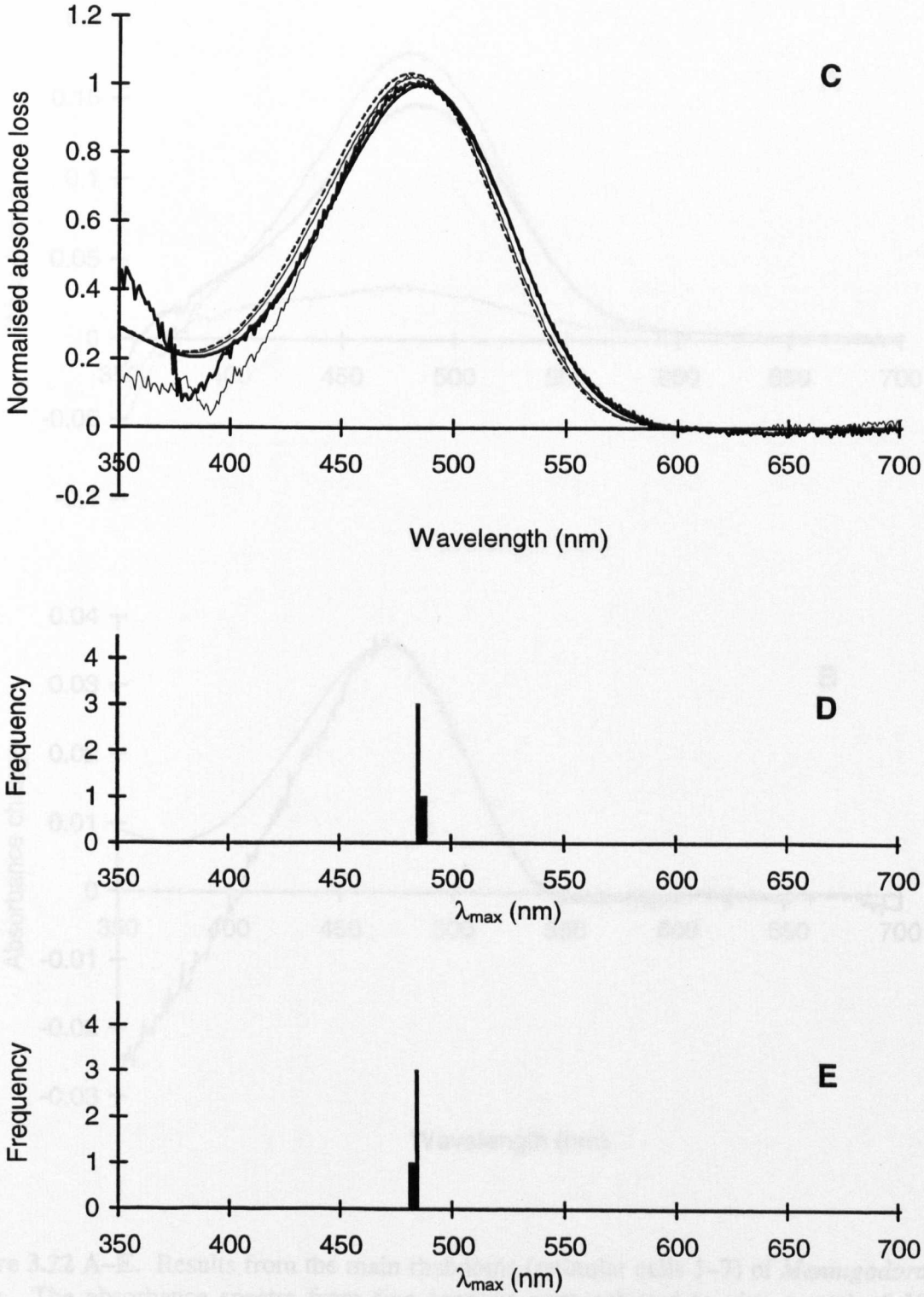

Figure 3.21 A–E. (Continued).

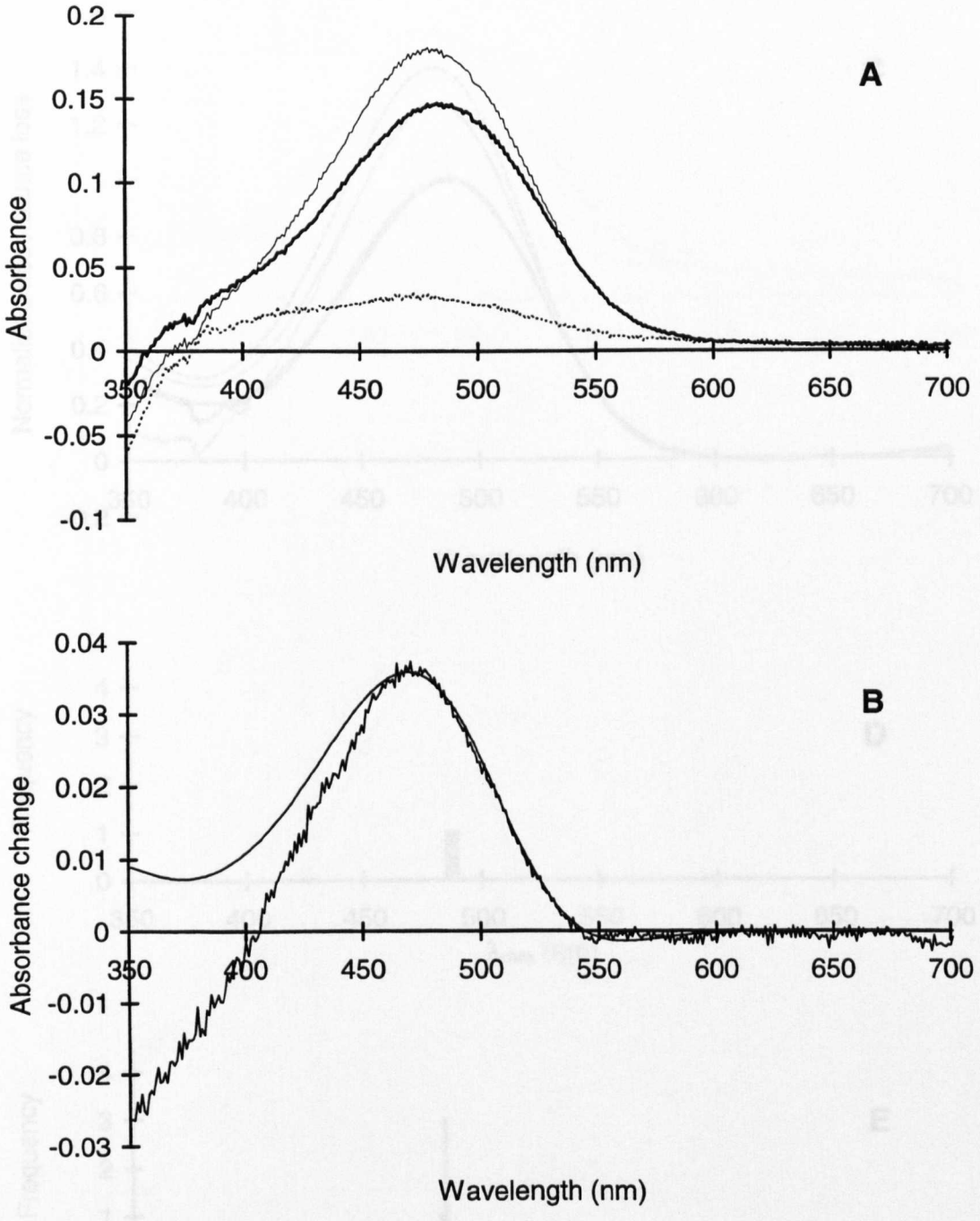

Figure 3.22 A–E. Results from the main rhabdoms (retinular cells 1–7) of *Meningodora vesca*. The absorbance spectra from five sections were selected to give a total of 18 difference spectra which constitute the average files of mix_1 and mix_2. The λ_{max} values of the best-fit templates for mix_1 and mix_2 are 487.2 and 482.4 nm, and the λ_{max} values of the *R* and *M* estimates are 487.1 and 480.8 nm with an estimated *M* to *R* extinction ratio of 1.402. The average maximum corrected absorbance loss for the mix_1 photobleach is 0.1237.

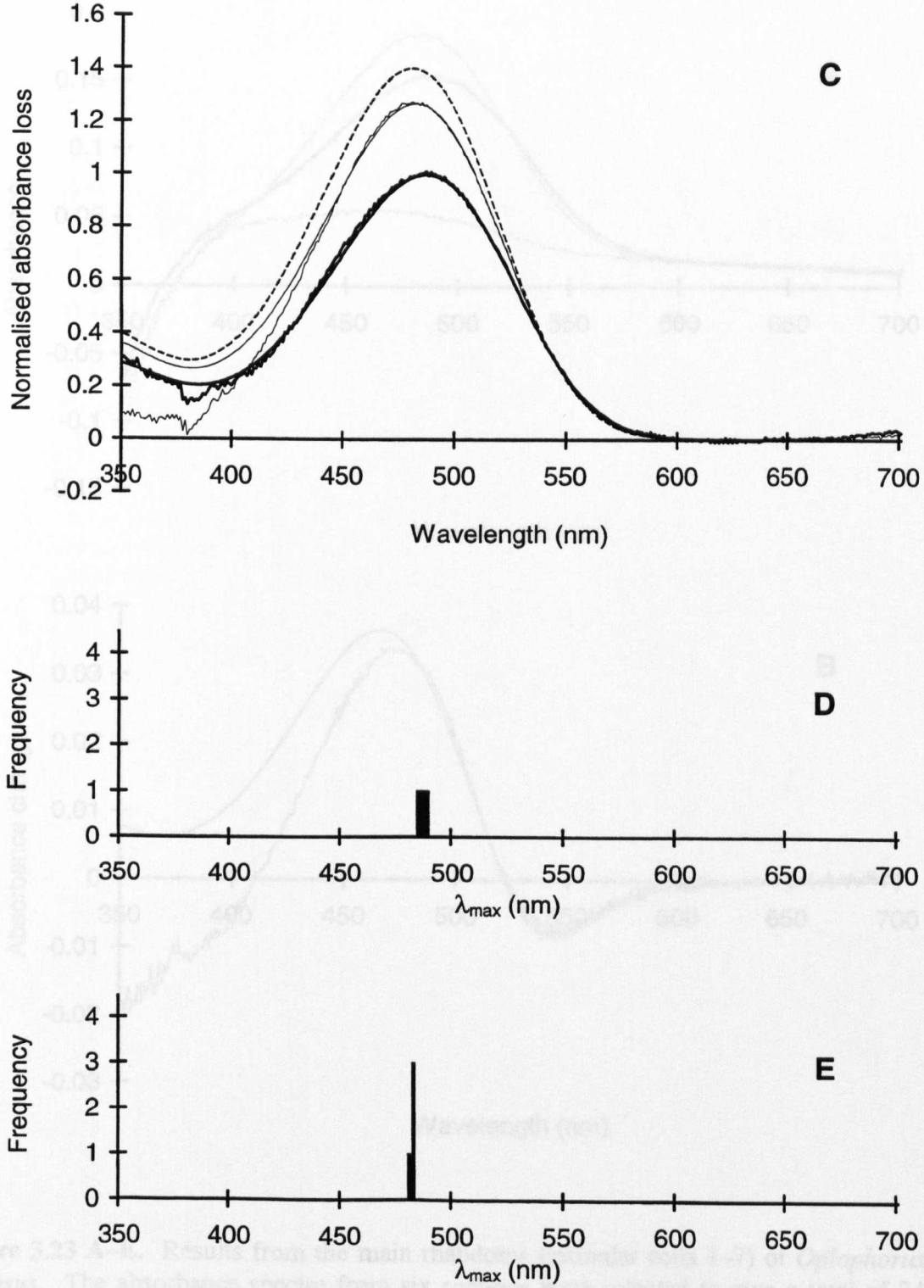

Figure 3.22 A–E. (Continued).

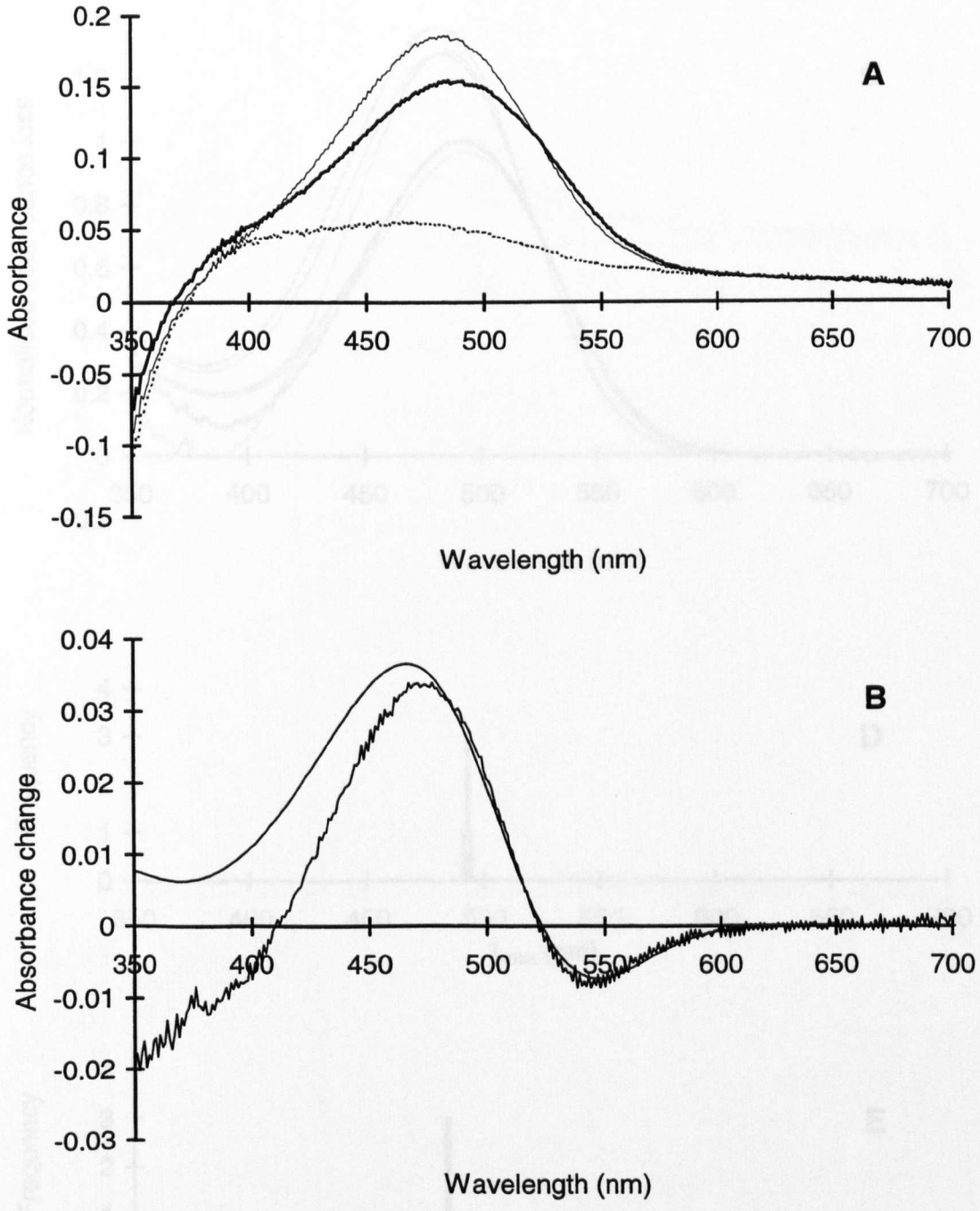

Figure 3.23 A–E. Results from the main rhabdoms (retinular cells 1–7) of *Oplophorus spinosus*. The absorbance spectra from six sections were selected to give a total of 24 difference spectra which constitute the average files of mix_1 and mix_2. The λ_{max} values of the best-fit templates for mix_1 and mix_2 are 492.0 and 482.8 nm, and the λ_{max} values of the *R* and *M* estimates are 493.8 and 481.1 nm with an estimated *M* to *R* extinction ratio of 1.416. The average maximum corrected absorbance loss for the mix_1 photobleach is 0.1043.

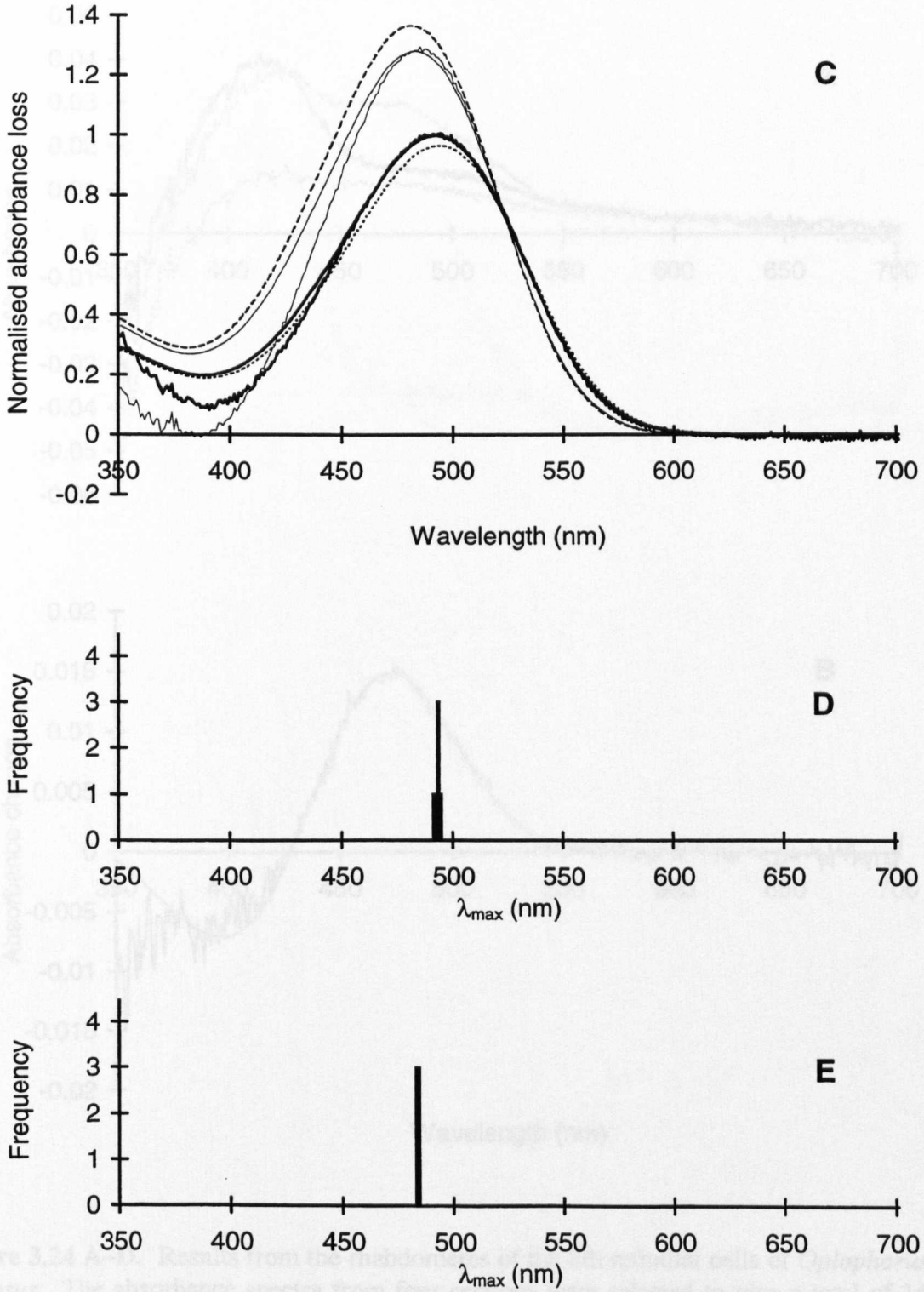

Figure 3.23 A–E. (Continued).

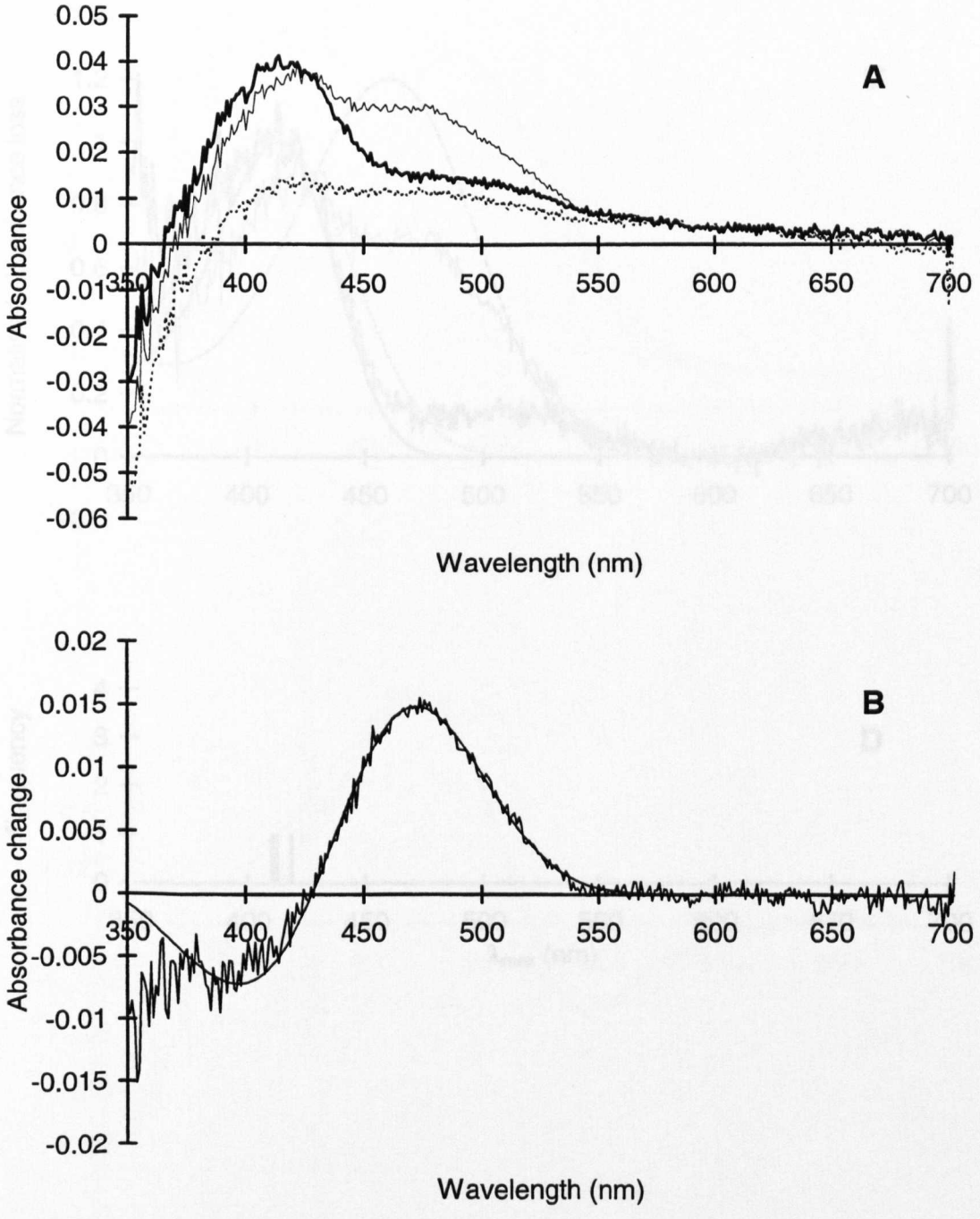

Figure 3.24 A–D. Results from the rhabdomeres of the 8th retinular cells of *Oplophorus spinosus*. The absorbance spectra from four sections were selected to give a total of 16 difference spectra which constitute the average files of mix_1 and mix_2. The running average λ_{max} of mix_1 is 413 nm, and the λ_{max} values of the *R* and *M* estimates are 412 and 460 nm with an estimated *M* to *R* extinction ratio of 1.2. The average maximum corrected absorbance loss for the mix_1 photobleach is 0.0265.

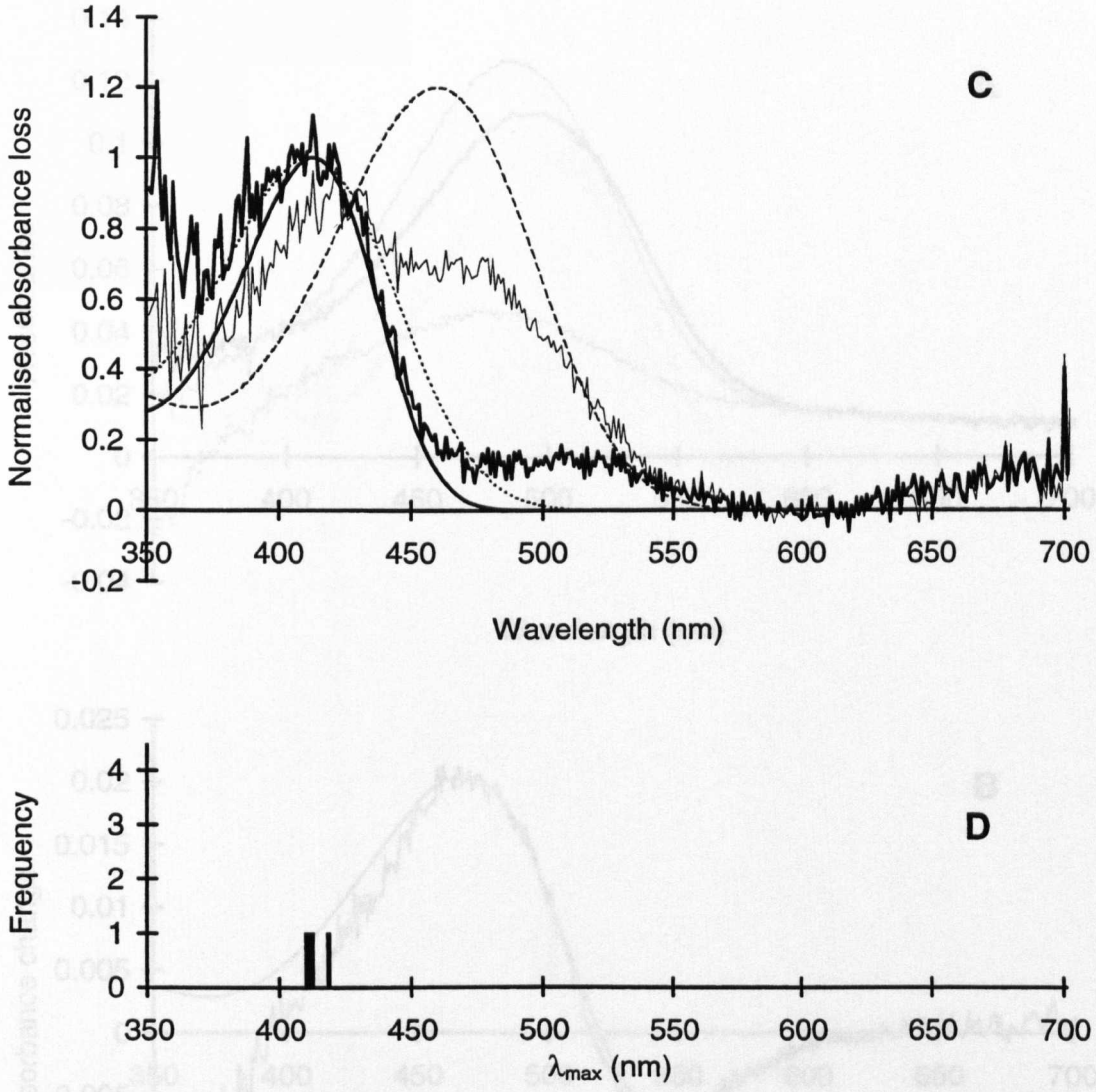

Figure 3.24 A–D. (Continued).

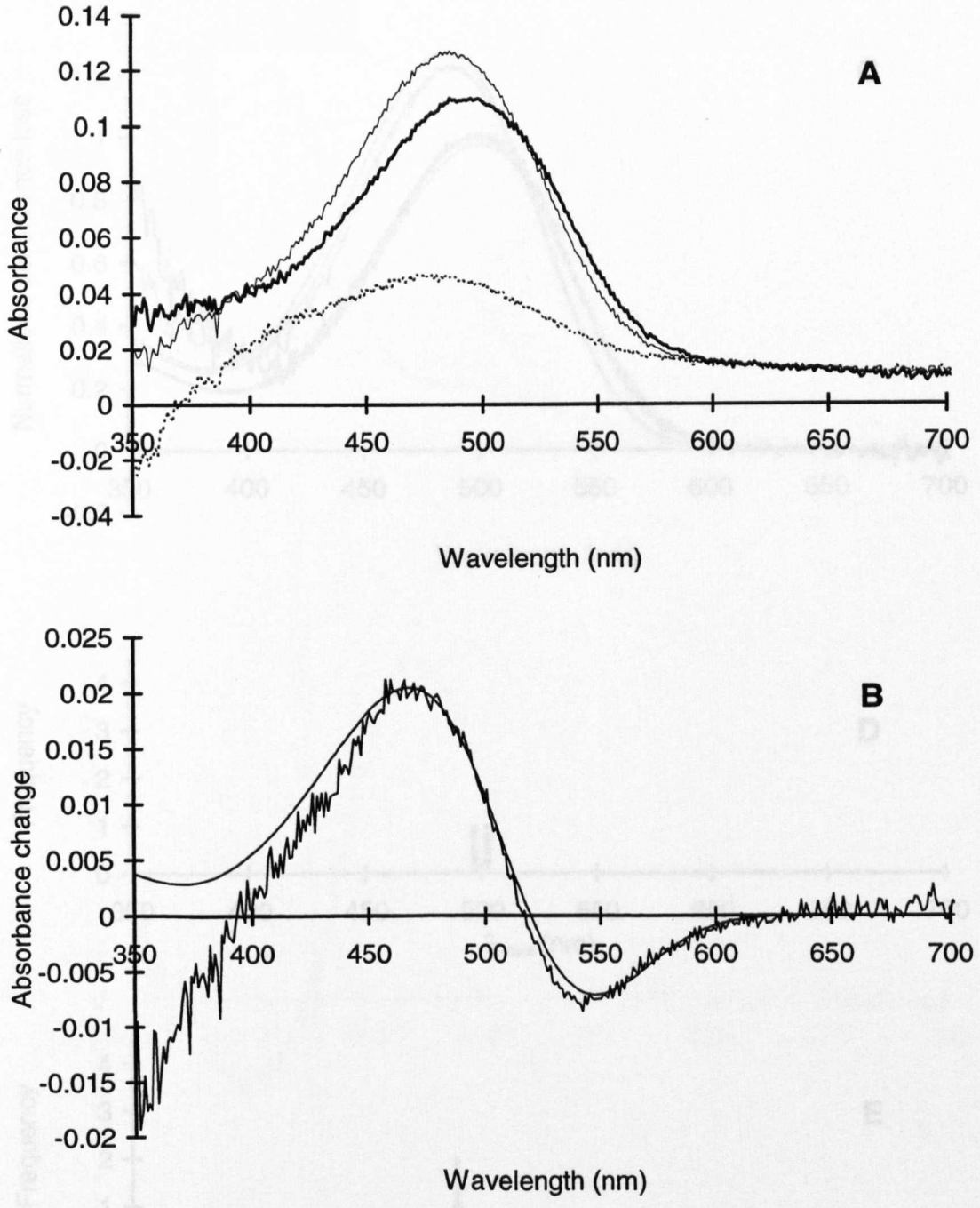

Figure 3.25 A–E. Results from the main rhabdoms (retinular cells 1–7) of *Systellaspis braueri*. The absorbance spectra from four sections were selected to give a total of 16 difference spectra which constitute the average files of mix_1 and mix_2. The λ_{max} values of the best-fit templates for mix_1 and mix_2 are 498.1 and 487.4 nm, and the λ_{max} values of the *R* and *M* estimates are 500.0 and 485.8 nm with an estimated *M* to *R* extinction ratio of 1.308. The average maximum corrected absorbance loss for the mix_1 photobleach is 0.0658.

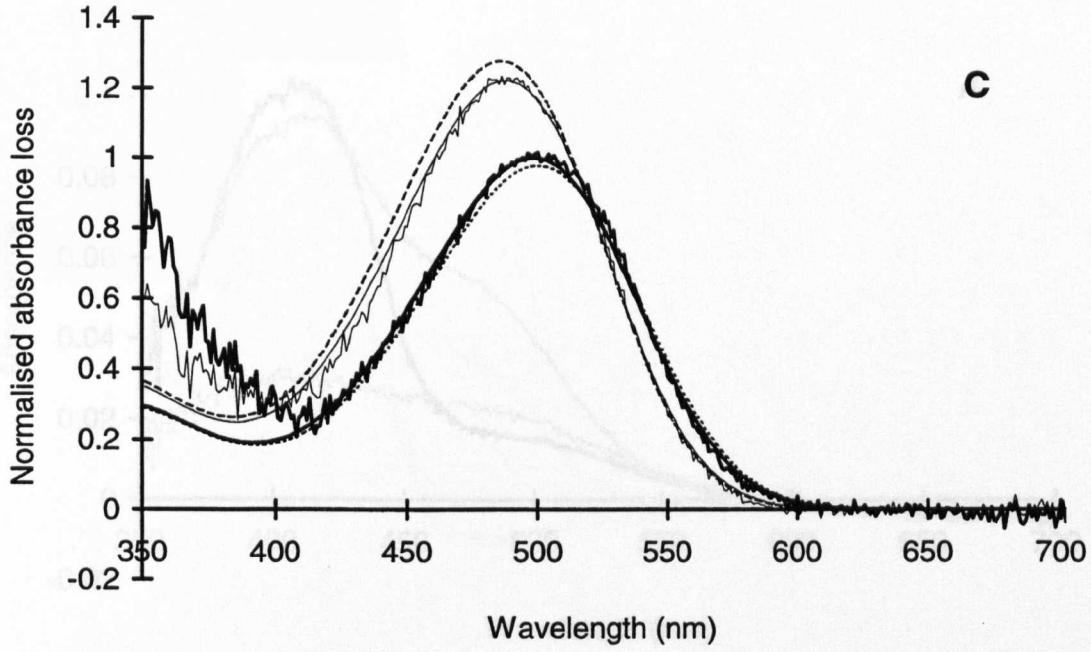

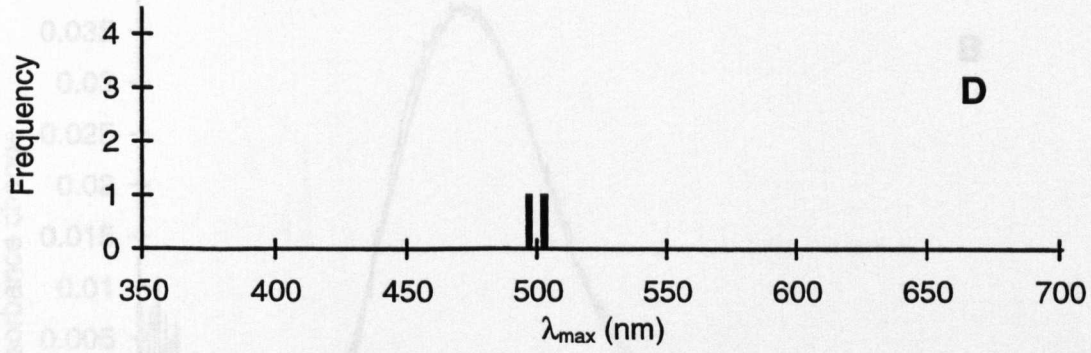

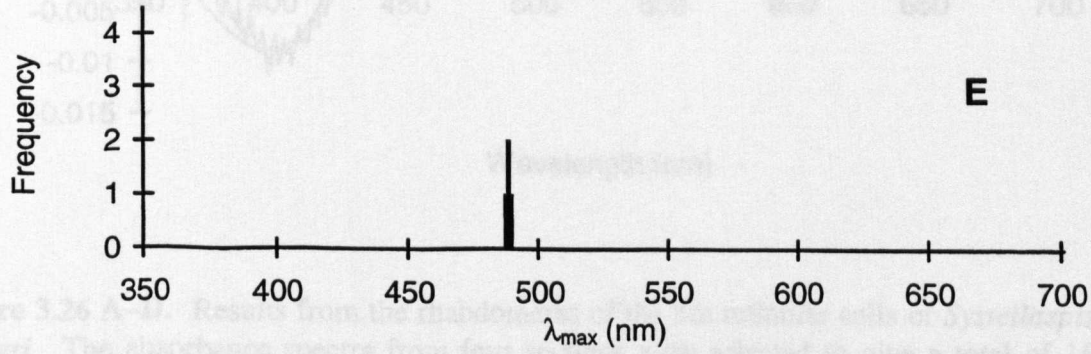

Figure 3.25 A–E. (Continued).

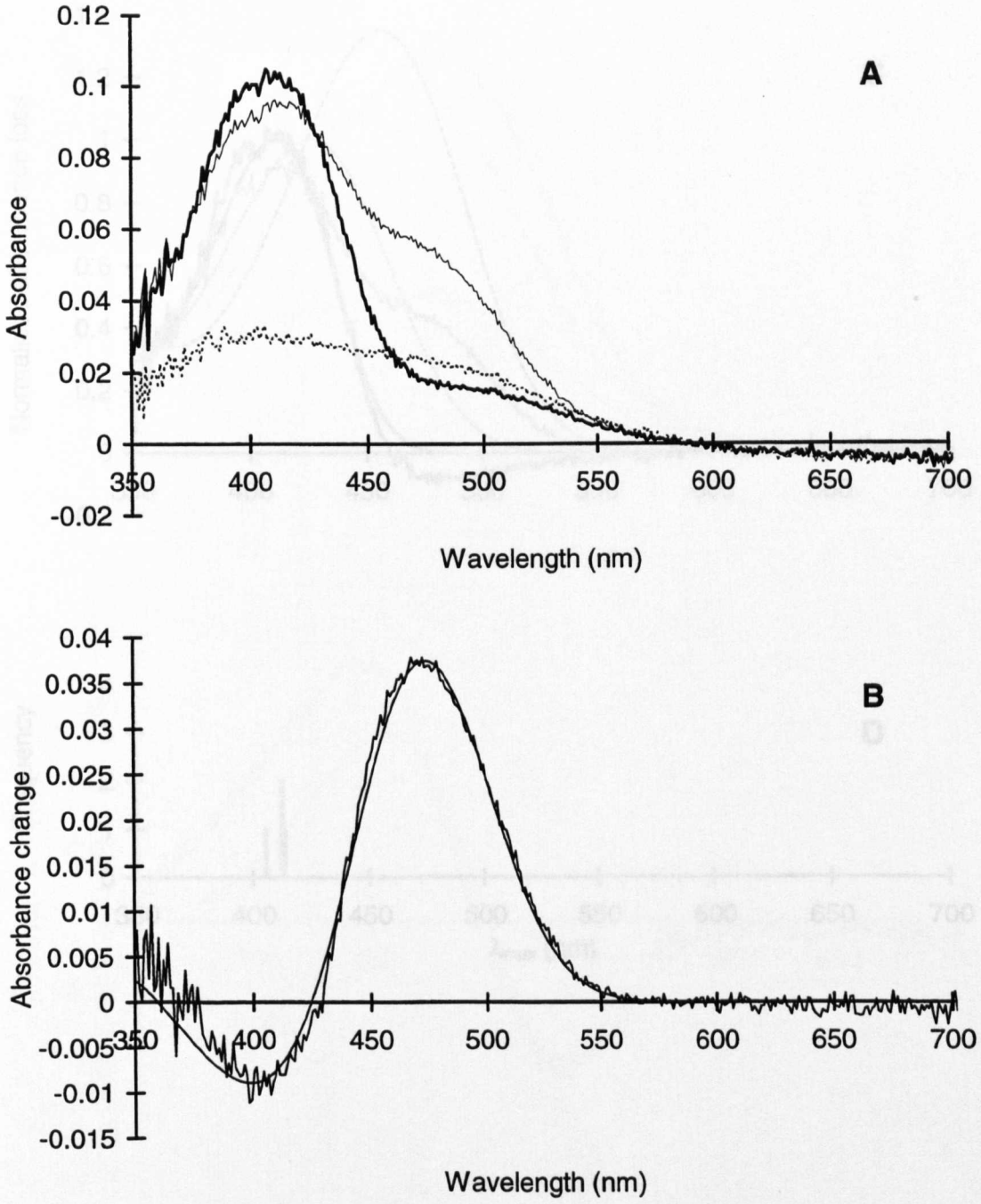

Figure 3.26 A–D. Results from the rhabdomeres of the 8th retinular cells of *Systellaspis braueri*. The absorbance spectra from four sections were selected to give a total of 16 difference spectra which constitute the average files of mix_1 and mix_2. The running average λ_{max} of mix_1 is 411 nm, and the λ_{max} values of the *R* and *M* estimates are 426 and 456 nm with an estimated *M* to *R* extinction ratio of 1.35. The average maximum corrected absorbance loss for the mix_1 photobleach is 0.0720.

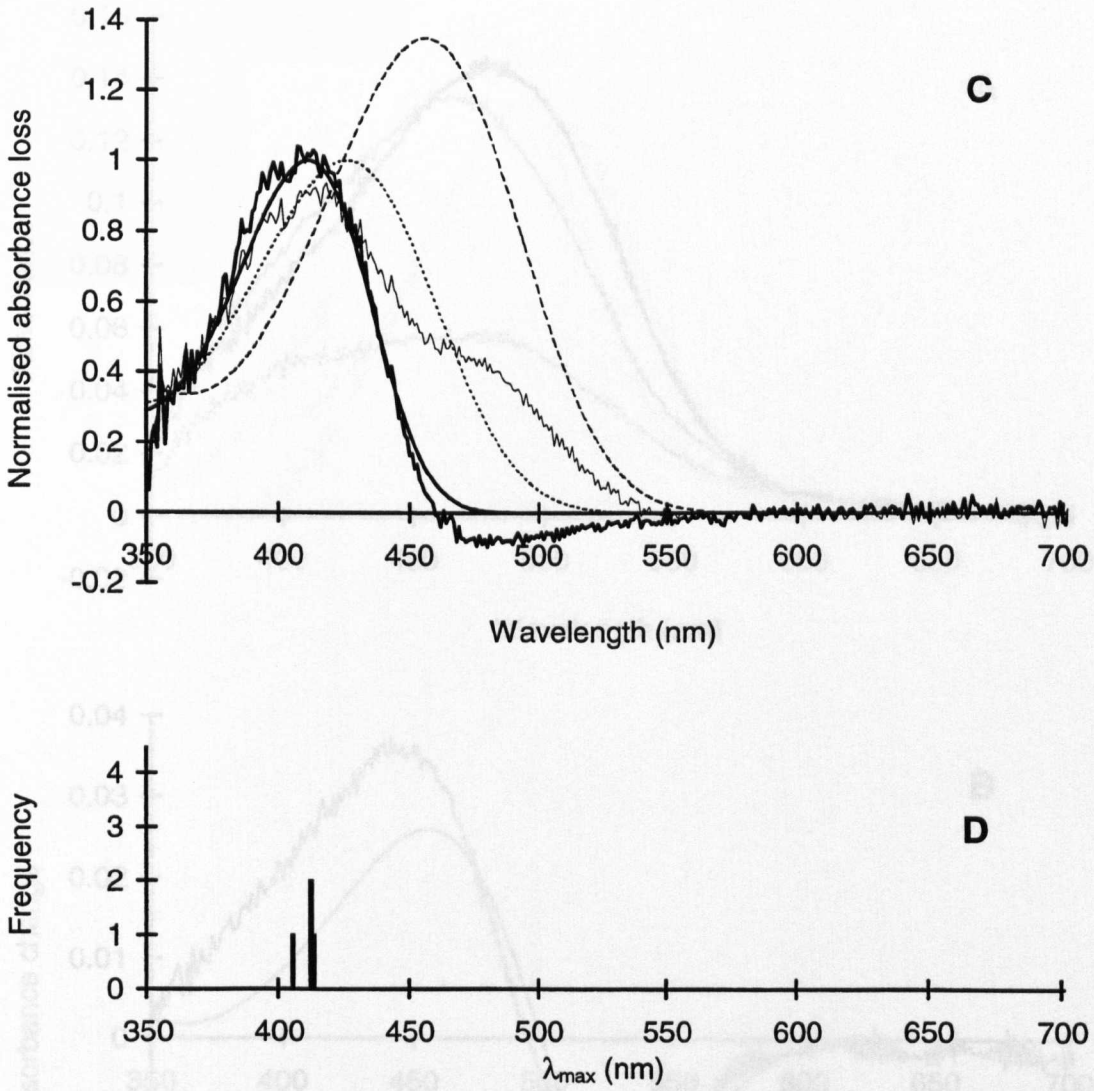

Figure 3.26 A–D. (Continued).

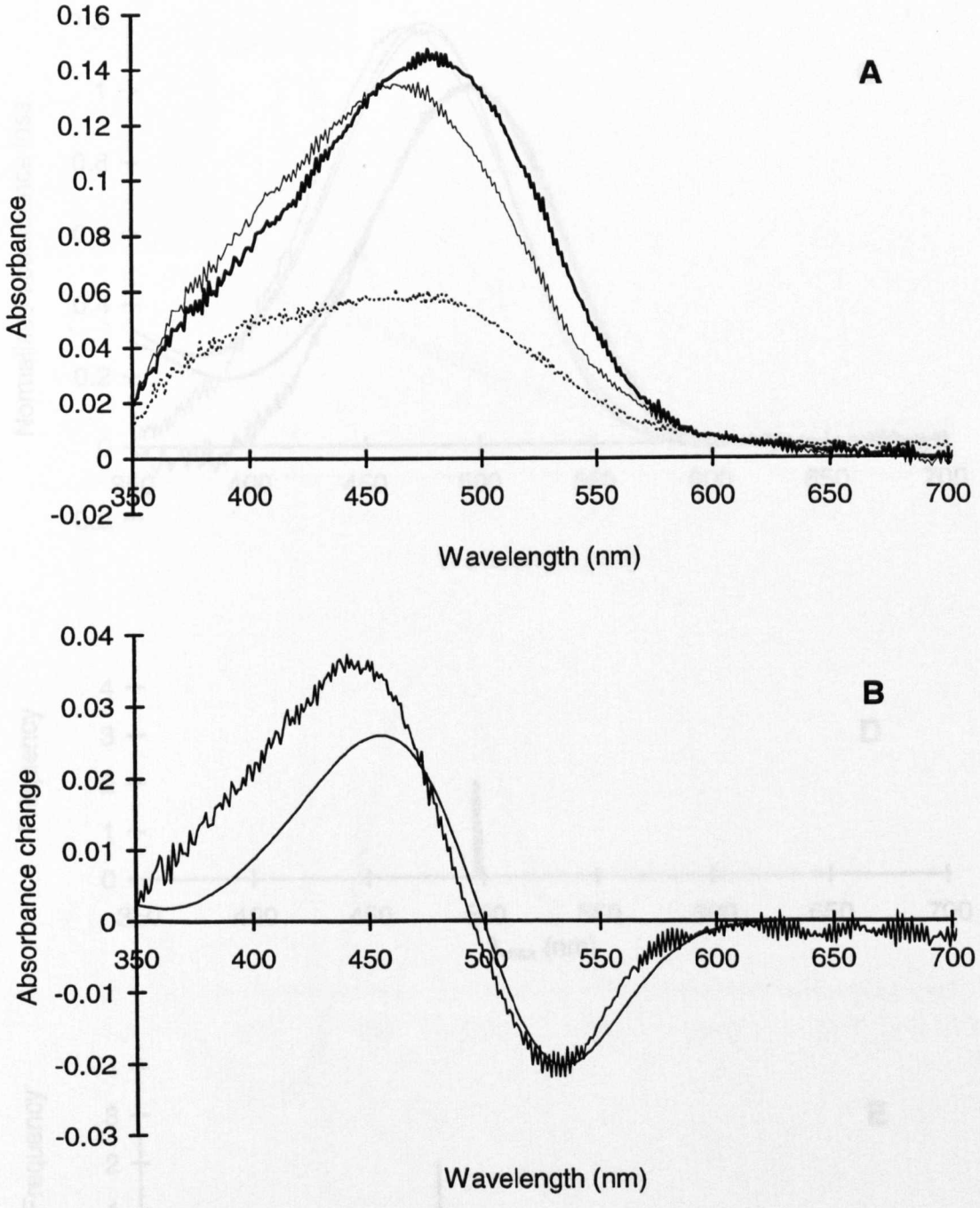

Figure 3.27 A–E. Results from the main rhabdoms (retinular cells 1–7) of *Systellaspis cristata*. The absorbance spectra from five sections were selected to give a total of 20 difference spectra which constitute the average files of mix_1 and mix_2. The λ_{max} values of the best-fit templates for mix_1 and mix_2 are 496.4 and 477.6 nm, and the λ_{max} values of the *R* and *M* estimates are 497.7 and 476.5 nm with an estimated *M* to *R* extinction ratio of 1.187. The average maximum corrected absorbance loss for the mix_1 photobleach is 0.0737.

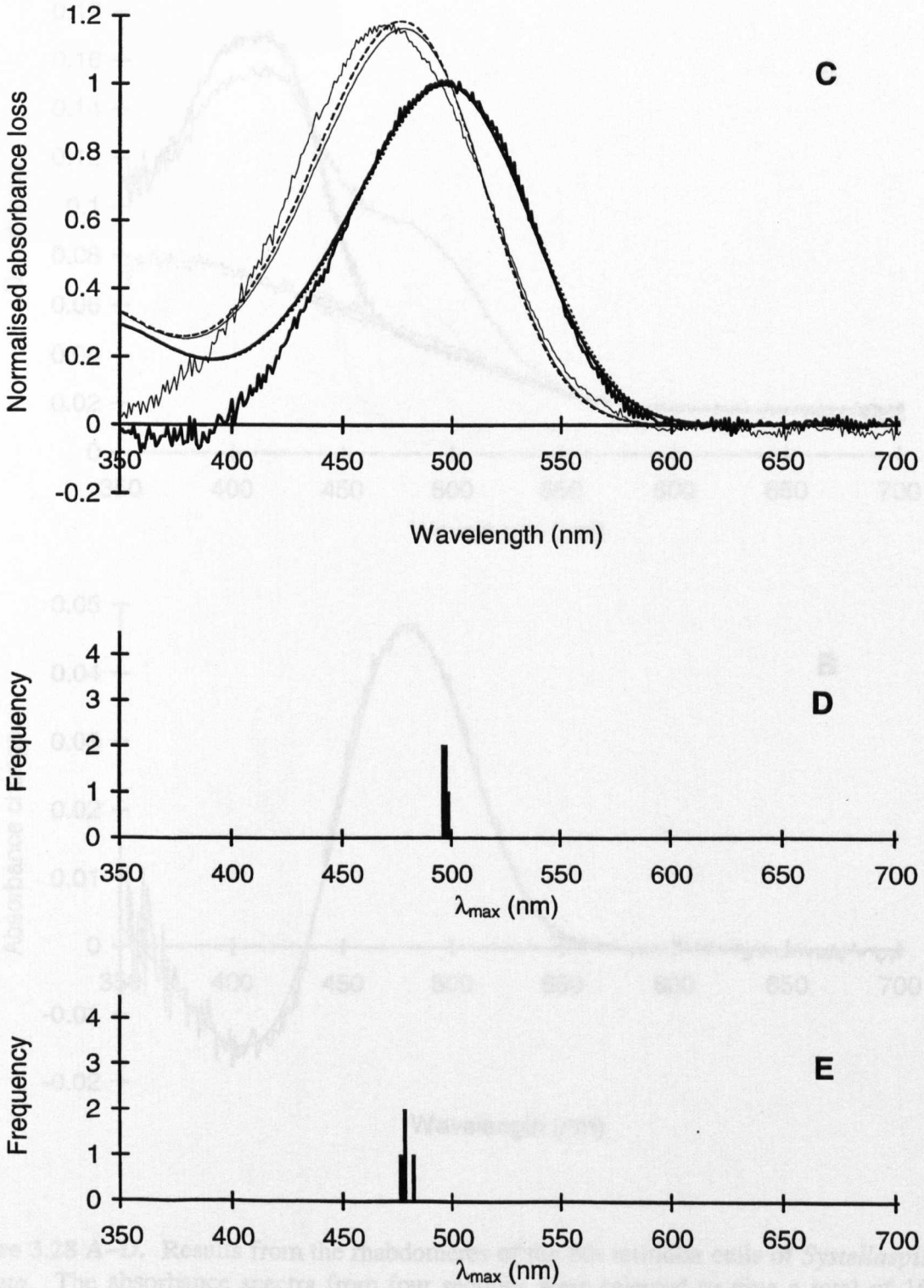

Figure 3.27 A–E. (Continued).

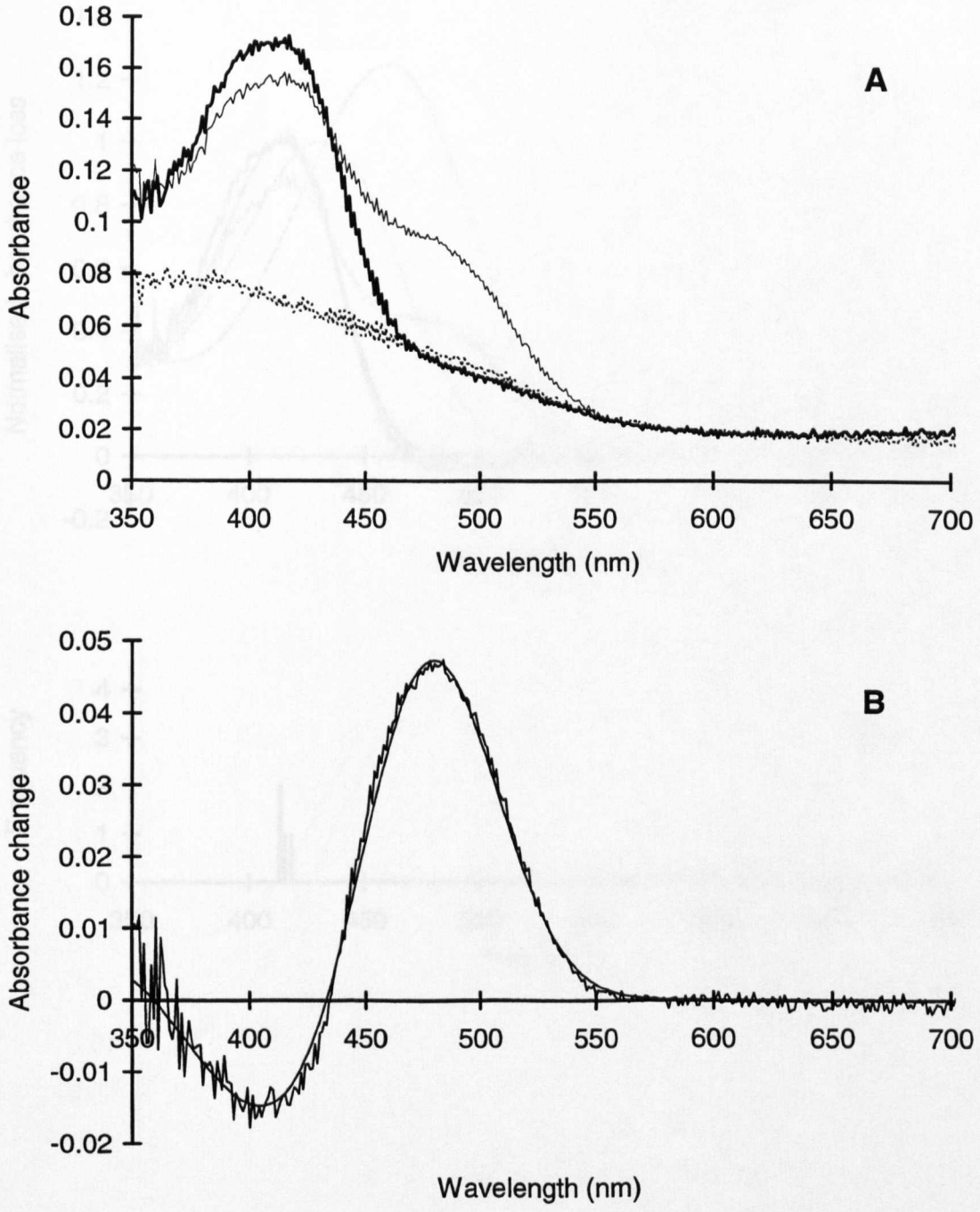

Figure 3.28 A–D. Results from the rhabdomeres of the 8th retinular cells of *Systellaspis cristata*. The absorbance spectra from four sections were selected to give a total of 16 difference spectra which constitute the average files of mix_1 and mix_2. The running average λ_{max} of mix_1 is 414 nm, and the λ_{max} values of the *R* and *M* estimates are 431 and 460 nm with an estimated *M* to *R* extinction ratio of 1.25. The average maximum corrected absorbance loss for the mix_1 photobleach is 0.1000.

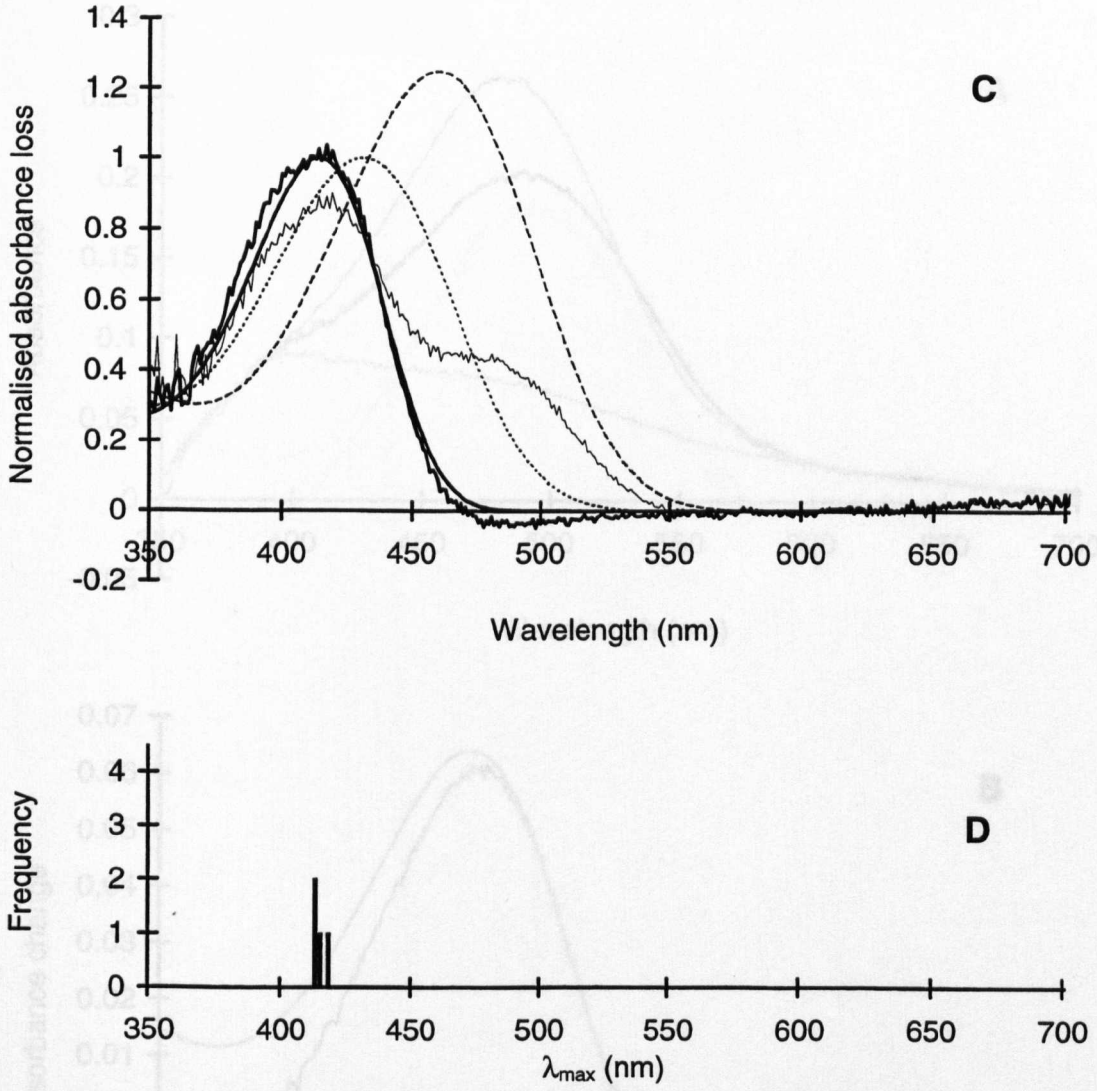

Figure 3.28 A–D. (Continued).

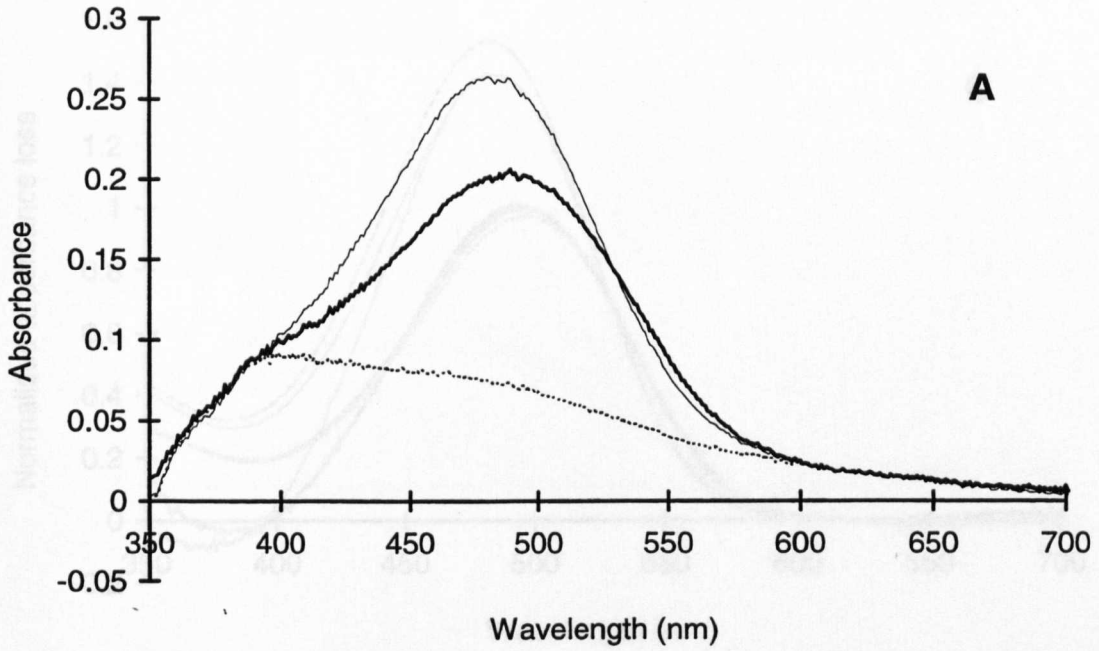

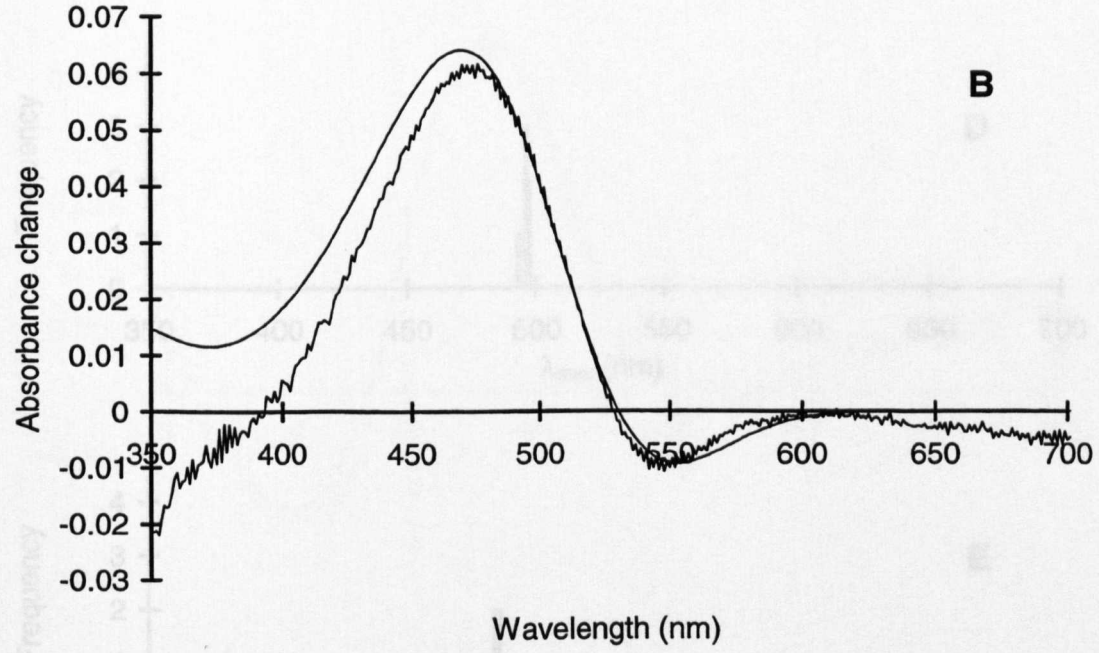

Figure 3.29 A–E. Results from the main rhabdoms (retinular cells 1–7) of *Systellaspis debilis*. The absorbance spectra from six sections were selected to give a total of 21 difference spectra which constitute the average files of mix_1 and mix_2. The λ_{max} values of the best-fit templates for mix_1 and mix_2 are 495.6 and 484.1 nm, and the λ_{max} values of the *R* and *M* estimates are 496.7 and 482.5 nm with an estimated *M* to *R* extinction ratio of 1.572. The average maximum corrected absorbance loss for the mix_1 photobleach is 0.1264.

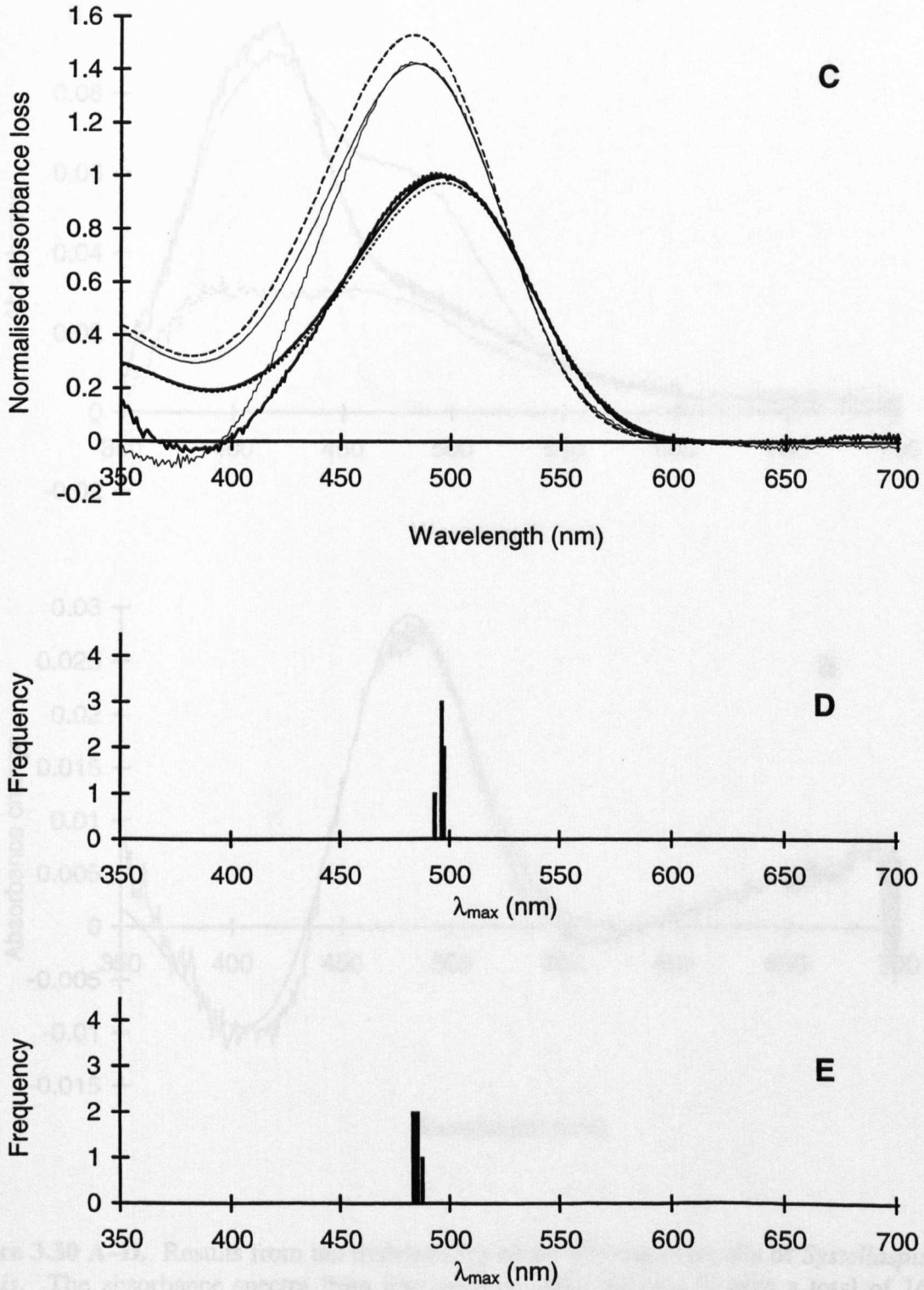

Figure 3.29 A–E. (Continued).

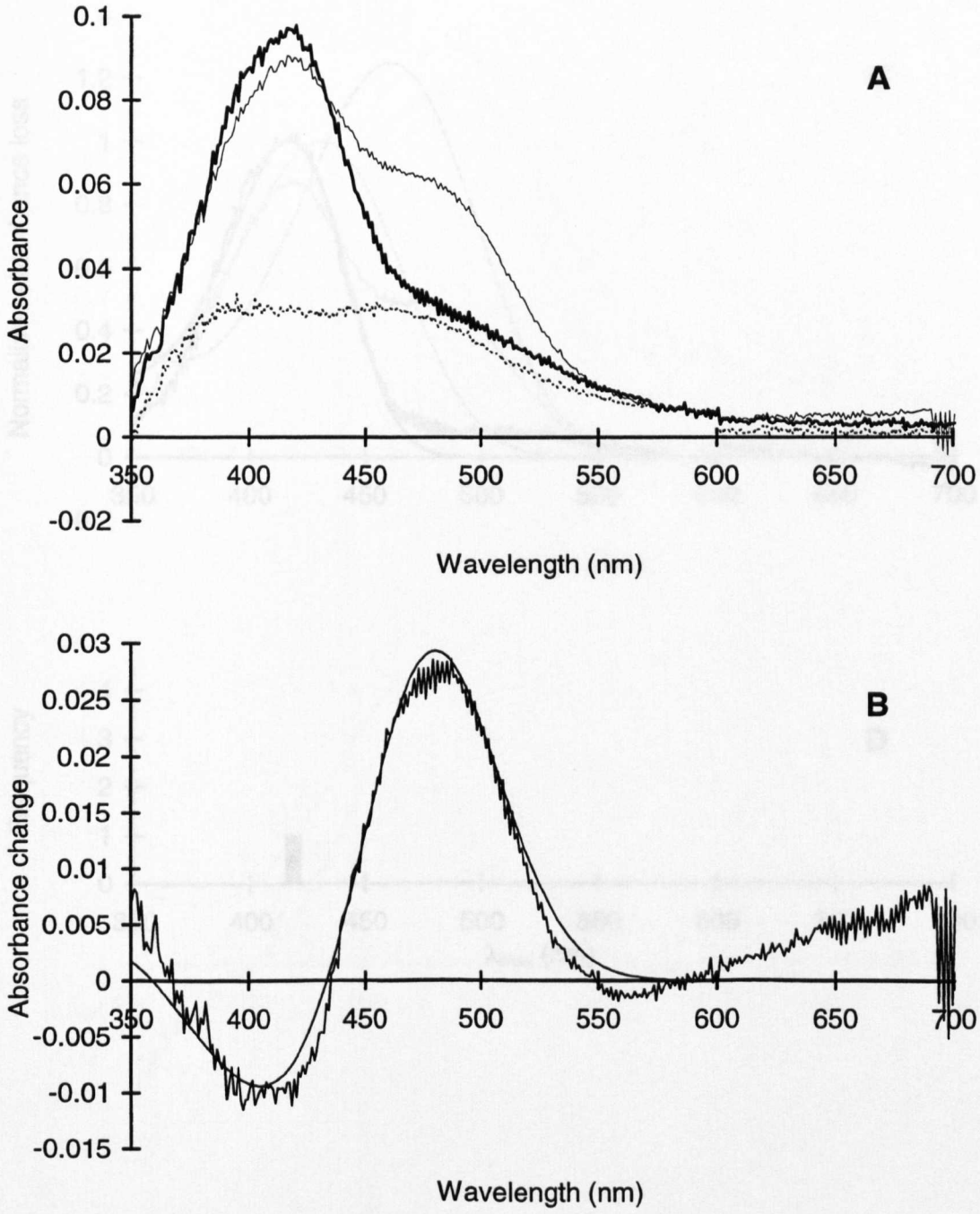

Figure 3.30 A–D. Results from the rhabdomeres of the 8th retinular cells of *Systellaspis debilis*. The absorbance spectra from four sections were selected to give a total of 16 difference spectra which constitute the average files of mix_1 and mix_2. The running average λ_{max} of mix_1 is 417 nm, and the λ_{max} values of the *R* and *M* estimates are 431 and 461 nm with an estimated *M* to *R* extinction ratio of 1.25. The average maximum corrected absorbance loss for the mix_1 photobleach is 0.0694.
The steps in the absorbance at 600 nm are due to averaging files with different upper wavelength limits. To counter this all files were normalised with the offset fixed at 600 nm.

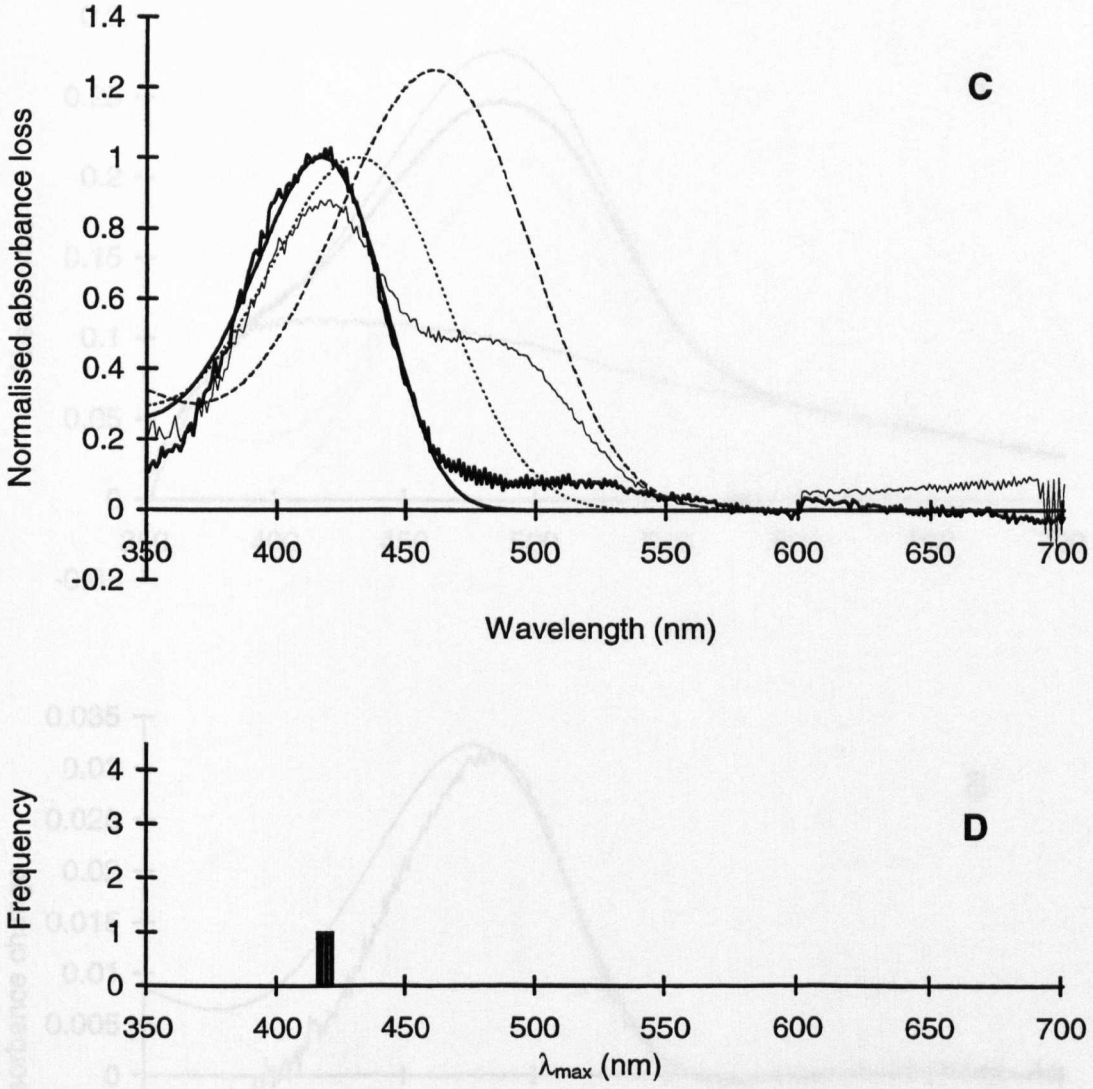

Figure 3.30 A–D. (Continued).

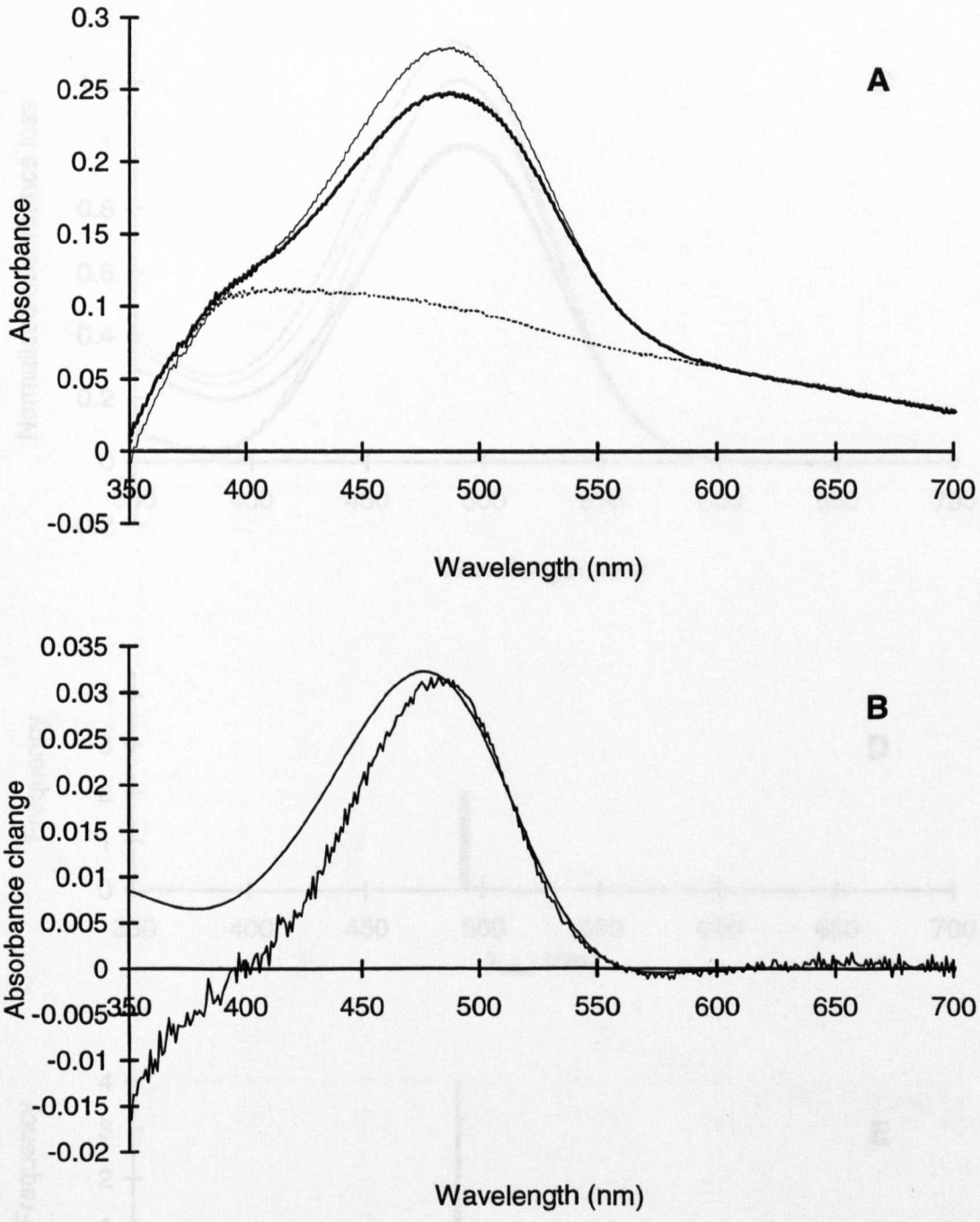

Figure 3.31 A–E. Results from the main rhabdoms (retinular cells 1–7) of *Stylopandalus richardii*. The absorbance spectra from five sections were selected to give a total of 20 difference spectra which constitute the average files of mix_1 and mix_2. The λ_{max} values of the best-fit templates for mix_1 and mix_2 are 491.2 and 488.2 nm, and the λ_{max} values of the *R* and *M* estimates are 491.1 and 486.8 nm with an estimated *M* to *R* extinction ratio of 1.333. The average maximum corrected absorbance loss for the mix_1 photobleach is 0.1482.

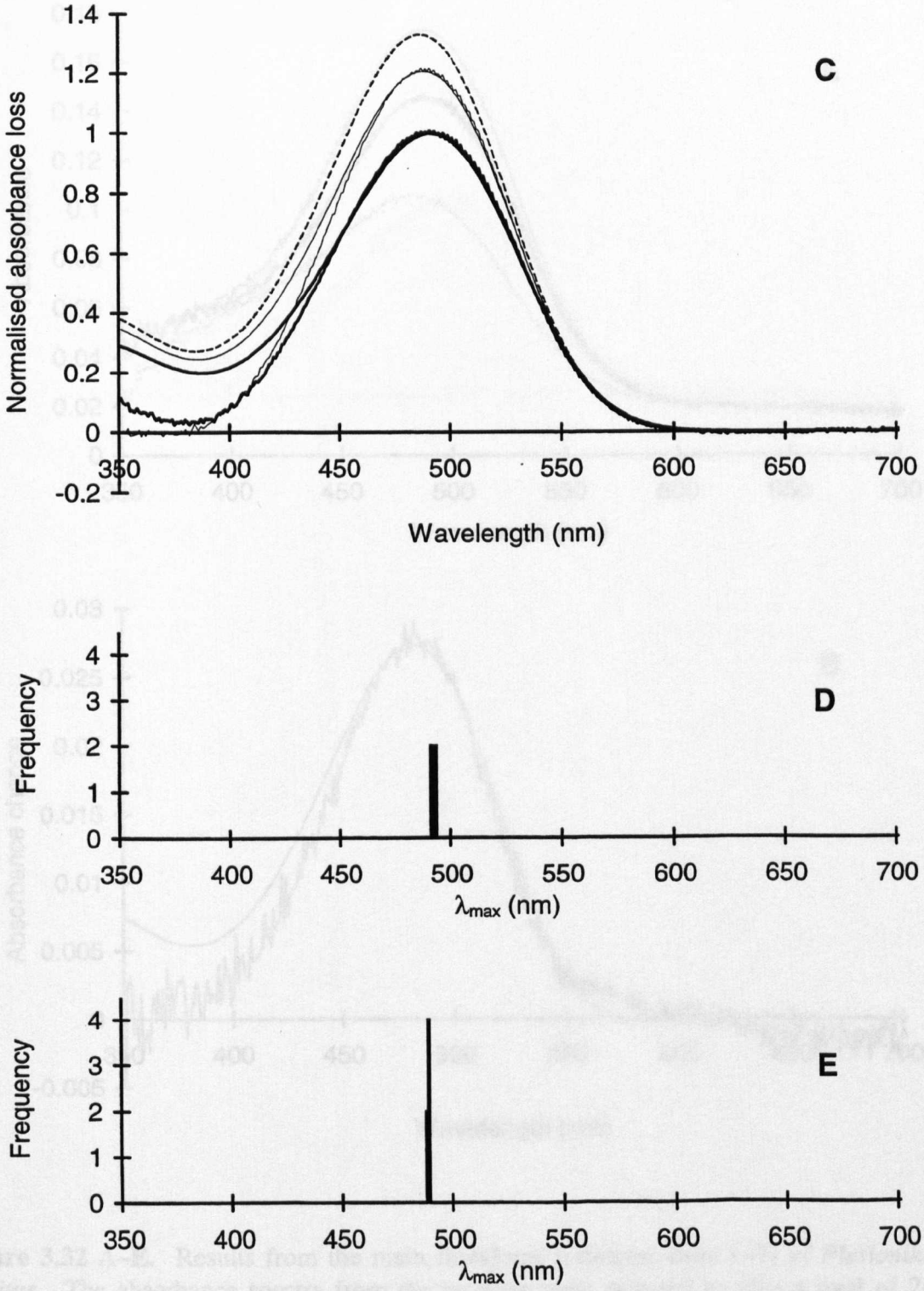

Figure 3.31A–E. (Continued).

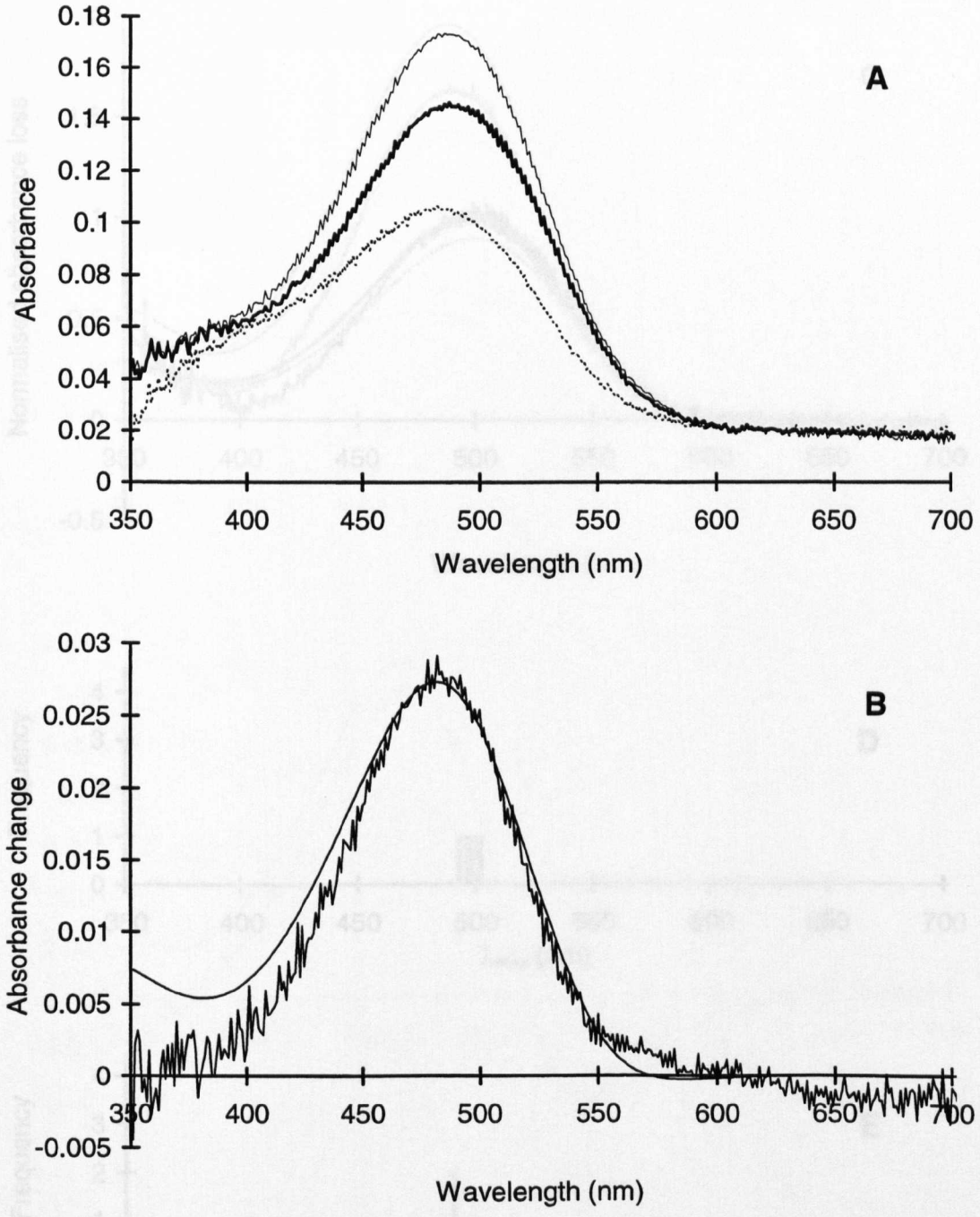

Figure 3.32 A–E. Results from the main rhabdoms (retinular cells 1–7) of *Plesionika maritus*. The absorbance spectra from six sections were selected to give a total of 24 difference spectra which constitute the average files of mix_1 and mix_2. The λ_{max} values of the best-fit templates for mix_1 and mix_2 are 497.1 and 490.2 nm, and the λ_{max} values of the *R* and *M* estimates are 499.3 and 488.5 nm with an estimated *M* to *R* extinction ratio of 2.185. The average maximum corrected absorbance loss for the mix_1 photobleach is 0.0417.

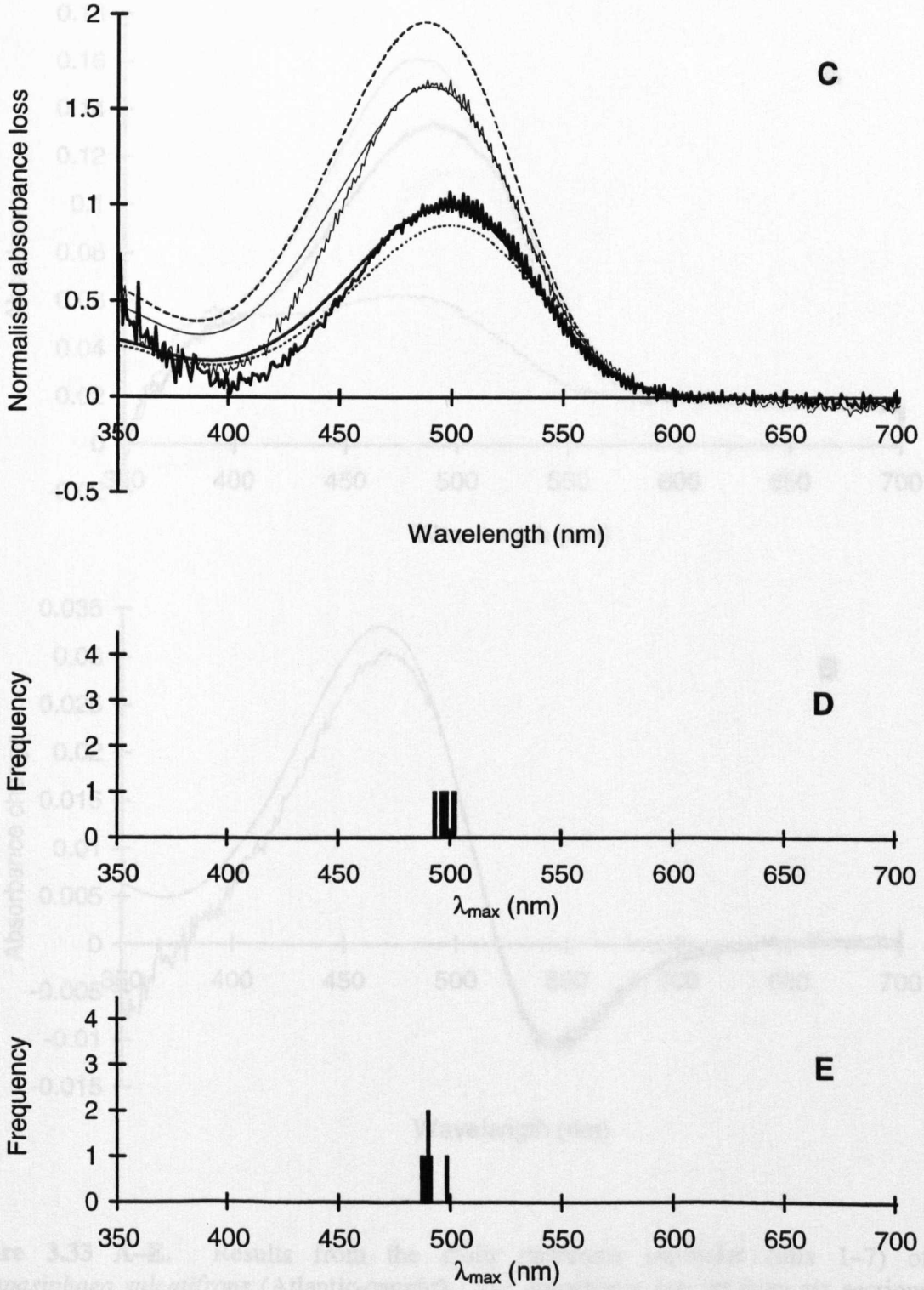

Figure 3.32 A–E. (Continued).

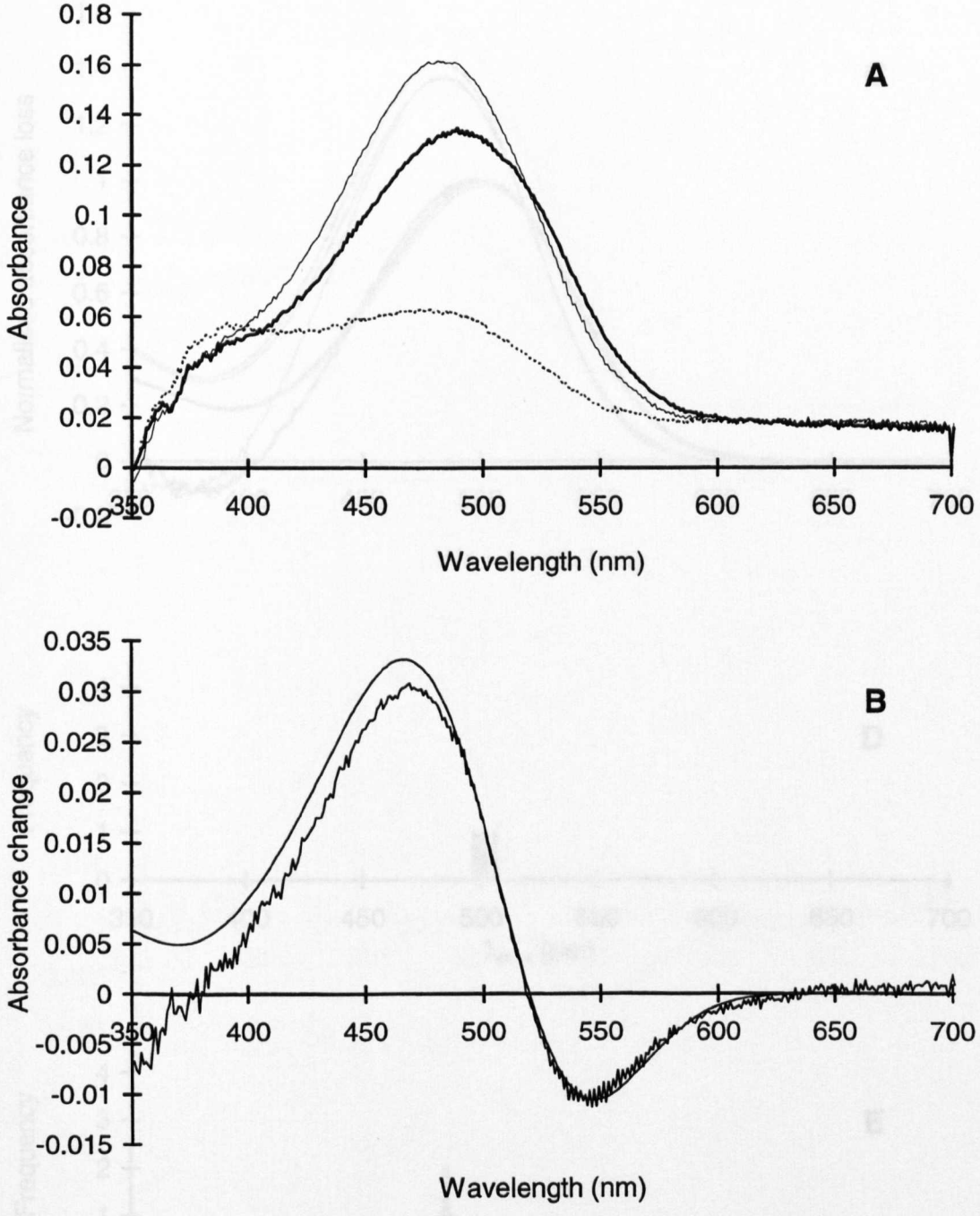

Figure 3.33 A–E. Results from the main rhabdoms (retinular cells 1–7) of *Parapasiphaea sulcatifrons* (Atlantic-caught). The absorbance spectra from six sections were selected to give a total of 20 difference spectra which constitute the average files of mix_1 and mix_2. The λ_{max} values of the best-fit templates for mix_1 and mix_2 are 499.6 and 483.7 nm, and the λ_{max} values of the *R* and *M* estimates are 501.0 and 482.4 nm with an estimated *M* to *R* extinction ratio of 1.450. The average maximum corrected absorbance loss for the mix_1 photobleach is 0.0660.

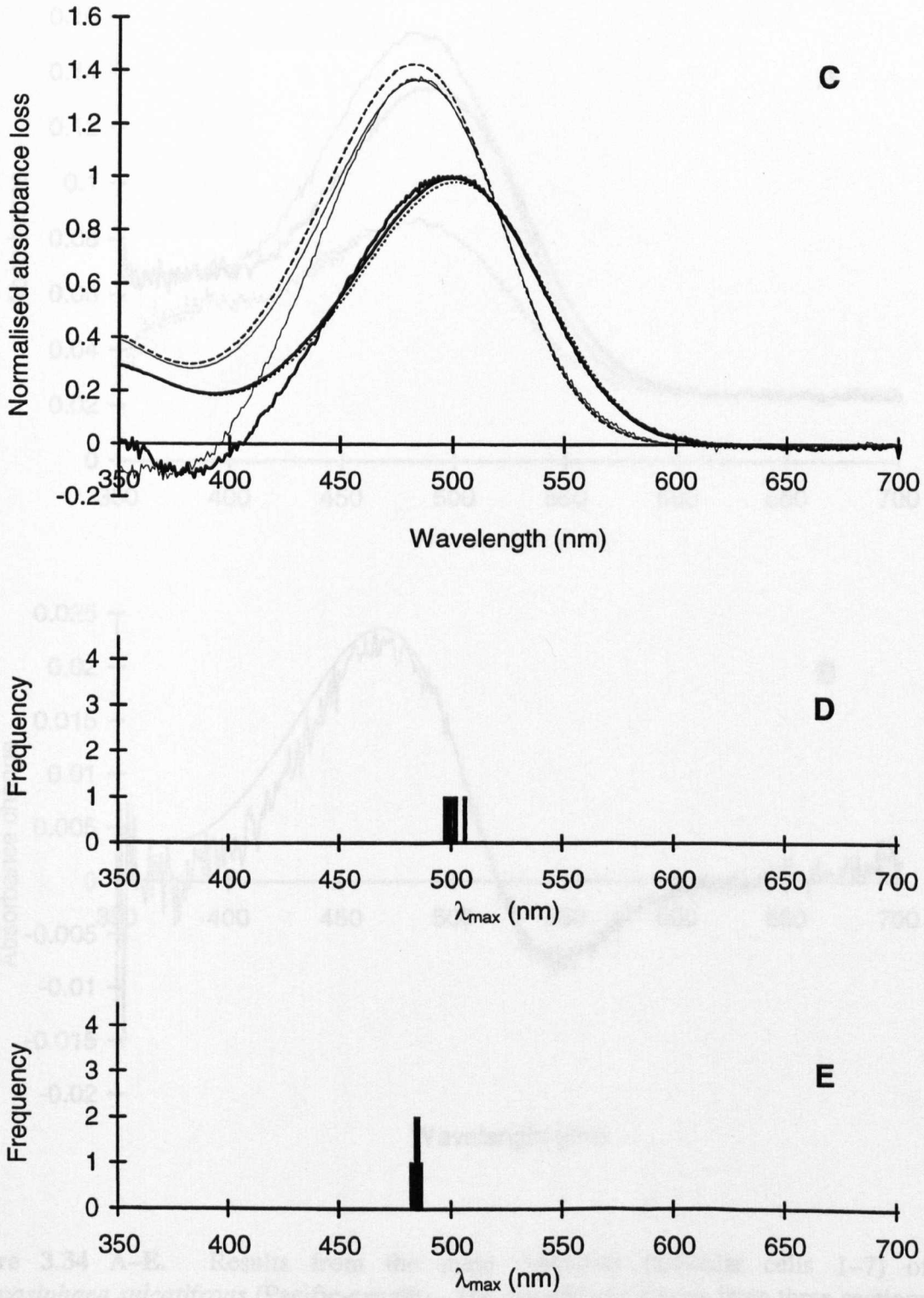

Figure 3.33 A–E. (Continued).

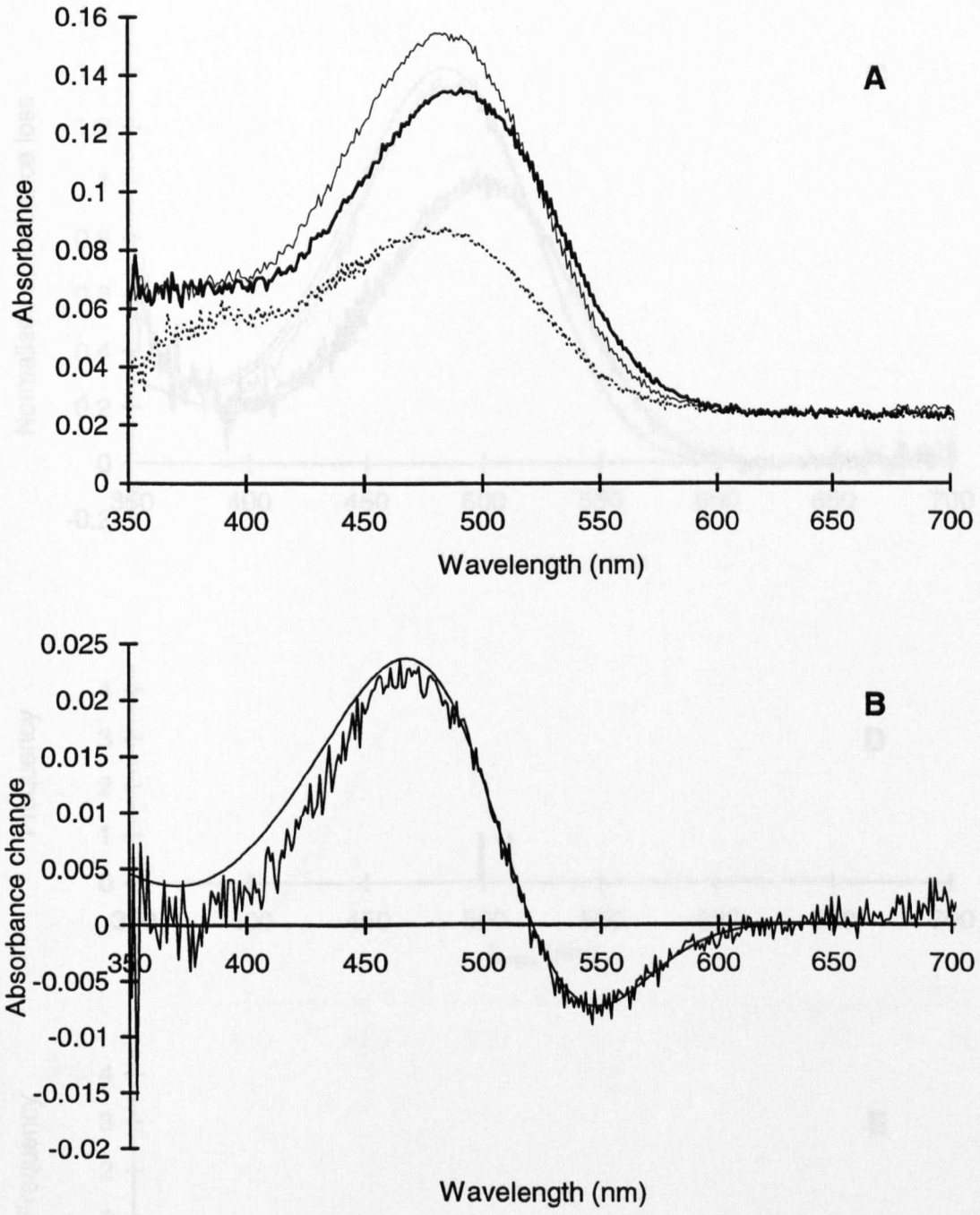

Figure 3.34 A–E. Results from the main rhabdoms (retinular cells 1–7) of *Parapasiphaea sulcatifrons* (Pacific-caught). The absorbance spectra from three sections were selected to give a total of 12 difference spectra which constitute the average files of mix_1 and mix_2. The λ_{max} values of the best-fit templates for mix_1 and mix_2 are 499.8 and 484.8 nm, and the λ_{max} values of the *R* and *M* estimates are 501.1 and 483.5 nm with an estimated *M* to *R* extinction ratio of 1.435. The average maximum corrected absorbance loss for the mix_1 photobleach is 0.0498.

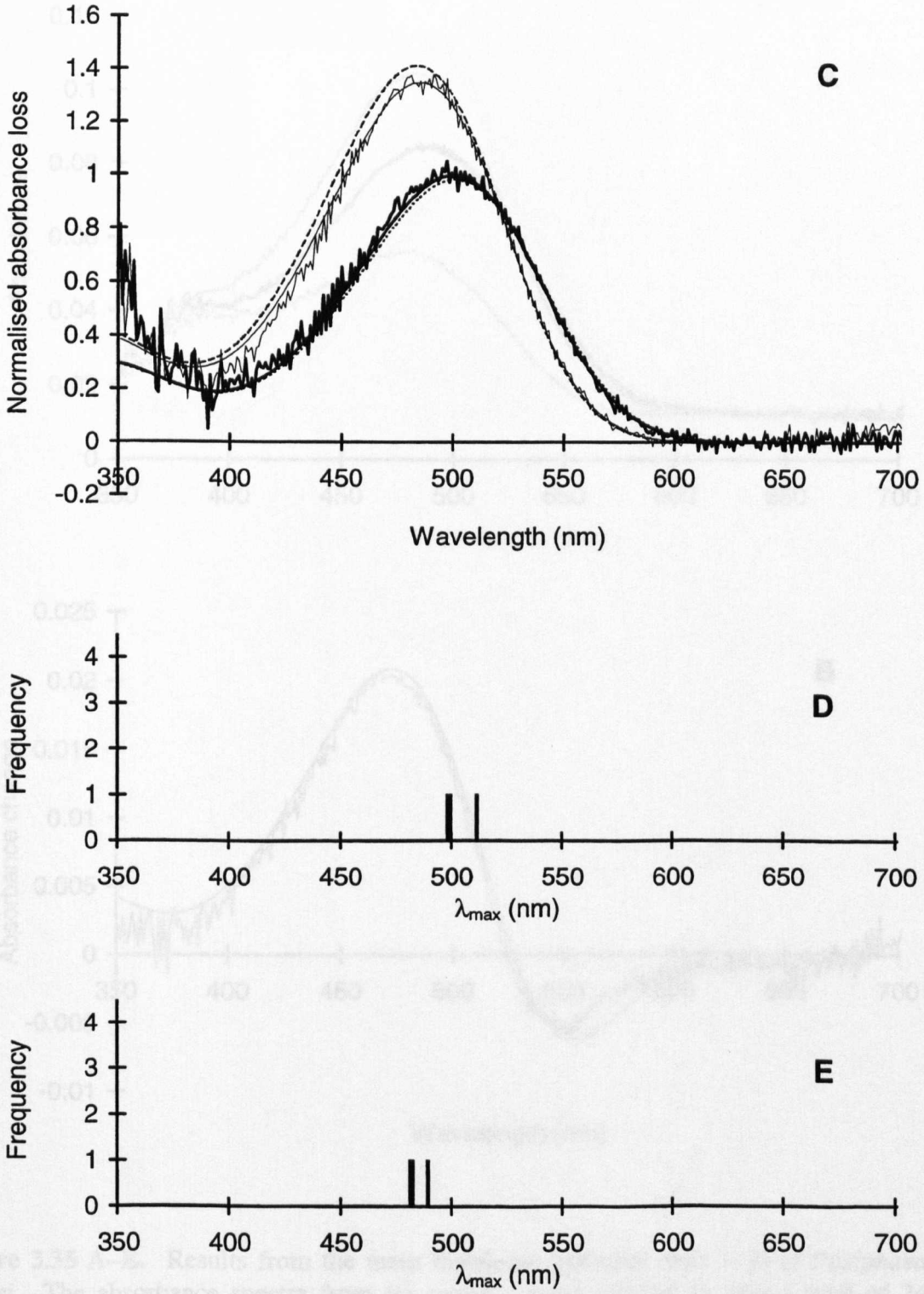

Figure 3.34 A–E. (Continued).

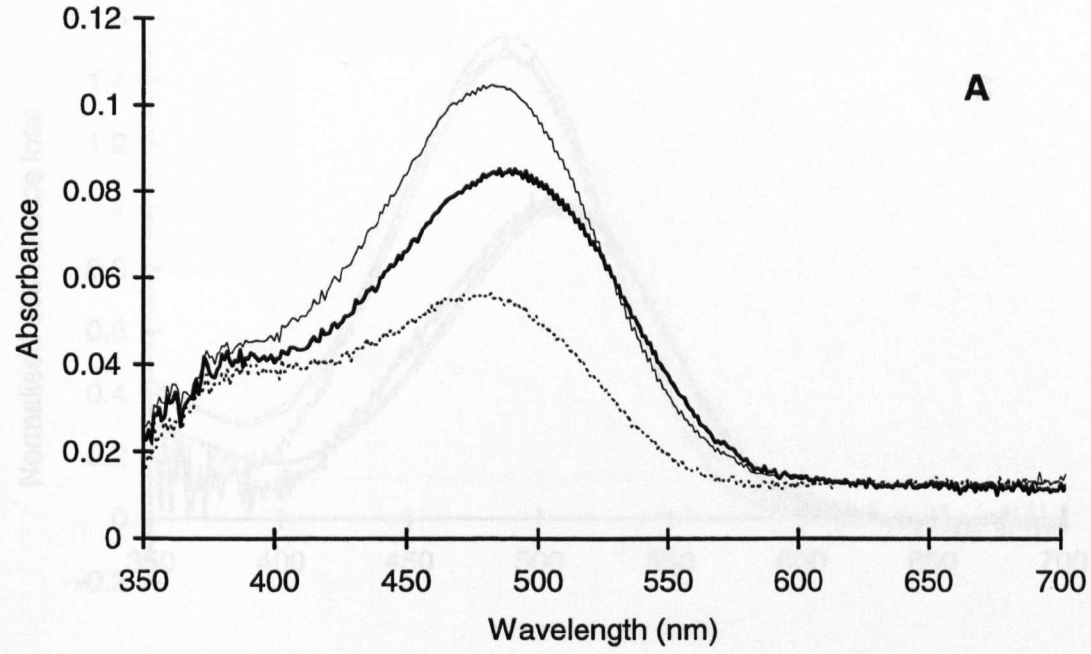

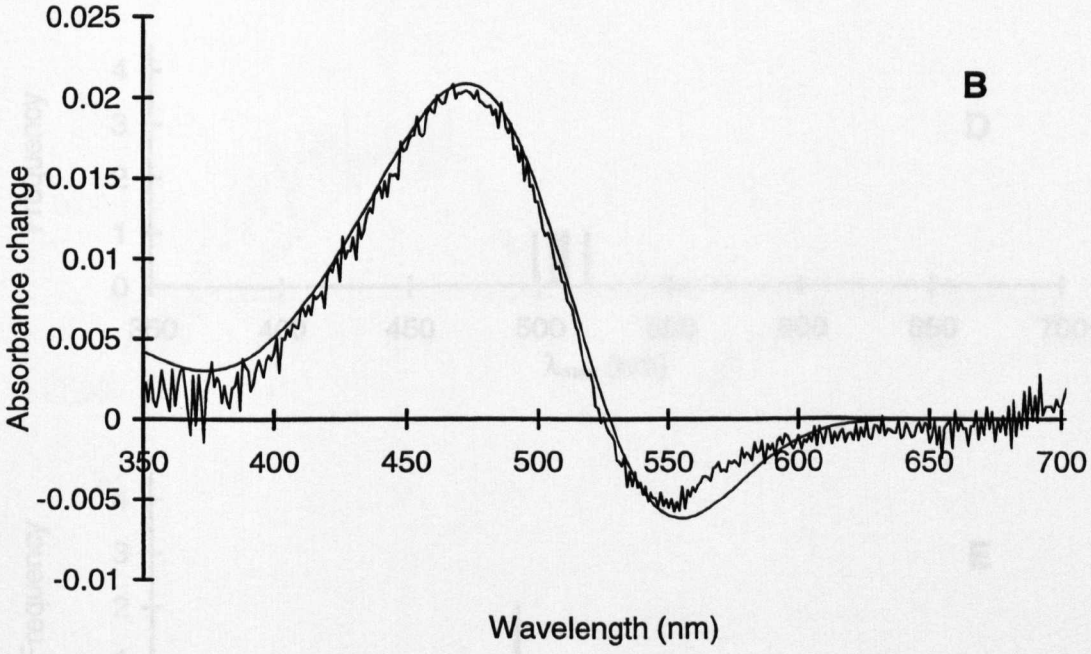

Figure 3.35 A–E. Results from the main rhabdoms (retinular cells 1–7) of *Pasiphaea chacei*. The absorbance spectra from six sections were selected to give a total of 24 difference spectra which constitute the average files of mix_1 and mix_2. The λ_{max} values of the best-fit templates for mix_1 and mix_2 are 507.5 and 488.4 nm, and the λ_{max} values of the *R* and *M* estimates are 509.2 and 487.3 nm with an estimated *M* to *R* extinction ratio of 1.573. The average maximum corrected absorbance loss for the mix_1 photobleach is 0.0325.

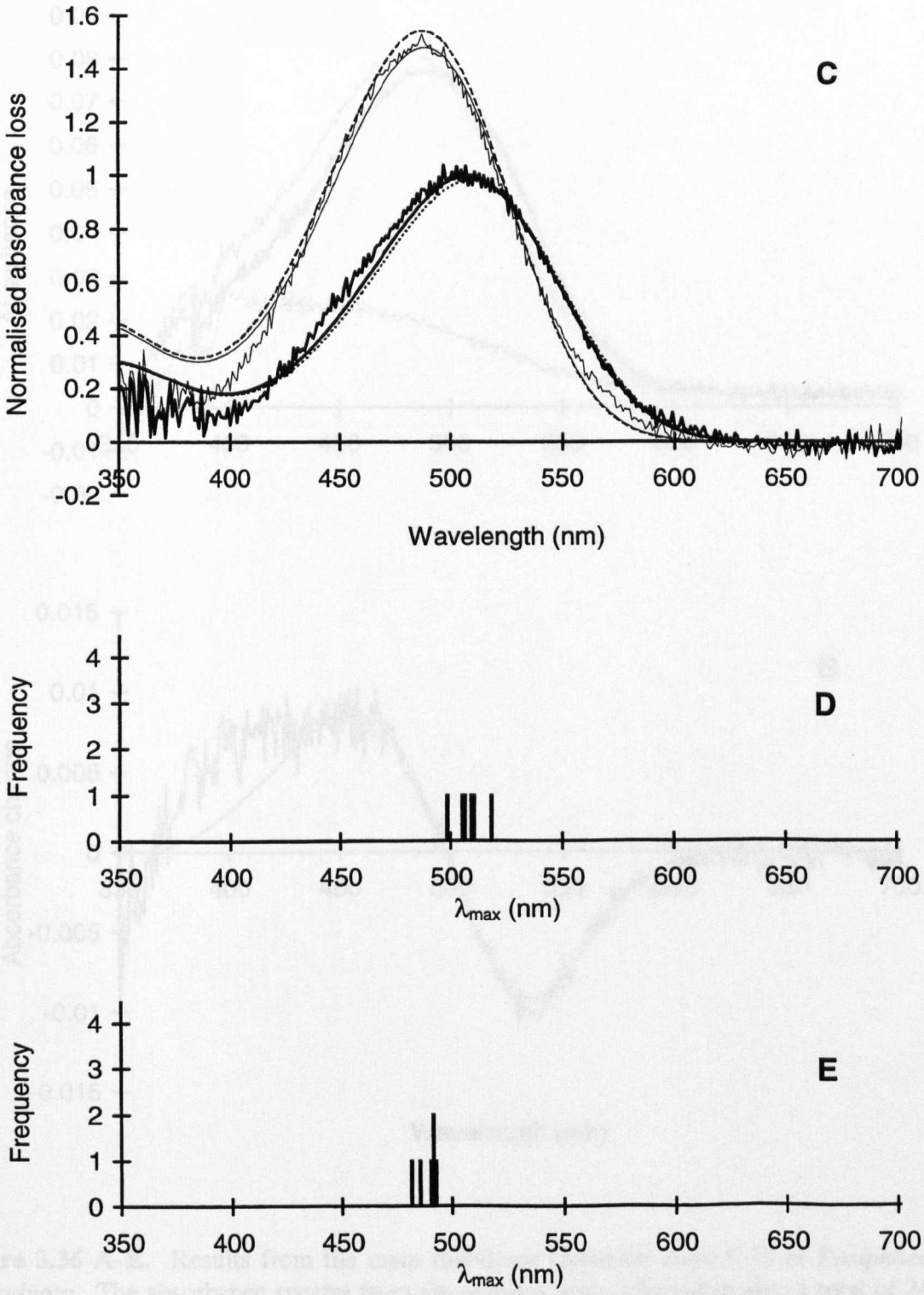

Figure 3.35 A–E. (Continued).

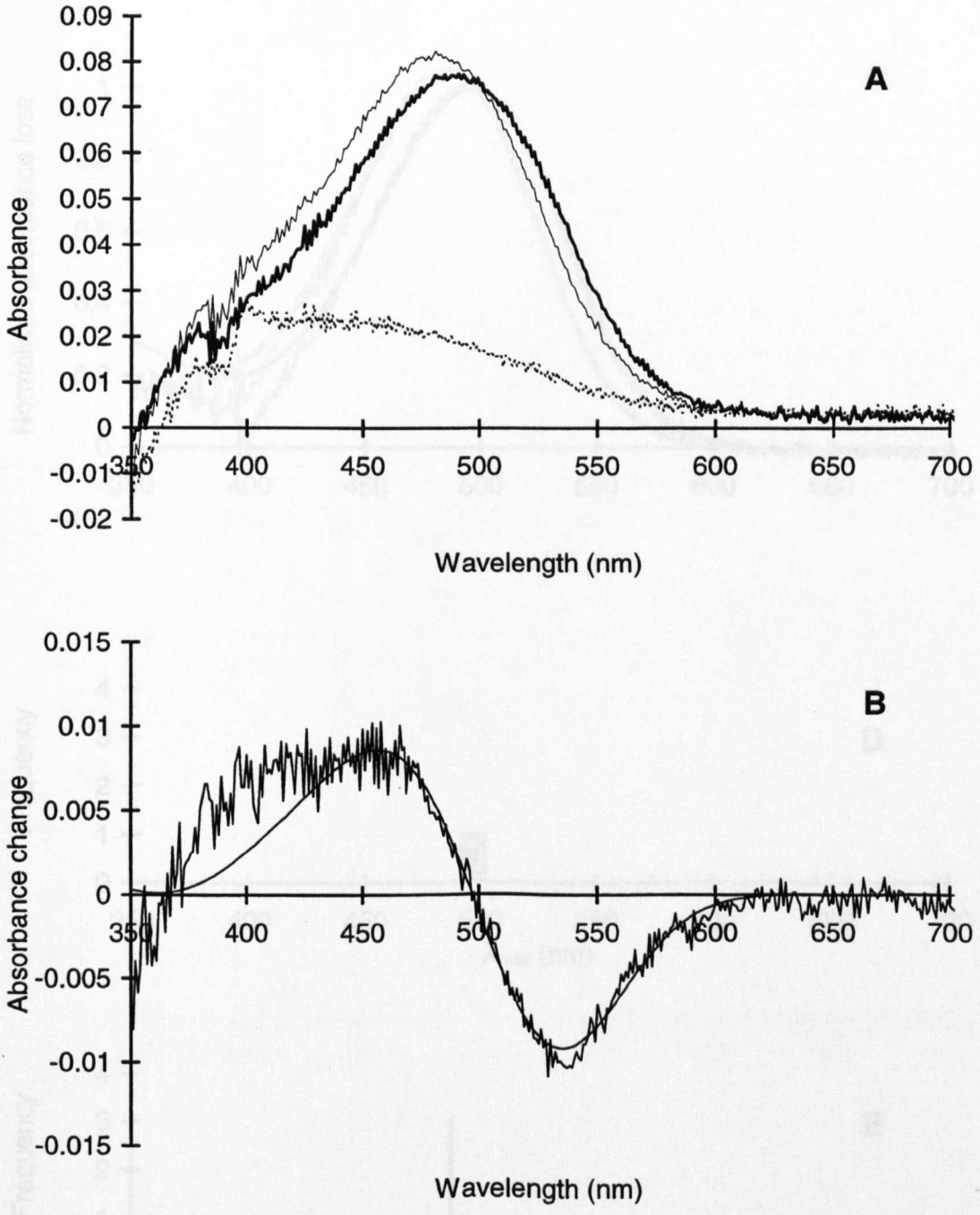

Figure 3.36 A–E. Results from the main rhabdoms (retinular cells 1–7) of *Pasiphaea emarginata*. The absorbance spectra from six sections were selected to give a total of 24 difference spectra which constitute the average files of mix_1 and mix_2. The λ_{max} values of the best-fit templates for mix_1 and mix_2 are 495.8 and 485.8 nm, and the λ_{max} values of the *R* and *M* estimates are 497.2 and 484.1 nm with an estimated *M* to *R* extinction ratio of 1.057. The average maximum corrected absorbance loss for the mix_1 photobleach is 0.0583.

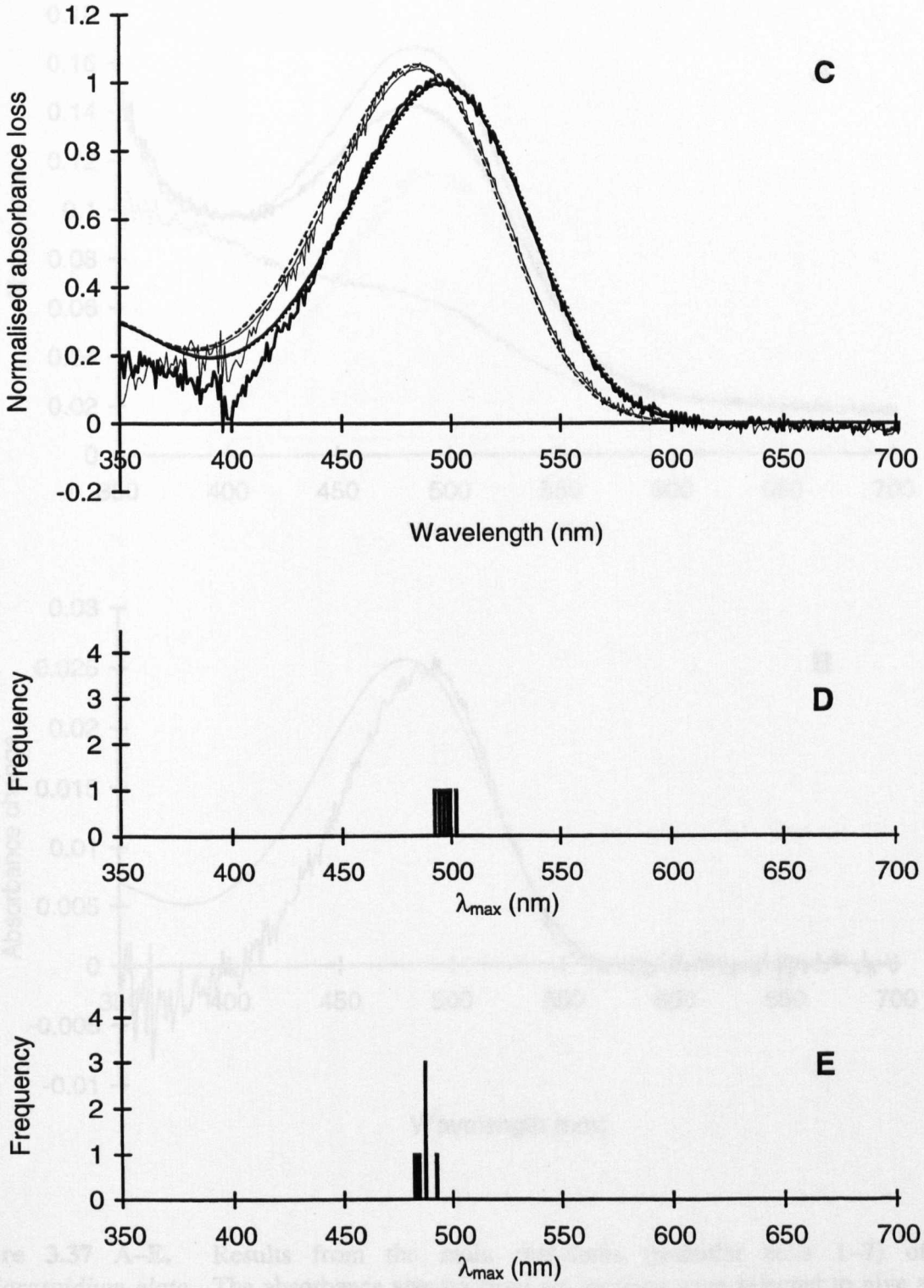

Figure 3.36 A–E. (Continued).

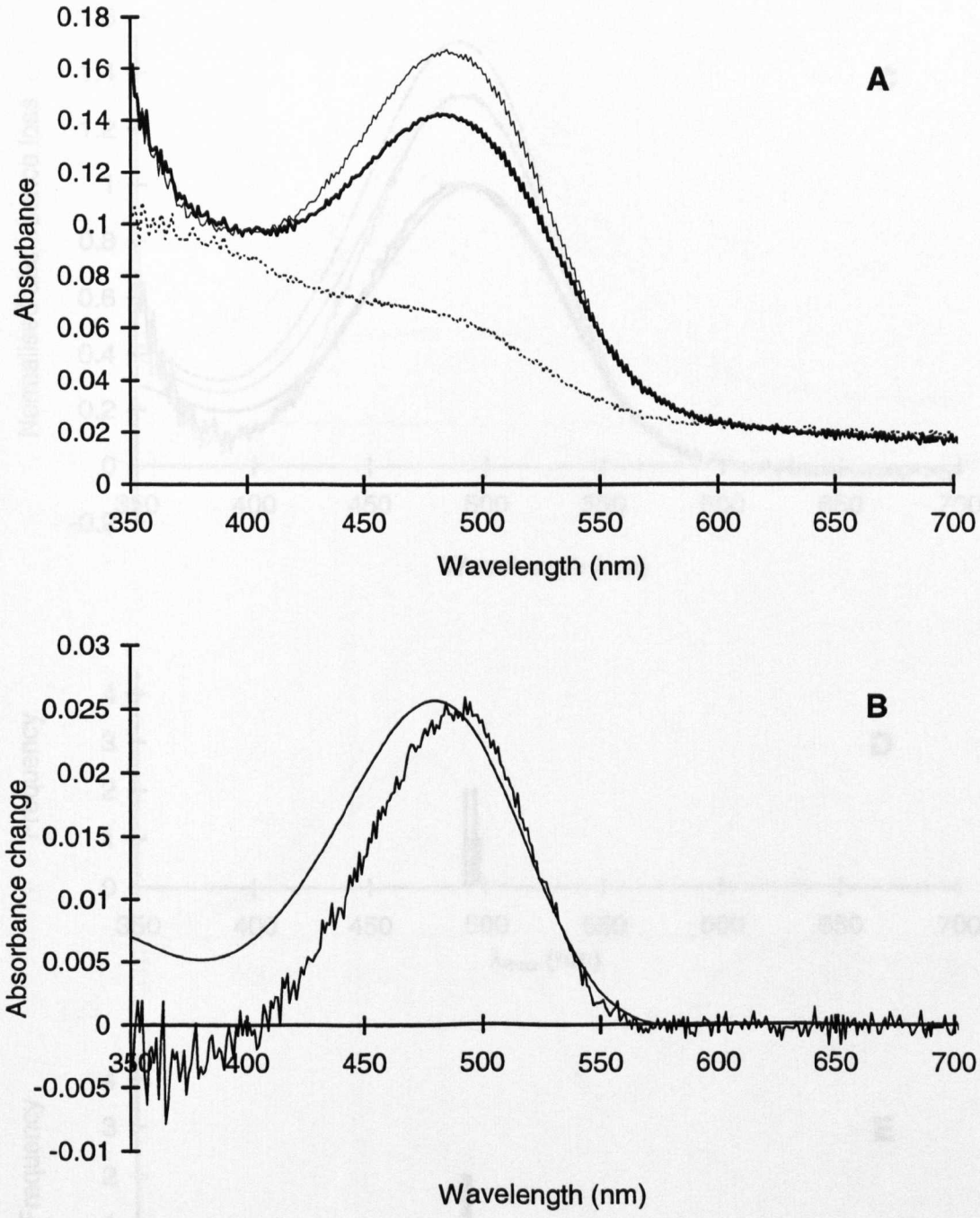

Figure 3.37 A–E. Results from the main rhabdoms (retinular cells 1–7) of *Chalaraspidium alata*. The absorbance spectra from six sections were selected to give a total of 24 difference spectra which constitute the average files of mix_1 and mix_2. The λ_{max} values of the best-fit templates for mix_1 and mix_2 are 493.4 and 489.6 nm, and the λ_{max} values of the *R* and *M* estimates are 493.3 and 488.1 nm with an estimated *M* to *R* extinction ratio of 1.516. The average maximum corrected absorbance loss for the mix_1 photobleach is 0.0774.

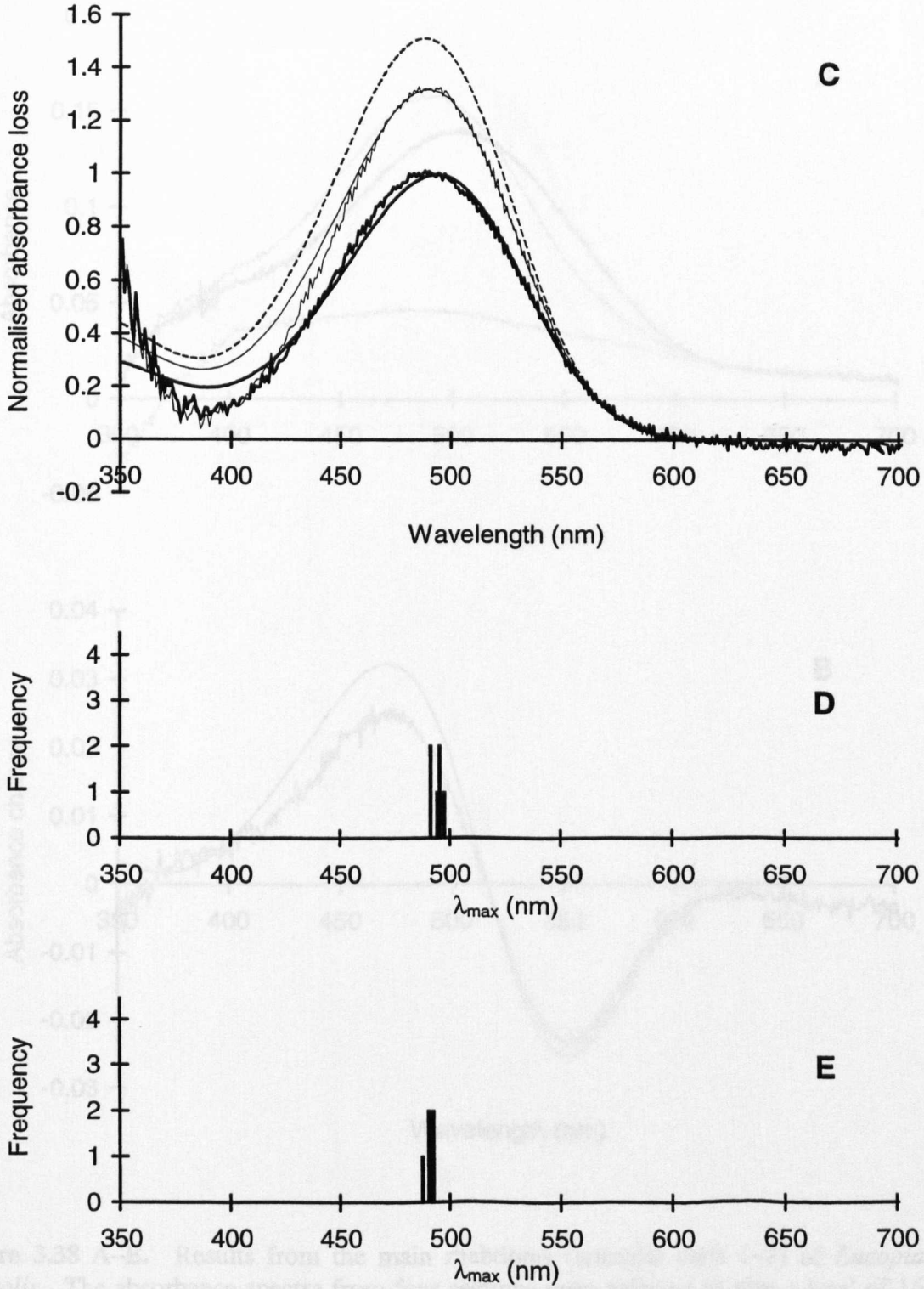

Figure 3.37 A–E. (Continued).

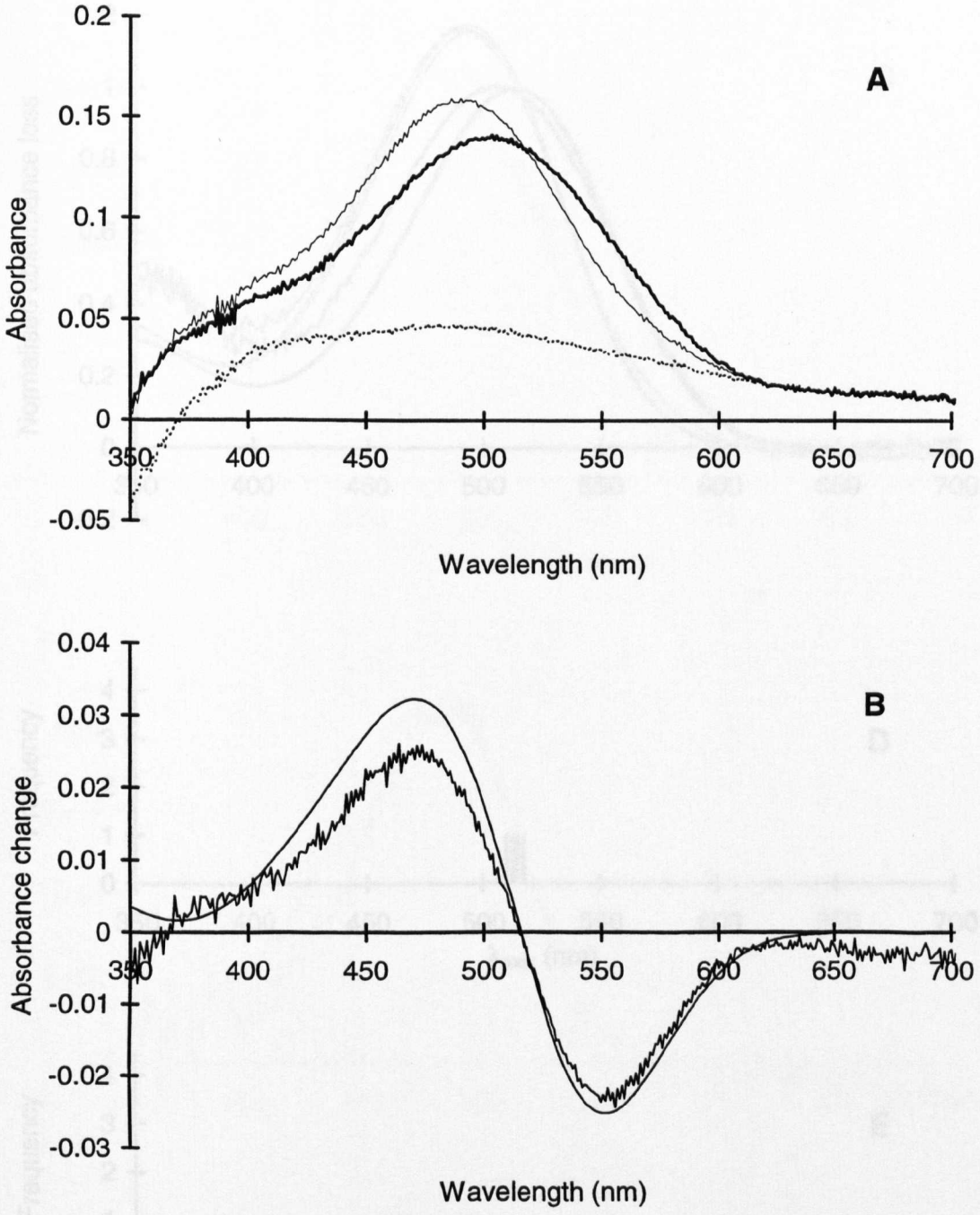

Figure 3.38 A–E. Results from the main rhabdoms (retinular cells 1–7) of *Eucopia australis*. The absorbance spectra from four sections were selected to give a total of 16 difference spectra which constitute the average files of mix_1 and mix_2. The λ_{max} values of the best-fit templates for mix_1 and mix_2 are 513.0 and 494.1 nm, and the λ_{max} values of the *R* and *M* estimates are 514.3 and 493 nm with an estimated *M* to *R* extinction ratio of 1.179. The average maximum corrected absorbance loss for the mix_1 photobleach is 0.0950.

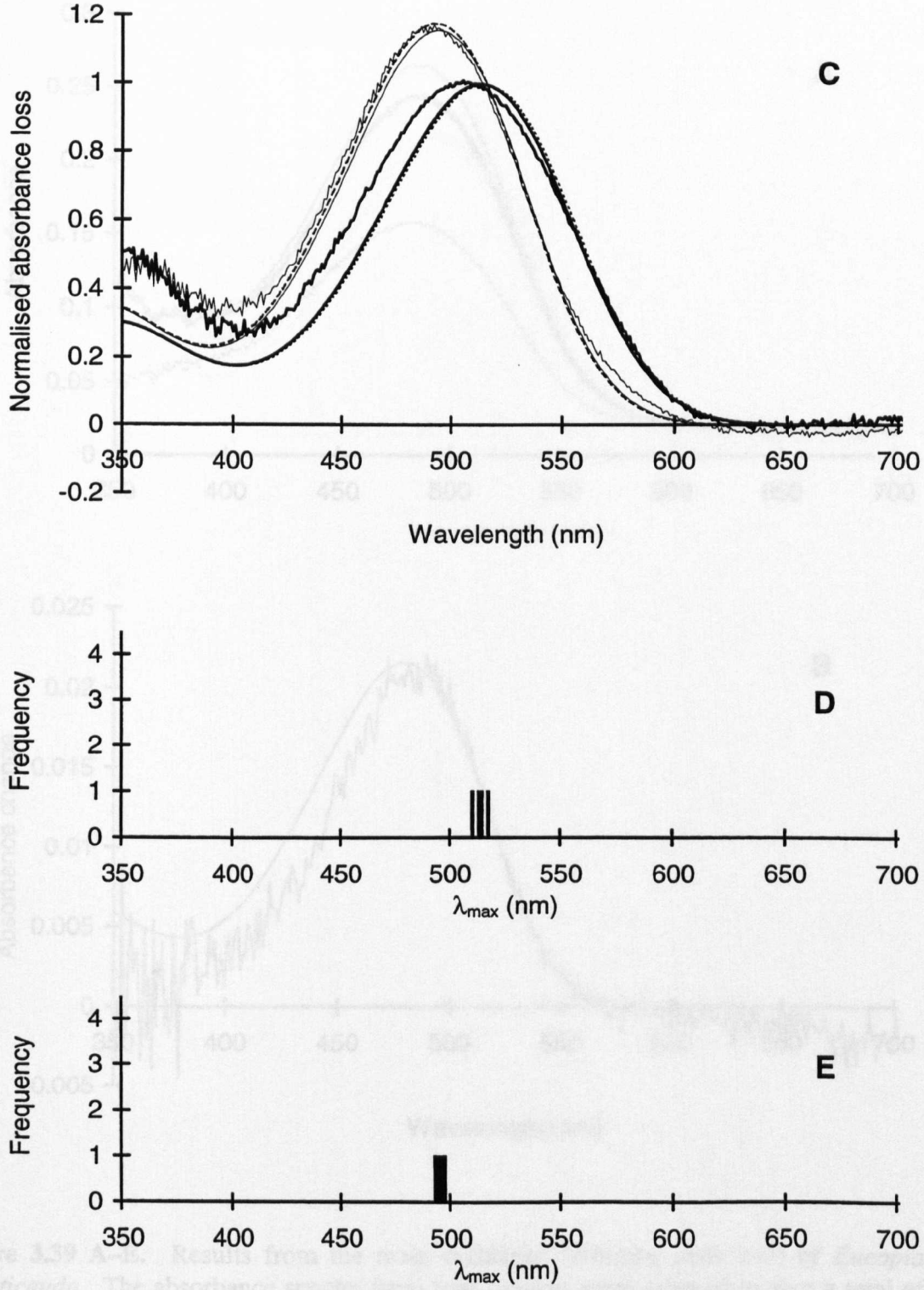

Figure 3.38 A–E. (Continued).

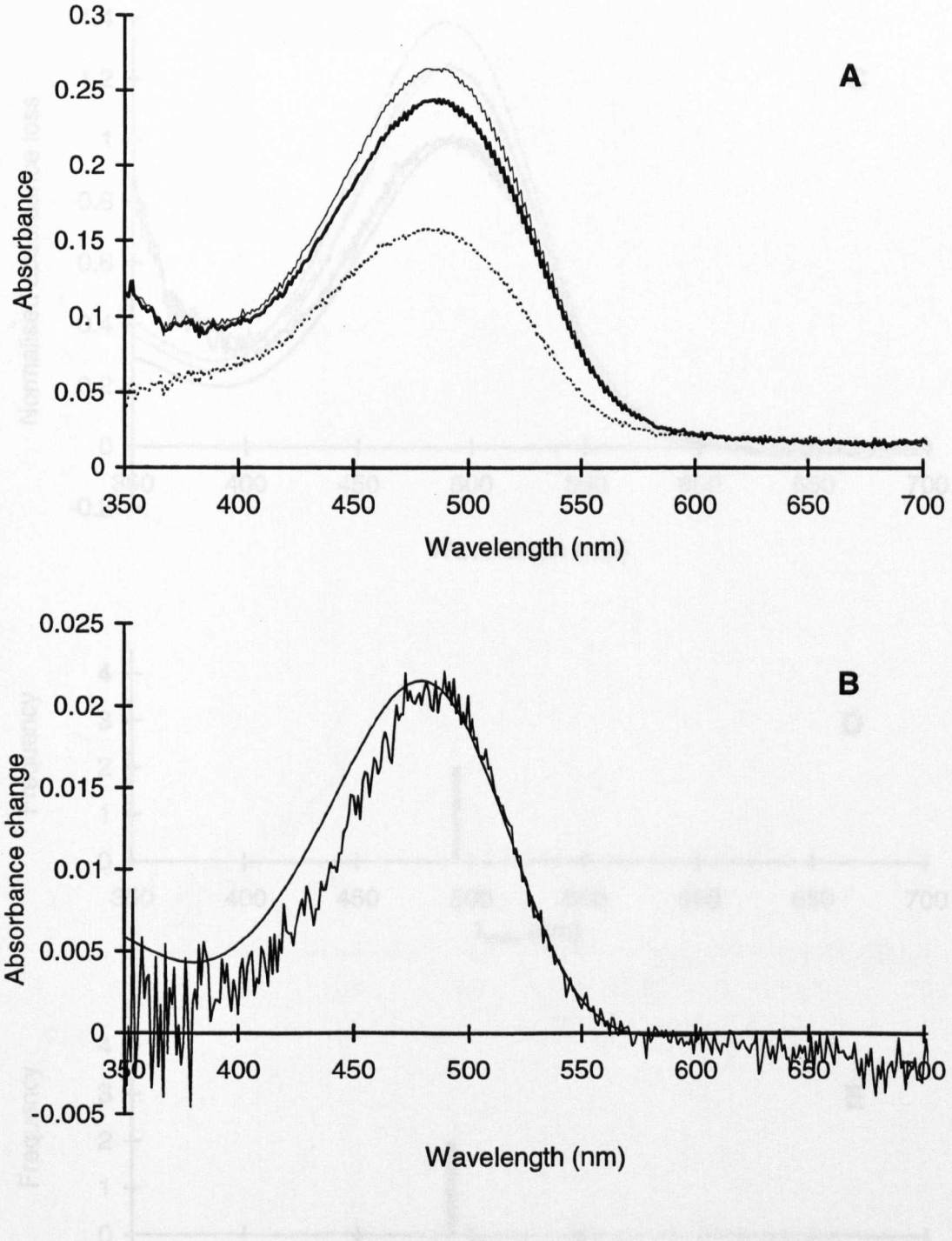

Figure 3.39 A–E. Results from the main rhabdoms (retinular cells 1–7) of *Eucopia sculpticauda*. The absorbance spectra from four sections were selected to give a total of 16 difference spectra which constitute the average files of mix_1 and mix_2. The λ_{max} values of the best-fit templates for mix_1 and mix_2 are 493.0 and 490.0 nm, and the λ_{max} values of the *R* and *M* estimates are 492.9 and 488.6 nm with an estimated *M* to *R* extinction ratio of 1.394. The average maximum corrected absorbance loss for the mix_1 photobleach is 0.0858.

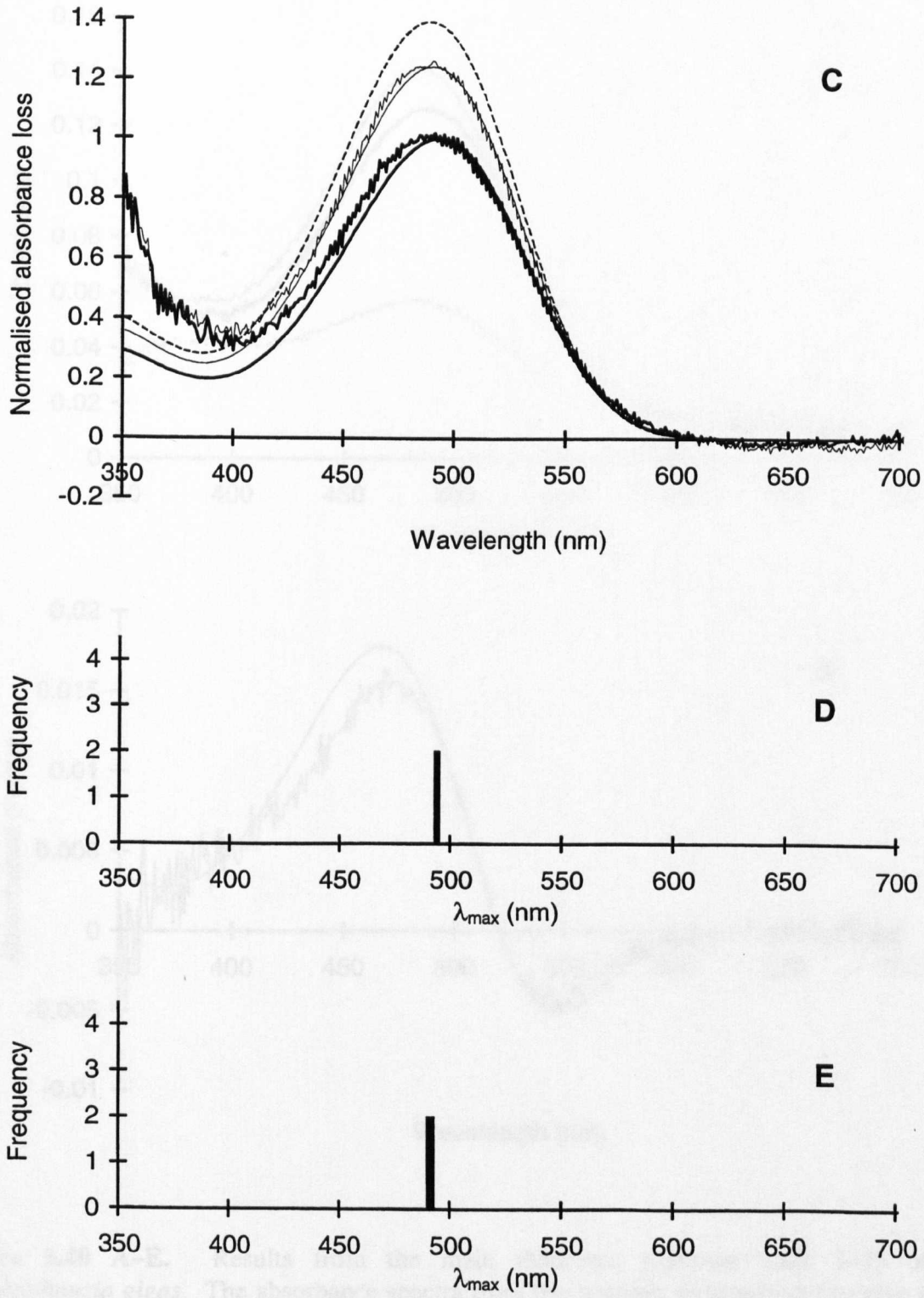

Figure 3.39 A–E. (Continued).

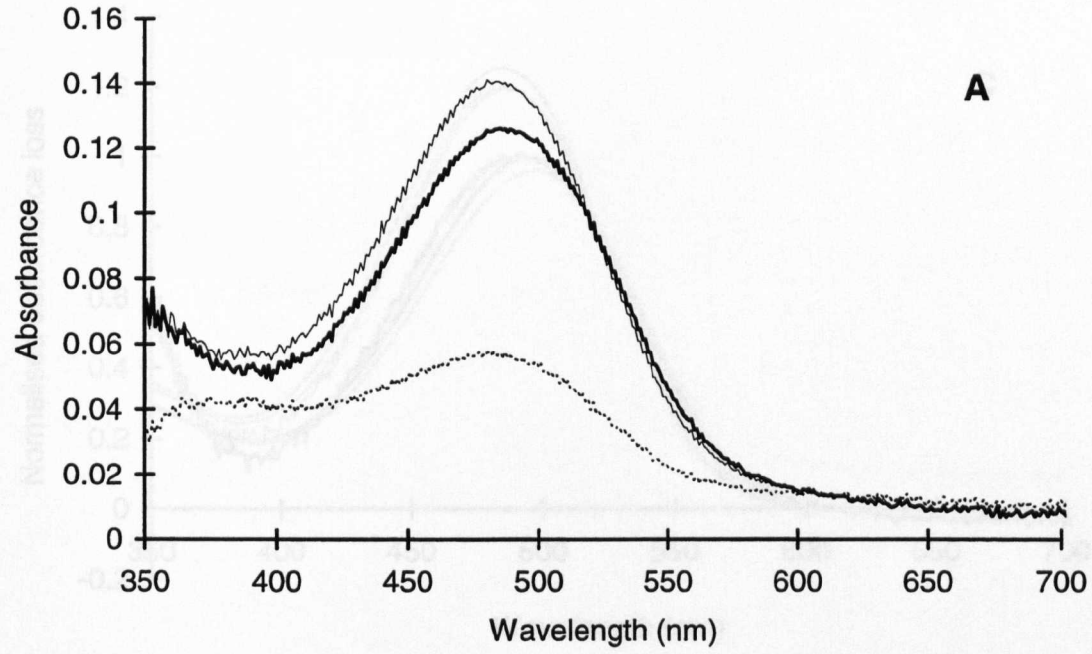

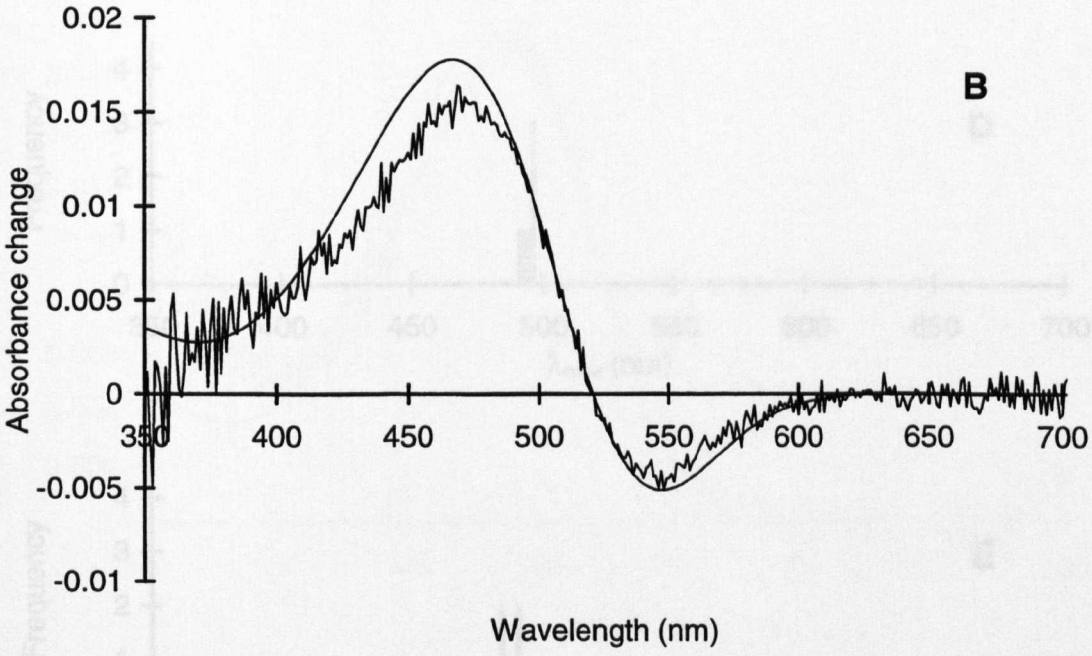

Figure 3.40 A–E. Results from the main rhabdoms (retinular cells 1–7) of *Gnathophausia gigas*. The absorbance spectra from five sections were selected to give a total of 20 difference spectra which constitute the average files of mix_1 and mix_2. The λ_{max} values of the best-fit templates for mix_1 and mix_2 are 491.4 and 489.7 nm, and the λ_{max} values of the *R* and *M* estimates are 491.3 and 488.7 nm with an estimated *M* to *R* extinction ratio of 1.318. The average maximum corrected absorbance loss for the mix_1 photobleach is 0.0699.

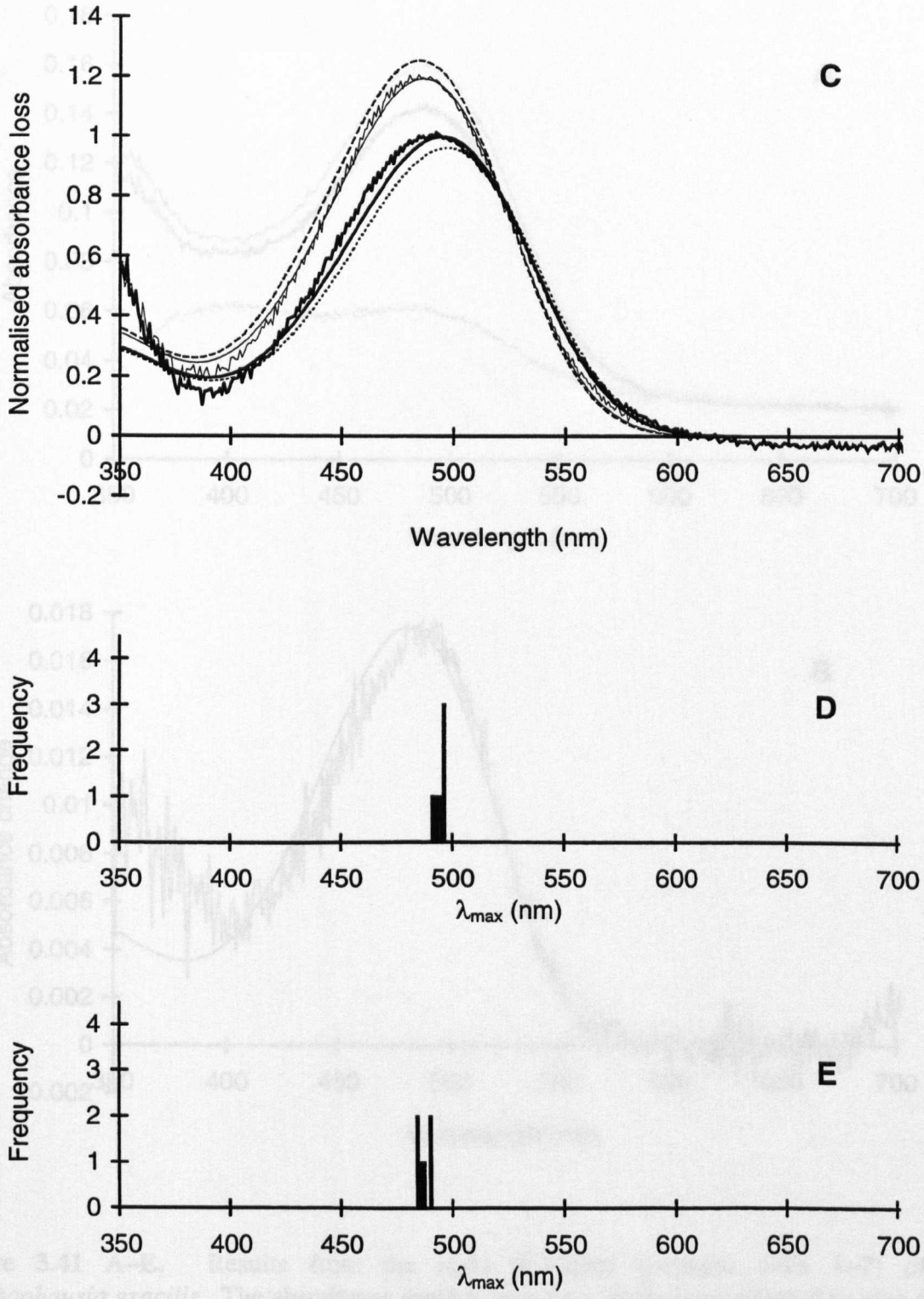

Figure 3.40 A–E. (Continued).

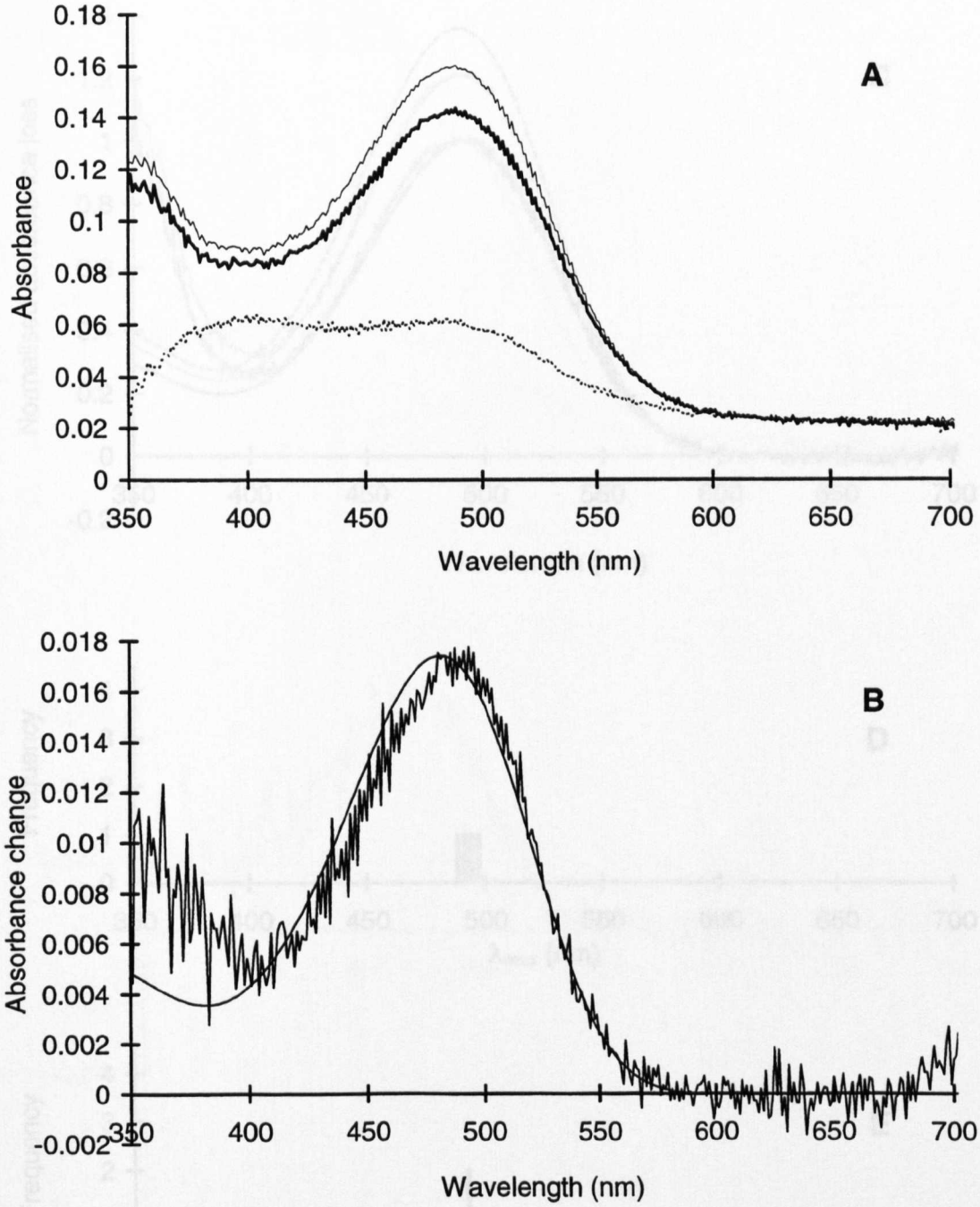

Figure 3.41 A–E. Results from the main rhabdoms (retinular cells 1–7) of *Gnathophausia gracilis*. The absorbance spectra from six sections were selected to give a total of 24 difference spectra which constitute the average files of mix_1 and mix_2. The λ_{max} values of the best-fit templates for mix_1 and mix_2 are 494.5 and 486.4 nm, and the λ_{max} values of the *R* and *M* estimates are 496.9 and 484.7 nm with an estimated *M* to *R* extinction ratio of 1.305. The average maximum corrected absorbance loss for the mix_1 photobleach is 0.0694.

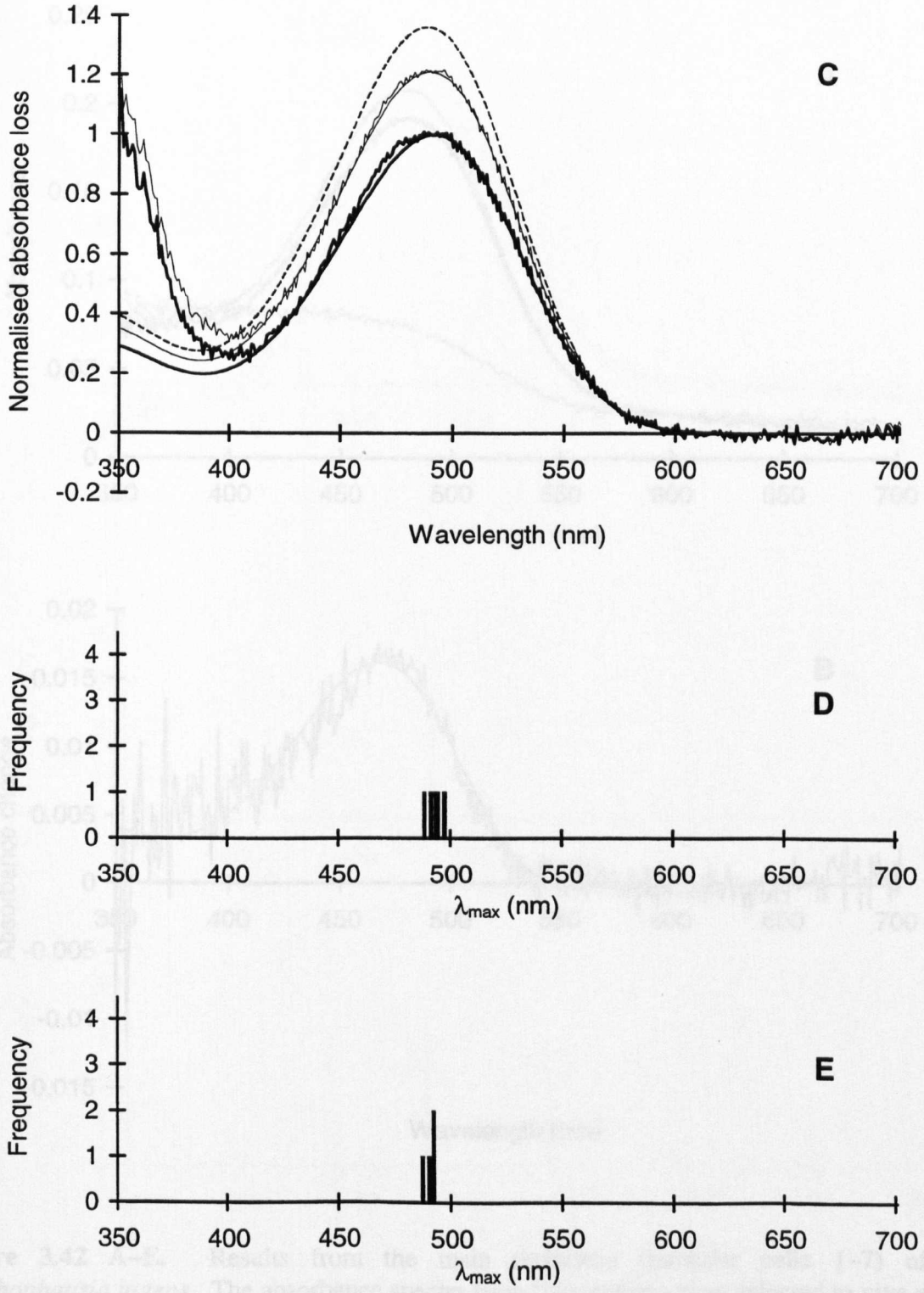

Figure 3.41 A–E. (Continued).

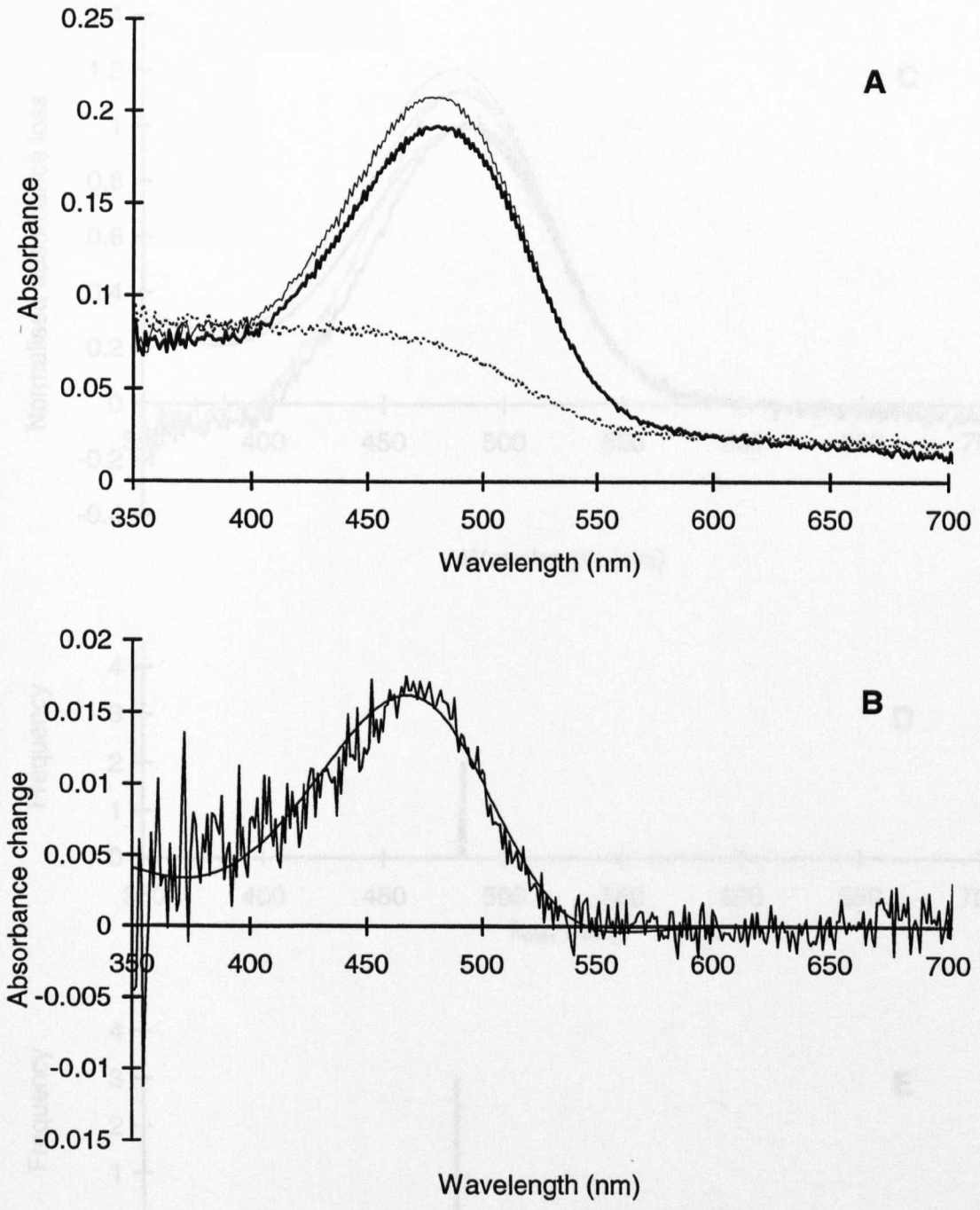

Figure 3.42 A–E. Results from the main rhabdoms (retinular cells 1–7) of *Gnathophausia ingens*. The absorbance spectra from five sections were selected to give a total of 20 difference spectra which constitute the average files of mix_1 and mix_2. The λ_{max} values of the best-fit templates for mix_1 and mix_2 are 491.7 and 489.8 nm, and the λ_{max} values of the *R* and *M* estimates are 491.6 and 488.7 nm with an estimated *M* to *R* extinction ratio of 1.363. The average maximum corrected absorbance loss for the mix_1 photobleach is 0.0810.

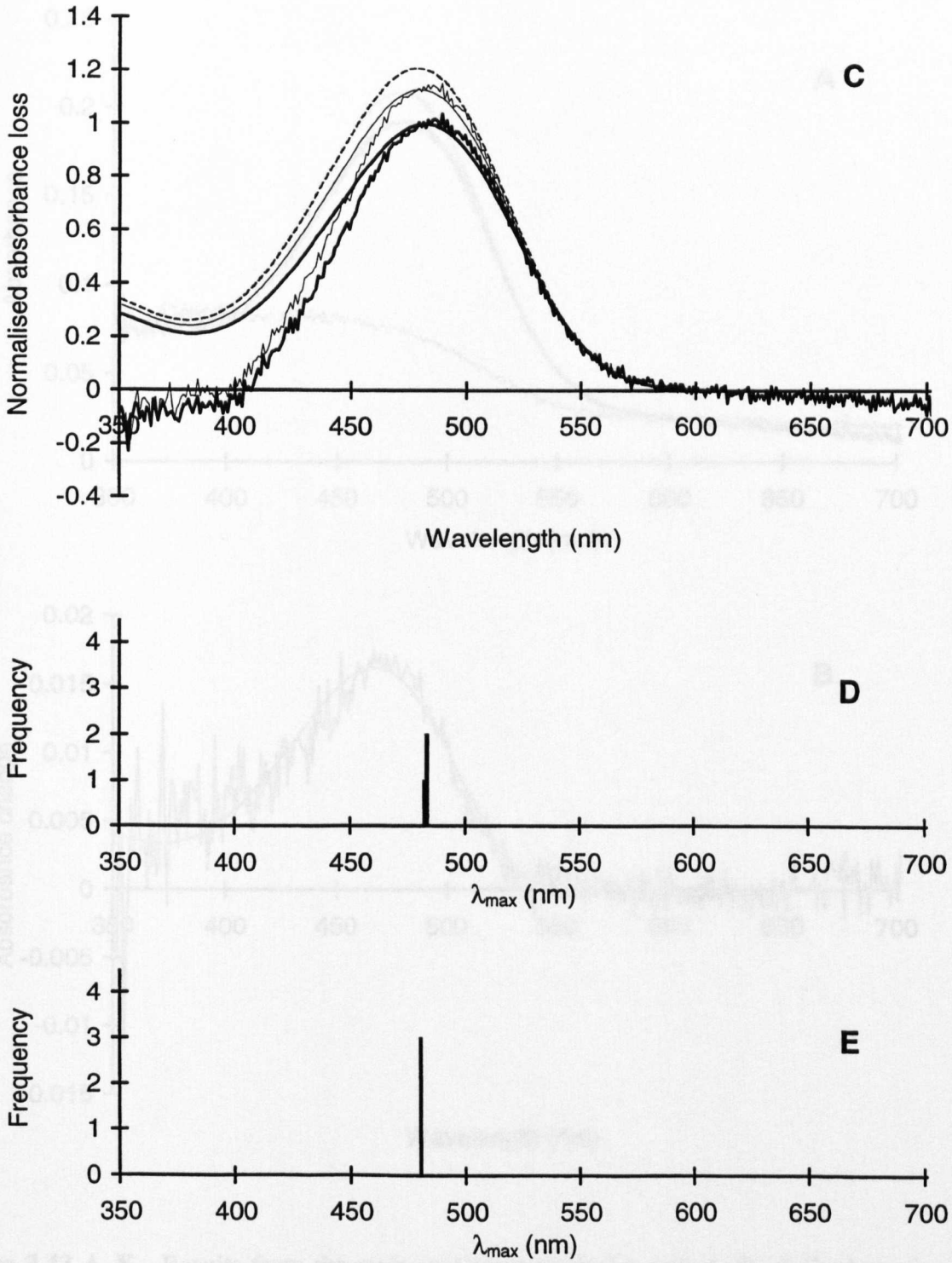

Figure 3.42 A–E. (Continued).

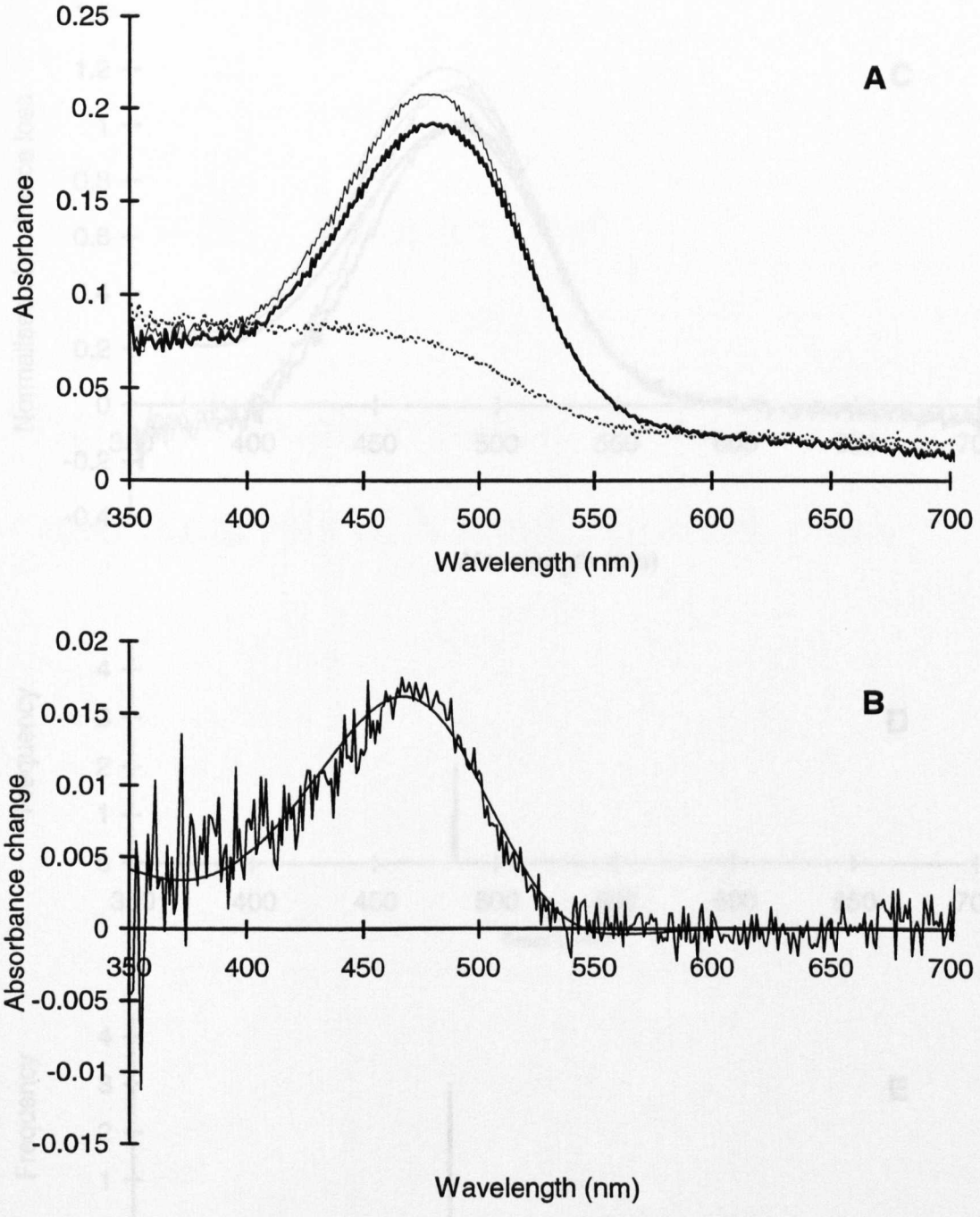

Figure 3.43 A–E. Results from the main rhabdoms (retinular cells 1–7) of *Cyphocaris richardi*. The absorbance spectra from three sections were selected to give a total of 12 difference spectra which constitute the average files of mix_1 and mix_2. The λ_{max} values of the best-fit templates for mix_1 and mix_2 are 481.8 and 479.7 nm, and the λ_{max} values of the *R* and *M* estimates are 481.7 and 478.6 nm with an estimated *M* to *R* extinction ratio of 1.210. The average maximum corrected absorbance loss for the mix_1 photobleach is 0.1181.

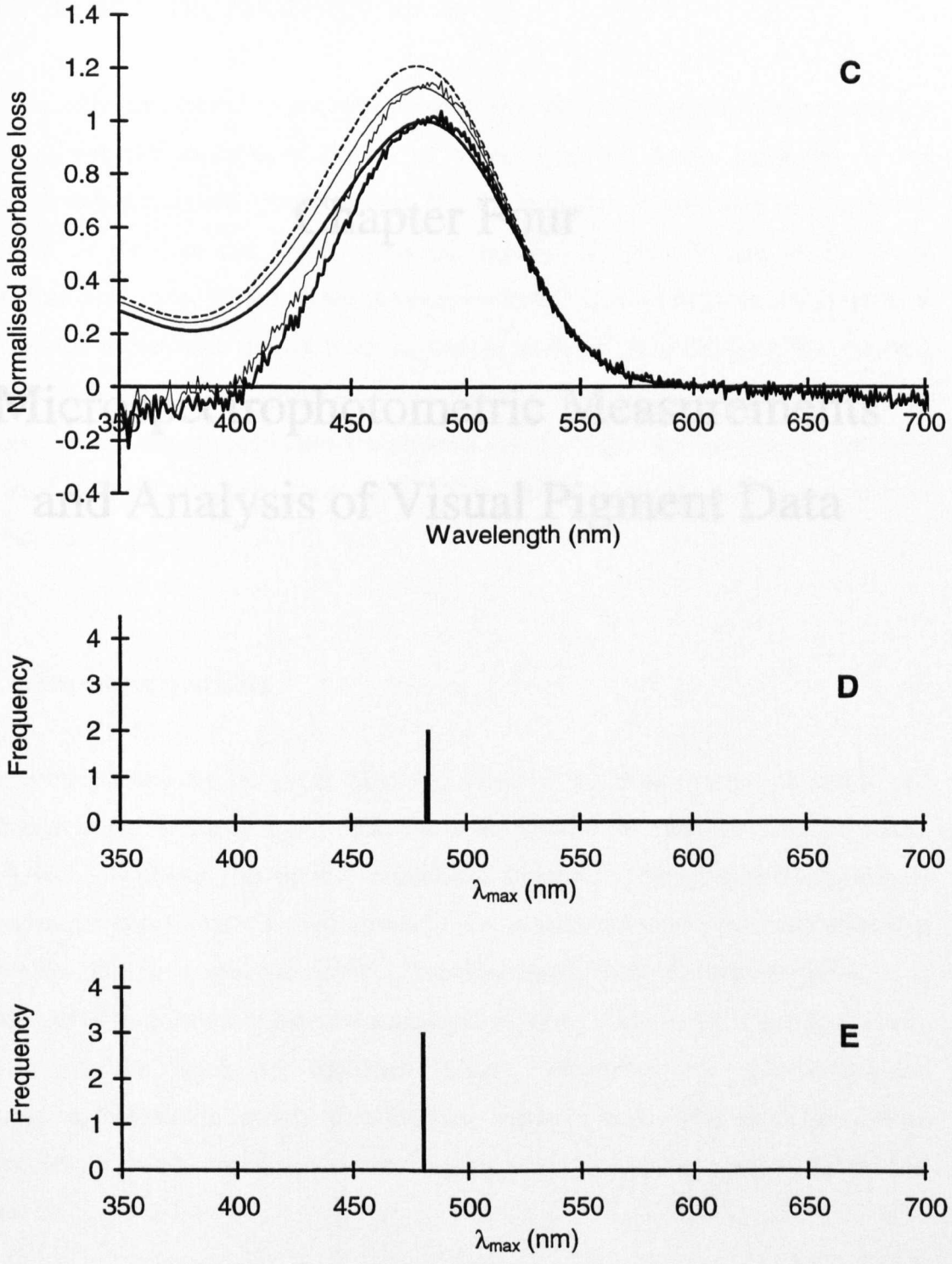

Figure 3.43 A–E. (Continued).

Chapter Four

Microspectrophotometric Measurements and Analysis of Visual Pigment Data

4.1 MICROSPECTROPHOTOMETRIC DATA

The main advantage of microspectrophotometry over all other methods currently used is that it allows the absorbance spectra of visual pigments to be measured in the photoreceptors, i.e. *in situ* (see Section 1.3). As such, one is not faced with potential distortions of the data due to the unnatural, experimental environment of the visual pigment molecule (i.e. during visual pigment extraction in detergents) or the process of deducing the absorbance spectra from another, behavioural measure (i.e. from spectral sensitivity recordings). However, the technique is often labour intensive and limited by the accuracy of the machinery used, the physical nature of light and the physical nature of the visual pigment molecules themselves. This section investigates the importance of such factors.

4.1.1 Absorbance precision

Microspectrophotometry of visual pigments involves the measurement of single cell absorbance using a beam of light which, due to the photolabile nature of visual pigments, must have a low photon flux density to minimise distortion of absorbance measurements by in-scan bleaching and/or photoconversion (i.e. bleaching and/or photoconversion that takes place during a spectral scan). The theoretical basis for the detection of a photosensitive substance has been discussed by Liebman (1972) and by Partridge (1986). Because of the need to minimise in-scan bleaching and photoconversion microspectrophotometric records often have low signal to noise (S/N) ratios (see Levine and MacNichol, 1985) and the absorbance values recorded will consequently have a low precision.

To measure the light absorption of a substance, it is necessary to detect the difference between the average incident light flux and the average transmitted light flux (i.e. the signal, S). For this to be possible the signal must sufficiently exceed in magnitude all random fluctuations in the signal (i.e. noise, N). Noise may be separated into signal induced noise, which is inevitable due to the quantum nature of light, and other extrinsic

noise sources which, to some extent, can be limited. For optimal operation it is preferable therefore to produce a microspectrophotometer whose accuracy and precision are only limited by photon noise.

4.1.1.1 Extrinsic noise

Noise other than photon noise may arise from a variety of sources including photomultiplier noise and drift, amplifier noise, extrinsic electrical noise, mechanical vibration, and movement of the retinal preparation. Strenuous efforts must be made to reduce or eliminate such sources of noise and the successful operation of the microspectrophotometer is fundamentally a question of maximising the signal to noise ratio of all measurements. These noise sources can be combated in a number of ways.

Photomultiplier intrinsic noise is due to current pulses produced within the photomultiplier which are not caused by noise in the light signal itself. This intrinsic noise includes dark noise (the current produced when the photocathode is shielded from the light), temperature dependent noise (thermionic emission and ionic gas release from metals related to increasing temperature), noise from cosmic rays and radioisotopes, and noise due to DC currents between electrodes or electrode high tension (HT) supply pins (e.g. via dust or fingerprints) etc. The noise rate of the photomultiplier tube is dependent on the type of photomultiplier used (e.g. bialkali photocathodes are considerably less noisy than trialkalis), the area of the photocathode and individual properties of the photocathode. The use of a permanent 'focusing' magnet will reduce the effective area of the photocathode, thereby reducing the dark current from the photomultiplier (MacNichol, Levine, Mansfield, Lipetz and Collins, 1983). Cooling the tube can give a substantial reduction in noise and has the additional advantage of eliminating temperature dependent drift in photomultiplier gain. If possible a tube with a particularly low noise and high quantum efficiency should be selected from a batch of tubes since photomultipliers are well known to show significant individual variation.

Noise inevitably arises in amplifier circuits as a result of thermal noise (including semiconductors), shot noise at p-n junctions and flicker or 1/f noise in transistors. While these sources cannot be entirely eliminated, the judicious selection of components in favour of 'low noise' types is essential. In addition it is important to isolate digital components from analogue circuitry where possible and provide separate power supplies. Although itself a source of some noise, the electronic rejection of noise by differential amplifiers or selective filtering is an important method for improving signal to noise ratios, and in the current microspectrophotometer a Butterworth 2-stage active filter is employed.

Extrinsic electrical noise arises from the switching in of high current devices either situated close to the microspectrophotometer's electronics or linked via the mains cable supply. Problems can be expected from such devices as thermostats or refrigerators housed in the same room as the microspectrophotometer. Where possible physical separation of such noise sources from the microspectrophotometer is beneficial. In addition the extensive use of earth-screened cables, for both digital control pulses and analogue signals, is advisable.

Mechanical vibration is frequently one of the most difficult noise sources to eliminate and high quality and robust engineering of all parts is essential. In addition the microspectrophotometer is mounted on a steel sheet (*ca.* 1 cm in depth) which rests on a cushion of small motorcycle inner tubes and foam-backed carpet. Together this arrangement provides some vibrational insulation of different frequencies from movement of people or machinery in adjoining rooms. Movement of cells in the preparation by convection currents, Brownian motion or even motile bacteria or protistans can be a problem with cell suspensions. However, such movement was not encountered when using the preserved ocular cryosections which thaw, and hence adhere, onto the coverslip. Preparation movements induced by focusing changes are reduced by eliminating as much excess medium from the preparation as is practically possible and sealing it between two coverslips with a ring of silicon grease.

4.1.1.2 Intrinsic, signal-induced noise

Signal-induced noise is the noise present in the signal from the photomultiplier. This is due primarily to the stochastic nature of photon flux which sets an irreducible upper limit to the signal to noise ratio attainable, i.e. the quantal nature of light, and the random nature of light emission from an incandescent source, leads to irreducible random modulation of the signal. In addition to this, the quantum efficiency of the photocathode will further reduce the signal to noise ratio by only registering a certain proportion of incident photons. Typically photocathode quantum efficiencies are about 10%, i.e. sampling 1 in 10 incident photons.

4.1.1.3 Intrinsic versus extrinsic noise

For the low light intensities used in the microspectrophotometry of visual pigments this intrinsic photo-electron noise should ideally be larger than noise due to all extrinsic sources. To test this the signal to noise ratio can be measured for different values of the signal. If the instrument is shot-noise limited then any change in light signal level should be accompanied by a square-root change in noise level, i.e.:

$$S/N \propto \sqrt{S} \qquad (1)$$

or $$\log_{10}(S/N) \propto 0.5\log_{10}(S) \qquad (2)$$

This relationship was tested with the microspectrophotometer of this study with changes in light level varying from transmission values of 1 to 0.13. The instrument was set up as if for normal use and the monochromator then stepped to an output of 730 nm and disconnected from the computer. Using the software normally used to control and record the scanning process, a file was then created storing the successive output from the V/F converter. These counts were then read into a spreadsheet and the values manipulated to give a value for the light signal, and the root-mean squared (RMS) noise of the signal. The light level was then changed by introducing increasing numbers of red acetate sheets

and the process repeated, until 13 such filters were scanned, corresponding to a transmission of *ca.* 0.13.

Once the linearity of the microspectrophotometer was confirmed (see Section 4.1.2 below) the inherent noise of the machine was investigated by plotting the logarithm of the RMS S/N ratios against the logarithm of the signal (see Figure 4.1). The regression line was then calculated which gave a gradient of 0.401 (with 95% confidence limits of $0.307 < x < 0.496$) and an intercept of 1.450 (with 95% confidence limits of $1.302 < x < 1.598$). Hence, from the confidence limits, this is significantly different from the theoretical gradient of 0.5 and it is concluded that the microspectrophotometer is not operating as a shot-noise limited device. While this does not affect the *accuracy* of the machine's recordings it does suggest that their *precision* could be improved, i.e. performance of the machine suffers some deterioration by extrinsic sources of electrical noise, photomultiplier dark noise or mechanical vibration noise etc. Due to the relatively large absorbances measured in this study achieving the maximum precision possible was not a limiting factor (see Sections 4.1.1.4 and 4.1.3 below). However, for the lower absorbances inherent when measuring vertebrate tissue optimisation of photon flux is often critical (see Partridge, 1986) and since this study the machine has undergone various modifications to reduce extrinsic noise.

4.1.1.4 In-scan photoconversion and photobleaching

The concentrations of visual pigments present in invertebrate photoreceptors (i.e. their specific absorbance) are generally lower than those found in vertebrates (see Land, 1981a). However, in the case of invertebrate tissue, presented either as a section through the eye or as dispersed cells, the photoreceptors are generally much larger (often greater than 100 x 20 μm) and present a greater optical pathlength (*ca.* 15 to 20 μm). The measuring beam can therefore be larger (typically 5 x 3 μm in this study, an area up to ten times that used with many vertebrate photoreceptors) and, overall, has a greater total photon flux which increases the signal to noise ratio. Thus, while invertebrate records have inherently higher signal to noise ratios, successful microspectrophotometry of

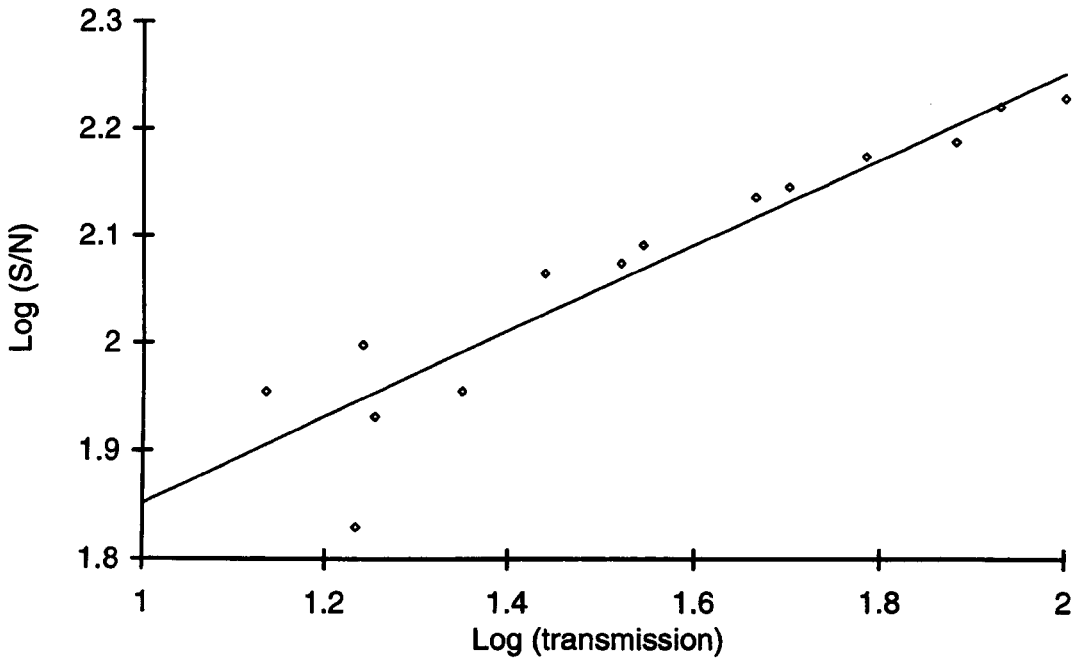

Figure 4.1 Signal to noise ratio versus signal of the microspectrophotometer used in this study. As the signal increases (here expressed as $\log_{10}(S)$) the S/N (here expressed as $\log_{10}(S/N)$) also increases. The regression line has a gradient of 0.401 (with 95% confidence limits of $0.307 < x < 0.496$) and an intercept of 1.450 (with 95% confidence limits of $1.302 < x < 1.598$). This is significantly different from the theoretical gradient of 0.5 and it is concluded that the microspectrophotometer is not operating as a shot-noise limited device.

invertebrate visual pigments still involves a careful optimisation of signal to noise ratios (Goldsmith, 1972; see also Liebman, 1972; Levine and MacNichol, 1985; Partridge, 1986).

Despite signal to noise optimisation the measurement of the absorption spectra of photoconvertable and photolabile pigments will inevitably cause some photoconversion and/or bleaching. Due to the relatively high levels of light needed to bleach invertebrate visual pigments, in-scan photoconversion is the greatest problem. Though scanning in both directions will help to counter this (i.e. from long to short wavelengths and back), the uneven spectral light flux of the measuring beam and the different absorbance characteristics of the two pigments (i.e. different λ_{max} values and extinction coefficients) will mean that some photoconversion is inevitable. During the preliminary study, multiple scans of invertebrate photoreceptors were made with increasing photon flux densities by varying a neutral density filter which restricts the light output from the exit slit of the monochromator. This was repeated until separation of the down–up and up–down scans was apparent. A neutral density filter with an absorbance greater than this value was then selected (peak absorbance of the filter selected is 1.07). Hence, this filter allows the maximum possible light flux of the measuring beam with levels of photobleaching and/or photoconversion lower than the noise inherent in the signal. Thus the level of photoconversion and bleaching during scanning has an insignificant effect on the overall shape of the measured absorption spectra.

4.1.1.5 Estimation of absorbance precision

When measuring visual pigment absorbance spectra one of the main characterising variables (along with the λ_{max}; see Section 4.2.4) is the maximum absorbance of the visual pigment (i.e. the absorbance at the λ_{max}). Due to the frequent necessity to subtract an offset, this is termed the maximum *corrected* absorbance (see Section 4.2.2) and its precision relies on the precision of the value of the absorbance at both the peak and at the longwave offset. The analysis software then indicates the precision of the maximum

corrected absorbance by combining the variability at the two points from which it is calculated (see Section 4.2.5.1).

In order to estimate an average value for this 80 typical difference spectra were selected (see Section 4.2.7.3), analysed with a 19 point running average, and their maximum corrected absorbances and associated standard deviations recorded. These values were then averaged to give an average maximum corrected absorbance of 0.102 with an average standard deviation of 0.003. Thus this implies that the microspectrophotometer, as used in this study, has an average measuring precision of *ca.* 3% for difference spectra with signals of this level. As these files were selected because they are typical of the ones obtained in this study, it can be further speculated that the average levels of in-scan photoconversion and/or photobleaching accounted for a change in absorbance of less than *ca.* 3%. Note that this refers to the microspectrophotometer as used in this study, i.e. measuring with two down–up, up–down spectral passes per record. The amount of photoconversion and/or photobleaching per spectral pass is thus less than 3% and, due to the uneven spectral light flux of the measuring beam and the different absorbance characteristics of the two pigments, the degree of photoconversion will depend on the direction of the spectral pass.

4.1.2 Absorbance accuracy

While the precision of the microspectrophotometer can be thought of as the repeatability of a given measurement, and is therefore governed by the noise in the signal, the accuracy is defined as the difference between the values recorded (averaged to reduce the effects of noise) and their actual values. Thus, the same filters used to test the signal to noise of the microspectrophotometer, incremented in the same order, were scanned using a Shimadzu UV-2101PC scanning spectrophotometer. The latter is known to be linear with a transmission accuracy of ± 0.3% and a repeatability of ± 0.1% in the transmittance range from 0.1 to 1. The transmission of the filters as measured by the microspectrophotometer were then plotted versus the transmission of the filters as measured by the Shimadzu spectrophotometer (Figure 4.2). The regression line was then calculated which gave a gradient of 1.023 (with 95% confidence limits of $0.972 < x < 1.074$) and an intercept of

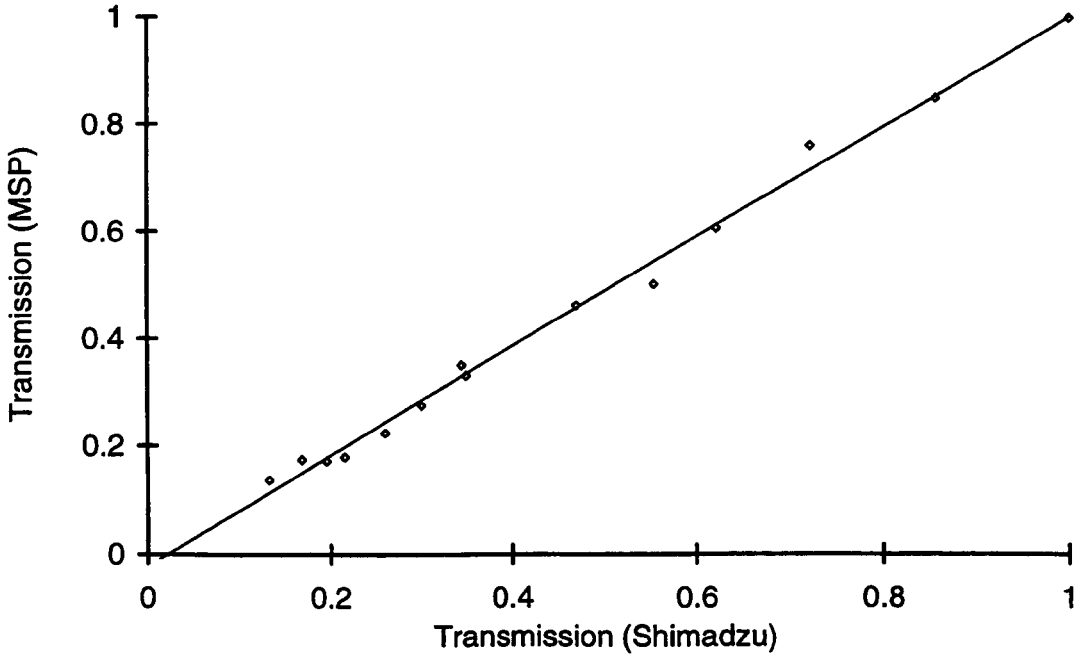

Figure 4.2 Linearity of the microspectrophotometer used in this study. The transmissions of a series of red acetate filters were measured at 730 nm by both the microspectrophotometer used in this study and a Shimadzu UV-2101PC scanning spectrophotometer. The regression line has a gradient of 1.023 (with 95% confidence limits of $0.972 < x < 1.074$) and an intercept of -0.022 (with 95% confidence limits of $-0.048 < x < 0.004$), indicating that the recordings of the microspectrophotometer are not significantly different from those of the spectrophotometer. Hence, because of the known linearity of the spectrophotometer, it is concluded that the microspectrophotometer is also linear over this transmission range.

-0.022 (with 95% confidence limits of $-0.048 < x < 0.004$). Hence, from the confidence limits, this is not significantly different from a gradient of 1 and an intercept of 0, indicating that the recordings of the microspectrophotometer are not significantly different from those of the Shimadzu spectrophotometer. Relative to the spectrophotometer, it is therefore concluded that the microspectrophotometer is both accurate and linear over this transmission range (equivalent to absorbance values from 0 to 0.866).

4.1.3 Other sources of distortions

Visual pigments measured by microspectrophotometry are subject to other potential artefacts caused by a number of factors including vibrations, tissue movement during measurement, the build up of photoproducts absorbing within the spectrum scanned, and the presence of other photolabile compounds. The tissue structure was also observed to deteriorate over time, causing the rhabdomeric tissue to take on a granular appearance. This is associated with scattering of shortwave light and an apparent increase in absorbance at the shortwave end of the spectrum. The damaged and thawed tissue structure also allows the migration of other, non-visual pigments such as screening pigments into the rhabdom. All of these factors may be responsible for wavelength dependent changes in absorbance of the tissue being measured in addition to the change due to the visual pigment present. Hence they may be included in, and therefore distort, the calculated absorbance spectrum of the visual pigment.

The absorbance due to non-visual pigments in the retinal tissue can be measured after all the visual pigment has been removed through bleaching with high photon flux density white light from the substage condenser. The absorbance of this photo-stable pigment can then be subtracted from the initial measurements, and those made after the red light treatment, to obtain the absorbance due to the visual pigment present. However, the calculation of such difference spectra relies on the assumption that any change is due only to visual pigments. While the build up of photoproducts, changes in tissue structure and migration of non-visual pigments will distort all of the recorded absorbance spectra, if these changes occur during the duration of the post-bleach bleach (from *ca.* 20 to 75 min)

they will also distort the difference spectra. Thus, all of these factors potentially explain any distortions seen between the calculated absorbance spectra of the visual pigments and their best-fit rhodopsin templates.

4.1.4 Wavelength precision and accuracy

The accuracy of the wavelengths as recorded by the microspectrophotometer is determined by the wavelength accuracy of the monochromator. According the manufacturer's specification the Jobin Yvon H-1061 VIS grating monochromator (Instruments S.A. Ltd., Middlesex, UK) is accurate to ± 0.5 nm. However, this is a best case and is only approached if the backlash is taken up (i.e. the slack in the drive cam between the monochromator and the stepper motor which drives it) and when stepping is in one direction only. Every precaution was taken to ensure the former, both mechanically and in the controlling software, and the latter was addressed by scanning only odd wavelengths on the 'downward' long- to shortwave spectral pass and only even wavelengths on the 'upward' short- to longwave spectral pass.

The wavelength precision of the microspectrophotometer can be controlled by the software because each wavelength reached by the monochromator is referenced to a wavelength calibration file, and it is the latter value that is recorded with the absorbance. To test the accuracy and calibration (i.e. precision) of the monochromator a didymium filter was used. Such filters are composed of mixtures of rare earth elements and have numerous absorption peaks and troughs at various wavelengths (see Figure 4.3). However, their exact absorption spectra vary from filter to filter and as a result must be calibrated themselves if they are to be used. Hence, the filter was first scanned using a Shimadzu UV-2101PC scanning spectrophotometer and then using the microspectrophotometer. Data from these scans were compared, the various minima and maxima recorded, and the discrepancies between the spectrophotometer and microspectrophotometer wavelengths noted assuming the spectrophotometer's values to be correct. No trend was apparent between discrepancies and the wavelengths at which they occurred, nor differences between the down–up and up–down spectral passes. All discrepancies were within ± 2 nm, with an average of + 0.9 nm. Hence, the wavelength

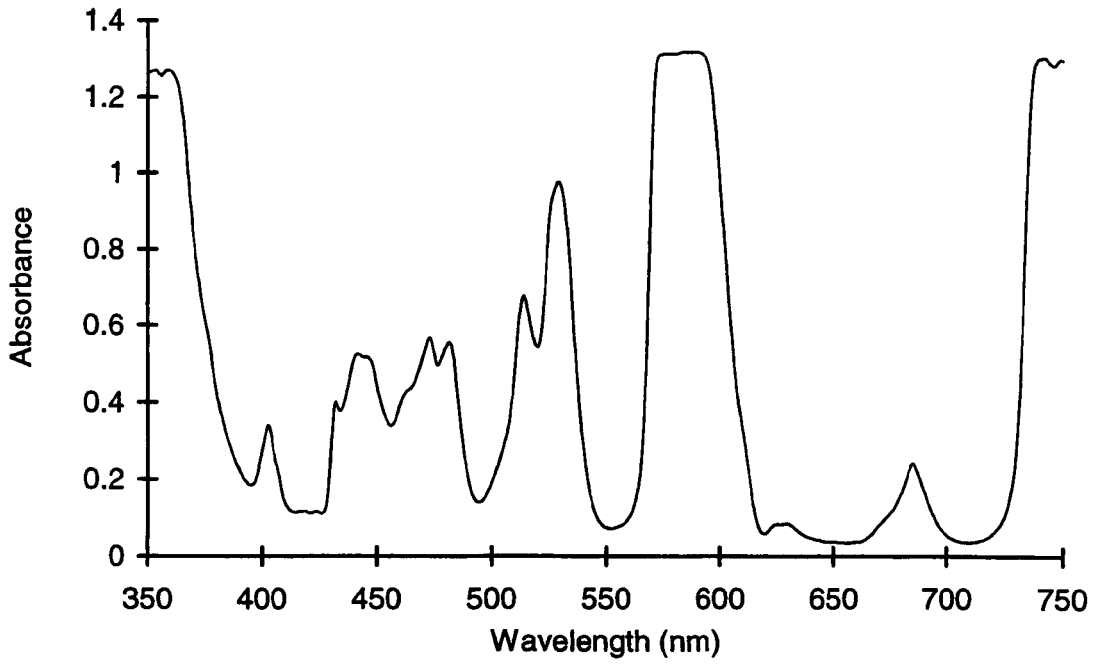

Figure 4.3 The absorbance spectrum of a didymium filter. Composed of mixtures of rare earth elements, it has numerous absorption peaks and troughs at various wavelengths specific to that filter. This filter was scanned using a Shimadzu UV-2101PC scanning spectrophotometer with a 1 nm FWHM bandwidth and numerically converted to represent a scan using an 8 nm FWHM bandwidth (i.e. equivalent to that of the microspectrophotometer). Such a scan was frequently compared to scans made by the microspectrophotometer to check wavelength accuracy and calibration (i.e. precision).

calibration file was created such that the true wavelength recorded was 1 nm greater than the wavelength as indicated by the monochromator and the wavelength accuracy of the microspectrophotometer is approximately ± 1 nm.

4.2 DATA ANALYSIS OF VISUAL PIGMENT ABSORBANCE SPECTRA

Microspectrophotometric records suffer from three consequences of the measurement process: 1) low signal to noise ratios, 2) distortions and 3) in-scan bleaching and/or photoconversion. The latter are discussed above (Section 4.1.1.4 and 4.1.3). To improve signal to noise ratios, many spectra from both the same and different photoreceptors, or areas of the retinal tissue, can be averaged together (see Section 4.2.7). Assuming the noise of the individual scans is equal between scans and entirely random, the signal to noise ratio of the average will be improved by the square root of the number of records in the average. However, some sources of noise, such as vibrations due to the scanning mechanism, may not be random in nature and will not be reduced by scan averaging (see Section 4.1.1.1). To avoid the inclusion of distorted measurements into averaged spectra, the microspectrophotometric data must be subjected to selection criteria (these have generally only been discussed for the microspectrophotometry of vertebrate systems; e.g. Hárosi, 1975; Levine and MacNichol, 1985; Partridge, 1986). These selection criteria often involve the use of template curves to describe the idealised absorbance spectrum of visual pigments. Such templates may be constructed as the sum of mathematical formulae (Hárosi, 1976; Levine and MacNichol, 1985, Partridge and DeGrip, 1991; Stavenga *et al.*, 1993) or may be based on transformed measurements of some carefully measured visual pigment (e.g. Bowmaker *et al.*, 1975).

The use of template curves for data selection presents the potential problem of circularity: i.e. only data fitting the template are selected so that the final average of the accepted data are bound to fit the template employed. However, Partridge and DeGrip (1991) have shown that this problem is unimportant if the selection criteria allow adequate departure of the data from the template being employed and yet allow some objective method by which seriously distorted data can be eliminated. Throughout this study a modified

rhodopsin visual pigment template given by Stavenga *et al.* (1993) has been used (see Section 4.2.4.4).

The rhodopsin template spectrum given by Stavenga *et al.* (1993) is based on the absorbance spectrum of purified bovine rhodopsin presented by Partridge and DeGrip (1991). Though the intermediate stable states of vertebrate and invertebrate visual pigments differ, the absorbance spectra of their rhodopsin states do not appear to (see Lipetz and Cronin, 1988). Thus the rhodopsin visual pigment template given by Stavenga *et al.* (1993) was used when analysing the initial minus post-bleach (mix_1) difference spectra. The absorbance spectra of invertebrate metarhodopsins have not been studied in depth but, from the data collected to date, appear to be identical to those of vertebrate rhodopsins with identical λ_{max} values. Hence, the rhodopsin visual pigment template given by Stavenga *et al.* (1993) was also used for analysis of the post-red light treatment minus post-bleach (mix_2) difference spectra.

Once the original microspectrophotometric files have been selected and averaged (see Section 4.2.7), there are still benefits in fitting a template to these average spectra, despite their high signal to noise ratios. Template fitting is often the most accurate way of determining both the λ_{max} and maximum absorbance of the data (see Sections 4.2.2 and 4.2.4). Further, if the data fit the template well, they can be described in terms of these two variables only and a representation of the data reproduced using the template formula without the need of the raw data. (Note that the *specific* maximum absorbance is preferable to the maximum absorbance measured as this takes into account the pathlength over which the visual pigment was measured and thus is a measure of pigment concentration.) In some cases, particularly in the modelling of visual pigment systems, it is preferable to use the template instead of the data as it is both easier to generate and has no associated noise.

4.2.1 Computer based analysis software

The analysis programs used during this project were written within Microsoft Excel 5.0c using Microsoft Visual Basic for Applications. It was decided that analysing the data within a spreadsheet would give users subsequent flexibility for data manipulation, incorporation and presentation, as well as the benefits of the familiar, user-friendly, 'Windows' presentation.

Each analysis workbook is saved as a read-only file split into a series of worksheets, each with their own specific function. A common plan was adopted so that a user familiar with one analysis program would soon be able to use any of the others available. Thus, most start with a 'Notes' sheet containing information for the user followed by a 'Control' sheet where the user may change certain variables, specify file details and initiate the analysis, often by simply clicking the mouse on the labelled button(s). Where appropriate the data are read into a 'Raw Data' sheet and data analysis carried out in the 'Calculations' sheet. The results of this analysis, together with relevant file information and control variables, are then presented in the 'Output' sheet which is often designed for printing. Various other data and analysis sheets may be present, as well as charts for graphical presentation. At the end of each workbook is a sheet named 'Procedures' which includes all the Visual Basic code used to automate Microsoft Excel through its macro functions.

The raw data are saved by the microspectrophotometer's PC as a comma delimited ASCII text file. This includes 'header information'; experimental variables needed for analysis and future reference. This is followed by three columns of wavelengths, baseline frequencies and sample frequencies in ascending wavelength order. The baseline and sample frequencies are the output of the microspectrophotometer's voltage to frequency converter as counted by the MetraByte CTM-05 counter/timer board in the microspectrophotometer's PC. The microspectrophotometric data file is read into the Microsoft Excel spreadsheet and the baseline and sample frequencies converted into absorbance values. The absorbance values are then normalised, a template fitted and various other variables calculated.

All visual pigment analysis programs are also capable of averaging files. Each file is first converted into absorbance values and then the average absorbance value at each wavelength is calculated. A new comma delimited file is then created, the average file, with reconstructed sample and baseline frequencies. Because the data are not normalised at any point the averaging process is not affected by any other variables (e.g. the position of longwave offset absorbance, or the number of points in the running average; see Sections 4.2.2.2 and 4.2.6) and has remained the same in all versions of the program. Thus it was not necessary to re-average all of the individual files each time a new version of the software was introduced. Simply, each average file was re-analysed.

4.2.2 Data normalisation

4.2.2.1 Finding a maximum

It is far easier to find the maxima and minima of smoothed (MacNichol, 1986) or noise-filtered data (e.g. Fourier transform filtering, Hárosi, 1987; Press, Flannery, Teukolsy and Vetterling, 1986) and this also helps to achieve consistent data normalisation necessary for subsequent template fitting. The 'box-car' running average used in the visual pigment analysis programs is designed to smooth the data so that fixing the peak and longwave offset absorbances is less affected by random noise at any particular point (see Sections 4.2.2 and 4.2.6). This is done by taking the average of a number of successive data points, all weighted evenly, and assigning this value to the middle datum point within this range. Thus the running average must always have an odd number of points. The running average 'half-bandwidth' is equal to the number of points minus one divided in half and represents the extremes of the average either side of the current datum point.

During analysis a box-car running average is passed through the absorbance values and the 'peak absorbance' value noted with its corresponding wavelength. This wavelength is then referred to as the 'running average λ_{max}'. The user can change both the number of points in the running average and its starting wavelength. Changing the number of points can significantly affect the normalisation of the data and is discussed below (Section

4.2.6). The latter option is useful if spectra show high absorbances at short wavelengths which might otherwise be used as the peak absorbance by the analysis program.

The running average λ_{max} is calculated not only because it indicates the wavelength at which the data are normalised, but also because it should be the same as the fitted template λ_{max} (see Section 4.2.4.1) if scans have a high signal to noise, the optimum number of points are used in the running average and the scans are not distorted. Since averaging results in high signal to noise ratios (see Section 4.2.7) and considerable effort was made to determine the optimum number of points needed in the running average (see Section 4.2.6), the running average λ_{max} can then be used as a check on data quality: i.e. it is independent of the calculation of the offset (see the following Section, 4.2.2.2) and is not dependent on the assumptions made when using a template (see Section 4.2.4.1). The results of such a comparison between λ_{max} estimates is discussed in Section 4.2.7.4.

4.2.2.2 Finding a minimum

Microspectrophotometric sample scans are frequently offset from the baseline scans principally because of optical differences between the tissue and tissue-free space which change the way in which light is focused onto the photomultiplier tube. Offset is also introduced by inert substances in the tissue also absorbing light. For difference spectra calculated from non-normalised raw data the offset may, in addition, reflect changes in the measuring apparatus with time (e.g. changes in room temperature affecting the output of electrical components) and the incomplete final bleaching of any visual pigment present. Both of the latter are likely to be wavelength dependent (due to the varying wavelength dependent signal) and such 'drift' is often noticeable as a positive or negative gradient at the longwave end of the spectrum which should otherwise be flat.

Due to these factors, it is often necessary to introduce an offset when normalising the absorbances measured. This offset is calculated at the longwave end of the spectrum where there is no absorbance due to the visual pigment. However, due to potential drift, it is not sufficient to simply set the offset at the longest wavelength(s) recorded. The

'longwave offset absorbance' is therefore set as the value of the running average at the closest wavelength equal to, or just longer than, the predicted wavelength at which the normalised absorbance of the visual pigment being measured is 0.005, plus the half-bandwidth of the running average (see Section 4.2.2). Thus, it effectively sets the offset as the average absorbance over a variable number of points at wavelengths longer than the predicted 0.005 maximum normalised absorbance wavelength. The 'maximum corrected absorbance' is taken as the peak absorbance minus the longwave offset absorbance and the data are normalised to this range for subsequent calculations and display. This method will result in an underestimation of the peak absorbance but, even with noise free data, this systematic error is just 0.5% (see Table 4.1).

The transform proposed by Mansfield (1985) and MacNichol (1986) produces an invariant rhodopsin template (see Section 4.2.4.1). If correct, then it follows that for all rhodopsin spectra there will be a consistent relationship between λ_{max} and any other wavelength of given absorbance on the short- or longwave limbs of the α-band. Thus, for the rhodopsin template used to analyse the data in this study (that given by Stavenga *et al.*, 1993; see Section 4.2.4.1) the wavelength at which the normalised absorbance is 0.005 is equal to $\lambda_{max}/0.8104$ nm (calculated using a λ_{max}/λ transformation based on a 500 nm λ_{max} template). During analysis only the running average λ_{max} can be determined before data normalisation and so, in practice, the offset wavelength is set relative to this wavelength.

With increasing number of points in the running average the longwave offset will shift to include longer wavelengths and the actual offset will decrease (see Table 4.1). An alternative method would be to simply fix the longwave offset at the closest wavelength equal to or just longer than the predicted wavelength at which the normalised absorbance of the visual pigment being measured is equal to 0.005. However, while the central wavelength of the longwave offset would remain unchanged (i.e. relative to the running average λ_{max}) the value itself would not. Though the running average would include data points both lower than 0.005 maximum normalised absorbance at longer wavelengths and those greater than 0.005 maximum normalised absorbance at shorter wavelengths, the overall effect would be to increase the absorbance of the running average at the offset

Table 4.1 The effect of varying the number of points in the running average on the longwave offset absorbance, with the longwave offset wavelength both fixed and allowed to shift.

Number of points in the running average	Fixed longwave offset [a]		Shifting longwave offset [b]	
	Wavelength at which offset is calculated (nm)	Offset absorbance (as % of peak)	Wavelength at which offset is calculated (nm)	Offset absorbance (as % of peak)
1	617	0.5	617	0.5
3	617	0.5	618	0.45
5	617	0.5	619	0.41
7	617	0.51	620	0.37
9	617	0.52	621	0.34
11	617	0.52	622	0.31
13	617	0.53	623	0.29
15	617	0.54	624	0.26
17	617	0.56	625	0.24
19	617	0.57	626	0.23
21	617	0.59	627	0.21
23	617	0.6	628	0.2
25	617	0.62	629	0.18
27	617	0.64	630	0.17
29	617	0.67	631	0.16
31	617	0.69	632	0.15
33	617	0.72	633	0.14
35	617	0.75	633	0.15
37	617	0.78	634	0.14
39	617	0.81	635	0.14
41	617	0.85	636	0.13
43	617	0.89	637	0.12
45	617	0.93	638	0.12
47	617	0.97	639	0.11
49	617	1.01	640	0.11

[a] The longwave offset is taken as the running average absorbance at 617 nm (equivalent to 0.005 maximum normalised absorbance). [b] The longwave offset absorbance shifts and is taken as the running average absorbance at the wavelength at which the normalised absorbance of the visual pigment being measured is 0.005, plus the half-bandwidth of the running average.

All other calculations were identical between the two methods and the data were produced by analysing noise-free, normalised rhodopsin template data with a 500 nm λ_{max}, generated using the equation given by Stavenga *et al.* (1993), and fixing the calculated maximum absorbance to unity.

wavelength as the number of points in the running average increased. This is due to the shape of the visual pigment spectrum which increases at a greater rate on the longwave limb before 0.005 maximum normalised absorbance than it decreases beyond it. Thus 'noisy' data that warrant a large number of points in the running average would be incorrectly normalised.

To show this effect, Table 4.1 was produced by analysing noise-free, normalised rhodopsin template data with a 500 nm λ_{max}, generated using the equation given by Stavenga *et al.* (1993), and fixing the calculated maximum absorbance to unity. Even in the worst case, when 49 points are used with a fixed longwave offset, this would produce an error in normalisation of just 1.01% (assuming that the maximum absorbance is accurately determined). The 'shifting longwave offset' was adopted and used because the analysis protocol also has a tendency to use too many points in the running average. This will start to flatten the peak of the visual pigment spectrum and further increase the underestimation of the total amplitude of the data (see Section 4.2.6.1). Also, by shifting the wavelength at which the offset is determined to increasingly longer wavelengths it introduces a greater margin of error should the position of the running average λ_{max} be incorrectly determined. Indeed, it is the setting of the offset wavelength relative to the wavelength of the running average λ_{max} that probably constitutes the largest error in data normalisation. This in turn will affect the main analysis process of template fitting (see Section 4.2.4.1 below).

4.2.3 Bandwidth

The full width at half maximum (FWHM) bandwidth of the data is determined by searching the running average absorbance values for those equivalent to half the maximum corrected absorbance. On the shortwave limb this will return the wavelength with an absorbance just under 0.5 normalised absorbance, thus half of the wavelength step interval is added and this wavelength listed. On the longwave limb the wavelength with an absorbance equivalent to just over 0.5 normalised absorbance will be returned, hence half of the wavelength step interval is subtracted and this wavelength listed. The FWHM

bandwidth is then equal to the wavelength of the longwave 50% point minus the wavelength of the shortwave 50% point.

4.2.4 Finding the λ_{max}

4.2.4.1 Using a rhodopsin template

The main visual pigment analysis involves the use of the polynomial given by Partridge and DeGrip (1991) to calculate the λ_{max} of a rhodopsin template that best-fits the data. Specifically, the λ_{max} values (nm) can be calculated from the wavelength (λ; nm) and the normalised absorbance of a data point (y) on the longwave limb between 80% and 20% of the maximum absorbance using the equation:

$$\lambda_{max} = \lambda\left(0.84628 + 0.20749y - 0.19932y^2 + 0.12486y^3\right) \qquad (3)$$

In effect, the template is moved mathematically to intersect each valid datum point on the longwave limb in a method similar to that described by Bowmaker *et al.* (1975), and the λ_{max} values noted for each. The average of these estimations is then taken as the best estimate of the λ_{max} of the data and is quoted as the template mean λ_{max} with the standard deviation, standard error and number of points used (or 'number of valid points') also calculated and listed. Only the longwave limb of a visual pigment absorbance spectrum is used to estimate the λ_{max} because this part of the spectrum is least affected by photoproduct build-up and light scattering at short wavelengths. It has the additional benefit of avoiding the overlapping regions of the α- and β-bands when the λ_{max} is at short wavelengths (see Section 4.2.4.3).

Partridge and DeGrip (1991) constructed their new template from the absorbance spectrum of purified bovine rhodopsin. Applying an abscissa transform of λ_{max}/λ as proposed by Mansfield (1985) and MacNichol (1986) they derived the cubic polynomial fitting the longwave limb as well as a Chebyshev polynomial accurately modelling the α-

band of the template. The rhodopsin template given by Stavenga *et al.* (1993) was derived using the same published bovine rhodopsin absorbance data of Partridge and DeGrip (1991). It assumes that the λ_{max}/λ transform holds for the α-band irrespective of the spectral position of the band, and that, relative to the α-band, the β- and γ-bands are constant with respect to both spectral location, shape and amplitude, at least for visual pigments with the same type of chromophore. In their treatment, each band is characterised by a modified lognormal function (Metzler and Harris, 1978):

$$\alpha_i = A_i \exp\left[-c_{0,i} x_i^2 \left(1 + c_{1,i} x_i + c_{2,i} x_i^2\right)\right] \tag{4}$$

where α is absorbance, the subscript i designates the absorption band (α, β or γ), $x_i = \log_{10}(\lambda/\lambda_{max,i})$, A_i is the absorbance at $\lambda_{max,i}$, $c_{0,i}$, $c_{1,i}$ and $c_{2,i}$ are coefficients characteristic of the ith absorption band, and $c_{2,i} = 3c_{1,i}^2/8$. The total visual pigment absorbance spectrum, ε, can then be resolved as the sum of the three individual functions (see Figure 4.4):

$$\varepsilon(\lambda) = \alpha_\alpha(\lambda) + \alpha_\beta(\lambda) + \alpha_\gamma(\lambda) \tag{5}$$

Thus it is advantageous in that it can be described in simple analytical expressions as well as parameter values, which are easily implemented in a computer program or worksheet.

The use of the Partridge and DeGrip (1991) polynomial to fit a rhodopsin template generated from the equation given by Stavenga *et al.* (1993) can therefore be justified because both are based on the same original bovine rhodopsin absorbance data. Indeed, when the polynomial given by Partridge and DeGrip (1991) was applied to a 497.63 nm λ_{max} rhodopsin template generated from the equation given by Stavenga *et al.* (1993) (i.e. equivalent to the bovine rhodopsin data of Partridge and DeGrip, 1991) the mean of the λ_{max} estimations was 497.60 nm (s.d. = 0.187 nm, n = 41 valid points at 1 nm intervals).

To check the longwave limb polynomial, the original Partridge and DeGrip (1991) absorbance data were used to generate a new longwave limb polynomial using the

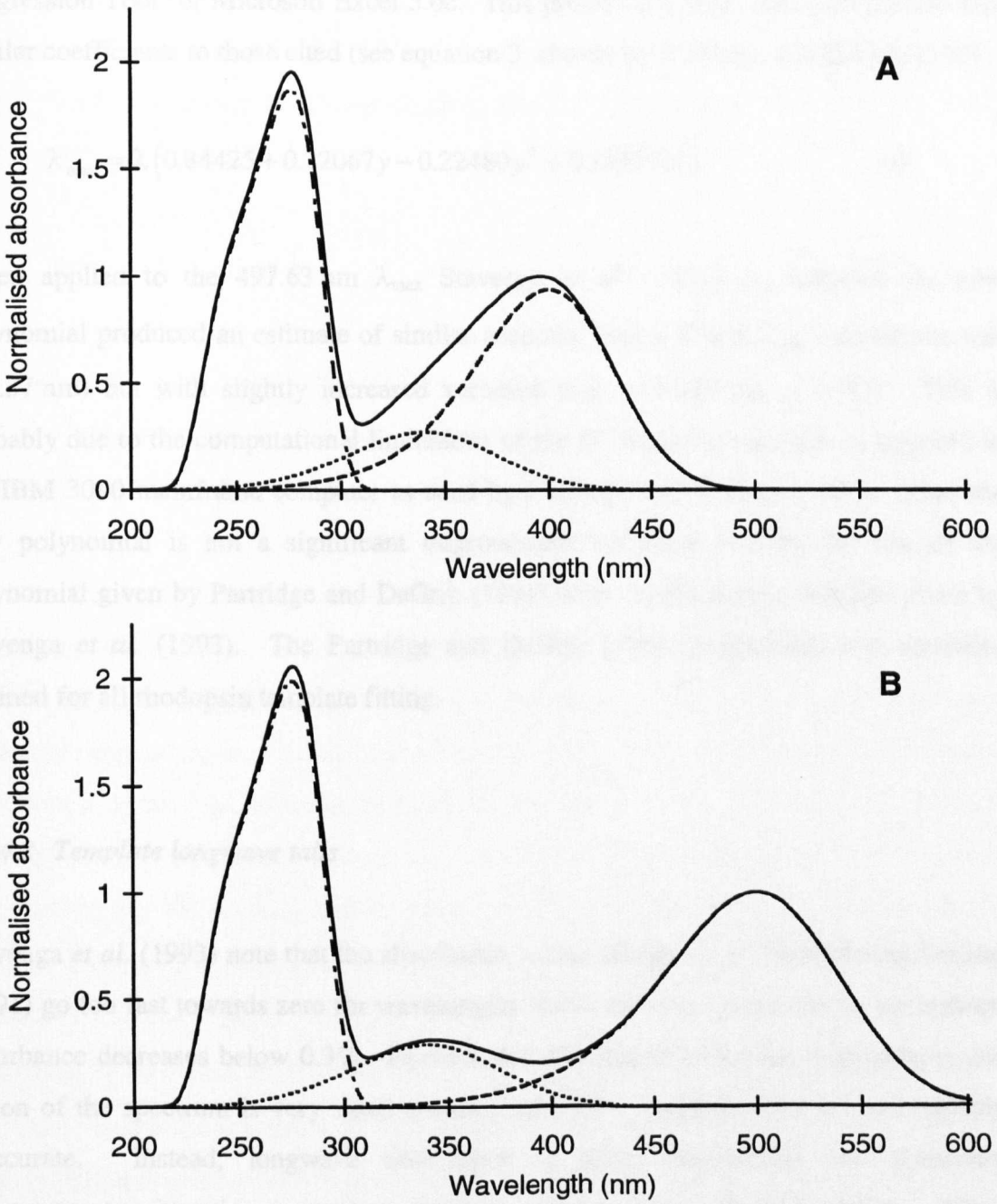

Figure 4.4 A, B. Examples of the rhodopsin visual pigment template given by Stavenga *et al.* (1993). The rhodopsin absorbance spectrum (solid trace) is the sum of the α-, β- and γ-bands, each expressed individually as lognormal functions (dashed, dotted and dash-dot traces, respectively). With a template λ_{max} of 500 nm (**B**) the λ_{max} of the template and the α-peak coincide. At lower λ_{max} values, e.g. with a λ_{max} of 400 nm (**A**), the template λ_{max} is shifted to shorter wavelengths than the α-peak as the overlap of the β-band becomes significant (see Section 4.2.4.3).
The data have been normalised to the absorbance at the template λ_{max}.

'Regression Tool' of Microsoft Excel 5.0c. This produced a new cubic polynomial with similar coefficients to those cited (see equation 3, above) by Partridge and DeGrip (1991):

$$\lambda_{max} = \lambda\left(0.84425 + 0.22067y - 0.22480y^2 + 0.13977y^3\right) \qquad (6)$$

When applied to the 497.63 nm λ_{max} Stavenga *et al.* (1993) A_1 template the new polynomial produced an estimate of similar accuracy (mean of the λ_{max} estimations was 497.57 nm) but with slightly increased variation (s.d. = 0.219 nm, n = 41). This is probably due to the computational limitations of the PC based spreadsheet as opposed to the IBM 3090 mainframe computer as used by Partridge and DeGrip (1991). Thus the new polynomial is not a significant improvement but does validate the use of the polynomial given by Partridge and DeGrip (1991) with the rhodopsin template given by Stavenga *et al.* (1993). The Partridge and DeGrip (1991) polynomial was therefore retained for all rhodopsin template fitting.

4.2.4.2 Template longwave tails

Stavenga *et al.* (1993) note that the absorbance values tabulated by Partridge and DeGrip (1991) go too fast towards zero for wavelengths above 620 nm, i.e. where the normalised absorbance decreases below 0.3%. Because the absorbance of bovine rhodopsin in this region of the spectrum is very small spectrophotometric measurements are unavoidably inaccurate. Instead, longwave absorbance is better determined via sensitivity measurements, assuming a constant quantum efficiency (see Dartnall, 1972). When comparing calculated absorbance spectra with sensitivity data, it becomes apparent that the modified lognormal function (i.e. as proposed by Stavenga *et al.*, 1993) fails on the longwave limb of the α-band when $\log(\lambda/\lambda_{max,\alpha})$ exceeds about 0.1 (*ca.* 630 nm with a 500 nm λ_{max}). Consequently, the longwave tail of the α-band must be 'patched' by the substitution of a fourth function in order to extend it into the range assessed by physiological measurements of spectral sensitivity. Specifically, the electrophysiologically measured sensitivity spectra of primate photoreceptors are found to decrease approximately log linearly, i.e. with a first degree exponential, at a long

wavenumber scale (Baylor, Nunn and Schnapf, 1987; Schnapf, Kraft and Baylor, 1987; Schnapf, Kraft, Nunn and Baylor, 1988; for a corresponding invertebrate case see Srebro, 1966). Thus, in this region, at wavelength x_α the spectral sensitivity, ε, is (after Stavenga *et al.*, 1993):

$$\log(\varepsilon) = s(x_\alpha - x_0) \qquad (7)$$

Stavenga *et al.* (1993) have shown that coefficients (x_0) derived for cattle rhodopsin describe well the spectral sensitivity of the α-band of rods and primate cones but adjustments must be made to the slope constant (s) for the linear tail of the α-band.

Recently, Lamb (1995) has presented a new (α-band only) rhodopsin template specifically constructed by initially concentrating on sensitivities in the longwave region, obtained from electrophysiological and psychophysical measurements, and then basing it primarily on the absorbance measurements of Partridge and DeGrip (1991) about the peak. Figure 4.5 shows a comparison between the rhodopsin templates given by Stavenga *et al.* (1993), with and without an added longwave tail, and the template given by Lamb (1995), each generated with a 500 nm λ_{max} and normalised at this peak. The longwave tail added to the template given by Stavenga *et al.* (1993) is that which the authors derived for cone visual pigment data and simply replaces the lognormal functions at long wavelengths ($\log(\lambda/\lambda_{max}) > ca.\ 0.1$). When the full absorbance range of the α-band is plotted the added tail is not discernible and the similarity between the α-band templates given by Stavenga *et al.* (1993) and Lamb (1995) is clear (see Figure 4.5A), as expected for templates based on the same data set. When the end of the longwave limb is enlarged (Figure 4.5B) the 'longwave tail' patch of Stavenga *et al.* (1993) is seen to initially have a lower absorbance than the template which it replaces (here it replaces the lognormal functions at $\log(\lambda/\lambda_{max}) = 0.080$). Towards longer wavelengths the patch joins the template given by Lamb (1995).

When fitting templates to microspectrophotometric measured absorbance data the presence of a longwave tail becomes irrelevant as the absorbance values in this range are less than the noise of the individual recordings. Thus the rhodopsin template given by

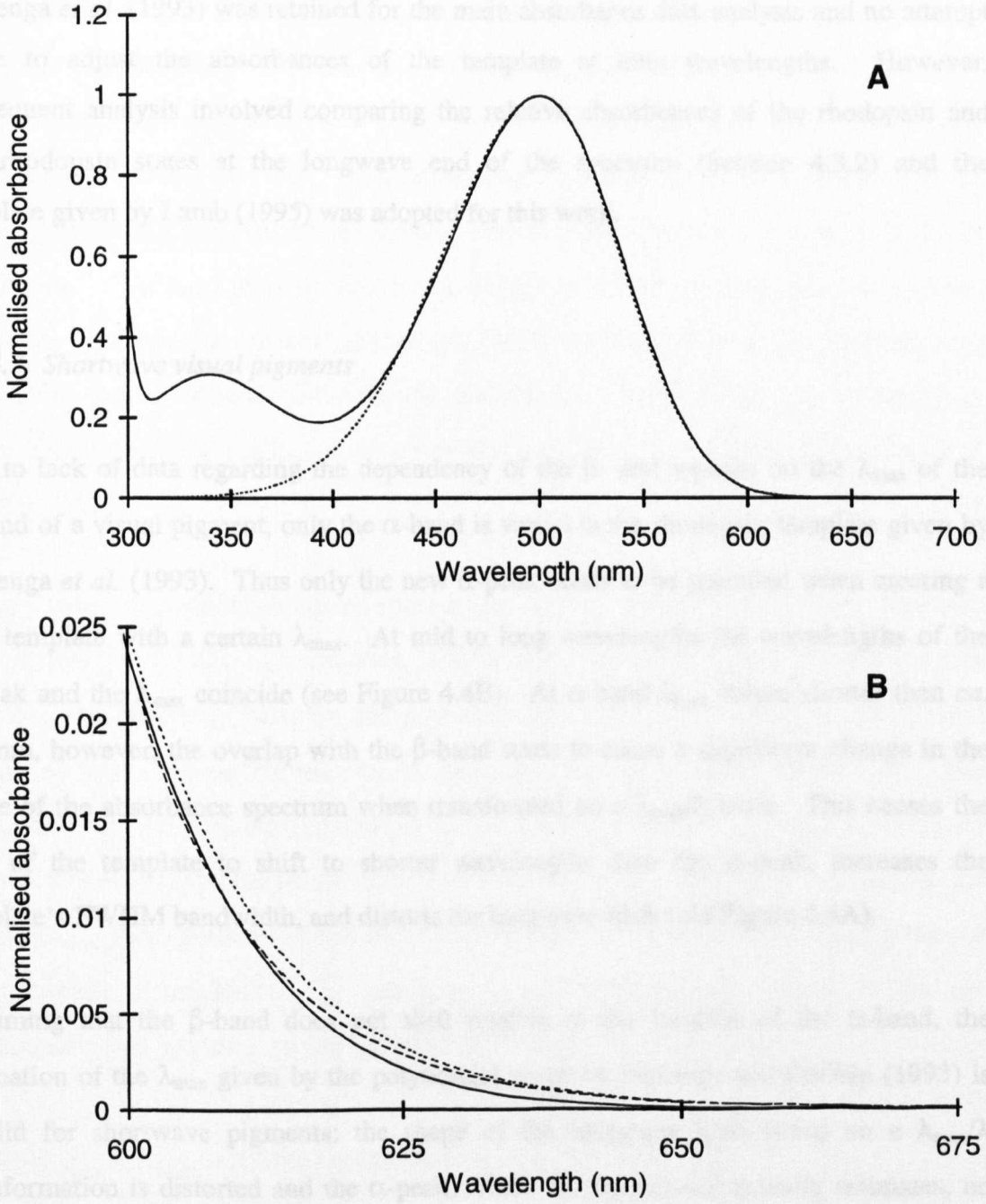

Figure 4.5 A, B. The rhodopsin template given by Stavenga *et al.* (1993) with (dashed trace) and without (solid trace) an added longwave tail (to fit cone visual pigment data) and the α-band only rhodopsin template given by Lamb (1995; dotted trace). In (**A**) the added tail is not discernible and the similarity between the α-band of the Stavenga *et al.* (1993) and Lamb (1995) is clear. When the end of the longwave limb is enlarged (**B**) the 'longwave tail' patch is seen to initially have a lower absorbance than the template which it replaces (here it replaces the lognormal functions at 601 nm) but towards longer wavelengths the patch joins the template given by Lamb (1995).
All three templates have a 500 nm λ_{max} and are normalised at this point.

Stavenga *et al.* (1993) was retained for the main absorbance data analysis and no attempt made to adjust the absorbances of the template at long wavelengths. However, subsequent analysis involved comparing the relative absorbances of the rhodopsin and metarhodopsin states at the longwave end of the spectrum (Section 4.3.2) and the template given by Lamb (1995) was adopted for this work.

4.2.4.3 Shortwave visual pigments

Due to lack of data regarding the dependency of the β- and γ-peaks on the λ_{max} of the α-band of a visual pigment, only the α-band is varied in the rhodopsin template given by Stavenga *et al.* (1993). Thus only the new α-peak needs to be specified when creating a new template with a certain λ_{max}. At mid to long wavelengths the wavelengths of the α-peak and the λ_{max} coincide (see Figure 4.4B). At α-band λ_{max} values shorter than *ca.* 430 nm, however, the overlap with the β-band starts to cause a significant change in the shape of the absorbance spectrum when transformed on a λ_{max}/λ basis. This causes the λ_{max} of the template to shift to shorter wavelengths than the α-peak, increases the template's FWHM bandwidth, and distorts the longwave limb (see Figure 4.4A).

Assuming that the β-band does not shift relative to the location of the α-band, the estimation of the λ_{max} given by the polynomial given by Partridge and DeGrip (1993) is invalid for shortwave pigments: the shape of the longwave limb based on a λ_{max}/λ transformation is distorted and the α-peak, which the polynomial actually estimates, no longer coincides with the template λ_{max}. Two methods were employed to overcome this. In the first, the scaled absorbance values of a template-generated β-band are subtracted from the normalised absorbance data being analysed. The remaining absorbance values are re-normalised and the polynomial given by Partridge and DeGrip (1993) applied to this 'α-band only' data.

The γ-band of the rhodopsin template spectrum given by Stavenga *et al.* (1993) has a λ_{max} of 276 nm and a FWHM bandwidth of *ca.* 50 nm. At a wavelength of 318 nm its

absorbance is less than 0.1% of the template's absorbance at the α-peak. Thus it does not contribute significantly to the absorbance of any rhodopsin visual pigments beyond this value and can effectively be ignored in this analysis. However, the scaling of the β-band is a weakness of this method. With decreasing λ_{max} values, the overlap between the α- and β-bands increases, increasing the absorbance at the template λ_{max} relative to that of the β-peak. This ratio must be estimated, using the running average λ_{max} as a guide, before the polynomial given by Partridge and DeGrip (1993) can be used. To avoid such estimations during calculation, the second method for calculating the λ_{max} at short λ_{max} values simply 'corrects' the λ_{max} estimate given by the polynomial given by Partridge and DeGrip (1993).

Using a series of rhodopsin template spectra generated by the equation given by Stavenga *et al.* (1993) at 0.1 nm λ_{max} intervals, a fifth order polynomial was produced which describes the difference between the predicted and actual λ_{max} values of the α-band (measured to the nearest 0.1 nm), in the template λ_{max} range of 340 to 500 nm. The polynomial was not used beyond 450 nm as the longwave limb is no longer distorted, no correction is needed and the polynomial becomes increasingly inaccurate. The λ_{max} of the α-peak ($\lambda_{max,\alpha}$; nm) needed to produce a template with the correct overall λ_{max}, given the mean α-peak estimation ($\lambda'_{max,\alpha}$ between 340 and 450 nm; nm) produced by the polynomial given by Partridge and DeGrip (1993), is then calculated as:

$$\begin{aligned}\lambda_{max,\alpha} = \lambda'_{max,\alpha} + \Big[&13443.4 - 150.028\left(\lambda'_{max,\alpha}\right) + 0.665764\left(\lambda'_{max,\alpha}\right)^2 \\ &-0.00146917\left(\lambda'_{max,\alpha}\right)^3 + 1.61287\times10^{-6}\left(\lambda'_{max,\alpha}\right)^4 \\ &-7.04899\times10^{-6}\left(\lambda'_{max,\alpha}\right)^5\Big]\end{aligned} \qquad (8)$$

In practice the equation of Partridge and DeGrip (1991), given above as equation (3), was used to estimate $\lambda'_{max,\alpha}$. A corrected λ_{max} value ($\lambda_{max,\alpha}$) was then calculated using equation (8) and this value used to generate the rhodopsin template which best-fits the recorded data. This method is advantageous over that of subtracting the β-band in that it involves less calculations per analysis of a visual pigment scan and avoids estimating the

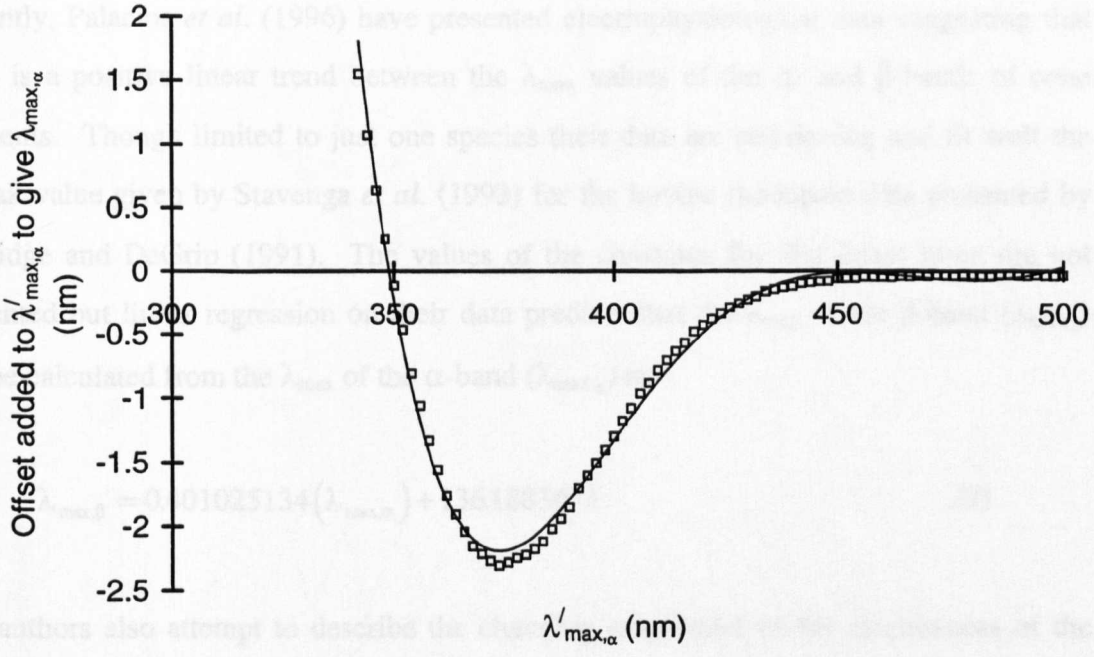

Figure 4.6 The 'offset' needed to shift the λ_{max} of the α-band as predicted by the polynomial given by Partridge and DeGrip (1991) ($\lambda'_{max,\alpha}$) to the α-peak value ($\lambda_{max,\alpha}$) needed to produce a rhodopsin template as given by Stavenga *et al.* (1993) with the same λ_{max} as that of the original data. For clarity the data points are shown at 1 nm intervals though they were obtained at $\lambda'_{max,\alpha}$ intervals of 0.1 nm. The best-fitting, fifth order polynomial is also shown which was used between $\lambda'_{max,\alpha}$ values of 340 to 450 nm.

ratio of the absorbances at the template λ_{max} and the β-peak during calculation.

4.2.4.4 Shifting β-band

Recently, Palacios *et al.* (1996) have presented electrophysiological data suggesting that there is a positive linear trend between the λ_{max} values of the α- and β-bands of cone pigments. Though limited to just one species their data are convincing and fit well the β-peak value given by Stavenga *et al.* (1993) for the bovine rhodopsin data presented by Partridge and DeGrip (1991). The values of the constants for this linear trend are not presented but linear regression on their data predicts that the λ_{max} of the β-band ($\lambda_{max,\beta}$) can be calculated from the λ_{max} of the α-band ($\lambda_{max,\alpha}$) as:

$$\lambda_{max,\beta} = 0.401025134\left(\lambda_{max,\alpha}\right) + 136.1883671 \qquad (9)$$

The authors also attempt to describe the changing amplitudes of the absorbances of the β- and γ-bands relative to the α-band. This is less convincing: their experimental measuring errors are very high in the shortwave end of the spectrum and there is no evidence that the photosensitivities of the β- and γ-bands follow their corresponding spectral absorbance spectra, as is considered the case for the α-band (see Morton, 1972; also Dartnall, 1972). Further, when analysed their data could not be described by a simple mathematical trend. A compromise was therefore adopted in which the relative amplitudes of the peaks were left as given by Stavenga *et al.* (1993) but with the λ_{max} of the β-band shifted relative to that of the α-band according to equation (9) above.

A series of rhodopsin templates were generated using the equation given by Stavenga *et al.* (1993) both with the λ_{max} of the β-band fixed at 340 nm (as given by Stavenga *et al.*, 1993) and linearly shifted relative to that of the α-band using equation (9) (Figure 4.7). The two series of templates appear quite similar, though the overlap of the fixed β-band at shortwave λ_{max} values is clear. To show the effect on the actual shape of the absorbance spectra these were then transformed on a λ_{max}/λ basis (Figure 4.8). This clearly shows

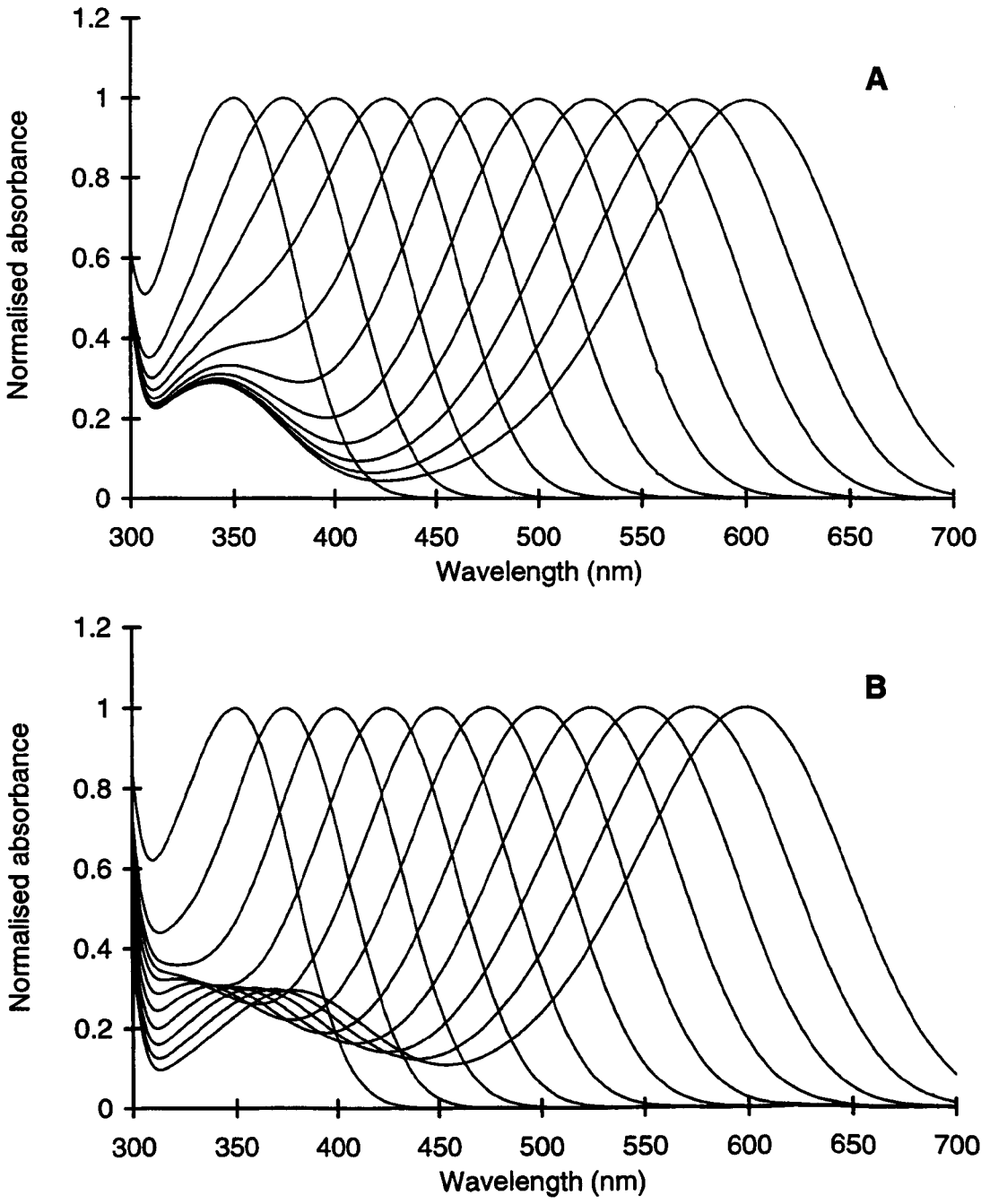

Figure 4.7 A, B. A series of rhodopsin visual pigment spectra plotted at 25 nm λ_{max} intervals from 350 to 600 nm, generated using the equation given by Stavenga *et al.* (1993). (**A**) The β-band remains fixed with a peak absorbance at 340 nm. (**B**) The β-band is linearly shifted relative to the α-band using the relationship given in equation (9).

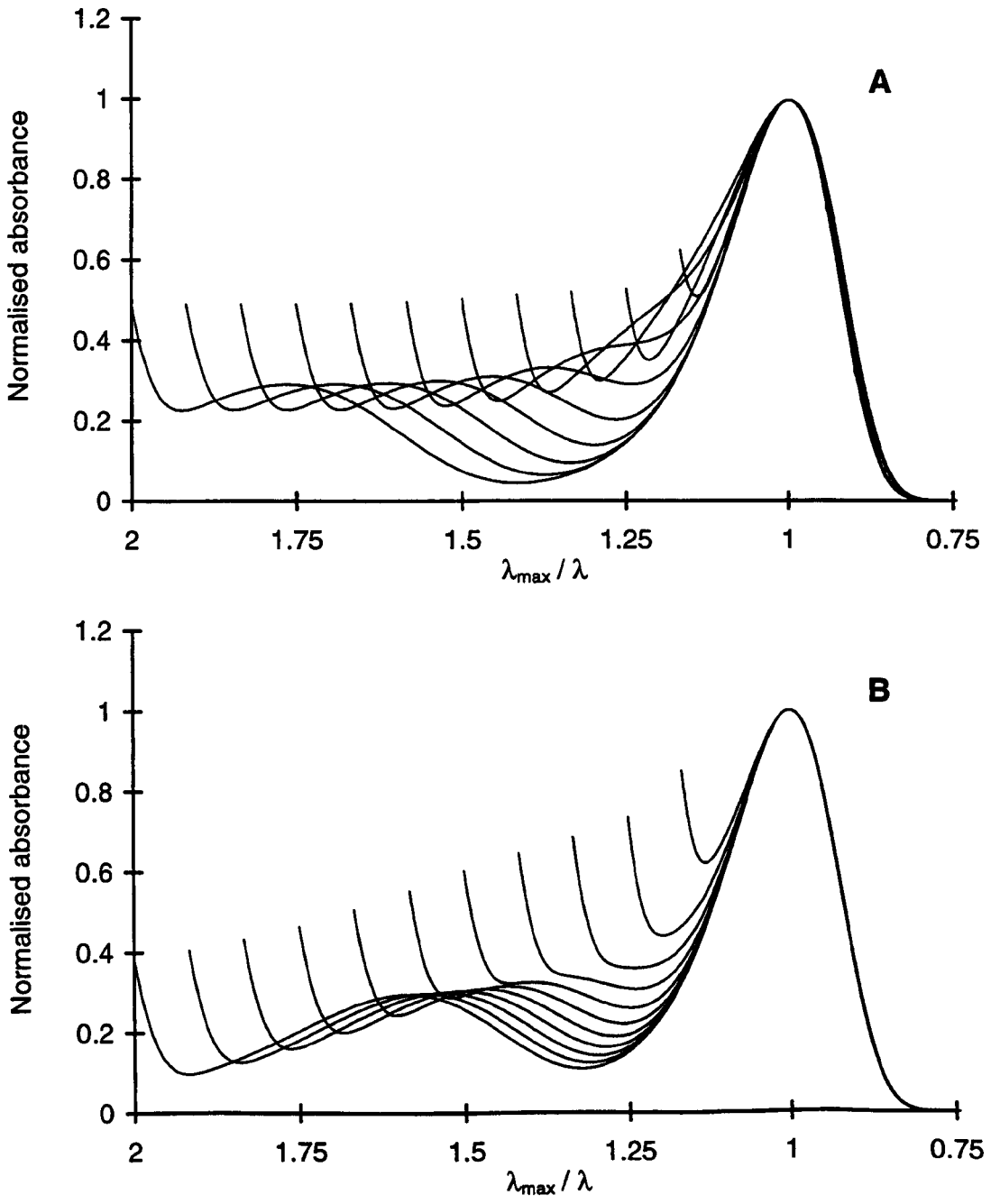

Figure 4.8 A, B. A series of rhodopsin visual pigment spectra plotted at 25 nm λ_{max} intervals from 350 to 600 nm, generated using the equation given by Stavenga *et al.* (1993) and expressed on a λ_{max}/λ abscissa (*cf.* Figure 4.7). (**A**) The β-band remains fixed with a peak absorbance at 340 nm. (**B**) The β-band is linearly shifted relative to the α-band using the relationship given in equation (9). Comparing (**A**) and (**B**) the distortion of the longwave limb and the increase in FWHM bandwidth caused by the overlap of the fixed β-band at short template λ_{max} values is clearly seen.
Note that the original absorbance values were truncated at 300 nm to avoid displaying the γ-band.

that the shortwave λ_{max} templates with a fixed β-band have distorted long- and shortwave limbs when compared to the longer λ_{max} templates which appear to have a uniform shape in the region of the α-band (i.e. $0.75 < \lambda_{max}/\lambda < 1.125$). However, with the shifting β-band, the longwave limb appears uniform for all λ_{max} values down to 350 nm and the shortwave limb is only affected at λ_{max} values of 400 nm and below. The overlap due to the β-band is effectively removed as its absorbance is shifted to shorter wavelengths.

The effect of the overlap between the α- and β-bands was further investigated by generating a series of rhodopsin templates at 1 nm λ_{max} intervals and calculating the percentage of the absorbance at the template λ_{max} due to the β-band, the FWHM bandwidth and the shortwave shift in the template λ_{max} relative to the α-band λ_{max}, with the β-band both fixed and shifting (see Figures 4.9, 4.10 and 4.11). Figure 4.9 shows how the overlap due to the fixed β-band at the template λ_{max} increases as the template λ_{max} decreases. However, when the β-band is shifted relative to the α-band, following the relationship given in equation (9), the overlap becomes insignificant even down to a λ_{max} of 350 nm (i.e. less than 1% of the maximum absorbance is due to the β-band absorbance at a template λ_{max} of 350 nm).

Many of the recent visual pigment templates are based on a λ_{max}/λ transformation which results in a linear decrease in the FWHM bandwidth with decreasing template λ_{max} (Mansfield, 1985; MacNichol, 1986). While this is true for the α-band, the overlap with the β-band at short wavelengths causes the main absorbance peak of the template spectrum to increase in width (Figure 4.10). With the β-band λ_{max} fixed at 340 nm this reaches a maximum when the λ_{max} is *ca.* 420 nm, where the FWHM bandwidth of 110 nm is comparable to that of a *ca.* 550 nm λ_{max} template. With a shifting β-band the FWHM bandwidth only increases at λ_{max} values below *ca.* 380 nm which is due to the overlap on the shortwave limb only. Below λ_{max} values of 352 and 364 nm, for the fixed and shifting β-band templates respectively, there is no template FWHM bandwidth as the shortwave limb never falls below 50% of the maximum absorbance.

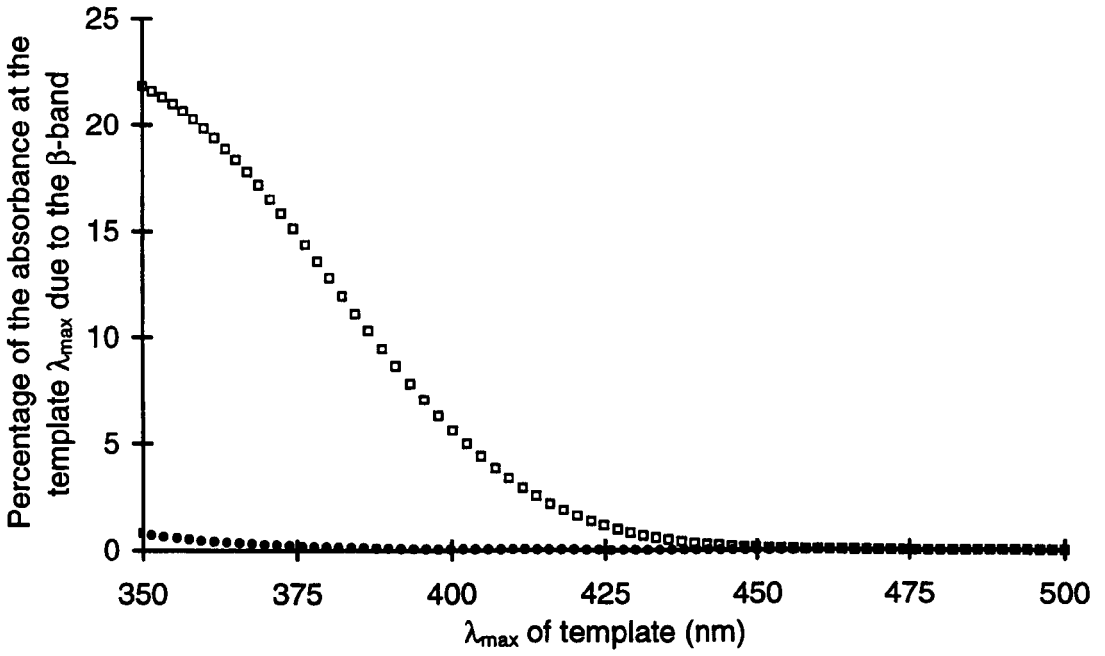

Figure 4.9 The percentage of the absorbance due to the β-band at the λ_{max} of a series of rhodopsin template spectra. These were generated using the equation given by Stavenga *et al.* (1993), with the β-band λ_{max} both fixed at 340 nm (squares) and shifted relative to the α-band λ_{max} (filled circles) following the relationship given in equation (9), and are plotted versus the template λ_{max}.
For clarity the data points are shown at 2 nm intervals.

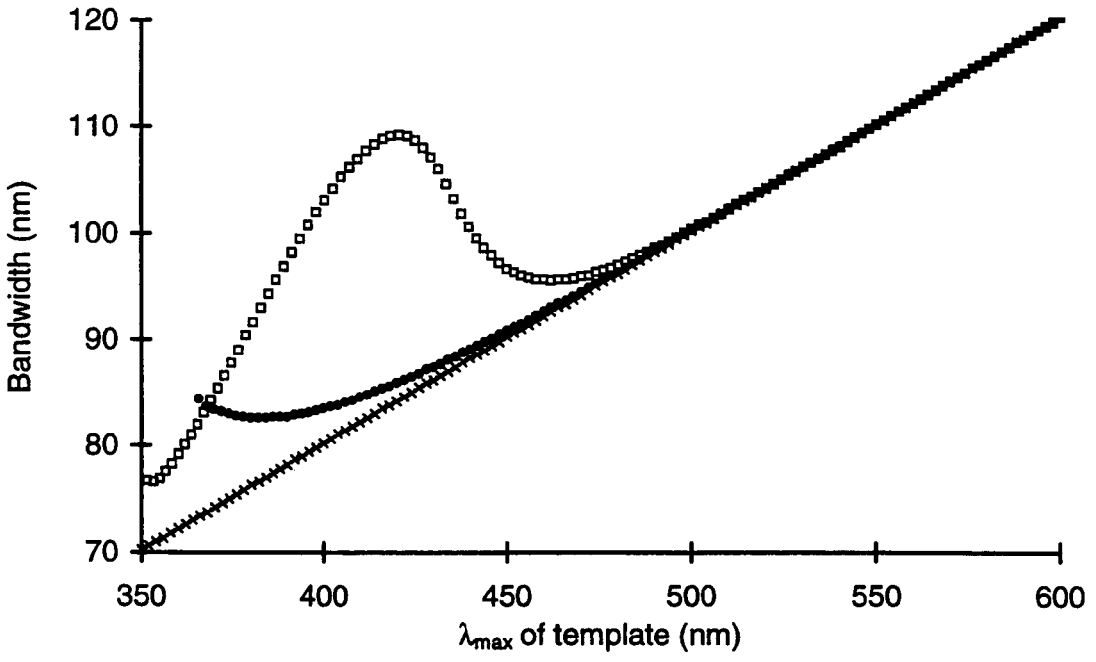

Figure 4.10 The FWHM bandwidths (measured to the nearest nanometer) of a series of rhodopsin template spectra. These were generated using the equation given by Stavenga *et al.* (1993), with the β-band λ_{max} both fixed at 340 nm (squares) and shifted relative to the α-band λ_{max} (filled circles) following the relationship given in equation (9), and are plotted versus the template λ_{max}. The FWHM bandwidths of the α-bands (crosses) are also shown.
For clarity the data points are shown at 2 nm intervals.

4.2.4.5 Generating rhodopsin templates

When the β-band is fixed at a λ_{max} of 340 nm the greatest discrepancy between the λ_{max} values of the template and of the α-band is 5.6 nm (at a template λ_{max} of 377 nm; see Figure 4.11). Producing a rhodopsin template by specifying the λ_{max} of the α-band only and assuming it coincides with the template λ_{max} would therefore introduce a significant error when analysing shortwave pigments. A fourth order polynomial was therefore produced which approximates the difference between the α-band and the template λ_{max} of a rhodopsin template generated using the equation given by Stavenga *et al.* (1993) with a β-band λ_{max} fixed at 340 nm, given the template λ_{max} required. The polynomial is not used for template λ_{max} values greater than 450 nm as the template and α-band λ_{max} values coincide, thus no 'correction' is needed, and the polynomial becomes increasingly inaccurate.

Between template λ_{max} values of 345 to 450 nm inclusive, the λ_{max} of the α-peak ($\lambda_{max,\alpha}$; nm) needed to produce a template with a given template λ_{max} (λ_{max}; nm) when the β-band λ_{max} is fixed at 340 nm, is calculated as:

$$\lambda_{max,\alpha} = \lambda_{max} + \left[-6322.94 + 58.4707(\lambda_{max}) - 0.201152(\lambda_{max})^2 + 3.05451\times10^{-4}(\lambda_{max})^3 - 1.72893\times10^{-7}(\lambda_{max,\alpha})^4\right] \quad (10)$$

The resulting templates have a maximum error in actual template λ_{max} of *ca.* 0.5 nm compared with the template λ_{max} required. A similar 'corrective polynomial' was produced for rhodopsin template spectra with a shifting β-band λ_{max}. For template λ_{max} values below 421 nm, the λ_{max} of the α-peak ($\lambda_{max,\alpha}$; nm) needed to produce a template with a given template λ_{max} (λ_{max}; nm) when the β-band λ_{max} is shifted relative to the α-band λ_{max}, is calculated as:

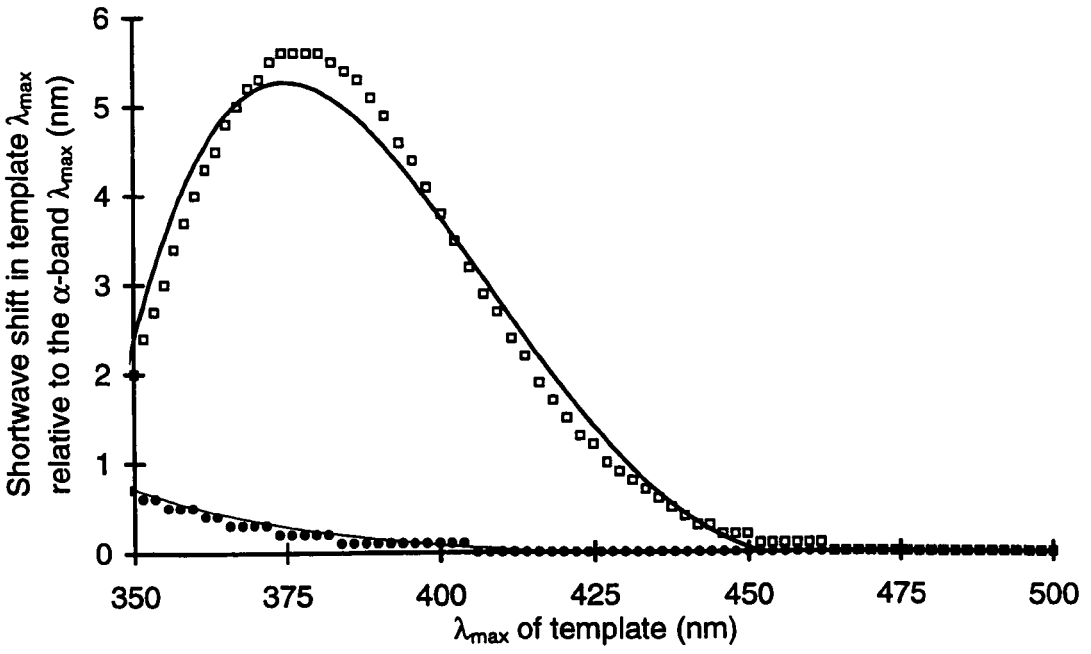

Figure 4.11 The shortwave shift of the template λ_{max} relative to the λ_{max} of the α-band for a series of rhodopsin template spectra. These were generated using the equation given by Stavenga *et al.* (1993), with the β-band λ_{max} both fixed at 340 nm (squares) and shifted relative to the α-band λ_{max} (filled circles) following the relationship given in equation (9). The best-fitting, 4th order polynomials are also shown which were used to predict the α-band λ_{max} values needed to generate templates with the desired template λ_{max} values (see equations 10 and 11).
For clarity the data points are shown at 2 nm intervals.

$$\lambda_{max,\alpha} = \lambda_{max} + \left[786.519 - 7.71969(\lambda_{max}) + 0.0284969(\lambda_{max})^2 \right.$$
$$\left. -4.68662 \times 10^{-5}(\lambda_{max})^3 + 2.89592 \times 10^{-8}(\lambda'_{max,\alpha})^4 \right] \quad (11)$$

However, the shortwave shift in template λ_{max} is still less than 1 nm at a template λ_{max} of 350 nm (see Figure 4.11) and thus correction of this discrepancy is probably not required.

All these attempts to improve template fitting at short λ_{max} values assume that the shape of the rhodopsin template spectrum given by Stavenga *et al.* (1993), with or without shifting the λ_{max} of the β-band, is accurate for shortwave pigments. There is mounting evidence (see Palacios *et al.*, 1996) that UV sensitive visual pigments, with λ_{max} values between 340 and 370 nm, have a smaller FWHM bandwidth than would be predicted with existing visual pigment templates. Thus they do not fit the λ_{max}/λ transformation which unifies the mid- to longwave pigments (Mansfield, 1985; MacNichol, 1986). Nevertheless, it appears likely that retinal-based UV sensitive pigments from widely separated taxa have the same spectral FWHM bandwidth and shape when plotted as λ_{max}/λ.

Recently, Palacios *et al.* (1996) published a separate template for UV visual pigment data as well as revised coefficients describing the α-band of UV sensitive pigments in the lognormal function given by Stavenga *et al.* (1993). Thus, the data now exist to generate retinal-based UV sensitive pigment template spectra. However, if shortwave templates with λ_{max} values between 380 and 450 nm are to be generated using the equation given by Stavenga *et al.* (1993) and fitted to measured absorbance data the following limitations must be noted and possible corrections made. If the β-band is fixed at a λ_{max} of 340 nm, the template spectra will be distorted below λ_{max} values of *ca.* 430 nm such that the template and α-band λ_{max} values no longer coincide. Thus the λ_{max} of the α-band must be determined before generating a rhodopsin template with a shortwave λ_{max} value and, together with the longwave limb distortion, the use of the polynomial given by Partridge and DeGrip (1993) to predict the template λ_{max} is no longer valid. However, polynomials can be used to correct these values (see equations 8 and 10 above).

If the linear relationship between the α- and β-band λ_{max} values given in equation (9) is incorporated into the equation given by Stavenga *et al.* (1993), however, the λ_{max} of the template and of the α-band now coincide and the longwave limb is no longer distorted based on a λ_{max}/λ transformation even down to λ_{max} values of *ca.* 350 nm. The resulting shortwave λ_{max} template spectra are narrower at the template peak and, if adopted as representative of the absorbance spectra of shortwave λ_{max} pigments, the polynomial given by Partridge and DeGrip (1993) can be used to estimate the template λ_{max} down to λ_{max} values of *ca.* 380 nm. Though the estimation of the λ_{max} appears accurate well below this value, the template itself should be modified at shorter λ_{max} values to reflect the narrower FWHM bandwidths of the UV sensitive pigments. This will alter the longwave limb of the α-band and the polynomial given by Partridge and DeGrip (1991) will no longer be valid.

4.2.4.6 The 'correct' rhodopsin template

In summary, the merits of various new templates were reviewed during this study. No single template was adopted as each has its own advantages for different parts of the analysis undertaken in this thesis. The equation given by Stavenga *et al.* (1993) remain the easiest to program, accurately describe the absorbance due to the α-, β- and γ-bands of still one of the most reliable sets of data (i.e. that of Partridge and DeGrip, 1991) yet offer the ability to change the given parameters as more accurate data are obtained. Hence, the linear relationship between the α- and β-band λ_{max} values (equation 9) calculated from the data presented by Palacios *et al.* (1996) was easily included and a switch to their own eighth order polynomial was unnecessary. Furthermore, when these authors proposed a new template for UV sensitive pigments, in addition to their own eighth order polynomial, they were also able to give revised coefficients which describe the new α-band and allow it to be generated using the equation given by Stavenga *et al.* (1993).

Thus, in the main analysis program written during this study, rhodopsin template spectra are generated using the equation given by Stavenga *et al.* (1993) modified to include the

linear relationship between the α- and β-band λ_{max} values as given in equation (9). The extinction coefficients of the three constituent bands (α, β and γ) are not altered from the values given by Stavenga *et al.* (1993), however, due to insufficient data presented in the study of Palacios *et al.* (1996). Once the λ_{max} values of the α- and β-bands have been calculated, the absorbance values of the three bands are calculated, summed and the total normalised to the maximum absorbance at wavelengths greater than the region of the γ-band (i.e. the 'template λ_{max}').

Retaining the template generating equation given by Stavenga *et al.* (1993) has also allowed us to retain the polynomial given by Partridge and DeGrip (1991) which predicts the λ_{max} from the absorbance values on the longwave limb. The majority of visual pigments analysed in this study have λ_{max} values from 470 to 510 nm. Thus, the use of the polynomial given by Partridge and DeGrip (1991) to estimate their λ_{max} values would be valid with or without the addition of the shifting β-band. The exceptions, the shortwave pigments of the Oplophorid deep-sea shrimps (λ_{max} values of *ca.* 414 nm), were found to have narrower bandwidths than rhodopsin templates with the equivalent λ_{max} (see Figures 3.24, 3.26, 3.28 and 3.30 and Section 4.3.3.2). Hence template-fitting using a predictive polynomial was abandoned and UV rhodopsin templates (generated using the equation of Stavenga *et al.* (1993) with the α-band coefficients altered as given by Palacios *et al.* (1996)) were fitted by manually iterating the λ_{max} values until the lowest RMS deviation between the template and the data was achieved.

The discrepancy between 80% and 20% normalised absorbance on the longwave limbs of the rhodopsin templates given by Stavenga *et al.* (1993) and Lamb (1995) is slight (less than 2% difference between the normalised absorbance values at any given wavelength within this range; see Section 4.2.4.2 and Figure 4.5). A new predictive polynomial was not calculated for the template given by Lamb (1995) as the use of such a template would not significantly affect the estimation of the λ_{max} obtained through template fitting. Further, the template given by Lamb (1995) only describes the absorbance due to the α-band and thus was not adopted for the main absorbance data analysis, i.e. this template was never fitted to raw or averaged data. However, this template does accurately describe

the longwave limb at the lower absorbance values at which the template given by Stavenga *et al.* (1993) fails. Assuming that the results of electrophysiological experiments can be directly related to a photopigment's absorbance, Lamb's template (1995) was therefore adopted when comparing the relative absorbances of the rhodopsin and metarhodopsin states at the longwave end of the spectrum (Section 4.3.2).

The use of two different templates, the first a modified version of that given by Stavenga *et al.* (1993) to incorporate the data of Palacios *et al.* (1996) and the second as given by Lamb (1995), for different methods of analysis is an informed compromise rather than an erroneous inconsistency. Such a compromise is likely to continue to be necessary while templates are generated through the process of fitting curves in an attempt to describe measured data. Ideally, such a curve should be based on firm theoretical principles, but a comprehensive mathematical description of light absorption by visual pigments has not yet been developed.

4.2.5 Estimation of signal to noise ratios

4.2.5.1 The variability of the data

To give a measure of the variability of the recorded data, and thus a degree of confidence in the output values, analysis methods included calculations of the standard deviations about the peak and longwave offset absorbances, using the number of points in the running average. The standard deviation of the maximum corrected absorbance is then calculated by sequentially pairing the data points used to calculate the peak and longwave offset absorbances. The mean of these pairs is then equal to the maximum corrected absorbance and n is the number of points in the running average. Note that the peak and maximum corrected absorbances (and associated standard deviations) are at the running average λ_{max} and not at the template λ_{max}. Similarly the position of the longwave offset absorbance is calculated relative to the running average λ_{max}. This is because the data must first be normalised before the template can be fitted and, although both will be

normalised to the same amplitude, the positions of the template and data λ_{max} may not coincide.

4.2.5.2 The noise of the data

The standard deviations at the peak and longwave offset absorbances indicate the range of the data at these points and thus the 'noise' of the data. (The standard deviation of the individual template λ_{max} estimates produced from successive points on the longwave limb also gives an indication of this noise but is complicated by the accuracy of the polynomial given by Partridge and DeGrip, 1991). Assessing the level of noise in the data is necessary to calculate the signal to noise ratio (Section 4.2.5.3) which in turn is needed to optimise the filtering of the data for further analysis (see Section 4.2.6 for a discussion on the running average). However, the relatively small number of points in the running average limits the accuracy of this estimation. Simply increasing the number of points is not valid as the data points do not lie evenly about the mean due to random noise alone, there is the additional underlying change in absorbance with wavelength. To isolate the variation in signal due to noise from that due to the wavelength dependent absorbance of the visual pigment the deviations between the normalised data and best-fit template were calculated at each wavelength interval. This method effectively subtracts the best-fit template data as a best estimate of the change in signal due to the visual pigment, leaving a horizontal line variations in which are then attributed to noise (see Figure 4.12).

Figure 4.12 clearly shows how, when the normalised template is subtracted from the normalised data, the noise that remains is wavelength dependent, probably as a direct consequence of the varying signal from the microspectrophotometer (i.e. due to the wavelength dependent changes in the measuring beam, transmission of the optics and sensitivity of the photomultiplier tube; see Section 2.2.2). Specifically, though the noise will also increase as the light intensity increases, the ratio of the intensity to the noise will decrease. Hence the signal to noise ratio will decrease. This suggests that a significant component of the noise is due to random photon events (see Section 4.1.1.2).

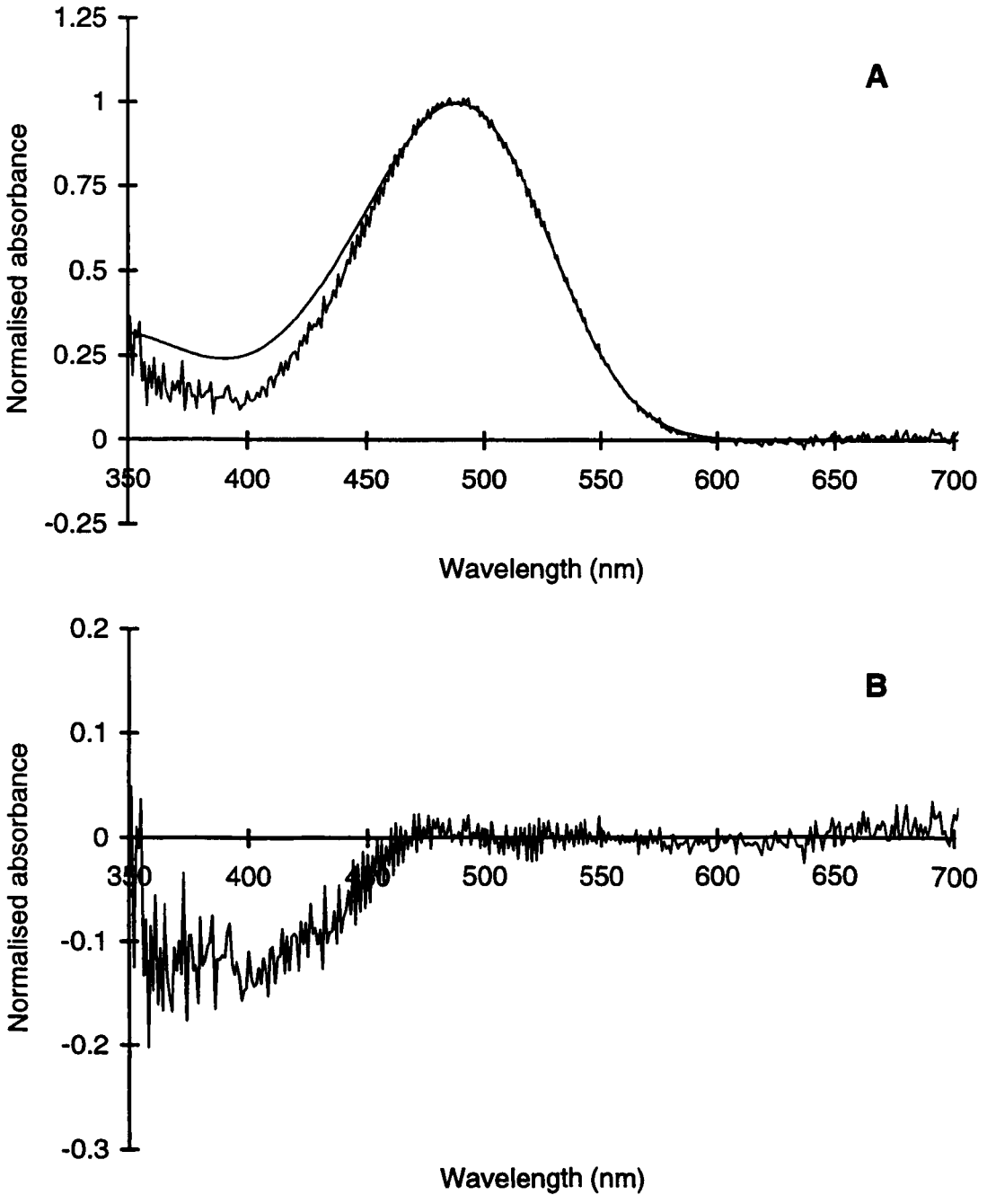

Figure 4.12 A, B. How the noise of a microspectrophotometric scan is calculated. (**A**) Normalised *Acanthephyra stylorostratis* mix_1 averaged difference spectrum (jagged trace) with best-fitting rhodopsin template (smooth trace) as analysed using the main visual pigment analysis program with 15 points in the running average. (**B**) Normalised template deviations (jagged trace) calculated by subtracting the absorbance values of the normalised best-fitting template from the normalised data. The remaining variations beyond *ca.* 460 nm can be attributed to noise and are clearly wavelength dependent. See text for further explanation and results.

To obtain an 'average level of noise' for the data the deviations between the normalised data and best-fit template were calculated over two ranges: 1) 80% to 20% normalised absorbance on the longwave limb, and 2) 80% normalised absorbance on the shortwave limb to the longwave offset absorbance (0.5% normalised absorbance). The former is a useful indicator of the noise over the region in which the most important variable, the λ_{max}, is estimated. The latter includes the regions used to set both the peak and longwave offset absorbances (and therefore the maximum corrected absorbance), the region in which the λ_{max} is estimated and, in essence, covers the absorbance due to the visual pigment which is of most biological interest. Thus it is seen as the best range for determining the 'overall noise' of the data. The wavelengths at which these normalised absorbances occur were calculated using a λ_{max}/λ transformation based on a 500 nm λ_{max} template:

80% normalised shortwave absorbance occurs at $\lambda_{max}/1.0627$

80% normalised longwave absorbance occurs at $\lambda_{max}/0.9488$

20% normalised longwave absorbance occurs at $\lambda_{max}/0.8803$

0.5% normalised longwave absorbance occurs at $\lambda_{max}/0.8104$

The mean normalised deviation from the template is then calculated for both ranges, complete with the standard deviation and the number of points used. If the template is a perfect fit to the data the average deviation will tend to zero as the variations represent noise either side of the fitted template. Thus the mean deviation from the template indicates the fit of the template irrespective of the noise of the data. However, the standard deviation of the these template deviations represents the spread of the deviations and is thus an accurate measure of the noise. These standard deviation values can then be used to produce normal distributions with means of zero which, when added to normalised template spectra, produce template data with noise equivalent to that of the original microspectrophotometric scan (albeit of even noise throughout the spectrum).

For the example presented in Figure 4.12, with the λ_{max} of the fitted template at 488.2 nm, the 80% to 20% longwave normalised absorbance range includes the wavelengths from 515 to 554 nm, inclusive. The 80% shortwave to 0.5% longwave normalised absorbance

range includes the wavelengths from 460 to 602 nm, inclusive. Thus, both avoid the regions where the template is obviously not a good fit (i.e. below *ca.* 460 nm) but still reflect the regions where the absorbance of the visual pigment is important and used for template fitting. The mean normalised deviations from the template over these two ranges are 0.14% and -0.28% of the maximum corrected absorbance, respectively, indicating the good fit of the template. The standard deviations are 0.0114 and 0.0108 (to give signal to noise ratios of 87.6 and 92.6; see the following section).

4.2.5.3 Signal to noise ratios

The signal to noise ratios of the average files from each species were calculated in order to optimise the filtering of the data for further analysis (see Section 4.2.6 and Table 3.17). To calculate a signal to noise ratio, the standard deviation of the deviations from the template (i.e. the noise calculated above) should be divided by the average signal over the same range. However, ignoring differences due to distortions in the measured data, the signal would then change depending on the range over which the standard deviation was calculated. To avoid this the signal used was taken to be that at the peak absorbance. Thus all signal to noise ratios presented in this study are actually estimates of the signal to noise ratio at the λ_{max} (note that the peak absorbance and fitted template λ_{max} will not necessarily coincide). Since the data are already normalised the signal to noise ratios of this study were simply calculated as the reciprocal of the standard deviation; i.e. the maximum signal being normalised to unity.

To convert the 'peak signal to mean noise' ratios quoted in this study to those reflecting the 'mean signal to mean noise' ratios usually used it is necessary to multiply the values in this study by the mean signal over the absorbance range used. For a 500 nm λ_{max} rhodopsin template (generated using the equation given by Stavenga *et al.*, 1993, and modified to incorporate a shifting β-band, after Palacios *et al.*, 1996), the mean signal is 0.484 between 80% to 20% normalised absorbance on the longwave limb, and 0.513 between 80% normalised absorbance on the shortwave limb to the longwave offset absorbance. As the ranges are specified by absorbance limits the mean signals for any

given range will not change dependent on the λ_{max}, though rounding errors will cause slight variation.

Intuitively, as the signal to noise ratio decreases the accuracy of fitting the template will decrease and thus so will the reliability of this method as an estimation of noise. A perfect measure of noise might only be expected when there is none! Further, due to measurement errors (e.g. photoproduct build-up, light scattering at short wavelengths, baseline drift etc.), it is unlikely that the template will be a perfect fit over the whole of the spectrum. Thus, if the original data analysis produced a best-fitting template from which the running average deviated significantly in certain regions (by more than *ca.* 5% of the normalised absorbance), these regions were then left out of the noise estimations. In many cases this resulted in the noise being estimated between the running average λ_{max} and the longwave offset, avoiding the shortwave limb, or just on the longwave limb between 80% and 20% normalised absorbance. It is expected that the latter region will always be a good fit to the template as it is over this region that the λ_{max} of the template to be fitted is determined. In all cases where the range was reduced the standard deviations of the mean normalised template deviations fell. This suggests that the previous values had been increased due to poor template fitting and did not reflect a greater level of noise.

4.2.6 The running average

4.2.6.1 Modelling the effect of the running average

The box-car running average used in the visual pigment analysis programs is designed to smooth the data so that fixing the peak and longwave offset absorbances is less affected by random noise at any particular point. The effect of varying the number of points on the longwave offset has already been shown (Table 4.1). An interesting by-product of this modelling is that the estimate of the template λ_{max} becomes increasingly more accurate as the magnitude of the offset absorbance becomes more accurate. When too few points are used the longwave offset absorbance is overestimated, the *remaining* data points are

distorted when normalised, and the λ_{max} wavelength estimate erroneously shifted to shorter wavelengths.

The effect on the peak absorbance is also of importance, however, an incorrect number of points in the running average will have opposing effects on the estimates of the maximum corrected absorbance and the template λ_{max} depending on whether too few or too many points are used. With too few points in the running average the data will not be smoothed enough and the peak absorbance of the data will be overestimated as it includes additional absorbance due to random noise (see Figure 4.13). If the longwave offset absorbance is set correctly, this will cause the maximum corrected absorbance to be overestimated and the absorbance data to be 'compressed' when normalised. This will decrease the gradient of the longwave limb of the α-band causing the estimate of the λ_{max} to be shifted erroneously to shorter wavelengths. However, the longwave offset absorbance is also likely to be overestimated which will appear to correct the maximum corrected absorbance estimate but will further shift the λ_{max} to erroneously shorter wavelengths.

Conversely, if the data are smoothed too much (too many points in the running average), the process will underestimate the peak absorbance as the running average includes additional points either side of the maximum on the short- and longwave limbs (see Figure 4.13). Again assuming the longwave offset is set correctly, this will cause the maximum corrected absorbance to be underestimated and the absorbance data to be 'stretched' when normalised. This will increase the gradient of the longwave limb of the α-band and the estimate of the λ_{max} will be erroneously shifted to longer wavelengths. However, the longwave offset absorbance is likely to be more accurate which will again appear to correct the maximum corrected absorbance estimate and will now shift the λ_{max} estimate back towards the correct wavelength. The overall effect of these conflicting factors is shown in Figure 4.14, produced by generating and individually analysing a series of ten rhodopsin templates each with a 500 nm λ_{max}, a maximum absorbance of unity, and a signal to noise ratio at the λ_{max} of 16.

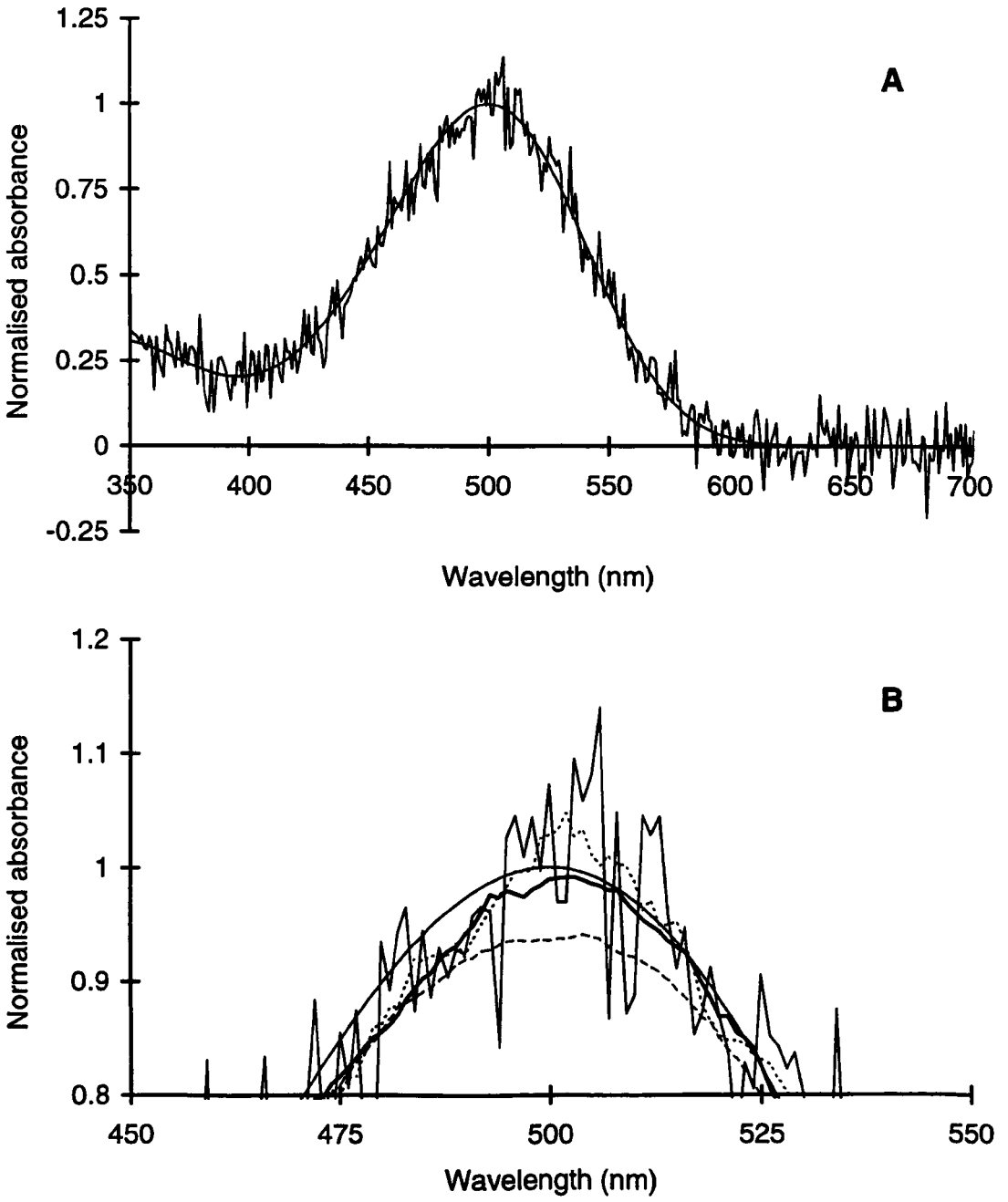

Figure 4.13 A, B. The effect of an incorrect running average at the peak absorbance. **(A)** A 500 nm λ_{max} template with a maximum absorbance of unity and added normally distributed (Gaussian) noise (to give a signal to noise ratio at the λ_{max} of 16) is shown (jagged trace), complete with the original 500 nm λ_{max} template (smooth trace). **(B)** The same data enlarged at the peak absorbance plus the results of a 9, 27 and 49 point running average (dotted, bold and dashed traces, respectively). When too few points are used the running average 'follows' the deviations due to the random noise in the data and the peak absorbance is overestimated. When too many points are used the peak is flattened and its absorbance underestimated as the average includes those points of decreasing absorbance on the short- and longwave limbs. Analysis calculated that, on average, a 27 point running average would be optimal with this level of noise (see Section 4.2.6.2).

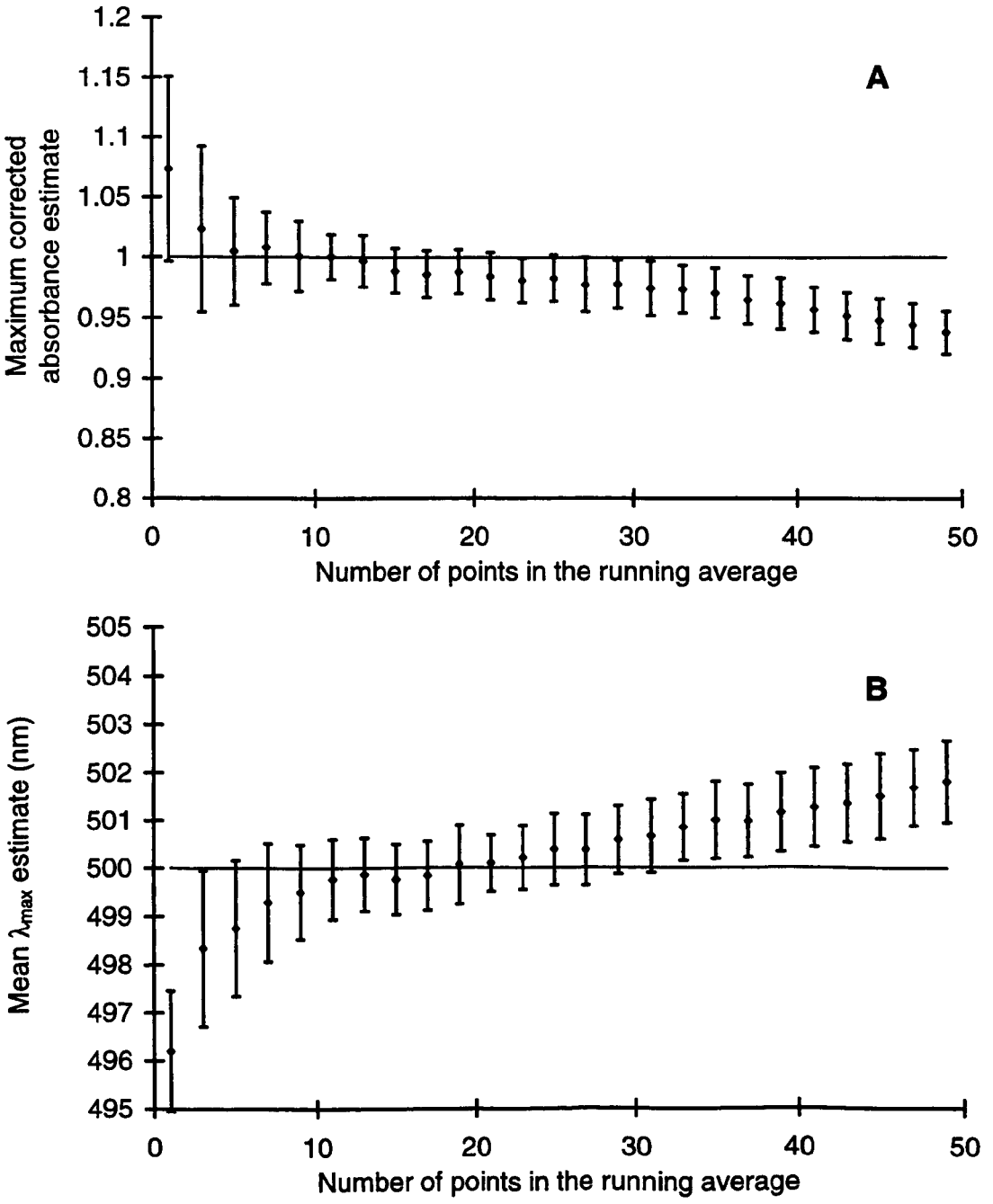

Figure 4.14 A, B. The effect of varying the number of points in the running average on (**A**) the maximum corrected absorbance and (**B**) the mean λ_{max}. Note that this is the average effect on ten individual spectra, each with a 500 nm λ_{max}, maximum absorbance of unity, and a signal to noise ratio at the λ_{max} of 16 produced by adding normally distributed (Gaussian) noise. The average values are plotted ± 1 s.d.

4.2.6.2 Optimising the running average

Varying the number of points in the running average clearly alters the outcome of the analysis (see Figure 4.14 above). The effect will depend not only on the overall signal to noise ratio of the data but also on the actual distribution of noise within that particular scan (i.e. the noise may be wavelength dependent). Further, it is not possible to quantify the accuracy of different analyses (e.g. different numbers of points in the running average) using variables for which the correct values are unknown. A compromise was necessary to simply these problems. Therefore, calculations were made to ascertain the *mean* optimum number of points in the running average needed to smooth known template data with a known level of non-wavelength dependent, normally distributed (Gaussian) added noise, as approximations to the microspectrophotometric data files.

In practice, the running averages were optimised for the average scans only. First the signal to noise ratio of each average file was estimated over the 80% shortwave to 0.5% longwave normalised absorbance range using the methods described in Section 4.2.5 (i.e. taking the signal as the maximum normalised value of one). The signal to noise ratios varied from 28.37 to 212.60 and the averages were then split into ten groups covering this range and more. The limits of, and mean signal to noise ratios within, these groups is shown in Table 4.2. These exponentially based divisions were the finest that could be used considering the number of trials (and therefore time) needed. A 489 nm λ_{max} rhodopsin template was then generated using the equation given by Stavenga *et al.* (1993) and normally distributed (Gaussian) noise added to give a signal to noise ratios equal to those of the means of the groups. (The same template data was used for all calculations as it approximates the average λ_{max} of both difference spectra for all deep-sea species.) Running averages with increasing numbers of points were then passed through the data and the results compared.

The optimum number for each template with added noise was selected as that which produced the running average spectrum with the least overall deviation from that of the original template spectrum without noise. Specifically, this 'best-fit' running average spectrum was chosen as that producing the least sum of squared differences with the

original template data points between 460 and 615 nm, inclusive. Equivalent to between 80% normalised absorbance on the shortwave limb and the longwave offset absorbance (based on analysis of the original template data) this fixed wavelength range meant that the sums of the squared differences were directly comparable between trials (i.e. changing the number of points in the running average would otherwise alter the wavelengths at which these two absorbance points are set). This process was repeated using new noise of the same level until a mean optimum number of points was determined with 95% confidence limits of less than ± 1. This in turn was repeated for each of the signal to noise ratios and the results shown in Table 4.2.

Variables calculated during the analysis (such as the mean λ_{max} estimate and the maximum corrected absorbance) were not used to select the optimum number of points in the running average as adding noise changes these variables which define a *specific* property of the underlying data. Thus when noise is added to 500 nm λ_{max} template data with a maximum corrected absorbance of unity, the new data might then have a maximum corrected absorbance of 0.975 and the best-fitting template might have a λ_{max} of 501 nm. By comparing the running average spectrum to the original template spectrum this effectively selected the running average which best smoothes the noise yet retains the underlying overall shape of the data.

As expected, the optimum number of points needed increases with increasing noise. The apparent jumps in the optimum number of points between groups is a consequence of having to round the means to the nearest odd number rather than the groups being too coarse. The average effect of increasing noise on the estimates of the maximum corrected absorbance and the mean λ_{max} were also noted. Thus, for each signal to noise ratio, ten individual spectra with a 489 nm λ_{max}, a maximum absorbance of unity and added noise were analysed using the optimum number of points determined for that signal to noise ratio. The results were averaged and are displayed as Figure 4.15. This shows that, on average, the estimates of the maximum corrected absorbances and mean λ_{max} values become less accurate with increasing noise, even when using the 'correct' number of points in the running average. Further, the estimates have greater associated variability.

Table 4.2 Optimum number of points needed in the running average to smooth data with the signal to noise ratios indicated (taking the signal as the maximum normalised value of one). The limits between these arbitrary groups are also shown.

Mean S/N ratio	S/N ratio limits for each group			Optimum number of points in the running average
11.31	9.51	< x <	13.45	31
16	13.45	< x <	19.03	27
22.63	19.03	< x <	26.91	23
32	26.91	< x <	38.05	23
45.25	38.05	< x <	53.82	17
64	53.82	< x <	76.11	17
90.51	76.11	< x <	107.63	15
128	107.63	< x <	152.22	13
181.02	152.22	< x <	215.27	13
256	215.27	< x <	304.44	13

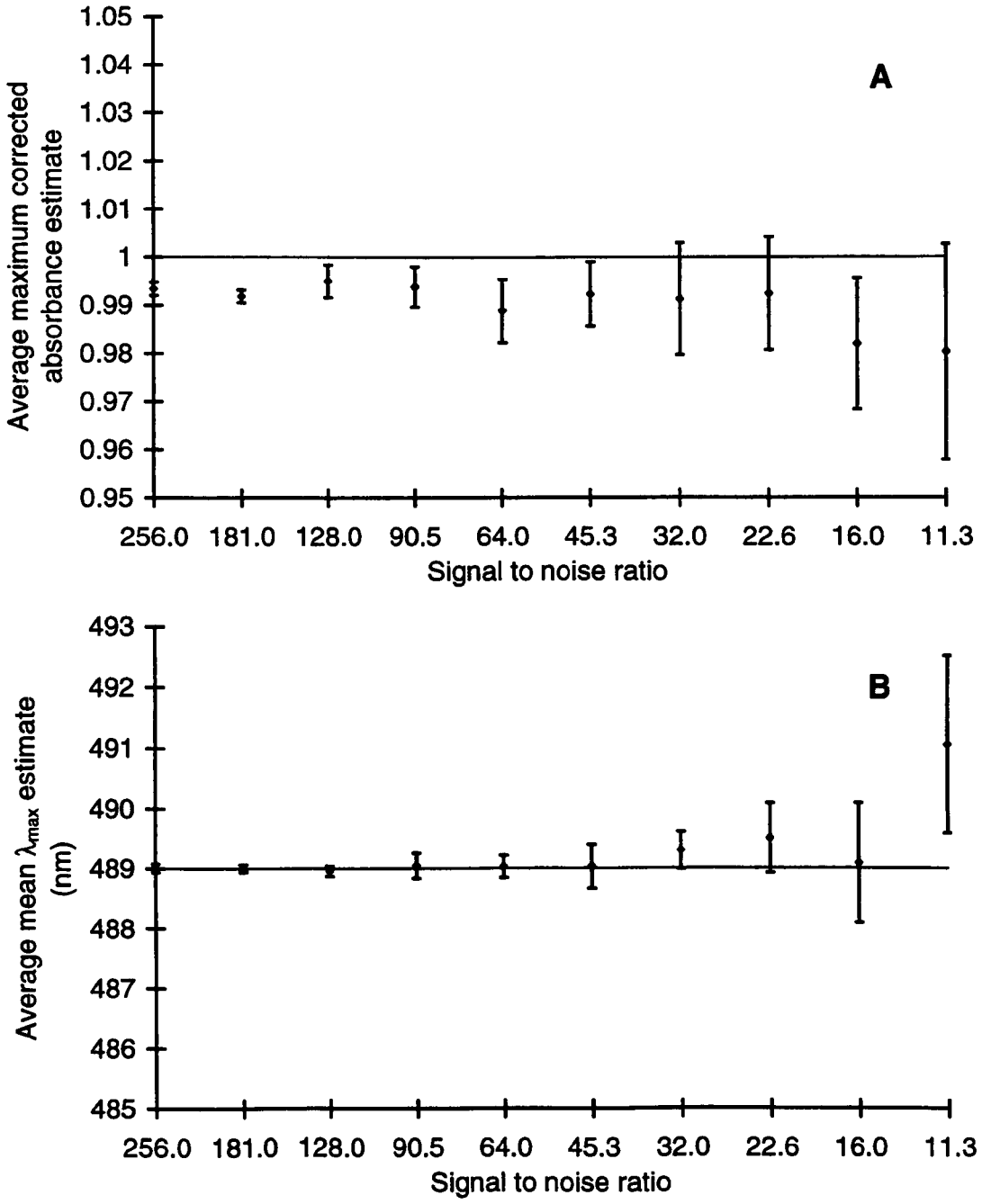

Figure 4.15 A, B. The average effect of increasing noise on the estimates of (**A**) the maximum corrected absorbance and (**B**) the mean λ_{max}. For each signal to noise ratio, ten individual spectra with a 489 nm λ_{max}, a maximum absorbance of unity and added normally distributed (Gaussian) noise were analysed using the optimum number of points for that signal to noise ratio, as determined using the method described in the text (Section 4.2.6). The average values are plotted ± 1 s.d.
This figure is in contrast to Figure 4.14 which shows the average effect of varying the number of points in the running average for a given signal to noise ratio.

Thus it appears that as the signal to noise ratio decreases the data are progressively over-smoothed, the maximum corrected absorbance increasingly underestimated and the template λ_{max} estimate erroneously shifted to longer wavelengths. Even with data with high signal to noise ratios the longwave offset is set too soon (i.e. at wavelengths which include some absorbance due to the visual pigment) and the peak is flattened. However, the errors are small (less that 1% of the actual maximum absorbance for signal to noise ratios of 90.5 and greater) and less than the measuring precision of the microspectrophotometer (Section 4.1.1).

As a result of this investigation, once the signal to noise ratio of any given data set is determined it is possible to categorise it and then re-analyse the data using the estimated optimum number of points in the running average. It would also be possible to correct for the errors observed in estimating variables such as the maximum corrected absorbance and the λ_{max}, by assuming an average condition. In practice this was not done as the errors involved are relatively small. Even the noisiest microspectrophotometric average file of this study would have an average error in normalising the data of just under 1% (i.e. an average maximum corrected absorbance of 0.9913 instead of 1 with a signal to noise ratio of 32), which shifts the average mean λ_{max} estimate by just *ca.* 0.3 nm, well within the *ca.* ± 1 nm accuracy of the microspectrophotometer (see Section 4.1.4).

4.2.6.3 Running average optimisation and microspectrophotometric data

Changing the number of points in the running average (i.e. as used in the main analysis program) will affect the normalisation of the data, the fitting of the template and therefore the original estimation of the noise of the data. An accurate estimation of the noise seems possible only when using the correct number of points in the running average, yet this measure of noise is needed to determine the correct number of points for the running average. Using these methods this circularity is unavoidable. In practice, the original analysis was done using an 11 point running average and the signal to noise ratios calculated were used to determine the optimum number of points needed. The data were

then re-analysed using the optimum number of points and the new estimates of the noise were found to be relatively unchanged.

For all species, the 95% confidence limits of the mean normalised deviations from the template, using both 11 and the optimum number of points in the running average, overlapped. This suggests that re-analysis using the optimum number of points in the running average did not produce a significantly better fitting template. However, the following should be noted: 1) The average scans are relatively noise free and thus do not require a high level of smoothing. With noisier data the effect of changing the number of points in the running average is likely to be more pronounced. 2) This is comparing the difference between smoothing the data with 11 points and the optimum number of points in the running average (i.e. from 13 to 23), not between non-smoothed and smoothed data. 3) The underlying data might not exactly follow the predicted template spectrum (e.g. if the data represent a mixture of different visual pigments). In these cases deviations between the template and increasingly smoothed data might increase.

Although there was apparently no significant change in the mean normalised deviations from the template the standard deviations, and thus the estimates of noise, did change slightly. However, in only three cases did these sufficiently alter the signal to noise ratios such that re-analysis was again suggested, i.e. using a different number of points in the running average (*Acanthephyra microphthalma* mix_1, *Gnathophausia gracilis* mix_2 and *Pasiphaea emarginata* mix_2; see Table 3.17). The first case involves a decrease in apparent noise while the latter two an apparent increase. All are borderline on the limit between 15 and 17 points (a 76.13 signal to noise ratio) and were left unchanged in subsequent analysis to avoid a potentially circular process (i.e. the noise estimates of these new values should then be used, and so on). Further, it must be noted that the boundaries between the noise levels are arbitrary and changes to the variables calculated are slight.

The 95% confidence limits of the final mean normalised deviations, calculated using the optimum number of points in the running average, suggest that of all the 74 average scans analysed (the main mix_1 and mix_2 averages for each species of deep-sea shrimp), 41 had mean deviations significantly different from zero. It follows that the shape of these

spectra are significantly different from that of the fitted template. However, the mean normalised deviations of the data from the templates for all of the average files are within ± 1% normalised absorbance and are therefore within the absorbance measuring accuracy of the microspectrophotometer (Section 4.1.4). Signal to noise ratios and the number of points used in the analysis of the average files are presented in Table 3.17.

Finally it must be noted that the entire process of optimising the number of points in the running average depends on making assumptions about the data. In some cases these assumptions can seem circular and care must obviously be taken. However, it is felt that the methods above represent a valid attempt to analyse the data more accurately, using quantitative methods to assess this.

4.2.7 Averaging microspectrophotometric data

It has already been stated that successful microspectrophotometry is a compromise between the conflicting requirements of high signal to noise and the need for low amounts of bleaching and/or photoconversion. Even when optimised, the data measured are still difficult to accurately quantify in terms of spectral location and amplitude due to the inherent noise. Assuming there is no cell to cell variation in pigment content, the solution is then to average the data obtained from the same photoreceptor type of a given species. As long as pseudoreplication is avoided (see Section 4.2.7.2), an average represents the best estimation of the underlying signal due to the visual pigment. However, there are two different ways in which an average can be calculated for these data, both with their own merits.

4.2.7.1 Average files

The microspectrophotometric data files as saved by the PC (i.e. the comma delimited ASCII text files) are already averages as the microspectrophotometer 'scans' by making repeated long- to shortwave and short- to longwave spectral passes, measuring at odd

wavelengths on the way down then even wavelengths on the way up (see Section 2.2.1). The number of spectral passes per recorded file can be varied by the user and the absorbances saved are the mean values at each wavelength. In practice the number of passes is limited by the time taken per spectral pass (*ca.* 20 s from 730 to 350 nm and back), the amount of photoconversion/bleaching per spectral pass and the diminishing return of the increase in single to noise (i.e. the signal to noise ratio increases by the square root of the number of scans). Two spectral passes per record was the compromise used during this study. Note that a 'scan' does not necessarily refer to a single down/up spectral pass and is used interchangeable with the terms 'file' and 'record' to refer to the output of the microspectrophotometer once it has completed a single measurement.

To check that a photostable state was being measured at each stage, and that levels of in-scan photoconversion/bleaching were not significant, consecutive files were compared by subtracting one from the other. If the resulting difference spectrum was 'flat' then both records were kept. The criterion for acceptance was that the signal underlying the noise of this difference spectrum was less than a *ca.* 2 to 3% of the signal amplitude of the original visual pigment mixture, or within half the amplitude of the noise, whichever was the greater. Though this judgement was not conducted statistically, with practice it was both consistent and relatively easy to assess. Note that a non-wavelength dependent 'drift' between records, resulting in a horizontal offset from zero, was accepted as this is a result of changes within the microspectrophotometer measuring equipment (e.g. due to room temperature fluctuations etc.) and not due to a change in the visual pigments and/or non-visual pigments present.

The protocol used (see Sections 2.2.3 and 2.2.4) produces two 'initial', two 'post-red' and two 'post-bleach' or 'final' files, each pair judged identical in all but random noise. Difference spectra for the initial and post-red light created pigment mixtures can then be created by subtracting the post-bleach files from the other two pairs. Using all possible combinations, four mix_1 (i.e. initial scans minus the post-bleach scans) and four mix_2 (i.e. post-red scans minus post-bleach scans) difference spectra are calculated and filed using the microspectrophotometer's PC, per section scanned. On average, for each species five

sections were scanned where the data were subsequently accepted. Nineteen of the 36 deep-sea species include data taken from more than one specimen.

Averaging these difference spectra, calculated as the mean absorbance at each wavelength, yields a single 'average spectrum' with a high signal to noise ratio. Fitting a template is then an accurate way of determining both the λ_{max} and maximum absorbance of the data, along with other important variables. The average spectra can then be used in subsequent analysis and the absorbances per wavelength may be regarded as independent data points (see Section 4.2.7.2 below).

4.2.7.2 A note on pseudoreplication

The independent data obtained for each *specimen* are the average absorbances per wavelength *per section*. The scans within each section are repeated measures and therefore not independent. Thus, the average file should be calculated by averaging the average data obtained per section, which themselves are the averages of the scans measured per section. The above method of calculating the average file avoids pseudoreplication only because the same number of scans was taken per section. Averaging all the scans together, in one step, does not then introduce any bias: it is correct to assign each scan the same weight. Thus it is the number of sections scanned that is quoted in the results in Chapter 3 (Tables 3.1 and 3.10).

When discussing species' populations, the average scans for each section are not independent if they are from the eye(s) of one individual specimen. In this case the average of the scans obtained from each specimen of each species is the independent datum point. Accepting this, the average file absorbance spectra obtained for approximately half of the species examined in this study are comprised of single independent data points per wavelength, as the retinae from only one individual were measured. No statistically based conclusions can thus be made regarding the visual pigments posed by the populations.

Whether considering the visual pigments possessed by individual specimens, or those of the species' populations, the body of independent data collected during this extensive survey of deep-sea shrimp visual pigments is small and represents a dramatic reduction of the raw data collected. This is typical of such an intensive measuring technique where the collection of independent data is constrained by both practical and time considerations. It is often necessary to then speculate about a species as a population based on the measurements from just one specimen. Hence, all discussion in Chapter 5 is made assuming that all of the specimens measured in this survey are representative of the population, but for approximately half of the species there is no evidence for this. Visual pigment polymorphism has been documented in primates (see Bowmaker, 1991) but is generally thought to be rare. Further, there are unlikely to be daily or seasonal visual pigment changes in adult specimens which inhabit such a constant photic environment (for an example of such a change see Wood *et al.*, 1992). Ontogenetic changes are possible and have been shown for eye design (e.g. Gaten and Herring, 1995) but only adult specimens were selected in this study.

4.2.7.3 File averages

The disadvantage of the 'averaged' files is that they give no indication of the variability of the individual files from which they are composed, and thus the variability of the data as measured by the microspectrophotometer. All the standard deviations calculated are due to the remaining noise in the average file only, the reduction of which is the sole purpose of averaging. Thus, a program was written to automate the individual analysis of the original difference spectra which comprise each average file. This then calculates the mean and range of each of the main variables between the individual files and tabulates the output. However, this method of 'averaging the individual files' is complicated by the results of the individual file analyses being influenced by the number of points in the running average (see Section 4.2.6). The time needed to determine the optimum number of points for each individual file is too great considering the slight gain in accuracy of the analysis. A compromise was reached by attempting to calculate the average optimum

number of points needed in the running average to analyse a model 'average' individual file. This number of points was then used for the analysis of all the individual files.

Using the data initially obtained using the main analysis program and an 11 point running average, the average signal to noise ratios of the *average* mix_1 and mix_2 difference spectra were calculated between all the deep-sea species. With values of 80.29 and 98.47, respectively, this gives an average signal to noise ratio for all of the average difference spectra files of 89.38. The average number of files per average file, for all species and both mixtures, was then calculated as 19.51. All those species with 20 files per average file were therefore selected, and the four mixtures with signal to noise ratios closest to the average value were chosen (see Table 3.17 for signal to noise data). The average signal to noise ratio of these four (*Gnathophausia ingens* mix_2, *Hymenodora frontalis* mix_2, *Sergestes similis* mix_2 and *Sergia maximus* mix_1) equals 90.55, less than 2% difference between that and the average of the averaged files from all of the deep-sea species.

The 20 individual files which make up each of the four selected average files were analysed individually using the main analysis program with 11 points in the running average. Their signal to noise ratios were noted (see Section 4.2.5 for the method), and the optimum number of points needed in the running average for that level of noise assigned using the limits previously calculated (see Section 4.2.6.2). Finally, the average optimum number of points for all 80 files was calculated by taking the mean value, namely 19.0.

Thus, the mean optimum number of points to use in a running average to analyse the individual difference spectra of this study is estimated at 19. Many assumptions were made in this estimation but this compromise is better than none at all. This estimation also suggests that the noise in the individual files is not solely due to random noise, i.e. the signal to noise ratio of the average is not equal to the average signal to noise ratio of the individual files multiplied by the square root of the number of files in the average. Thus the microspectrophotometer appears not to be limited by random photon noise (the ideal situation) but by other factors as has previously been determined (see Section 4.1.1).

All individual mix_1 and mix_2 difference spectra selected for inclusion in the average difference spectra were then analysed individually for each species, using the main analysis program with a 19 point running average, and the results averaged. The values associated with this method of analysis are then referred to as those of the 'average of the files' or 'file averages', as opposed to those of the 'average files'. Thus, a value for each variable can be calculated in two ways: 1) by analysing the single average file, or 2) by analysing the individual files which passed the selection criteria and averaging the values for each. The standard deviations associated with the file averages now indicate the spread of the data encountered for each photoreceptor type per species. These are much higher than the standard deviations of the average files which only reflect the noise remaining in those single files.

4.2.7.4 The 'average' λ_{max} value

The standard deviations of the average files and file averages are measures of two different ranges (see Section 4.2.7.3 above). However, the mean values of calculated variables should be very similar between the two methods of averaging. The calculation of the λ_{max} deserves special attention as it is arguably the most important variable to measure and attempt to define. Two methods of determining the λ_{max} are available: 1) fitting a template to the data and quoting its λ_{max} (the λ_{max} of the fitted template or 'template λ_{max}'), or 2) finding the maximum absorbance value after attempting to remove the noise (the 'running average λ_{max}'). This is then complicated by the two methods of averaging available. To investigate this, paired two sample t-tests were used to compare the two mean λ_{max} values calculated for the file averages and averages of file as presented in Tables 3.12 to 3.15.

Comparing the differences between the two λ_{max} estimates within each method of averaging, the template λ_{max} is, on average, at longer wavelengths than the running average λ_{max}. For the mix_1 difference spectra, this difference is significant for both methods of averaging (the mean difference between the template λ_{max} values and the

running average λ_{max} values of the average files is 1.47 nm, s.d. = 2.13 nm, $t_{36} = 4.185$, $p < 0.01$, and for the file averages is 1.20 nm, s.d. = 2.22 nm, $t_{36} = 3.277$, $p < 0.01$). For the mix_2 difference spectra, the difference is only significant for the file averages (the mean difference between the template λ_{max} values and the running average λ_{max} values of the average files is 0.44 nm, s.d. = 2.29 nm, $t_{36} = 1.181$, $p = 0.25$, and for the files averages is 0.70 nm, s.d. = 2.04 nm, $t_{36} = 2.091$, $p < 0.05$).

The longwave shift in template λ_{max} relative to the running average λ_{max} is probably due to the difference spectra representing the absorbance of a mixture of rhodopsin and metarhodopsin pigments. A mixture is likely to have a wider absorbance spectrum and fixing the λ_{max} relative to the longwave limb will not take this into account (see Figure 4.16). As observed, this is likely to be more pronounced in the mix_1 difference spectra, the mix_2 difference spectra representing the absorbance of mixtures which were created to be dominated by one pigment, i.e. the metarhodopsin. Further, normalising the data is always slightly biased towards underestimating the amplitude (i.e. setting the offset too soon and too many points in the running average; see Section 4.2.6.3). This stretches the data, steepens the longwave limb and shifts the λ_{max} to longer wavelengths.

Although the fitted template λ_{max} assumes the data fit a template and have been normalised correctly, it is still thought of as a better estimate than the running average estimate. It uses more points (*ca.* 40 points on the longwave limb as opposed to between *ca.* 13 and 23 at the peak) and uses the more accurate, steeper gradient of the longwave limb. It is therefore less likely to be affected by optical distortions, scattering and photoproduct build-up at short wavelengths. Both are still calculated and quoted in the analysis for completeness, and because the running average λ_{max} indicates the wavelength at which the data are normalised.

The template λ_{max} estimations for both the mix_1 and the mix_2 difference spectra were not found to be statistically different between the two methods of averaging (mean differences between the average files' template λ_{max} values minus the file averages' template λ_{max} values are -0.17 nm, s.d. = 0.64 nm, $t_{36} = -1.655$, $p = 0.11$, and 0.04 nm, s.d. = 0.37 nm,

t_{36} = -0.733, p = 0.47, respectively). The mean running average λ_{max} values for the mix_1 difference spectra did differ significantly between the two methods of averaging, whilst those for the mix_2 difference spectra did not (mean differences are -0.44 nm, s.d. = 1.16 nm, t_{36} = -2.327, $p < 0.05$, and 0.21 nm, s.d. = 0.87 nm, t_{36} = 1.471, p = 0.15, respectively).

These tests suggest that the template λ_{max} values as determined by either averaging method are equally good estimates for the λ_{max} of the data being analysed. The advantage of the file average value is that the associated standard deviation indicates the range of variation amongst the individual files accepted for that species. It is thought to represent measuring error and, where more than one animal was measured, possible variations between individuals of the same species. Though the running average λ_{max} values for the mix_2 difference spectra did prove significantly different between the two methods of averaging, the differences are very small (i.e. within the measuring accuracy of the microspectrophotometer; Section 4.1.4). Again, either would be a good estimate and the standard deviation of the file average values indicate the range of variation amongst the individual files accepted.

However, the average file has distinct advantages over the file average: 1) its calculation is independent of any parameters such as the number of points in the running average, however, 2) when subsequently analysed it is possible to assess and use the optimum value of such parameters, and 3) the average file spectrum, which consists of single average absorbance values per wavelength, is a single record of independent data points which can then be used in further analysis. Thus, the mean values of the average files are thought to be the most accurate for *all* calculated variables. Further, during all such discussion it should be remembered that the microspectrophotometer's monochromator has a λ calibration of $\pm$ 1 nm (see Section 4.1.4), so all computational λ_{max} 'errors' are generally within this.

It is accepted that such multiple testing of the same data set is susceptible to producing a significant result by chance alone. However, allowing for this (decreasing the probability level at which things are judged to be significant, or performing a single test, i.e. an

ANOVA) would decrease the likelihood of a difference being detected. The best way to compare the methods of averaging and analysis would be to create model data and process them using all available methods. The results of each method could then be compared to the known original data. This was not done as the relative merits of each method can clearly be seen and all differences are slight.

4.2.7.5 The 'average' extinction ratio

As with the λ_{max} estimates, the maximum corrected absorbances of the average files are thought to be the most accurate and the true independent data. For this reason, although the extinction ratios were found to be significantly different between the two methods of averaging (mean difference between the ratios of the average files compared to the ratios of the file averages is 0.004, s.d. = 0.012, $t_{36} = 2.320$, $p < 0.05$, with a mean extinction ratio between the average files of 1.261), those calculated using the maximum corrected absorbances of the file averages are the values used. Again, as with the average differences observed in measured wavelengths, these differences in absorbance are nevertheless slight and within the measuring precision of the microspectrophotometer (Section 4.1.1).

The average extinction ratios for each species could be estimated by calculating all possible ratio combinations per section scanned. With four difference spectra per section this would create sixteen ratios, and a total of 80 ratios with 5 sections per species. However, each of the maximum corrected absorbance values would then have been obtained using a non-optimal number of points in the running average. Further, this method suffers from pseudoreplication and could distort the data.

4.2.7.6 Average files versus file averages

In summary, the results of both average file and file average analysis are presented (see Tables 3.12 to 3.15), as both contain useful information. The former are the mean values

thought to be most accurate for each species and represent the independent data values and spectra used in further analysis. The means of the latter are also good estimates but their merit is in indicating the spread of the data encountered for each photoreceptor type per species. The template λ_{max} of the average file is the best estimate of the λ_{max} of the data and the extinction ratio is taken as the ratio of the average files' absorbances.

4.3 CHARACTERISING THE RHODOPSIN AND METARHODOPSIN

The sequence of analysis detailed above (Section 4.2) is a valid attempt to determine the λ_{max} and other descriptive variables given the absorbance spectrum of pure visual pigments. However, it is likely, due to their dual photostable state system, that the absorbances measured in this study represent mixtures of rhodopsins and metarhodopsins as a result of exposure to natural light before capture, bioluminescence in the trawl, red light exposure during experimental manipulations and in-scan photoconversion (though the effects of the latter two are estimated to be negligible; see Sections 2.2.2 and 4.1.1.4). Deep-sea specimens were not dark-adapted prior to experimentation and thus photoreceptors cannot be assumed to possess 100% rhodopsin. Hence further analysis was required to ascertain the absorbances of the rhodopsin and metarhodopsin pigments.

4.3.1 Analysing visual pigment mixtures with template fitting programs

If two pigments differ in λ_{max} and/or absorbance maxima, then the absorbance spectrum of a mixture of these will not follow a typical rhodopsin absorbance spectrum. Specifically, it will have too broad a FWHM bandwidth and fitting a template using the polynomial given by Partridge and DeGrip (1991) will tend to be increasingly erroneous, estimating the λ_{max} at increasingly longer wavelengths. This is shown in Figure 4.16, where the values have been chosen to represent an extreme, worst-case scenario.

Conversely, such a mixture may only be apparent when template fitting is attempted and

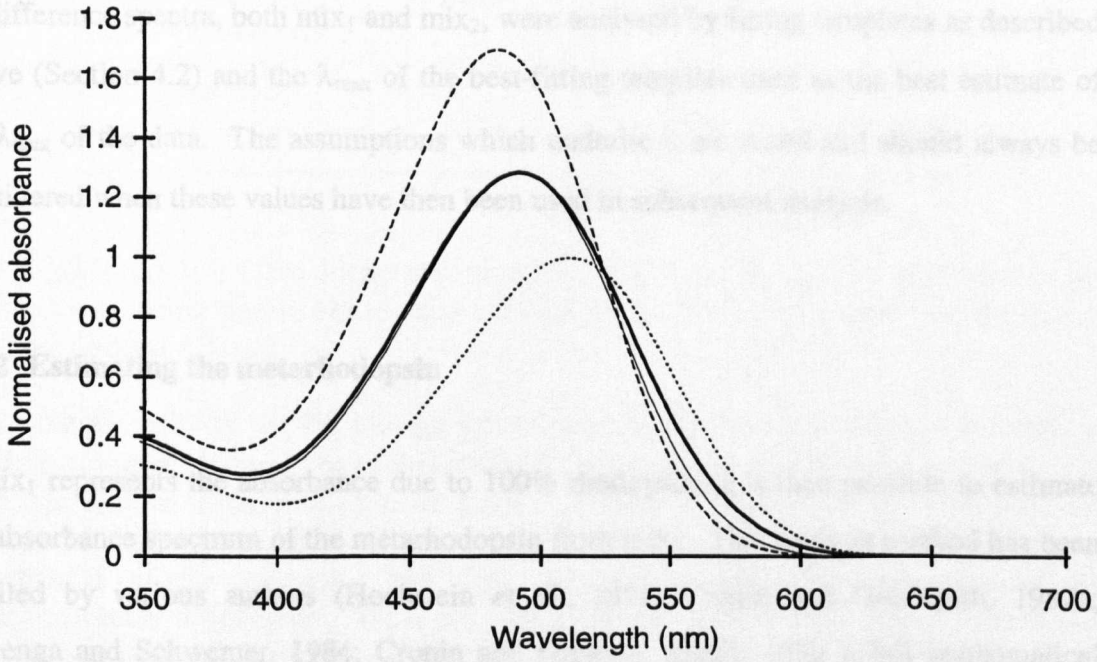

Figure 4.16 The absorbance spectrum of a mixture of two visual pigments compared to a rhodopsin template spectrum with the same λ_{max}. In this example two templates were generated using the equation given by Stavenga *et al.* (1993), with shifting β-bands, to represent a rhodopsin and a metarhodopsin with λ_{max} values of 511 nm (dotted trace) and 483.5 nm (dashed trace), respectively, with an extinction ratio of 1.7. A 50:50 mixture was then created, the λ_{max} found to be 491.7 nm (to the nearest 0.1 nm; bold trace), and a new rhodopsin template generated with this λ_{max} and scaled to the mixture's maximum absorbance (*ca.* 1.29; light trace). The FWHM bandwidth of the absorbance spectrum of the mixture is clearly greater and the polynomial given by Partridge and DeGrip (1991) erroneously estimates the λ_{max} to be at 495.4 nm due to the altered slope of the longwave limb.

mixtures with one predominant pigment, and a sufficiently low signal to noise ratio, might still be analysed with more accuracy than, say, by simply finding the running average λ_{max}. It is also assumed that a metarhodopsin pigment has the same shaped absorbance spectrum as that of a rhodopsin. However, no author has ever proposed a distinct 'metarhodopsin template' and there is no data that suggests one is needed. Thus, all difference spectra, both mix_1 and mix_2, were analysed by fitting templates as described above (Section 4.2) and the λ_{max} of the best-fitting template used as the best estimate of the λ_{max} of the data. The assumptions which underlie it are noted and should always be considered when these values have then been used in subsequent analysis.

4.3.2 Estimating the metarhodopsin

If mix_1 represents the absorbance due to 100% rhodopsin, it is then possible to estimate the absorbance spectrum of the metarhodopsin from mix_2. This analysis method has been detailed by various authors (Hochstein *et al.*, 1978; Cronin and Goldsmith, 1982a; Stavenga and Schwemer, 1984; Cronin and Forward, 1988). (For a full mathematical treatment of the invertebrate visual pigment system the reader is referred to Hamdorf (1979).) In brief, templates are used to model the rhodopsin (mix_1) and mix_2 absorbance spectra and the fraction of rhodopsin in the second photosteady state mixture is estimated by comparing the total absorbances of the two templates in the region of the saturating, red light exposure. This fraction is then subtracted from mix_2, the remaining absorbance rescaled and the λ_{max} and extinction coefficient of this 'metarhodopsin estimate' noted.

Some of the assumptions underlying the use of templates to model this process have already been noted (Section 4.3.1). Ideally the measured absorbance data should be used, however, the absorbance levels at the red end of the spectrum are so low as to be indistinguishable from the inherent noise of the system. Thus the recent template given by Lamb (1995) was selected for this work as it specifically models the sensitivities observed at these longer wavelengths (see Section 4.2.4.2). Templates were generated to model mix_1 and mix_2 such that they had the same λ_{max} as those estimated by the polynomial given by Partridge and DeGrip (1991). Templates generated using the

Table 4.3 The effect of the absorbance template employed on the estimate of the metarhodopsin.

Template authors	F_R in mix_2	Est. M λ_{max} (nm)	Extinction ratio: $\varepsilon_{max}M$ / $\varepsilon_{max}R$
Stavenga *et al.* (1993) - without longwave tail	0.039	485.0	1.272
Stavenga *et al.* (1993) - with longwave tail [a]	0.216	483.6	1.340
Lamb (1996)	0.227	483.5	1.344

[a] At $\log(\lambda/\lambda_{max}) > 0.1$ the lognormal functions describing the α-, β- and γ-bands are replaced with a first degree exponential with the slope adjusted to fit cone visual pigment data (see Section 4.2.4.2).

This example is based on the average values obtained for the main pigment mixtures of the deep-sea species measured in this study: i.e. a mix_1 λ_{max} of 493.8 nm, a mix_2 λ_{max} of 485.2 nm and an extinction ratio of 1.261. Assuming mix_1 is 100% rhodopsin, the fraction of rhodopsin in mix_2 (F_R in mix_2), is equal to the overlap of the mixtures' absorbances at the saturating red light, divided by one plus the ratio of the photoconversion efficiencies. Thus, the overlap of the absorbances is clearly much less when a longwave tail is not included as the absorbance due to mix_2 will then effectively be zero at such long wavelengths. The shift in the λ_{max} and extinction ratio of the estimated metarhodopsin is then reduced. The longwave tails produced by the patch given by Stavenga *et al.* (1993) and the template given by Lamb (1995) are very similar at the red end of the spectrum (see Figure 4.5) and produce similar metarhodopsin estimates. See text for equations and further details.

equation presented by Lamb (1995) were not fitted to the average difference spectra because the two templates are so similar about the peak (see Section 4.2.4.2). Note that this also assumes that the metarhodopsin has an identical 'longwave tail' to that of the rhodopsin. Though there might well be some differences in the ultimate slope, this could only be determined via sensitivity measurements which are, of course, not available for metarhodopsin pigments (i.e. photoconversion from the metarhodopsin to the rhodopsin does not elicit a physiological response which could be measured). Thus, though a longwave tail for metarhodopsin has never been shown, let alone measured, it is very likely to be present and similar to that of the rhodopsin given the observed similarities in the absorbances of rhodopsins and metarhodopsins about the peak, and the fact that the absorbances of these pigments are due to different molecular configurations of the same molecule (Cronin and Goldsmith, 1982b; Stavenga and Schwemer, 1984; Cronin, 1986a). The importance of the longwave tail, and thus the selection of the appropriate template, for such modelling is demonstrated in Table 4.3.

4.3.2.1 Calculation of the metarhodopsin

The following derivation of the equations used to estimate the metarhodopsin absorbance spectrum is reproduced from Cronin and Forward (1988) and included here for reference:

When a visual pigment system containing stable end points R (i.e. the rhodopsin) and M (i.e. the metarhodopsin) has been brought to a photosteady state mixture by a saturating exposure of light to wavelength λ, the fraction of M in the mixture, $F_M(\lambda)$, is:

$$F_M(\lambda) = \frac{\alpha_R(\lambda)\phi}{\alpha_R(\lambda)\phi + \alpha_M(\lambda)} \qquad (12)$$

where α is the molecular absorbance at λ and ϕ is the ratio of the quantum efficiency of the photoconversion $R \rightarrow M$ to that of the photoconversion $M \rightarrow R$. Defining $a(\lambda)$ as the absorbance of the mixture of R and M, divided by pathlength and pigment concentration (see Cronin and Goldsmith, 1982a):

$$a(\lambda) = \alpha_R(\lambda) F_R(\lambda) + \alpha_M(\lambda) F_M(\lambda) \tag{13}$$

Rearranging:

$$\alpha_M(\lambda) = \frac{a(\lambda) - \alpha_R(\lambda) F_R(\lambda)}{F_M(\lambda)} \tag{14}$$

Substituting (14) in (12):

$$F_M(\lambda) = \frac{\alpha_R(\lambda)\phi}{\alpha_R(\lambda)\phi + \left(a(\lambda) - \alpha_R(\lambda) F_R(\lambda)\right)/F_M(\lambda)} \tag{15}$$

After simplifying and dividing through by F_M:

$$1 = \frac{\alpha_R(\lambda)\phi}{\alpha_R(\lambda)\phi F_M(\lambda) + a(\lambda) - \alpha_R(\lambda) F_R} \tag{16}$$

Since $F_R + F_M = 1$, F_M may be replaced by $(1 - F_R)$:

$$1 = \frac{\alpha_R(\lambda)\phi}{\alpha_R(\lambda)\phi - \alpha_R(\lambda)\phi F_R + a(\lambda) - \alpha_R(\lambda) F_R} \tag{17}$$

Which may be rearranged to:

$$\alpha_R(\lambda)\phi - \alpha_R(\lambda)\phi F_R + a(\lambda) - \alpha_R(\lambda) F_R = \alpha_R(\lambda)\phi \tag{18}$$

Finally, this expression may be simplified and solved for F_R:

$$F_R = \frac{a(\lambda)}{\alpha_R(\lambda)\phi - \alpha_R(\lambda)}$$

$$= \frac{a(\lambda)}{\alpha_R(\lambda)(1+\phi)} \qquad (19)$$

In words, the fraction of rhodopsin in any photosteady state mixture is equal to the ratio of the absorbances at the saturating wavelength of the mixture and the rhodopsin, divided by (1 + ϕ). Once F_R in the mixture is known, the metarhodopsin absorption spectrum is easily obtained by subtracting the contribution of rhodopsin (mix_1) from the spectrum of the mixture (mix_2) and dividing the result by F_M.

In this study the λ_{max} of this metarhodopsin estimate was determined by simply finding the wavelength of maximum absorbance (to the nearest 0.1 nm). Representative templates were then generated using this λ_{max} and the absorbances scaled to that at the peak. Template fitting (i.e. using the polynomial given by Partridge and DeGrip, 1991) was not employed because it is not an exercise in trying to determine the λ_{max} given a signal with noise: when using smooth templates the maximum absorbance will be at the λ_{max}, by definition.

Relationship (19) strictly holds for a single wavelength. To estimate the F_R in mix_2 created by the broad-band saturating irradiation used in this study (see Section 2.2.2 for their spectra) equation (19) was used to calculate a series of F_R values which would result if the mixture (mix_2) was created by monochromatic light at 1 nm wavelength intervals, covering the full spectrum from 350 to 800 nm. A weighted average was then calculated by multiplying the F_R at each irradiating wavelength by the relative amount of irradiance at that wavelength (in normalised quanta s^{-1} m^{-2}). This average F_R value is considered to represent the fraction of rhodopsin that would be present in the photosteady state mix_2, given the irradiance spectrum used to create it.

This weighted average is regarded as an improvement over the method of the original authors who simply compute an overall absorption ratio using the total area under the spectra from 600 to 700 nm, though their point that not knowing the precise spectral distribution of the saturating light is not in practice a problem since visual pigment spectra (with λ_{max} values of *ca.* 500 nm) are almost parallel in this region (see Section 4.2.4.2) is

conceded. Varying the wavelength limits over which the absorption ratio is calculated then makes little difference on the spectral location or extinction ratios of the metarhodopsin estimate. However, incorporating the spectrum of the saturating light source allowed this analysis to be subsequently modified in an attempt to model the mixtures that would result given different sources of saturating illumination and the visual pigments present (see Section 5.2.10).

This estimation, and that of Cronin and Forward (1988), does assume that the quantity ϕ is constant within the band of saturating irradiance. The value of ϕ is wavelength-independent in the main absorption band of visual pigments (Dartnall, 1972) and the value previously determined for crayfish photopigments, $\phi = 1.41$ (Cronin and Goldsmith, 1982a), was used in this study. This value was measured using crayfish maintained under conditions that maximise ocular retinal:dehydroretinal ratios (Suzuki *et al.*, 1984) and is consistent with other known arthropod values for ϕ (Cronin and Goldsmith, 1982a).

In practice the estimate of the metarhodopsin absorbance spectrum is not significantly affected by the actual value of ϕ. To demonstrate this the average values obtained for the main pigment mixtures of the deep-sea species measured in this study were used to generate estimates of metarhodopsin using different values of ϕ. Even when ϕ was varied by 50% either side of its predicted value (1.41) the estimated λ_{max} of the metarhodopsin varied by just 0.5 nm and the extinction coefficient by just 0.03, both within the original measuring accuracy of the microspectrophotometer (see Table 4.4, and Sections 4.1.1 and 4.1.4).

4.3.2.2 Metarhodopsin estimates calculated in this study

When applied to the deep-sea species' data obtained in this study, on average, the above method results in an estimate of the metarhodopsin spectrum whose λ_{max} is shortwave shifted by 1.45 nm (s.d. = 0.28 nm) and the extinction coefficient increased by 7.49% (s.d. = 4.31%), relative to that of mix_2. Thus the shift is relatively small and the accuracy

Table 4.4 The effect of varying ϕ on the estimate of the metarhodopsin.

ϕ	F_R in mix_2	Est. M λ_{max} (nm)	Extinction ratio: $\varepsilon_{max}M$ / $\varepsilon_{max}R$
0.94	0.282	483.0	1.373
1.41	0.227	483.5	1.344
2.115	0.176	483.9	1.321

This example is based on the average values obtained for the main pigment mixtures of the deep-sea species measured in this study: a mix_1 λ_{max} of 493.8 nm, a mix_2 λ_{max} of 485.2 nm and an extinction ratio of 1.261. See the text for details on the calculation of the metarhodopsin estimate, M. Even when ϕ, the ratio of the quantum efficiency of the photoconversion $R \rightarrow M$ to that of the photoconversion $M \rightarrow R$, is varied by 50% from its predicted value (1.41) the estimated λ_{max} of M varies by just 0.5 nm and the extinction coefficient by just 0.03.

of the calculations are in practice limited by the accuracy of the original absorbance measurement. Both spectral location and relative absorbance of the metarhodopsin estimate appear correlated to the calculated F_R in mix_2 (see Figure 4.17). The shift in λ_{max} increases up to $F_R \approx 0.25$ as the increase in overlap results in more R being subtracted from mix_2 to create the estimate of the metarhodopsin. Beyond this the shift decreases as the λ_{max} values of the two measured absorbance mixtures converge (i.e. the overlap of their absorbances increases but the shift is decreased as the λ_{max} of mix_1 is so close to that of mix_2). The proportional increase in the extinction coefficient appears approximately linearly related to the F_R in mix_2.

In summary, the metarhodopsin estimates presented in the Chapter 3 (Tables 3.7 and 3.18) were calculated using equation (19), taking into account the spectrum of the saturating, red light irradiance that produced the mix_2 data. This analysis assumes that mix_1 represents the absorbance due to 100% rhodopsin and, given this assumption, the absorbance spectra of the two photostable states of the visual pigment are now known. Though the actual values of ϕ are not known, the metarhodopsin absorbance presumed to fit a rhodopsin template and the absorbance mixtures modelled by rhodopsin templates, all of these factors result in a maximum error of similar amplitude to that of the accuracy of the absorbances originally measured.

4.3.3 Estimating the rhodopsin

Although often claimed, or assumed due to periods of dark-adaptation, there is little direct evidence to support the assumption that the invertebrate visual pigments scanned initially are predominated by the rhodopsin. In this study, the discrepancy between the running average λ_{max} and the template λ_{max} of the mix_1 records (see Section 4.2.7.4) suggests that this is not the case. Further, when the standard deviations of the file averages' template λ_{max} values for mix_1 and mix_2 were compared using a paired two sample t-test, the former were found to be very highly significantly greater (mean of mix_1 s.d.'s = 2.77 nm, mean of mix_2 s.d.'s = 2.07 nm, $t_{36} = 3.730$, $p < 0.01$; see Tables 3.12 and 3.13). Within a species, the standard deviations of the mix_2 records are thought to represent measurement error as

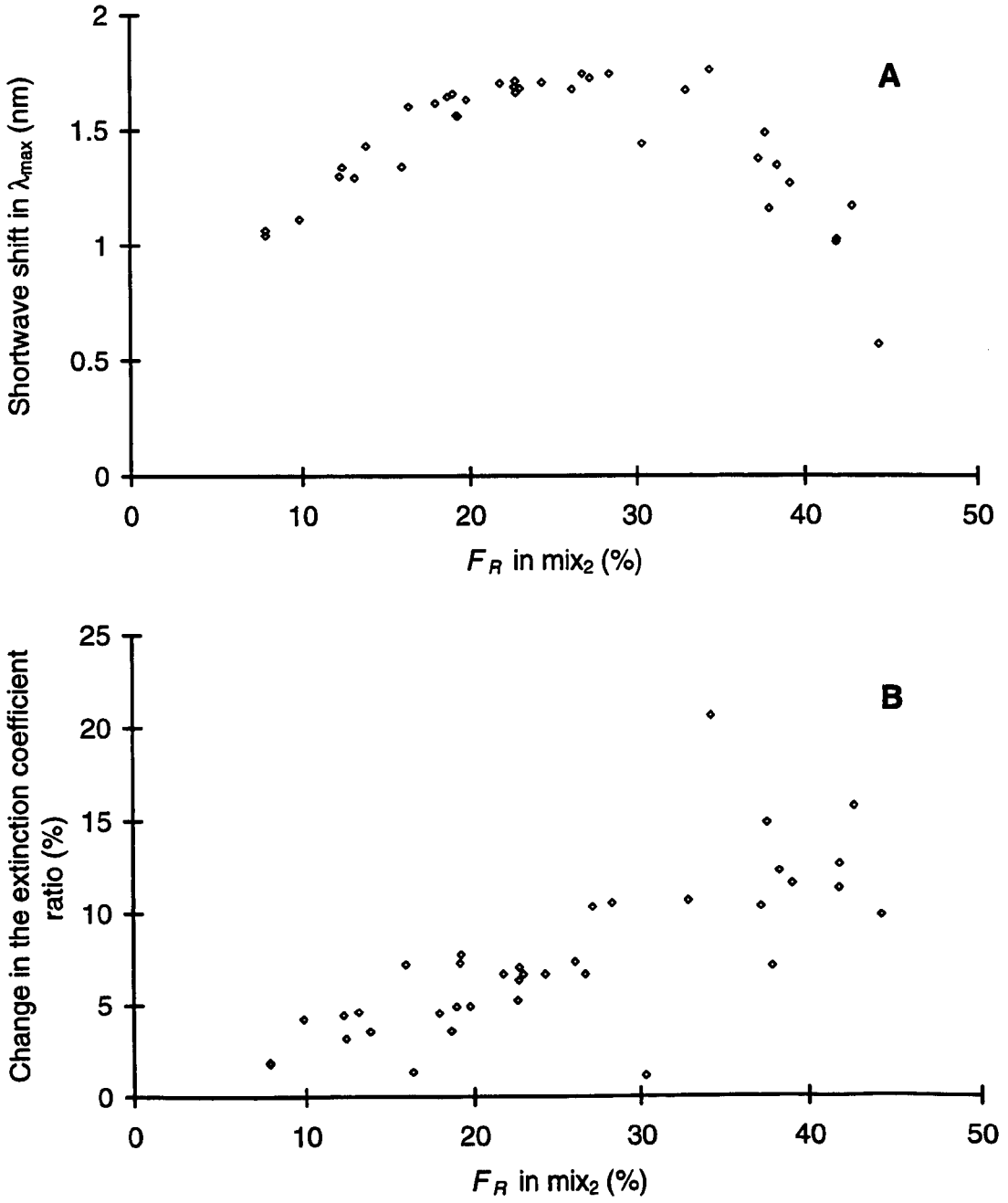

Figure 4.17 A, B. The shortwave shift in λ_{max} and the increase in the extinction coefficient between mix_2 and the estimated metarhodopsin (see text for analysis method). Each datum point represents a deep-sea shrimp recorded in this study. Both spectral location and relative absorbance appear correlated to the calculated F_R in mix_2. **(A)** The shift in λ_{max} increases up to $F_R \approx 0.25$ as the increase in overlap results in more R being subtracted from mix_2 to create the estimate of metarhodopsin. Beyond this the shift decreases as the λ_{max} values of the two measured absorbance mixtures converge. **(B)** The proportional increase in the extinction coefficient appears approximately linearly related to the F_R in mix_2.

the photosteady mixtures created should be identical. As the mix_1 standard deviations are significantly greater, this suggests that there is additional variation due, perhaps, to the initial mixture varying in the fractions of rhodopsin and metarhodopsin present. This increase in standard deviation would not be expected if the initial mixture were 100% rhodopsin, or was always the same fraction of rhodopsin. In contrast, the fact that many of the mix_1 mixtures are a good fit to a rhodopsin template is evidence of mix_1 being close to 100% rhodopsin (see Section 4.3.3). Further investigation was needed.

If mix_1 is also treated as a mixture of rhodopsin and metarhodopsin, it cannot be assumed that it has been brought to a photosteady state either naturally, before being caught, nor during subsequent experimental manipulations. In this case too many variables are unknown and calculating their absorbance spectra becomes an exercise in approximation. Some possible methods and their merits are discussed in this section before the final method adopted in this study is described (Section 4.3.3.3).

If mix_1 is not 100% rhodopsin then a mixture of rhodopsin and metarhodopsin will only fit a template nomogram exactly if the rhodopsin and metarhodopsin share the same absorbance spectra in both spectral location and amplitude. As this has never been found, one possible way to determine rhodopsin and metarhodopsin would be to fit combinations of templates representing rhodopsin and metarhodopsin estimates to both mix_1 and mix_2. However, though it is clear from Figure 4.16 that the absorbance spectrum of pigment mixtures will not fit a rhodopsin template with the same λ_{max} perfectly, it will be very close. Thus, while one pair of rhodopsin and metarhodopsin values will best-fit the measured absorbance spectra (i.e. by producing the least sum of squared differences between the template mixture and the measured data), there is little discrepancy for the method to 'home-in' on, and many other combinations will produce spectra which are not significantly inferior fits to the measured data. Coupled with the vast number of combinations that could be considered (i.e. factors that can be varied are the λ_{max} values of the rhodopsin and metarhodopsin, the extinction ratio of the rhodopsin to the metarhodopsin, and the F_R/F_M in both mix_1 and mix_2), this method is clearly neither robust nor practical.

Photoconversion difference spectra, calculated as the average absorbance spectrum of mix_2 minus that of mix_1, represent the change in absorbance produced when the fraction of the rhodopsin and metarhodopsin pigments is changed by the saturating, red light irradiance. Their shape is then unique given the λ_{max} values and extinction ratio of the rhodopsin and metarhodopsin pigments. Thus, it should be possible to determine the constituent pigments by fitting model photoconversion difference spectra to the data photoconversion difference spectra. This has the advantage over fitting rhodopsin and metarhodopsin combinations to the mix_1 and mix_2 data in that only one data spectrum is being modelled. Further, this analysis can be used if there are practical difficulties in effectively bleaching the pigments present, if the production of photoproducts distorts the difference spectra, or if it is not possible to convert a short wavelength λ_{max} rhodopsin to a mixture predominated by its longer wavelength λ_{max} metarhodopsin due to the overlap of their absorbances. Such analysis was used by Cronin and Frank (1996) to determine the rhodopsin and metarhodopsin pigments in the R8 cells of *Systellaspis debilis* for this last reason (see Section 4.3.3.2).

However, while the shape of a photoconversion difference spectrum is unique for any given rhodopsin and metarhodopsin combination, the amplitude is linearly related to the fraction of pigment that changes state. For example, if half of the molecules present change from the rhodopsin to the metarhodopsin state the measured photoconversion difference spectrum will have half the total amplitude compared to that if all of the molecules changed from rhodopsin to metarhodopsin. Thus template photoconversion difference spectra must also be scaled to fit that of the data. This factor has not been considered by the authors who have previously used photoconversion difference spectra and may invalidate their conclusions. The scaling needed to fit a model photoconversion difference spectrum to measured data could be used to calculate the F_R (or F_M) in one of the mixtures if the F_R in the other mixture was known. For example, if F_R in the post-red scan was calculated to be 20% and the photoconversion difference spectrum was best-fit by a rhodopsin and metarhodopsin combination whose photoconversion difference spectrum was scaled by 75%, it implies that 75% of the molecules that were in the rhodopsin state converted to metarhodopsin, leaving 20% as rhodopsin. Therefore, the original mixture was 95% rhodopsin. Note that in reality photoconversion involves

molecules changing continually between both photostable states but, if the irradiance is saturating, a photosteady *ratio* of the pigments will result.

Considerable effort was put into using photoconversion difference spectra to estimate the rhodopsin and metarhodopsin pigments. Spreadsheets were written which both varied all possible factors and others which 'anchored' the values of metarhodopsin as estimated by the method above (Section 4.3.2). In brief, model photoconversion difference spectra were generated for a range of rhodopsin, metarhodopsin and extinction coefficient values, scaled to the amplitude of the data photoconversion difference spectra (i.e. varying the number of pigment molecules changing state, or effectively varying the F_R in both mix_1 and mix_2), and the sum of the squared differences between the model and the measured data noted. In practice such analysis failed because, by allowing the amplitudes of the photoconversion difference spectra to change, this reduced their individuality (see Figure 4.18). As with fitting template mixtures to the measured data, while one combination will best-fit the photoconversion difference spectrum generated from the measured data, others will not be significantly inferior. As the example in Figure 4.18 shows, these 'equally good' combinations could be comprised from very different rhodopsin and metarhodopsin values and there is no way of selecting which are correct.

In conclusion, though iterative methods of analysis can be useful, the two examples above will fail because too many factors were unknown and different combinations of the variables produce very similar model spectra. The latter indicates that there would be no 'confidence' in the analyses output, i.e. the tests are not 'robust', while the former suggests that additional data needs to be collected at the time when the absorbance spectra are recorded (see Section 4.3.3.1 below). Thus, both attempts had to be abandoned. It was then clear that any analysis which did not assume that mix_1 is essentially 100% rhodopsin would require additional estimations to reduce the number of unknown factors.

4.3.3.1 Metarhodopsin fluorescence

Cronin and Goldsmith (1981) have shown that the metarhodopsin chromophore site of the crayfish (*Procambarus, Orconectes*) is fluorescent, with an emission spectrum which

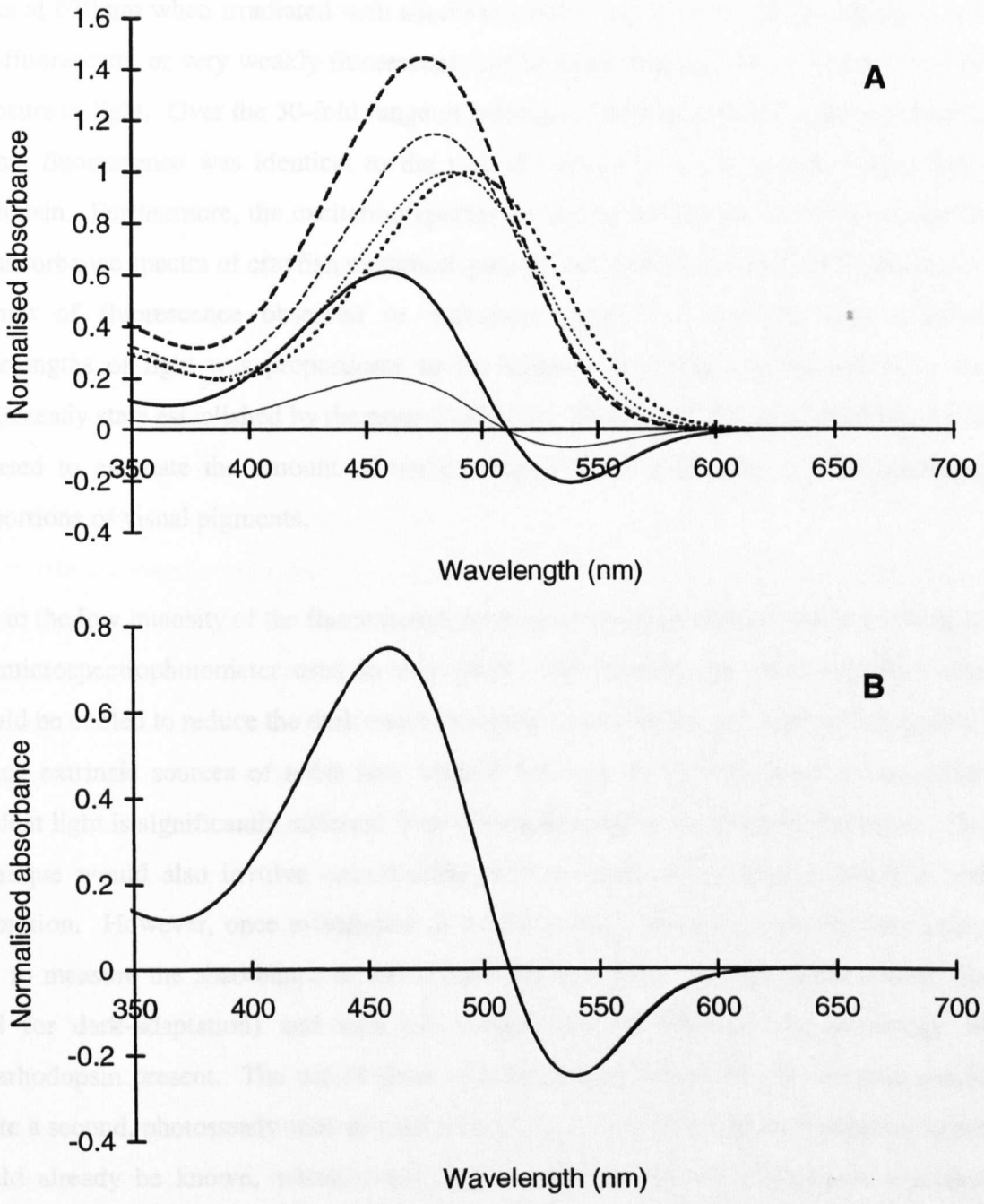

Figure 4.18 A, B. The similarity between photoconversion difference spectra when normalised. (**A**) The absorbance spectra of the rhodopsin templates, generated using the equation given by Stavenga *et al.* (1993) with a shifting β-band, used to model two invertebrate visual pigment systems. The first consists of a 487 nm λ_{max} rhodopsin (light, dotted trace) and a 480 nm λ_{max} metarhodopsin (light, dashed trace) with an extinction ratio of 1.15. The second consists of a 494 nm λ_{max} rhodopsin (bold, dotted trace) and a 475 nm λ_{max} metarhodopsin (bold, dashed trace) with an extinction ratio of 1.45. The photoconversion difference spectra for the two systems are also calculated (light and bold

peaks at 670 nm when irradiated with shortwave light. Fully dark-adapted rhabdoms are non-fluorescent, or very weakly fluorescent, but an increasing emission was observed on exposure to light. Over the 30-fold range of intensities studied, the rate of the appearance of this fluorescence was identical to the rate of formation of the metarhodopsin from rhodopsin. Furthermore, the excitation spectra for the observed emission were similar to the absorbance spectra of crayfish metarhodopsin at both neutral and acid pH. Finally, the amount of fluorescence observed in rhabdoms previously irradiated with selected wavelengths of light was proportional to the amount of metarhodopsin present in the photosteady state established by the prior irradiation. Hence, this linear relationship could be used to estimate the amount of metarhodopsin present in samples with unknown proportions of visual pigments.

Due to the low intensity of the fluorescence some modifications would have to be made to the microspectrophotometer used in this study. Specifically the photomultiplier tube should be cooled to reduce the dark count (housing are available) and every effort made to reduce extrinsic sources of noise (see Section 4.1.1.1), i.e. the threshold above which incident light is significantly different from the background noise should be lowered. The technique would also involve considerable trials in order to establish a baseline and calibration. However, once established, it would prove a powerful tool, the user being able to measure the absorbance of the sample initially (mix_1, i.e. as caught without the need for dark-adaptation) and then use fluorescence to estimate the percentage of metarhodopsin present. The use of short wavelengths to induce the fluorescence would create a second, photosteady state mixture (i.e. mix_2), of which the metarhodopsin content would already be known, which could also be scanned and its absorbance spectrum obtained. The mathematical deduction of the rhodopsin and metarhodopsin absorbance spectra would then be relatively straightforward as the proportion of the pigments present in both mixtures would be known. Not needing to dark-adapt animals prior to

Figure 4.18 (Continued).

solid traces, respectively) and all spectra are normalised to the peak absorbances of the rhodopsin pigments. In this example the photoconversion difference spectra are clearly different. However, when the photoconversion difference spectra are normalised to their peak to peak amplitudes (**B**) they are indistinguishable.

measurement would not only remove the need for animal maintenance, but would also allow the recording of rhodopsin:metarhodopsin ratios *in vivo*. Knowledge of these ratios may prove of considerable importance when relating calculated spectral sensitivities to visual tasks (Section 5.2.11).

However, it may be that it is not possible to modify the microspectrophotometer so that it can measure both absorbance and fluorescence sequentially. In this case, absorbance measurements could be taken as described above (Section 2.2.3) and then fluorescence measurements taken afterwards. Average mix_1 and mix_2 absorbance spectra would be obtained as before, and the proportions of rhodopsin and metarhodopsin within them estimated from the average fluorescence measurements. Ideally, the fluorescence and absorbance measurements should be from alternate eye sections/retinal preparations from the same animal. However, fluorescence measurements could be taken much later if the tissue was appropriately preserved, for example the frozen samples of this study. Although whole eyes were sectioned in this study and the unused sections destroyed, for many species the other eye is still frozen. Fluorescence could thus be done on the second eye to estimate the proportions of rhodopsin and metarhodopsin and these values compared with the results of the statistical analysis described in Section 4.3.3.4.

4.3.3.2 Characterising the visual pigments of the R8 cells

It has already been noted that the rhodopsins of the R8 cells measured in this study appear to have narrower FWHM bandwidths than their corresponding rhodopsin templates (see Figures 3.24, 3.26, 3.28 and 3.30). Therefore, new templates were generated using the equation given by Stavenga *et al.* (1993) but with the parameters altered to produce a narrowed α-band as predicted for UV sensitive pigments (Palacios *et al.*, 1996). Template fitting using a predictive polynomial was therefore abandoned and templates fitted by manually iterating the λ_{max} of the template until the lowest RMS deviation between the template and the data was achieved. In all but one case this resulted in a λ_{max} value equivalent to the running average λ_{max}. The one exception, the R8 pigment of *Systellaspis braueri*, resulted in a λ_{max} just 2 nm longer than the running average λ_{max} (i.e.

a 413 nm template λ_{max} compared to a 411 nm running average λ_{max}). These UV templates clearly fit the data: the implication is that such shortwave pigments (i.e. with λ_{max} values around *ca.* 410 nm) are more closely related to the UV sensitive pigments (i.e. with λ_{max} values below 400 nm) than to those with longer λ_{max} values and there is also genetic evidence for this (see Tovee, 1995 for a review of UV sensitivity in animals).

The R8 rhodopsin absorbance spectrum presented by Cronin and Frank (1996) is similarly narrowed. These authors suggest that the reason for this is the production of photoproducts absorbing at short wavelengths and the inability to convert most of the shortwave sensitive rhodopsin to its metarhodopsin because of their absorbance overlap. However, the latter should not affect the rhodopsin spectrum as this is calculated by subtracting the initial scan from the post-bleach scan. These spectra are also presented and, while the post-bleach scan appears slightly lower on the shortwave limb (indicating some photoproduct formation which has then been bleached), the initial scan is still clearly too narrow. This suggests that the narrowing is not a consequence of distortions through experimentation and/or photoproduct.

Given their conclusions, Cronin and Frank (1996) determined the absorbance spectra of the rhodopsin and metarhodopsin by analysing the average difference spectrum for the photoconversion of rhodopsin to metarhodopsin (see above). A virtually perfect fit was found using a 410 nm λ_{max} rhodopsin, a 474 nm λ_{max} metarhodopsin and an extinction ratio of 1.45. This analysis was repeated using the R8 data obtained in this study (generating rhodopsin templates using the equation given by Stavenga *et al.* (1993) modified to include a shifting β-band) and the results are presented in Table 4.5. Only one set of data, that of *Oplophorus spinosus*, produced estimates that appeared correct, the other three sets all predicting the rhodopsin λ_{max} at *ca.* 430 nm, clearly 15 nm or more towards too long a wavelength. Two main reasons could explain this discrepancy. The first is that if the R8 rhodopsins do have narrower FWHM bandwidths then appropriately shaped templates must be used to model them. The photoconversion difference spectra used in these examples (and presumably by Cronin and Frank, 1996) were calculated using standard rhodopsin templates and thus are not representative. Secondly, given the similarity of such photoconversion difference spectra when normalised (see Figure 4.18

Table 4.5 Estimation of the rhodopsin and metarhodopsin pigments present in the R8 cells of the deep-sea species studied.

Species	Est. R λ_{max} (nm)	Est. M λ_{max} (nm)	F_R in mix_2	Extinction ratio: $\varepsilon_{max}M$ / $\varepsilon_{max}R$
Oplophorus spinosus	412	460	0.57	1.2
Systellaspis braueri	426	456	0.61	1.35
Systellaspis cristata	431	460	0.63	1.25
Systellaspis debilis (data from this study)	431	461	0.55	1.25
Systellaspis debilis (Cronin and Frank, 1996)	410	475	-	1.45

The absorbance spectra of the rhodopsin and metarhodopsin were determined by analysing the average difference spectrum for the photoconversion of rhodopsin to metarhodopsin. For this study, in all but one case (*Oplophorus spinosus*) these estimates are thought to be incorrect. The results obtained by Cronin and Frank (1996) using apparently identical methods are also given. See text for details.

above), it is not then surprising that a difference spectrum calculated from inaccurate templates still fits the data.

Cronin and Frank (1996) note that their photoconversion difference spectra rapidly became distorted as the variables changed from the best-fit combination. However, they do not state how their template photoconversion difference spectra were scaled. It is clear that all of the rhodopsin was not fully converted to the metarhodopsin and it is this factor which determines the scaling. (It is interesting to note that the blue light used in this study photoconverted less rhodopsin to metarhodopsin that the violet light used by Cronin and Frank (1996).) Finally, if the narrowing of the R8 absorbance spectra are due to photoproducts, as suggested by Cronin and Frank (1996), one would not expect the continued fit of the template generated photoconversion difference spectrum to the data at wavelengths down to 350 nm as presented by these authors. This suggests that photoproducts were not distorting the spectra in this region and again implies that the narrowed α-band is real and not an artefact.

Due to the problems inherent with fitting photoconversion difference spectra this analysis method was abandoned, though the photoconversion difference spectra of the R8 cell pigments are still presented in Chapter 3 (Figures 3.24, 3.26, 3.28 and 3.30). Neither could the metarhodopsin be estimated by comparing the absorbance overlap of the rhodopsin and the rhodopsin and metarhodopsin mixture (Section 4.3.2) due to the uncertainty of the rhodopsins' absorbance spectra. However, the mix_1 spectra clearly indicate a pigment absorbing with a λ_{max} close to 410 nm and the mix_2 spectra clearly suggest the presence of a second pigment absorbing at mid-wavelengths. In conclusion, the λ_{max} values of the R8 cells' rhodopsin pigments were determined by fitting UV rhodopsin templates until the lowest RMS deviations were achieved. These λ_{max} values correlate closely with the R8 cells' rhodopsin running average λ_{max} values. The metarhodopsin pigments could not be characterised but, from the mix_2 spectra, appear to have λ_{max} values at *ca.* 475 nm.

Finally, in both this study and the absorbance spectra presented by Cronin and Frank (1996) the longwave limbs of the R8 rhodopsin difference spectra show a longwave rise

in absorbance between *ca.* 475 and 550 nm. This 'shoulder' may reflect the presence of some metarhodopsin in the initial scan. The fact that it is more apparent in the data presented in this study (Figures 3.24, 3.26, 3.28 and 3.30) adds to this conclusion as the specimens were not deliberately dark-adapted as were the specimens used by Cronin and Frank (1996).

4.3.3.3 'Anchoring' the metarhodopsin

Once the metarhodopsin has been estimated using the method above (see Section 4.3.2.1) it is tempting to use it to estimate which rhodopsin values it could be paired with in order to create the mix_1 and mix_2 pigment mixtures actually measured. Thus, a new value for the F_R in mix_1 could be assumed and the new rhodopsin calculated by subtracting the F_M from mix_1 and dividing this by the F_R. Indeed, this is how the metarhodopsin spectrum is obtained from the mix_2 absorption spectrum once the F_R in mix_2 has been determined. However, the estimation of the metarhodopsin using equation (19) is only valid for the case where mix_1 is 100% rhodopsin, as it compares the relative overlap of the mixture and the *rhodopsin* absorbance spectra in the region of the saturating irradiance. Thus, the estimate of the metarhodopsin will change as the estimate of the rhodopsin does.

No analytical method appears to exist which will calculate the rhodopsin and metarhodopsin from two unknown mixtures. Thus it was decided to model how erroneous it would be to first estimate the metarhodopsin using a F_R in mix_1 of 1 and then 'anchor' this value to determine new estimates of rhodopsin. Using the average values of the deep-sea species studied, analysing a 493.8 nm λ_{max} mix_1 and a 485.2 nm λ_{max} mix_2, with a 1.261 extinction ratio, produces an estimated metarhodopsin with a 483.5 nm λ_{max} and a new extinction ratio of 1.344 (assuming mix_1 is 100% rhodopsin). If it is then suspected that mix_1 is in fact a 50% rhodopsin:metarhodopsin mix (i.e. a worst case scenario), subtracting 50% of the estimated metarhodopsin from mix_1 produces a 511.1 nm λ_{max} pigment with a peak absorbance of 0.788 relative to mix_1 (equivalent to a 1.707 metarhodopsin to rhodopsin extinction ratio). To check this value, a mixture created with equal proportions of the templates representing these new rhodopsin and

metarhodopsin estimations produces an absorbance spectrum with a 491.1 nm λ_{max} and a maximum absorbance of 1.018. Using the new rhodopsin template and the mix_2 template then produces a new metarhodopsin estimate with a λ_{max} of 484.5 nm and a metarhodopsin to rhodopsin extinction ratio of 1.646. Thus, 'anchoring' the first metarhodopsin estimation in order to determine possible values of rhodopsin does not drastically affect subsequent estimations of the metarhodopsin if the new value for rhodopsin is used, even if the F_R in mix_1 is as high as 50%. In practice, because the new value for the metarhodopsin could then be used to determine another estimate of the rhodopsin given mix_1, the first estimation of the metarhodopsin was recorded to avoid potentially unlimited circularity.

Accepting that the assumptions made above are not too erroneous, possible rhodopsin and metarhodopsin combinations can be calculated given the mix_1 and mix_2 data and varying the F_R in mix_1. This is illustrated in Figure 4.19 in which the average values of the deep-sea species studied have been used and the F_R in mix_1 varied from 90% to 50% at 10% intervals. Note that while the estimations of the rhodopsin are also subject to the value of ϕ (i.e. because ϕ is used in the initial calculation of the metarhodopsin), again changing its value has little effect because it has such a slight effect on the first metarhodopsin estimate. Using the example above, when ϕ is 1.41 and the F_R in mix_1 is 50%, the rhodopsin estimate has a λ_{max} of 511.1 nm and an extinction coefficient of 0.788 relative to mix_1. If ϕ is changed to 0.94, the rhodopsin estimate has a 512.1 nm λ_{max} and an extinction coefficient of 0.778; when ϕ is 2.115, the rhodopsin estimate has a 510.3 nm λ_{max} and an extinction coefficient of 0.797. Hence the change in the rhodopsin estimate is of approximately equal amplitude to the measuring accuracy of the original scans made by the microspectrophotometer (see Section 4.1). The effect of potential errors in the value of ϕ is therefore insignificant.

4.3.3.4 Photoconversion difference spectra

Though estimating possible rhodopsin spectra from the mix_1 and mix_2 data is an interesting exercise in its own right, the actually rhodopsin present in the animal has still

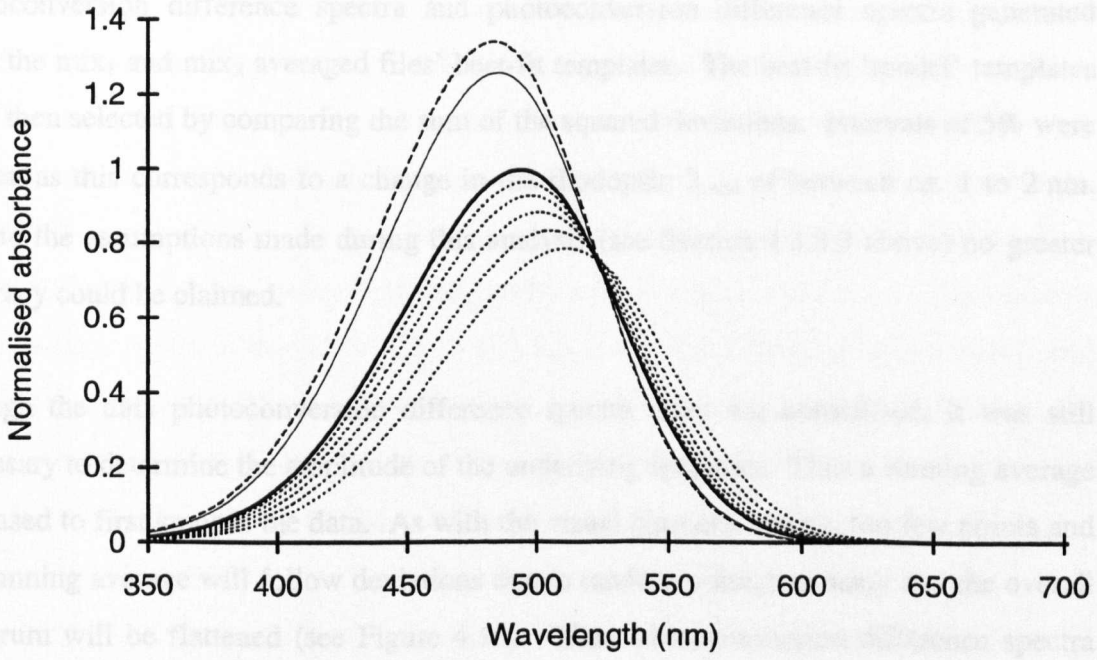

Figure 4.19 The change in λ_{max} and extinction coefficient of the rhodopsin estimate versus the F_R in mix_1. Using the average values of the deep-sea species studied, a 493.8 nm λ_{max} mix_1 (bold trace) and a 485.2 nm λ_{max} mix_2 (light trace) with a 1.261 extinction ratio produces an estimated metarhodopsin (dashed trace) with a 483.5 nm λ_{max} and a new extinction ratio of 1.344 (assuming mix_1 is 100% rhodopsin). Varying F_R from 90% to 50% at 10% intervals then produces rhodopsin estimates (dotted traces) with λ_{max} values and extinction coefficients relative to mix_1 of: 495.5 nm and 0.968; 497.9 nm, 0.930; 501.1 nm, 0.886; 505.6 nm, 0.837; and 511.1 nm, 0.788, respectively.
All templates are generated using the equation given by Lamb (1995).

not been determined. In order to select one rhodopsin value as the best estimate, the photoconversion difference spectra were again considered. In brief, using rhodopsin and metarhodopsin estimates generated at F_R in mix_1 intervals of 5% it was possible to create a restricted number of template photoconversion difference spectra. These 'model' template photoconversion difference spectra were then fitted to both the data photoconversion difference spectra and photoconversion difference spectra generated from the mix_1 and mix_2 averaged files' best-fit templates. The best-fit 'model' templates were then selected by comparing the sum of the squared deviations. Intervals of 5% were chosen as this corresponds to a change in the rhodopsin λ_{max} of between *ca.* 1 to 2 nm. Due to the assumptions made during this analysis (see Section 4.3.3.3 above) no greater accuracy could be claimed.

Though the data photoconversion difference spectra were not normalised, it was still necessary to determine the amplitude of the underlying spectrum. Thus a running average was used to first smooth the data. As with the visual pigment spectra, too few points and the running average will follow deviations due to random noise, too many and the overall spectrum will be flattened (see Figure 4.13). Thus, photoconversion difference spectra were created using two visual pigment templates with λ_{max} values, added random noise and an extinction ratio equal to those of the mix_1 and mix_2 average files (as estimated using the main visual pigment analysis program with an 11 point running average; see Section 4.2). Running averages with varying numbers of points were then passed through these spectra and the optimum chosen as that which produced the least sum of squared deviations with the original template photoconversion difference spectrum without noise (in the range 450 to 650 nm). Individual trials were repeated until the mean optimum number of points was calculated with an associated 95% confidence limit of less than one. As expected, for spectra with increasing signal to noise the optimum number of points increased. The actual numbers of points in the running averages used to smooth the photoconversion difference spectra of each species are presented in Table 3.17.

The amplitude of each model photoconversion difference spectrum was determined by scaling the constituent rhodopsin and metarhodopsin templates relative to the actual absorbance of the mix_1 photobleach. This scaled photoconversion difference spectrum

then represents the change in absorbance across the spectrum which would occur if all of the visual pigment molecules were photoconverted from 100% rhodopsin to 100% metarhodopsin. Since the F_R in mix_1 is being assumed (i.e. it is the main variable in generating these photoconversion difference spectra) and the F_R in mix_2 can be calculated, subtracting the latter from the former gives the fraction of molecules which have changed from rhodopsin to metarhodopsin between mix_1 and mix_2. The photoconversion difference spectrum representing '100% change' was therefore multiplied by this fraction to give the actual amplitude of the model photoconversion difference spectrum. This process was repeated generating different model photoconversion difference spectra for every 5% change in the F_R present in mix_1. The best-fit model photoconversion difference spectrum was defined as that producing the least sum of squared differences with the data points in the range 425 to 675 nm (i.e. to include both the maximum and minimum absorbance change regions). There was no need to introduce an offset as the data photoconversion difference spectra were generated from the normalised mix_1 and mix_2 averaged data and then scaled to reflect the actual absorbance changes.

4.3.3.5 Rhodopsin estimates calculated in this study

In practice, all of the photoconversion difference spectra calculated from the averaged files were best-fit by model photoconversion difference spectra generated using rhodopsin and metarhodopsin templates assuming the F_R in mix_1 was 100%. However, it was evident that the photoconversion difference spectra calculated from the averaged data were often distorted. Many of the deviations between the absorbance spectra of the averaged difference spectra and the best-fit templates (e.g. at short wavelengths due to an incomplete final bleach and/or the build-up of photoproducts) are present in either or both of the mix_1 and the mix_2 spectra. These deviations can be additive when the two spectra are subtracted from each other. In addition, the relative amplitudes of these deviations increases as the overall amplitude of the photoconversion difference spectrum is *ca.* 2 to 4 times less than that of the maximum corrected absorbance loss for the mix_1 photobleach (see Figure 4.20).

For pigment systems like those of the deep-sea species studied, in which the metarhodopsin is displaced to shorter wavelengths with a greater extinction coefficient than the rhodopsin, the positive region of the photoconversion difference spectrum represents the increase in absorbance due to the presence of the metarhodopsin in mix_2. The negative region is then the absorbance lost due to the rhodopsin molecules being photoconverted to the metarhodopsin. As the F_R in mix_1 increases the estimate of the rhodopsin shifts to longer wavelengths and the photoconversion difference spectrum will show most change in the region of negative absorbance. The maximum to minimum gradient remains approximately constant as does the overall amplitude (see Figure 4.20). Hence it is not surprising that the best-fit photoconversion difference spectra do not follow the data at short wavelengths, particularly the first limb of the peak, where distortions of the original files as scanned by the microspectrophotometer are most apparent. However, the region of the minimum might still be used to select the most appropriate rhodopsin.

To use the photoconversion difference spectra to select the most appropriate estimate of the rhodopsin, spectra were created using the mix_1 and mix_2 best-fit templates. The photoconversion spectra thus produced were advantageous compared to those produced using the averaged data files in that they did not have any distortions (though they might be incorrect if the rhodopsin templates are not truly representative of the mix_1 and mix_2 absorbance spectra). Further, the change in the absorbance about the minimum of the model photoconversion difference spectra was sufficient for one to obviously best-fit the mix_2 minus mix_1 generated photoconversion difference spectra (the best-fitting model was defined as that producing the least sum of squared deviations with the mix_2 minus mix_1 spectrum).

The results of this template based modelling are shown in Table 3.19. All species have predicted F_R in mix_1 between 100% and 85% and, further, all model mix_1 absorbance spectra (calculated using the new rhodopsin and metarhodopsin estimates) have λ_{max} values within 0.3 nm of the original values with extinction ratios within 0.0002. This apparent accuracy is not surprising: this process is effectively the reverse of the way in which the estimate of rhodopsin is calculated above. The re-estimated λ_{max} values for the

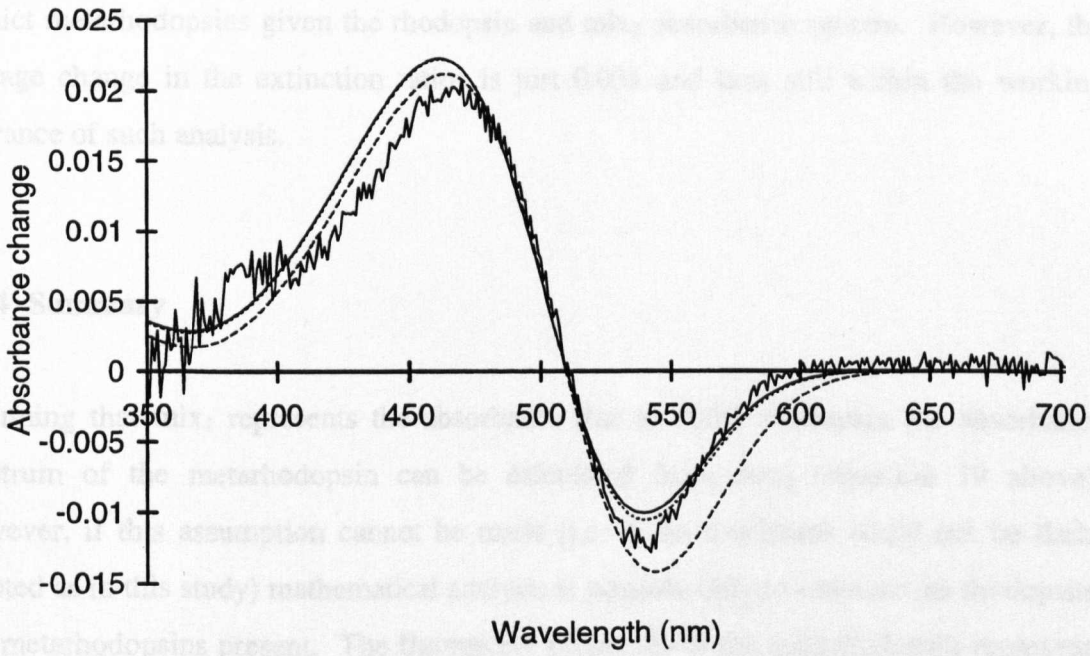

Figure 4.20 The effect of the F_R in mix_1 on the template generated photoconversion difference spectra. This example is based on the data from *Sergia phorcus* which has best-fit template λ_{max} values for the mix_1 and mix_2 averaged data at 493.6 and 483.9 nm, an extinction ratio of 1.152, an estimated metarhodopsin λ_{max} at 482.2 nm and a metarhodopsin to mix_1 extinction ratio of 1.193. The data photoconversion difference spectrum (jagged trace) was best-fit by a template photoconversion difference spectrum based on the mix_1 and estimate metarhodopsin values, i.e. assuming F_R in mix_1 is 100% (smooth trace), and corresponds to 81.4% of the visual pigment molecules present changing state from rhodopsin to metarhodopsin between mix_1 and mix_2.
Based on template photoconversion difference spectra only (see Section 4.3.3.4 for details) the F_R in mix_1 was estimated to be 90%, giving a 495.2 nm λ_{max} rhodopsin estimate and a metarhodopsin to rhodopsin extinction ratio of 1.212, which corresponds to 73.8% of the visual pigment molecules changing state from rhodopsin to metarhodopsin. The new photoconversion difference spectrum is clearly very similar (dotted trace). Finally, to show more clearly how the shape of the photoconversion difference spectrum changes with different rhodopsins, the photoconversion difference spectrum based on a F_R in mix_1 of 50% is also shown (dashed trace; 508.4 nm λ_{max} rhodopsin and a metarhodopsin to rhodopsin extinction ratio of 1.287). Note how the gradient between the maximum and minimum is unaffected with most change occurring about the minimum.

metarhodopsin, using the new rhodopsin estimate and mix_2, are a more appropriate check. All re-estimated metarhodopsins were within 0.1 nm of the first estimate but with a maximum change in extinction ratio of 0.220 (relative to the first $\varepsilon_{max}M$ / $\varepsilon_{max}mix_1$ ratio). This indicates that this method is more robust for λ_{max} values than for extinction ratios. This was also noted by Cronin and Forward (1988) when they used equation (19) to predict metarhodopsins given the rhodopsin and mix_2 absorbance spectra. However, the average change in the extinction ratios is just 0.031 and thus still within the working tolerance of such analysis.

4.3.4 Summary

Assuming that mix_1 represents the absorbance due to 100% rhodopsin the absorbance spectrum of the metarhodopsin can be calculated from mix_2 (equation 19 above). However, if this assumption cannot be made (i.e. if the specimens could not be dark-adapted as in this study) mathematical analysis is possible only to *estimate* the rhodopsins and metarhodopsins present. The fluorescent properties of the metarhodopsin represents an alternative method of determining the concentration, and therefore ratios, of pigments present. However, this would involve substantial modifications to the microspectrophotometer used in this study and additional measurements during experimentation.

Both of the methods used to fit prospective rhodopsin and metarhodopsin combinations to the photoconversion difference spectra, either template or average file based, suggest that the initial scans are predominated by rhodopsin. The data are summarised in Table 3.20 and it can be seen that even when the F_R in mix_1 is at its lowest value of 0.85, the change in the λ_{max} and extinction coefficient of the estimated value for the rhodopsin is slight. For all subsequent discussion (Chapter 5) the estimated rhodopsin and metarhodopsin values are used based on the template only modelling. However, it must be noted that even if this analysis is incorrect (and/or readers prefer to rely on the assumption that the initial scans do represent 100% rhodopsin) the values will be, on average, just 1.6 nm

shorter than the rhodopsin estimates quoted here and all will be within 3 nm of the mix_1 values recorded.

Chapter Five

The Visual Pigments of Deep-Sea Crustaceans

5.1 PRELIMINARY STUDY: *HOMARUS* AND *NEPHROPS*

Homarus gammarus and *Nephrops norvegicus* were selected for preliminary study as they were both relatively accessible and easy to maintain in aquaria. Their visual pigments were then measured to confirm the operation of the microspectrophotometer used during this study. Specimens with intact eyeshine were used and the spectral absorbances recorded were consistent with a typical invertebrate visual pigment system, i.e. mixtures containing different proportions of the rhodopsin and metarhodopsin states were created on exposure to different saturating irradiances and the visual pigments were bleached on exposure to bright 'white' light (see Cronin and Forward, 1988). Eyeshine, or eyeglow, is a characteristic feature of superposition compound eyes, particularly when they are in the dark-adapted state, and results from the reflection of incident light out of the eye. In most species this reflection is thought to occur at the tapetum and is thus a convenient, non-invasive method of assessing the internal structure of the eye (e.g. Loew, 1976; Land, 1981a). The experimental protocol was perfected during this initial study and the data produced used to test and modify the analysis procedures. Only the main rhabdoms were scanned and no attempt made to identify or record from putative R8 cells.

The visual pigments of *N. norvegicus* have already been determined by microspectrophotometry (Loew, 1976). Though the results are similar, 498 nm for the rhodopsin λ_{max} and 484 nm for the metarhodopsin (*cf.* the 499 nm and 478 nm values recorded in this study; see Table 3.9), various aspects of the protocol and observations imply that excessive light was used by Loew (1976) during the production of the photosteady state mixture. The eyes of *N. norvegicus* are known to suffer irreversible damage on exposure to bright illumination, both to the photoreceptor tissue (Loew, 1976, 1979; Shelton, *et al.*, 1985; Gaten, Shelton, Chapman and Shanks, 1990) and the dioptric apparatus (Gaten, 1988). Photoreceptor damage following the creation of a predominantly metarhodopsin mixture was noted by Loew (1976) and gradual, progressive deterioration occurred in the dark in both exposed and unexposed rhabdoms. This is interpreted as the metarhodopsin reducing the structural integrity of the photoreceptor, higher levels being created by the experimental procedures than would be expected *in vivo*.

Presumably because the rhabdoms showed such damage, Loew (1976) did not attempt to bleach the visual pigment present. Hence, difference spectra were not calculated and rhodopsin templates fitted directly to the absorbance spectra recorded initially (i.e. in the dark-adapted state) and post-'light exposure' (of unknown spectral radiance). This may be done if the final post-bleach scan is effectively flat (i.e. there are no other pigments present which absorb in the spectrum scanned or, if there are, their absorption is the same over this range) but there is no evidence given to support this. Figure 3.2 clearly shows that the average post-bleach spectrum recorded for *Nephrops* in this study was not flat, absorbance increasing approximately linearly towards shorter wavelengths. Fitting templates to the initial and post-red light treatment average scans in this study (Figure 3.2A) would reveal a poor fit to the best-fit rhodopsin templates on the shortwave limb due to the additional absorbance of other, non-visual pigments which are present (not shown). However, because the templates are fitted to the longwave limb, using these templates as estimates of the rhodopsin and metarhodopsin spectra results in predicted λ_{max} values of 496 and 480 nm, respectively, similar to the values obtained by Loew (1976). In contrast, the running averages of the average initial and post-red light treatment absorbance spectra peak at 488 and 474 nm, respectively, indicating the poor fit of the rhodopsin templates. Finally, it is unlikely that the unspecified 'light exposure' used by Loew (1976) created a mixture which was 100% metarhodopsin, potentially explaining the *ca.* 6 nm longwave shift in λ_{max} relative to the 479 nm calculated in this study.

Although *H. gammarus* has not been previously studied its American relative, *H. americanus*, has yielded pigments (a 515 nm λ_{max} rhodopsin and a 490 nm λ_{max} metarhodopsin, Wald and Hubbard, 1957; Bruno *et al.*, 1977) that are similar to the 522 and 482 nm λ_{max} pigments recorded in this study. The differences of 7 to 8 nm are unlikely to be due to wavelength calibration errors between studies and more likely reflect actual differences in the visual pigments possessed. Alternatively the data recorded for *H. americanus* may represent the absorbance spectra of unknown visual pigment mixtures, often not investigated in previous studies. However, whatever the reasons for the discrepancy between these two species, the values obtained here are within the range

of the λ_{max} values recorded for other members of the Family Astacidea and thus support the recordings and analysis of this study.

Though conclusions from a sample size of just two species cannot be firm, it does appear that these two species have rhodopsins complying with the Sensitivity Hypothesis. Thus, *N. norvegicus* possesses a blue sensitive rhodopsin, matched to the limited light at the depths and times at which it is active (Chapman and Rice, 1971; Loew, 1976; Loew, 1979; Gaten *et al.*, 1990), while *H. gammarus* possesses a longer λ_{max} rhodopsin presumably matched to the coastal waters in which it is found. Further, the separation between the rhodopsin and metarhodopsin pigments is greater for the shallower living *H. gammarus*, perhaps due to the widening spectrum available. This separation would serve to lessen the filtering effect by the metarhodopsin in the photoreceptor (and thus leave the spectral sensitivity of the photoreceptor unaltered; see Section 5.2.6 and Goldsmith, 1978a) and reduce the 'conflict' between light absorbed by the rhodopsin to elicit a response and by the metarhodopsin to photoconvert it back to the rhodopsin. Further analysis could be applied to any species whose visual pigments have been studied by microspectrophotometry to determine the effects of the transmission properties of the cornea and the filtering effects of the metarhodopsin and other non-visual pigments on the organism's actual spectral sensitivity.

Retinal tissue from *H. gammarus* was fixed for *ca.* 3 h in 2.5% glutaraldehyde in seawater to enable subsequent photobleaching of the normally photostable visual pigments (for discussion of this technique see Hays and Goldsmith, 1969; Bruno *et al.*, 1977; Goldsmith, 1978b; Cronin, 1985). In contrast, the visual pigments from the deeper living *N. norvegicus* were rendered so unstable with *any* glutaraldehyde fixation that the red light treatment photobleached the pigment rather than photoconverting it to a rhodopsin/metarhodopsin mixture. Though susceptibility to glutaraldehyde fixation is clearly not of importance in nature it may be correlated with visual pigment instability. A more 'unstable' visual pigment may be adaptive at the lower light intensities in which *N. norvegicus* is active if this indicates a higher quantum efficiency and/or reduced activation energies needed for photoisomerization.

It is difficult to relate a comparison of the times taken to induce full photoconversion and photobleaching to the visual processes which occur *in vivo*. While analysis of the former could yield information regarding the efficiencies of the visual pigments within the photoreceptors, the latter is simply an experimental procedure to obtain a reference scan. However, due to this procedure it was noted that the absorbance due to non-visual pigments (i.e. photostable pigments present after the bright, white light bleach) is greater in *H. gammarus* than in *N. norvegicus* (*cf.* Figures 3.1 and 3.2), despite similar magnitudes of photobleach due to the rhodopsin. Thus, the rhabdoms of *H. gammarus* appear to be covered in more screening pigment than those of *N. norvegicus*, adaptations expected given the different photic environments they inhabit.

5.2 THE SPECTRAL SENSITIVITIES OF DEEP-SEA CRUSTACEANS

The main emphasis of this study is the measurement of the absorbances of the visual pigments of deep-sea crustaceans, these data being used to gain an understanding of their spectral sensitivities. This study has characterised the visual pigments of four of those species previously studied (see Section 5.2.1 below) and added a further 32 new species, including 5 additional mysids and, for the first time, the visual pigments of a deep-sea amphipod, *Cyphocaris richardi*. (In all the discussions below the data obtained from the Atlantic- and Pacific-caught specimens of *Parapasiphaea sulcatifrons* will be treated as one and no distinctions made between the two populations; see Section 3.2.2.) Thus, while the deep-sea fishing used to obtain the species in this study represents a random sampling technique, sufficient samples were obtained to cover the main representatives of the deep-sea decapod shrimps.

5.2.1 Previous studies

Prior to this study, the spectral sensitivities of just eleven species of deep-sea shrimp had been published (see Table 1.1). These include nine decapods of the families Sergestidae, Oplophoridae and Alvinocarididae (the unusual deep-sea hydrothermal vent shrimp,

Rimicaris exoculata), and the deep-sea mysid, *Gnathophausia ingens*. The spectral sensitivities of all of the deep-sea shrimps now measured are summarised in Table 5.1 (excluding that of *R. exoculata* as it is proposed that its visual pigment, whose λ_{max} is 500 nm, may be used to see the black-body radiation produced by the heat associated with hydrothermal vents and not visible light; Pelli and Chamberlain, 1989). The distributions of the rhodopsin and metarhodopsin pigments as measured by microspectrophotometry, including those of the R8 cells, are shown as histograms in Figure 5.1. Only those pigment pairs recorded by microspectrophotometry are included to avoid discrepancies between different techniques.

Comparing the three deep-sea decapod species previously studied by other authors and duplicated in this study (and those of *H. gammarus* and *N. norvegicus*; see Section 5.1 above) suggests that the results of this study are very similar. Specifically, the rhodopsin and metarhodopsin λ_{max} values reported by microspectrophotometry (Hiller-Adams *et al.*, 1988) for *Acanthephyra curtirostris* and of *Systellaspis debilis* (presumably the R1–7 cells) are all within 5 nm of the values obtained in this study. The near-UV sensitive pigment later found in *S. debilis* was not found by Hiller-Adams *et al.* (1988) however, highlighting one of the weaknesses of microspectrophotometry, i.e. that photoreceptor classes can be missed. The greatest discrepancy between the microspectrophotometric data is for the rhodopsin of *S. debilis* (here estimated to have a λ_{max} of 497 nm). However, the shortwave shifted λ_{max} (493 nm) reported by Hiller-Adams *et al.* (1988) is probably due to some of the visual pigment already being present in the metarhodopsin state, the specimens used having been maintained in the dark for periods of only *ca.* 4½ h prior to study. This was recently confirmed when Cronin and Frank (1996) reported a λ_{max} of 498 nm in specimens which had been maintained in darkness for up to a week and which are therefore presumed to have regenerated a full complement of 100% rhodopsin molecules.

Comparisons between the microspectrophotometric data obtained in this and previous studies and electrophysiological data are made in Section 5.2.4.

Table 5.1 Spectral sensitivities of the deep-sea shrimps measured in this and previous studies.

Species	Method of study	λ_{max} of R or S_{max} (nm)	λ_{max} of M (where measured) (nm)	Author(s)
Superorder Eucarida				
Order Decapoda				
Suborder Dendrobranchiata				
Infraorder Penaeidea				
Family Penaeidae				
Bentheogennema intermedia	MSP	494	481	Present study
Bentheogennema pasithea	MSP	500	486	Present study
Gennadas sp.	MSP	495	478	Present study
Gennadas valens	MSP	495	478	Present study
Petalidium suspirosum	MSP	501	490	Present study
Plesiopenaeus armatus	MSP	493	480	Present study
Family Sergestidae				
Sergestes curvatus	MSP	493	484	Present study
Sergestes similis	MSP	495	484	Present study
Sergestes tenuiremis	MSP	495	487	Hiller-Adams, Widder & Case, 1988
Sergia maximus	MSP	495	482	Present study
Sergia phorcus	MSP	495	482	Present study
Sergia robustus	MSP	496	484	Present study
Sergia splendens	MSP	497	485	Present study
Suborder Pleocyemata				
Infraorder Caridea				
Family Oplophoridae				
Acanthephyra curtirostris	MSP	485	482	Present study
	ERG	510	-	Frank & Case, 1988a
	MSP	485	480	Hiller-Adams, Widder & Case, 1988
Acanthephyra microphthalma	MSP	482	480	Present study

Table 5.1 (Continued).

Species	Method of study	λ_{max} of R or S_{max} (nm)	λ_{max} of M (where measured) (nm)	Author(s)
Acanthephyra purpurea	MSP	492	481	Present study
Acanthephyra smithi	ERG	510	-	Frank & Case, 1988a
	MSP	491	482	Hiller-Adams, Widder & Case, 1988
Acanthephyra stylorostratis	MSP	489	484	Present study
Hymenodora frontalis	MSP	495	483	Present study
Hymenodora glacialis	MSP	500	483	Present study
Janicella spinicauda	ERG	400 & 500	-	Frank & Case, 1988a
Meningodora miccyla	MSP	486	481	Present study
Meningodora vesca	MSP	487	481	Present study
Notostomus elegans	ERG	490	-	Frank & Case, 1988a
Notostomus gibbosus	ERG	490	-	Frank & Case, 1988a
Oplophorus gracilirostris	ERG	400 & 500	-	Frank & Case, 1988a
Oplophorus spinosus	MSP	413, 494	*ca.* 475, 481	Present study
	ERG	400 & 500	-	Frank & Case, 1988a
Systellaspis braueri	MSP	411, 500	*ca.* 475, 486	Present study
Systellaspis cristata	MSP	414, 498	*ca.* 475, 477	Present study
Systellaspis debilis	MSP	417, 497	*ca.* 475, 483	Present study
	MSP	410 & 498	474 & 484	Cronin & Frank, 1996
	B	nr-UV & blue-green	-	Frank & Widder, 1994a
	ERG	400 & 500	-	Frank & Case, 1988a
	MSP	493	481	Hiller-Adams, Widder & Case, 1988
Family Pandalidae				
Plesionika maritus	MSP	499	489	Present study
Stylopandalus richardii	MSP	491	487	Present study

Table 5.1 (Continued).

Species	Method of study	λ_{max} of R or S_{max} (nm)	λ_{max} of M (where measured) (nm)	Author(s)
Family Pasiphaeidae				
Parapasiphaea sulcatifrons (Atl)	MSP	501	482	Present study
Parapasiphaea sulcatifrons (Pac)	MSP	501	484	Present study
Pasiphaea chacei	MSP	509	487	Present study
Pasiphaea emarginata	MSP	497	484	Present study
Superorder Percarida				
Order Mysida				
Chalaraspidium alata	MSP	493	488	Present study
Eucopia australis	MSP	514	493	Present study
Eucopia sculpticauda	MSP	493	489	Present study
Gnathophausia gigas	MSP	491	489	Present study
Gnathophausia gracilis	MSP	497	485	Present study
Gnathophausia ingens	MSP	492	489	Present study
	ERG	490 & 520	-	Frank & Case, 1988b
Order Amphipoda				
Cyphocaris richardi	MSP	482	479	Present study

Abbreviations as follows: MSP - microspectrophotometry; ERG - electroretinogram; B - behavioural. Where microspectrophotometry has been used λ_{max} values are quoted, the rest represent S_{max} values.

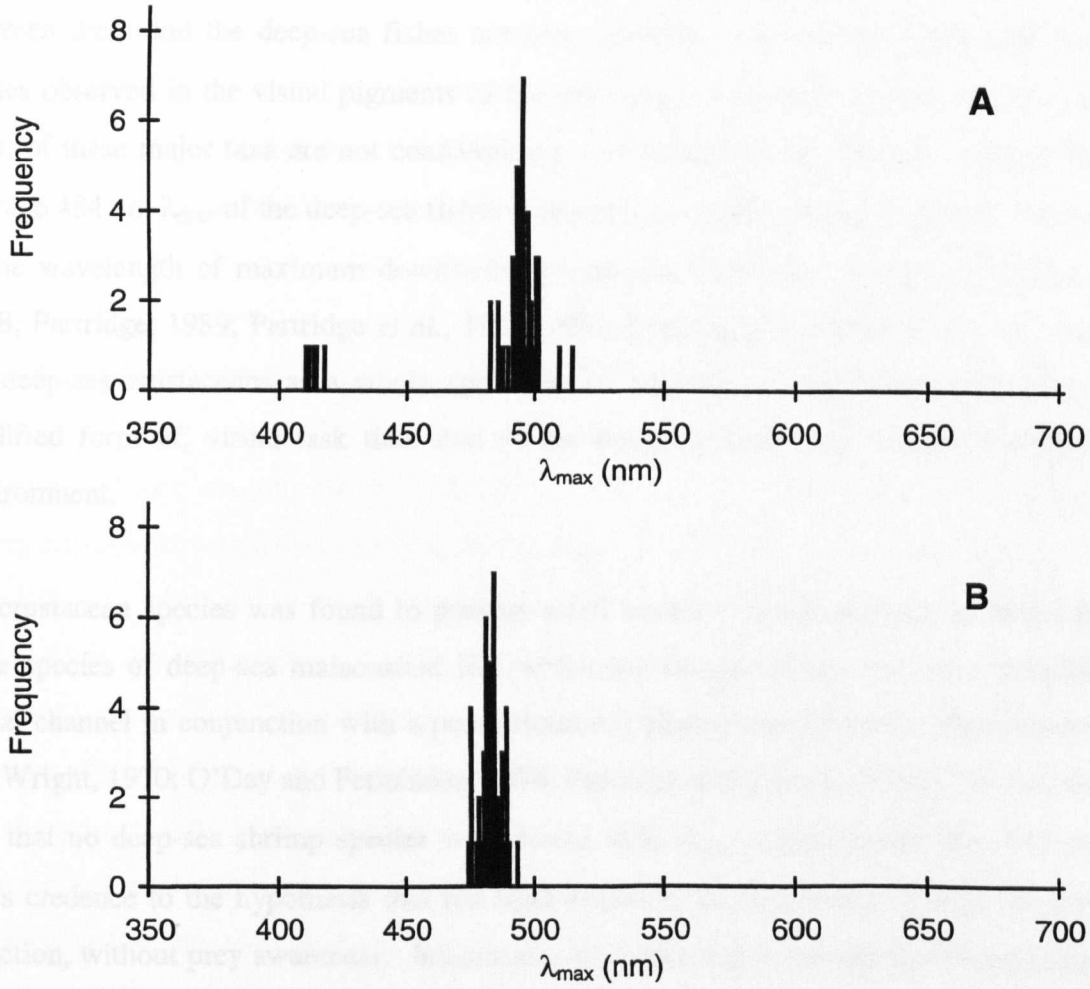

Figure 5.1 Histograms showing the distributions of the λ_{max} values of (**A**) rhodopsin and (**B**) metarhodopsin pigments recorded in the photoreceptors of deep-sea crustaceans by microspectrophotometry.

5.2.2 Deep-sea fishes

In characterising the visual pigments of so many of the deep-sea decapods, comparisons between them and the deep-sea fishes are now possible. The longer wavelength λ_{max} values observed in the visual pigments of the deep-sea crustaceans suggests that one, or both, of these major taxa are not conforming to the Sensitivity Hypothesis. Indeed, the average 484 nm λ_{max} of the deep-sea fishes is already *ca.* 10 nm longwave shifted relative to the wavelength of maximum downwelling light (see Partridge, Archer and Lythgoe, 1988; Partridge, 1989; Partridge *et al.*, 1989, 1992; Douglas and Partridge, 1997). Thus the deep-sea crustaceans as a whole appear to be adapted to a different, or at least a modified form of, visual task than that of the deep-sea fish which inhabit the same environment.

No crustacean species was found to possess a red sensitive visual pigment as found in three species of deep-sea malacosteid fish which are thought to use this as a 'private' visual channel in conjunction with a post-orbital red photophore (Denton, Gilpin-Brown and Wright, 1970; O'Day and Fernández, 1974; Partridge and Douglas, 1995). Hence, the fact that no deep-sea shrimp species were found with λ_{max} values greater than 515 nm lends credence to the hypothesis that red light emission and sensitivity is used for prey detection, without prey awareness. In contrast, no deep-sea fish species have been found to possess the shortwave visual pigments now identified in some deep-sea shrimp species. Though the reasons for sensitivity to shortwave light in the deep-sea is still a matter of debate (see Section 5.2.12), the presence of two blue–green sensitive visual pigments in some species of deep-sea fish may also serve as a system for discriminating between different bioluminescent sources using the spectral bandwidth as the basis for discrimination (Partridge *et al.*, 1988, 1989, 1992). Bioluminescence has been described in terms of both intensity and duration (e.g. Mensinger and Case, 1990) and spectral composition (e.g. Widder *et al.*, 1983; Frank and Case, 1988a; Latz *et al.*, 1988). Differences in bioluminescence emission properties may yet explain the variety of visual systems both within and between these taxa.

In general the data regarding the behaviours of both deep-sea fishes and crustaceans are scarce and explaining the disparity between these taxa will no doubt depend on identifying and characterising their visual tasks. Possible reasons for the possession of the visual pigments observed in the deep-sea crustaceans are explored throughout the rest of this discussion. This culminates in a simplified model which provides a possible explanation for the λ_{max} values observed, based on maximising photon capture when viewing bioluminescence (Section 5.3).

5.2.3 Taxonomic and depth comparisons

The range of deep-sea shrimps now studied, especially within the Order Decapoda, also allows comparisons to be made within this group. Although the members of taxonomic classes have traditionally been grouped together largely in terms of their similar morphology, this still relates, to some extent, to their phylogeny. Thus families represent a convenient taxonomic level at which to compare groups of probably very closely related animals. For subsequent comparisons only those species listed in Table 5.1 and whose visual pigments have been studied by microspectrophotometry are considered. Note that no statistical analyses have been applied due to the constraint that, in many cases, the value quoted as representative for a species is often actually an average from just one specimen of that species (see Section 4.2.7.2).

Within the Decapoda there is little difference between the average λ_{max} of the R1–7 rhodopsin pigments possessed by the members of the different families. Hence, the average rhodopsin λ_{max} values of the members of the families Penaeidae, Sergestidae and Pandalidae are 496, 495 and 495 nm, respectively, with all the λ_{max} values within a 10 nm range from 491 to 501 nm. In particular the range within the Sergestidae is particularly tight, spanning just 4 nm (n = 7). Though the range within the families Oplophoridae and Pasiphaeidae are slightly greater, the former including species with slightly more R1–7 shortwave rhodopsin pigments and the latter slightly more longwave pigments (i.e. ranges of 482 to 500 nm and 497 to 509 nm) the mean values are still 492 and 499 nm, respectively. The total range of λ_{max} values for the decapods' R1–7 pigments is therefore

482 to 509 nm, with the majority within ± 5 nm of the overall average decapod rhodopsin λ_{max} value of 494 nm.

The only obvious difference between members of the Decapoda is that four Oplophorid species, *Oplophorus spinosus*, *Systellaspis braueri*, *S. cristata* and *S. debilis* possess a second, shortwave sensitive visual pigment. The technique of microspectrophotometry is such that it is possible to miss sub-sets of photoreceptor classes and this would be particularly relevant concerning the smaller R8 cells in which these pigments are found. Indeed, some members of the Sergestidae appear to possess degenerate R8 cells distal to their functional R1–7 cells (P.M.J. Shelton, pers. comm.) which were not identified during this study. Although it was often not possible to view the R8 cells as distinct structures, the presence of a different pigment was immediately obvious, and the occurrence of a shortwave sensitive pigment was investigated in all species by recording from the far distal end of the rhabdom layer. It is likely that the degenerative R8 cells of the Sergestidae are therefore non-functional or do not contain a different visual pigment to that found in the main, R1–7 rhabdom. Hence, though the presence of a shortwave sensitive pigment may have been missed in some species this is unlikely. Further, its possession by just four, closely related species is unlikely to be the result of missing such pigments in other species. The uses of shortwave spectral sensitivity are discussed in Section 5.2.12.

With the exception of *Eucopia australis*, within the Order Mysida the range of λ_{max} values is similar to that of the decapods, spanning 491 to 497 nm. On closer examination of the *E. australis* absorbance spectra (Figure 3.38) it is clear that the mix_1 absorbance spectrum is relatively broad (perhaps reflecting an incomplete final bleach) and, as a consequence of the analysis, the λ_{max} of the best-fit rhodopsin template is 8 nm longer than the running average λ_{max} of the data. The estimated value of the rhodopsin λ_{max} (514 nm) is similarly distorted and hence little significance should be given to this outlier, the closely related *E. sculpticauda* having a more typical rhodopsin λ_{max} of 493 nm. Finally, the single amphipod recorded in this study, *Cyphocaris richardi*, has the lowest rhodopsin λ_{max} recorded in this study (482 nm), though this is still equal to that recorded in a decapod (e.g. *Acanthephyra microphthalma*).

No significant differences are therefore apparent in the rhodopsin λ_{max} values found in the R1–7 cells of the deep-sea shrimps measured in this, and previous studies by microspectrophotometry, despite including the main representatives of the decapods found in the deep-sea and including six mysids and a single amphipod. If differences between taxa are not apparent it is unlikely that there will be correlations with physical parameters such as depth. Though depth distributions of many deep-sea species are known they are not consistent in all areas, often depending on many other physical parameters, for example the shallowing of the sea floor near a continental slope (Hargreaves, 1984). For vertical distributions regarding decapods from the infraorders Caridea and Penaeidea refer to papers by Foxton (1970a, b, respectively), for mysids to Hargreaves (1985 and 1989) and for pelagic amphipods to Thurston (1976). Many of the species obtained while on board the RV New Horizon are listed, with depth ranges, by Childress (1975).

The depth which a species inhabits not only changes with location but for many it also changes by day, various species undergoing large vertical migrations to shallower water at twilight and back to deeper water again at sunrise. If statistical analysis is to be done, for example to correlate depth and λ_{max}, depth ranges cannot be used. The decision must then be made whether to use the depth by day, by night, or during the migrations etc. The size of the depth ranges themselves may well be of importance and the use of a mean will lose this information. Indeed, if a single value is needed a mode is probably more representative. However, any selection of a value that represents an animal's depth in the deep-sea given a certain range is already making assumptions about the importance of that depth to the animal.

Depth is a physical parameter that is relatively easy for us both to measure and comprehend. The reality is that such factors may not, in themselves, be of importance to the animals which experience them. Hence, depth will be an important factor determining an animal's visual pigment absorbance spectra only if it is related to a variable (or variables) which defines the visual tasks of such animals. One factor that is linked to depth which could influence visual pigment spectral absorbance is downwelling light, its spectral composition (Figure 1.1) and flux changing systematically with depth (see

Section 1.4.1). Indeed, the data set presented can be split into two sets of species, those above and those below the threshold of downwelling light perception. The depth of this threshold will depend on the sensitivity of the species' eyes but the calculation of this appears unnecessary, no difference in λ_{max} values is observed between even the most extreme examples. Thus, no appreciable difference is observed between the λ_{max} values of the vertically migrating species *O. spinosus* (λ_{max} of 494 nm) and those of the deepest benthic species *Plesiopenaeus armatus* (λ_{max} of 493 nm). Neither are species which inhabit the same depth ranges necessarily similar. For example, the two Oplophorids, *P. armatus* and *A. microphthalma*, are both epibenthic (*ca.* 4000 m in depth) yet have λ_{max} values of 494 and 482 nm, covering approximately two-thirds of the total range found within this family.

In conclusion, no differences or correlations with taxonomy or depth are apparent between the rhodopsin λ_{max} values of the deep-sea decapods, mysids and the amphipod recorded in this, and previous studies, by microspectrophotometry: the range of R1–7 rhodopsin values being constrained between 482 and 509 nm (ignoring the data obtained from *E. australis*). However, the absence of such trends is not surprising as neither taxonomy nor depth (with the possible exception of its link to downwelling light) are necessarily representative of visual tasks which change in a progressive manner. It is the visual tasks of an animal which will act as the selection pressures for the evolution of a suitable visual pigment.

5.2.4 Spectral sensitivities versus visual pigment absorptions

That the spectral sensitivity of a photoreceptor is largely determined by the spectral absorbance of the visual pigment that it contains is thought to be particularly true for the superposition eyes of the deep-sea crustaceans (i.e. due to their presumed permanently dark-adapted state and relatively low levels of proximal shielding pigment; Hiller-Adams *et al.*, 1988; Gaten *et al.*, 1992). Comparing the λ_{max} values recorded by microspectrophotometry in this and other studies (Hiller-Adams *et al.*, 1988; Cronin and Frank, 1996) to the spectral sensitivities previously recorded by ERG (Frank and Case,

1988a) demonstrates that in many cases this is indeed true. That is, the effective spectral absorptance characteristics of the rhodopsins *in vivo* appear relatively unaltered by other pigments within the eye. The disparity between the 500 nm S_{max} reported by Frank and Case (1988a) for *O. spinosus* and *S. debilis* and the 494 and 497 nm λ_{max} rhodopsin pigments estimated in this study could be explained by wavelength calibration errors, different methods of analysis (e.g. template fitting) or simply the inherent reduced accuracy of ascertaining the S_{max} by ERG (i.e. due to experimental protocol the spectral sensitivity spectra are often comprised of a restricted number of data points spanning the visible spectrum). Alternatively, the shift in S_{max} may reflect slight changes due to screening pigments and/or the absorption characteristics of the optical components of the eye (though the dioptric structures in most crustaceans are assumed to have negligible absorption except in the violet and ultraviolet; Goldsmith, 1978a; see also Hiller-Adams *et al.*, 1988). Similarly, though the λ_{max} of their rhodopsin pigments is unknown, the S_{max} values of 490 nm reported for *Notostomus gibbosus* and *N. elegans*, and the 500 nm S_{max} values reported for the main pigments (again, presumably situated in the R1–7 cells) for *Janicella spinacauda* and *Oplophorus gracilirostris* (Frank and Case, 1988a) fit the current data set of λ_{max} values reported for other species within the Family Oplophoridae.

Greater disparity between the spectral sensitivity and the visual pigment absorbance of a photoreceptor has been observed in several species of the Crustacea, however, including two species of deep-sea shrimp. Specifically, the spectral sensitivities of *Acanthephyra curtirostris* and *A. smithi* were found to peak at 510 nm (Frank and Case, 1988a), seemingly more appropriate for shallow water crustaceans than for species that maintain daytime depths of greater than 500 m. Their absorbance spectra (see Figure 3.15 and Hiller-Adams *et al.*, 1988) match the shape of the spectral sensitivity spectrum recorded by Frank and Case (1988a) but are offset by *ca.* 20 nm to shorter wavelengths. This suggests that these species may possess some type of immobile distal screening pigment, as found in *A. purpurea* (Welsh and Chace, 1937), that would shift the S_{max} away from the visual pigment's λ_{max}. In crayfish and lobsters, this 'pigment screen' is believed to be responsible for the 10 to 30 nm difference between the S_{max} and λ_{max} (Goldsmith, 1978a). Why such a screening pigment shield would be needed, particularly in *A. curtirostris* which never migrates to shallower waters, remains obscure. The superposition optics of

such species are presumably adaptive to increase sensitivity, and are assumed to permanently remain in a dark-adapted state (Gaten *et al.*, 1990, 1992), unlike the eyes of coastal species whose spectral sensitivities are known to shift with the movement of screening pigments which accompany light- and dark-adaptation (Stowe, 1980b).

It is unlikely that screening by metarhodopsin contributed significantly to the longwave shift in spectral sensitivity reported by Frank and Case (1988a) although both *A. curtirostris* and *A. smithi* possess metarhodopsins with λ_{max} values at shorter wavelengths (482 nm) than those of their rhodopsins, so that screening by metarhodopsin would shift the spectral sensitivity to longer wavelengths (see Section 5.2.6). According to Goldsmith (1978a), screening by metarhodopsin should be negligible if: 1) the eye is dark-adapted, 2) near-threshold flashes are used to stimulate the eye (preventing conversion of a sizeable fraction of rhodopsin to metarhodopsin), and 3) the organism has other mechanisms than photo-regeneration for restoring a full titer of rhodopsin. The first two conditions were met by the experimental protocol of Frank and Case (1988a), and while these two species have not yet been studied with respect to dark-regeneration, such a system was found in another oplophorid occupying the same depth range (Hiller-Adams *et al.*, 1988). In addition, specimens tested within three hours of capture demonstrated the same spectral sensitivity as those that were maintained in the dark for 24 h before testing. Thus the authors reasonably conclude that screening by metarhodopsin is not the explanation for the shift in S_{max} observed (Frank and Case, 1988a).

5.2.5 *Gnathophausia* visual pigments

When previously studied by electroretinography, the deep-sea mysid *Gnathophausia ingens* was found to have sensitivity extending, unusually, to orange light (S_{max} at *ca.* 510 nm) and the results of chromatic adaptation and silent substitution experiments were not compatible with either a one or two pigment visual system (Frank and Case, 1988b). In contrast, this study revealed only single visual pigments in the rhabdoms of *G. ingens* specimens and specimens of the related *G. gigas* and *G. gracilis*. Though the estimated λ_{max} values of their rhodopsin pigments are consistent with the rest of the deep-sea

shrimps measured (rhodopsin λ_{max} values of 491, 497 and 492 nm for *G. gigas*, *G. gracilis* and *G. ingens*, respectively) the discrepancy between the λ_{max} and S_{max} values could be explained by the filtering effects of other pigments present in the eyes. However, this would have been revealed by its visual physiology. Frank and Case (1988b) were forced to conclude that "we are left with the enigma of a deep-sea crustacean with unusually high sensitivity to orange light that cannot be explained by known combinations of visual and/or screening pigments". Unfortunately, all this study can add is that this is true despite the evidence that a single, typical deep-sea crustacean visual pigment is possessed by *G. ingens* and two other members of the same genera. Clearly, further investigation is needed.

5.2.6 The effect of metarhodopsin on spectral sensitivity

Although it has already been noted that the screening effects of metarhodopsin within a rhabdom do not explain the disparity observed between the S_{max} and λ_{max} values recorded for both shallow living and deep-sea crustacean species (see Goldsmith, 1978a; Frank and Case, 1988a), it is still interesting to model this phenomenon as significant levels of metarhodopsin may occur in the rhabdom *in vivo*. It is the presence of other pigments, both within the eye and the photoreceptor cell itself, which will change the spectral sensitivity from that of the visual pigment's absorptance. In invertebrates such pigments include the metarhodopsin configuration of the visual pigment molecule itself. The theoretical effects of inert pigment screens have been explored by Goldstein and Williams (1966), who considered two limiting cases. In the first, the receptor, with an *in situ* rhodopsin absorbance $\alpha_R(\lambda)$, is overlain by a screen of metarhodopsin with *in situ* absorbance $\alpha_M(\lambda)$ (i.e. these values represent the actual absorbances of the pigments present, the 'rhabdomeric absorbance', and are calculated by multiplying the normalised absorbance by the specific absorbance per unit length and the total length of the photoreceptor). In this case the absorptance of the rhodopsin, $A_R(\lambda)$, is given by (after Goldsmith, 1978a):

$$A_R(\lambda) = 10^{-\alpha_M(\lambda)}\left[1 - 10^{-\alpha_R(\lambda)}\right] \qquad (20)$$

The first function outside of the brackets is the transmittance of the overlying pigment filter, whilst the function inside the brackets is the absorptance of the rhodopsin in an unscreened photoreceptor. In the absence of neural or optical coupling between cells (see Schiff, 1987), the normalised function $A_R(\lambda)/A_R\,\lambda_{max}$ should describe the spectral sensitivity of the receptor.

In the second case, the metarhodopsin is mixed homogeneously within the photoreceptor with the rhodopsin. Under these conditions (after Goldsmith, 1978a):

$$A_R(\lambda) = \left[\frac{\alpha_R(\lambda)}{\alpha_R(\lambda) + \alpha_M(\lambda)}\right]\left[1 - 10^{-[\alpha_R(\lambda)+\alpha_M(\lambda)]}\right] \qquad (21)$$

In equation (21) the expression between the second pair of brackets is the total absorptance of the receptor, and the first term in brackets is the fraction of this absorptance due to the rhodopsin. As before, the normalised function $A_R(\lambda)/A_R\,\lambda_{max}$ should describe the spectral sensitivity of the receptor. Note that if $A_M(\lambda) = 0$, both equations (20 and 21) reduce to the absorptance of the rhodopsin present, and the only screening is then 'self-screening' (see Goldsmith, 1978a). Self-screening is inevitable in any photoreceptor, but only becomes significant in long photoreceptors, depending on the optical density, D, of the pigment ($D = c.l.E(\lambda)$, where c is the concentration, l the path length, and $E(\lambda)$ the molar absorption coefficient). Other factors being equal, self-screening will then be greater for long receptors. Thus this is a particularly important consideration in deep-sea shrimps which can possess rhabdoms from *ca.* 70 to 150 μm in length, explaining their broad-band spectral sensitivities (see Section 5.3). The changes in spectral sensitivity with increasing amounts of metarhodopsin are shown in Figures 5.2 and 5.3.

[Note that these equations could be applied to any photostable pigment present either as an overlying filter (equation 20; e.g. the intrarhabdomal filters found in the stomatopods)

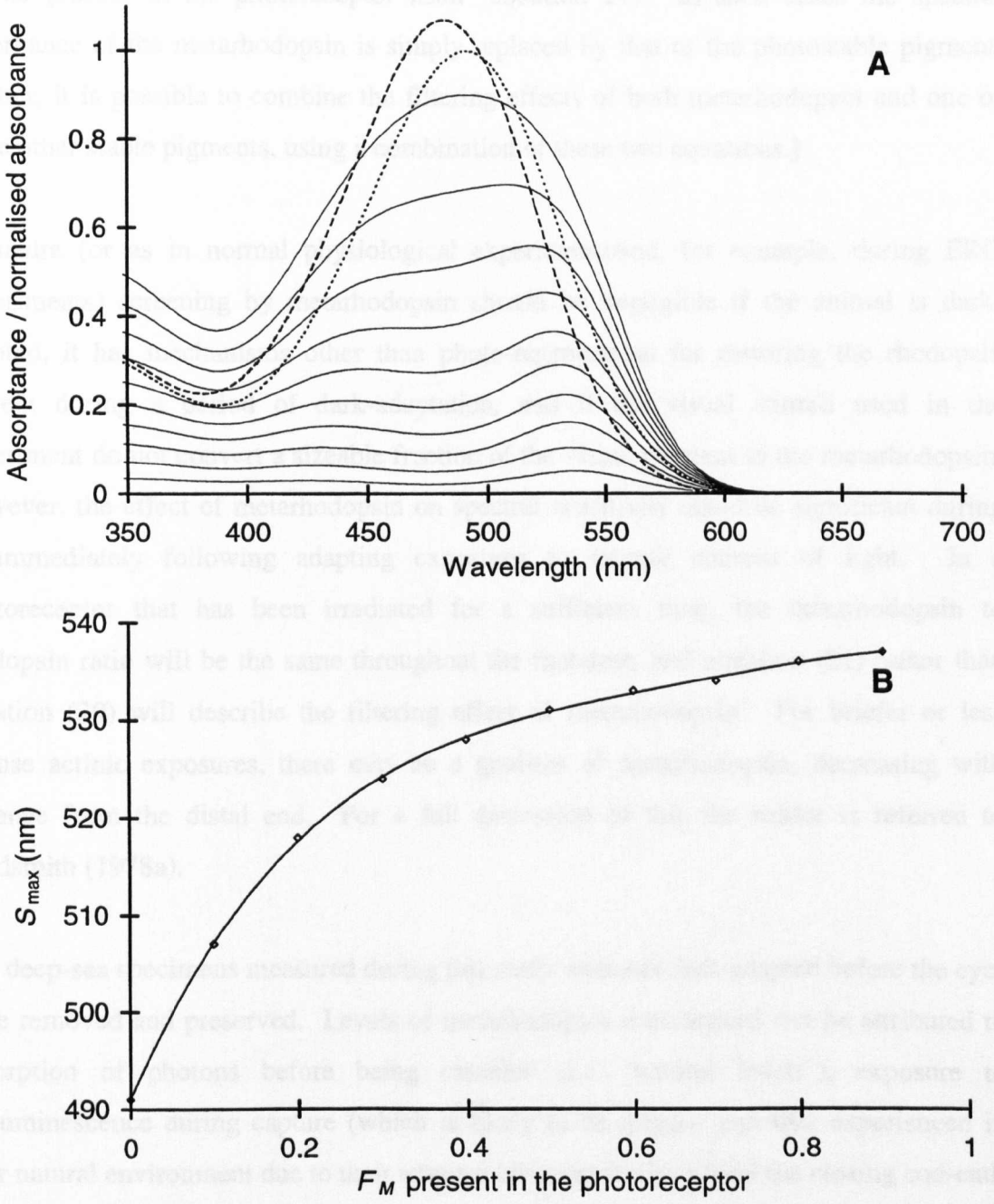

Figure 5.2 A, B. The change in rhabdomeric absorptance (equivalent to spectral sensitivity) with increasing levels of metarhodopsin, modelled as overlying the remaining rhodopsin (after Goldsmith, 1978a). (**A**) A 491 nm λ_{max} rhodopsin (dotted trace) and a 482 nm λ_{max} metarhodopsin (dashed trace) with an extinction ratio of 1.07 are used to model the pigment system as measured in *A. smithi* by Hiller-Adams *et al.* (1988). The first (highest) solid trace represents the absorptance due to 100% rhodopsin with a specific absorbance of 0.01 μm^{-1} and a pathlength of 100 μm. Note the broad spectral sensitivity due to self-screening by the rhodopsin. Successive solid traces (with

or one present in the photoreceptor itself (equation 21). In such cases the spectral absorbance of the metarhodopsin is simply replaced by that of the photostable pigment. Further, it is possible to combine the filtering effects of both metarhodopsin and one or more other stable pigments, using a combination of these two equations.]

In nature (or as in normal physiological experimentation, for example, during ERG experiments) screening by metarhodopsin should be negligible if the animal is dark-adapted, it has mechanisms other than photo-regeneration for restoring the rhodopsin content during a period of dark-adaptation, and if the visual stimuli used in the experiment do not convert a sizeable fraction of the visual pigment to the metarhodopsin. However, the effect of metarhodopsin on spectral sensitivity could be significant during or immediately following adapting exposures to intense sources of light. In a photoreceptor that has been irradiated for a sufficient time, the metarhodopsin to rhodopsin ratio will be the same throughout the rhabdom, and equation (21) rather than equation (20) will describe the filtering effect of metarhodopsin. For briefer or less intense actinic exposures, there may be a gradient of metarhodopsin, decreasing with distance from the distal end. For a full discussion of this the reader is referred to Goldsmith (1978a).

The deep-sea specimens measured during this study were not dark-adapted before the eyes were removed and preserved. Levels of metarhodopsin encountered can be attributed to absorption of photons before being captured (i.e. 'natural levels'), exposure to bioluminescence during capture (which is likely to be greater than that experienced in their natural environment due to their extreme close proximity within the closing cod-end) and red light exposure during experimental procedures (which is estimated to be

---

Figure 5.2 A, B. (Continued).

decreasing absorptance) represent the spectral absorptance which results from the filtering of an overlying screen of metarhodopsin, increasing at 10% intervals, over the remaining, decreasing layer of rhodopsin. Overall spectral sensitivity is clearly reduced and, though the spectrum remains broad, (**B**) the wavelength of maximum spectral sensitivity (S_{max}) shifts to longer wavelengths with increasing fractions of metarhodopsin (F_M) present.
The best-fit line through the S_{max} values is a fourth order polynomial and the original rhodopsin and metarhodopsin templates were generated using the equation given by Stavenga *et al.* (1993), incorporating a shifting β-band (after Palacios *et al.*, 1996).

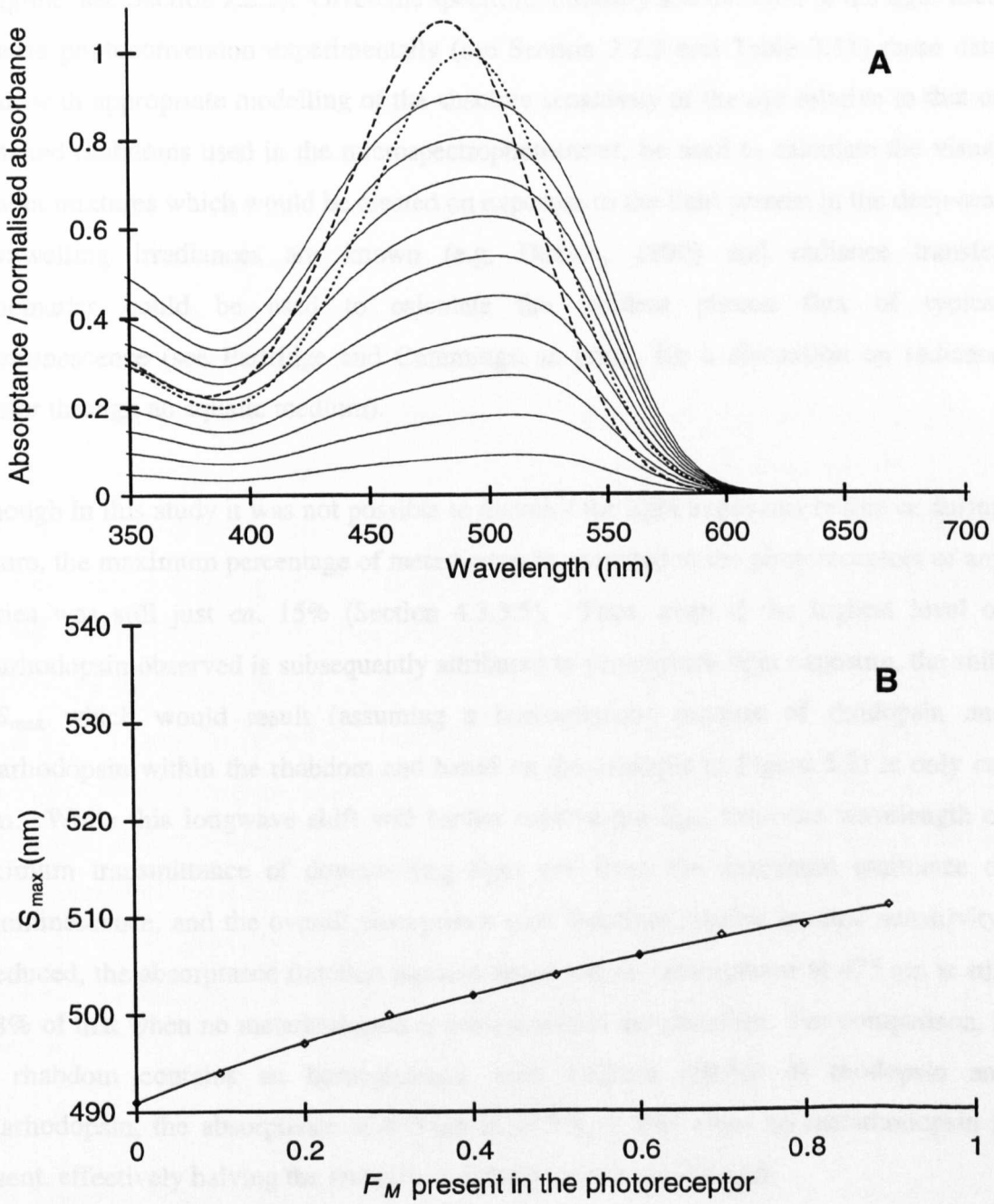

Figure 5.3 A, B. The change in rhabdomeric absorptance (equivalent to spectral sensitivity) with increasing levels of metarhodopsin homogeneously mixed with the rhodopsin (after Goldsmith, 1978a). (**A**) A 491 nm λ_{max} rhodopsin (dotted trace) and a 482 nm λ_{max} metarhodopsin (dashed trace) with an extinction ratio of 1.07 are used to model the pigment system as measured in *A. smithi* by Hiller-Adams *et al.* (1988). The first (highest) solid trace represents the absorptance due to 100% rhodopsin with a specific absorbance of 0.01 μm^{-1} and a pathlength of 100 μm. Note the broad spectral sensitivity due to self-screening by the rhodopsin. Successive solid traces (with

negligible; see Section 2.2.2). Given the spectrum, intensity and duration of the light used to cause photoconversion experimentally (see Section 2.2.2 and Table 3.11) these data could, with appropriate modelling of the absolute sensitivity of the eye relative to that of the naked rhabdoms used in the microspectrophotometer, be used to calculate the visual pigment mixtures which would be created on exposure to the light present in the deep-sea. Downwelling irradiances are known (e.g. Denton, 1990) and radiance transfer mathematics could be used to calculate the incident photon flux of typical bioluminescence (see Partridge and Cummings, in prep., for a discussion on radiance transfer through an aquatic medium).

Although in this study it was not possible to quantify the light exposures before or during capture, the maximum percentage of metarhodopsin recorded in the photoreceptors of any species was still just *ca.* 15% (Section 4.3.3.5). Thus, even if the highest level of metarhodopsin observed is subsequently attributed to pre-capture light exposure, the shift in S_{max} which would result (assuming a homogeneous mixture of rhodopsin and metarhodopsin within the rhabdom and based on the example in Figure 5.3) is only *ca.* 4 nm. While this longwave shift will further remove the S_{max} from the wavelength of maximum transmittance of downwelling light and from the maximum emittance of bioluminescence, and the overall absorptance (and therefore relative spectral sensitivity) is reduced, the absorptance function remains broad and the absorptance at 475 nm is still 83.8% of that when no metarhodopsin is present within the rhabdom. For comparison, if the rhabdom contains an homogeneous, even mixture (50:50) of rhodopsin and metarhodopsin, the absorptance at 475 nm is 47.7% of that when no metarhodopsin is present, effectively halving the animal's sensitivity at this wavelength.

Figure 5.3 A, B. (Continued).

decreasing absorptance) represent the spectral absorptance which results from the filtering by the metarhodopsin, increasing at 10% intervals, homogeneously mixed with the remaining, decreasing rhodopsin. Compared to Figure 5.2, the spectral sensitivity is again reduced and remains broad, however, (**B**) the shift in the wavelength of maximum spectral sensitivity (S_{max}) with increasing fractions of metarhodopsin (F_M) is reduced.
The best-fit line through the S_{max} values is a third order polynomial and the original rhodopsin and metarhodopsin templates were generated using the equation given by Stavenga *et al.* (1993), incorporating a shifting β-band (after Palacios *et al.*, 1996).

Using equation (21) the 20 nm longwave shift in S_{max} observed by Frank and Case (1988a) for *A. smithi* relative to the λ_{max} of its rhodopsin (as measured by Hiller-Adams *et al.*, 1988) would require 90% of the pigment present to be in the metarhodopsin state. For *A. curtirostris* such a shift would require less than 1% of the total pigment present being rhodopsin. Clearly, screening by metarhodopsin is unlikely to be responsible for this shift. However, one can speculate that such a large shift could be produced in those deep-sea shrimps which possess a functional R8 cell. Specifically, while the rhodopsins present in the R8 cells have λ_{max} values at *ca.* 414 nm and are unlikely to dramatically alter the spectral sensitivity of the underlying R1–7 cells (containing a rhodopsin with a λ_{max} at *ca.* 495 nm), the same cannot be said for their metarhodopsins. The metarhodopsins of the R8 cells have a λ_{max} at *ca.* 475 nm and would thus have similar effects to that shown in Figure 5.2. As the function of the R8 cells in such animals is still disputed and the natural levels of metarhodopsin in the R8 cells unknown, modelling of this phenomenon is not attempted. However, whatever the magnitude of this effect, the shift in S_{max} of the underlying R1–7 cells will again be to longer wavelengths, away from the wavelength of maximum transmittance of downwelling light and from the maximum emittance of bioluminescence. In conclusion, the presence of *any* metarhodopsin within the photoreceptors, be it in the R8 or the R1–7 cells themselves, will shift the S_{max} of the R1–7 cells to longer wavelengths and seemingly further invalidate the Sensitivity Hypothesis for the deep-sea crustaceans as far as sensitivity to downwelling irradiance is concerned.

5.2.7 Metarhodopsin spectral location

The average λ_{max} of the crustacean rhodopsin pigments measured by microspectrophotometry in the studies included in Table 1.1 is 488.3 nm (± s.d. of 50.6 nm, n = 84) with a range from 325 to 551 nm, inclusive (including the pigments of both R8 and R1–7 cells). The corresponding data for the metarhodopsins measured is a mean of 494.5 nm (± s.d. of 11.4 nm, n = 47) with a range from 460 to 515 nm. Thus the metarhodopsin state appears much more constrained in terms of spectral location with a total range in λ_{max} value of less than a quarter of that shown by the rhodopsin

configuration. However, this comparison is biased as most of the pigments measured in the stomatopods have not been characterised in their metarhodopsin state. Thus, those crustacean visual pigments showing the greatest variation in spectral location have only been described in terms of their rhodopsins.

To address this, the λ_{max} of all crustacean visual pigments recorded by microspectrophotometry in both their rhodopsin and metarhodopsin states were selected and plotted in a scatter-graph (Figure 5.4). Excluding the near-UV sensitive pigments, a highly significant, positive trend between the spectral location of the absorbance of the two structural conformations is apparent (using a product moment correlation test, $r = 0.283$ with 81 d.f., $p < 0.01$). Because data from other studies may, in fact, be measures of pigment mixtures, due to incomplete dark-adaptation and/or photoconversion, the actual correlation may be higher.

That the spectral absorbance of the metarhodopsin state is related to that of the rhodopsin is not surprising given that they are simply different conformational states of the same molecule: the chromophore is isomerized and the opsin is unchanged during the process of invertebrate visual perception. How the amino acid sequence of the opsin influences the absorbance of the rhodopsin is the subject of intense research (for examples see Nathan, 1990; Nakayama and Khorana, 1991; Merbs and Nathans, 1993; Asenjo, Rim and Oprian, 1994). How this relates to the spectral absorbance of the metarhodopsin state is unclear, but the basic mechanism is unlikely to be different from that for the rhodopsin. Specific amino acid residues have special roles within the opsin protein, either maintaining the structural conformation of the protein, or interacting with the chromophore and 'tuning' the spectral absorption of the visual pigment (see Hope, Partridge, Dulai and Hunt, 1997). The tuning of each visual pigment depends on the ionic interactions between the chromophore and the neighbouring amino acids. Thus, the conformational change observed in the chromophore of invertebrate visual pigments during rhodopsin $\Leftrightarrow$ metarhodopsin transformations might alter the relative effect of this ionic-interaction, and therefore the spectral absorption.

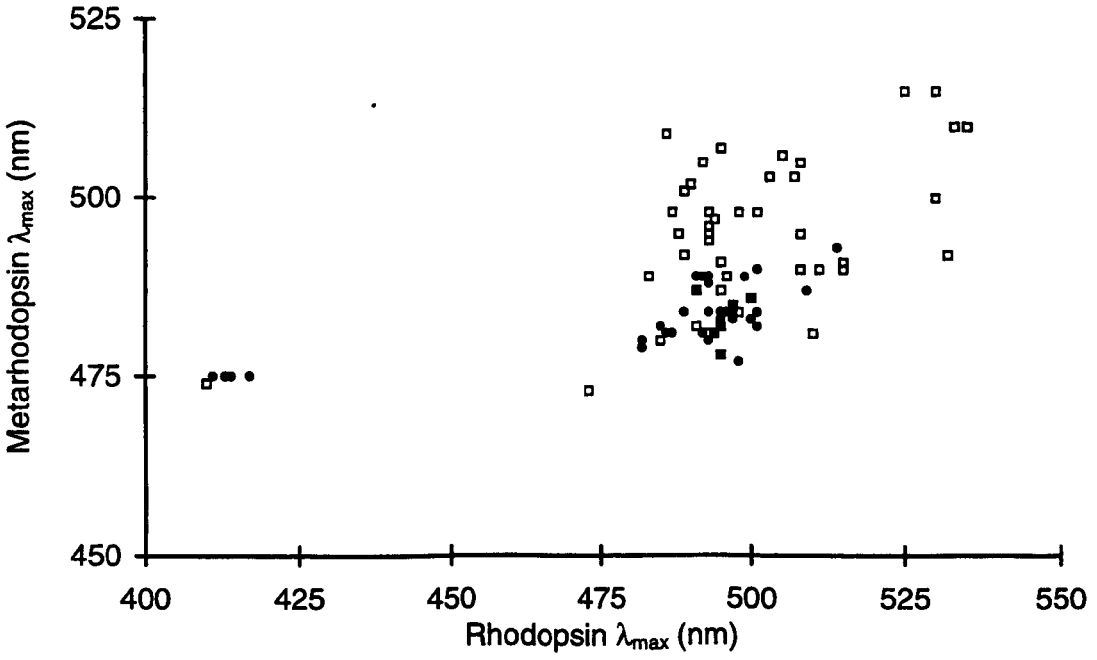

Figure 5.4 A plot of metarhodopsin λ_{max} versus rhodopsin λ_{max} values for visual pigments as measured by microspectrophotometry. These data include all the deep-sea crustaceans recorded during this study (filled circles). Excluding the near-UV sensitive pigments, a highly significant, positive trend between the spectral location of the absorbance of the two structural conformations is apparent (using a product moment correlation test, $r = 0.283$ with 81 d.f., $p < 0.01$). Data from other studies may, in fact, be measures of pigment mixtures due to incomplete dark-adaptation and/or photoconversion and thus the actual correlation may be higher.

The spectral location of the metarhodopsins of the near-UV rhodopsin pigments (found in the R8 cells of species within the Family Oplophoridae) do not fit the correlation observed in the rest of the crustacean pigments. However, the observation that the absorbance spectra of such shortwave pigments, both vertebrate and invertebrate, do not fit the templates based on abscissa transformations formulated for non-shortwave pigments (see Section 4.3.3.2), suggests that their spectral characteristics are in some ways modified. Thus, the ionic interactions between the chromophore and the neighbouring amino acids may be different and this may be reflected in the spectral location of the metarhodopsin. As only a few such shortwave invertebrate pigments have been characterised further investigation is needed.

5.2.8 Specific absorbances

While the importance of polarization sensitivity has not been considered in this study, calculations regarding its occurrence at depth have been made (see Waterman, 1981). These show that, like the radiance, the polarization in shallow waters is determined by the incident light on the water's surface. However, below a certain depth (the 'asymptotic' depth, between 150 and 400 m in clear waters, depending on the wavelength of light; Jerlov, 1968) the polarization in this region depends only on the optical properties of the medium. Waterman (1981) has suggested that polarization sensitive animals should be able to detect both the degree and E-vector of polarized light throughout the photic zone in natural waters. In surface layers and down to a level above the asymptotic depth, the E-vector could be used to determine the sun's azimuth. Below this depth polarization could still provide visual information useful for the animal's spatial orientation.

Though polarization sensitivity was not investigated in this study, the inherent dichroic nature of the invertebrate rhabdom requires investigation in order to calculate the specific absorbances of the pigments measured *in vivo*. In most Crustacea the fused rhabdoms consist of microvilli orientated perpendicular to the ommatidial axis. The rhabdom is divided into layers, each consisting of tightly packed, parallel arrays of microvilli whose long axes are perpendicular to the microvilli in the immediately adjacent layers (Eakin,

1968). Transverse measurements (i.e. when a rhabdom has been detached from its surrounding retinular cells or in a section through the eye cut parallel to the ommatidial axis) can then be made through one or more of these layers. When the rhabdom is orientated properly with respect to rotation about its long axis, the measuring beam will be incident perpendicular to the microvillar axes in half the layers and will be parallel to the microvilli when placed in any one of the alternate bands (see Goldsmith, 1972).

The visual pigment chromophore is a dipole and as such exhibits maximal absorption when the E-vector of incident light is parallel to the long axis of the molecule. In vertebrate photoreceptors the visual pigment molecules maintain a fixed angle relative to the membrane surface, but are free to rotate within the tangent plane of the membrane (Poo and Cone, 1974; reviewed by Laughlin, Menzel and Snyder, 1975). The resulting random orientation in this plane explains why vertebrate photoreceptors exhibit no dichroic absorption under normal conditions of illumination. The visual pigments of invertebrates are embedded within the membranes of the rhabdomeric microvilli. Due to their tubular structure, dichroic absorption will result even when the visual pigments rotate freely within the membrane plane, as those pigments localised in the side parts of the microvilli can be activated only when the E-vector of plane polarized light is parallel to the microvillar axis. This arrangement predicts a dichroic ratio of 2 (Moody and Parriss, 1961) which was then confirmed by microspectrophotometry (Waterman, Fernández and Goldsmith, 1969). Specifically, for a transverse beam, those layers where the microvilli are illuminated with plane polarized light from the side show positive dichroism, the absorptance being maximal when the E-vector is parallel to the axes of the microvilli. For those layers illuminated axially, absorptance is essentially independent of the E-vector and is about the same magnitude as the absorptance obtained when illuminating microvilli side-on with the E-vector perpendicular to the microvillar axes (i.e. the minimum absorptance).

However, later measurements showed that the dichroic ratios can be significantly higher than 2 (e.g. 2 to 3.5 in crayfish photoreceptors; Goldsmith, 1975), indicating that some dipole alignment with the microvillar axis does indeed occur. Theoretical analysis of their results led Goldsmith and Wehner (1977) to predict that crustacean visual pigments

should have a dichroic ratio of 5 to 7 with the visual pigments making an angle no greater than 50° relative to the long axis of the microvilli. Similar values have been recorded by physiological measurements and the reason for the discrepancy with previous microspectrophotometric measurements is still unknown (for a full discussion see Rossel, 1989). It has been suggested, however, that some degradation of pigment orientation may occur during microspectrophotometry due to the lability of the microvillar cytoskeleton which may be critical for the alignment of the visual pigment molecules (Blest, Stowe and Eddey, 1982; Stowe, 1983).

When light passes down the axis of the rhabdom, as it does in the living eye, it is always propagating perpendicular to the microvillar axes. Therefore, absorption measured with a transverse beam at right angles to the microvilli is the same, for a given pathlength within a given layer, as absorption of naturally incident light. Assuming the naturally incident light is unpolarized, the absorbance to axial light will then be equal to the maximum absorbance measured transversely (i.e. with light perpendicular to the microvillar axes and the plane of the E-vector equal to that of the microvilli). The retinas of deep-sea shrimps are typically almost fully occupied by the main rhabdoms so, in this study (and that of Cronin and Frank, 1996), measurements of rhabdoms were taken at various angles relative to their long axes, depending on the depth of the section being examined (see Section 3.2.1). Further, it was not possible to distinguish alternating layers of microvilli within the rhabdoms. The latter may be a functional adaptation in some deep-sea shrimps (see Gaten, *et al.*, 1992) or a consequence of tissue damage during preparation, preservation and/or sectioning. Hence, in this study the E-vector of the measuring beam was simply orientated perpendicular to the ommatidial axis in order to maximise *potential* dichroism.

The alternating bands of microvilli observed in certain species of the Family Oplophoridae are approximately 2 μm in width (measurements taken from the light micrographs presented by Gaten *et al.*, 1992). The measuring beam used in this study was *ca.* 5 x 3 μm, orientated parallel to the ommatidial axis (see Section 2.2.3). Thus, even if the beam entered the rhabdom orthogonally to its axis and microvillar banding was present, it would still sample from at least one of each of the alternate microvillar bands

and, on average, would sample equally from both. Further, given that the rhabdoms would have been differentially rotated about their ommatidial axes, on average the measuring beam will have recorded from microvilli orientated at 45° to the transverse beam, in any given band. If banding was not present, either due to damage or it being the natural condition, then the microvilli will not be in any preferential orientation and, on average, will again be orientated at 45° to a transverse beam.

Hence, all the factors outlined above (i.e. the beam covering from more than one band, the rhabdom rotation about its ommatidial axis, the possible microvillar disarray, and the unknown angle of the measuring beam relative to the ommatidial long axis) will mean that the average dichroism will lie between the *ca.* 5–7:1 limits predicted (Goldsmith and Wehner, 1977) and the absorption measured will be less than the maximum possible. Thus the specific absorbance values recorded in Table 3.16 do not reflect the absorbances which would occur to axial, naturally incident light. However, it is not possible to quantify these factors and the only conclusion is that the specific absorbances of the photoreceptors *in vivo* will be equal to or greater than those values recorded. Moreover, the values given in Table 3.16 are the specific absorbances measured for the visual pigment mixtures. To calculate the specific absorbance of the rhodopsin or metarhodopsin the absorbance due to the other state must be subtracted. Due to the uncertainties regarding the absorption values this was not done. However, because the fraction of metarhodopsin in mix_1 was never greater than *ca.* 15% (Section 4.3.3.5) the specific absorbance of mix_1 is a close approximation to that of the rhodopsin as measured *in situ.*

The range of specific absorbances recorded (from 0.0022 to 0.0106 μm^{-1}; see Table 3.16) may reflect the influence of all of these factors and not actual differences of visual pigment concentrations. In addition, there may be variable break-down of visual pigments during preparation and preservation, varying section thickness when cryosectioning the eyes which would result in the specific absorbances being miscalculated (see Section 2.1.5), and incomplete photobleaching which would underestimate the maximum absorbance of the pigment present. No attempt was made to investigate the relative importance of these factors. It is likely that the packing of visual

pigment molecules within a rhabdom will be constrained by physical and/or biochemical factors (e.g. the ionic events of visual excitation, including transmembrane flow; see Krebs, 1974). However, reaching this limit might be expected by the deep-sea crustaceans which are presumably highly adapted to maximise photon capture. The large variation recorded suggests this is due to experimental factors and therefore no significance is attached to differences in specific absorbances between species.

Cronin and Frank (1996) recorded an *in situ* specific absorbance of 0.01 μm^{-1} in the R1–7 cells of *S. debilis*, greater than the 0.0077 μm^{-1} value recorded in this study but equal to the highest values recorded, and slightly higher than the usual crustacean value of 0.008 μm^{-1} (Cronin and Forward, 1988; Hiller-Adams *et al.*, 1988). However, their measuring beam was also not necessarily transverse relative to the long axes of the rhabdoms and their 5 μm diameter measuring beam is, again, likely to have sampled from more than one band of microvillar orientations. Thus this value is also likely to be less than the absorption of naturally occurring, axially incident light. However, without further investigation it is the best estimate available and a specific absorbance of 0.01 μm^{-1} is used in the modelling which follows (Section 5.3.2).

5.2.9 Metarhodopsin to rhodopsin extinction ratios

Not only do metarhodopsins have different λ_{max} values from their analogous rhodopsins, but they also differ in extinction coefficient (i.e. a measure of a molecule's efficiency at absorbing a photon of any given wavelength). No absolute measures of extinction coefficients were made in this study, but it was possible to estimate the *ratio* of the metarhodopsin to rhodopsin extinction coefficients (i.e. the ratio of their absorbances at their λ_{max} values). However, as the fraction of visual pigment molecules present in the photostable state produced by red light irradiance (i.e. mix_2) approaches 50% it becomes increasingly difficult to determine the precise absorption characteristics of the metarhodopsin because the absorption spectra of the mixture is so close to that of the rhodopsin. Under these conditions, the analytical method employed in this study (Section 4.3.2) is very sensitive to small changes in λ_{max} or in the relative absorption ratios of the

mixture spectra. This was found by Cronin and Forward (1988), though their results were further complicated by their glutaraldehyde treatments. Crustacean metarhodopsins readily photobleach on glutaraldehyde fixation, so as the mixture forms during red light irradiation visual pigment in the metarhodopsin state may be preferentially destroyed. The range in $\varepsilon_{max}M / \varepsilon_{max}R$ in Table 3.20 is thus, no doubt due, in part, to these uncertainties. However, even when mix_2 is predominantly metarhodopsin the ratios still show considerable variation.

Cronin and Forward (1988) propose that the variability in the ratio $\varepsilon_{max}M / \varepsilon_{max}R$ also arises from changes in the preferential absorption vector of the chromophore when metarhodopsin is formed from rhodopsin. Such changes occur in crayfish and lobster visual pigments (Goldsmith and Wehner, 1977; Bruno *et al.*, 1977), leading to decreased dichroic ratios in rhabdoms containing metarhodopsin as compared to those with only rhodopsin. Therefore, absorption of polarized light whose E-vector is parallel to the microvillar axes is relatively reduced. In this study unpolarized red (or blue) light was used to saturate the photopigment system, thus affecting all chromophoric orientations equally. In contrast, polarized light with an E-vector parallel to the axes of the rhabdomeric microvilli was used to measure absorbance, so chromophores having that preferred absorption vector would dominate the measurements. Decreased dichroism, due either to reduced alignment of chromophores within the microvillar axes or to increased randomness in overall chromophoric orientation (see Section 5.2.8 above; Goldsmith and Wehner, 1977) would then explain the low $\varepsilon_{max}M / \varepsilon_{max}R$ recorded in, for example, *Meningodora miccyla* and *Pasiphaea emarginata* (see Table 3.20). The more unusual results from *Plesionika maritus* for example, in which the absorbance of the mix_2 was substantially increased, suggests the opposite change, i.e. much closer alignment of metarhodopsin than rhodopsin chromophoric absorption axes to the microvilli.

5.2.10 Consequences of the presence of metarhodopsin

Maximum sensitivity will always be achieved when a photoreceptor contains 100% rhodopsin, however, metarhodopsin levels will increase as irradiance continues and a

saturating source of irradiance will eventually produce a photostable mix of the two. For a given spectral distribution, the light intensity does not influence the photoequilibrium itself, but rather determines the rate at which the photoequilibrium is reached. The presence of a hypochromatic metarhodopsin will then both reduce the overall sensitivity of the cell and shift its effective S_{max} to longer wavelengths (see Section 5.2.6). The possible effects of this will now be considered.

Using equation (12) (Section 4.3.2.1) it is possible to calculate the visual pigment mixture that will result given a spectrum of saturating irradiance (i.e. by comparing the overlap of the rhodopsin and metarhodopsin absorbance spectra in the region of the saturating light). Thus, this can be used to predict the mixtures of pigments present in photoreceptors, albeit without taking into account the transmittance of the such structures as the crystalline cones etc. within the eye. Based on the absorbance characteristics of the average visual pigments measured in the R1–7 cells of deep-sea shrimps, equation (12) predicts that if a shrimp observes saturating levels of either bioluminescence (specifically an average fish bioluminescence emittance spectrum based on Herring, 1983) or downwelling sunlight (normalised photon flux density at 500 m depth as shown in Figure 1.1) the rhabdoms will contain an approximately even mixture of rhodopsin and metarhodopsin (i.e. *ca.* 50:50). If the λ_{max} of the metarhodopsin was displaced to shorter wavelengths then the resulting mixture would contain a greater proportion of metarhodopsin. As only the rhodopsin to metarhodopsin conversion elicits a response, such a shift would appear to be advantageous: i.e., if more visual pigment molecules are photoconverted from the rhodopsin to the metarhodopsin state a greater response from each individual photoreceptor might be expected. In a light-limited environment such as the deep-sea the animals present are presumed to have every adaptation possible to increase a photoreceptor's signal (in addition to the optical adaptations observed which increase absolute sensitivity; see Land, 1981a).

As the spectral location of a metarhodopsin's λ_{max} appears correlated to that of the rhodopsin (see Section 5.2.7 above), it may be that adaptations are not possible to shift the metarhodopsin's absorbance to shorter wavelengths (and thus reduce the relative overlap between its absorption spectrum and that of the rhodopsin) independent of the λ_{max} of the

rhodopsin. In other words, the λ_{max} of the metarhodopsin maybe constrained. However, it would be possible to possess a rhodopsin/metarhodopsin combination that would still result in a mixture containing more metarhodopsin. Alternatively, it must be considered if a shift towards a predominance of metarhodopsin on exposure to saturating irradiance really is advantageous. The presence of metarhodopsin clearly affects the S_{max} and in this sense would appear to be disadvantageous, shifting it away from the maximum of the downwelling or bioluminescent incident light (see Section 5.2.6). Perhaps this limits the end-point of the photostable mixture, a homogeneous mixture of 50:50 rhodopsin/metarhodopsin shifting the S_{max} by 13 nm in the example shown in Figure 5.3.

An alternative explanation is found when considering the formation of a photosteady state: some molecules are being photoconverted back to the rhodopsin state and are thus being made available to absorb photons and elicit a response. Though never studied directly in deep-sea crustaceans, the dark-regeneration of rhodopsin in those arthropods studied is an active metabolic process involving the replacement of photoreceptor membranes and thus the insertion of newly synthesised rhodopsin (see Blest, 1980; Stowe, 1980a, 1981; Piekos and Waterman, 1983; Waterman and Piekos, 1983). These membrane turnover events are commonly associated with the ambient light:dark cycle (e.g. Nässel and Waterman, 1979; Shelton, *et al.*, 1985) though complete recovery of rhabdoms following intense adaptations to orange light has been shown in crayfish maintained in the dark over a period of several days (Cronin and Goldsmith, 1984). During a study of deep-sea crustaceans, the initial absorbance spectra of *S. debilis* specimens examined post-capture were shown to peak at shorter wavelengths than those of specimens maintained in the dark for 68 h (Hiller-Adams *et al.*, 1988). This suggests that dark-regeneration also occurs in these deep-sea shrimps (and that photoisomerization occurs during capture as a result of exposure to bioluminescence; see Section 5.2.11). Whether this process also occurs in those bathypelagic and epibenthic animals too deep to experience the daily fluctuations of downwelling light is unknown.

Photoconversion, through the absorption of photons by the metarhodopsin, remains a metabolically inexpensive way to regenerate rhodopsin molecules. The formation of a 50:50 mixture could be viewed as a compromise: on average, half of the incident photons

are absorbed by the metarhodopsin molecules and the other half by the rhodopsin. Thus, while only half of the incident photons are available for visual perception, the rest are used to constantly regenerate rhodopsin without metabolic expense and with relative speed. In this way visual perception can continue indefinitely though at a reduced overall sensitivity. Although rapid regeneration of visual pigment often may not be necessary to maintain visual sensitivity in the mesopelagic environment, since relatively little metarhodopsin may be generated by dim or infrequent light, photoregeneration may be expected to facilitate a more rapid restoration of visual sensitivity when larger amounts of metarhodopsin are present. This could occur when an individual is exposed to bright bioluminescence including, for example, the secretion from oplophorids and the bright and long-lived flashes of other mesopelagic invertebrates. The process of photoregeneration may be very important given the limited sources of energy and narrow spectra of light sources present in the deep-sea.

A consequence of the extensive overlap of the rhodopsin and metarhodopsin absorbance spectra observed in the deep-sea crustaceans, however, is that photoregeneration alone cannot fully restore maximum sensitivity. The data obtained for *S. debilis* suggest that dark-regeneration would restore rhabdoms to their full rhodopsin content within a few days (Hiller-Adams, *et al.*, 1988). Thus, the different rhodopsin and metarhodopsin λ_{max} values present in different species may reflect a fine tuning of both their spectral sensitivities, given varying proportions of metarhodopsin in their photoreceptors, and the capacity for photoregeneration.

5.2.11 Metarhodopsin levels *in vivo*

The entrance pupil of deep-sea crustaceans possessing reflecting superposition eyes is often larger than the radius of the eye, giving F-numbers[5] less than 0.5 (Land, 1976,

[5] F-number is a measure of the relative area over which an eye receives incident light. It is calculated as f/A (as in photography), where f is the principal focal length, or posterior nodal distance, of an optical system and A is the diameter of the aperture of the optical system. Its reciprocal, A/f, is referred to as the relative aperture (see Land, 1981a).

1981a). This large effective pupil area confers high retinal illuminance and it is clear that this is the *raison d'être* for superposition optics. However, it is equally true that high aperture systems of whatever kind bring the attendant disadvantages of poor geometrical image quality (aberrations) and scattered, non-image forming light. Evidence suggests that an evolutionary 'trade-off' exists: where photon capture is all important, resolution is sacrificed for the sake of a wide aperture and vice versa.

Land (1976) has measured the optical apparatus of *Oplophorus spinosus* and calculated an F-number of *ca.* 0.4 (Land, 1981a). This suggests that it is likely to have an absolute threshold of vision to downwelling light similar to that calculated for deep-sea fishes (Denton, 1990). *O. spinosus* itself, and many others, lives hundreds of metres above this threshold and thus might well be able to detect downwelling light. To model the actual photon capture is beyond the scope of this study but will be described in brief (see Lythgoe, 1979; Partridge and Cummings, in prep.). First the spectral irradiance of the downwelling light, or the spectral emittance of the bioluminescent source, must be known. For downwelling light this represents the spectrum incident at the observer's eye. For bioluminescence seen at a distance, its passage through the water towards the observer will change the observed irradiance spectrum as the light is absorbed or scattered and background light itself scattered into the pathway. As these are the very factors which reduce the broad sunlight irradiance at the ocean surface to the homochromatic irradiance at depth, bioluminescence spectra will converge on that of downwelling light at depth, especially given the fact that such emission spectra are already centred about those wavelengths of maximum transmittance (for this reason). However, the pathlengths involved in seeing sources of bioluminescence are orders of magnitude less than the depths to which sunlight penetrates due to the lower intensity of the bioluminescent sources, and this filtering effect is relatively low. The photon capture of the eye can then be calculated by integrating the incident photon flux at the observer's eye by the sensitivity of the eye at each wavelength interval, the latter incorporating the rhabdomeric absorptance due to the visual pigment, the possible presence of a tapetum and the transmittance of the overlying optics and screening pigments.

Given that many of the shallower mesopelagic species experience downwelling light throughout the day, one might expect a photosteady rhodopsin/metarhodopsin mixture to be created. As for bioluminescence, simple modelling predicts a 50:50 mixture should result (i.e. using equation 12 as described above). Thus, the fact that none of the animals obtained during this study had metarhodopsin levels above *ca.* 15% (Section 4.3.3.5) suggests that the downwelling light does not occur at saturating levels, i.e. the intensity is such that the rate of photon capture is relatively low and, during any 24 h period, is less than the rate at which rhodopsin molecules are regenerated (metabolic, dark-regeneration). Further, many of the specimens collected were caught during the day when dark-regeneration appears to stop in shallower living crustaceans (e.g. Nässel and Waterman, 1979; Shelton, *et al.*, 1985). If active regeneration does only occur at night (or is reduced during the day) then the photon flux of the downwelling light coupled with the sensitivity of the eyes of the mesopelagic species must result in a very low rate of photon capture indeed.

In many cases apparently healthy specimens were exposed to bioluminescent secretion during capture and subsequent sorting (especially the active *O. spinosus* and *S. debilis*; see also Hiller-Adams *et al.*, 1988 for a discussion of this), but again were only found to have levels of metarhodopsin between 5 and 10%. This suggests that even repeated bioluminescent secretions, experienced at very close distances, are not enough to saturate the visual pigments present in the photoreceptors. Though the effects are estimated to be negligible (Section 2.2.2), the dim red light used during specimen preparation (both on-board ship and in the laboratory) will eventually produce a visual pigment mixture biased towards metarhodopsin. The levels observed during this study can therefore be thought of as a 'worst case', metarhodopsin biased, scenario with levels of metarhodopsin being lower *in vivo*.

Thus the apparent discrepancy between these observations and the predictions of simple modelling suggests that the light sources experienced by the deep-sea shrimps (both downwelling light and bioluminescence) are never saturating. Subsequent models, incorporating actual photon flux densities, exposure times and eye photon capture rates, may calculate the actual fraction of the visual pigment molecules which absorb the

incident photons. The observations of this study predict that the majority of the visual pigment will remain in the rhodopsin state. Thus, the effects of metarhodopsin screening will always be small and the spectral sensitivity will remain close to that observed in dark-adapted specimens. Indeed, the maintenance of high levels of rhodopsin *in vivo* may be adaptive for this very reason, i.e. to preserve the spectral sensitivity function. More likely, given the light-limited environment, this may simply be a consequence of increasing overall sensitivity and/or the broadening of the spectral sensitivity function in order to compensate for the apparent disparity between the λ_{max} of the rhodopsin and the wavelengths of maximum downwelling and bioluminescent light transmission.

[The maintenance of high levels of rhodopsin/low levels of metarhodopsin may not be possible for shallower living species exposed to higher levels of irradiance, or indeed any invertebrate active by day. In such a case one might expect a photosteady mixture of rhodopsin and metarhodopsin to always be present, dependent on the spectrum of the irradiance. Studies of mantis shrimps inhabiting different photic conditions suggests that they are optically adapted to function at a certain rate of visual pigment stimulation (Cronin *et al.*, 1994e). This may well be proven for many other species of invertebrates. However, spectral sensitivities recorded in dark-adapted specimens (e.g. by ERG) do not include the effect of metarhodopsin screening and thus may not be representative of the organism's spectral sensitivity in nature. I am not aware of any study in which this has been addressed directly though it may be of significant importance when linked to visual ecology.]

5.2.12 Near-UV pigments

In this study four Oplophorid species, *Oplophorus spinosus*, *Systellaspis braueri*, *S. cristata* and *S. debilis* were confirmed to possess a second, shortwave sensitive visual pigment in their distal R8 cells, with an average λ_{max} of 414 nm. Previously, near-UV sensitivity had only been found in the shallower living mesopelagic species, *S. debilis*, *Janicella spinicauda*, *O. spinosus* and *O. glacilirostris* (Frank and Case, 1988a; Frank and Widder, 1994a; Cronin and Frank, 1996). These four are all photophore-bearing species

which undergo daily, vertical migrations and are active predators. This apparent correlation, and the changes in swimming speed and body tilt exhibited by tethered *S. debilis* specimens to changes in ambient light (Frank and Widder, 1994a), led to the idea that the shortwave sensitivity may be used to mediate vertical migrations.

The behavioural threshold for *S. debilis* to UV light (Frank and Widder, 1994a) was 2 log units lower than the intensity of UV light theoretically available at the depths in which they inhabit by day (i.e. 600 m; Frank and Widder 1996). Further, the ratio of UV–violet to blue–green light (i.e. those wavelengths that the visual pigments of the R8 and R1–7 cells are tuned to) were thought to change with both depth and time of day (Frank and Case, 1988a). Thus comparing the ratio of these wavelengths could act as a depth gauge, either absolute or relative (Wald and Rayport, 1977), or simply trigger migrations (Frank and Case, 1988a). Further, it has also been predicted that polarization will change during twilight and the two sensitivity channels may be optimised to detect this. However, this hypothesis has now largely been discarded as recent measurements of light in the deep-sea demonstrate that below the euphotic zone there is little change in spectral composition with time or depth (Frank and Widder, 1996). It is also clear that these daily migrations are not an attempt to inhabit a constant light intensity ('isolume') as the animals cannot swim quickly enough to match the changing intensities at dusk and dawn.

It has also been proposed that such a visual system would be well suited not only to enhance the visibility of, but also to discriminate between, bioluminescent spectra from each other and from the downwelling light. Different bioluminescent sources are often spectrally diverse (Widder *et al.*, 1983; Frank and Case, 1988a; Latz *et al.*, 1988) and the spectral sensitivities of the R8 and R1–7 photoreceptors appear optimally placed to maximise the differences between them, i.e. to maximise contrast (Cronin *et al.*, 1996a). Hence this visual system could be used to detect and distinguish potential prey, predators and congeners, and variations in these visual tasks may be linked to directional, anatomical differences observed in the eyes of some of these Oplophorids (Gaten *et al.*, 1992). The recognition of congeners (i.e. by their cuticular photophores) is thought to be particularly important in those species which undertake vertical migrations in congener swarms.

Oplophorid species, such as *S. debilis* and *O. spinosus*, produce a second type of bioluminescent emission in the form of a secretion (Herring, 1983). This is thought to act as a defensive signal, alerting secondary predators, either different species or larger conspecific cannibals, to potential prey in the form of the predator or grazer (the 'burglar alarm' hypothesis; Burkenroad, 1943). The value of such predator interference through visual flashes has recently been demonstrated (Mensinger and Case, 1992; Fleisher and Case, 1995) and its application in the deep-sea explored by Herring (1997). Clearly, it would be advantageous for congeners of the original prey to distinguish between such an alarm and a simple identification signal, and this may not be possible with a single visual pigment. Finally, the ability to distinguish the spectra of different light sources present in the mesopelagic zone may simply aid such species when producing bioluminescence from their ventral photophores. These are presumed to act as counter-illumination camouflage avoiding them from creating an obvious silhouette to upward looking, potential predators (Herring, 1977; Frank and Case, 1988a).

All of the above hypotheses have been specifically constructed to apply to mesopelagic, vertically migrating species, however, one of the species found to possess a shortwave sensitive pigment in this study, *S. braueri*, lives at depths of 1000 m and below and is not thought to ever undergo vertical migrations at any stage of its life cycle (P.J. Herring, pers. comm.). Further, it is likely to hatch in an advanced stage and therefore always inhabit deeper waters, below the threshold at which downwelling light is perceived. Thus many of the hypotheses formulated for its shallower relatives cannot apply. Specifically, shortwave sensitivity in *S. braueri* cannot be used for mediating vertical migrations nor for judging either absolute or relative depth. Neither does this species possess photophores, so shortwave sensitivity is not used for conspecific recognition nor controlling counter illumination even if it should venture into shallower waters. However, it may still be used to perceive bioluminescent sources, either to distinguish between them or simply increase total photon capture (the latter may be particularly relevant if the β-band of a visual pigment's spectral absorbance is not part of its photosensitivity; see Dartnall, 1972; Morton, 1972).

The possession of a shortwave visual pigment by a bathypelagic species may simply be a phylogenetic relic, all of the species shown to possess shortwave sensitivity being members of three closely related genera. Further, no species of these genera have been shown to *not* possess such sensitivity (i.e. studies where a shortwave pigment/sensitivity was not found originally have subsequently been corrected). However, the R8 cells of *S. braueri* were in no way degenerate and possessed an equal pigment concentration to that found in *S. debilis* (see Table 3.16). In conclusion, while shortwave sensitivity by a bathypelagic, non-vertically migrating species which lacks photophores may be vestigial, equally it could still be used to perceive and distinguish different sources of bioluminescence. Neither does it rule out the additional uses hypothesised for its shallower living, mesopelagic, vertically migrating relatives which do possess photophores.

5.2.13 Other pigments within the compound eye

The amount of proximal shielding pigment found in the retinal cells of most deep-sea species is low (see Gaten *et al.*, 1992), as expected for animals from deep water (Gaten *et al.*, 1990). However, even in relatively unpigmented eyes some light that passes obliquely through the eye will encounter granules of screening pigment (both non-migratory and migratory, if present). If some of this light is then transmitted through these granules or is reflected from their surfaces (i.e. not absorbed by them) and absorbed by the visual pigments, this will affect the spectral sensitivity of the photoreceptors. This is equally true for those accessory pigments with high refractive indices which surround the base of rhabdoms and function as a tapetum (see Shelton *et al.*, 1992).

The transmission properties of non-retinal ocular structures have been measured for four mesopelagic decapods by Hiller-Adams *et al.* (1988). The cornea, cones and clear zone appeared translucent in white light and have nearly flat absorbance spectra. Proximal and distal screening pigments were dark reddish-brown in transmitted light and spectra revealed increasing transmission at longer wavelengths, as has been reported for screening pigments of other crustaceans (e.g. Bruno *et al.*, 1973; Goldsmith, 1978a; Stowe, 1980b).

The tapetum was white in reflected light and black in transmitted light. Its optical density spectrum, probably more an indication of the tapetum's reflectivity than its absorbance, indicates a maximum between 400 and 500 nm and decreasing at longer wavelengths. Thus it appears well suited to reflecting downwelling light and the majority of bioluminescence. The authors conclude that non-retinal structures may be expected to have little effect on the spectral sensitivity of these four species when fully dark-adapted. The screening pigments would shift spectral sensitivity to slightly longer wavelengths in light-adapted individuals but it is unknown if the mechanisms needed for pigment movement even exist.

The data recorded in this study are similar to those recorded in many other species of Crustacea (e.g. Cronin and Forward, 1988) in that the spectra often depart from the standard rhodopsin template. Cronin and Forward (1988) suggest that this indicates the presence of up to two other photosensitive pigments in the rhabdoms of some species. The first is often suggested by the additional decrease in absorption at short wavelengths (350 to 450 nm) following photobleaching, beyond the decrease expected from the removal of the rhodopsin alone (see Figure 3.16 as a typical example). This observed departure is likely to be caused by the presence of a photoproduct, perhaps with an all-*trans* chromophore, which absorbs in this region (Lipetz and Cronin, 1988). The absorbing compounds may occur naturally in the crustacean visual cycle, or it may be produced only under the special circumstances of experimental treatments (i.e. high light intensities delivered for long durations, etc.). Alternatively, the appearance of this photoproduct could be an artefact due to increased light scattering at short wavelengths produced during the phototreatments of each rhabdom. However, the form of departure of the rhodopsin (i.e. mix_1) photobleach spectrum from the best-fitting rhodopsin template is similar in all measurements and therefore correlates with large differences in the magnitude of the photobleach. Thus it is unlikely to be due to scattering changes alone (see Cronin and Forward, 1988).

Rises in the photobleaching spectrum above the best-fit template may be associated with the photobleaching of small particles of retinular cell pigment. The measuring beam of the microspectrophotometer was only placed in clear regions of the rhabdomeric

microvilli, but occasionally there may have been some absorption by pigment particles lying out of focus or in regions transmitting photons scattered from the focused beam. This interpretation is supported by the observations of Cronin and Forward (1988) that screening pigment within the rhabdoms of some crab species photobleaches. A comparison of their estimated extent of pigment granule content revealed that long wavelength departures from their nomogram template were well correlated with the presence of pigment granules on isolated rhabdoms. Crustacean screening pigments have broad absorption spectra extending beyond 650 nm (Scott and Mote, 1974; Goldsmith, 1978b; Stowe, 1980b). Thus, at long wavelengths their normalised absorbance spectra become apparent above the decreasing absorbance of a typical rhodopsin spectrum. The rhabdoms of the deep-sea crustaceans in this study were relatively unpigmented and those scans which did show deviations from the rhodopsin template at long wavelengths (i.e. beyond 600 nm) were not included for subsequent averaging.

5.3 THE SENSITIVITY HYPOTHESIS

For the deep-sea crustaceans measured by microspectrophotometry in this and other studies (i.e. those included in Table 5.1), the average λ_{max} of the rhodopsins present in the R1–7 cells is 494.7 nm (s.d. = 6.23 nm, n = 42) with a range from 482 to 514 nm. Including other methods of study, these equate to a S_{max} range from 482 to 520 nm. The corresponding average λ_{max} range for the R1–7 metarhodopsins is 483.5 nm (s.d. = 3.84 nm, n = 42) with a range from 475 to 493 nm. The distribution of these pigments, including those of the R8 cells, are shown as histograms in Figure 5.1. Only those pigment pairs recorded by microspectrophotometry are included to avoid discrepancies between different techniques.

Comparing the λ_{max} values of deep-sea shrimp visual pigments, deep-sea bioluminescent emissions and, for comparison, the λ_{max} of deep-sea fish visual pigments, the Sensitivity Hypothesis is inconsistent with the current data in several ways. Firstly, the average λ_{max} of the deep-sea shrimps' R1–7 cells is *ca.* 20 nm longer than 475 nm, which, from past work, is presumed to the be the wavelength of maximum light flux at depth in the open

oceans (McFarland and Munz, 1975a; Lythgoe, 1979; Levine and MacNichol, 1982). Thus, the average deep-sea shrimp visual pigment is apparently not optimal for maximum sensitivity to downwelling light. Also, if crustacean visual pigments are tuned to downwelling light or bioluminescence, which has an average emission at 479 nm (data from Widder *et al.*, 1983; Latz *et al.*, 1988), one would not expect the 482 nm to 520 nm diversity of S_{max} values. Potential self-screening by metarhodopsin and other photostable pigments could shift the S_{max} values to even longer wavelengths *in vivo* (see Sections 5.2.6 and 5.2.13). The λ_{max} of the visual pigments of fish inhabiting the same photic region averages 484 nm, so, although better matched to downwelling light or bioluminescence, the same basic problem applies.

A possible explanation for the λ_{max} values measured in the Crustacea emerges when one considers their sensitivity function, taking into account the length and optical density of photoreceptors, in addition to their λ_{max} values. For example, by having a 150 μm long photoreceptor with a relatively high density (0.01, compared to 0.008 μm^{-1} in most crustaceans; see Section 5.2.8 and Cronin and Frank, 1996) the mesopelagic decapod *S. debilis,* whose λ_{max} is at 498 nm, catches virtually as many photons at 475 nm as it does at 498 nm (98.1%). Within 25 nm either side of the λ_{max} the spectral sensitivity at any one wavelength of such a pigment is at least 95% of that at the λ_{max}. Thus, within a 30 to 40 nm window around 475 nm, the exact λ_{max} placement is not important. Other mesopelagic crustaceans examined anatomically also possess long photoreceptors (e.g. Gaten *et al.,* 1992) and perhaps this results in a low selection pressure for the exact position of the λ_{max} of their visual pigments.

5.3.1 Photon capture

Due to their light-limited environment the long photoreceptors and frequently high specific absorbances found in deep-sea crustaceans are probably adaptive to maximise photon capture at all wavelengths available. The presence of these specialisations, and the maintenance of an eye at all, suggests that visual perception is of great importance.

Hence, it is difficult to concede that the λ_{max} values are unmatched to the wavelengths of maximum transmittance simply because they are *almost* as efficient as a matched visual pigment. Given the range of rhodopsin λ_{max} values found in shallower living species, and the deep-sea fish, one might expect even a comparatively low selection pressure to take effect and shift the λ_{max} to shorter wavelengths. Further, this does not explain why the rhodopsins found in the deep-sea shrimps (of various taxa, and thus probably of different phylogeny) are *all* longwave shifted. If their spectral positioning is relatively unimportant, then λ_{max} values could be spread either side of 475 nm for example. Indeed, given the recent findings which suggest higher levels of UV and near-UV light than was previously envisaged in the mesopelagic zone (Frank and Widder, 1996), a rhodopsin shorter than 475 nm may be better matched to the downwelling light.

Also, simply increasing the length of a photoreceptor and/or increasing visual pigment concentration to achieve a broader spectral sensitivity is not necessarily advantageous over optimising the absorbance of the visual pigment. Evidence suggests (Barlow, Birge, Kaplan and Tallent, 1993) that in a light-limited environment such as the deep-sea, the limit to scotopic vision is the noise in the photoreceptors, due to a two-step process in which an unprotonated, 'activated' form of the rhodopsin undergoes spontaneous thermal isomerization. Photoreceptors therefore generate discrete electrical events in the dark (i.e. when photons are not being absorbed) indistinguishable from those evoked by the absorption of light. For visual perception at low light levels the stimulus intensity must be statistically significantly above this level (see Land, 1981a; Barlow, 1988). Thus, while increasing the visual pigment content potentially increases the signal (i.e. the number of photons which are absorbed) this is also raises the spontaneous noise and therefore the threshold of stimulus perception. To a first approximation, photoreceptor cell volume will correlate with the number of molecules of rhodopsin present and thus with photoreceptor noise.

A compromise between the number of rhodopsin molecules per photoreceptor available to absorb incident light and the noise which they then create is clearly reached, which might be expected to be optimal in deep-sea animals. Thus a tapetum is a very efficient adaptation which, by reflecting those photons not absorbed by the visual pigment

molecules on their first passage through the rhabdom back through the rhabdom again, effectively doubles the pathlength of the rhabdom without increasing the number of visual pigment molecules (see Land, 1981a). Finally, theory suggests that shortwave sensitive visual pigments are the most thermally stable (Barlow, 1957), and this is supported by limited experimental evidence (Firsov and Govardovskii, 1990). Once again it is hard to conceive why such a factor has seemingly not influenced the pigments possessed by both deep-sea fishes and crustaceans.

The answer to the anomaly of the Sensitivity Hypothesis and the deep-sea animals which appear to contradict it may be due to the emphasis that has been placed on matching the λ_{max} or S_{max} of the photoreceptor with that of the maximum transmitted wavelength of either downwelling or bioluminescent light. If the spectra of incident light and spectral sensitivity are symmetrical the greatest photon capture (calculated by integrating the overlap between the two) is indeed achieved when the maxima of both are matched. However, due to the asymmetrical shape of both the visual pigment absorptance and the spectra of incident light the maximum photon capture may be achieved when the λ_{max} (or S_{max}) is seemingly offset. In this regard the S_{max} is as misleading as the λ_{max}, both describing a single characteristic of an otherwise unknown spectral function.

5.3.2 Modelling photon capture

To investigate relative photon capture by deep-sea crustaceans a simple model was produced which compares the relative overlap between a spectrum representing the average bioluminescence from a survey of deep-sea fish (Herring, 1983) and the absorptance of a visual pigment with a fixed specific absorbance of 0.01 μm^{-1} (see Section 5.2.8) and an effective pathlength of 240 μm. The latter reflects a typical rhabdom length of 120 μm (see Table 5.2), doubled to take into account the presence of a tapetum (see Land, 1981a). This assumes the tapetum reflects 100% of the incident light back through the rhabdom though in reality the actual value can only be less than or equal to this. The λ_{max} of the rhodopsin absorbance template was then varied at 1 nm intervals and the relative photon capture calculated. This model does not take into account the

change in the emission spectra that would occur with increasing distance from the observer, nor factors within the eye which might change the spectral sensitivity (though the effects of non-retinal pigments are thought to be negligible in at least the mesopelagic species; see Section 5.2.13). Both factors require substantial additional information beyond the scope of this study, but are unlikely to dramatically alter the results of the model given the relatively short visualisation distances over which a deep-sea shrimp is thought to observe bioluminescence (J.C. Partridge, pers. comm.) and the dark-adapted, relatively unpigmented superposition optics of most deep-sea crustaceans (see Gaten *et al.*, 1992).

Examples of this model are shown in Figure 5.5. Though the absorptance spectrum is relatively broad it is seen to fall off even more sharply on the longwave limb than that of the absorbance spectrum from which it is calculated. In contrast, at short wavelengths spectral sensitivity remains high due, in part, to the absorptance of the β-band. (Note that this is assuming that the photosensitivity spectrum follows the absorbance spectrum, for which limited evidence is available (see Dartnall, 1972; Morton, 1972).) There may, in fact, be a fall off in photosensitivity at such short wavelengths though the effect on the following examples will be relatively small given the steeper gradient of the bioluminescence emission spectrum on the shortwave limb.) Thus, although shifting the λ_{max} to longer wavelengths results in less photons being captured about the peak of the emission spectrum, this is compensated by more of the longwave photons being absorbed. With the parameters as stated above, a λ_{max} of 498 nm is found to be optimal with the total relative photon capture *ca.* 5% greater than for a pigment matched to the emission maximum at 470 nm. Though the modelling was not done, a similar result might be expected for downwelling light due again to the asymmetry of the visual pigment's absorptance function.

Optimising photon capture, particularly from bioluminescent sources, therefore appears to explain the spectral location of the rhodopsin pigments observed in deep-sea crustaceans. That bioluminescence, and not downwelling light, is of greater importance is suggested by the fact that this shift is seen in species which live both above and below the threshold at which downwelling light is thought to be perceived (Land, 1981a; Denton, 1990). No

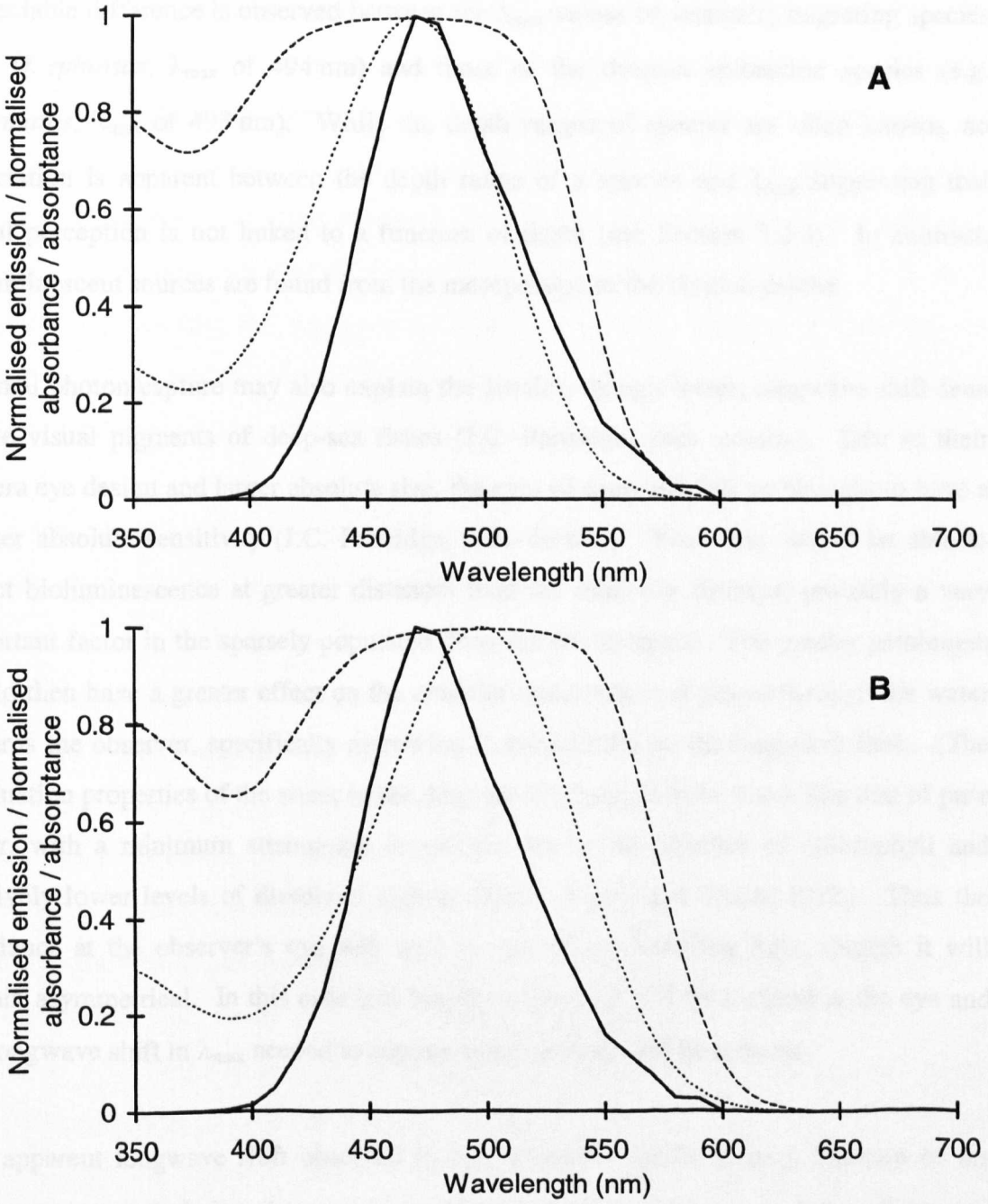

Figure 5.5 A, B. A simple model to show the relative photon catch when observing a typical deep-sea fish bioluminescence emittance spectrum (bold trace; adapted from Herring, 1983). In both (**A**) and (**B**) the absorptance spectra (or spectral sensitivity; dashed trace) are calculated given a rhodopsin absorbance template (dotted trace) calculated using the equation given by Stavenga *et al.* (1993) with a shifting β-band (after Palacios *et al.*, 1996), a specific absorbance of 0.01 μm^{-1} and a pathlength of 240 μm. In (**A**) the λ_{max} of the rhodopsin is matched to the wavelength of maximum emission (470 nm). In (**B**) the λ_{max} is offset at 498 nm. Comparing the overlap between the

appreciable difference is observed between the λ_{max} values of vertically migrating species (e.g. *O. spinosus*, λ_{max} of 494 nm) and those of the deepest epibenthic species (e.g. *P. armatus*, λ_{max} of 493 nm). While the depth ranges of species are often known, no association is apparent between the depth range of a species and λ_{max} suggesting that visual perception is not linked to a function of depth (see Section 5.2.3). In contrast, bioluminescent sources are found from the mesopelagic to the benthic depths.

Optimal photon capture may also explain the similar, though lesser, longwave shift seen in the visual pigments of deep-sea fishes (J.C. Partridge, pers. comm.). Due to their camera eye design and larger absolute size, the eyes of deep-sea fish are thought to have a greater absolute sensitivity (J.C. Partridge, pers. comm.). Thus they would be able to detect bioluminescence at greater distances than the deep-sea shrimps, probably a very important factor in the sparsely populated deep-sea environment. The greater pathlength would then have a greater effect on the emission spectrum as it passes through the water towards the observer, specifically narrowing it, particularly on the longwave limb. (The attenuation properties of the water in the deep-sea are thought to be much like that of pure water, with a minimum attenuation at 460 nm due to the absence of chlorophyll and relatively lower levels of dissolved organic matter; Baker and Smith, 1982). Thus the irradiance at the observer's eye will tend to that of downwelling light, though it will remain asymmetrical. In this case less longwave photons will be incident at the eye and the longwave shift in λ_{max} needed to capture these photons will be reduced.

The apparent longwave shift observed in λ_{max} therefore seems to be a function of the emittance spectrum being observed, its pathlength through the water (together these give the spectrum incident at the eye) and the spectral sensitivity of the organism's eye itself. As a further test of this hypothesis the effect of the latter was investigated by varying the

---

Figure 5.5 A, B. (Continued).

absorptance with the emission spectrum, the longwave shift results in less photons being captured about the peak of the emission spectrum but this is more than compensated by the absorption of the longwave photons. With these parameters a λ_{max} of 498 nm is optimal, being 5.0% more efficient at capturing the total incident photons than the 470 nm λ_{max} visual pigment.

effective pathlength of the photoreceptor and then calculating the relative photon capture using visual pigments of varying λ_{max}. Once again, this simple model did not include the change in the radiance spectrum that would occur with increasing distance from the observer, nor factors within the eye which might change the spectral sensitivity from that of the absorptance of the visual pigment. Two typical results are shown in Figure 5.6. Using a specific absorbance of 0.01 μm^{-1}, doubling the effective pathlength to 240 μm (equivalent to doubling the length of the rhabdom, adding a tapetum, or doubling the specific absorbance of the visual pigment) the optimum λ_{max} is shifted from 493 nm to 498 nm, and the maximum relative photon capture increased by *ca.* 13%.

Given that rhabdom length and/or visual pigment specific absorbance changes the optimum rhodopsin λ_{max} needed for maximal photon capture, the relationship between rhabdom length and λ_{max} was investigated for 14 of the deep-sea decapod species examined in this study for which rhabdom dimensions were also available (M.L. Johnson, pers. comm.). These species, their rhodopsin λ_{max} values, rhodopsin specific absorbances (calculated by multiplying the specific absorbances of the mix_1 spectra by the rhodopsin to mix_1 extinction ratios; see Tables 3.16, 3.18 and 3.19) and rhabdom lengths are given in Table 5.2. Rhabdomeric absorbances at the λ_{max} (specific absorbance multiplied by rhabdom length) were also calculated to incorporate both of the latter into one function. No correlation was found between rhabdomeric absorbance and rhodopsin λ_{max} ($r = -0.357$ with 14 d.f., $p > 0.05$; see Figure 5.7). Due to the lack of confidence in the specific absorbances recorded in this study (Section 5.2.8), this factor was removed and the data replotted against rhabdom length only. Again no correlation was found ($r = 0.324$ with 14 d.f., $p > 0.05$; see Figure 5.7). However, when the data for *Hymenodora glacialis* is removed, a highly significant, positive correlation of rhodopsin λ_{max} versus rhabdom length results ($r = 0.653$ with 13 d.f., $p < 0.01$).

[Note that during this particular study the two sampled populations of *Parapasiphaea sulcatifrons* were treated separately to see if any differences would become apparent. Although none did, they are still presented separately in this section. Hence 15 data sets were used in this modelling representing, probably, 14 different species.]

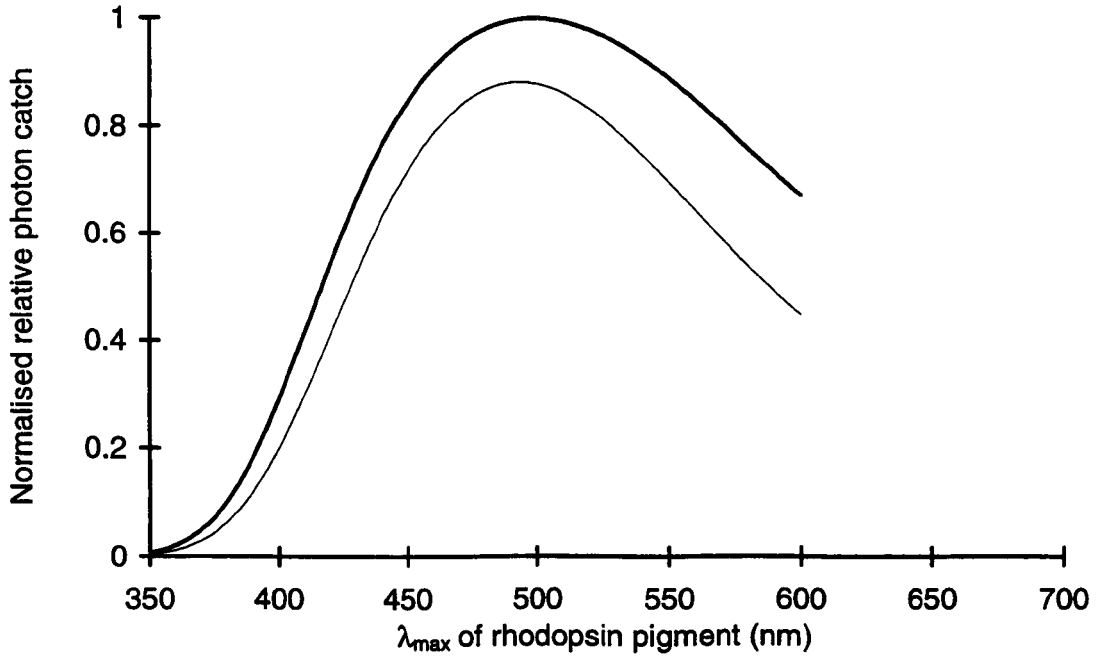

Figure 5.6 The effect of varying the rhodopsin λ_{max} on the relative photon capture of a typical deep-sea fish bioluminescent emission, given two different photoreceptor lengths. Using a specific absorbance of 0.01 μm^{-1} and a pathlength of 120 μm (light trace) the maximum photon capture is achieved with a λ_{max} of 493 nm, photon capture decreasing as the λ_{max} is both short- and longwave shifted from this value. Doubling the effective pathlength to 240 μm (equivalent to doubling the length of the rhabdom, adding a tapetum, or doubling the specific absorbance of the visual pigment; bold trace) shifts the optimum λ_{max} to 498 nm, and increases the maximum relative photon capture by 13.4%. See text for full details of the model used.

Table 5.2 The rhodopsin λ_{max} values, specific absorbances, rhabdom lengths and calculated rhabdomeric absorbances of 14 species of deep-sea decapods.

Species	*R* λ_{max} (nm)	*R* specific absorbance (μm^{-1})	Rhabdom length [a] (μm)	Rhabdomeric absorbance
Bentheogennema intermedia	494	0.0053	145	0.763
Gennadas sp.	495	0.0044	100	0.442
Gennadas valens	495	0.0048	100	0.477
Sergestes curvatus	493	0.0077	129	0.992
Sergestes similis	495	0.0070	129	0.905
Sergia robustus	496	0.0070	120	0.836
Acanthephyra stylorostratis	489	0.0061	113	0.688
Hymenodora glacialis	500	0.0021	70	0.150
Oplophorus spinosus	494	0.0068	100	0.676
Systellaspis braueri	500	0.0050	135	0.673
Systellaspis cristata	498	0.0061	135	0.823
Systellaspis debilis	497	0.0075	150	1.128
Stylopandalus richardii	491	0.0099	93	0.921
Parapasiphae sulcatifrons (Atl)	501	0.0043	150	0.650
Parapasiphae sulcatifrons (Pac)	501	0.0035	150	0.532

[a] M.L. Johnson, pers. comm.

The eyes of *Gennadas* are refracting superposition, *H. glacialis* has no apparent optics and therefore possesses essentially naked retinas, and those of the other species are of the reflecting, superposition type (see Figure 1.2). The average λ_{max} of these species is 495.9 nm, with an average specific absorbance of 0.0058 μm^{-1} and an average rhabdom length of 121 μm.

To model this correlation, the optimal rhodopsin λ_{max} values for viewing an average deep-sea fish bioluminescence spectrum (adapted from Herring, 1983; see text above for details), given varying rhabdom lengths were also plotted (Figure 5.7). Using a specific absorbance of 0.01 μm^{-1} and the lengths of the rhabdoms of the 14 species, the data appear to have longwave shifted rhodopsin λ_{max} values. When the effective pathlength is doubled (to model the presence of a tapetum) the species data are shortwave shifted relative to the data. Thus, the species lie between the limits modelled suggesting that the model could be improved to 'fit' the species data, i.e. by varying the effective pathlength and/or the specific absorbance. The former is particularly attractive as a tapetum is unlikely to be 100% efficient. Thus doubling the effective pathlength to incorporate the presence of a tapetum is clearly an ideal scenario. In reality the effective pathlength will be less than this and the model may then be a better fit to the data. However, the merits of adjusting such parameters is limited given the other factors not even considered in this model (e.g. attenuation of the bioluminescence emission spectrum through the water towards the observer, transmission of the optics of the eye, etc.).

Though the sample size is not large, and thus conclusions must be tentative, no discernible difference is apparent between those species possessing reflecting and those species possessing refracting superposition eyes. (The data set is too small to apply a statistical test to quantify this observation.) In contrast, the naked-retina of *H. glacialis* does not fit this model, apparently possessing too longwave a rhodopsin pigment given its short rhabdom lengths. However, by not incorporating it as a factor, this model is assuming that the effects of different optics are identical. Though reduced in both size and image forming optics, the eye of *H. glacialis* achieves a very high sensitivity to extended fields (M.L. Johnson, pers. comm.) and may well be optimal for the animal's visual tasks. Other limitations of this model must also be noted. For example, many mesopelagic shrimps have been shown to lack a tapetum in specific regions of the eye (Shelton *et al.*, 1992) and the lengths of the photoreceptors are also often found to vary about the eye (Gaten *et al.*, 1992). Both are thought to be adaptive and these two factors alone would change the effective pathlength of the photoreceptors and thus the predicted λ_{max} of the optimal rhodopsin pigment.

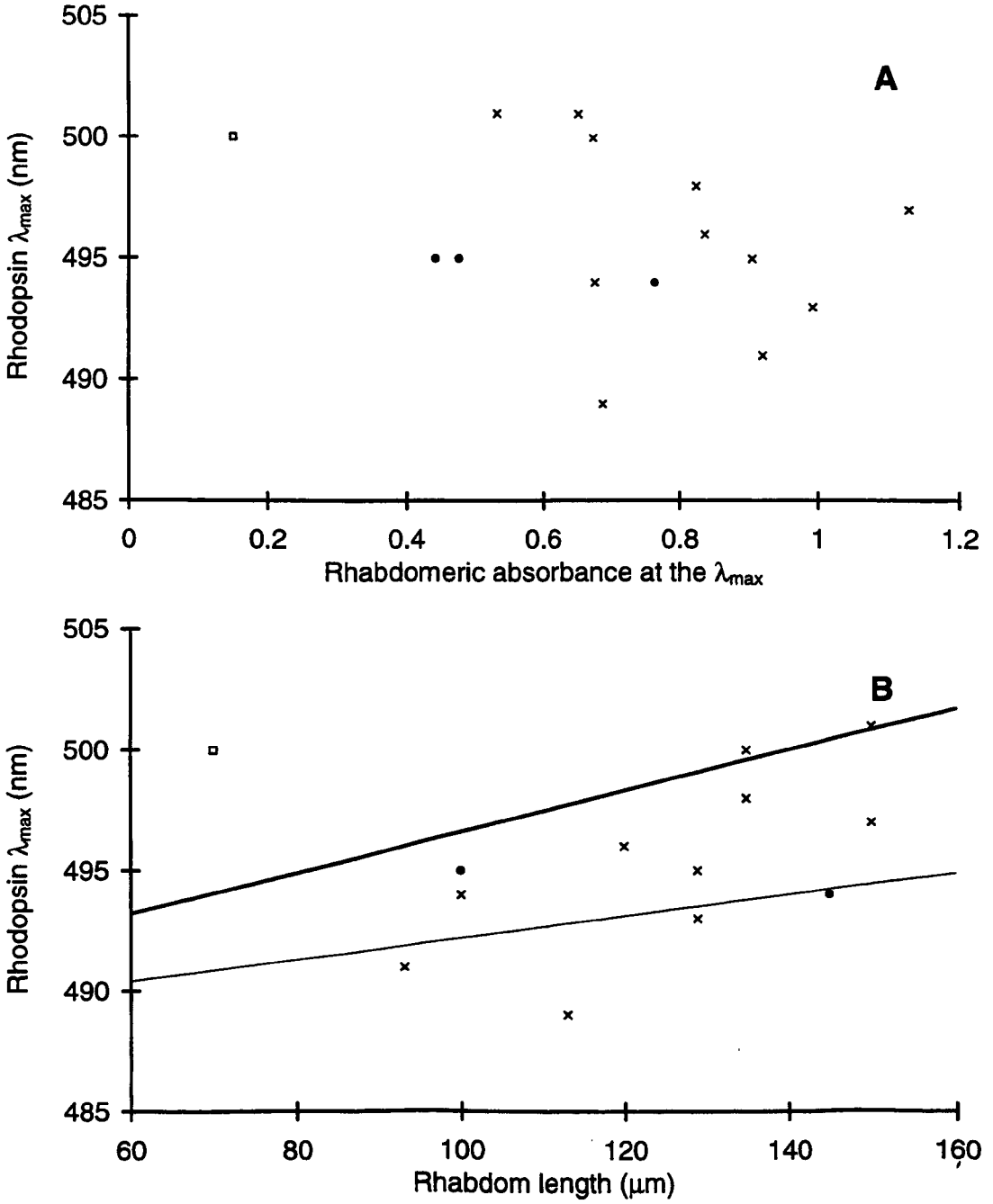

Figure 5.7 A, B. The rhodopsin λ_{max} values of 14 species of deep-sea decapods plotted against (**A**) rhabdomeric absorbance and (**B**) rhabdom length. See Table 5.2 for the species and parameters used. (**A**) The relationship between λ_{max} and rhabdomeric absorbance (specific absorbance multiplied by rhabdom length) revealed no significant correlation ($r = -0.357$ with 14 d.f., $p > 0.05$). Equally, (**B**) no correlation is found between rhodopsin λ_{max} and rhabdom length ($r = 0.324$ with 14 d.f., $p > 0.05$). However, when the *H. glacialis* data point is removed (square), a highly significant, positive correlation of rhodopsin λ_{max} versus rhabdom length results ($r = 0.653$ with 13 d.f.,

To investigate the model further, the relative photon catches for the 14 species in Table 5.2 were calculated, using their actual rhodopsin λ_{max} values and rhabdom lengths. The results are tabulated in Table 5.3 and displayed in Figure 5.8. All are calculated to be efficient at capturing the photons emitted by an average deep-sea fish bioluminescent source (adapted from Herring, 1983) and, again, no discernible difference is apparent between those species possessing reflecting and those species possessing refracting superposition eyes. However, while the other species all catch at least 94.9% of that of the maximum, the naked-retina of *H. glacialis* has a relative photon capture of 89.8% of that of the maximum. Thus, although its rhodopsin pigment is more longwave shifted than might be expected given its relatively short rhabdom length (see Figure 5.7), the overall photon capture is still high.

5.3.3 Perception of point sources

Variations in the relative photon catch shown in Figure 5.8 are small and could be due to other constraints or specialisations linked to the optimisation of the animal's eye to its own visual tasks. While all of the modelling above is concerned with the maximisation of photon capture at the rhabdom, no allowance has been made for the other parameters of the eyes. If these species are indeed adapted to observe bioluminescent 'point sources' then another factor which should be considered is the surface area of the eye over which

---

Figure 5.7 A, B. (Continued).

$p < 0.01$). To test these values against the results of a simple model used to predict photon capture when viewing an average deep-sea fish bioluminescence spectrum (adapted from Herring, 1983; see text for details), the optimal rhodopsin λ_{max} values given a certain rhabdom length are also plotted. With a specific absorbance of 0.01 μm^{-1} and the actual rhabdom lengths (light trace) the species considered appear to have longwave shifted rhodopsin λ_{max} values. When the effective pathlength is doubled (to model the presence of a tapetum) the species data are shortwave shifted relative to the data (bold trace).
Although the sample size is not large, no discernible difference is apparent between those species possessing reflecting (crosses) and those species possessing refracting (filled circles) superposition eyes. The naked-retina of *H. glacialis* (square), however, does not fit the model.

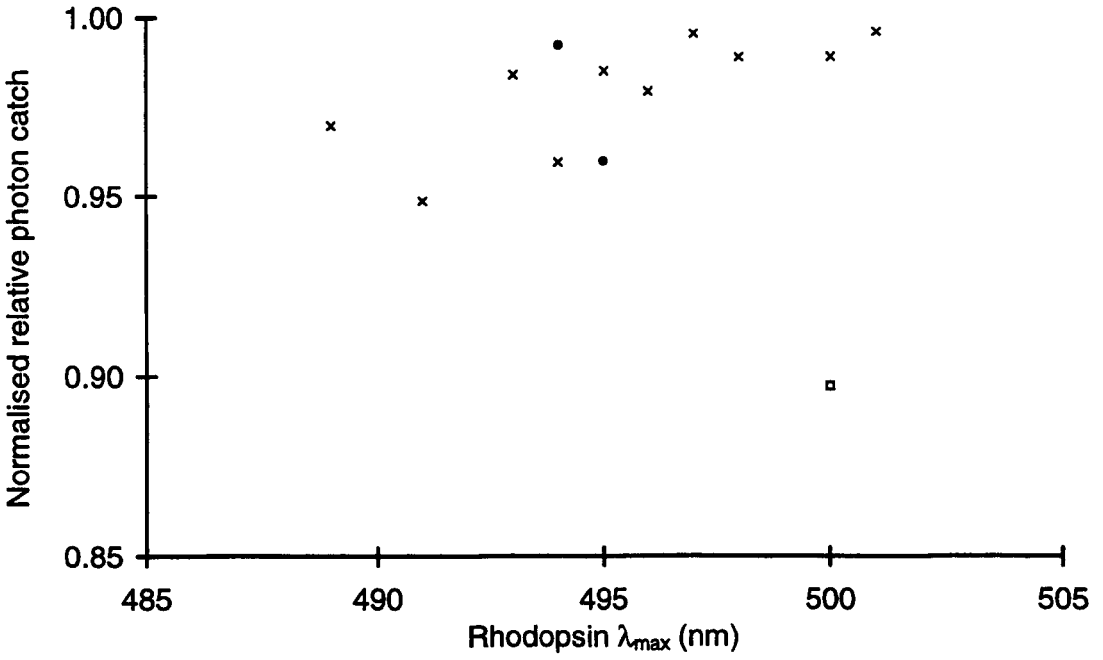

Figure 5.8 The normalised relative photon capture of 14 species of deep-sea decapods. See Table 5.2 for the species and parameters used. When rhodopsin λ_{max} and rhabdom length are modelled, all of the species included appear to be highly efficient at capturing the photons emitted by an average deep-sea fish bioluminescent source (adapted from Herring, 1983; see text for details). A specific absorbance of 0.01 μm^{-1} was used for all of the species.

Although the sample size is not large, no discernible difference is apparent between those species possessing reflecting (crosses) and those species possessing refracting (filled circles) superposition eyes. The naked-retina of *H. glacialis* (square), however, has a relative photon capture of 89.8% of that of the maximum.

Table 5.3 The eye parameters of 14 species of deep-sea decapods used to calculate relative sensitivities and relative signal to noise levels.

Species	Normalised relative photon catch	Aperture diameter [a] (mm)	Rhabdom length [a] (μm)	Rhabdom width [a] (μm)	Normalised relative sensitivity	Normalised S/N ratio
Bentheogennema intermedia	0.996	1.28	145	15	0.667	1.000
Gennadas sp.	0.963	0.52	100	13	0.106	0.267
Gennadas valens	0.963	0.52	100	13	0.106	0.267
Sergestes curvatus	0.988	0.49	129	10	0.097	0.245
Sergestes similis	0.989	0.49	129	10	0.097	0.245
Sergia robustus	0.983	1.08	120	15	0.469	0.849
Acanthephyra stylorostratis	0.973	0.47	113	25	0.088	0.101
Hymenodora glacialis	0.901	0.46	70	38	0.078	0.095
Oplophorus spinosus	0.963	1.02	100	32	0.409	0.417
Systellaspis braueri	0.993	0.87	135	25	0.307	0.297
Systellaspis cristata	0.993	1.57	135	25	1.000	0.966
Systellaspis debilis	0.999	0.74	150	25	0.224	0.194
Stylopandalus richardii	0.952	0.48	93	18	0.090	0.175
Parapasiphae sulcatifrons (Atl)	1.000	0.24	150	38	0.024	0.013
Parapasiphae sulcatifrons (Pac)	1.000	0.24	150	38	0.024	0.013

[a] M.L. Johnson, pers. comm.

The eyes of *Gennadas* are refracting superposition, *H. glacialis* has no apparent optics and therefore possesses essentially naked retinas, and those of the other species are of the reflecting, superposition type (see Figure 1.2).

the incident light falls (in addition to other factors still not included in this model including the spectral changes induced by the presence of a tapetum and screening pigments, and corneal transmittance etc.). Sensitivity is then proportional to the aperture of the system (Kirschfeld, 1974) and the reflecting superposition eye, with its wide aperture, will be most efficient at detecting point sources against a dark background. However, this optical arrangement would be less efficient for viewing objects in silhouette against downwelling light. In this situation, a narrow aperture would result in the greatest change in response of the ommatidium, from a maximum (the unattenuated downwelling light) to a minimum (the silhouette of the object). It is for this reason that some workers argue the retention of some apposition optics in the dorsal part of adult mesopelagic shrimp eyes is adaptive (Gaten and Herring, 1995).

For animals with superposition optics the aperture of the eye is easily measured by observing the area over which an incident light source is reflected back towards the viewer (i.e. the area of eyeshine; see Shelton *et al.*, 1992). The relative sensitivity of the eye can then be calculated by multiplying this pupil area by the relative photon capture as calculated above (Section 5.3.2 above). The results of this are presented in Table 5.3 and Figure 5.9. However, since all the species have been shown to possess very similar relative photon catches without this factor, this effectively reduces this to investigating trends in species' eye apertures. No obvious trends are then apparent amongst these 14 species. However, a number of factors are still not included in this model, including the change in the spectral sensitivity function due to transmission properties of the optics and the filtering due to the presence of other pigments (though this will be small in dark-adapted, superposition eyes; see Section 5.2.13), the distance of the viewer from the source (and therefore the attenuation of the emission spectrum through the water towards the observer) and finally the actual emission spectrum of the source being observed (rather than an average as used here).

5.3.4 Signal to noise optimisation

One other factor was included in this investigation. While the model above calculates the relative sensitivity, and thus the signal, it doesn't take into account the noise of the

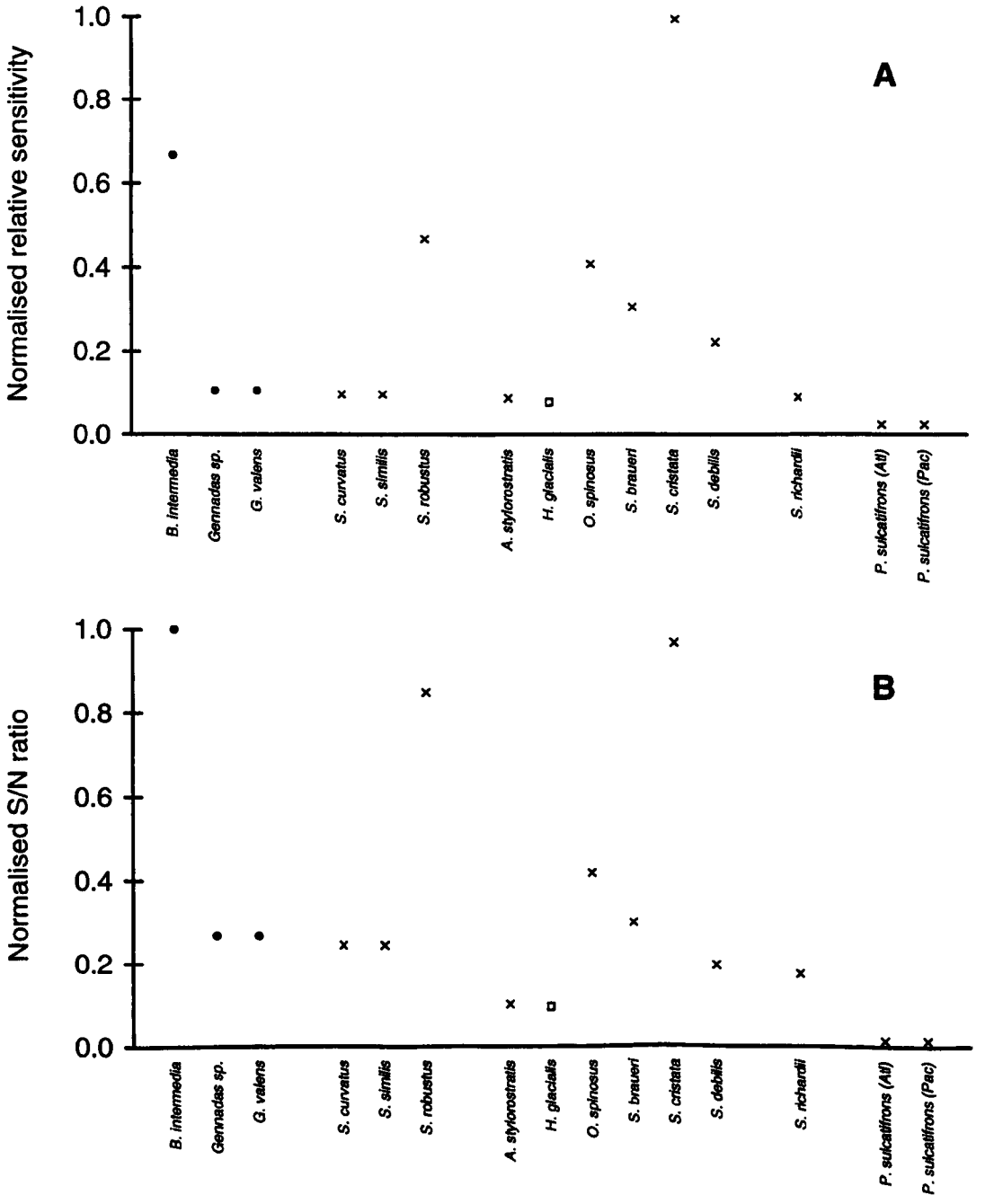

Figure 5.9 A, B. The normalised relative sensitivities and normalised signal to noise ratios of 14 species of deep-sea decapods. (**A**) Calculating relative sensitivity to a bioluminescent 'point source' as the relative photon capture calculated above (see Section 5.3.3) divided by eye aperture reveals no apparent trend between species. (**B**) Dividing the results of (**A**) by the total volume of a typical rhabdom for each species, to give a relative signal to noise ratio, leaves the data equally ambiguous.

system. As photoreceptors narrow they increasingly behave as waveguides, greater proportions of the incident light propagating outside rather than within the structure. However, the rhabdoms of the deep-sea crustaceans are relatively wide (see Table 5.3) and certainly greater than the 1 μm limit below which the majority of light would pass outside a photoreceptor and hence not be absorbed (Land, 1981a). Thus wide photoreceptors may be adaptive to maximise the photons which travel inside the rhabdom which can then be absorbed, as well as presenting a greater surface area over which incident photons fall. However, this will also increase photoreceptor volume, the number of visual pigment molecules and thus spontaneous thermal isomerization (i.e. noise; see Section 5.3.1). If a trade off between increasing signal and increasing noise exists, animals inhabiting a light-limited environment such as the deep-sea might be optimising their signal to noise ratios.

To investigate the possible importance of signal to noise ratio the relative sensitivities calculated above (Section 5.3.3) were divided by rhabdom volume as a measure of total visual pigment content. This assumes that all photoreceptors contain the same concentration of visual pigment throughout their photoreceptors (see Section 5.2.8) and that the rhodopsins all have the same thermal stability. The latter is not thought to be the case (Aho, Donner, Hydén, Larson and Reuter, 1988; Donner, Firsov and Govardovskii, 1990), however, as all of the λ_{max} values of the 14 species modelled here are within a 12 nm range and the species all inhabit a light-limited environment, the visual pigments might be expected to have very similar thermal stabilities. The results of this are, again, presented in Table 5.3 and Figure 5.9B. Including noise and estimating signal to noise ratios does not significantly alter the pattern between species observed for relative sensitivity: i.e. the distribution is still mainly due to variations in eye aperture.

5.3.5 Modelling conclusions

The last two examples (Sections 5.3.3 and 5.3.4) highlight the main problem of such simple modelling: the inclusion of an increasing number of factors, while ignoring the effects of others, can quickly lead to ambiguous results which seem to refute the

importance of the factors considered. The aperture of the eye *is* an important optical property which *will* determine the absolute sensitivity of the eye. Increased visual pigment content *will* increase the amount of photoreceptor dark noise which *will* determine the threshold above which a signal will be perceived. The lack of correlation between the species investigated does not change these. The benefit of such a model is that when a correlation is found, such as that between rhabdom length and rhodopsin λ_{max} (Section 5.3.2), the possible biological significance can then be explored. Further, the model can be used to make predictions for other species and again the significance of similarities and disparities explored.

It has already been noted that this model does not include the distance of the viewer from the source nor the actual emission spectrum of the source being observed (rather than an average as used here). Both of these factors describe properties of the visual task of the animal and it is likely that these will be species specific. The incorporation of these alone might re-group the species considered. The model also lacks anatomical and physiological considerations. For example, pooling is common in crustacean vision, both pooling in a single ommatidium and pooling inputs from many ommatidia by overlapping visual fields. Such optical and neural pooling work together, often subdividing the eye into different surface regions with different tasks (Schiff, 1987). Regional anatomical differentiation of decapod shrimp eyes is also well known, including variations in the tapetum (Shelton *et al.*, 1992), R8 to R1–7 size ratio and rhabdom form in mesopelagic shrimps (Gaten *et al.*, 1992). All of these factors are worthy of consideration.

Anatomical and physiological variations are likely to be adaptive and, for example, the varying tapetum and overlying R8 cells (where present) will alter the spectral sensitivity of the underlying R1–7 cell. The presence of only one visual pigment in the main rhabdom throughout the eye may reflect a compromise throughout the visual field otherwise adapted for different, directional visual tasks. Again, the importance of knowing the visual tasks of the animal are central to such an investigation. The limitation of time meant that the overall morphology of deep-sea shrimp eyes was not investigated in this study. However, this has been addressed by other investigators, including the comparison of trends in benthic, coastal species (Hiller-Adams and Case, 1985) and in

deep-sea species (Hiller-Adams and Case, 1988; Johnson, in prep.). In benthic decapods and mesopelagic deep-sea species there is a tendency towards increasing eye size with depth presumably to increase overall sensitivity (i.e. both eye aperture and rhabdom width will increase with increasing eye size). In contrast, some species, such as the aptly named *A. microphthalma* have eyes markedly reduced in size. However, the retention of eyes at all in such a bathypelagic species emphasises the importance of bioluminescent cues.

Eye structure has also been studied in deep-sea species of the euphausiids (e.g. Hiller-Adams and Case, 1984) and of the mysids (e.g. Hiller-Adams and Case, 1988). Both possess refracting superposition eyes, which have also been identified in a few species of deep-sea decapods (Nilsson, 1990b), and are thought to involve less aberrations than the reflecting superposition design (Nilsson, 1988, 1989a). Further, many deep-water euphausiids have 'double' eyes, usually with a region of enlarged facets pointing upwards and covering a narrow angle, and a downward pointing region covering a wider angle (Land *et al.*, 1979). Such optical arrangements are clearly adaptive though interpretation of their functions is often still speculative. It is also unknown why such an externally differentiated eye has not evolved using superposition optics. Again, only when the visual tasks that these regions are adaptive towards are identified will the significance of the visual pigment or pigments present (as yet unmeasured) be apparent.

Modelling may also be used to investigate the relative efficiencies of larval eyes. During growth the apposition eyes of the larval stages, and the superposition eyes of the young adults are clearly smaller than those of the mature adult. In most cases the rhabdoms will then be smaller, rather than reduced in number. Though some species are known to change their visual pigments during development (Cronin *et al.*, 1995a) this might not be the case in the deep-sea shrimps. Instead the λ_{max} of the rhodopsin may be optimal only for a specific stage of development (i.e. a specific size of the rhabdom) when visual tasks are most important (e.g. perhaps during periods of potentially higher predation and/or competition as a larval stage). In this case trying to correlate visual pigments possessed by the adult with any factor relevant only to that stage in its life cycle may prove futile.

It is clear that the identification of a species' visual tasks is essential to gain a full understanding of the visual apparatus it possesses. Modelling of the factors involved may then indicate their relative importance and allow predictions to be made. However, no additional factors may offer correlations in themselves and the prediction that the rhodopsins of the deep-sea shrimps are spectrally located to maximise photon capture when observing bioluminescence may remain unchallenged. That the specific λ_{max} is correlated to the effective length of their photoreceptors (i.e. rhabdom length and the effect of a tapetum) may also prove final.

5.4 SUMMARY

The light environment of the deep-sea varies from the predominance of downwelling light by day to that of only bioluminescence at depth and at night. The eyes of deep-sea animals, both fishes and crustaceans, are clearly not the vestigial remnants of the complex eyes of their shallow water ancestors but are highly specialised organs that deal with the particular demands of the deep-sea environment. Integral to this is the spectral sensitivity of their photoreceptors, governed mainly by the spectral location of the visual pigments they contain and adaptive to their visual tasks.

On average the λ_{max} of the main visual pigments of the deep-sea crustaceans studied are shifted to longer wavelengths than those of the deep-sea fishes. With the λ_{max} values of the deep-sea fishes also slightly longwave shifted in comparison to the wavelengths of maximum downwelling light and of maximum bioluminescent emissions, one or both of these taxa are apparently not conforming to the Sensitivity Hypothesis. Differences between or among the families of the deep-sea crustacean species measured in this study show no apparent correlations with taxa or the depth which they inhabit. Some families are very constrained in the λ_{max} range of their rhodopsins while others show almost as much as that of the deep-sea crustaceans in total. Further this total range is spanned by species which occupy apparently identical depths. The additional shortwave sensitivity found in related members of the Family Oplophoridae has previously been suggested to mediate daily vertical migrations and conspecific recognition. The demonstration here of

its presence in a bathypelagic, non-vertically migrating species which lacks photophores questions these ideas. However, the fact remains that, coupled with the main rhodopsin pigment, it appears optimally located to distinguish between different sources of bioluminescence. All of this evidence points to the importance of considering an animal's specific visual tasks.

Simple modelling allows possible visual tasks to be investigated and the results of this study indicate that the main deep-sea crustacean visual pigments may be spectrally located to maximise photon capture when viewing bioluminescence. The model also reveals a correlation between rhabdom length and rhodopsin pigment which may explain differences in visual pigment complement between species. No trends were apparent when factors relevant to the perception of point sources or signal to noise ratios were investigated. Further modelling may be expected to integrate all possible factors including the use of absolute, rather than relative, photon fluxes. Deep-sea shrimps represent an attractive group of invertebrates to which such complex modelling can be applied as their extreme photic environment suggests they should be highly adapted. With high evolutionary pressures correlations should be clear. Further, levels of metarhodopsin and screening pigments *in vivo* are apparently low leaving spectral sensitivity almost totally a function of visual pigment spectral absorbance.

In conclusion, as in most areas of visual ecology, the identification and importance of the visual tasks of the deep-sea animals need investigation. Many ecological factors are still unknown, or poorly known, and it is with these and not the physical factors often measured that data concerning visual pigment λ_{max} values are likely to correlate. The perception of downwelling light is unlikely to be important *per se*, but equally will be related to ecological factors such as prey and predator visualisation. All previous studies have attempted to match λ_{max} values with the wavelengths of maximum available light (either downwelling or bioluminescence). This study is the first to propose the idea of a visual pigment being spectrally located to maximise photon capture for the visualisation of bioluminescence and this approach now validates the Sensitivity Hypothesis, over sixty years after it was first suggested.

References

Aho, A-C., Donner, K., Hydén, E., Larsen, L.O. and Reuter, T. (1988) Low retinal noise in animals with low body temperature allows high visual sensitivity. *Nature*, **334**, 348–350.

Aiken, R.B. and Hailman, J.P. (1978) Positive phototaxis of the brine shrimp *Artemia salina* to monochromatic light. *Canadian Journal of Zoology*, **56**, 708–711.

Archer, S.N. (1988) *Microspectrophotometric study of visual pigment polymorphism in the guppy*. Ph.D. thesis, University of Bristol.

Archer, S.N., Endler, J.A., Lythgoe, J.N. and Partridge, J.C. (1987) Visual pigment polymorphism in the guppy, *Poecilia reticulata*. *Vision Research*, **27**, 1243–1252.

Arikawa, K., Kawamata, K., Suzuki, T. and Eguchi, E. (1987) Daily changes of structure, function, and rhodopsin content in the compound eye of the crab *Hemigrapsus sanguineus*. *Journal of Comparative Physiology A*, **161**, 161–174.

Asenjo, A.B., Rim, J. and Oprian, D.D. (1994) Molecular determinants of the human red/green color discrimination. *Neuron*, **12**, 1131–1138.

Baker, K.S. and Smith, R.C. (1982) Bio-optical classification and model of natural waters. 2. *Limnology and Oceanography*, **27**, 500–509.

Barlow, H.B. (1957) Purkinje shift and retinal noise. *Nature*, **179**, 255–256.

Barlow, H.B. (1988) The thermal limits of seeing. *Nature*, **344**, 296–297.

Barlow, R.B., Birge, R.R., Kaplan, E. and Tallent, J.R. (1993) On the molecular origin of photoreceptor noise. *Nature*, **366**, 64–66.

Barnes, H. and Klepal, W. (1972) Phototaxis in stage I nauplius larvae of two cirripedes. *Journal of Experimental Marine Biology and Ecology*, **10**, 267–273.

Baylor, D.A., Nunn, B.J. and Schnapf, J.L. (1987) Spectral sensitivity of cones of monkeys *Macaca fasicularis*. *Journal of Physiology*, **390**, 145–160.

Bayliss, L.E., Lythgoe, R.J. and Tansley, K. (1936) Some new forms of visual purple found in sea fishes, with a note on the visual cells of origin. *Proceedings of the Royal Society of London B*, **816**, 95–113.

Blest, A.D. (1980) Photoreceptor membrane turnover in arthropods: Comparative studies of breakdown processes and their implications. In *The Effects of Constant Light on Visual Processes* (eds. T.P. Williams and B.N. Baker), Plenum Press, New York, London, pp. 217–245.

Blest, A.D., Stowe, S. and Eddey, W. (1982) A labile, Ca^{2+}-dependent cytoskeleton in rhabdomeral microvilli of blowflies. *Cell and Tissue Research*, **223**, 553–573.

Boden, B.P., Kampa, E.M. and Abott, B.C. (1961) Photoreception of a planktonic crustacean in relation to light penetration in the sea. In *Progress in Photobiology* (eds. B. Christensen and B. Buchamann), Elsevier North-Holland Inc., New York, pp. 189–196.

Bowmaker, J.K. (1990) Visual pigments and colour vision in primates. In *From Pigments to Perception* (eds. A. Valberg and B.B. Lee), Plenum Press, New York, pp. 1–9.

Bowmaker, J.K. (1991) Visual pigments of fishes. In *The Visual System of Fishes* (eds. R.H. Douglas and M.B.A. Djamgoz), Chapman and Hall, London, pp. 81–107.

Bowmaker, J.K. and Kunz, Y.W. (1987) Ultraviolet receptors, tetrachromatic colour vision and retinal mosaics in the brown trout (*Salmo trutta*): age dependent changes. *Vision Research*, **27**, 2101–2108.

Bowmaker, J.K., Loew, E.R. and Liebman, P.A. (1975) Variation in the λ_{max} of rhodopsin from individual frogs. *Vision Research*, **15**, 997–1003.

Bradley, D.J. and Forward, R.B. Jr. (1984) Phototaxis of adult brine shrimp, *Artemia salina*. *Canadian Journal of Zoology*, **62**, 2357–2359.

Bridges, C.D.B. (1964) Periodicity of absorption properties in pigments based on vitamin A_2 from fish retinae. *Nature*, **203**, 303–304.

Bridges, C.D.B. (1972) The rhodopsin-porphyropsin visual system. In *Handbook of Sensory Physiology Volume VII/1, Photochemistry of vision* (ed. H.J.A. Dartnall), Springer-Verlag, Berlin, Heidelberg, New York, pp. 417–480.

Bridges, C.D.B. and Yoshikama, S. (1970) The rhodopsin-porphyropsin system in fresh-water fishes. *Vision Research*, **10**, 1333–1345.

Briggs, M.H. (1961) Visual pigment of grapsoid crabs. *Nature*, **190**, 784–786.

Bruno, M.S. and Goldsmith, T.H. (1974) Rhodopsin of the blue crab *Callinectes*: evidence for absorption differences in *vitro* and *in vivo*. *Vision Research*, **14**, 653–658.

Bruno, M.S., Mote, M.I. and Goldsmith, T.H. (1973) Spectral absorption and sensitivity measurements in single ommatidia of the green crab, *Carcinus*. *Journal of Comparative Physiology*, **82**, 151–163.

Bruno, M.S., Barnes, S.N. and Goldsmith, T.H. (1977) The visual pigment and visual cycle of the lobster, *Homarus*. *Journal of Comparative Physiology*, **120**, 123–142.

Buchanan, C. and Goldberg, B. (1981) The action spectrum of *Daphnia magna* (Crustacea) phototaxis in a simulated natural environment. *Photochemistry and Photobiology*, **34**, 711–717.

Burkenroad, M.D. (1943) A possible function of bioluminescence. *Journal of Marine Research*, **5**, 161–164.

Caldwell, R.L. and Dingle, H. (1976) Stomatopods. *Scientific American*, **234**, 80–89.

Chapman, C.J. and Rice, A.L. (1971) Some direct observations on the ecology and behaviour of the Norway lobster *Nephrops norvegicus*. *Marine Biology*, **10**, 321–329.

Childress, J.J. (1975) The respiratory rates of midwater crustaceans as a function of depth of occurrence and relation to the oxygen minimum layer off Southern California. *Comparative Biochemical Physiology A*, **50**, 787–799.

Childress, J.J. and Price, M.H. (1978) Growth rate of the bathypelagic crustacean *Gnathophausia ingens*. I. Dimensional growth and population structure. *Marine Biology*, **50**, 47–62.

Childress, J.J., Barnes, A.T., Quetin, L.B. and Robison, B.H. (1977) Thermally protecting cod ends for the recovery of living deep-sea animals. *Deep-Sea Research*, **25**, 419–422.

Chittka, L. (1996) Does bee color-vision predate the evolution of flower color? *Naturwissenschaften*, **83**, 136–138.

Clarke, G.L. (1936) On the depth at which fishes can see. *Ecology*, **17**, 452–456.

Consi, T.R. and Macagno, E.R. (1985) The spectral sensitivity of eye movements in response to light flashes in *Daphnia magna*. *Journal of Comparative Physiology A*, **156**, 135–143.

Crandall, K.A. and Cronin T.W. (in press) The molecular evolution of visual pigments of freshwater crayfishes (Decapoda: Cambaridae). *Journal of Molecular Evolution*.

Crescitelli, F., McFall-Ngai, M. and Horwitz, J. (1985) The visual pigment sensitivity hypothesis: further evidence from fishes of varying habitats. *Journal of Comparative Physiology A*, **156**, 679–687.

Cronin, T.W. (1985) The visual pigment of a stomatopod crustacean, *Squilla empusa*. *Journal of Comparative Physiology A*, **156**, 679–687.

Cronin, T.W. (1986a) Photoreception in marine invertebrates. *American Zoologist*, **26**, 403–415.

Cronin, T.W. (1986b) Optical design and evolutionary adaptation in crustacean compound eyes. *Journal of Crustacean Biology*, **61**, 1–23.

Cronin, T.W. (1989) Application of intracellular optical techniques to the study of stomatopod crustacean vision. *Journal of Comparative Physiology A*, **164**, 737–749.

Cronin, T.W. (1990) Pigments in crustacean compound eyes. In *Frontiers in Crustacean Neurobiology* (eds. K. Wiese, W.-D. Kreuse, J. Tautz, H. Reichert and B. Mulloney). Birkhäuser, Basel, pp. 58–65.

Cronin, T.W. and Forward, R.B. Jr. (1988) The visual pigments of crabs - I. Spectral characteristics. *Journal of Comparative Physiology A*, **162**, 463–478.

Cronin, T.W. and Frank, T. (1996) A short-wavelength photoreceptor class in a deep-sea shrimp. *Proceedings of the Royal Society of London B*, **263**, 861–865.

Cronin, T.W. and Goldsmith, T.H. (1981) Fluorescence of crayfish metarhodopsin studied in single rhabdoms. *Biophysical Journal*, **35**, 653–664.

Cronin, T.W. and Goldsmith, T.H. (1982a) Quantum efficiency and photosensitivity of the rhodopsin ⇔ metarhodopsin conversion in crayfish photoreceptors. *Photochemistry and Photobiology*, **36**, 447–454.

Cronin, T.W. and Goldsmith, T.H. (1982b) Photosensitivity spectrum of crayfish rhodopsin measured using fluorescence of metarhodopsin. *Journal of General Physiology*, **79**, 313–332.

Cronin, T.W. and Goldsmith, T.H. (1984) Dark regeneration of rhodopsin in crayfish photoreceptors. *Journal of General Physiology*, **84**, 63–81.

Cronin, T.W. and King, C.A. (1989) Spectral sensitivity of vision in the mantis shrimp, *Gonodactylus oerstedii*, determined using noninvasive techniques. *Biological Bulletin*, **176**, 308–316.

Cronin, T.W. and Marshall, N.J. (1989a) Multiple spectral classes of photoreceptors in the retinas of gonodactyloid stomatopod crustaceans. *Journal of Comparative Physiology A*, **166**, 267–275.

Cronin, T.W. and Marshall, N.J. (1989b) A retina with at least ten spectral types of photoreceptors in a stomatopod crustacean. *Nature*, **339**, 137–140.

Cronin, T.W. and Marshall, N.J. (in press) Lateral filtering in photoreceptors of two species of stomatopod crustaceans. *Vision Research.*

Cronin, T.W., Marshall, N.J. and Caldwell, R.L. (1993) Photoreceptor spectral diversity in the retinas of squilloid and lysiosquilloid stomatopod crustaceans. *Journal of Comparative Physiology A*, **172**, 339–350.

Cronin, T.W., Marshall, N.J. and Land, M.F. (1994a) The unique visual system of the mantis shrimp. *American Scientist*, **82**, 356–365.

Cronin, T.W., Marshall, N.J. and Caldwell, R.L. (1994b) The intrarhabdomal filters in the retinas of mantis shrimps. *Vision Research*, **34**, 279–291.

Cronin, T.W., Marshall, N.J., Quinn, C.A. and King, C.A. (1994c) Ultraviolet photoreception in mantis shrimp. *Vision Research*, **34**, 1443–1452.

Cronin, T.W., Marshall, N.J. and Caldwell, R.L. (1994d) The retinas of mantis shrimps from low-light environments (Crustacea, Stomatopoda, Gonodactylidae). *Journal of Comparative Physiology A*, **174**, 607–619.

Cronin, T.W., Marshall, N.J., Caldwell, R.L. and Shashar, N. (1994e) Specialization of retinal function in the compound eyes of mantis shrimps. *Vision Research*, **34**, 2639–2656.

Cronin, T.W., Marshall, N.J., Caldwell, R.L. and Pales, D. (1995a) Compound eyes and ocular pigments of crustacean larvae (Stomatopoda and Decapoda, Brachyura). *Marine and Freshwater Behavior and Physiology*, **26**, 219–231.

Cronin, T.W., Shashar, N. and Wolff. L. (1995b) Imaging technology reveals the polarized light fields that exist in nature. *Biophotonics International*, **2**, 38–41.

Cronin, T.W., Kent, J., Frank, T., Widder, E., Partridge, J.C., Herring, P., Robinson, P. (1996a) Visual pigments and photoreceptor classes of deep-sea shrimps. *Society for Neuroscience Abstracts.*

Cronin, T.W., Marshall, N.J. and Caldwell, R.L. (1996b) Visual pigment diversity in two genera of mantis shrimps implies rapid evolution (Crustacea; Stomatopoda). *Journal of Comparative Physiology A*, **179**, 371–384.

Cummins, D. and Goldsmith, T.H. (1981) Cellular identification of the violet receptor in the crayfish eye. *Journal of Comparative Physiology*, **142**, 199–202.

Cummins, D.R., Chen, D-M., and Goldsmith, T.H. (1984) Spectral sensitivity of the spiny lobster, *Panulirus argus*. *Biological Bulletin*, **166**, 269–276.

Dartnall, H.J.A. (1953) The interpretation of spectral sensitivity curves. *British Medical Bulletin*, **9**, 24–30.

Dartnall, H.J.A. (1972) Photosensitivity. In *Handbook of Sensory Physiology Volume VII/1, Photochemistry of vision* (ed. H.J.A. Dartnall), Springer-Verlag, Berlin, Heidelberg, New York, pp. 122–145.

Dartnall, H.J.A. (1975) Assessing the fitness of visual pigments for their photic environments. In *Vision in Fishes* (ed. M.A. Ali), Plenum Press, New York, pp. 543–564.

Dartnall, H.J.A. and Lythgoe, J.N. (1965) The spectral clustering of visual pigments. *Vision Research*, **5**, 81–100.

Dartnall, H.J.A., Goodeve, C.F. and Lythgoe, R.J. (1936) The quantitative analysis of the photochemical bleaching of visual purple solutions in monochromatic light. *Proceedings of the Royal Society of London A*, **156**, 158–170.

Dawis, S.M. (1981) Polynomial expressions of pigment nomograms. *Vision Research*, **21**, 1427–1430.

Denton, E.J. (1990) Light and vision at depths greater than 200 metres. In *Light and Life in the Sea* (eds. P.J. Herring, A.K. Campbell, M. Whitfield and L. Maddock), Cambridge University Press, Cambridge, New York, pp. 127–148.

Denton, E.J., Gilpin-Brown, J.B. and Wright, P.G. (1970) On the 'filters' in the photoreceptors of mesopelagic fish and on a fish emitting red light and especially sensitive to red light. *Journal of Physiology (London)*, **208**, 72–73.

Denys, C.J. (1982) Ommochrome pigments in the eyes of *Euphausia superba* (Crustacea, Euphausiacea). *Polar Biology*, **1**, 69–76.

Denys, C.J. and Brown, P.K. (1982) The rhodopsins of *Euphausia superba* and *Meganyctiphanes norvegica* (Crustacea, Euphausiacea). *Journal of General Physiology*, **80**, 451–472.

Donner, K., Firsov, M.L. and Govardovskii, V.I. (1990) The frequency of isomerization-like dark events in rhodopsin and porphyropsin rods of the bullfrog retina. *Journal of Physiology*, **428**, 673–692.

Donner, K.O., Langer, H., Lindström, M. and Schlecht, P. (1994) Visual pigment, dark adaptation and rhodopsin renewal in the eye of *Pontoporeia affinis* (Crustacea, Amphipoda). *Journal of Comparative Physiology A*, **174**, 451–459.

Douglas, R.H and Partridge, J.C. (1997) On the visual pigments of deep-sea fish. *Journal of Fish Biology*, **50**, 68–85.

Douglass, J.K. (1986) Ph.D. thesis, Duke University, Durham, North Carolina, U.S.A.

Douglass, J.K. and Forward, R.B. Jr. (1989) The ontogeny of facultative superposition optics in a shrimp eye: hatching through metamorphosis. *Cell and Tissue Research*, **258**, 289–300.

Eakin, R.M. (1968) Evolution of photoreceptors. *Evolutionary Biology*, **2**, 194–242.

Eakin, R.M. (1972) Structure of invertebrate photoreceptors. In *Handbook of Sensory Physiology Volume VII/1, Photochemistry of vision* (ed. H.J.A. Dartnall), Springer-Verlag, Berlin, Heidelberg, New York, pp. 625–684.

Eaton, B.P. and Brown, C.M. (1970) Photoreception in the nauplius eye of *Pandalus borealis* Kröger: Decapoda, Crustacea. *Canadian Journal of Zoology*, **48**, 119–121.

Ebrey, T. and Honig, B. (1977) New wavelength dependent visual pigment nomograms. *Vision Research*, **17**, 147–151.

Eguchi, E. and Waterman, T.H. (1973) Orthogonal microvillus pattern in the eighth rhabdomere of the rock crab *Grapsus*. *Zeitschrift fuer Zellforschung und Mikroskopische Anatomie*, **137**, 145–157.

Exner, S. (1891) *Die Physiologie der facettirten Augen von Krebsen und Insecten.* Liepzig-Wein, Deuticke.

Fernández, H.R. (1965) *A survey of the visual pigments of decapod crustacea of South Florida.* Ph.D. thesis, University of Miami, Coral Gables, Florida.

Fernández, H.R. (1973) Spectral sensitivity and visual pigment of the compound eye of the galatheid crab *Pleuroncodes planipes*. *Marine Biology*, **20**, 148–153.

Fincham, A.A. (1980) Eyes and classification of malacostracan crustaceans. *Nature (London)*, **287**, 729–731.

Fincham, A.A. (1984) Ontogeny and optics of the eyes of the common prawn *Palaemon (Palaemon) serratus* (Pennant, 1777). *Zoological Journal of the Linnean Society*, **81**, 89–113.

Firsov, M.L. and Govardovskii, V.I. (1990) Dark noise of visual pigments with different absorption maxima. *Sensory Systems*, **4**, 25–34 (In Russian).

Fisher, L.R. (1967) Pigments of the euphausiid eyes. *Journal of the Marine Biological Association of India*, **2**, 1074–1080.

Fisher, L.R. and Goldie, E.H. (1959) The eye pigments of a euphausiid crustacean, *Meganyctiphanes norvegica* (M. Sars). *Proceedings of the International Congress on Zoology (London)*, **15**, 533–535.

Fisher, L.R. and Goldie, E.H. (1961) Pigments of compound eyes. In *Progress in Photobiology* (eds. B. Christensen and B. Buchamann), Elsevier North-Holland Inc., New York, pp. 153–154.

Fleisher, K.J. and Case, J.F. (1995) Cephalopod predation facilitated by dinoflagellate luminescence. *Biological Bulletin*, **189**, 263–271.

Forward, R.B. Jr. (1987) Comparative study of crustacean larval photoresponses. *Marine Biology*, **94**, 589–595.

Forward, R.B. Jr. and Costlow, J.D. (1974) The ontogeny of phototaxis by the larvae of the crab *Rhithropanopeus harrisi*. *Marine Biology*, **26**, 27–33.

Forward, R.B. Jr. and Cronin, T.W. (1979) Spectral sensitivity of larvae from intertidal crustaceans. *Journal of Comparative Physiology*, **133**, 311–315.

Forward, R.B. Jr. and Douglass, J.K. (1989) Crustacean larval visual sensitivity during diel vertical migration. *Proceedings of the 21st EMBS*, 59–66.

Forward, R.B. Jr., Cronin, T.W. and Douglass, J.K. (1988) The visual pigments of crabs - II. Environmental adaptations. *Journal of Comparative Physiology A*, **162**, 479–490.

Foxton, P. (1970a) The vertical distribution of pelagic decapods (Crustacea: Natantia) collected on the Sond Cruise 1965. I. The Caridea. *Journal of the Marine Biological Association of the United Kingdom*, **50**, 939–960.

Foxton, P. (1970b) The vertical distribution of pelagic decapods (Crustacea: Natantia) collected on the Sond Cruise 1965. II. The Penaeidea and General Discussion. *Journal of the Marine Biological Association of the United Kingdom*, **50**, 961–1000.

Frank, T.M. and Case, J.F. (1988a) Visual spectral sensitivities of bioluminescent deep-sea crustaceans. *Biological Bulletin*, **175**, 261–273.

Frank, T.M. and Case, J.F. (1988b) Visual spectral sensitivities of the bioluminescent deep-sea mysid, *Gnathophausia ingens*. *Biological Bulletin*, **175**, 274–283.

Frank, T.M. and Widder, E.A. (1994a) Evidence for behavioural sensitivity to near-UV light in the deep-sea crustacean *Systellaspis debilis*. *Marine Biology*, **118**, 279–284.

Frank, T.M. and Widder, E.A. (1994b) Comparative study of behavioural-sensitivity thresholds to near UV and blue–green light in the deep-sea crustaceans. *Marine Biology*, **121**, 229–235.

Frank, T.M. and Widder, E.A. (1996) UV light in the deep-sea: *in situ* measurements of downwelling irradiance in relation to the visual threshold sensitivity of UV-sensitive crustaceans. *Marine and Freshwater Behavior and Physiology*, **27**, 189–197.

Frisch, K. von and Kupeiwieser, H. (1913) Über den einfluss der lichtfarbe auf die phototaktischen reaktionen niederer krebse. *Biol. Centrabl.*, **33**, 517–552.

Gaten, E. (1988) Light-induced damage to the dioptric apparatus of *Nephrops norvegicus* (L.) and the quantitative assessment of the damage. *Marine Behaviour and Physiology*, **13**, 169–183.

Gaten, E. and Herring, P.J. (1995) Morphology of the reflecting superposition eyes of larval oplophorid shrimps. *Journal of Morphology*, **225**, 19–29.

Gaten, E., Shelton, P.M.J., Chapman, C.J. and Shanks, A.M. (1990) Depth related variation in the structure and functioning of the compound eye of the Norway lobster *Nephrops norvegicus*. *Journal of the Marine Biological Association of the United Kingdom*, **70**, 343–355.

Gaten, E., Shelton, P.M.J. and Herring, P.J. (1992) Regional morphological variations in the compound eyes of certain mesopelagic shrimps in relation to their habitat. *Journal of the Marine Biological Association of the United Kingdom*, **72**, 61–75.

Glantz, R.M. (1996) Polarization sensitivity in Crayfish lamina monopolar neurons. *Journal of Comparative Physiology A*, **178**, 413–425.

Goddard, S.M. and Forward, R.B. Jr. (1991) The role of underwater polarised light patterns in sun compass navigation of the grass shrimp *Palaemonetes vulgaris*. *Journal of Comparative Physiology A*, **169**, 479–491.

Goldsmith, T.H. (1972) The natural history of invertebrate photoreceptors. In *Handbook of Sensory Physiology Volume VII/1, Photochemistry of vision* (ed. H.J.A. Dartnall), Springer-Verlag, Berlin, Heidelberg, New York, pp. 685–719.

Goldsmith, T.H. (1975) The polarization sensitivity-dichroic absorption paradox in arthropod photoreceptors. In *Photoreceptor Optics* (eds. A.W. Snyder and R. Menzel), Springer, Berlin, Heidelberg, New York, pp. 392–409.

Goldsmith, T.H. (1978a) The effects of screening pigments on the spectral sensitivity of some Crustacea with scotopic (superposition) eyes. *Vision Research*, **18**, 475–482.

Goldsmith, T.H. (1978b) The spectral absorption of crayfish rhabdoms: Pigment, photoproduct, and pH sensitivity. *Vision Research*, **18**, 463–473.

Goldsmith, T.H. (1991) The evolution of visual pigments and colour vision. In *The Perception of Colour* (ed. P. Gouras). *Vision and visual dysfunction, Volume 6* (ed. gen. J. Cronly-Dillon), Macmillan, pp. 62–89.

Goldsmith, T.H. and Bruno, M.S. (1973) Behavior of rhodopsin and metarhodopsin in isolated rhabdoms of crabs and lobster. In *Biochemistry and Physiology of Visual Pigments* (ed. H. Langer), Springer-Verlag, Berlin, Heidelberg, New York, pp. 147–153.

Goldsmith, T.H. and Wehner, R. (1977) Restrictions on rotational and translational diffusion of pigment in the membranes of rhabdomeric photoreceptor. *Journal of General Physiology*, **70**, 453–490.

Greenberg, A.D., Honig, B. and Ebrey, T.G. (1975) Wavelength dependence of the bandwidths of visual pigment spectra. *Nature*, **257**, 823–824.

Hamacher, H. and Stieve, H. (1984) Spectral properties of the rhodopsin-system of the crayfish *Astacus leptodactylus*. *Photochemistry and Photobiology*, **39**, 379–390.

Hamacher, K.J. and Kohl, K.D. (1981) Spectroscopical studies of the *Astacus* visual pigment. *Biophys. Struct. Mech.*, **7**, 338.

Hamdorf, K. (1979) The physiology of invertebrate visual pigments.. In *Handbook of Sensory Physiology Volume VII/6A, Vision in invertebrates* (ed. H. Autrum), Springer-Verlag, Berlin, Heidelberg, New York, pp. 145–224.

Hargreaves, P.M. (1984) The distribution of Decapoda (Crustacea) in the open ocean and near-bottom over an adjacent slope in the northern North-east Atlantic Ocean during autumn 1979. *Journal of the Marine Biological Association of the United Kingdom*, **64**, 829–857.

Hargreaves, P.M. (1985) The distribution of Mysidacea in the open ocean and near-bottom over slope regions in the northern North-east Atlantic Ocean during 1979. *Journal of Plankton Research*, **7**, 241–261.

Hargreaves, P.M. (1989) The vertical and horizontal distribution of four species of the genus Gnathophausia (Crustacea: Mysidacea) in the eastern North Atlantic Ocean. *Journal of Plankton Research*, **11**, 687–702.

Hariyama, T., Tsukahara, Y. and Meyer-Rochow, V.B. (1993) Spectral responses including a UV-sensitive cell type in the eye of the isopod *Ligia exotica*. *Naturwissenschaften*, **80**, 233–235.

Hárosi, F.I. (1975) MSP: The technique and some of its pitfalls. In *Vision in Fishes* (ed. M.A. Ali), Plenum Press, New York, pp. 43–55.

Hárosi, F.I. (1976) Spectral relations of cone pigments in goldfish. *Journal of General Physiology*, **68**, 65–68.

Hárosi, F.I. (1987) Application of Fourier transform smoothing and statistical techniques to the determination of spectral parameters. *Journal of General Physiology*, **89**, 717–743.

Hays, D. and Goldsmith, T.H. (1969) Microspectrophotometry of the visual pigment of the spider crab *Libinia emarginata*. *Zeitschrift fuer Vergleichende Physiologie*, **65**, 218–232.

Herring, P.J. (1977) Luminescence in cephalopods and fish. *Symposia of the Zoological Society of London*, **38**, 127–159.

Herring, P.J. (1983) The spectral characteristics of luminous marine organisms. *Proceedings of the Royal Society of London B*, **220**, 183–217.

Herring, P.J. (1997) Aaaargh, no! - in lights. *Nature*, **387**, 140.

Herring, R.J. and Roe, H.S.J. (1988) The photoecology of pelagic oceanic decapods. *Symposia of the Zoological Society of London*, **59**, 263–290.

Hertel, H. (1980) The compound eye of *Artemia salina* (Crustacea). II. Analysis by electrophysiological methods. *Zoological Journal of Physiology B*, **84**, 15–25.

Hiller-Adams, P. and Case, J.F. (1984) Optical parameters of euphausiid eyes as a function of habitat depth. *Journal of Comparative Physiology A*, **154**, 307–318.

Hiller-Adams, P. and Case, J.F. (1985) Optical parameters of the eyes of some benthic decapods as a function of habitat depth (Crustacea, Decapoda). *Zoomorphology*, **105**, 108–113.

Hiller-Adams, P. and Case, J.F. (1988) Eye size of pelagic crustaceans as a function of habitat depth and possession of photophores. *Vision Research*, **28**, 667–680.

Hiller-Adams, P., Widder, E.A. and Case, J.F. (1988) The visual pigments of four deep-sea crustacean species. *Journal of Comparative Physiology A*, **163**, 63–72.

Hillman, P., Dodge, F.A., Hochstein, S., Knight, B.W. and Minke, B. (1973) Rapid dark recovery of the invertebrate early receptor potential. *Journal of General Physiology*, **62**, 77–86.

Hobson, E.S., McFarland, W.N. and Chess, J.R. (1981) Crepuscular and nocturnal activities of Californian nearshore fishes, with consideration of their scotopic visual pigments and the photic environment. *Fisheries Bulletin*, **79**, 1–30.

Hochstein, S., Minke, B., Hillman, P. and Knight, B.W. (1978) The kinetics of visual pigment systems. I. Mathematical analysis. *Biological Cybernetics*, **30**, 23–32.

Hope, A.J., Partridge, J.C., Dulai, K.S. and Hunt, D.M. (1997) Mechanisms of wavelength tuning in the rod opsins of deep-sea fishes. *Proceedings of the Royal Society of London B*, **264**, 155–163.

Horridge, G.A. (1967) Perception of polarization plane, colour, and movement in two dimensions by the crab, *Carcinus*. *Zeitschrift fuer Vergleichende Physiologie*, **55**, 207–224.

Hyatt, G.W. (1975) Physiological and behavioural evidence for colour discrimination by fiddler crabs (Brachyura, Ocypodidae, Genus, Uca). In *Physiological Ecology of Estuarine Organisms* (ed. J. Vernberg), University of South Carolina Press, Columbia.

Ivanoff, A. and Waterman, T.H. (1958) Factors, mainly depth and wavelength, affecting the degree of underwater light polarization. *Journal of Marine Research*, **16**, 283–307.

Jerlov, N.G. (1968) *Optical Oceanography*. Elsevier, Amsterdam.

Jerlov, N.G. (1976) *Marine Optics*. Elsevier, Amsterdam.

Johnson, M.L. (in prep.) Ph.D. thesis, Leicester University.

Kampa, E.M. (1955) Euphausiopsin, a new photosensitive pigment from the eyes of euphausiid crustaceans. *Nature (London)*, **175**, 996–998.

Kampa, E.M. (1965) The euphausiid eye - a re-evaluation. *Vision Research*, **5**, 475–481.

Kay, R.H. (1965) Light-stimulated and light-inhibited bioluminescence of the euphausiid *Meganyctiphanes norvegica* (G.O. Sars). *Proceedings of the Royal Society of London B*, **162**, 365–386.

Kirschfeld, K. (1974) The absolute sensitivity of lens and compound eyes. *Zeitschrift fuer Naturforschung C*, **29**, 592–596.

Knowles, A. and Dartnall, H.J.A. (1977) Photobiology of vision. In *The Eye, Volume IIB* (ed. H. Davson), Academic Press, New York, London, San Francisco, pp. 1–689.

Kong, K.-L., Yau, M.-F. and Wasserman, G.S. (1980) Filter-mediated color vision with one visual pigment. *Science*, **207**, 783–786.

Krebs, W. (1974) Area and volume relationship in the crayfish retina. *Vision Research*, **14**, 441–442.

Krebs, W. and Lietz, R. (1982) Apical region of the crayfish retinula. *Cell and Tissue Research*, **222**, 409–415.

Lall, A.B. and Cronin, T.W. (1987) Spectral sensitivity of the compound eyes in the purple land crab, *Gecarcinus lateralis*. *Biological Bulletin*, **173**, 398–406.

Lamb, T.D. (1995) Photoreceptor spectral sensitivities: common shape in the long-wavelength region. *Vision Research*, **35**, 3083–3091.

Land, M.F. (1976) Superposition images are formed by reflection in the eyes of some oceanic decapod crustacea. *Nature*, **263**, 764–765.

Land, M.F. (1978) Animal eyes with mirror optics. *Scientific American*, **239**, 126–134.

Land, M.F. (1980) Compound eyes: old and new optical mechanisms. *Nature*, **287**, 681–686.

Land, M.F. (1981a) Optics and vision in invertebrates. In *Handbook of Sensory Physiology Volume VII/6B, Vision in invertebrates* (ed. H. Autrum), Springer-Verlag, Berlin, Heidelberg, New York, pp. 471–594.

Land, M.F. (1981b) Optical mechanisms in the higher Crustacea with a comment on their evolutionary origins. In *Sense Organs* (eds. M.S. Laverack and D.J. Cosens), Blackie, London, Glasgow, pp. 31–48.

Land, M.F. (1984) Crustacea. In *Photoreception and Vision in Invertebrates* (ed. M.A. Ali), Plenum Press, pp. 401–438.

Land, M.F. (1988) Paradoxical superposition. *Nature*, **332**, 15–16.

Land, M.F. (1989a) Variations in the structure and design of compound eyes. In *Facets of Vision* (eds. D.G. Stavenga and R.C. Hardie), Springer-Verlag, Berlin, Heidelberg, pp. 89–111.

Land, M.F. (1989b) The eyes of hyperiid amphipods: relation so optical structure to depth. *Journal of Comparative Physiology A*, **164**, 751–762.

Land, M.F. (1989c) The sight of deep wet heat. *Nature*, **337**, 404.

Land, M.F. (1990) Optics of the eyes of marine animals. In *Light and Life in the Sea* (eds P.J. Herring, A.K. Campbell, M. Whitfield and L. Maddock), Cambridge University Press, Cambridge, New York, pp. 149–166.

Land, M.F., Burton, F.A. and Meyer-Rochow, V.B. (1979) The optical geometry of euphausiid eyes. *Journal of Comparative Physiology*, **130**, 49–62.

Land, M.F., Marshall, N.J. and Diebel, C. (1995) Tracking of blue lights by hyperiid amphipods. *Journal of the Marine Biological Association of the United Kingdom*, **75**, 71–81.

Lang, W.H., Forward, R.B. Jr. and Miller, D.C. (1979) Behavioural responses of *Balanus improvisus* nauplii to light intensity and spectrum. *Biological Bulletin*, **157**, 166–181.

Latz, M.I., Frank, T.M. and Case, J.F. (1988) Spectral composition of bioluminescence of epipelagic organisms from the Sargasso Sea. *Marine Biology*, **98**, 441–446.

Laughlin, S.B., Menzel, R. and Snyder, A.W. (1975) Membranes, dichroism and receptor sensitivity. In *Photoreceptor Optics* (eds. A.W. Snyder and R. Menzel), Springer, Berlin, Heidelberg, New York, pp. 237–259.

Leggett, L.M.W. (1979) A retinal substrate for colour discrimination in crabs. *Journal of Comparative Physiology*, **133**, 159–166.

Levine, J.S. and MacNichol, E.F. Jr. (1982) Color vision in fishes. *Scientific American*, **246**, 108–117.

Levine, J.S. and MacNichol, E.F. Jr. (1985) Microspectrophotometry of primate photoreceptors: Art, artifact and analysis. In *The Visual System* (eds. A. Fein and J.S. Levine), Liss, New York, pp. 73–87.

Levine, J.S., Lobel, P.S. and MacNichol, E.F. Jr. (1980) Visual communication in fishes. In *Environmental Physiology of Fishes* (ed. M.A. Ali), Plenum Press, New York, pp. 447–475.

Liebman, P. (1972) Microspectrophotometry of photoreceptors. In *Handbook of Sensory Physiology Volume VII/1, Photochemistry of vision* (ed. H.J.A. Dartnall), Springer-Verlag, Berlin, Heidelberg, New York, pp. 481–528.

Lindström, M. and Nilsson, H.L. (1988) Eye function of *Mysis relicta* Lóven (Crustacea) from two photic environments. Spectral sensitivity and light tolerance. *Journal of Experimental Marine Biology and Ecology*, **120**, 23–37.

Lipetz, L. E. and Cronin, T. W. (1988) Application of an invariant spectral form to the visual pigments of crustaceans: Implications regarding the binding of the chromophore. *Vision Research*, **28**, 1083–1093.

Loew, E.R. (1976) Light, and photoreceptor degeneration in the Norway lobster, *Nephrops norvegicus* (L.). *Proceedings of the Royal Society of London B*, **193**, 31–44.

Loew, E.R. (1979) Visual pigment regeneration rate and susceptibility to photic damage. In *The Effects of Constant Light on Visual Processes* (eds. T.P. Williams and B.N. Baker), Plenum Press, New York, London, pp. 297–306.

Loew, E.R. and Lythgoe, J.N. (1978) The ecology of cone pigments in teleost fishes. *Vision Research*, **18**, 715–722.

Loew, E.R. and McFarland, W.N. (1990) The underwater visual environment. In *The visual system of fish* (eds. R.H. Douglas and M.B.A. Djamgoz), Chapman and Hall, London, pp. 1–49.

Lythgoe, J.N. (1966) Visual pigments and underwater vision. In *Light as an Ecological Factor* (ed. R. Bainbridge, G. C. Evans and O. Ruckham), Blackwell, Oxford, pp. 375–391.

Lythgoe, J.N. (1968) Visual pigments and visual range underwater. *Vision Research*, **8**, 997–11012.

Lythgoe, J.N. (1972) The adaptation of visual pigments to the photic environment. In *Handbook of Sensory Physiology Volume VII/1, Photochemistry of vision* (ed. H. J. A. Dartnall), Springer-Verlag, Berlin, Heidelberg, New York, pp. 566–603.

Lythgoe, J.N. (1976) The ecology, function and phylogeny of iridescent multilayers in fish cones. In *Light as an Ecological Factor, Volume II* (eds. G.C. Evans, R. Bainbridge and O. Rackham), Blackwell, Oxford, pp. 211–247.

Lythgoe, J.N. (1979) *The Ecology of Vision.* Claredon Press, Oxford.

McFarland, W.N. (1986) Light in the sea - correlation with behaviors of fishes and invertebrates. *American Zoologist*, **26**, 389–401.

McFarland, W.N. and Munz, F.W. (1975a) Part II: The photic environment of clear tropical seas during the day. *Vision Research*, **15**, 1063–1070.

McFarland, W.N. and Munz, F.W. (1975b) Part III: The evolution of photopic visual pigments in fishes. *Vision Research*, **15**, 1071–1080.

MacNichol, E.F. Jr. (1986) A unifying presentation of photopigment spectra. *Vision Research*, **26**, 1543–1556.

MacNichol, E.F. Jr., Levine, J.S., Mansfield, R.J.W., Lipetz, L.E. and Collins, B.A. (1983) Microspectrophotometry of visual pigments in primate photoreceptors. In *Colour Vision* (eds. J.D. Mollon and L.T. Sharpe), Academic Press, London, New York, pp. 13–38.

Manning, R.B. (1969) *Stomatopod crustacea of the Western Atlantic. Studies in Tropical Oceanography 8.* University of Miami Press, 380 pp.

Manning, R.B. and Camp, D.K. (1983) Erythrosquilloidea, a new superfamily, and tetrasquillidae, a new family of stomatopod crustaceans. *Proceedings of the Biological Society of Washington*, **106**, 85–91.

Manning, R.B., Schiff, H. and Abbott, B.C. (1984) Eye structure and the classification of stomatopod crustacea. *Zoologica Scripta*, **13**, 41–44.

Mansfield, R.J.W. (1985) Primate photopigments and cone mechanisms. In *The Visual System* (eds. A. Fein and J.S. Levine), Liss, New York, pp. 89–106.

Marshall, N.B. (1979) *Developments in deep-sea biology*. Blandford, Dorset.

Marshall, N.J. (1988) A unique colour and polarization vision system in mantis shrimps. *Nature*, **333**, 557–560.

Marshall, N.J. and Land, M.F. (1993) Some optical features of the eyes of stomatopods. I. Eye shape, optical axes and resolution. *Journal of Comparative Physiology A*, **173**, 565–582.

Marshall, N.J., Land, M.F., King, C.A. and Cronin, T.W. (1991a) The compound eyes of mantis shrimps (Crustacea, Hoplocarida, Stomatopoda). I. Compound eye structure: the detection of polarised light. *Philosophical Transactions of the Royal Society of London B*, **334**, 33–56.

Marshall, N.J., Land, M.F., King, C.A. and Cronin, T.W. (1991b) The compound eyes of mantis shrimps (Crustacea, Hoplocarida, Stomatopoda). II Colour pigments in the eyes of stomatopod crustaceans: polychromatic vision by serial and lateral filtering. *Philosophical Transactions of the Royal Society of London B*, **334**, 57–84.

Marshall, N.J., Land, M.F., Oberwinkler, J., Jones, J.P. Horwood, J and Cronin, T.W. (1994) Mantis shrimps - sixteen visual pigments in one eye. Why? *The Ecology of Vision Conference, Abstracts. IMC, Sardinia, April 1994.*

Marshall, N.J., Jones, J.P. and Cronin, T.W. (1996) Behavioural evidence for colour vision in stomatopod crustaceans. *Journal of Comparative Physiology A*, **197**, 473–481.

Martin, F.G. and Mote, M.I. (1982) Colour receptors in marine crustaceans: a second class of retinular cell in the compound eyes of *Callinectes* and *Carcinus*. *Journal of Comparative Physiology*, **145**, 549–554.

Mensinger, A.F. and Case, J.F. (1990) Luminescent properties of deep sea fish. *Journal of Experimental Marine Biology and Ecology*, **144**, 1–15.

Mensinger, A.F. and Case, J.F. (1992) Dinoflagellate luminescence increases susceptibility of zooplankton to teleost predation. *Marine Biology*, **112**, 207–210.

Menzel, R. (1981) Spectral sensitivity and colour vision in invertebrates. In *Handbook of Sensory Physiology Volume VII/6A, Vision in invertebrates* (ed. H. Autrum), Springer-Verlag, Berlin, Heidelberg, New York, pp. 503–580.

Merbs, S.L. and Nathans, J. (1993) Role of hydroxyl-bearing amino acids in differentially tuning the absorption spectra of the human red and green cone pigments. *Photochemistry and Photobiology*, **58**, 706–710.

Merrett, N.R. and Marshall, N.B. (1981) Observations on the ecology of deep-sea bottom living fishes collected off North West Africa (08°27' N). *Progress in Oceanography*, **9**, 185–244.

Metzler, D.E. and Harris, C.M. (1978) Shapes of spectral bands of visual pigments. *Vision Research*, **18**, 1417–1420.

Meyer-Rochow, V.B. and Walsh, S. (1977) The eyes of mesopelagic crustaceans: I. *Gennadas sp.* (Penaeidae). *Cell and Tissue Research*, **184**, 87–101.

Minke, B. and Kirschfield, K. (1978) Microspectrophotometric evidence for two photo-interconvertible states of visual pigment in the barnacle lateral eye. *Journal of General Physiology*, **71**, 37–45.

Minke, B., Hochstein, S. and Hillman, P. (1973) Early receptor potential evidence for the existence of two thermally stable states in the barnacle visual pigment. *Journal of General Physiology*, **62**, 87–104.

Moody, M.F. and Parriss, J.R. (1961) The discrimination of polarized light by *Octopus*: a behavioral and morphological study. *Zeitschrift fuer Vergleichende Physiologie*, **44**, 268–291.

Moon, P. (1940) Proposed standard solar radiation curves for engineering use. *Journal of the Franklin Institute*, **230**, 583–617.

Morel, A. (1974) Optical properties of pure water and pure sea water. In *Optical Aspects of Oceanography* (ed. N.G. Jerlov and E. Steeman Nielsen), Academic Press, London, pp. 1–24.

Morton, R.A. (1972) The chemistry of the visual pigments. In *Handbook of Sensory Physiology Volume VII/1, Photochemistry of vision* (ed. H.J.A. Dartnall), Springer-Verlag, Berlin, Heidelberg, New York, pp. 33–68.

Muntz, W.R.A. and Mouat, G.S.V. (1984) Annual variations in the visual pigment of brown trout inhabiting lochs providing different light environments. *Vision Research*, **24**, 1575–1580.

Munz, F.W. and McFarland, W.N. (1973) The significance of spectral position in the rhodopsins of tropical marine fishes. *Vision Research*, **13**, 1829–1874.

Munz, F.W. and McFarland, W.N. (1977) Evolutionary adaptations of fishes to the photic environment. In *Handbook of Sensory Physiology Volume VII/5, The visual system in vertebrates* (ed. F. Crescitelli), Springer-Verlag, Berlin, Heidelberg, New York, pp. 193–274.

Nakayama, T.A. and Khorana, H.G. (1991) Mapping of the amino acids in membrane-embedded helices that interact with the retinal chromophore in the bovine rhodopsin. *Journal of Biological Chemistry*, **266**, 4269–4275.

Nässel, D.R. (1976) The retina and the retinal projection on the lamina ganglionaris of the crayfish *Pacifasticus leniusculus* (Dana). *Journal of Comparative Physiology A*, **167**, 341–360.

Nässel, D.R. and Waterman, T.H. (1979) Massive diurnally modulated photoreceptor turnover in crab light and dark adaptation. *Journal of Comparative Physiology*, **131**, 205–216.

Nathans, J. (1990) Determinants of visual pigment absorbances - role of charged amino acids in the putative transmembrane segments. *Biochemistry (Washington)*, **29**, 937–942.

Nathans, J., Thomas, D. and Hogness, D.S. (1986) Molecular genetics of human vision: the genes encoding blue, green , and red pigments. *Science*, **232**, 193–202.

Neville, A.C. and Luke, B.M. (1971) Form optical activity in crustacean cuticle. *Journal of Insect Physiology*, **17**, 519–526.

Nilsson, D.-E. (1983) Evolutionary links between apposition and superposition optics in crustacean eyes. *Nature*, **302**, 818–821.

Nilsson, D.-E. (1988) A new type of imaging optics in compound eyes. *Nature*, **332**, 76–78.

Nilsson, D.-E. (1989a) Optics and evolution of the compound eye. In *Facets of Vision* (eds. D.G. Stavenga and R.C. Hardie), Springer-Verlag, Berlin, Heidelberg, New York, pp. 30–73.

Nilsson, D.-E. (1989b) Vision optics and evolution. *Bioscience*, **39**, 298–307.

Nilsson, D.-E. (1990a) From cornea to retinal image in invertebrate eyes. *Trends in Neuroscience*, **13**, 55–64.

Nilsson, D.-E. (1990b) Three unexpected cases of refracting superposition eyes in crustaceans. *Journal of Comparative Physiology A*, **167**, 71–78.

Nilsson, D.-E. and Modlin, R.F. (1994) A mysid shrimp carrying a pair of binoculars. *Journal of Experimental Biology*, **189**, 213–236.

Nilsson, D.-E. and Pelger, S. (1994) A pessimistic estimate of the time required for an eye to evolve. *Proceedings of the Royal Society of London B*, **256**, 53–58.

Nilsson, H.L. and Lindström, M. (1983) Retinal damage and sensitivity loss of a light-sensitive crustacean compound eye (*Cirolana borealis*): electron microscopy and electrophysiology. *Journal of Experimental Biology*, **107**, 277–292.

O'Day, W.T. and Fernández, H.R. (1974) *Aristostomias scintillans* (Malacosteidae): a deep-sea fish with visual pigments apparently adapted to its own bioluminescence. *Vision Research*, **14**, 545–550.

Osorio, D. and Vorobyev, M. (1997) *Sepia* tones, stomatopod signals and the uses of colour. *Trends in Ecology and Evolution*, **12**, 167–168.

Osorio, D., Marshall, N.J. and Cronin, T.W. (in press) Stomatopod photoreceptor spectral tuning as an adaptation for colour constancy in water. *Vision Research.*

Palacios, A.G., Goldsmith, T.H. and Bernard, G.D. (1996) Sensitivity of cones from a cyprinid fish (*Danio aequipinnatus*) to ultraviolet and visible light. *Visual Neuroscience*, **13**, 411–421.

Partridge, J.C. (1986) *Microspectrophotometry of vertebrate photoreceptors.* Ph.D. thesis, University of Bristol.

Partridge, J.C. (1989) The visual pigments of deep-sea fishes: Ecophysiology and molecular biology. *Progress in Underwater Science*, **14**, 17–31.

Partridge, J.C. (1990) The colour sensitivity and vision of fishes. In *Light and Life in the Sea* (ed. P. J. Herring, A. K. Campbell, M. Whitfield, and L. Maddock), Cambridge University Press, pp. 167–184.

Partridge, J.C. and Cummings, M.E. (in prep.) Adaptation of visual pigments to the aquatic environment. In *Adaptive mechanisms in the ecology of vision* (eds. S.N. Archer, M.B.A. Djamgoz, E. Loew, J.C. Partridge and S. Vallerga). Chapman and Hall.

Partridge, J.C. and DeGrip, W.J. (1991) A new template for rhodopsin (vitamin A_1 based) visual pigments. *Vision Research*, **31**, 619–630.

Partridge, J.C. and Douglas, R.H. (1995) Far-red sensitivity of dragon fish. *Nature (London)*, **375**, 21–22.

Partridge, J.C., Archer, S.N. and Lythgoe, J.N. (1988) Visual pigments in the individual rods of deep-sea fishes. *Journal of Comparative Physiology A*, **162**, 543–550.

Partridge, J.C., Shand, J., Archer, S.N., Lythgoe, J.N., and van Groningen-Luyben, W.A.H.M. (1989) Interspecific variation in the visual pigments of deep-sea fishes. *Journal of Comparative Physiology A*, **164**, 513–529.

Partridge, J.C., Archer, S.N. and Van Oostrum, J. (1992) Single and multiple visual pigments in deep-sea fishes. *Journal of the Marine Biological Association of the United Kingdom*, **72**, 113–130.

Pelli, D.G. and Chamberlain, S.C. (1989) The visibility of 350 °C black-body radiation by the shrimp *Rimicaris exoculata* and man. *Nature*, **337**, 460–461.

Piekos, W.B. and Waterman, T.H. (1983) Nocturnal rhabdom cycling and retinal hemocyte functions in crayfish (*Procambarus*) compound eyes. I. Light microscopy. *Journal of Experimental Zoology*, **225**, 209–217.

Poo, M-M. and Cone, R.A. (1974) Lateral diffusion of rhodopsin in the photoreceptor membrane. *Nature*, **247**, 438–441.

Press, W.H., Flannery, B.P., Teukolsy, S.A. and Vetterling, W.T. (1986) *Numerical recipes*. University Press, Cambridge.

Rebach, S. and Dunham, D.W. (1983) *Studies in adaptation. The behaviour of higher Crustacea*. Wiley Interscience Publication, New York, 282 pp.

Reuter, T.E., White, R. and Wald, G. (1971) Rhodopsin and porphyropsin fields in the adult bullfrog retina. *Journal of General Physiology*, **58**, 351–371.

Roe, H.S.J. and Shale, D.M. (1979) A new multiple rectangular midwater trawl (RMT 1+8M) and some modifications to the Institute of Oceanographic Sciences' RMT 1+8. *Marine Biology*, **50**, 283–288.

Rossel, S. (1989) Polarization sensitivity in compound eyes. In *Facets of Vision* (eds. D.G. Stavenga and R.C. Hardie), Springer-Verlag, Berlin, Heidelberg, pp. 298–316.

Schehr, R.S. (1984) *Spectral sensitivities of anatomically identified photoreceptors in the compound eye of Daphnia magna*. Ph.D. thesis, Columbia University.

Schiff, H. (1963) Dim light vision of *Squilla mantis* L. *American Journal of Physiology*, **205**, 927–940.

Schiff, H. (1987) Optical and neural pooling in visual processing in crustacea. *Comparative Biochemical Physiology A*, **88**, 1–13.

Schnapf, J.L., Kraft, T.W. and Baylor, D.A. (1987) Spectral sensitivity of human cone photoreceptors. *Nature*, **325**, 439–441.

Schnapf, J.L., Kraft, T.W., Nunn, B.J. and Baylor, D.A. (1988) Spectral sensitivity of primate photoreceptors. *Visual Neuroscience*, **1**, 255–261.

Schwemer, J. (1984) Renewal of visual pigment in photoreceptors of the blowfly. *Journal of Comparative Physiology* A, **154**, 535–547.

Scott, S. and Mote, M.I. (1974) Spectral sensitivity in some marine crustacea. *Vision Research*, **14**, 659–663.

Seliger, H.H., Lall, A.B. and Biggley, W.H. (1994) Blue through UV polarisation sensitivities in insects. Optimizations for the range of atmospheric polarization conditions. *Journal of Comparative Physiology A*, **175**, 475–486.

Shand, J. (1993) Changes in the spectral absorption of cone visual pigments during the settlement of the goatfish *Upeneus tragula*: the loss of red sensitivity as a benthic existence begins. *Journal of Comparative Physiology A*, **173**, 115–121.

Shashar N., Rutledge, P.S. and Cronin, T.W. (1996) Polarization vision in cuttlefish - a concealed communication channel? *Journal of Experimental Biology*, **199**, 2077–2084.

Shelton, P.M.J., Gaten, E. and Chapman, C.J. (1985) Light and retinal damage in *Nephrops norvegicus* (L.) (Crustacea). *Proceedings of the Royal Society of London B*, **226**, 217–236.

Shelton, P.M.J., Gaten, E. and Herring, P.J. (1992) Adaptations of tapeta in the eyes of mesopelagic decapod shrimps to match the oceanic irradiance distribution. *Journal of the Marine Biological Association of the United Kingdom*, **72**, 77–88.

Smith, F.E. and Baylor, E.R. (1953) Colour responses in the cladocera and their ecological significance. *American Naturalist*, **87**, 49–55.

Smith, K.C. and Macagno, E.R. (1990) UV photoreceptors in the compound eye of *Daphnia magna* (Crustacea, Branchiopoda). A fourth spectral class in a single ommatidium. *Journal of Comparative Physiology A*, **166**, 597–606.

Snyder, A.W., Menzel, R. and Laughlin, S.B. (1973) Structure and function of the fused rhabdom. *Journal of Comparative Physiology*, **87**, 99–135.

Srebro, R. (1966) A thermal component of excitation in the lateral eye of *Limulus*. *Journal of Physiology A*, **187**, 417–425.

Stavenga, D.G. and Schwemer, J. (1984) Visual pigments of invertebrates. In *Photoreception and Vision in Invertebrates* (ed. M.A. Ali), Plenum Press, New York and London, pp. 11–61.

Stavenga, D.G., Smits, R.P. and Hoenders, B.J. (1993) Simple exponential functions describing the absorbance bands of visual pigment spectra. *Vision Research*, **33**, 1011–1017.

Stearns, D.E. and Forward, R.B. Jr. (1984) Photosensitivity of the calanoid copepod, *Acartia tonsa*. *Marine Biology*, **82**, 85–90.

Stearns, S.C. (1975) Light responses of *Daphnia pulex*. *Limnology and Oceanography*, **20**, 564–570.

Stowe, S. (1980a) Rapid synthesis of photoreceptor membrane and assembly of new microvilli in a crab at dusk. *Cell and Tissue Research*, **211**, 419–440.

Stowe, S. (1980b) Spectral sensitivity and retinal pigment movement in the crab *Leptograspsus variegatus* (Fabricius). *Journal of Experimental Biology*, **87**, 73–98.

Stowe, S. (1981) Effects of illumination changes on rhabdom synthesis in a crab. *Journal of Comparative Physiology*, **142**, 19–25.

Stowe, S. (1983) A theoretical explanation of intensity-independent variation of polarization sensitivity in Crustacean retinula cells. *Journal of Comparative Physiology A*, **153**, 435–441.

Suzuki, T. and Eguchi, E. (1987) A survey of 3-dehydroretinal as a visual pigment chromophore in various species of crayfish and other crustaceans. *Experientia*, **43**, 1111–1113.

Suzuki, T., Makino-Tasaka, M. and Eguchi, E. (1984) 3-dehydroretinal (vitamin A_2 aldehyde) in crayfish eye. *Vision Research*, **24**, 783–787.

Suzuki, T., Arikawa, K. and Eguchi, E. (1985) The effects of light and temperature on the rhodopsin-porphyropsin visual system of the crayfish, *Procambarus clarkii*. *Zoological Science*, **2**, 455–461.

Swift, M.C. and Forward, R.B. Jr. (1983) Photoresponses of the copepod *Mesocyclops edax*. *Journal of Plankton Research*, **5**, 407–415.

Thurston, M.H. (1976) The vertical distribution and diurnal migration of the Crustacea Amphipoda collected during the Sond Cruise, 1965. I. The Gammaridea. *Journal of the Marine Biological Association of the United Kingdom*, **56**, 359–382.

Tovee, M.J. (1995) Ultraviolet photoreceptors in the animal kingdom - their distribution and function. *Trends in Ecology and Evolution*, **10**, 455–460.

Tyler, J.E. (1959) Natural water as a monochromator. *Limnology and Oceanography*, **4**, 102–105

Tyler, J.E. and Smith, R.C. (1970) *Measurement of spectral irradiance underwater*. Gordon and Breach, New York.

Van Dover, C.L., Szuts, E.Z., Chamberlain, S.C. and Cann, J.R. (1989) A novel eye in the 'eyeless' shrimp from hydrothermal vents of the Mid-Atlantic Ridge. *Nature*, **337**, 458–460.

Via, S.E. and Forward, R.B. Jr. (1975) The ontogeny and spectral sensitivity of polarotaxis in the larvae of the crab *Rhithropanopeus harrisi* (Gould). *Biological Bulletin*, **149**, 251–166.

Vogt, K. (1975) Zur Optik des Flußkrebsauges. *Zeitschrift fuer Naturforschung C*, **30**, 691.

Vogt, K. (1977) Ray path and reflection mechanisms in crayfish eyes. *Zeitschrift fuer Naturforschung*, **32**, 466–468.

Vogt, K. (1980) Die Spiegeloptik des Flußkrebsauges. The optical system of the crayfish eye. *Journal of Comparative Physiology*, **135**, 1–19.

Wald, G. (1968) Single and multiple visual systems in arthropods. *Journal of General Physiology*, **51**, 125–156.

Wald, G. and Hubbard, R. (1957) Visual pigment of a decapod crustacean: the lobster. *Nature (London)*, **180**, 278–280.

Wald, G. and Rayport, S. (1977) Vision in annelid worms. *Science*, **196**, 1434–1439.

Wald, G. and Seldin, E.B. (1968) Spectral sensitivity of the common prawn, *Palaemonetes vulgaris*. *Journal of General Physiology*, **51**, 694–700.

Waterman, T.H. (1981) Polarization sensitivity. In *Handbook of Sensory Physiology Volume VII/6C, Vision in invertebrates* (ed. H. Autrum), Springer-Verlag, Berlin, Heidelberg, New York, pp. 566–603.

Waterman, T.H. and Piekos, W.B. (1983) Nocturnal rhabdom cycling and retinal hemocyte functions in crayfish (*Procambarus*) compound eyes. II. Transmission electron microscopy and acid phosphatase localization. *Journal of Experimental Zoology*, **225**, 219–231.

Waterman, T.H., Fernández, H.R. and Goldsmith, T.H. (1969) Dichroism of photosensitive pigment in rhabdoms of crayfish *Orconectes*. *Journal of General Physiology*, **54**, 415–432.

Wehner, R. (1983) The perception of polarized light. In *The Biology of Photoreception* (eds. D.J. Cosens and D. Vince-Prue), Symposia of the Society for Experimental Biology. Symposium XXXVI. Cambridge University Press, Cambridge, London, New York. pp. 331–369.

Welsh, J.H. and Chace, F.A., Jr. (1937) Eyes of deep sea crustaceans. I. Acanthephyridae. *Biological Bulletin*, **72**, 57–74.

Widder, E.A., Latz, M.I. and Case, J.F. (1983) Marine bioluminescence spectra measured with an optical multichannel detection system. *Biological Bulletin*, **165**, 791–810.

Widder, E.A., Hiller-Adams, P. and Case, J.F. (1987) A multichannel microspectrophotometer for visual pigment investigations. *Vision Research*, **27**, 1047–1055.

Wild, R.A., Darlington, E. and Herring, P.J. (1985) An acoustically controlled cod-end system for the recovery of deep-sea animals at *in situ* temperatures. *Deep-Sea Research*, **32**, 1583–1589.

Wood, P., Partridge, J.C. and De Grip, W.J. (1992) Rod visual pigment changes in the elver of the eel *Anguilla anguilla* (L.) measured by microspectrophotometry. *Journal of Fish Biology*, **41**, 601–611.

Zeiger, J. and Goldsmith, T.H. (1989) Spectral properties of porphyropsin from an invertebrate. *Vision Research*, **29**, 519–527.

Appendix I

Photographs of Selected Deep-Sea Decapods

Figure 6.1 *Bentheogennema intermedia* (Family Penaeidae). Scale bar = 10 mm.

Figure 6.2 *Gennadas valens* (Family Penaeidae). Scale bar = 10 mm.

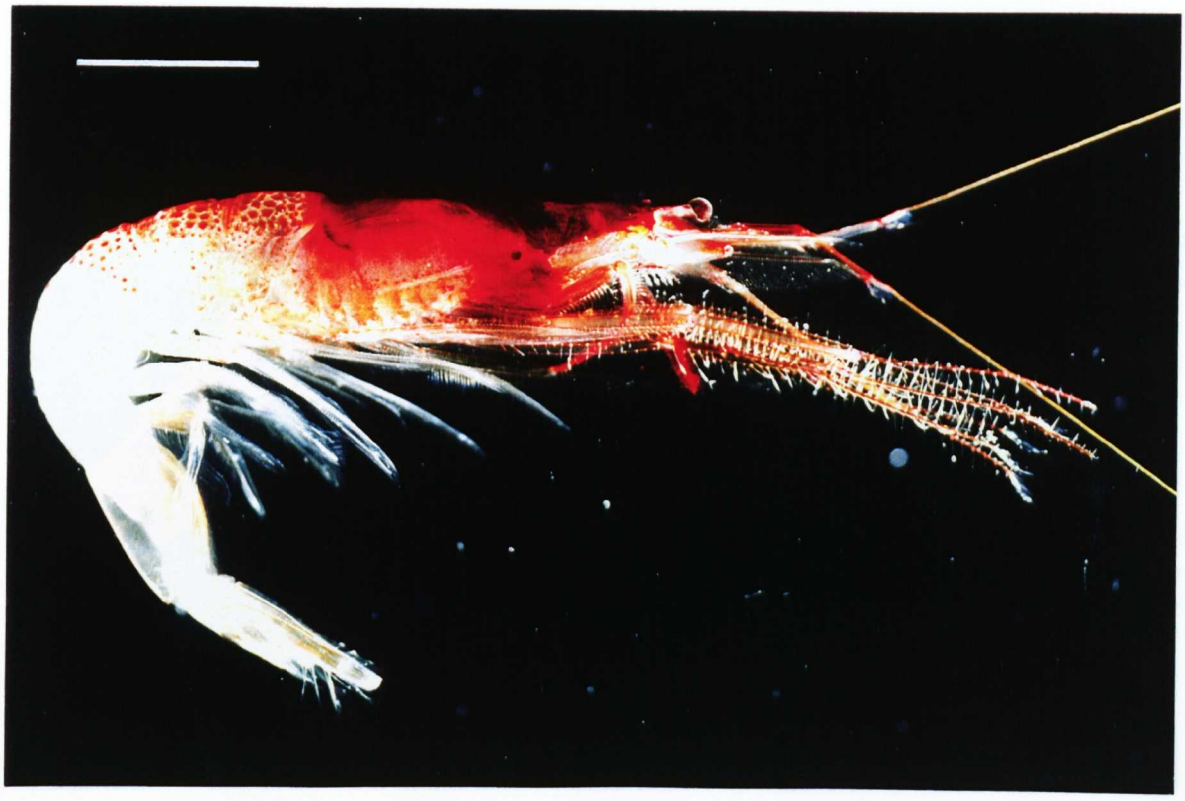

Figure 6.3 *Sergestes curvatus* (Family Sergestidae). Scale bar = 10 mm.

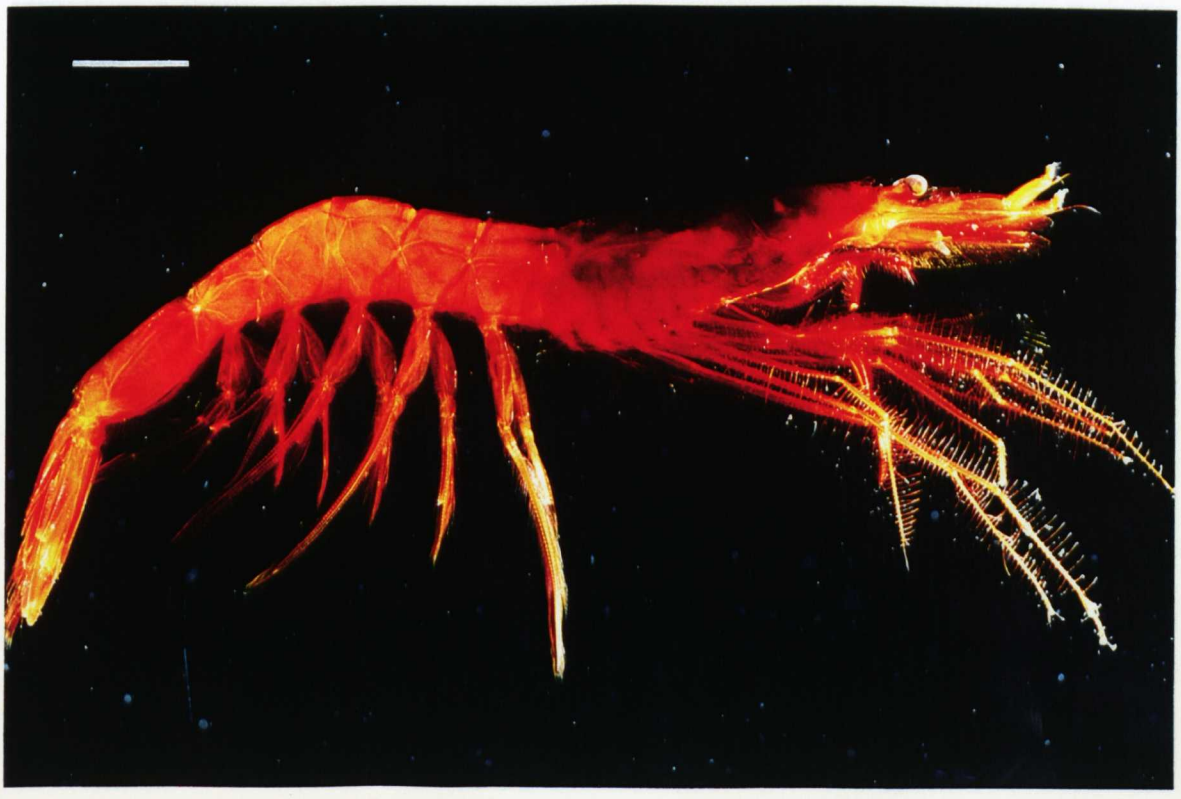

Figure 6.4 *Sergia maximus* (Family Sergestidae). Scale bar = 10 mm.

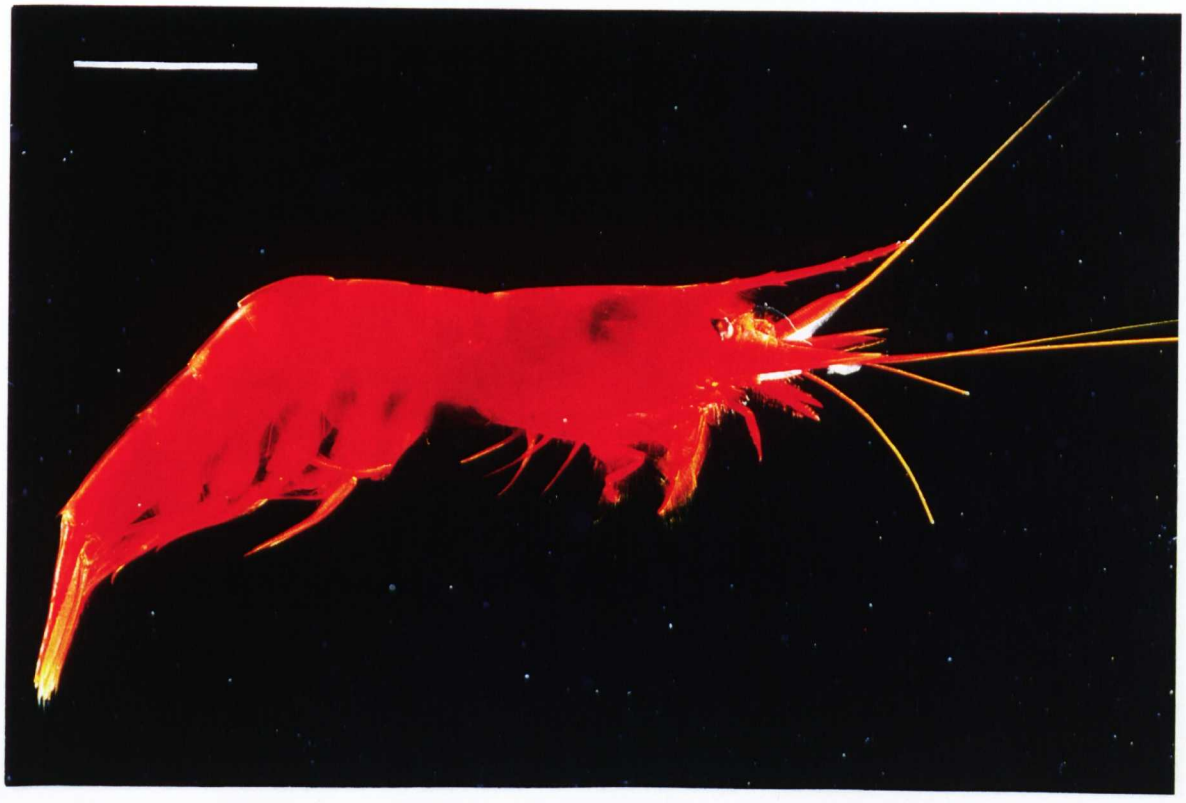

Figure 6.5 *Acanthephyra purpurea* (Family Oplophoridae). Scale bar = 10 mm.

Figure 6.6 *Meningodora vesca* (Family Oplophoridae). Scale bar = 5 mm.

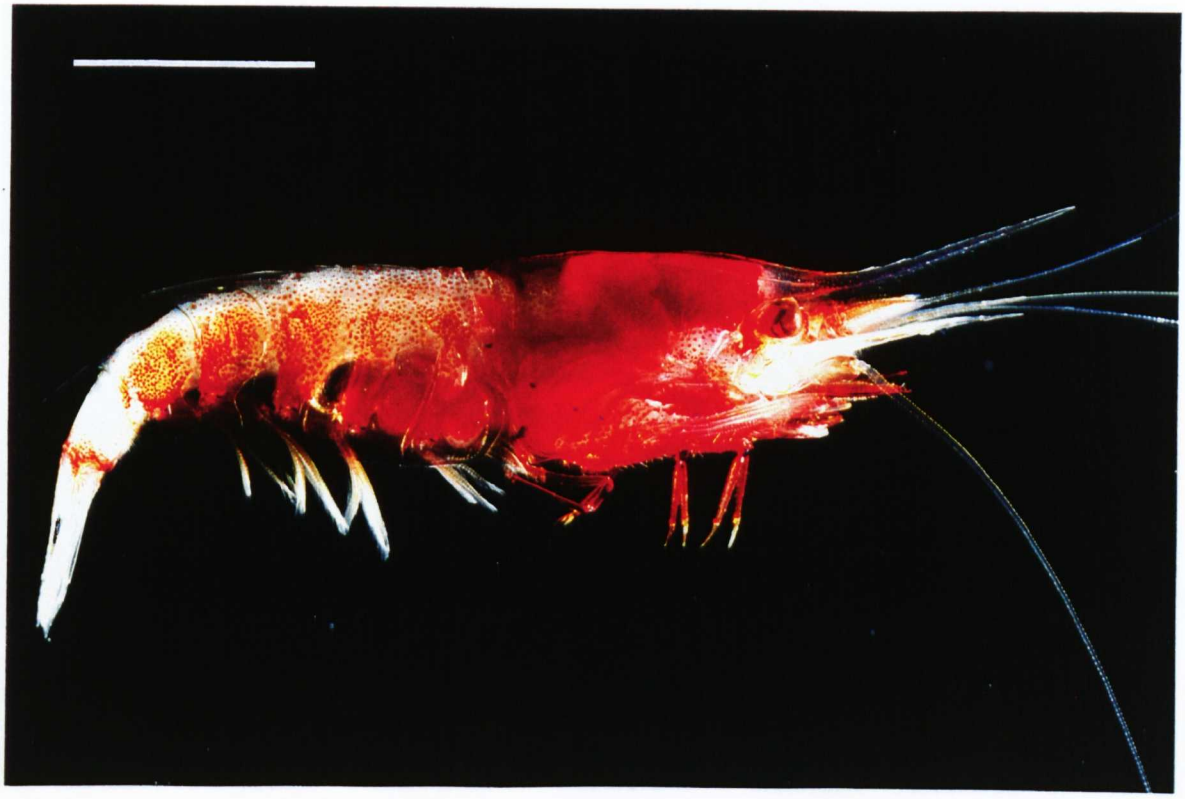

Figure 6.7 *Oplophorus spinosus* (Family Oplophoridae). Scale bar = 10 mm.

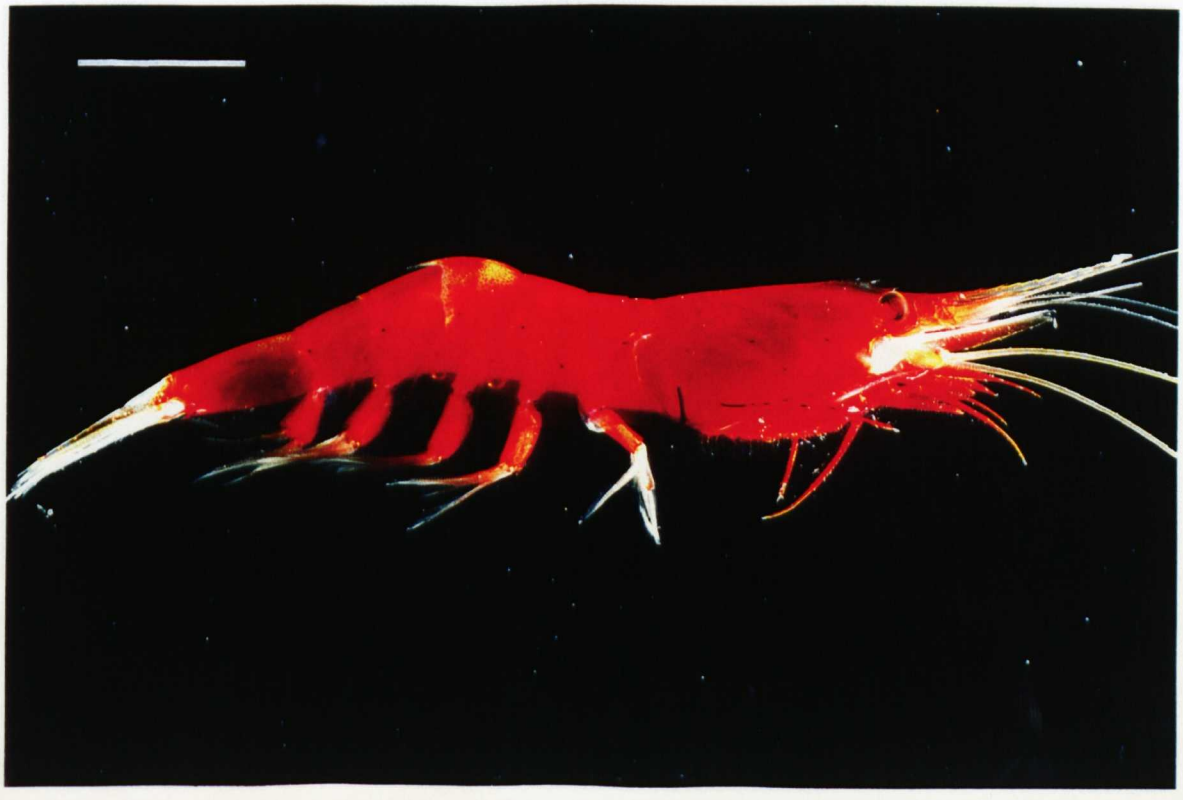

Figure 6.8 *Systellaspis debilis* (Family Oplophoridae). Scale bar = 10 mm.

Figure 6.9 *Stylopandalus richardii* (Family Pandalidae). Scale bar = 10 mm.

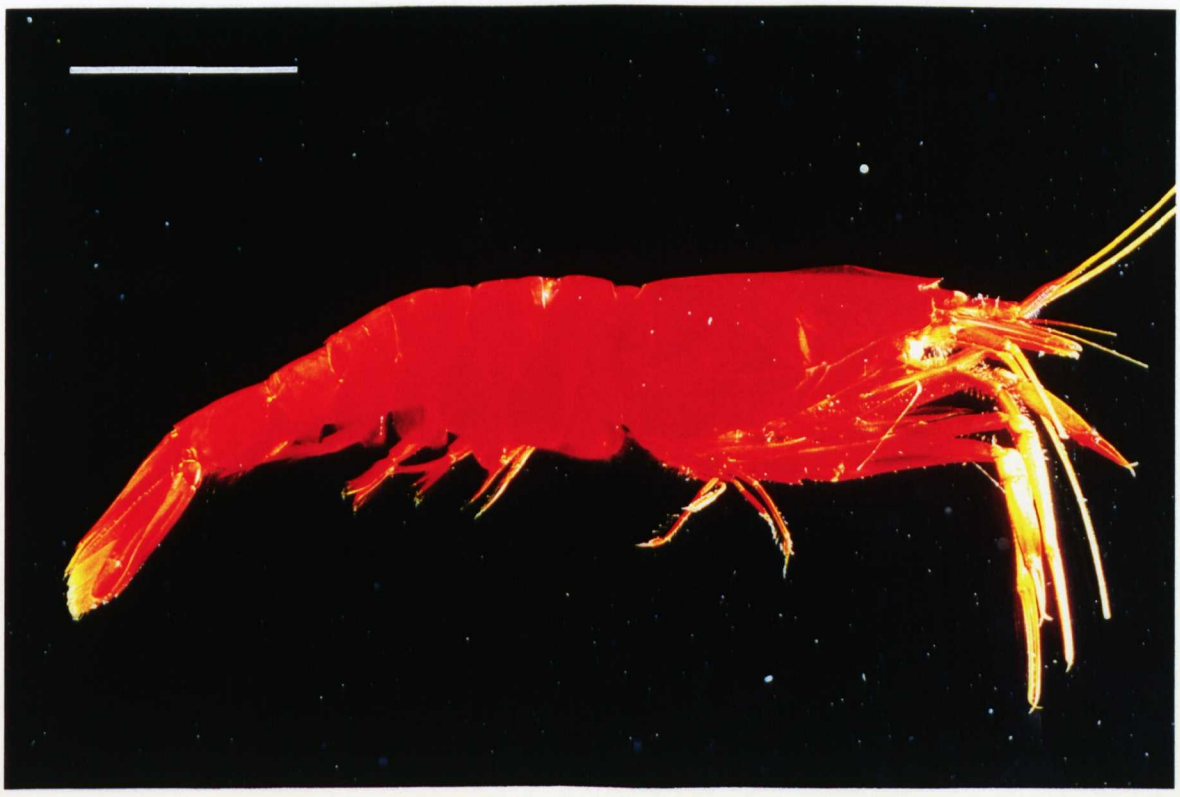

Figure 6.10 *Parapasiphaea sulcatifrons* (Family Pasiphaeidae). Scale bar = 20 mm.

Appendix II

Abstracts of Conference Posters

VISUAL PIGMENTS OF DEEP-SEA CRUSTACEANS.

J. Kent†, J.C. Partridge†, T.W. Cronin‡ and P.J. Herring§.

†School of Biological Sciences, University of Bristol.
‡School of Biological Sciences, University of Maryland Baltimore County Campus, USA.
§ Southampton Oceanography Centre.

The deep-sea presents an unique visual environment; either a dim, monochromatic blue world or, at greater depths and at night, a virtually lightless environment broken only by bioluminescent emissions. The suggestion that deep-sea fishes have their retinal spectral sensitivities tuned to the light available at depth, the sensitivity hypothesis, has been a topic frequently reassessed as new data become available. We have recently started a comparative study of the visual pigments of deep-sea crustaceans. During Challenger cruise 122 (September/October 1995) we collected sixteen species of deep-sea decapod crustaceans. On board ship, specimens were sorted under dim red illumination, the eyes removed and preserved by rapid freezing with cryospray. Following the cruise, at the University of Bristol, frozen eyes were sectioned on a cryostat and the spectral absorbances of the rhabdomeric visual pigments measured using a purpose-modified microspectrophotometer (MSP). As with deep-sea fish, we found that most deep-sea crustaceans have a single visual pigment approximately matched to the spectrum of light available in the deep-sea. However, two species also have a second, short wavelength sensitive visual pigment conferring broader spectral sensitivity and the potential for hue discrimination.

(The Society for Experimental Biology's Annual Meeting, Lancaster, UK. March 1996)

VISUAL PIGMENTS AND PHOTORECEPTOR CLASSES OF DEEP-SEA SHRIMPS.

T.W. Cronin, **J. Kent**, T. Frank, E. Widder, J.C. Partridge, P. Herring and P. Robinson.

Dept. of Biological Sciences, University of Maryland Baltimore County, Baltimore, MD 212228; Harbour Branch Oceanographic Institute, Fort Pierce, FL 34946; School of Biological Sciences, University of Bristol, Bristol BS8 1UG, UK.

The photic environment of the deep-sea contains the remains of downwelling sunlight, filtered by the overlying water to a limited waveband centered near 475 nm, together with a diversity of bioluminescent emitters. The visual pigments of the deep-sea fishes tend to absorb maximally in the waveband transmitted by the water and emitted by bioluminescent animals, and thus have λ_{max} in the spectral range between 450 and 500 nm. We collected a diversity of deep-sea shrimps using midwater sampling gear capable of maintaining living specimens in total darkness, as well as a benthic trawl sampling at depths near 4500 m. Visual pigments were determined using microspectrophotometry of cryosections from eyes quick-frozen and stored at low temperature immediately after collection. Most species have a single visual pigment (λ_{max} $\approx$ 490 nm) throughout the retina, but two oplophorid shrimp species (*Systellaspis debilis* and *Oplophorus spinosus*) possessed a second, unexpectedly short-wavelength photoreceptor class peaking near 410 nm. An analysis comparing the spectrum of downwelling light with typical bioluminescent emission spectra suggests that these species may be capable of discriminating bioluminescence from downwelling light, enabling them to counter bioluminescent camouflage systems.

Supported by NSF Grant IBN-9413357, NERC Grant GR3/9329 and studentship GT4/93/3/A, and by the Harbour Branch Oceanographic Institute.

(Society for Neuroscience, Annual Meeting, Washington D.C., USA. November 1996)

VISUAL PIGMENTS IN DEEP-SEA CRUSTACEANS.

Jeremy Kent, Julian Partridge, Peter Herring* and Tom Cronin‡.

School of Biological Sciences, University of Bristol, Woodland Road, Bristol, BS8 1UG, UK. (email: j.c.partridge@bristol.ac.uk)
*Southampton Oceanography Centre, Empress Dock, Southampton, SO14 3ZH, UK.
‡School of Biological Sciences, University of Maryland Baltimore County Campus, Catonsville, Maryland 21228, USA.

The deep-sea presents a unique visual environment. Due to spectral filtering by overlying water, the downwelling light is reduced to homochromatic blue light. At greater depths and at night, downwelling sunlight is insignificant and the visual environment is limited to bioluminescent emissions. The suggestion that deep-sea animals have their retinal spectral sensitivities matched to the light available at depth, the Sensitivity Hypothesis, has largely been investigated using species of deep-sea fishes. To test the hypothesis further it has now been applied to another taxon which inhabits the same environment. This poster presents a comparative study of the visual pigments of deep-sea crustaceans, concentrating on the caridean and penaeidean decapods.

During RRS Challenger cruise 122 (September to October 1995) and a cruise on the RV New Horizon (May 1996) a total of thirty six species of deep-sea crustaceans were collected. Specimens included twenty nine species of decapods, six mysids and a single amphipod. On board ship, specimens were sorted under dim red illumination, the eyes removed and preserved by rapid freezing. Following the cruises, at the University of Bristol, frozen eyes were sectioned on a cryostat and the spectral absorbances of the rhabdomeric visual pigments measured using a purpose-modified microspectrophotometer. Computer spread-sheet based analysis methods were written to fully characterise the visual pigments present.

Most deep-sea crustaceans investigated have a single visual pigment with a wavelength of peak absorbance (λ_{max}) between 482 and 509 nm, on average *ca.* 10 nm longer than those of the deep-sea fishes. Thus, on first investigation, deep-sea crustacean visual pigments are not matched to the spectrum of downwelling sunlight available in the deep-sea, nor the wavelength of maximum bioluminescent emissions. No correlation is apparent with depth and the total range of pigments limited. However, simple modelling describing the viewing of bioluminescence suggests that, due to the asymmetries of both visual pigment and bioluminescent spectra, these pigments are, in fact, spectrally located to maximise photon capture. This model also reveals a correlation between rhabdom length and rhodopsin pigment which may explain differences in visual pigment complement between species. In contrast to the majority of species, four Oplophorid species also have a second, short wavelength sensitive visual pigment (λ_{max} *ca.* 414 nm), conferring broader spectral sensitivity and the potential for hue discrimination. The demonstration of such a pigment in a bathypelagic, non-vertically migrating species which lacks photophores questions the use of such a pigment in mediating daily migrations and conspecific recognition. However, its presence still indicates its possible advantage in increasing perception to, and distinguishing between, different sources of bioluminescence.

(The Eighth Deep Sea Biology Symposium, MBARI, USA. September 1997)